UNIVERSITY OF SOUTHAMPTON

FACULTY OF NATURAL AND ENVIRONMENTAL SCIENCES

School of Chemistry

Active-Template Synthesis of Small Functionalised Rotaxanes for Sensing Applications

by

Mathieu Denis

Thesis for the degree of Doctor of Philosophy

December 2017

UNIVERSITY OF SOUTHAMPTON

ABSTRACT

FACULTY OF NATURAL AND ENVIRONMENTAL SCIENCE

Chemistry

Thesis for the degree of Doctor of Philosophy

ACTIVE-TEMPLATE SYNTHESIS OF SMALL FUNCTIONALISED ROTAXANES FOR SENSING APPLICATIONS

Mathieu Denis

Interlocked molecules, the archetypal examples of which are catenanes, and rotaxanes, have progressed over the last half-century from a significant synthetic challenge to readily accessible chemical species. The interest for these supramolecular architectures, which started from a purely aesthetic point of view, has further developed due to the high degree of freedom between its individual components. Controlling this motion *via* chemical or physical stimuli has resulted in the development of many stimuli-responsive interlocked systems with applications in wide range of field such as switches, molecular machinery and sensing. The latter is of particular interest as the mechanical bond within a catenane or rotaxane molecule creates a well-defined three-dimensional environment that can be readily functionalised to accommodate a variety of guest molecules. This thesis presents an investigation into the design and synthesis of novel functional rotaxane receptors and their application in the sensing of metal ions, anions and small chiral molecules.

The introductory chapter presents the active template approach to interlocked molecules. It highlights its key advantages and outline recent advances that have been made using this methodology. The following three chapters focus on the study of rotaxane receptors synthesised using this approach. Chapter two reports the synthesis of a sulfur-functionalised rotaxane and the investigation of its selective response for Zn^{2+} ion over other transition metal cations. Chapter three on the other hand focuses on a urea-based rotaxane that binds ion-pairs. This section will introduce preliminary results obtained with a simple model rotaxane before presenting its evolution into a stimuli-responsive receptor. The binding behaviour of both the rotaxane and related non-interlocked axle will be investigated to demonstrate the impact of the mechanical bond on the properties of the receptor. In the fourth chapter, the project was expanded toward chirality and more specifically enantioselective sensing. The development of a novel synthetic route to access functionalised mechanically planar chiral rotaxanes will be presented and it will conclude on preliminary binding studies of simple chiral anionic guest that shows enantioselectivity.

Table of Contents

DECLARATION OF AUTHORSHIP

I, MATHIEU DENIS

declare that this thesis and the work presented in it are my own and has been generated by me as the result of my own original research.

ACTIVE-TEMPLATE SYNTHESIS OF SMALL FUNCTIONALISED ROTAXANES FOR SENSING APPLICATIONS

I confirm that:

1. This work was done wholly or mainly while in candidature for a research degree at this University;
2. Where any part of this thesis has previously been submitted for a degree or any other qualification at this University or any other institution, this has been clearly stated;
3. Where I have consulted the published work of others, this is always clearly attributed;
4. Where I have quoted from the work of others, the source is always given. With the exception of such quotations, this thesis is entirely my own work;
5. I have acknowledged all main sources of help;
6. Where the thesis is based on work done by myself jointly with others, I have made clear exactly what was done by others and what I have contributed myself;
7. Parts of this work have been published as: M. Denis and S. M. Goldup, "*The Active Template Approach to Interlocked Molecules: Principles, Progress and Applications*", Nat. *Chem. Rev.*, 2017, **1**, 61. doi:10.1038/s41570-017-0061

Signed: Mathieu Denis .....

Date: 12/12/2017.....

Acknowledgements

The first and most important acknowledgment of all goes to the one I have been calling "Boss" for the past three years now, my supervisor Steve. Thank you for putting your trust in me, for your guidance and for the chance to visit amazing places during my PhD.

A second big thank you goes to every single person that has been part of "The Team", no matter if it was for a few years or a few days. Without you this journey would not have been the same and you have made it an unforgettable experience, with all its ups and downs.

A very special thank you goes to Marzia. Thank you for everything, I could not be more specific!

I would also like to address a special thank you to Jamie, my Bro. You have been a great co-worker obviously but more importantly, you now are an amazing friend and I am glad I met you. Also, I guess that we could say you introduced me to one of the best thing the British culture has to offer, thank you for that!

Cath and Elise, you two have been without a doubt the best lab neighbours I could have ever wished for. You taught me a lot and were always here when I needed a break. Those coffee/sporcle moments were the best, thank you.

Florian for the nice morning talks while listening to French music. Peggy for being Peggy, certainly one of the most caring person that I know. My office neighbour Ellen for her energy, the sweets she brought to group meeting and her funny accent!

Thank you to Mike for proof reading on his own my entire thesis and Ed for the template. Both things were very useful and much appreciated.

A special thank you to Wim. It is a shame that you had to leave only a few months after I started. You have most certainly had an impact on my PhD at its very beginning and I am grateful I met you.

Pour conclure sur une note plus personnelle, je tiens à remercier ma famille. Vous avez toujours été là pour moi et soutenu chacune de mes décisions, même les plus folles. Sans vous rien de tout cela n'aurait été possible. Je vous dédie ce travail.

Definitions and Abbreviations

δ ..... Chemical shift

Ac ..... Acetyl

AT-CuAAC ..... Active-template Cu-catalysed azide-alkyne cycloaddition

Aq. ..... Aqueous

BINOL .....1,1'-binaphthyl-2,2'-diyl

Boc .....*t*-Butyloxycarbonyl

CD ..... Circular dichroism

CDI .....1,1'-carbonyldiimidazole

CIP ..... Cahn-Ingold-Prelog

COSY .....Correlation spectroscopy

DDQ 2,3-Dichloro-5,6-dicyano-1,4-benzoquinone

DEAD .....Diethyl azodicarboxylate

DIPEA .....*N,N'*-diisopropylethylamine

DMAP 4-Dimethylaminopyridine

DMF ..... *N,N'*-Dimethylformamide

DMSO ..... Dimethylsulfoxide

DPP .....diketopyrrolopyrrole

EDTA .....*N,N,N',N'*-ethylenediamine tetraacetate

ee ..... Enantiomeric excess

EI ..... Electron Ionisation

Equiv. ..... Equivalent

EtOAc ..... Ethyl acetate

EtOH .....Ethanol

h .....Hours

HMBC .....Heteronuclear multiple-bond correlation

HPLC ..... High performance liquid chromatography

HRMS .....High resolution mass spectrometry

HSQC .....Heteronuclear single quantum correlation

IR .....Infrared radiation

J ..... Coupling constant

J-MOD ..... J-modulation spin-echo

LAH .....Lithium aluminium hydride

LRMS .....Low resolution mass spectrometry

M ..... Molar

Me .....Methyl

min ..... Minute

MLCT .....Metal-to-ligand charge transfer

m.p. ..... Melting point

Ms .....Methanesulfonyl

MS ..... Mass spectrometry

NMR ..... Nuclear magnetic resonance

NOESY .....Nuclear Overhauser effect spectroscopy

PET .....Photoinduced electron transfer

Ppm .....Parts per million

quant. .....Quantitative

R_{mp} .....*R* isomer (mechanically planar chiral)

ROESY ..... Rotating-frame NOE Spectroscopy

r.t. ..... Room temperature

S_{mp} ..... *S* isomer (mechanically planar chiral)

TBA .....Tetrabutylammonium

TBDMS .....*Tert*-butyldimethylsilyl

TEA .....Triethylamine

TFA ..... Trifluoroacetic acid

THF .....Tetrahydrofuran

TLC .....Thin layer chromatography

Ts 4-Toluenesulfonyl

UV-Vis ..... Ultraviolet-visible radiation

Chapter 1: Introduction

Abstract: << The active template approach to interlocked molecules takes advantage of the ability of metal ions to both organise precursor fragments for mechanical bond formation and to mediate the final covalent bond forming reaction that captures the interlocked structure. Since its inception just a decade ago, this new methodology has expanded rapidly from a single reaction for rotaxane synthesis to a range of metal-mediated bond formations for the synthesis of complex interlocked molecules. Here we introduce the active template concept, its key advantages for the synthesis of interlocked molecules and outline recent advances that have been made using this technology. We will conclude with comments about future directions and challenges.>>

Acknowledgements: I would like to thank my supervisor Prof Stephen Goldup for giving me the opportunity to write the review on the active template approach to interlocked molecules with him.

Prior publication: The majority of this chapter was previously published as part of:

M. Denis and S. M. Goldup, "*The Active Template Approach to Interlocked Molecules: Principles, Progress and Applications*", Nat. *Chem. Rev.*, 2017, **1**, 61. doi:10.1038/s41570-017-0061

1.1. Introduction

Interlocked molecules, the archetypal examples of which are catenanes, and rotaxanes, have progressed over the last half-century from a significant synthetic challenge to readily accessible chemical species[1]. The first synthetic breakthroughs in the field were provided by Wasserman, who demonstrated in 1960 that catenane formation could be achieved simply by taking advantage of the random threading of macrocycle precursors through pre-formed rings prior to cyclisation[2], and soon after by Schill and Lüttringhaus, who showed in 1964 that the low yield of the Wasserman's approach could be significantly improved by employing a covalent template[3]. Although successful, both of these approaches foundered on low synthetic efficiencies: Wasserman's statistical approach employed simple building blocks but led to inherently low yields of the interlocked target; Schill and Lüttringhaus' covalent template directed approach led to significantly higher yields in the mechanical bond forming step but required the laborious synthesis of complex precursors.

The synthetic "big bang" moment for the field came in 1983 when Sauvage and co-workers disclosed the first metal ion templated synthesis of a catenane[4]. Sauvage's approach was revolutionary because it demonstrated for the first time that interlocked molecules could be obtained in an efficient manner from relatively simple building blocks by employing non-covalent interactions to orient the covalent components prior to mechanical bond formation. This "passive template" synthetic philosophy has driven research on interlocked molecules for over three decades, with a small number of privileged non-covalent templates that deliver the interlocked structure in high yield dominating the field, including Stoddart's electron-deficient/electron-rich π-π template, Leigh's hydrogen bonding tetralactam macrocycles, Beer's anion-directed approach, and various systems that take advantage of hydrophobic binding[1]. This has allowed the study of the mechanical bond for a range of applications, perhaps most famously as components of molecular machines for which Sauvage and Stoddart received the 2016 Nobel Prize for Chemistry along with Feringa[5].

The metal ion-directed methods developed by Sauvage employed metal-ligand interactions as a passive "glue" to organise the covalent components prior to mechanical bond formation by "stoppering" of the axle component (in the case of rotaxane synthesis; Figure 1. 1 a) or "clipping" of the macrocycle (applicable in both rotaxane and catenane synthesis). Arguably however, this fails to take full advantage of the chemistry of metal ions, the

dominant application of which in modern chemistry is as catalytically active species for the synthesis of complex molecules. In 2006, Leigh and co-workers introduced the active template (AT) concept[6] in which the full potential of the templating moiety is realised; a metal ion bound in the cavity of a macrocycle mediates the formation of a new covalent bond between two suitably functionalised half axles *through* the cavity of the ring, leading to efficient mechanical bond formation (Figure 1. 1 b).

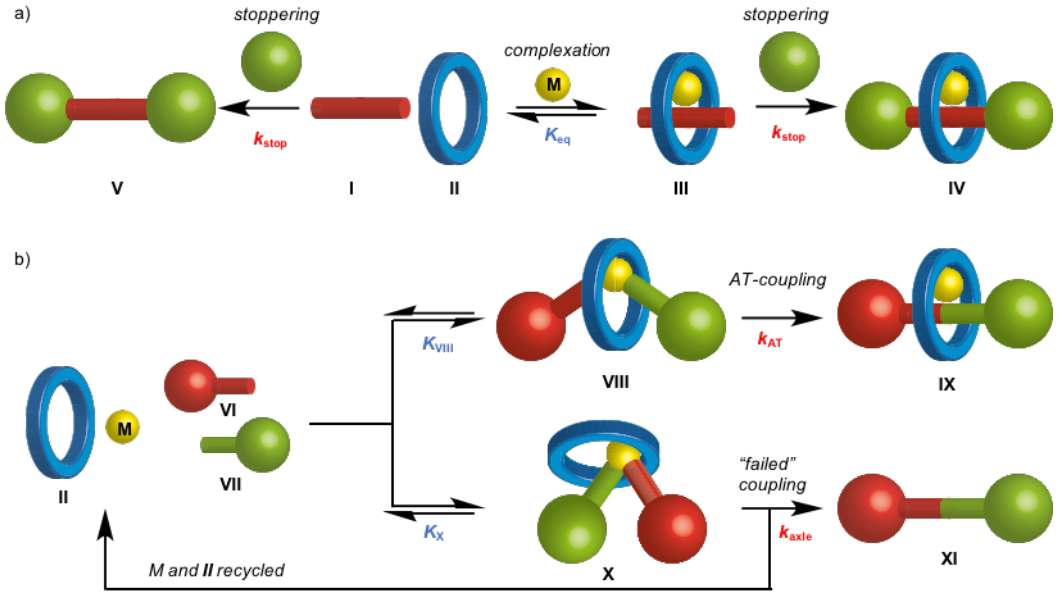

Figure 1. 1 Schematic representations of the passive and active template synthesis of rotaxanes indicating the key steps leading to reaction selectivity and examples of the AT-CuAAC reaction. a) Cartoon representation of the metal ion-directed passive template approach to rotaxanes by stoppering. b) Cartoon representation of the active template approach to rotaxanes.

In this chapter, we will introduce the active template concept and chart its development from the original report to a powerful synthetic tool for the production of a range of complex interlocked molecules. Along the way, we will discuss the key differences and advantages of this novel methodology from those previously developed, the chemical requirements of a successful active template reaction, recent applications of the methodology and future directions for this relatively new synthetic approach.

1.2. Development of the Active Template Approach - the AT-CuAAC Reaction

The Cu-mediated alkyne-azide cycloaddition reaction[7,8] has rapidly become a tool of choice in the synthesis of functional non-natural products due its broad substrate scope and typically high synthetic efficiency. The active template (AT-CuAAC) modification of this ubiquitous "click"[9] reaction was the first example to be reported by Leigh and co-workers in 2006 and is the best-developed of current active template methodologies[10]. In the original report, a Cu^{I} ion bound to a pyridine ligand disposed endotopically in the cavity of the macrocycle mediated the formation of a triazole linkage. The reaction was proposed to proceed by coordinating the alkyne and azide moieties of the half-axle components to the Cu ion on opposite faces of the macrocycle, which activates them to the 1,3-dipolar cycloaddition reaction (Figure 1. 2 a). A respectable 57% isolated yield of rotaxane **4** was achieved when one equivalent of all components was used, the balance of the material being the non-interlocked axle and recovered macrocycle **3**. The yield based on macrocycle **3** could be raised to 94% when 5 equivalents of alkyne **1** and azide **2** were employed. Even when a sub-stoichiometric quantity of the Cu^{I} ion was added, yields as high as 82% were obtained demonstrating that the metal ion can turn over in an active template process.

Soon after[11], Leigh and co-workers extended the AT-CuAAC reaction to a range of pyridine-containing macrocycles. The key finding of this study was that, although macrocycle rigidity, number of Lewis basic donor atoms and steric hindrance near the binding site all affected the yield of the interlocked product, as long as the endotopic ligand was reasonably unencumbered and mono- or bi-dentate the desired rotaxane was indeed formed. This suggested that the active template approach could be relatively tolerant to modification of the macrocycle component. The one variable that was not explored in this report was the effect of macrocycle size on the reaction outcome, an important factor in rotaxane synthesis as the diameter the macrocyclic cavity determines the size of the stoppers required to hold it on the axle. An educated first "guess" of the effect of macrocycle size in an active template reaction might be that reaction efficiency would fall as the space within the macrocycle available for the bond formation to take place is reduced. In 2011 Goldup and co-workers published the first study of macrocycle size in the AT-CuAAC reaction and reached the surprising conclusion that instead, smaller bipyridine macrocycles led to enhanced yields of [2]rotaxane products; the smallest macrocycle investigated produced [2]rotaxanes with up to 100% selectivity[12]. This finding allowed the synthesis of a selection of functionalised rotaxanes in excellent yield based on a range of simple, small stopper units (Figure 1. 2 b). Subsequently, the same authors demonstrated that by modifying the reaction conditions

essentially quantitative yields could be obtained with all macrocycle sizes, increasing the generality of the AT-CuAAC reaction still further[13].

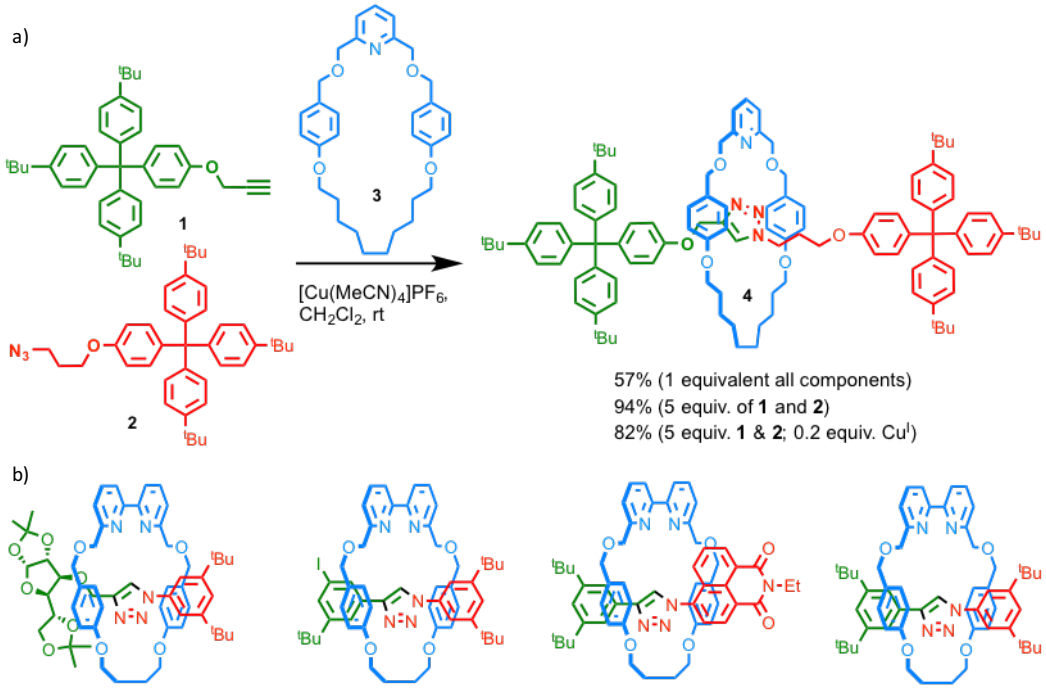

Figure 1. 2 a) Leigh's original active template CuAAC reaction. b) Examples of functionalised rotaxanes synthesised using the AT-CuAAC reaction with small macrocycles.

The simplicity of the AT-CuAAC, its generality with respect to substrates and macrocycle size, and the ready availability of the reaction components has led to this being the most studied and applied of all active template procedures published to date.

1.3. Key Differences Between the Passive and Active Template Approach

Although there are superficial similarities between metal ion-based passive template syntheses and the AT-CuAAC reaction (both require the metal ion to bind in the cavity of the macrocycle and coordinate the axle precursors), the passive and active template approaches differ fundamentally in the underlying driving force for mechanical bond formation. The passive template approach relies on the formation of a thermodynamically stable, suitably pre-organised complex between the covalent components (Figure 1. 1 a, intermediate **III**). The interlocked architecture is then captured by a final covalent bond forming reaction (stoppering) that is, to a first approximation, independent of the threading state of the molecule[14]. Thus, in the passive template process shown in Figure 1. 1 a, the yield of the product can be superficially linked to the position of the equilibrium between threaded complex **III** and non-productive species **I** and the yield optimised by designing conditions that bias the equilibrium to favour the former.

In contrast, the active template approach (Figure 1. 1 b) relies on the metal ion that mediates the final covalent bond formation being sequestered within the macrocycle, leading to bond formation taking place through the cavity of the macrocycle faster than it takes place in bulk solution. In this analysis, the active template phenomenon is fundamentally kinetically driven with the selectivity for the threaded product depending on the same factors that determine selectivity in catalytic processes; the position of the pre-equilibrium between the starting materials and activated complexes (e.g. **VIII** and **X**), the relative rates with which these complexes progress towards products, and any background reactions that compete with the desired bond formation (e.g. the direct reaction of substrates **VI** and **VII** without the involvement of the metal ion or off-ligand reactions mediated by metal ions not ligated by a macrocycle). In the case of the process shown in Figure 1.1 b the yield of rotaxane will depend on the relative values of $K_{\mathbf{VIII}}$, k_{AT}, $K_{\mathbf{X}}$ and k_{axle} all of which are expected to vary with the conditions of the reaction.

The distinction between the thermodynamic nature of the passive template phenomenon and the kinetic nature of the active template approach may seem somewhat philosophical but it has direct practical consequences, including the different considerations required when optimising passive and active template syntheses.

1.3.1. Role of Mechanism in the Active Template Approach

Based on the above discussion it should be clear that the detailed mechanism of the bond formation employed in an active template reaction is extremely important as it determines the availability and relative rate of pathways that lead to mechanical bond formation and competing pathways that lead to non-interlocked products. These different pathways can be superficially grouped as those that involve bond formation from opposite faces of the macrocycle (productive intermediate **VI**, Figure 1. 1 b), bond formation from the same face of the macrocycle (unproductive intermediate **VIII**) and background reactions not involving the macrocycle which necessarily lead to non-interlocked axle. In the case of the original AT-CuAAC reaction, the latter was determined to be the origin of the incomplete conversion of macrocycle **3**[11]; kinetic studies demonstrated that "free" Cu^{I} is both catalytically competent and indeed mediates the CuAAC reaction that leads to non-interlocked products faster than the corresponding AT-CuAAC reaction leading to rotaxane **4**. Thus, even when the quantity of unbound Cu^{I} is extremely low, the CuAAC pathway is competitive with the AT-CuAAC pathway. Having identified this trend, Leigh and co-workers were able to optimise the reaction further by employing 10 equivalents of macrocycle **3** to significantly reduce the

concentration of unbound Cu^{I}. Under these conditions the yield of rotaxane **4** based on half-axle components **1** and **2** rose to >95%.

The situation becomes more complicated when more than one viable active template pathway is present leading to different interlocked structures as Leigh and co-workers observed in the case of rigid pyridine macrocycle **9**. When **9** was employed in excess over Cu^{I} in the AT-CuAAC reaction of alkyne **1** and azide **3**, [3]rotaxane **10** was also isolated in addition to the expected [2]rotaxane (Figure 1. 3 a). This provides strong evidence for a di-Cu pathway in the triazole forming step[10]. Later work by Goldup and co-workers with bipyridine macrocycles **11** of varying size and substituents allowed a detailed model of the key intermediate in the bipyridine-mediated AT-CuAAC reaction to be derived (Figure 1. 3 b)[13]. The results suggest that, at least in the case of the smallest macrocycles, a mono-metallic pathway via intermediate **I** is favoured leading to [2]rotaxanes. However, when larger macrocycles bearing a benzylic ether linkage were employed at high temperature, a bimetallic pathway via intermediate **II** becomes important. By optimising the conditions of the reaction, the yield of the [3]rotaxane can be raised to ~50% based on the macrocyclic component or the [2]rotaxane can be formed in >95% yield in all cases.

These examples demonstrate that the active template approach can be used as a relatively unusual mechanistic probe in which the mechanical state of the product provides insight into the composition of key intermediates en route to the mechanical bond formation. Conversely this insight can be used to allow the synthesis of new interlocked products. Goldup and co-workers used the detailed mechanistic model to design a kinetic self-sorting approach to hetero[3]rotaxanes in which the order of macrocycles on the axle is determined by the mechanism of the reaction[15].

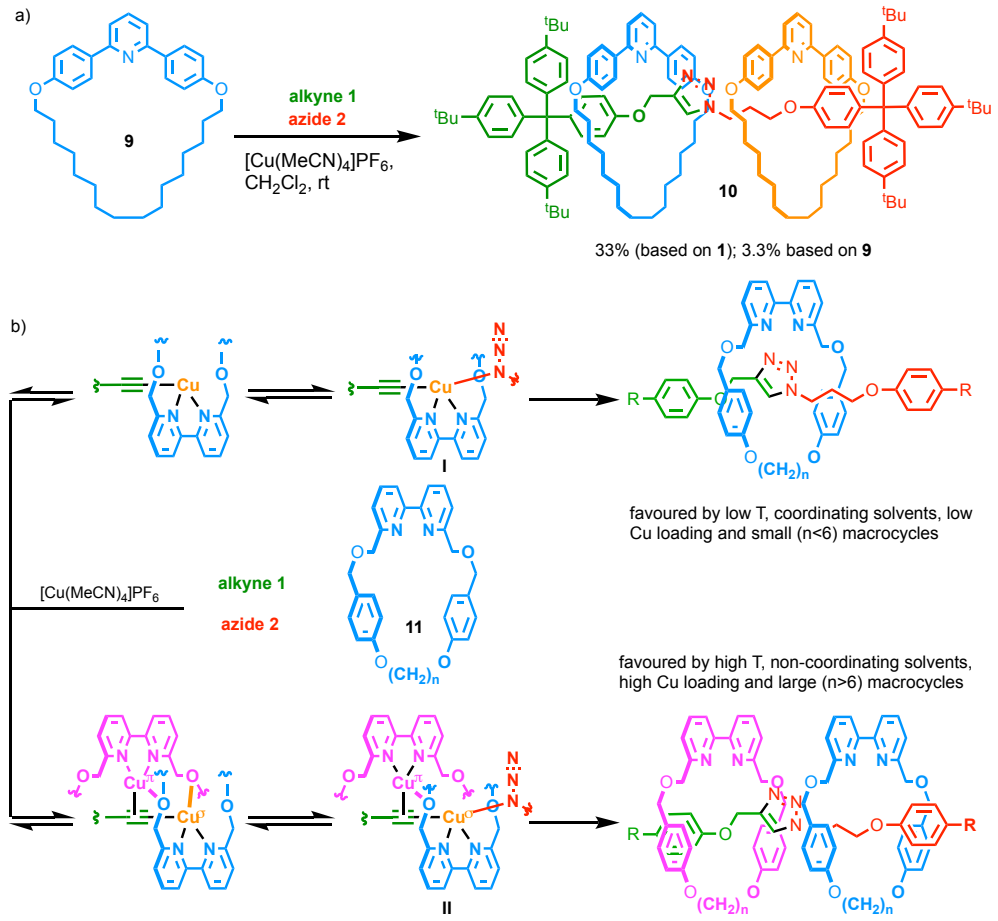

Figure 1. 3 The formation of [3]rotaxanes in the AT-CuAAC reaction. a) Formation of [3]rotaxanes **10** in the AT-CuAAC reaction with pyridine macrocycle **9**. b) A detailed mechanistic model for the formation of [3]rotaxanes in the bipyridine-mediated AT-CuAAC reaction in which the pathway followed depends on ring size, temperature, Cu loading and solvent.

1.3.2. Turnover of reaction components

One consequence of the kinetic nature of AT methodologies is that there is no requirement that the axle and macrocycle combine to form a stable complex with the metal ion in either the interlocked or non-interlocked arrangements. This is in contrast to passive template syntheses in which both components bind the metal ion to form a stable complex both before and, importantly, after the final covalent bond forming reaction. As a consequence, regardless of the inherent selectivity for the interlocked product, an active template reaction can in theory be driven to complete conversion with respect to the macrocycle (typically the more synthetically expensive component) by addition of excess half-axle components; any macrocycle complex resulting in "failed" bond formations will not necessarily remain associated with the products and can thus be recycled back into the reaction and ultimately go on to produce the interlocked product. Similarly, it is theoretically possible to employ substoichiometric quantities of the metal ion in an active template

reaction as it can be recycled from interlocked product to unreacted macrocycle. Both of these key synthetic advantages were demonstrated in the Leigh group's first report of the AT-CuAAC reaction[10] (Figure 1. 2 a) and have been exploited in many subsequent reports of active template processes.

1.3.3. Access to unstable interlocked molecules

Whereas the initial product of a successful passive template synthesis is typically more thermodynamically stable than the non-interlocked components, the product in an active template reaction need not be and can even be significantly *less* thermodynamically stable than its non-interlocked components. All that is required is that the active template pathway proceed with an appreciable rate. The ability to form [2]rotaxanes in high yield using the bipyridine macrocycles in the AT-CuAAC reaction provides a striking example of this. Although the products of reactions with the smallest macrocycle are extremely sterically hindered (e.g. Figure 1. 2 b[12]) and expected to be unstable with respect to de-threading, they are still formed in excellent yield. This is in part due to the favourable free energy of triazole formation, which compensates for the build-up of repulsive steric interactions, and in part because the steric interactions in the rotaxane are not fully developed in the transition state leading to the interlocked product[16]. In contrast, when macrocycles of a similar size were employed in Sauvage's passive template approach the yield of the interlocked product fell dramatically[17], presumably because steric interactions disfavour formation of the threaded complex.

1.4. Generality of the Active Template Concept – Scope and Considerations

As discussed above, the active template approach requires the final covalent bond formation to take place through the cavity of the macrocycle with the functionalised half-axle components disposed on opposite faces of the ring. If these requirements are met, almost any bond formation can, with some caveats, be harnessed to generate a new active template reaction. This principle has been amply demonstrated over the last decade: since the AT-CuAAC reaction[10] was first disclosed, active template couplings based on bond formations mediated by Cu[18–25], Pd[26–28], Ni[29–31], Zn[32] and more recently Ru[33] ions have been developed with a large variety of functional groups produced in the coupling step (Figure 1. 4). The relatively rapid development of a range of active template couplings might suggest that such developments are "easy" to achieve and that simply substituting a similar macrocyclic ligand in an established metal-mediated bond formation will result in a

successful active template coupling. This view is unfortunately naïve; as suggested above, the detailed mechanism of the reaction is extremely important.

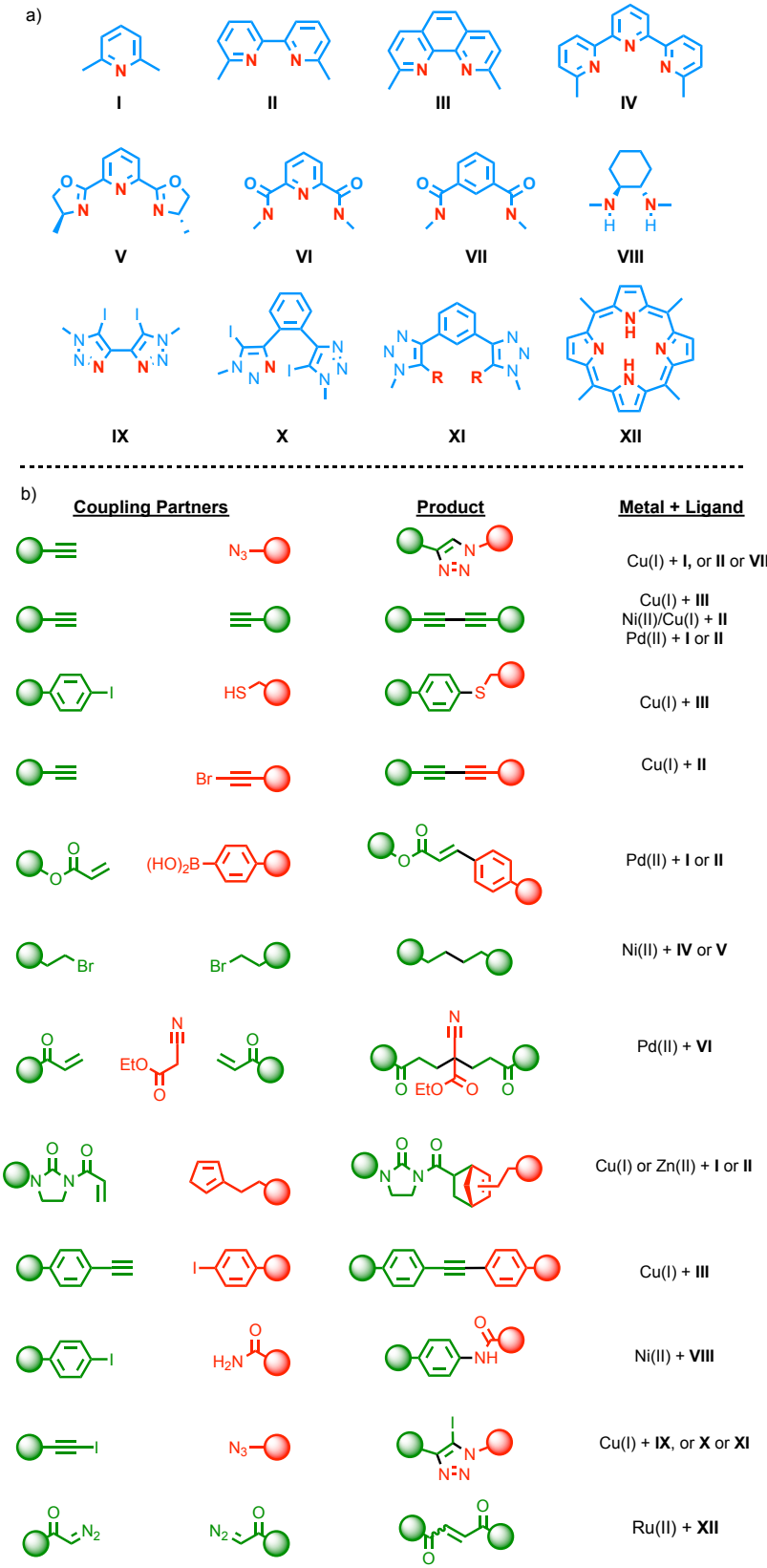

Figure 1. 4 a) Ligands employed to date in the AT approach (donor atoms in red). b) AT bond forming reactions published to date.

Firstly, it is a necessary pre-requisite that at least one of the axle components, the metal ion and the macrocycle are in some way associated during the step that leads to mechanical bond formation. Secondly, it is typically desirable that the final covalent bond forming reaction is irreversible as, all other factors being equal, the non-interlocked product is entropically favoured. Thirdly, the intermediate leading to the proposed mechanical bond formation must be stereoelectronically biased to lead to reaction through the macrocycle cavity. Not all reactions meet these three basic criteria, for example (Figure 1. 5) the attack of nucleophiles on aldehyde electrophiles bearing a proximal chelating unit activated by a Lewis acidic Cu^{II} PyBox complex is reported to proceed via complex **A**[34]. This model suggests that if this process were designed to take place within a macrocycle, as in **B**, then the aldehyde will be disposed such that nucleophilic attack will take place on the same face of the macrocycle as that to which the aldehyde is coordinated, leading to non-interlocked products. Thus, it is wise to consider the detailed mechanism of a proposed new active template process.

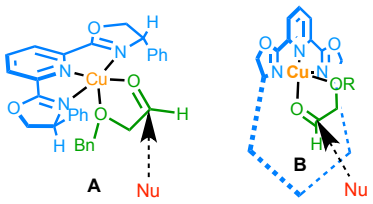

Figure 1. 5 Example of a stereoelectronically disfavoured AT Reaction

The points above notwithstanding, the potential to design active template reactions based on existing catalytic processes is an extremely powerful and attractive. Indeed, it is impressive that active template couplings leading to 10 different axle functional groups have been disclosed in the last decade alone. This increases the synthetic diversity of interlocked molecules available as the only restriction on the axle moiety is that it contains the functional group produced in the coupling step (c.f. the passive template approach in which both axle *and* macrocycle must contain the components required for efficient templation).

Looking to the future, given the diversity of reactions presented, it is striking that almost all active template reactions rely on aromatic-N ligands. This may in part be due to the relative ease with which endotopic aromatic-N ligands can be designed, in contrast, for instance, to the tetrahedral P ligands commonly used in catalysis. Furthermore, it is noteworthy that to date no $Pd^{II/0}$ cross coupling active template reactions have been disclosed; the Pd-mediated sp-sp and oxidative Heck active template couplings published rely on Pd^{II} to gather the reaction components with oxidation of the Pd^{0} by-product taking place off-cycle. It seems

likely that diversification of the ligand motifs in the active template approach will lead to further developments in the types of bond formations that can be employed.

1.4.1. Dual Template Effect

Earlier this year Hayashi, Weiss and co-workers utilised the AT-CuAAC reaction in the formation of strapped-porphyrin [2]rotaxanes [M(**15**)][35]. They investigated the role played by the metal in the porphyrin core and showed no reactivity with the nickel porphyrin, in contrast to the copper and zinc derivatives that formed the interlocked product $[Cu(\mathbf{15})]^{2+}$ and $[Zn(\mathbf{15})]^{2+}$ in 16 and 50% yield respectively (Figure 1. 6). Interestingly, these results matched the behaviour of each porphyrin toward the binding of an axial ligands. Indeed, hard oxophilic porphyrin-Cu^{II} complexes formed $[Cu(\mathbf{15})]^{2+}$ in low yield whereas soft porphyrin-Zn^{II} complexes, which display enhanced affinity for nitrogen containing axial ligands, gave higher conversion to the interlocked system. Nickel porphyrins in contrast are known to be inert in nature toward the axial binding of exogenous ligands and did not form any rotaxane product. The authors concluded on the presence of a productive dual template effect in the reaction and postulated that the assistance of the click reaction occurs *via* coordination of the azide on the strapped-side of the zinc porphyrin. The latter can be favoured by the binding of a fifth ligand in fast exchange to the open-face as they demonstrated it varying the base in the reaction (Figure 1. 7). Using 4-picoline, which strongly binds to zinc and thus competes with the binding of the azide moiety, resulted in 11% yield. Conversely 2,6-lutidine, which cannot bind to either face of the porphyrin for steric reasons, allows for the non-productive binding of the azide to the open-face of the porphyrin which translated in a 18% yield. Finally, using a stronger yet non-nucleophilic base such as DIPEA, the weak interaction of the base itself with zinc favoured the binding of the azide ligand with Zn *via* the strapped-face of the porphyrin, giving $[Zn(\mathbf{15})]^{2+}$ in 50% yield.

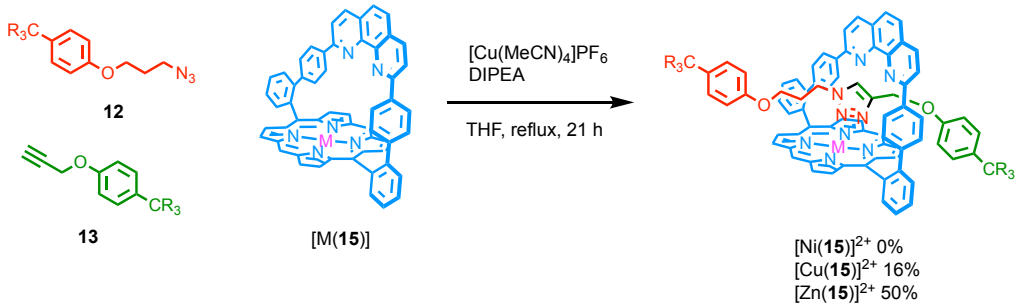

Figure 1. 6 Active-Template synthesis of strapped-porphyrin [2]rotaxanes $[Ni(\mathbf{15})]^{2+}$, $[Cu(\mathbf{15})]^{2+}$ and $[Zn(\mathbf{15})]^{2+}$.

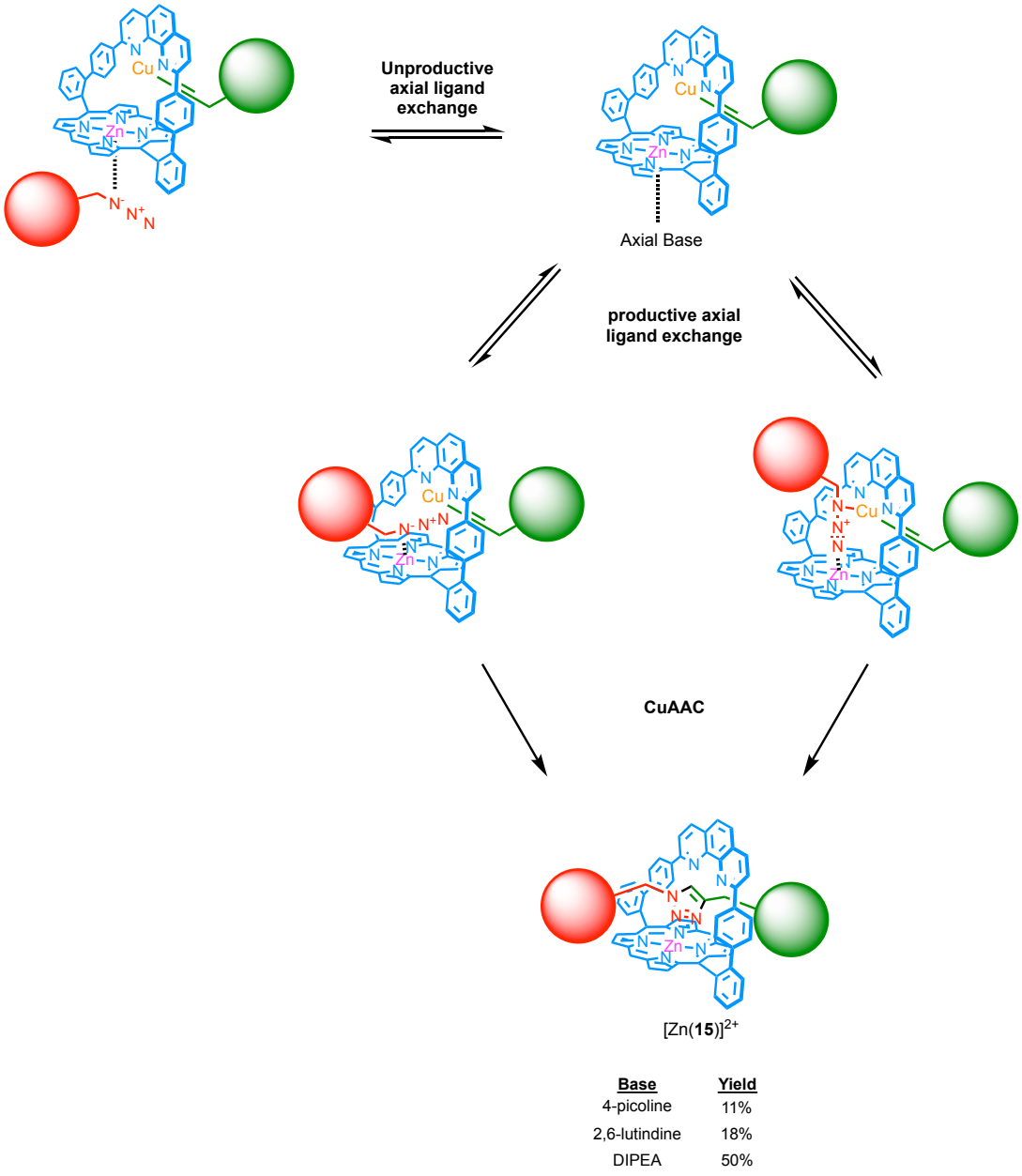

Figure 1. 7 Proposed tandem actions of a Zn organising template and a Cu active metal template.

1.5. Organo-Catalysed Active Template Approach

Although up until now the discussion focused on active template approaches using one or two metal ions to template and catalyse the mechanical bond formation reaction, metal ions are not a condition *sine qua none*. Indeed, earlier this year the groups of Credi and Leigh reported independently what they refer to as the 'metal-free active template synthesis' in which the macrocycle has the dual role of pre-organising the interlocked system and increasing the rate of the mechanical bond formation reaction.

Credi's system (Figure 1. 8) employs a calix[6]arene macrocycle derivative **16** that is a host for the stoppered pyridylpyridinium unit but also accelerates the alkylation step that gives

the axle by a factor of 16[36]. Mixing macrocycle **16** and half-thread **17** in toluene they observed mixture of free molecular components and the two pseudorotaxane isomers P'[**16**⊃**17**] and P''[**16**⊃**17**] in which the pyridylpyridinium guest inserts inside the ring through the upper and lower rim respectively. The ratio of each species could not be assessed due to the complexity of the spectra, but it was already an interesting result as bipyridinium axles in contrast are known to enter the wheel selectively through the upper rim. They postulated that the urea moieties of the upper side play a less significant role in threading/dethreading processes when in presence of a monocationic guest compare to a dicationic one. Upon alkylation of the half-thread in the pseudorotaxane followed with a direct capping of the interlocked system, they observed only the formation of R'[**16**⊃**18**] and isolated it in 63% yield. It indicates that under the conditions employed the active template effect of macrocycle **16** only takes place when the pyridyl nitrogen is oriented towards the upper rim of the calixarene. They tentatively assigned the latter as being a combination of steric (the nitrogen is more exposed to the bulk) and electronic (enhancement of the nitrogen nucleophilicity by stabilisation of the positive charge in the electron-rich ethyloxy cavity) factors. Moreover, it is also possible that the urea moieties play a role in stabilising the transition state by binding the tosylate anion. In the end, their methodology allows for the metal free synthesis of oriented calix[6]arene-based rotaxanes in which the threading direction of molecular axles is controlled. They built on this result and synthesised an interlocked system in which the longer alkyl chain is orientated toward the lower rim of the ring[37], a feature that cannot be obtained *via* standard kinetically controlled threading of the dicationic type guest into the macrocycle with subsequent capping of both extremities with bulky stoppers.

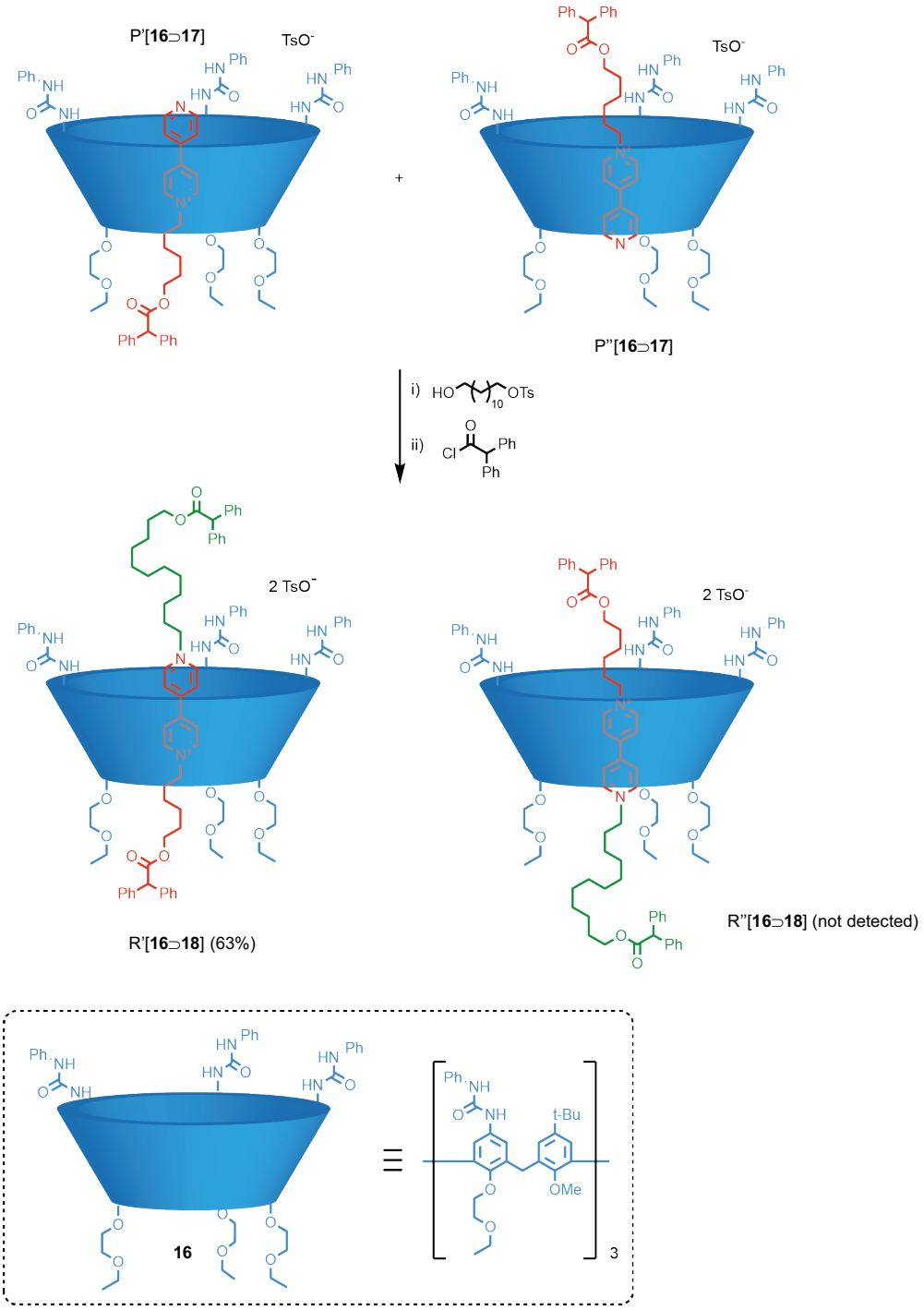

Figure 1. 8 [2]rotaxane R'[**16**⊃**18**] by Credi and co-workers synthesised *via* an organo-catalysed active template approach.

The work presented by Leigh and co-workers relies on the stabilisation of the transition state of the axle-forming reaction by macrocycle **20** containing both a hydrogen-bond donor unit (pyridyl-2,6-dicarboxyamide) and a hydrogen-bond acceptor crown ether part that weakly interacts with amino half thread **21**[38]. They postulated that the initial complex between **20** and **21**, which is too weak to be used in a classical passive template (K_a = 25 M^{-1}), strengthens during the nucleophilic attack of **21** to the cyclic sulfate second axle component **19** as the

macrocycle stabilises both positive and negative charges developing during the course of the reaction (Figure 1. 9). Using a 5-fold excess of both half-threads they achieved a 57% conversion to rotaxane **22** under optimised reaction conditions (8 °C, 22 h). The presence of the crown ether region in the ring is mandatory as macrocycle **24** did not show any rotaxane product under similar conditions, whereas **23** that differs from **20** by the replacement of ester units for the amide formed the interlocked system in a much lower yield (25%, 26 h).

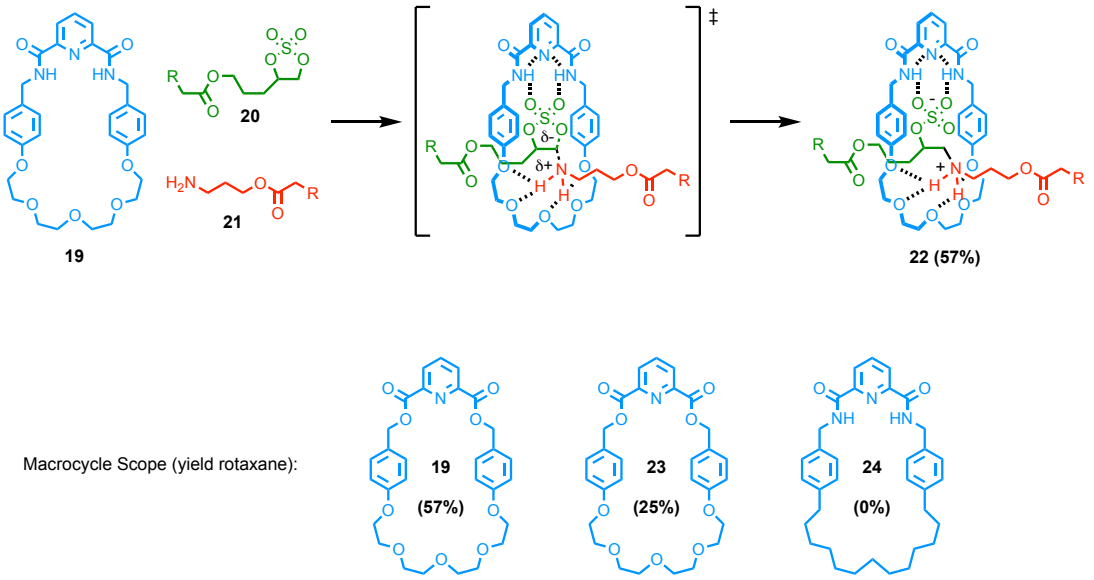

Figure 1. 9 Organo-catalysed active template synthesis of [2]rotaxane **22** proceeding *via* stabilisation of the axle-forming transition state step, and comparison of the yield of the interlocked-system using macrocycle **19**, **23** or **24**.

1.6. Recent Applications of the Active Template Approach

1.6.1. Synthesis of complex targets

Although many of the early studies focussed on rotaxane synthesis, the active template concept is clearly applicable to other interlocked and entangled targets; embedding a metal ion in any looped portion of a molecule can permit the formation of a molecular crossing point and thus a mechanical bond. Active template catenane formation was reported simultaneously in 2009 by the groups of Saito[39,40] and Leigh[41] using AT-Glaser and AT-CuAAC reactions respectively (Figure 1. 10 a). In both cases the yields reported are relatively low compared with the corresponding rotaxane forming reaction (50-64%) even with five equivalents of the pre-macrocycle component and relatively extended reaction times (~5 days) due to the need to work under high-dilution conditions. These results highlight the dual challenge in catenane synthesis; the need to form a new macrocycle while also templating

mechanical bond formation. Thus, although catenane synthesis is possible using the active template approach, it is yet to be turned into a genuinely useful and general tool.

In 2011, the AT-CuAAC reaction was extended to knotted structures by Leigh and co-workers in an approach that combines passive and active templating methodologies. Looped intermediate **27** was formed by coordination of the bipyridine moieties to Cu^{I} and the second Cu^{I} ion bound to the pyridine unit mediated the AT-CuAAC reaction to capture knotted structure **28**[42] (Figure 1. 10 b). In addition to the novelty of the approach, it is worth noting that trefoil knot **28** (Figure 1. 10 b) was the smallest reported to date. That such a small knot can be produced in reasonable yield is once again thanks to the fact that the intermediate leading to the knot need not be thermodynamically favoured in the equilibrium, simply kinetically viable in the AT-CuAAC bond formation.

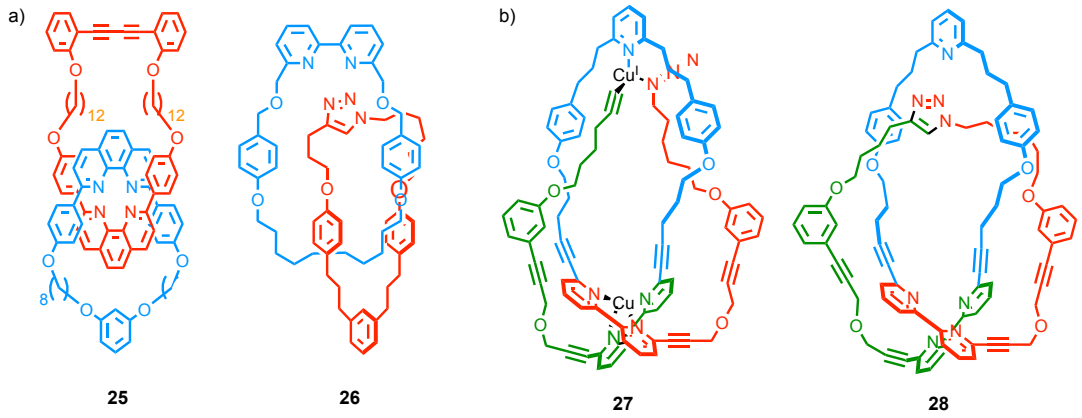

Figure 1. 10 Complex interlocked molecules synthesised using the active template approach: a) Catenanes **25** and **26** produced by AT-Glaser and AT-CuAAC couplings in moderate yield. b) Molecular knot **28** synthesised by a mixed active/passive template approach via intermediate **27**.

An extension of the observation that the metal ion can turn over in the active template approach is that the same metal ion-ligand motif can mediate more than one covalent bond formation to generate more than one mechanical bond. This was first demonstrated in the formation of "handcuff" [3]rotaxanes in which the ligand employed in active template CuAAC or Cadiot-Chodkiewicz couplings bridged the two macrocyclic units[43]. More recently, this result has been extended to the synthesis of true "molecular sheaf" systems in which multiple axles are threaded through a single macrocycle[30],[44] (Figure 1. 11). The first successful approach reported by Leigh and co-workers made use of an active template Ni-mediated sp^3-sp^3 homo-coupling to thread up to three axles through a terpyridine macrocycle to give [4]rotaxane **29** (Figure 1. 11 a). Similarly, Anderson and co-workers achieved the synthesis of doubly threaded [3]rotaxane **30** using an AT-Glaser coupling (Figure 1. 11 a). Rotaxanes **29** and **30** are notable because the threading of multiple

axles through a single macrocycle is a longstanding challenge that has been hard to address using passive template methodologies; passive template syntheses require that a stable complex is formed with all axles present, necessitating extremely large macrocycles and thus extremely large stoppering units[45]. The active template approach to some extent alleviates this problem and thus makes access to such multiply threaded species possible. In contrast, when Saito and co-workers took a mixed active/passive template approach to the synthesis of doubly threaded [3]rotaxane **31**[46,47] (Figure 1. 11 b) and related rotacatenanes[48], the use of a passive template step necessitated the use of larger macrocycles and thus extremely large stoppering units.

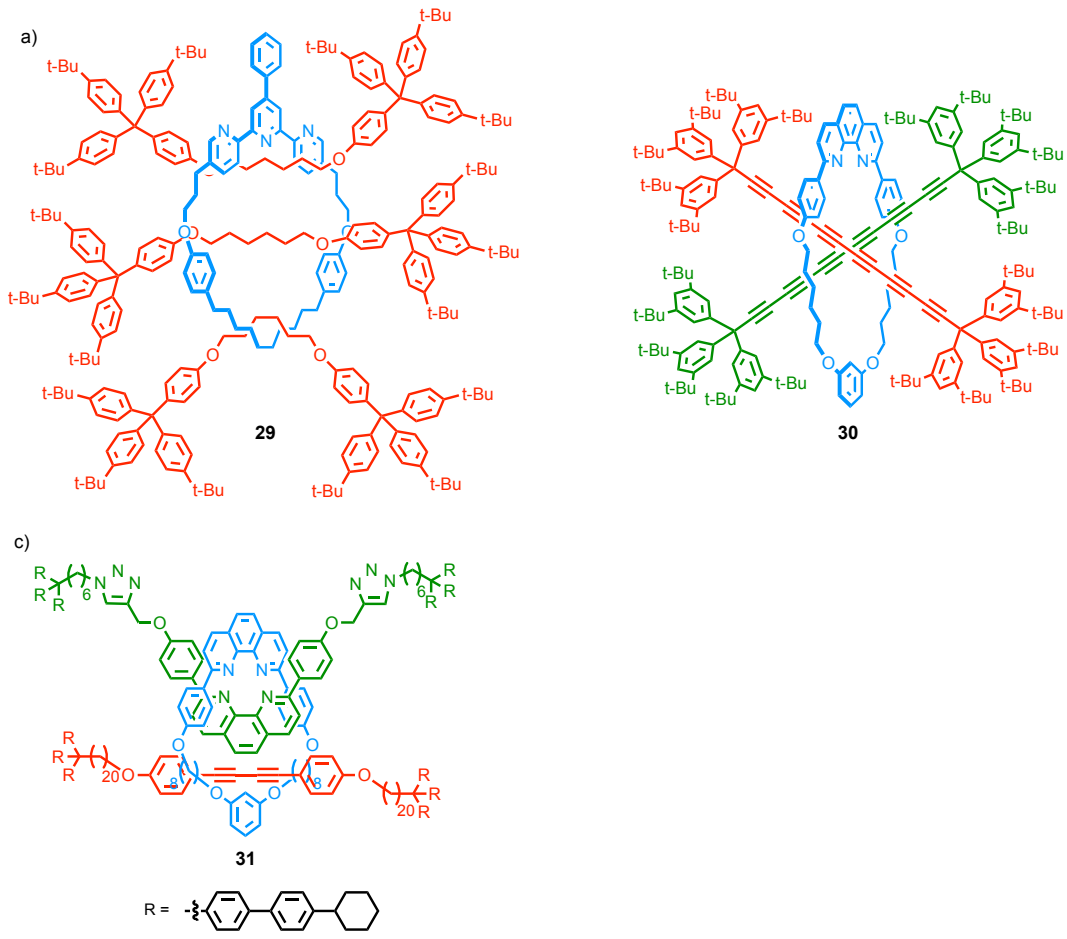

Figure 1. 11 Complex interlocked molecules synthesised using the active template approach: a) Multiply-threaded [4]rotaxane **29** and [3]rotaxane **30** synthesis by AT-sp^3-sp^3 homocoupling of alky bromides and AT-Glaser coupling respectively. b) Doubly threaded [3]rotaxane **31** synthesised by AT-Glaser coupling and subsequent passive template threading.

The ability to synthesise small, crowded rotaxanes using the active template approach was exploited by Goldup and co-workers in the synthesis of mechanically planar chiral rotaxanes using a chiral auxiliary approach[49]. Their synthesis relies on the crowded nature of diastereoisomers (D-R_{mp})-**32** and (D-S_{mp})-**32** (Figure 1. 12) in which the elements of

mechanical and covalent chirality are forced into close proximity and so interact strongly. Although mechanically epimeric rotaxanes have previously been reported[50] this was the first example of their separation using standard chromatographic techniques. Once separated, the diastereoisomers were converted to the corresponding enantiomers by a grafting reaction[51] that replaces the chiral sugar-derived stopper with an achiral amine nucleophile.

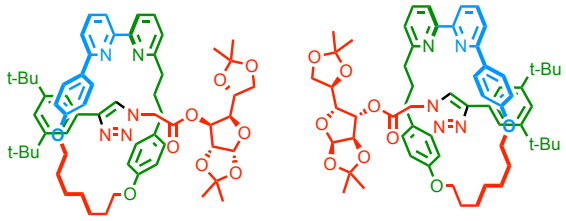

Figure 1. 12 Separable crowded mechanical epimers (D-R_{mp})-**32** and (D-S_{mp})-**32** used in the auxiliary synthesis of enantiopure mechanically planar chiral rotaxanes.

One of the most complex molecules synthesised so far using the AT-CuAAC reaction is a rotaxane pro-drug **33** disclosed by Papot and co-workers (Figure 1. 13)[52]. Rotaxane **33** contains a hydrophilic sugar-derived stopper group (green), a sugar-derived enzyme-cleavable group (orange), a self-imolative linker (grey) and a stopper derived from the complex anti-cancer natural product paclitaxel (purple). Rotaxane **33** was synthesised in a respectable 27% yield for such a complex molecule after preparative HPLC. The mechanical diastereoisomers (see above) of **33** were not separated. The authors demonstrated that the mechanical bond of **33** prevents enzymatic cleavage of the ester bond between the paclitaxel unit and the stopper, which in turn suppresses the antimitotic activity of the drug. However, in the presence of β-galactosidase, the enzyme cleavable group (orange) is removed which results in cleavage of the self-imolative linker (grey) and ultimately cleavage of the macrocycle (blue) and disassembly of the rotaxane. The axle, freed from the rotaxane, is subsequently saponified to produce free, biologically active paclitaxel. Thus, rotaxane **33** is a β-galactosidase-dependent pro-drug form of paclitaxel that relies on the mechanical bond for its function.

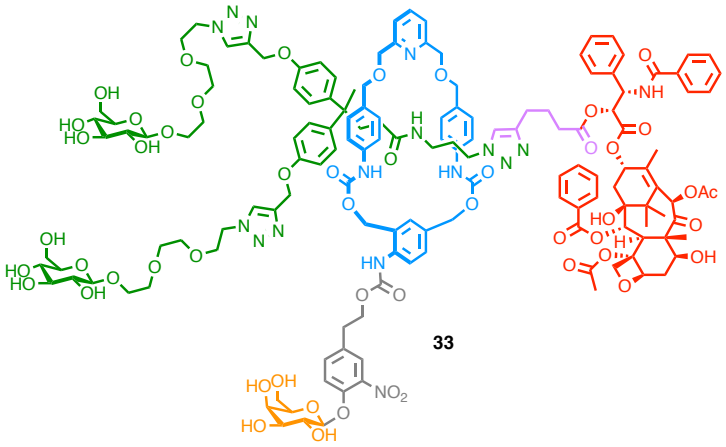

Figure 1. 13 Papot's rotaxane prodrug **33** that demonstrates the level of molecular complexity that can be achieved using the AT-CuAAC reaction

The examples presented demonstrate the potential of the active template approach in the synthesis of complex interlocked structures including systems with multiple mechanical bonds and complex mechanical stereochemistry. This in turn opens up new structures for study and will hopefully lead to new applications of interlocked molecules in various areas.

1.6.2. The Active Template Approach in the Synthesis of Interlocked Materials

Materials based on interlocked molecules have been the source of much attention for the past three decades. In recent years, the active template approach has been bought to bear on the synthesis of molecules with potential materials applications. In 2012, the groups of Anderson[53] and Gladysz[54–56] independently reported the synthesis of conjugated oligoyne rotaxanes using the AT-Glaser reaction. This approach has since been extended by Anderson and co-workers to active template Cadiot-Chodkiewicz sp-sp heterocouplings and increasingly complicated examples including conjugated porphyrin nano-rings (**34**)[57], longer polyynes up with up to 12 conjugated triple bonds[58] (**35**), doubly threaded oligoyne rotaxanes[54] (**30**), and [9]cumulenes (**36**)[59] by isomerisation of the oligoyne product of the Glaser coupling (Figure 1. 14 a). Studies of the properties of these insulated conjugated molecules revealed that encapsulation by the macrocycles stabilised the conjugated structures; dodecayne rotaxane **35** was stable to temperatures >220 °C[58], [9]cumulene rotaxane **36** was sufficiently stable to allow the detailed study of its electronic properties[55], and a modified hexa-yne rotaxane was stable enough to be used in single molecule conductance experiments[60]. Encapsulation was also shown to lead to efficient energy transfer between the threaded components[53,61,62].

Poly[n]rotaxanes have previously been synthesised by threading of macrocycles onto pre-formed polymers or polymerisation of threaded monomers. However, the precision synthesis of oligomeric rotaxanes, including those with distinguishable and precisely placed macrocycles remains an outstanding challenge. In 2016 Goldup and co-workers demonstrated an iterative AT-CuAAC approach to rotaxane oligomers (Figure 1. 14 b) that takes advantage of the use of small macrocycles, removing the need for bulky groups between the reactions sites. By employing a monomer unit containing an azide and a protected alkyne function, [7]rotaxane **37** containing six identical macrocycles was produced with >90% synthetic efficiency over each round of coupling[63]. Furthermore, varying the macrocycle in each AT-CuAAC coupling step allowed the synthesis of [4]rotaxane **38** containing three distinct macrocycles precisely placed on the axle in 75% yield over 9 chemical steps. Aside from demonstrating the power of the active template approach for the precision engineering of interlocked structures, this study suggests that formation of the mechanical bond alters the conformation of the axle significantly by favouring an extended all *syn* arrangement that minimises steric repulsion between the macrocycles. More recently, by exploiting the crowded nature of these small rotaxanes Goldup and co-workers extended this approach to the stepwise protecting group free synthesis of [3] and [4]rotaxanes[64].

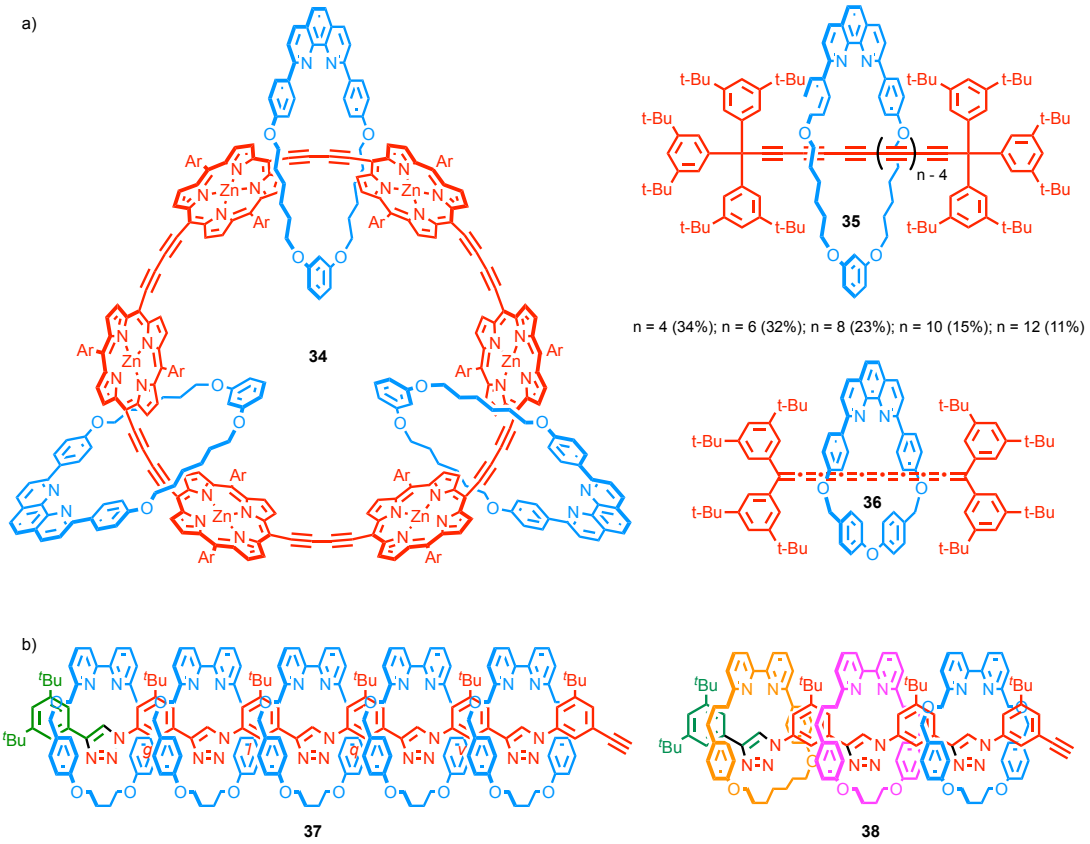

Figure 1. 14 Interlocked electronic and oligomeric materials can be synthesised using the active template approach: a) insulated conjugate structures synthesised using AT-Glaser and AT-Cadiot-Chodkiewicz couplings (conjugated porphyrin nanoring , oligoyne [2]rotaxanes **35**, cumulene rotaxane **36**). b) homo[6]rotaxane **37** and hetero[4]rotaxane **38** synthesised using an iterative AT-CuAAC coupling strategy.

An alternative approach to extended interlocked materials is the use of metalo-supramolecular chemistry to assemble suitably functionalised building blocks using metal ligand interactions[65]. Crowley and co-workers demonstrated this in the context of rotaxanes synthesised using the AT-CuAAC reaction by post-synthetically modifying a rotaxane to include a terpyridine unit in both the macrocycle and axle. Addition of an Fe^{II} salt to **39** led to the assembly of oligomeric species of between 11 and 13 monomer units (Figure 1. 15)[66].

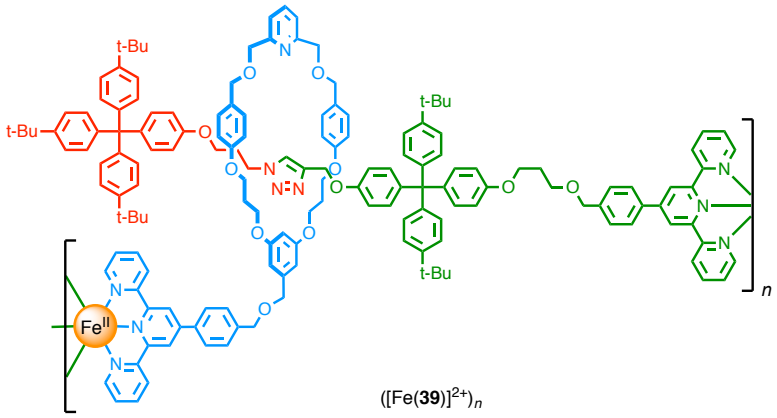

Figure 1. 15 Crowley's interlocked metallosupramolecular polymer ([Fe(**39**)]$^{2+}$)*n* (*n* = 11–13) obtained using an AT-CuAAC strategy.

The application of active template reactions in the synthesis of interlocked materials is still in its infancy but important lead results have already been reported. Hopefully these will inspire further developments that exploit the unusual properties of the active template approach.

1.6.3. Functional Interlocked Molecules

1.6.3.1. Catalysts

Although a great many interlocked ligands have been synthesised since Sauvage's first passive template synthesis, the application of these systems as ligands to support catalytically competent metal ions has not been reported. This is perhaps unsurprising because interlocked ligands synthesised using the passive template approach typically lead to coordinatively saturated complexes that are poorly suited to catalysis. In 2015, the groups of Goldup and Leigh independently reported the first examples of rotaxane ligands in catalysts synthesised using active template methodologies. Leigh and co-workers reported an active template Goldberg reaction to synthesise rotaxane **40** that contains a chiral macrocycle with an endotopic metal-binding site[21]. The Michael addition reaction between diethyl malonate and nitrostyrene proceeded with higher enantioselectivity in the presence of the Ni complex of chiral rotaxane **40** than that of chiral acyclic ligand **41 (**Figure 1. 16 a**)**. However, this study also highlighted one of the key challenges in the development of rotaxane ligands for catalysis; the reaction with rotaxane **40**, although more selective was over an order of magnitude slower than acyclic ligand **41** (27 days vs 2 days). Thus, although complexes of **40** are coordinatively unsaturated and the crowded nature of the cavity formed by the mechanical bond bears attractive similarities with an enzyme active site (flexible, well-defined 3D space), it appears this same crowding can lead to low catalytic activity.

Goldup and co-workers took a different approach to the development of rotaxane catalysts by placing the catalytic function near to but not directly within the macrocycle[67] (Figure 1. 16 b). Rotaxane gold complex [Au(**42**)Cl] was synthesised in excellent yield using the AT-CuAAC reaction and its activity in an Au-mediated cyclopropanation reaction studied. Surprisingly, precatalyst [Au(**42**)Cl] was found to be inactive but non-interlocked axle complex [Au(**43**)Cl] was catalytically competent. Subsequent studies revealed this to be due to inhibition by the Lewis basic N-donors in the macrocycle. This inhibition could be reversed by competitive binding of catalytically innocent cations into the cavity of the macrocycle which resulted in a catalyst species that was both highly active *and* more diastereoselecitve than non-interlocked complex. The increased selectivity was attributed to the sterically hindered environment provided by the threaded macrocycle. Importantly, the nature of the cationic guest controlled the degree of diastereoselectivity, presumably by altering the steric environment around the metal centre, demonstrating that [Au(**42**)Cl] produces an allosterically regulated catalyst in which the guest controls both activity and selectivity.

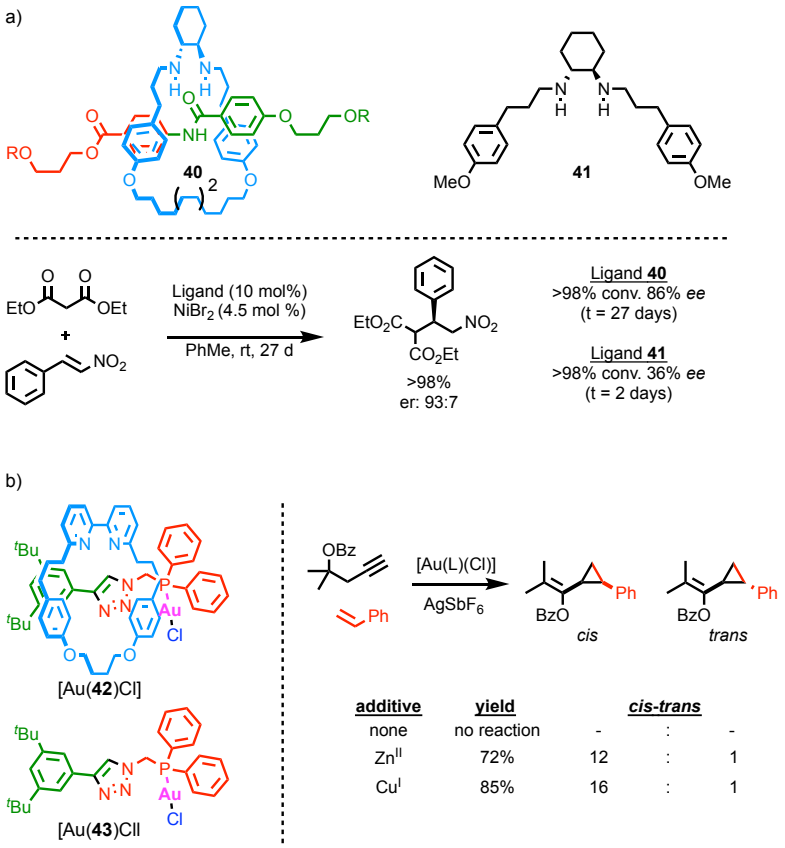

Figure 1. 16 : Catalysts interlocked molecules synthesised using the active template approach: a) Leigh's chiral interlocked ligand and its performance in a Ni-mediated Michel addition. b) Goldup's rotaxane-AuCl complex and its behaviour as a stimuli-responsive cyclopropanation catalyst.

Leigh and Goldup's interlocked catalysts use the mechanical bond to control the action of a catalyst on exogenous substrates. There is also significant interest in interlocked systems which control functionalisation of the axle component, for instance as a potential method for post synthetic modification of polymers[68]. Saito and co-workers demonstrated that a Cu^{I} ion bound within the cavity of a phenanthroline macrocycle was able to mediate a double hydro-amination reaction of the threaded diyne functionality generated in an AT-Glaser reaction to produce a pyrrole moiety (Figure 1. 17)[69]. The conversion of diyne rotaxane **44** to pyrrole rotaxane **45** was found to be significantly more efficient than the corresponding reaction of the non-interlocked macrocycle and axle suggesting that the mechanical bond plays a role in the transformation. Key to the success of this approach is that the axle does not contain ligating functionality that would inhibit the activity of the metal ion, an important benefit of the active template approach.

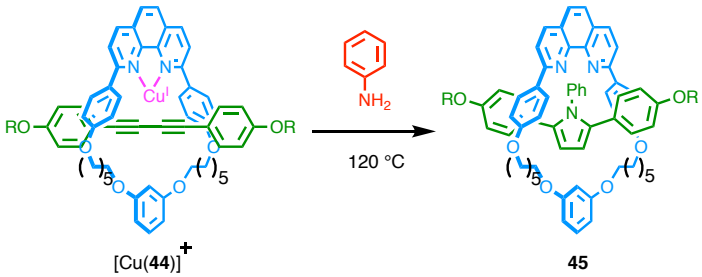

Figure 1. 17 Conversion of the diyne-containing axle of rotaxane **44** to a pyrrole axle in **45** by a reaction with aniline catalysed by a Cu(I) ion that is coordinated by the macrocycle.

Another example of control of reactivity brought by the mechanical bond was published this year by Elemans, Nolte, Rowan and co-workers. In their work, they used ruthenium porphyrin macrocycle **47**(Ru) to catalyse the formation of rotaxanes **48a** and **48b** *via* dimerization reaction of diazo compounds **46a** and **46b** (Figure 1. 18)[33]. In the case of the shorter half thread they only observed the formation of interlocked product **48a** (50%) and corresponding free axle **49a** using a large excess of half-thread (50 equiv.). However, when a longer stopper was employed under similar reaction conditions, **49b** was obtained along with rotaxane **48b** (41%) and other products of molecular masses higher than the one of **48b** based on MALDI-ToF analyses (masses = m(**48b**) + (n x 346) amu with n =1, 2, 3, 4). Based on this result as well as HSQC, HMBC and ROESY NMR spectroscopy analyses, they proposed the latter side product to result from insertion of α-diazoester **46b** either to the double bond of the alkene of a preformed linear thread, or into the alkyl spacer *via* C-H insertion, or both cases. The fact that a model ruthenium porphyrin complex, which is not incorporated into a ring architecture, produced only the axle **49b** without any other insertions product suggests

that the latter result from the increase in effective molarity of the axle component **49b** when inside the cavity of **47**(Ru). The system with the shorter axle **48a** did not show any insertion product most probably due to the close proximity in space of the bulky 3,5-di-*tert*-butyl stoppers to the ring (confirmed by ROESY NMR analysis) that would prevent further half-thread **46a** accessing the ruthenium metal ion.

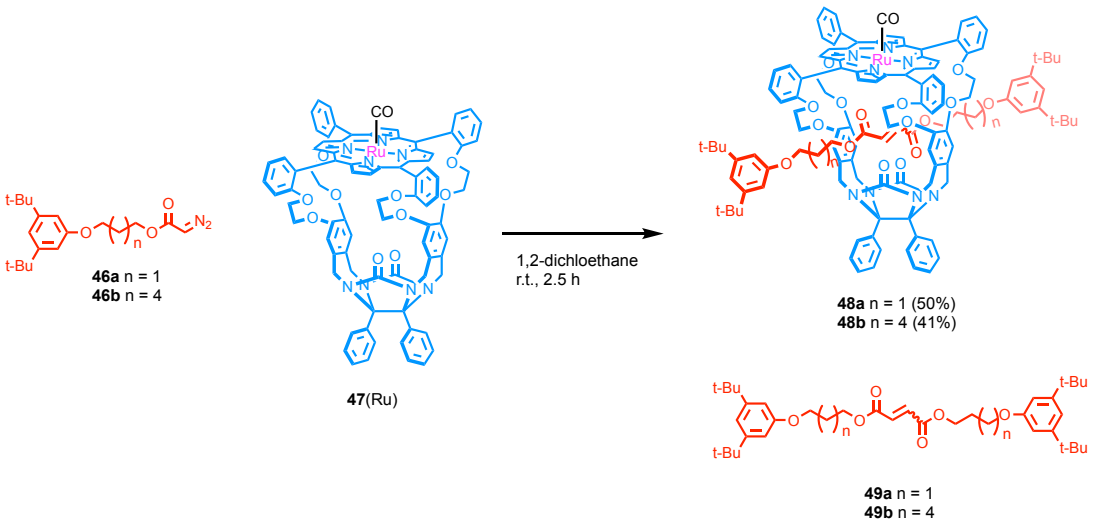

Figure 1. 18 Active-Template synthesis of rotaxane **48a** and **48b** using a Ru catalysed carbenoid transfer reaction.

1.6.3.2. Hosts

Beer and co-workers have pioneered the use of active template couplings in the synthesis of hosts for anions by developing a modification of the AT-CuAAC reaction in which the terminal acetylene coupling partner is replaced with an iodoacetylene, leading to formation of an iodotriazole product[22]. The first examples reported employed bis-iodotriazole macrocycles that coordinate to Cu^{I} through the triazole ligand. These complexes then mediate active template formation of the iodotriazole to produce the interlocked product in reasonable yield (18-41%). The triazole donors were subsequently coordinated to Re^{I} to orient the C-I bonds into the cavity of the rotaxane **50** and generate a cavity containing three polarised C-I bonds that readily participated in halogen bonding interactions with a range of anions (Figure 1. 19 a). Rotaxane **50** selectively binds halide anions over harder oxy-anions (Figure 1. 19 a), in line with other halogen bonding hosts[70]. Later work extended this approach to systems with up to four polarised C-I bonds and these hosts were found to bind anions even in the presence of water[23]. In competitive solvents, the relative order of binding was reversed with iodide binding more strongly than chloride.

Following this work, they extended this approach to chalcogenido-triazole macrocycles **51b** and **51c**, which bind Cu in a bidentate manner through the Se and Te atoms respectively

(Figure 1. 19 b)[24]. These macrocycles were then employed in the AT-CuAAC reaction to produce rotaxanes **51b** and **51c** and their ability to bind anions through chalcogen bonding interactions was investigated. Rotaxane **51c** was found to bind anions more strongly than the corresponding protonated system **51a** through a X•••Te chalcogen bond whereas the less polarised C-Se bond of **51b** was found to be ineffective. Not only does this work introduce a new interaction to the field of rotaxane anion hosts, it is also the first and only example of a non-N ligand based macrocycle for use in an active template process.

More recently, they used the AT-CuAAC methodology to synthesis of the interlocked receptor **52** in which the triazole moiety is not involved in the binding process but instead an indolo-carbazole unit incorporated within the axle (Figure 1. 19 c)[71]. Although the latter functionality is a well-known bi-dentate hydrogen-bond donor motif with fluorescent anion sensing ability, its incorporation in a [2]rotaxane scaffold *via* anion-templating approach is yet to be achieved. Rotaxane **52** demonstrated an increase in anion binding affinity compare to the non-interlocked thread with a preference for $H_2PO_4^-$ and SO_4^{2-}, which suggests a most suited topological arrangement of the hydrogen-bond donor groups in the cavity for oxoanions of tetrahedral geometry. Interestingly, whereas the binding model is 1:1 stoichiometry for $H_2PO_4^-$, it is composite in the case of sulfate anions starting with a 2:1 binding stoichiometry that is replaced by a 1:1 complex at higher anion concentration. Finally, the binding event triggered changes in fluorescence and in particular substantial bathochromic shifts (15-40 nm) in the maximum of the emission band, which to date has been observed only once for indolo-carbazole-based anion receptors and is still under investigation.

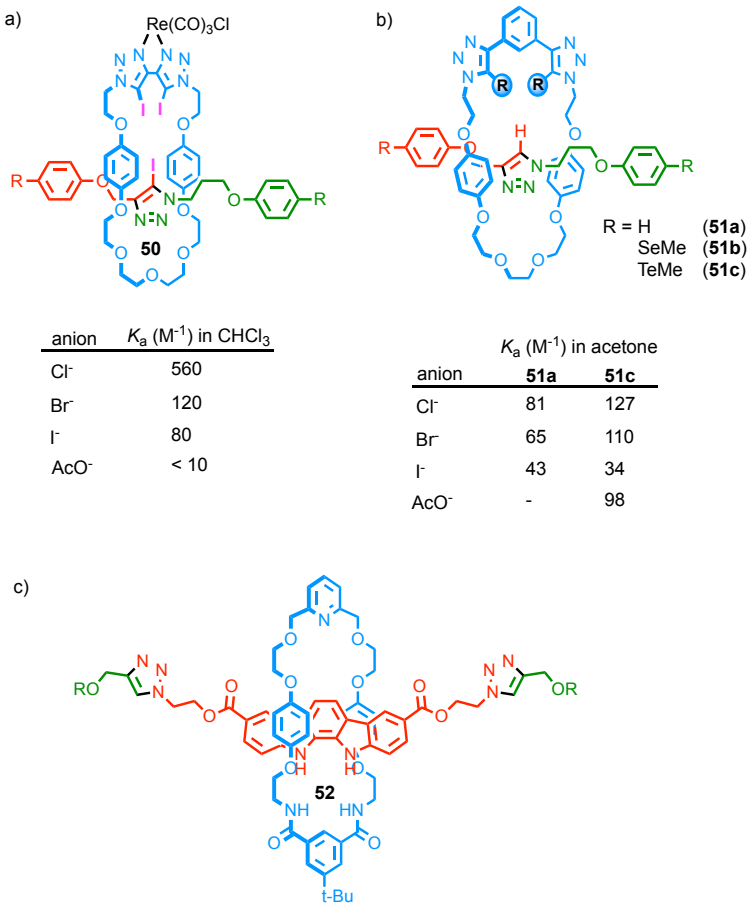

anion	K_a (M^{-1}) in $CHCl_3$
Cl^-	560
Br^-	120
I^-	80
AcO^-	< 10

anion	K_a (M^{-1}) in acetone	
	51a	**51c**
Cl^-	81	127
Br^-	65	110
I^-	43	34
AcO^-	-	98

anion	K_a (M^{-1}) in acetone-water 95:5
F^-	739
Cl^-	516
Br^-	142
AcO^-	2359
$H_2PO_4^-$	2049
SO_4^{2-}	4518

Figure 1. 19 Beer's host interlocked molecules synthesised using the active template approach: a) halogen bonding anion host **50** and the binding constant with selected anions. b) chalcogen-bonding host **51c** and a comparison between the binding constants with various anions and the hydrogen bonding-only host **51a**. c) indolo-carbazole host **52**.

Tucker and McClenaghan applied the active template approach to develop a host for small molecules. They synthesised rotaxanes based on the Hamilton receptor for barbital using the AT-Glaser (**54**) and AT-CuAAC (**55**) reactions (Figure 1. 20)[72]. While diyne rotaxane **54** bound barbital (**53**), albeit with a reduced binding constant compared with the non-interlocked macrocycle, triazole rotaxane **55** did not bind the guest at all. The reduced binding of **54** for barbital compared with the macrocyclic host was attributed to the steric hindrance provided by the mechanical bond. However, the failure of **55** to bind is harder to rationalise using steric arguments alone and is likely to be due to competing interactions between the Lewis basic triazole moiety and the hydrogen bond donor sites in the macrocycle.

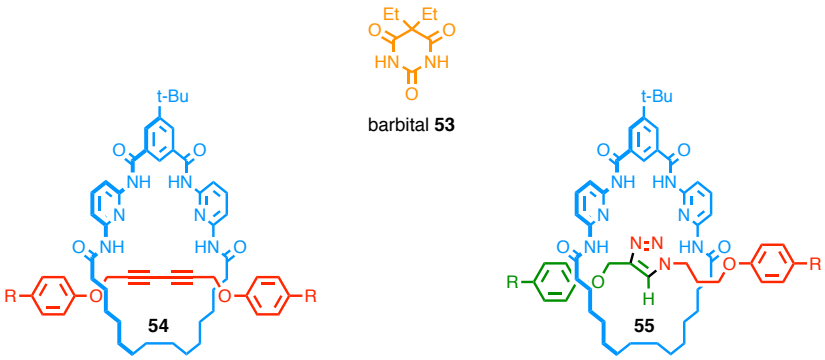

Figure 1. 20 Tucker and McClenaghan's Hamilton-receptor rotaxanes synthesized through active template Glaser (**54**) and AT-CuAAC (**55**) reactions. Only **54** is a host for barbital (**53**).

In 2014 Goldup and co-workers serendipitously observed stabilisation of a reactive organometallic species during in the AT-CuAAC synthesis of a simple rotaxane[73]; when base was added to accelerate the reaction between azide **56**, alkyne **57** and macrocycle **58** the isolated product was triazolide **59** *even after* aqueous work up with EDTA and column chromatography. Triazolide **59** could even be produced in high yield under aqueous conditions (Figure 1. 21)! The dramatic stabilisation of the Cu^{I}-C bond in **59** is attributed to the steric hindrance provided by the crowded mechanical bond between the short axle and small macrocycle. Indeed, when a larger macrocycle or more a flexible axle were employed the corresponding triazolide was not isolated. In addition to providing mechanistic evidence for a Cu^{I} triazolide intermediate in the AT-CuAAC reaction (**59** appears to be a "trapped" intermediate of the reaction rather than the product of Cu^{I} insertion as readdition of Cu^{I} to the corresponding rotaxane fails to lead to formation of **59**), the unexpected stability of **59** suggests that sterically hindered rotaxanes accessible using active template approaches may allow the design of kinetically stabilised ligands for various applications (*cf* Sauvage's "catenand" effect[74]).

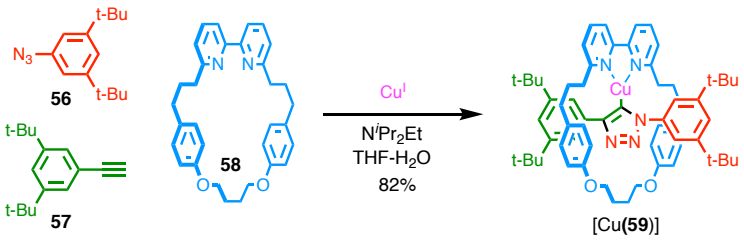

Figure 1. 21 Goldup's rotaxane Cu^{I}–triazolide [Cu(**59**)], which can be synthesized under aqueous conditions owing to the stabilization that is provided by the mechanical bond.

The above examples demonstrate that, in addition to high synthetic efficiency, the active template approach offers opportunities to generate interlocked molecules with diverse functionality and function. The reduced synthetic restrictions on structure compared with

passive template approaches will hopefully lead to new applications of mechanically bonded structures and the production of optimised interlocked catalysts, hosts, ligands and sensors.

1.6.4. Molecular Machines

Soon after the development of the AT-CuAAC reaction Leigh and co-workers disclosed a degenerate molecular shuttle in which two triazole ligands in the axle act as stations for a metal ion bound in the cavity of the macrocycle[11]. This first report set the scene for much of the later work on bistable stimuli responsive molecular shuttles in which the functional group formed in an active template reaction typically acts as one of the stations[28],[32],[75]. One of the most recently disclosed of these, but perhaps most obvious given the history of the field, is shuttle **60**[75] which is a triazole-pyridine analogue of Sauvage's seminal phenanthroline-terpyridine shuttle[76]; the bidentate pyridine-triazole station is formed in the final AT-CuAAC coupling that forms the mechanical bond (Figure 1. 22). When bound to Cu^{I} the macrocycle predominantly occupies the bidentate station but is translocated to the tridentate station when Cu^{I} is replaced by Zn^{II}.

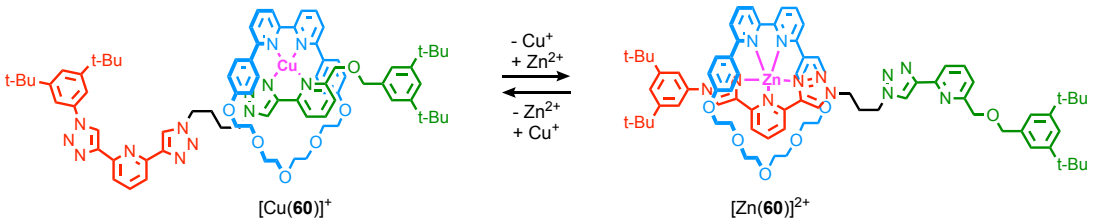

Figure 1. 22 Sauvage-like shuttle **60** synthesised using the AT-CuAAC reaction.

Historically, molecular shuttles have typically taken advantage of the templating motif used in the passive template synthesis of the interlocked molecule as one of the macrocycle binding sites. Although this alignment between the method of synthesis and the function of the target is elegant it comes with a disadvantage; typically, the templating interaction is extremely favourable and so the activation barrier to shuttling is often relatively high. One of the principle advantages of the active template approach to shuttles is to allow the synthesis of molecular shuttles with significantly reduced intermolecular interactions and thus lower barriers to molecular motion while still maintaining good positional integrity; a preference of just 7.3 $kJ.mol^{-1}$ is sufficient for >95% of the molecules to exist in the preferred co-conformation. Leigh and co-workers disclosed the first example of such a shuttle by employing single H-bond contacts as the primary non-covalent interaction between the macrocycle and station (Figure 1. 23)[19,77]. Shuttle **61** was synthesised using an AT-Cadiot Chodkiewicz reaction that produces a diyne functional group in the axle that does not have

significant attractive interactions with the macrocycle. The stations in the shuttle are the amide unit and the dimethylaminopyridine (DMAP) unit. In the neutral state the macrocycle predominantly occupies the amide station due to the hydrogen bond between the amide N-H and the bipyridine macrocycle. Protonation of the DMAP station results in a new preferred co-conformation in which the macrocycle is hydrogen bonded to pyridinium unit. Calculations suggest that the preferred co-conformations in the neutral and protonated states are favoured by 16.3 kcalmol^{-1} and 3.8 kcalmol^{-1} respectively suggesting reasonable co-conformational integrity in both states.

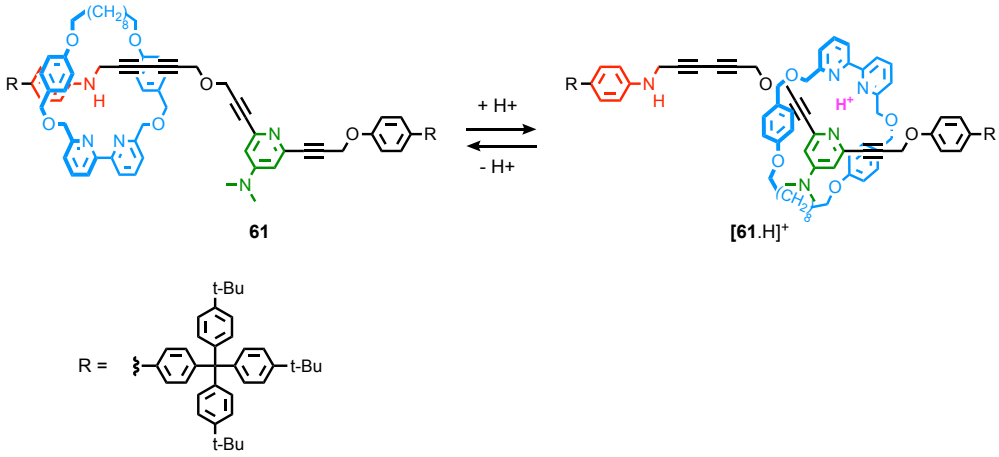

Figure 1. 23 Leigh's "low interaction" shuttle **61** synthesised using the AT-Cadiot-Chodkiewicz coupling.

The most complex molecular machine synthesised using the active template approach to date is undoubtedly Leigh and co-workers' "peptide synthesiser" rotaxane **65** (Figure 1. 24)[78], in which a catalyst bound to macrocycle sequentially transforms functional groups in the axle component to produce a sequence-specific peptide product. The role of the AT-CuAAC in the synthesis is to allow the assembly of the interlocked structure in high yield from macrocycle **62**, alkyne **63** and azide **64**, loading the macrocyclic on to the axle information strand, without introducing significant inter-component interactions that would hinder or slow the operation of the machine. The catalyst unit was then attached to the macrocycle by

hydrazone formation. The application of the active template approach in the synthesis of such a complex structure demonstrates the synthetic power of this methodology.

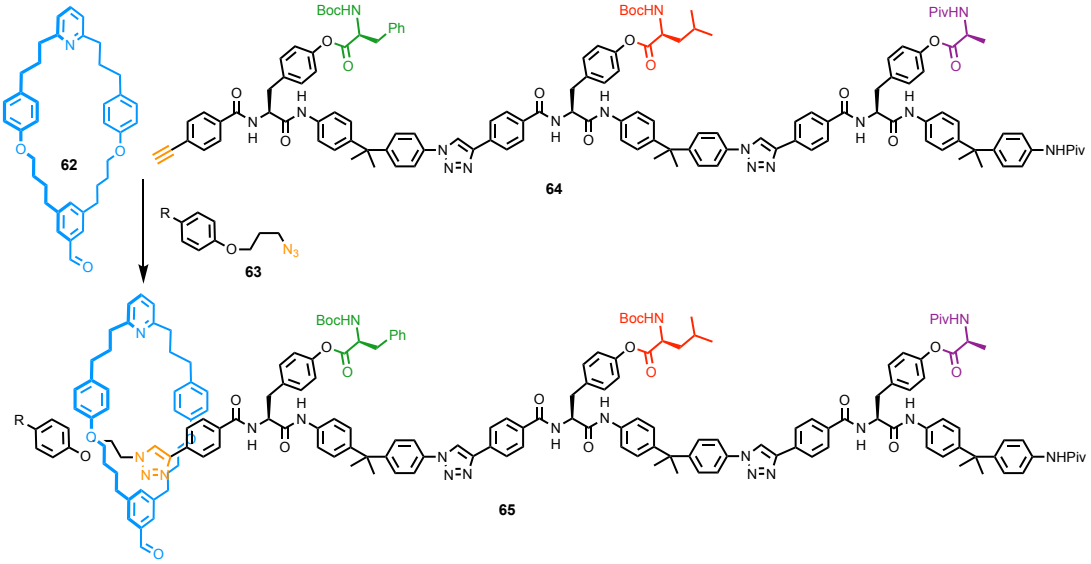

Figure 1. 24 "Peptide synthesiser" **65** molecular machine precursor assembled using the AT-CuAAC reaction.

1.7. Conclusions and future challenges

To conclude, the active template approach has come a long way in the decade since the principle was established by Leigh and co-workers; 10 new active template bond forming reactions have been developed; the approach has been extended to a range of other structures including catenanes and knots; and active template reactions have been applied to the synthesis of functional architectures and interlocked materials. For comparison, it took a decade from Sauvage's first report of a catenane for his Cu-phenanthroline template to be extended to a rotaxane[79]! While the high rate of progress in the active template approach surely reflects the larger and more developed community of modern synthetic supramolecular chemistry, not to mention the improved analytical techniques available to characterise the products, it is still an impressive start for a new field.

However, this progress has been largely driven by a relatively small number of groups, and the majority of publications concerning the active template approach focus on the development of new AT methodologies, rather than their application to new targets and functions. That such a useful methodology has not been applied more widely may simply reflect the conservative nature of synthetic chemistry but may also relate to the availability of the key starting material, the macrocycle. Indeed, in many cases macrocycles required for the active template approach, particularly small bipyridine macrocycles, were typically only

available in relatively low yield (10% or less in the macrocyclisation step). Recent efforts have improved this significantly however and this will hopefully open the field up to new entrants[70].

Future directions will surely include the application of the approach to new and challenging targets and ever more complex structures, including those with applications in catalysis, sensing and materials. The extension of the AT approach to non-N ligands, as demonstrated by Beer and co-workers is surely overdue, in particular, ligands capable of supporting cross coupling reactions such as Pd and Ni-mediated processes, given the power and ubiquity of these reactions in synthetic chemistry more widely. Another opportunity that has so far remained overlooked is the possibility of developing organocatalytic active template reactions by embedding suitable organocatalytic functionality within the cavity of a macrocycle. The extension of the approach to a general and high-yielding catenane forming reaction is also yet to be achieved. Finally, a clear understanding of the role of macrocycle size in reactions other than the bipyridine-mediated AT-CuAAC reaction is also desirable[13].

To achieve this, one aim of this introduction is to highlight the potential for researchers in the field of catalysis to contribute the development of new methods for the synthesis of interlocked molecules; the detailed understanding they would bring to the area would surely significantly accelerate progress. Conversely, the application of active template reactions to the analysis of reactions mechanisms could contribute significantly to the field of catalysis.

Finally, the greatest challenge in organic synthesis is to be able to make any molecule efficiently, regardless of the structure. Arguably, the active template approach takes us one step closer to this lofty aim in the context of mechanically bonded molecules by allowing, in principle, almost any axle to be included in the cavity of a macrocycle. Although this has in the past been termed a "traceless" synthesis, because it is not obvious where the bond formation has taken place or how it was templated, the macrocycle still bears the ligand unit used to direct the reaction and this still serves to reduce the structural diversity of the available products. Perhaps in future, a truly traceless active template reaction in which no component of the interlocked structure retains the tell-tale signature of the synthesis will become available and the ultimate aim of being able to achieve any target with little or no limitations on the covalent structure of the components will be within our grasp.

1.8. Bibliography

[1] C. J. Bruns, J. F. Stoddart, *"The Nature of the Mechanical Bond: From Molecules to Machine"*, Wiley, **2016**.

[2] E. Wasserman, *J. Am. Chem. Soc.* **1960**, *82*, 4433–4434.

[3] G. Schill, A. Lüttringhaus, *Angew. Chem. Int. Ed. Engl.* **1964**, *3*, 546–547.

[4] C. . Dietrich-Buchecker, J. . Sauvage, J. . Kintzinger, *Tetrahedron Lett.* **1983**, *24*, 5095–5098.

[5] S. Erbas-Cakmak, D. A. Leigh, C. T. McTernan, A. L. Nussbaumer, *Chem. Rev.* **2015**, *115*, 10081–10206.

[6] J. D. Crowley, S. M. Goldup, A.-L. Lee, D. a. Leigh, R. T. McBurney, *Chem. Soc. Rev.* **2009**, *38*, 1530.

[7] C. W. Tornøe, C. Christensen, M. Meldal, *J. Org. Chem.* **2002**, *67*, 3057–3064.

[8] V. V Rostovtsev, L. G. Green, V. V Fokin, K. B. Sharpless, *Angew. Chem. Int. Ed.* **2002**, *41*, 2596–2599.

[9] H. C. Kolb, M. G. Finn, K. B. Sharpless, *Angew. Chem. Int. Ed.* **2001**, *40*, 2004–2021.

[10] V. Aucagne, K. D. Hänni, D. A. Leigh, P. J. Lusby, D. B. Walker, *J. Am. Chem. Soc.* **2006**, *128*, 2186–2187.

[11] V. Aucagne, J. Berná, J. D. Crowley, S. M. Goldup, K. D. Hänni, D. a. Leigh, P. J. Lusby, V. E. Ronaldson, A. M. Z. Slawin, A. Viterisi, et al., *J. Am. Chem. Soc.* **2007**, *129*, 11950–11963.

[12] H. Lahlali, K. Jobe, M. Watkinson, S. M. Goldup, *Angew. Chem. Int. Ed.* **2011**, *50*, 4151–4155.

[13] E. A. Neal, S. M. Goldup, *Chem. Sci.* **2015**, *6*, 2398–2404.

[14] X. Hou, C. Ke, J. Fraser Stoddart, *Chem. Soc. Rev.* **2016**, *45*, 3766–3780.

[15] E. A. Neal, S. M. Goldup, *Angew. Chem. Int. Ed.* **2016**, *55*, 12488–12493.

[16] A. Noor, W. K. C. Lo, S. C. Moratti, J. D. Crowley, *Chem . Commun.* **2014**, *50*, 7044–7047.

[17] C. O. Dietrich-Buchecker, A. Edel, J. P. Kintzinger, J. P. Sauvage, *Tetrahedron* **1987**, *43*, 333–344.

[18] S. Saito, E. Takahashi, K. Nakazono, *Org. Lett.* **2006**, *8*, 5133–5136.

[19] J. Berná, S. M. Goldup, A.-L. Lee, D. A. Leigh, M. D. Symes, G. Teobaldi, F. Zerbetto, *Angew. Chem. Int. Ed.* **2008**, *47*, 4392–4396.

[20] K. Ugajin, E. Takahashi, R. Yamasaki, Y. Mutoh, T. Kasama, S. Saito, *Org. Lett.* **2013**, *15*, 2684–2687.

[21] S. Hoekman, M. O. Kitching, D. a. Leigh, M. Papmeyer, D. Roke, *J. Am. Chem. Soc.* **2015**, *137*, 7656–7659.

[22] M. J. Langton, Y. Xiong, P. D. Beer, *Chem. Eur. J.* **2015**, *21*, 18910–18914.

[23] J. Y. C. Lim, T. Bunchuay, P. D. Beer, *Chem. Eur. J.* **2017**, *23*, 4700–4707.

[24] J. Y. C. Lim, I. Marques, A. L. Thompson, K. E. Christensen, V. Félix, P. D. Beer, *J. Am. Chem. Soc.* **2017**, *139*, 3122–3133.

[25] B. E. Fletcher, M. J. G. Peach, N. H. Evans, *Org. Biomol. Chem.* **2017**, *15*, 2797–2803.

[26] J. Berná, J. D. Crowley, S. M. Goldup, K. D. Hänni, A.-L. Lee, D. A. Leigh, *Angew. Chem. Int. Ed.* **2007**, *46*, 5709–5713.

[27] J. D. Crowley, K. D. Hänni, A. Lee, D. A. Leigh, *J. Am. Chem. Soc.* **2007**, *129*, 12092–12093.

[28] S. M. Goldup, D. A. Leigh, P. J. Lusby, R. T. McBurney, A. M. Z. Slawin, *Angew. Chem. Int. Ed.* **2008**, *47*, 3381–3384.

[29] S. M. Goldup, D. A. Leigh, R. T. McBurney, P. R. McGonigal, A. Plant, *Chem. Sci.* **2010**, *1*, 383.

[30] J. D. Crowley, S. M. Goldup, N. D. Gowans, D. a Leigh, V. E. Ronaldson, A. M. Z. Slawin, *J. Am. Chem. Soc.* **2010**, *132*, 6243–6248.

[31] J. J. Danon, D. A. Leigh, P. R. McGonigal, J. W. Ward, J. Wu, *J. Am. Chem. Soc.* **2016**, *138*, 12643–12647.

[32] J. D. Crowley, K. D. Hänni, D. A. Leigh, A. M. Z. Slawin, *J. Am. Chem. Soc.* **2010**, *132*, 5309–5314.

[33] O. I. van den Boomen, R. G. E. Coumans, N. Akeroyd, T. P. J. Peters, P. P. J. Schlebos, J. Smits, R. de Gelder, J. A. A. W. Elemans, R. J. M. Nolte, A. E. Rowan, *Tetrahedron* **2017**, *73*, 5029–5037.

[34] D. A. Evans, M. C. Kozlowski, J. A. Murry, C. S. Burgey, K. R. Campos, B. T. Connell, R. J. Staples, *J. Am. Chem. Soc.* **1999**, *121*, 669–685.

[35] Y. Miyazaki, C. Kahlfuss, A. Ogawa, T. Matsumoto, J. A. Wytko, K. Oohora, T. Hayashi, J. Weiss, *Chem. Eur. J.* **2017**, *4*, 13579–13582.

[36] G. Orlandini, G. Ragazzon, V. Zanichelli, A. Secchi, S. Silvi, M. Venturi, A. Arduini, A. Credi, *Chem . Commun.* **2017**, *53*, 6172–6174.

[37] V. Zanichelli, G. Ragazzon, G. Orlandini, M. Venturi, A. Credi, S. Silvi, A. Arduini, A. Secchi, *Org. Biomol. Chem.* **2017**, *15*, 6753–6763.

[38] G. De Bo, G. Dolphijn, C. T. McTernan, D. A. Leigh, *J. Am. Chem. Soc.* **2017**, *139*, 8455–8457.

[39] Y. Sato, R. Yamasaki, S. Saito, *Angew. Chem. Int. Ed.* **2009**, *48*, 504–507.

[40] S. Saito, *J. Incl. Phenom. Macrocycl. Chem.* **2015**, *82*, 437–451.

[41] S. M. Goldup, D. A. Leigh, T. Long, P. R. McGonigal, M. D. Symes, J. Wu, *J. Am. Chem. Soc.* **2009**, *131*, 15924–15929.

[42] P. E. Barran, H. L. Cole, S. M. Goldup, D. A. Leigh, P. R. McGonigal, M. D. Symes, J. Wu, M. Zengerle, *Angew. Chem. Int. Ed.* **2011**, *50*, 12280–12284.

[43] S. M. Goldup, D. A. Leigh, P. R. McGonigal, V. E. Ronaldson, A. M. Z. Slawin, *J. Am. Chem. Soc.* **2010**, *132*, 315–320.

[44] H. M. Cheng, D. A. Leigh, F. Maffei, P. R. McGonigal, A. M. Z. Slawin, J. Wu, *J. Am. Chem. Soc.* **2011**, *133*, 12298–12303.

[45] A. I. Prikhod'ko, J.-P. Sauvage, *J. Am. Chem. Soc.* **2009**, *131*, 6794–6807.

[46] R. Hayashi, Y. Mutoh, T. Kasama, S. Saito, *J. Org. Chem.* **2015**, *80*, 7536–7546.

[47] Y. Yamashita, Y. Mutoh, R. Yamasaki, T. Kasama, S. Saito, *Chem. Eur. J.* **2015**, *21*, 2139–2145.

[48] R. Hayashi, K. Wakatsuki, R. Yamasaki, Y. Mutoh, T. Kasama, S. Saito, *Chem . Commun.*

2014, *50*, 204–206.

[49] R. J. Bordoli, S. M. Goldup, *J. Am. Chem. Soc.* **2014**, *136*, 4817–4820.

[50] T. Schmidt, R. Schmieder, W. M. Müller, B. Kiupel, F. Vögtle, *Eur. J. Org. Chem.* **1998**, *1998*, 2003–2007.

[51] S. J. Rowan, J. F. Stoddart, *J. Am. Chem. Soc.* **2000**, *122*, 164–165.

[52] R. Barat, T. Legigan, I. Tranoy-Opalinski, B. Renoux, E. Péraudeau, J. Clarhaut, P. Poinot, A. E. Fernandes, V. Aucagne, D. A. Leigh, et al., *Chem. Sci.* **2015**, *6*, 2608–2613.

[53] L. D. Movsisyan, D. V. Kondratuk, M. Franz, A. L. Thompson, R. R. Tykwinski, H. L. Anderson, *Org. Lett.* **2012**, *14*, 3424–3426.

[54] N. Weisbach, Z. Baranová, S. Gauthier, J. H. Reibenspies, J. A. Gladysz, *Chem. Commun.* **2012**, *48*, 7562.

[55] H. Sahnoune, Z. Baranová, N. Bhuvanesh, J. A. Gladysz, J.-F. Halet, *Organometallics* **2013**, *32*, 6360–6367.

[56] Z. Baranová, H. Amini, N. Bhuvanesh, J. A. Gladysz, *Organometallics* **2014**, *33*, 6746–6749.

[57] M. J. Langton, J. D. Matichak, A. L. Thompson, H. L. Anderson, *Chem. Sci.* **2011**, *2*, 1897.

[58] L. D. Movsisyan, M. Franz, F. Hampel, A. L. Thompson, R. R. Tykwinski, H. L. Anderson, *J. Am. Chem. Soc.* **2016**, *138*, 1366–1376.

[59] M. Franz, J. A. Januszewski, D. Wendinger, C. Neiss, L. D. Movsisyan, F. Hampel, H. L. Anderson, A. Görling, R. R. Tykwinski, *Angew. Chem. Int. Ed.* **2015**, *54*, 6645–6649.

[60] D. C. Milan, M. Krempe, A. K. Ismael, L. D. Movsisyan, M. Franz, I. Grace, R. J. Brooke, W. Schwarzacher, S. J. Higgins, H. L. Anderson, et al., *Nanoscale* **2017**, *9*, 355–361.

[61] L. D. Movsisyan, M. D. Peeks, G. M. Greetham, M. Towrie, A. L. Thompson, A. W. Parker, H. L. Anderson, *J. Am. Chem. Soc.* **2014**, *136*, 17996–18008.

[62] D. R. Kohn, L. D. Movsisyan, A. L. Thompson, H. L. Anderson, *Org. Lett.* **2017**, *19*, 348–351.

[63] J. E. M. Lewis, J. Winn, L. Cera, S. M. Goldup, *J. Am. Chem. Soc.* **2016**, *138*, 16329–

16336.

[64] J. Lewis, J. Winn, S. Goldup, *Molecules* **2017**, *22*, 89.

[65] J. E. M. Lewis, P. D. Beer, S. J. Loeb, S. M. Goldup, *Chem. Soc. Rev.* **2017**, *46*, 2577–2591.

[66] A. Noor, S. C. Moratti, J. D. Crowley, *Chem. Sci.* **2014**, *5*, 4283–4290.

[67] M. Galli, J. E. M. Lewis, S. M. Goldup, *Angew. Chem. Int. Ed.* **2015**, *54*, 13545–13549.

[68] P. Thordarson, E. J. A. Bijsterveld, A. E. Rowan, R. J. M. Nolte, *Nature* **2003**, *424*, 915–918.

[69] Y. Matsuoka, Y. Mutoh, I. Azumaya, S. Kikkawa, T. Kasama, S. Saito, *J. Org. Chem.* **2016**, *81*, 3479–3487.

[70] L. C. Gilday, S. W. Robinson, T. A. Barendt, M. J. Langton, B. R. Mullaney, P. D. Beer, *Chem. Rev.* **2015**, *115*, 7118–7195.

[71] A. Brown, T. Lang, K. M. Mullen, P. D. Beer, *Org. Biomol. Chem.* **2017**, *15*, 4587–4594.

[72] A. Tron, P. J. Thornton, B. Kauffmann, J. H. R. Tucker, N. D. McClenaghan, *Supramol. Chem.* **2016**, *28*, 733–741.

[73] J. Winn, A. Pinczewska, S. M. Goldup, *J. Am. Chem. Soc.* **2013**, *135*, 13318–13321.

[74] A. M. Albrecht-Gary, Z. Saad, C. O. Dietrich-Buchecker, J. P. Sauvage, *J. Am. Chem. Soc.* **1985**, *107*, 3205–3209.

[75] J. E. M. Lewis, R. J. Bordoli, M. Denis, C. J. Fletcher, M. Galli, E. A. Neal, E. M. Rochette, S. M. Goldup, *Chem. Sci.* **2016**, *7*, 3154–3161.

[76] J.-P. Collin, C. Dietrich-Buchecker, P. Gaviña, M. C. Jimenez-Molero, J.-P. Sauvage, *Acc. Chem. Res.* **2001**, *34*, 477–487.

[77] B. Hesseler, M. Zindler, R. Herges, U. Lüning, *Eur. J. Org. Chem.* **2014**, *2014*, 3885–3901.

[78] B. Lewandowski, G. De Bo, J. W. Ward, M. Papmeyer, S. Kuschel, M. J. Aldegunde, P. M. E. Gramlich, D. Heckmann, S. M. Goldup, D. M. D'Souza, et al., *Science* **2013**, *339*, 189–193.

[79] C. Wu, P. R. Lecavalier, Y. X. Shen, H. W. Gibson, *Chem. Mater.* **1991**, *3*, 569–572.

Chapter 2: << Chelating Rotaxane Ligand as Fluorescent Metal Ion Sensors >>

Abstract: This chapter reports on the synthesis and study of a proof-of-concept fluorescent rotaxane sensor for metal ions. During the investigation, it was found that the interlocked system selectively reports the binding of Zn^{2+} over other divalent metals ions and in particular Cd^{2+}, an interesting feature given the analogous co-ordination chemistry and d^{10} electronic configuration of the two metal ions. Using x-ray crystallography techniques as well as fluorescence and NMR spectroscopy analyses, we studied the binding behaviour of the receptor and gained knowledge that would explain both the switch-on of the fluorescence and the selectivity for Zn^{2+}. Interestingly, it emerged that the mechanical bond has an impact on both features and in particular the latter for steric reasons.

Acknowledgements: I would like to thank Drs Kajally Jobe, Jessica Pancholi and Michael Watkinson for the preliminary work they provided as well as their help during this study.

I would like to thank Dr James Lewis for the crystal structure determination of rotaxane **83**.

I would like to thank the members of the Goldup group for providing macrocycle **78**.

Prior publication: None of this work has been previously published.

2.1. Introduction

What makes small molecule sensors such a powerful tool for the detection of metal cations in living cell is their fast response, as well as their potential for non-invasive, high resolution imaging[1–4]. They are commonly based on a multi-dentate ligand linked to a fluorophore whose response is modulated upon the binding event of the guest of interest[5]. In mechanically interlocked systems[6], such as catenanes and rotaxanes, it has been shown for many years now that mechanical motion (pirouetting, shuttling Figure 2. 1) can be induced between its two components in response to guest binding. This unique feature of mechanically interlocked molecules makes it possible to alter the photophysical properties of the whole system in relation to its non-interlocked components[7,8]. Making good use of mechanical motion, a number of rotaxanes and catenanes chemosensors have already been published. They are usually based on a commonly available luminescent unit which is introduced within the axle or the ring and its photophysical response is recorded as a result of binding events. This approach has been successful, particularly for the development of anions sensors as it has been shown by the groups of Beer and Ma, pioneers in the field. However, the literature contains a very limited number of papers where this methodology has been applied to the detection of cationic guests. A surprising fact given that mechanically interlocked molecules, especially those obtain through metal-mediated approaches, possess well-defined cavities containing multiple donor atoms for metal ions[9].

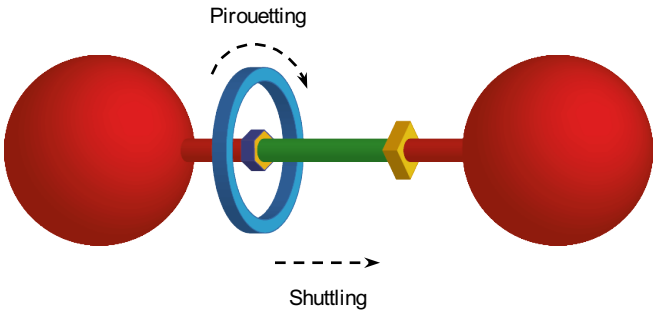

Figure 2. 1 Cartoon representation of pirouetting and shuttling motions in a rotaxane.

One of the first examples comes from Swager and co-workers. In 1997 they synthesised a polyrotaxane 66 containing a phenantroline unit within ring and a bipyridine moiety inside the axle[10] (Scheme 2. 1). They demonstrated that upon binding of Cu^{2+}, the conductivity of polymer increased by 10^6 to 10^7 fold along with a red-shift of the UV-vis absorption.

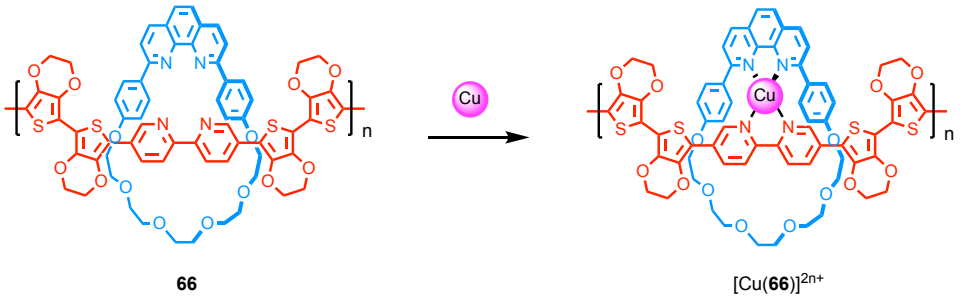

66 [Cu(**66**)]$^{2n+}$

Scheme 2. 1 Cu^{2+} polyrotaxane **66** sensor synthesised by Swager and co-workers.

In 2004, Hiratani and co-workers synthesised [1]rotaxane (or lariat structure) **67** bearing an anthracene unit as a stopper (Scheme 2. 2)[11]. They demonstrated that upon addition of Li^+ the system exhibited conformational rearrangement that brought the stopper closer to the ring. As a result, the fluorescence from 400 to 500 nm was enhanced due to increase in the charge transfer from the naphthalene to the anthryl group. Since the system only responding to Li^+, it made it a candidate for lithium ion sensing agent.

Building up on this work, they developed a [3]rotaxane **68** (Scheme 2. 2) that formed a 1:2 complex upon addition Li^+. With Cs^{2+} however a 1:1 complex was observed with a concomitant increase of the fluorescence. They hypothesised, based on NOESY NMR data, that addition of Cs^+ promoted a change in orientation of the two macrocycles to form a sandwich complex where the cation is located in between the two rings[12].

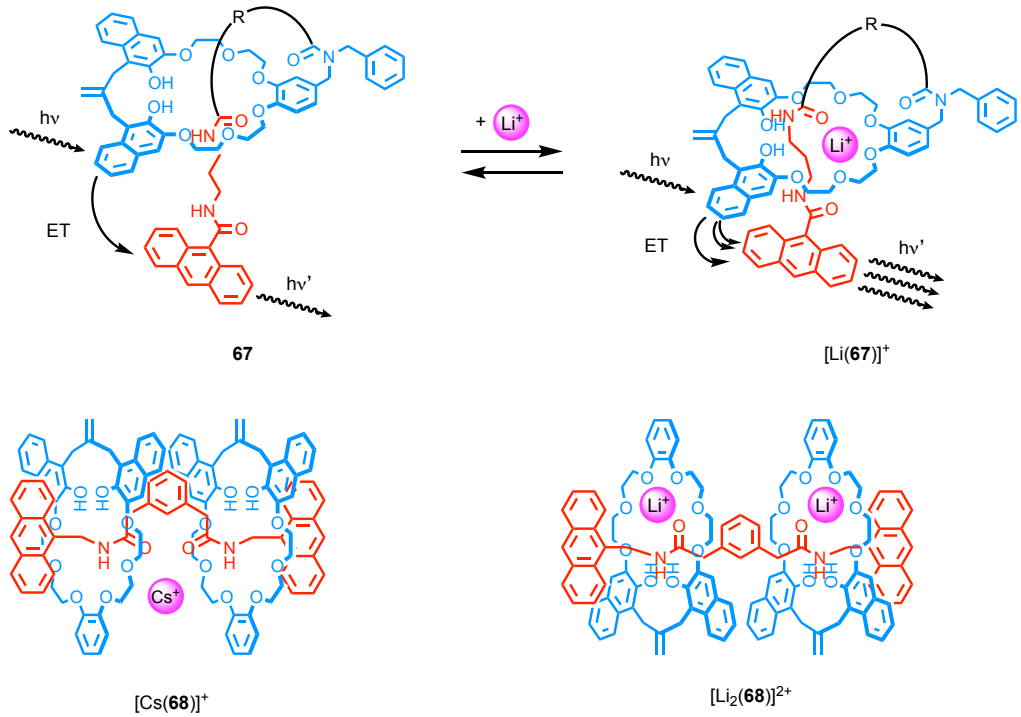

67 [Li(**67**)]$^+$ [Cs(**68**)]$^+$ [Li_2(**68**)]$^{2+}$

Scheme 2. 2 Pseudorotaxane **67** and [3]rotaxane **68** synthesised by Hiratani and co-workers.

Although devoid of photophysical properties, another interesting interlocked example came from Chen and co-workers with the synthesis of a [2]rotaxane-based ^{1}H NMR spectroscopy probe for metal ions[13]. The molecule **69** contained a bis-*p*-xylyl[26]crown-6 macrocycle and bipyridine unit within its axle (Figure 2. 2). They showed that **69** formed complexes with Li^{+}, Na^{+}, Mg^{2+}, Ca^{2+} and K^{+} ions, each complex displaying a unique set of signals by ^{1}H NMR spectroscopy. The fact that it was also the case in a complex mixture (Figure 2.2) made **69** a potential sensor for these physiologically important cations.

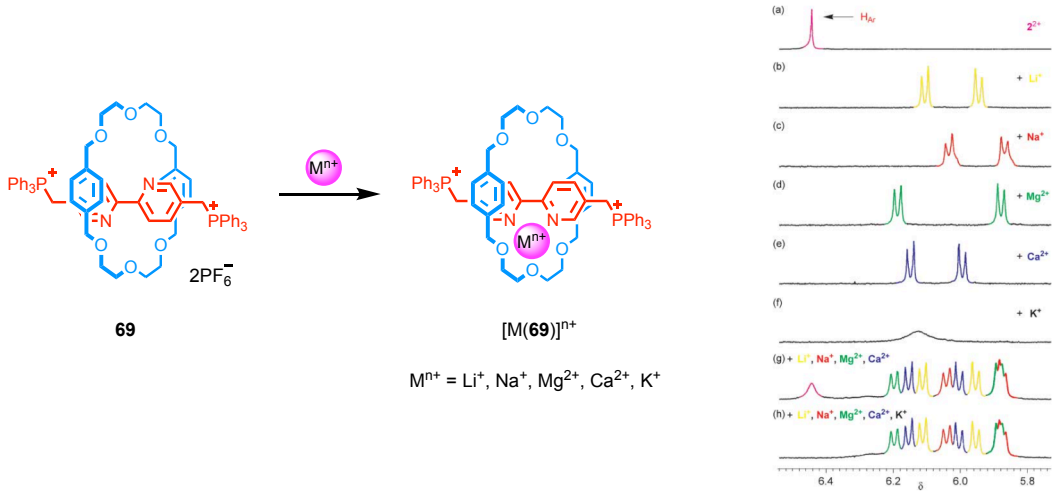

Figure 2. 2 ^{1}H NMR spectroscopy [2]rotaxane probe **69** developed by Chen and co-workers.

In 2008, Li *and co-workers* synthesised a fluorescent switchable [2]rotaxane incorporating two stations within its axle, an amine and an amide (Scheme 2. 3)[14]. The shuttling motion of the ring from one station to the other could be triggered by acid/base addition (protonating/de-protonating the amine site) but also with the use of Zn^{2+} or Li^{+} ions. In the presence of the latter, the macrocycle sat at the amide station and photoinduced electron transfer (PET) between the amine and the anthracene stopper resulted in a weak fluorescent response. Upon addition of Zn^{2+}, Li^{+} was displaced and the ring shuttled to the amine station. In $[Zn(\mathbf{70})]^{2+}$, PET was suppressed and resulting in an enhancement of the fluorescence at 422 nm.

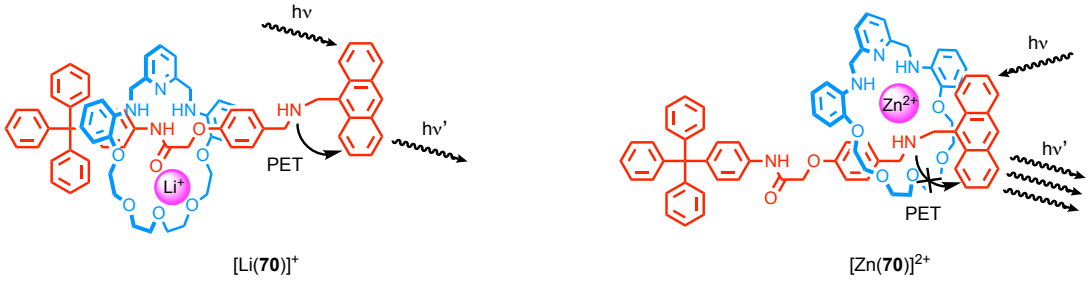

Scheme 2. 3 Fluorescent shuttle **70** synthesised by Li and co-workers.

Another example of photo-responsive molecular switches come from Chiu and co-workers. In 2010, they synthesised a two-station [2]rotaxane containing a squaraine and a bipyridinium unit (Scheme 2. 4)[15]. They demonstrated that upon addition and removal of Na^+ it was possible to selectively encapsulate or expose the squaraine unit, resulting in an enhancement or quenching of its long-wavelength emission at 641 nm, respectively.

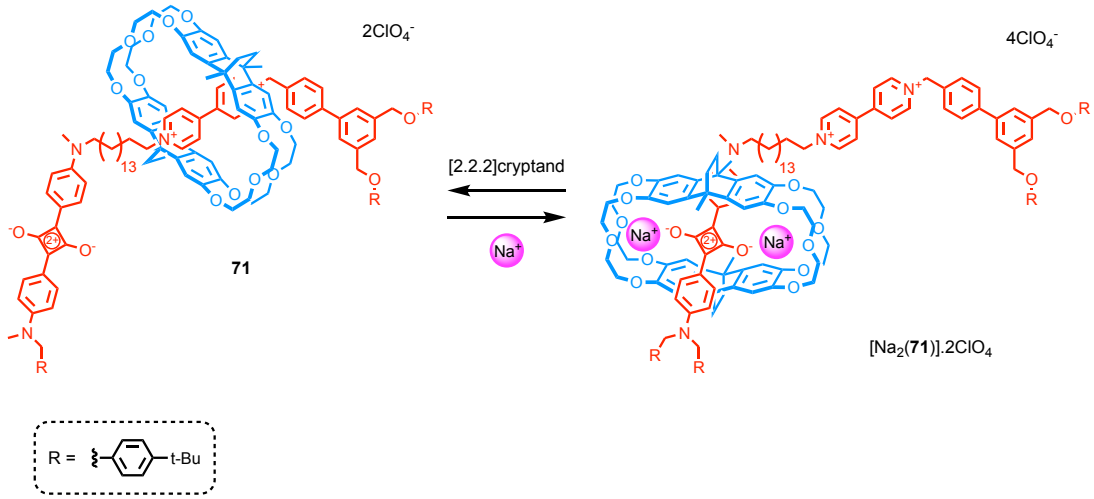

Scheme 2. 4 Fluorescent shuttle **71** synthesised by Chiu and co-workers.

The same year, Yashima and co-workers reported the optically active catenane **72** based on an amidinium carboxylate salt bridge lock (Scheme 2. 5)[16]. The chiral substituents on the amidine nitrogen atoms control the twist sense of the m-terphenyl ligand in its lock state, which resulted in a strong CD response from the system. Upon addition of 2 equivalents of TFA the bridge was 'unlocked' and the two macrocycles were allowed to freely rotate around each other, resulting in the CD spectrum becoming identical to the one of the TFA salt of the amidine macrocycle on its own. Addition of base restored the bridge between the two components and the chiroptical properties. The switch could also be observed using 1 equivalent of $Zn(ClO_4)_2$, the metal cation forming a complex with the amidine ligand which unlocked the two rings and affected the CD signal. Moreover, addition of Zn^{2+} also caused enhancement of the fluorescence of the m-terphenyl units with a concomitant red-shift, leading to a change in colour from purple to bright yellow. Subsequent addition of [2.2.1] cryptand trapped the Zn^{2+} cations, which restored the CD and fluorescent spectra of the salt bridge system, making the switch a reversible process.

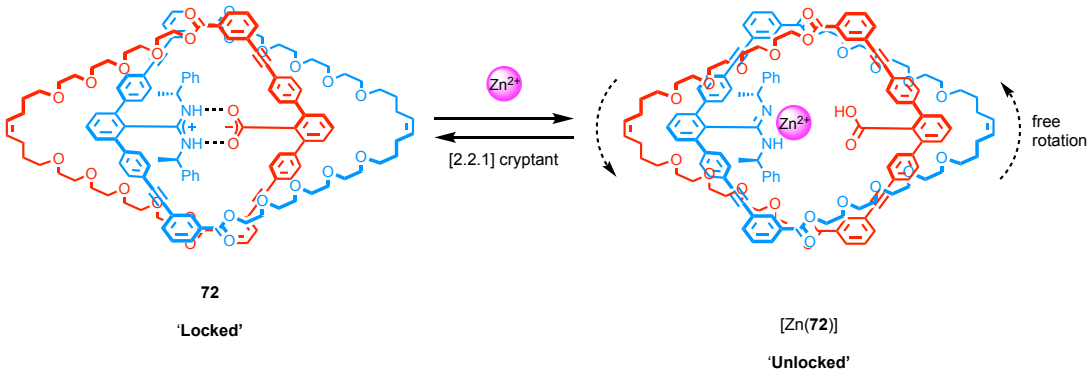

Scheme 2. 5 Catenane sensor **72** synthesis by Yashima and co-workers.

More recently, Smith and co-workers worked on squaraine rotaxane endoperoxides containing sites for metal chelation[17]. They tested their metal binding behaviour and showed that upon coordination of Co^{2+}, Zn^{2+} and Ni^{2+} with to the dipicolylamine site (Figure 2. 3) the fluorescence was quenched. However, no selectivity was reported toward any of the three metal cations.

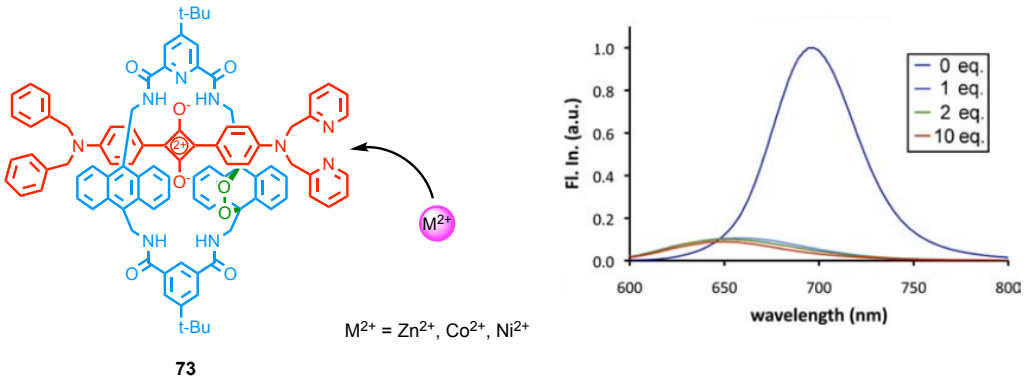

Figure 2. 3 Example of [2]rotaxane endoperoxide synthesised by Smith and co-workers and its fluorescence response upon binding of Zn^{2+} ions.

Project Aim

An efficient chemosensor must show a selective response for a guest on interest in a complex mixture containing many other competitive analytes. In the past, the Goldup group have successfully demonstrated the synthesis of a small fluorescent receptor showing a selective response for Zn^{2+} cations (Scheme 2. 6)[18]. The interest for selective optical sensing of zinc comes from the spectroscopically silent nature of d^{10} Zn ions, combined with the fact that changes in zinc homeostasis are associated with diseases with high morbidity rate such as Alzheimer's disease[19], Type II diabetes[20] and age related macular degeneration[21].

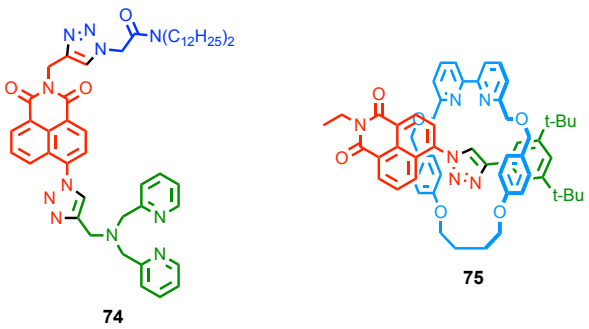

74 75

Scheme 2. 6 Zn^{2+} selective sensor and small naphthalimide rotaxane synthesised by Goldup and co-workers.

In 2011, a novel fluorescent small rotaxane containing a naphthalimide unit at one end of the axle (Scheme 2. 6) was synthesised using the AT-CuAAC reaction[22]. As mentioned earlier, mechanically interlocked molecules obtained through metal-mediated approaches possess well-defined cavities containing multiple donor atoms for metal ions. Moreover, they offer the possibility to readily modify the periphery of the binding site in order to finely tune the binding behaviour without affecting the binding site on its own. These features together make them interesting candidates for the development of mechanically chelating ligand for metal cation.

We therefore aimed to develop a family of [2]rotaxane probes, targeting Zn^{2+} as analyte of interest.

Preliminary work

This work was begun by Drs Kajally Jobe and Jessica Pancholi during their studies. Below I have outlined their key results that served as the starting point for my work.

The study started with the synthesis of rotaxane **79** and axle **80** and the investigation of its photophysical properties in the presence of various metal. The synthetic route was very straightforward as macrocycle **78** and both half threads **76** and **77** were known in the literature. Using the AT-CuAAC methodology rotaxane **79** was obtained (88%) as well as the non-interlocked counterpart **80** (40%) (Scheme 2. 7).

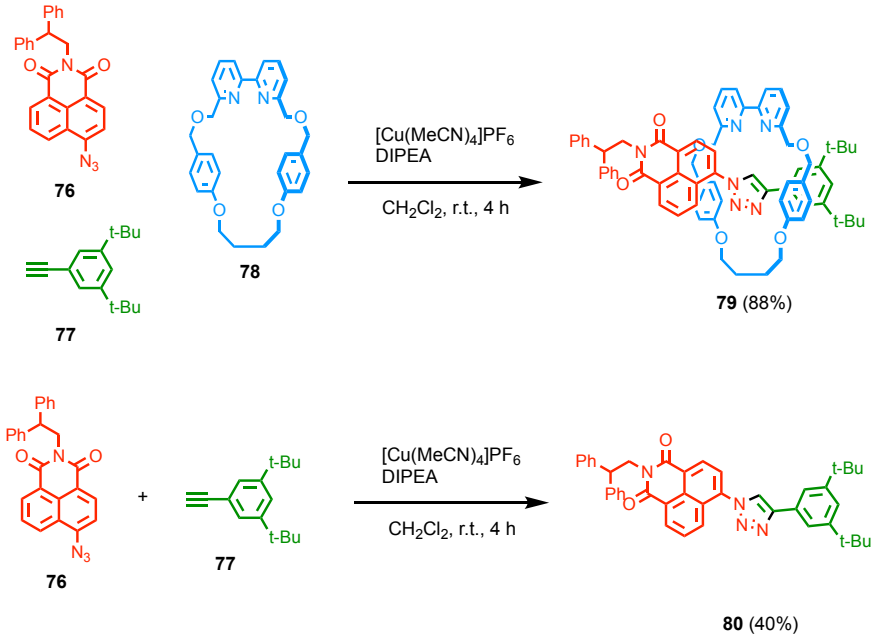

Scheme 2. 7 Active-Template synthesis of rotaxane **79** and axle **80**.

Its absorption spectra displayed a band centred at 344 nm in MeCN attributed to the naphthalimide unit, and more interesting perhaps, two emission bands were observed in fluorescence spectroscopy (λ_{em} = 430 and 560 nm) (Figure 2. 4 a). The potential behaviour of **79** as a sensor was investigated by fluorescence spectroscopy and it was shown that portion-wise additions of $Zn(ClO_4)_2.6H_2O$ to a solution of **79** in MeCN led to quenching of the emission at 560 nm that plateaued after 1 equivalent of metal had been added (Figure 2. 4 a). It is worth noting that the emission property of the axle on its own did not show any response to Zn^{2+} (Figure 2. 4 b), a promising result for the potential application of **79** as a 'switch-off' sensor for Zn^{2+}. Unfortunately, this feature was not unique to Zn^{2+} and other divalent metal cations (V^{2+}, Mn^{2+}, Fe^{2+}, Co^{2+}, Ni^{2+}, Cu^{2+}, Cd^{2+} and Hg^{2+}) showed similar quenching effect (Figure 2. 4c), ruling **79** out as a metal ion sensor.

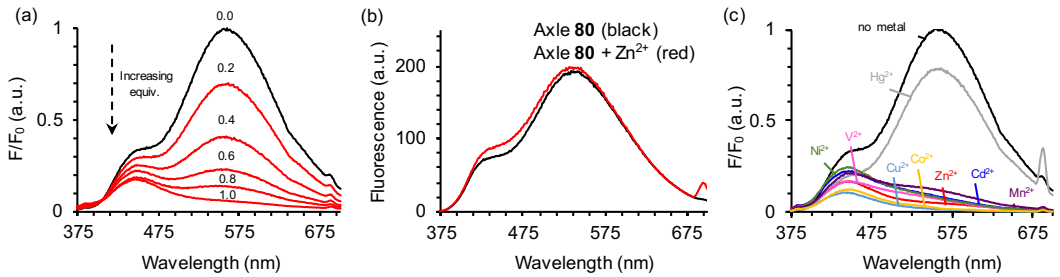

Figure 2. 4 Fluorescence response in MeCN (298 K) at C = 100 μM of (a) **79** upon addition of increasing amount of $Zn(ClO_4)_2.6H_2O$, (b) axle **80** upon in the presence of 1 equiv. $Zn(ClO_4)_2.6H_2O$ and (c) rotaxane **79** in the presence of 5 equiv. of $M(ClO_4)_2$ (M = V^{2+}, Mn^{2+}, Fe^{2+}, Co^{2+}, Ni^{2+}, Cu^{2+}, Cd^{2+} and Hg^{2+}). No emission was observed in the case of $Fe(ClO_4)^{2+}$.

Having confirmed the optical response of the system to endotopic binding of metal cations, the investigation was extended to a family of heteroatom-substituted naphthalimide rotaxane (Scheme 2. 8). Within these new receptors, a possible direct interaction between the heteroatom and the metal ion could affect the photophysical properties of the fluorophore.

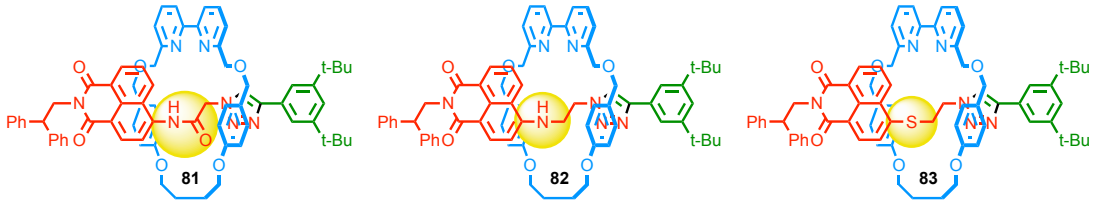

Scheme 2. 8 heteroatom-substituted naphthalimide rotaxanes studied in this work.

The three rotaxanes **81**, **82** and **83** were synthesised in good to excellent yields (62%, 72% and 86% respectively) the AT-CuAAC. ^{1}H NMR spectroscopy confirmed the ligand behaviour of the three compounds with the clear formation of a 1:1 complex upon addition of 1 equivalent of Zn^{2+} to a solution **81**, **82** or **83** in CD_3CN (Figure 2. 5).

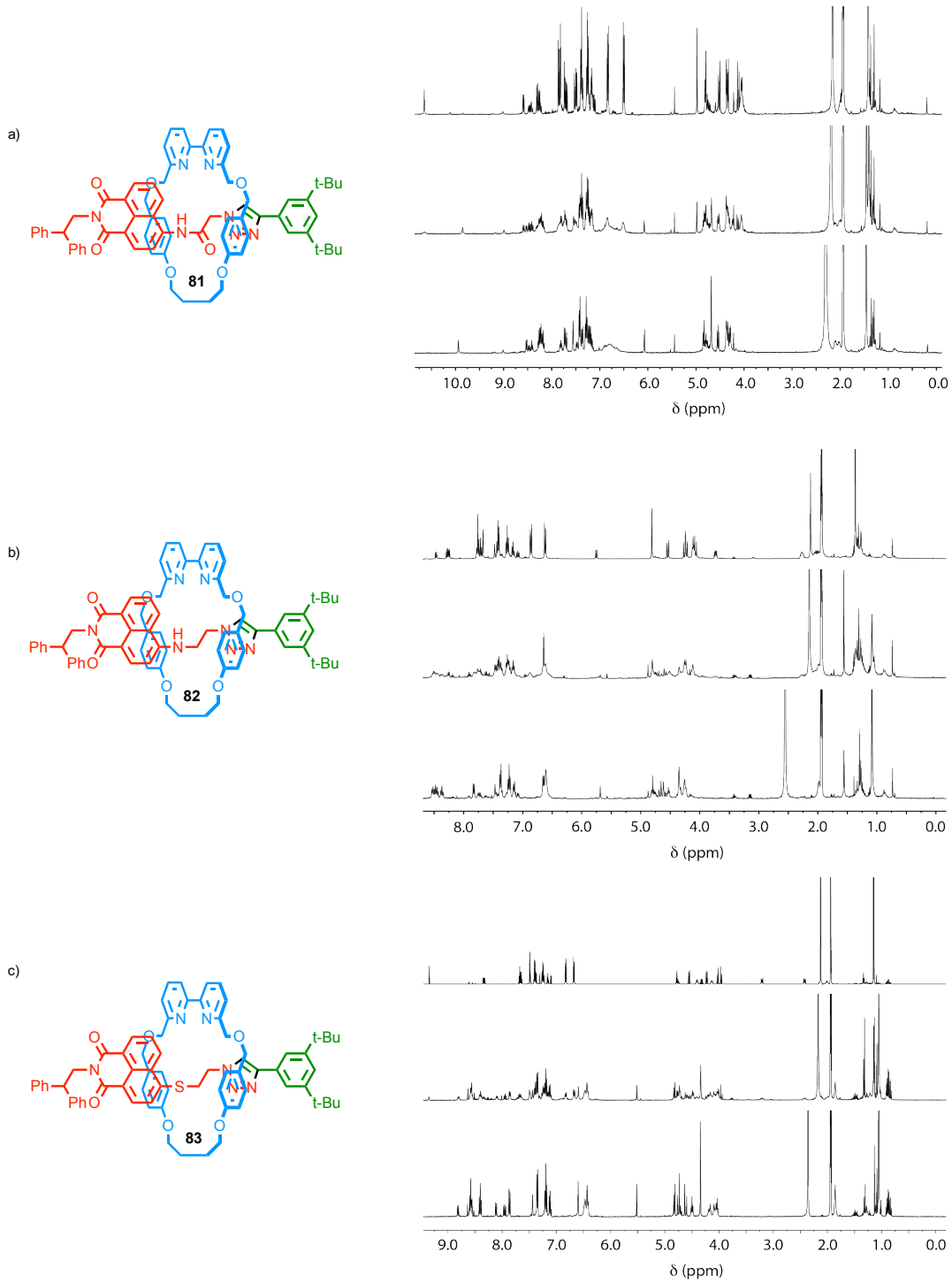

Figure 2. 5 ^{1}H NMR titrations (CD_3CN, 400 MHz, 298 K) of (a) **81**, (b) **82** and (c) **83** with $Zn(ClO_4)_2.6H_2O$ in CD_3CN. Each stack plot shows (top) rotaxane, (middle) rotaxane with 0.5 equivalent of Zn^{2+} and (bottom) rotaxane with 1 equivalent of Zn^{2+}.

Their photophysical properties were then investigated in MeCN. Whereas the naphthalimide absorbance band was centered at 377 and 380 nm for **81** and **83** respectively, it appeared significantly redshifted in rotaxane **82** (433 nm) (Figure 2. 6). A shoulder at 450 nm could also be noticed in the case of rotaxane **81** bearing the amino group within the thread, possibly due to PET between the amine and the naphthalimide. Portion-wise addition of

$Zn(ClO_4)_2.6H_2O$ to a solution of each rotaxane in MeCN resulted in the appearance of new absorbance bands in the 310-330 nm region, corresponding to the metal bound to the bipyridine ligand. Moreover, the absorbance of the naphthalimide experienced a hypsochromic in all three cases ($\Delta\lambda$ = 29, 15 and 5 ppm for **81**, **82** and **83** respectively) with a concomitant slight decrease in intensity for **81**, **82** and an increase for **83** (Figure 2. 6).

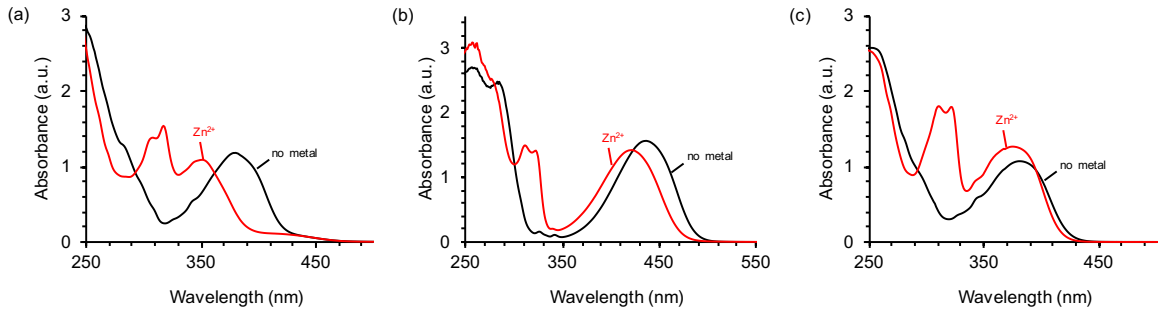

Figure 2. 6 Changes in the UV-Visible spectra upon addition of $Zn(ClO_4)_2.6H_2O$ (red lines) for (a) **81**, (b) **82** and (c) **83** in MeCN, C = 100 μM.

Fluorescence studies however displayed very different behaviours. Whereas rotaxane **82** responded to the presence the majority of divalent metal cations with a "switch-off" of the emission (Figure 2. 7 b), **81** in contrast showed little to no response to Mg^{2+}, Ca^{2+}, Mn^{2+}, Zn^{2+} and Hg^{2+} but a "switch-off" in the presence of Ni^{2+}, Co^{2+}, Cu^{2+} and on to Fe^{2+} (weak) Hg^{2+} with an impressive five-fold increase in emission (Figure 2. 7 a). Although not entirely selective and therefore not useful in itself as a metal ion probe, the diversity in the outcome of fluorescence observed for **81** were promising results for the development of sensors for Hg^{2+}.

Pleasingly, titration of rotaxane **83** with Zn^{2+} resulted a two-fold increase in the emission with a concomitant blue shift of 15 nm, whereas all other metal ions tested decreased it or left it unaffected (Figure 2. 7 c). Furthermore, competition experiment suggested that in many cases Zn^{2+} was able to displaced other metal ions from ligand **83**, resulting in recovery of fluorescence in the case on Mn^{2+}, Fe^{2+}, and Co^{2+}. Finally, it was notable that the sensor was selective for Zn^{2+} over Cd^{2+}.

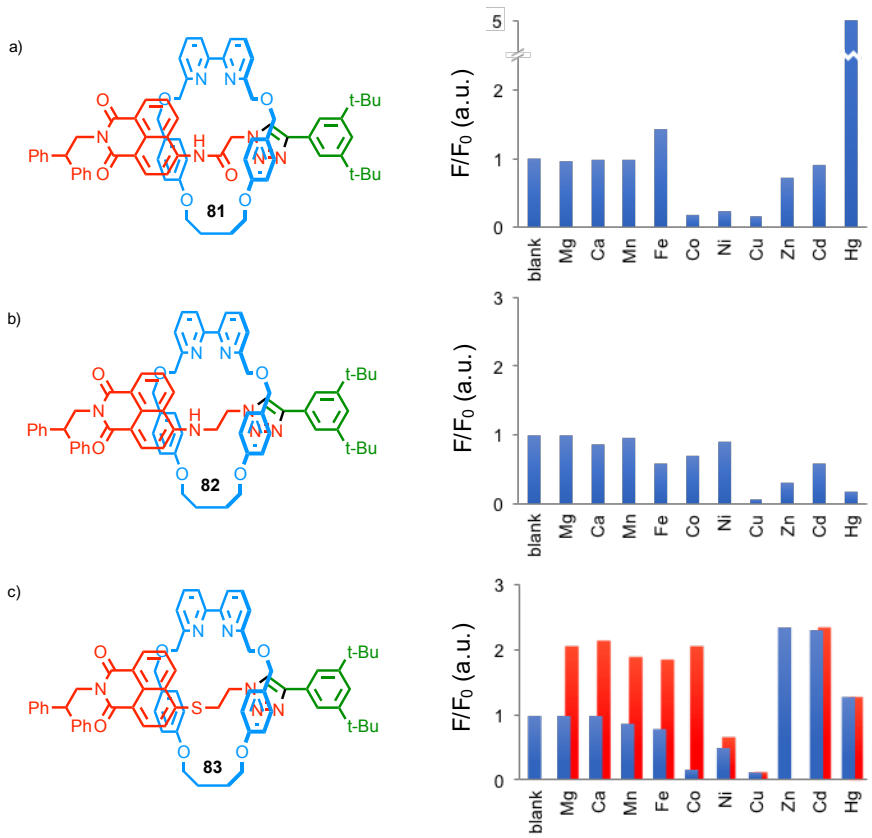

Figure 2. 7 Rotaxanes a) **81**, b) **82** and c) **83** and their fluorescence response to $M(ClO_4)_2$ (MeCN, 100 μM). Blue bars refer to the response of the ligand to 5 equiv. of metal ion. Red bars in c) refer to the fluorescence response on sequential addition of M^{2+} indicated followed by Zn^{2+} (5 equiv. each).

This selectivity for Zn^{2+} over Cd^{2+} observed with **83** was surprising given the similarity of both metal cation. Indeed, Zn^{2+} sensors reported in the literature often show a similar response to both metals due to their analogous co-ordination chemistry and d^{10} electronic configuration. For this reason, we decided to investigate this particular behaviour of our sensor more in detail.

2.2. Results and Discussion

2.2.1. Starting material and rotaxane synthesis

The synthesis of sulfur-containing half-thread was performed in a single step starting from the alcohol intermediate **84** previously made by Dr Jessica Pancholi. The alcohol was transformed to the azide was using diphenylphosphoryl azide in a Mitsunobu-type reaction, affording half-thread **85** in 60% yield (Scheme 2. 9).

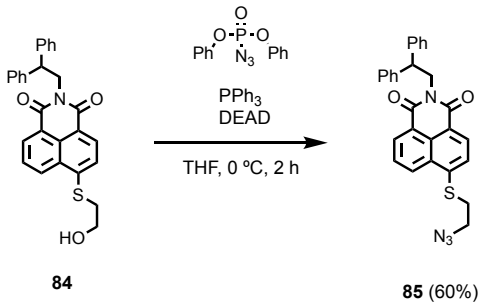

Scheme 2. 9 Synthesis of sulfur-containing half-thread **85**.

The 3,5-di-*tert*-butylalkyne stopper **88** was synthesised in two steps starting with a Sonogashira coupling between 3,5-di-*tert*-butylbromobenzene **86** and ethynyltrimethylsilane. The TMS protecting group on **87** was then removed under basic conditions, affording **88** in 97% yield without the need for any further purification (Scheme 2. 10).

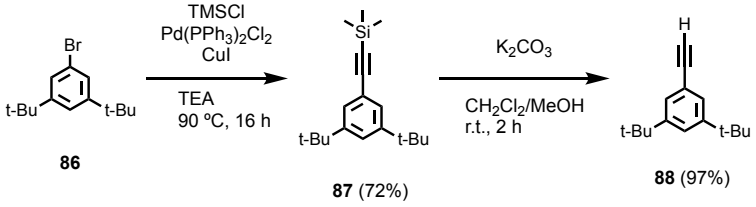

Scheme 2. 10 Synthesis of alkyne **88**.

With the two half threads in hand and macrocycle **78** being provided by members of the group, sulfur-containing rotaxane **83** was obtained in good yields 83% *via* our AT-CuAAC methodology (Scheme 2. 11).

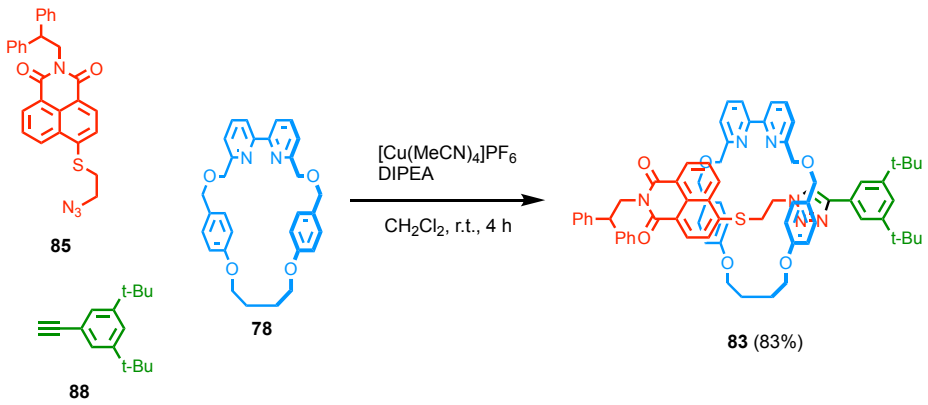

Scheme 2. 11 Synthesis of sulfur-containing rotaxane **83**.

2.2.2. Study of the binding behaviour of **83**

Having identified rotaxane **83** as a potential switch-on sensor for Zn^{2+}, we investigated its behaviour more in detail starting with the structure of the host itself. Comparing the ^{1}H NMR spectra of both the axle **89** and rotaxane **83** in CD_3CN, a number of key differences were noted (Figure 2. 8). Firstly, a significant deshielding of the triazole proton H_m ($\Delta\delta$ = 1.36 ppm) in the interlocked system that we attribute to C-H•••N hydrogen bond with the bipyridine moiety, as has previously been observed in similar structures.[21] Secondly, the alkyl protons H_k and H_l appear at lower ppm, which could be the result of C-H•••π interactions with the flanking aromatic rings in the macrocycle.

Pleasingly, single crystals suitable for X-ray analysis were obtained from slow evaporation of a solution of **83** in MeCN and confirmed the proposed interactions in solution. In the solid state (Figure 2. 9 a), short distances were measured between H_m and N1 (2.46 Å) and perhaps more interestingly between one of H_k and the second bipyridine nitrogen N2 (2.71 Å). Finally, one each of proton H_k and H_l appeared to be in close contact with the flanking aromatic rings in the macrocycle (2.66 and 2.79 Å respectively) (Figure 2. 9 b), which is interesting because H_k experienced a lesser upfield shield ($\Delta\delta$ = 1.36 ppm) compare to H_l despite a shorter C-H•••π contact by 0.13 Å.

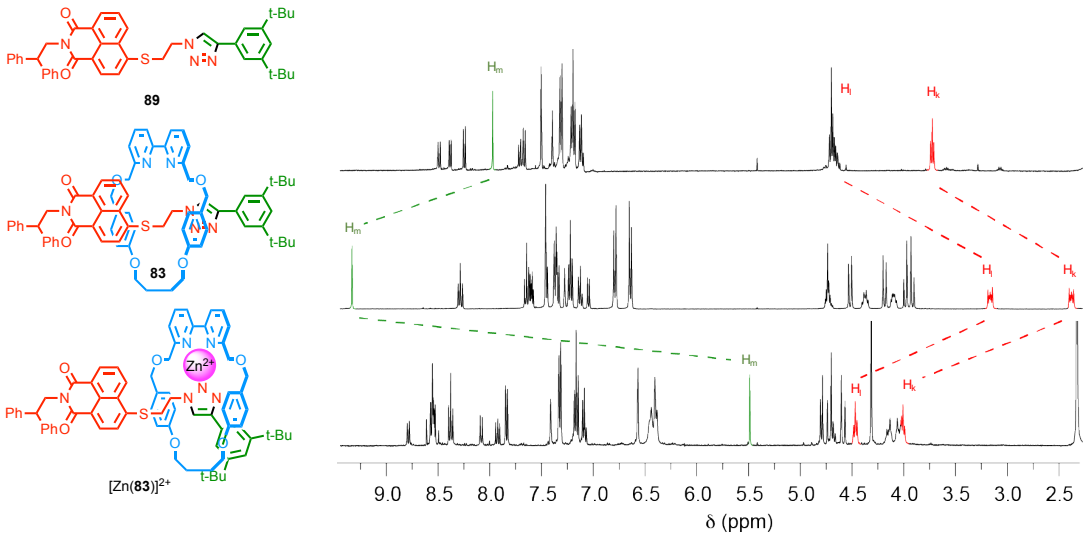

Figure 2. 8 Partial ^{1}H NMR spectra (CD_3CN, 400 MHz, 298 K) of a) axle **89**, b) rotaxane **83** and c) rotaxane **83** with 1 equiv. of $Zn(ClO_4)_2.6H_2O$.

Portion-wise addition of $Zn(ClO_4)_2.H_2O$ to a solution of **83** in CD_3CN, resulted first in broadening of the ^{1}H NMR peaks of **83** and the appearance of a new set of signals that was tentatively assigned to [Zn(**83**)]$^{2+}$. Once one equivalent of the metal ion had been added, no further changes were observed confirming the formation of a 1:1 complex. Looking at the ^{1}H NMR of [Zn(**83**)]$^{2+}$ in detail (Figure 2. 8), a significant upfield shift was observed for the triazole proton H_m, now appearing at 5.52 ppm ($\Delta\delta$ = 3.84 ppm). Meanwhile proton H_k and H_l from the thread shifted to higher ppm, reaching values closer to the one found in the non-interlocked axle and suggesting the disappearance of the proposed C-H•••π interactions in **83.** Single crystals suitable for X-ray analysis were grown from slow evaporation of a solution of [Zn(**83**)]$^{2+}$ in MeCN. The solid-state structure of the complex confirmed the important structural rearrangement induced by binding of the metal ion (Figure 2. 9 b). The zinc ion is bound to the bipyridine nitrogen atoms as well as one of the nitrogen of the triazole ring and one of the ether oxygens in the side chain of the ring. Perhaps of interest, the sulfur atom was not involved in the binding, instead a water molecule completed a five-coordinate environment around the zinc. As a consequence of metal coordination, the short contact interactions between the triazole proton H_m and the bipyridine nitrogen atoms are interrupted and instead it engages in C-H•••π contacts (2.74 Å) with one of the flanking aromatics of the ring. Moreover, the macrocycle shifted to fully encircle the triazole moiety, breaking the C-H•••π contacts between H_k, H_l and the ring in the meantime. Interestingly, the axle experience a 90º bend upon metal binding and a short C-H•••π contact (2.86 Å) was measured between one of the flanking aromatic proton H_F and the naphthalimide core.

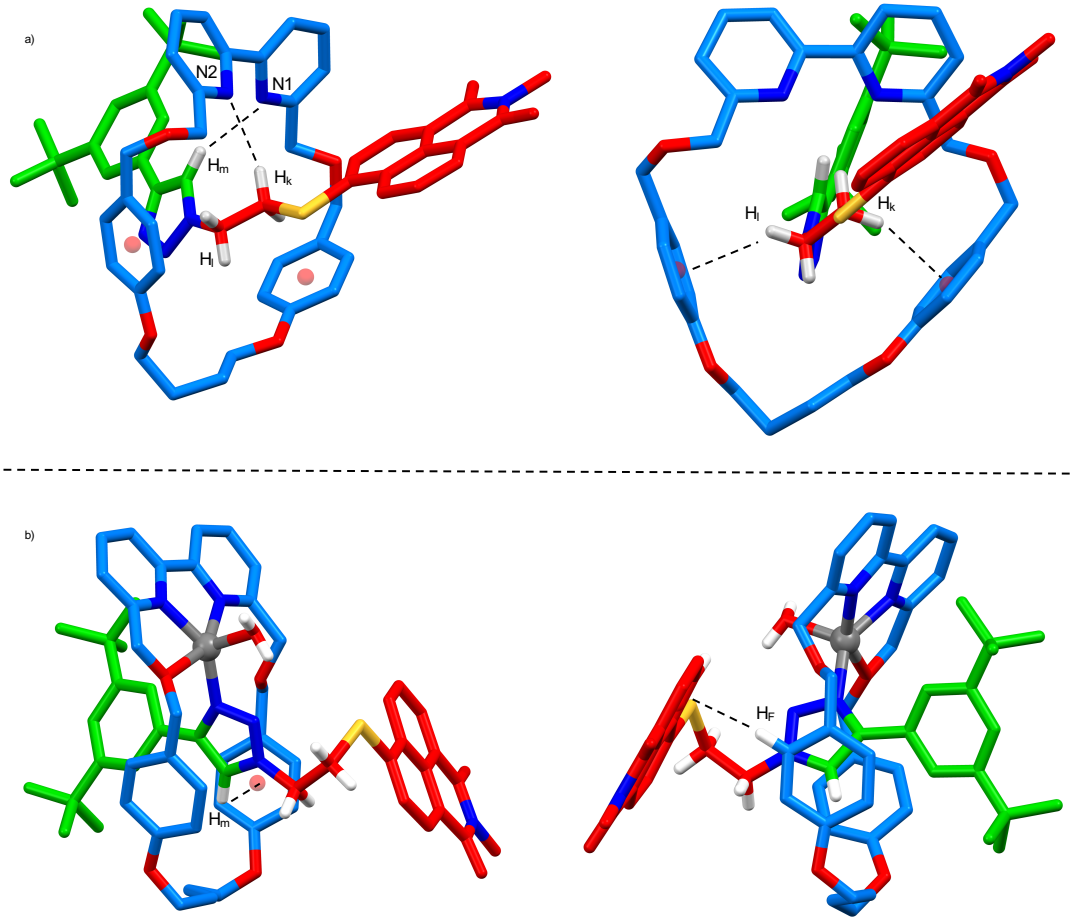

Figure 2. 9 Solid state structures of a) rotaxane **83** (selected distances in Å: C-H_m•••N1 = 2.46, C-H_k•••N2 = 2.71, C-H_k•••π = 2.66, C-H•••π = 2.79, dihedral b) $[Zn(\mathbf{83})]^{2+}$ (selected distances in Å: C-H_m•••π = 2.74, C-H_F•••π = 2.86). The diphenyl top unit of the naphthalimide as well as the non-relevant protons have been hidden for clarity.

2.2.3. The influence of water

Having successfully assessed the structure and binding mode of our receptor, we investigated its potential use as a selective sensor for Zn^{2+} ions. However, when repeating the metal screening experiment in MeCN, **83** showed a positive response for both Zn^{2+} and Cd^{2+} with two-fold increase of the emission with a concomitant hypsochromic shift of $\Delta\lambda_{em}$ = 14 and 9 nm, respectively (Figure 2. 10 a). We then decided to investigate the nature of the salt used for the study and quickly realized the key role it played. Whereas in the presence of 100 equivalents of $M(ClO_4)_2.6H_2O$ (M = Zn^{2+}, Cd^{2+}) an enhancement of the fluorescence was observed by naked-eye (Figure 2. 10 b), $Zn(ClO_4)_2.xH_2O$, where x is an unknown value presumed to be significantly greater than 6, induced an apparent quenching (Figure 2. 10 b). However, used in a smaller excess (5 equiv.) both $Zn(ClO_4)_2.6H_2O$ and $Zn(ClO_4)_2.xH_2O$ triggered a similar response (Figure 2. 10 a).

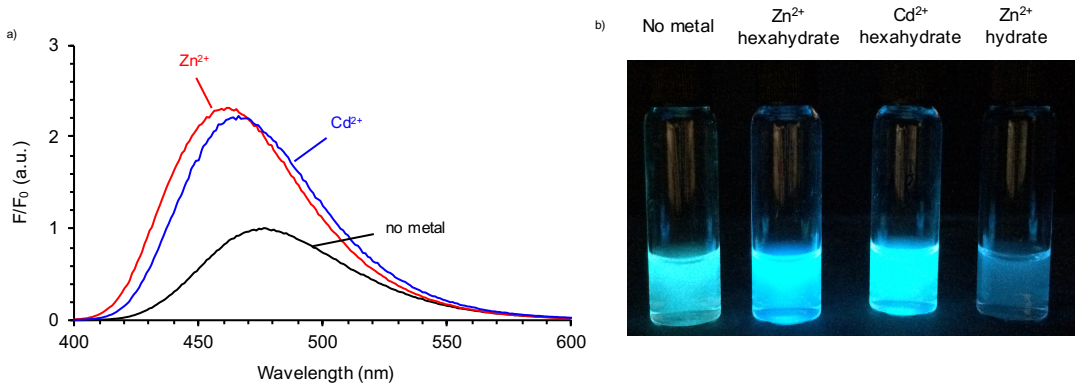

Figure 2. 10 a) normalized fluorescence of **83** (λ_{ex} = 380 nm) in MeCN at 100 μM without any metals (black), in the presence of $Zn(ClO_4)_2.6H_2O$ or $Zn(ClO_4)_2.xH_2O$ (red), in the presence of $Cd(ClO_4)_2.6H_2O$ (blue) (5 equiv. of each), b) picture of (from left to right) **83** on its own and in the presence of $Zn(ClO_4)_2.6H_2O$ (red), $Cd(ClO_4)_2.6H_2O$ and $Zn(ClO_4)_2.xH_2O$ in MeCN (100 equiv. of each).

Taking in account these new results we then investigated the effect of water on the binding behavior and photophysical properties of **83**. It was observed that the addition of known amount of water to a solution of **83** in MeCN resulted in a significant decrease in the emission signal with ~30% of the intensity being lost with only 2% of water added. Interestingly, addition of $M(ClO_4)_2.6H_2O$ (M = Zn^{2+}, Cd^{2+}) gave us the expecting switch-on response. However, where 6 equivalents of Zn^{2+} produced a two-fold increase in intensity, 10 equivalents of Cd^{2+} created only a 30% enhancement leading to an apparent 'non-response' in comparison to the emission in neat MeCN (Figure 2. 11). These results would explain the 'switch-off' previously reported by Dr Pancholi for Cd^{2+} if an old sample of $Cd(ClO_4)_2.xH_2O$ containing a significant amount of water was used for the study. Finally, we pushed this investigation further and observed that upon addition of $Zn(ClO_4)_2.6H_2O$ and $Cd(ClO_4)_2.6H_2O$ (5 equiv.) to a solution of **83** in MeCN/H_2O (98:2), the system responded in the same way it did with Zn^{2+} alone. Taking these results in consideration, we then decided to study the potential selectivity of **83** for Zn^{2+} over Cd^{2+}.

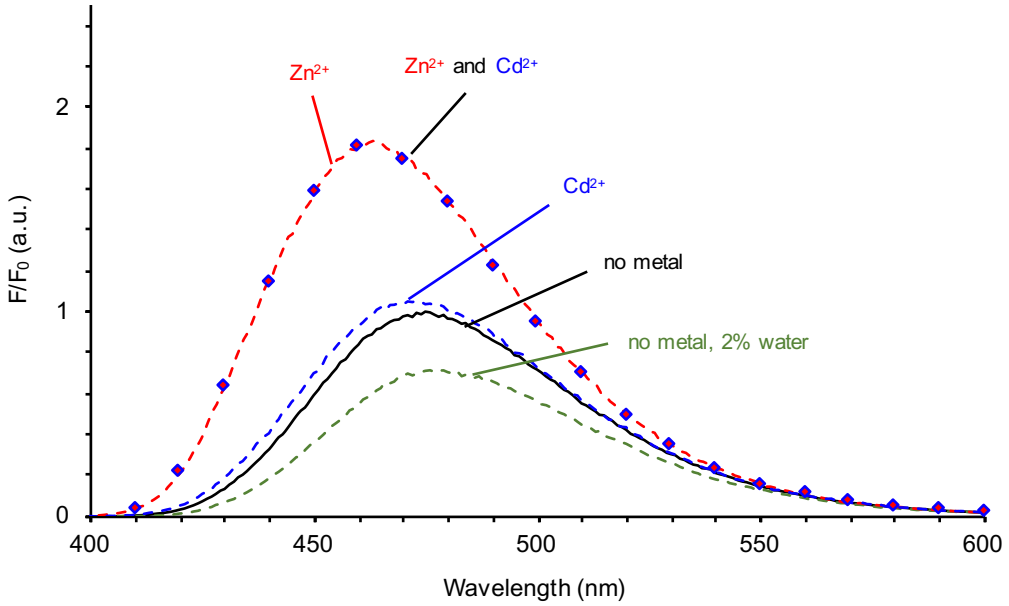

Figure 2. 11 Normalized fluorescence of **83** (λ_{ex} = 380 nm) in MeCN at 100 μM (black), in presence of increasing amount of water (dotted green lines), with 5 equiv. of $M(ClO_4)_2.6H_2O$ in $MeCN/H_2O$ (98:2) (M = Zn^{2+} (red), Cd^{2+} (blue)) and with both metals (red and blue markers).

2.2.4. Selectivity for Zn^{2+} over Cd^{2+}

In the study, we investigated the potential relative selectivity of **83** for Zn^{2+} ions and the impact of the mechanically chelating triazole within the interlocked structure.

UV-visible titrations of $Zn(ClO_4)_2.6H_2O$ and $Cd(ClO_4)_2.6H_2O$ were performed for both receptor **78** and **83** in MeCN and the data were fitted with a non-linear regression analysis (Equation 2.1)[23] plotting the new absorption of the bipyridine unit bound to the metal. Whereas a strong binding was observed for Zn^{2+} with a dissociation constant $K_d < 10^{-8}$ M^{-1} for both the macrocycle **78** and rotaxane **83** (Figure 2. 12 a and c), Cd^{2+} showed some differences. Indeed macrocycle **78** still displayed a strong binding affinity to Cd^{2+} ions ($K_d < 10^{-8}$, Figure 2. 12 b), but a dissociation constant of 3.6×10^{-5} M^{-1} was obtained for rotaxane **83** (Figure 2. 12 d). A significant drop in binding strength by at least three order of magnitude that was further confirmed by fluorescent titrations, plotting the maxima of emission in relation to the amount of metal ion added (Figure 2. 12 e and f).

$$\frac{F}{F(0)} = 1 + \left(\frac{F(max)}{2F(0)} - 0.5\right) \times \left(1 + \frac{CM}{CL} + \frac{Kd}{CL} - \left[\left(1 + \frac{CM}{CL} + \frac{Kd}{CL}\right)^2 - \frac{4CM}{CL}\right]^{0.5}\right)$$

Equation 2.1 Equation used to determine K_d value for rotaxanes, where CM and CL concentrations of Zn^{2+} and rotaxane respectively, F is the observed absorbance, F(0) is the observed absorbance of the rotaxane alone (i.e. CM = 0). Non-linear regression analysis was used to determine F(max)/F(0) and K_d.

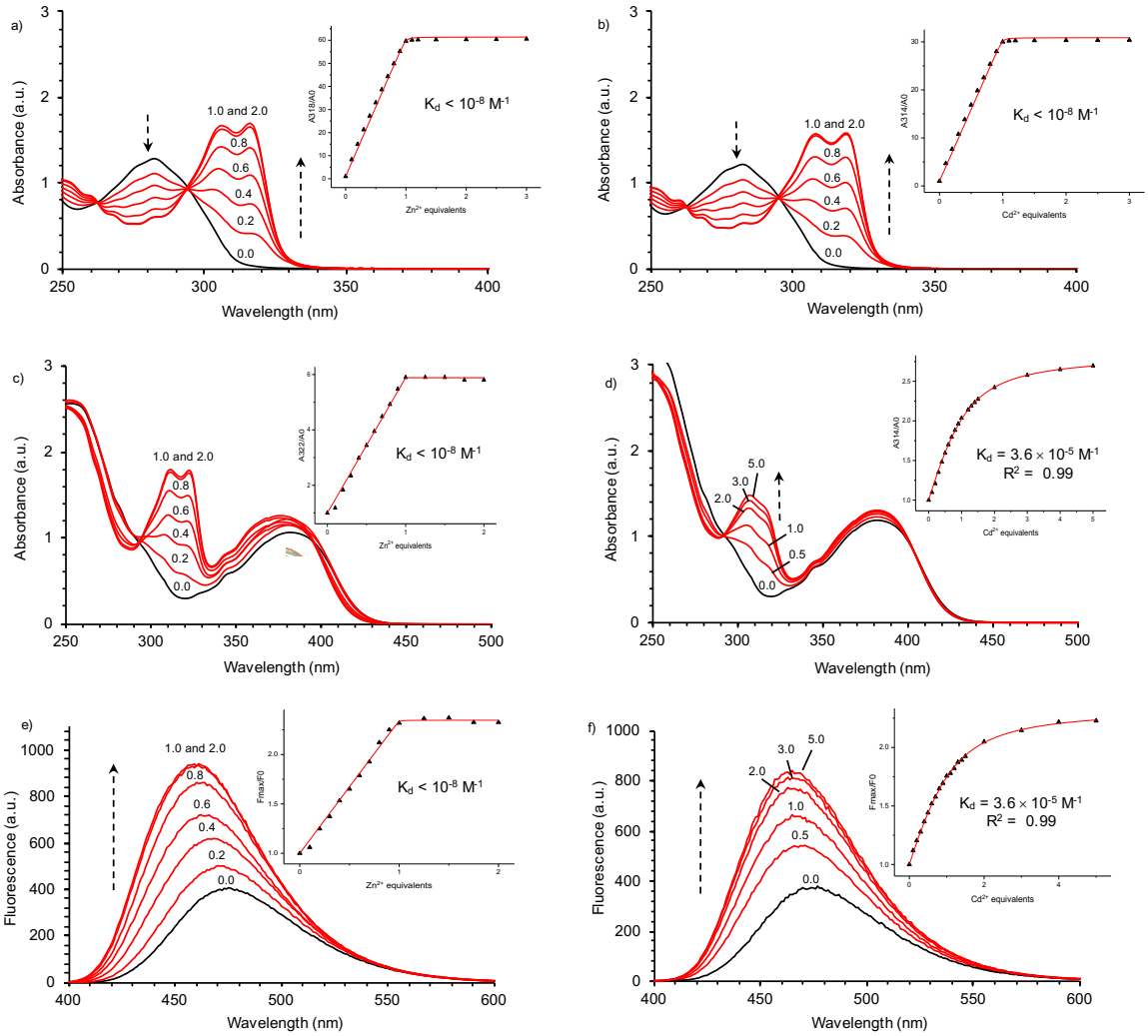

Figure 2. 12 UV-visible titrations (MeCN, C = 100 μM) of a) **78** with $Zn(ClO_4)_2.6H_2O$, b) **78** with $Cd(ClO_4)_2.6H_2O$, c) a) **83** with $Zn(ClO_4)_2.6H_2O$, b) **83** with $Cd(ClO_4)_2.6H_2O$, and fluorescence titrations (MeCN, C = 100 μM). of **83** with e) $Zn(ClO_4)_2.6H_2O$ and f) $Cd(ClO_4)_2.6H_2O$.

The difference in binding affinity of **83** for Zn^{2+} and Cd^{2+} was also corroborated by ^{1}H NMR spectroscopy analysis. After addition of one equivalent of each metal cation to a sample of **83** in CD_3CN, only the signals of $[Zn(\mathbf{83})]^{2+}$ were observed (Figure 2. 13); whereas the same experiment performed with macrocycle **78** showed a 4:1 mixture of Zn^{2+} and Cd^{2+} complexes (Figure 2. 14). These results demonstrated that the mechanical bond has an impact on the degree of selectivity on the binding of metal ions of similar nature. This could be attributed to difference in sizes of Zn^{2+} and Cd^{2+} (with respective ionic radii of 88 and 109 pm), or to the exclusion of additional ligands from the coordination sphere of the metal ion for steric reasons.

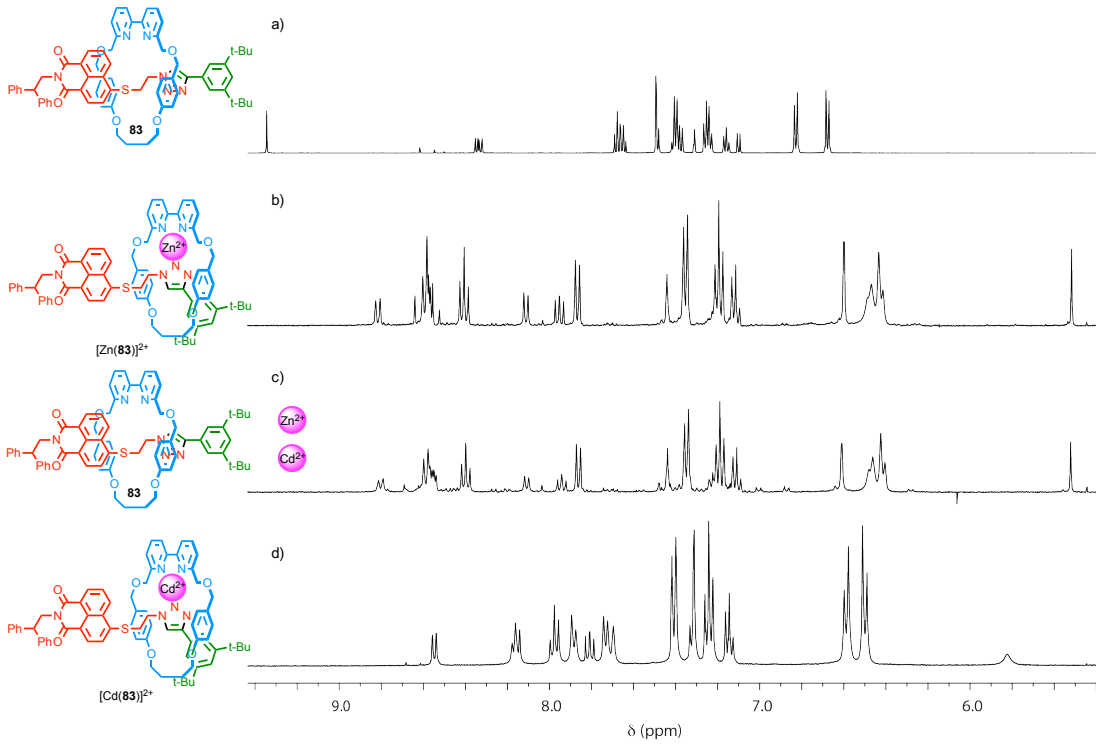

Figure 2. 13 Partial ^{1}H NMR stack plot (CD_3CN, 400 MHz, 298 K) of a) rotaxane **83**, b) [Zn(**83**)]$^{2+}$ complex, c) **83** in the presence of Zn^{2+} and Cd^{2+} (1 equiv. of each) and d) [Cd(**83**)]$^{2+}$.

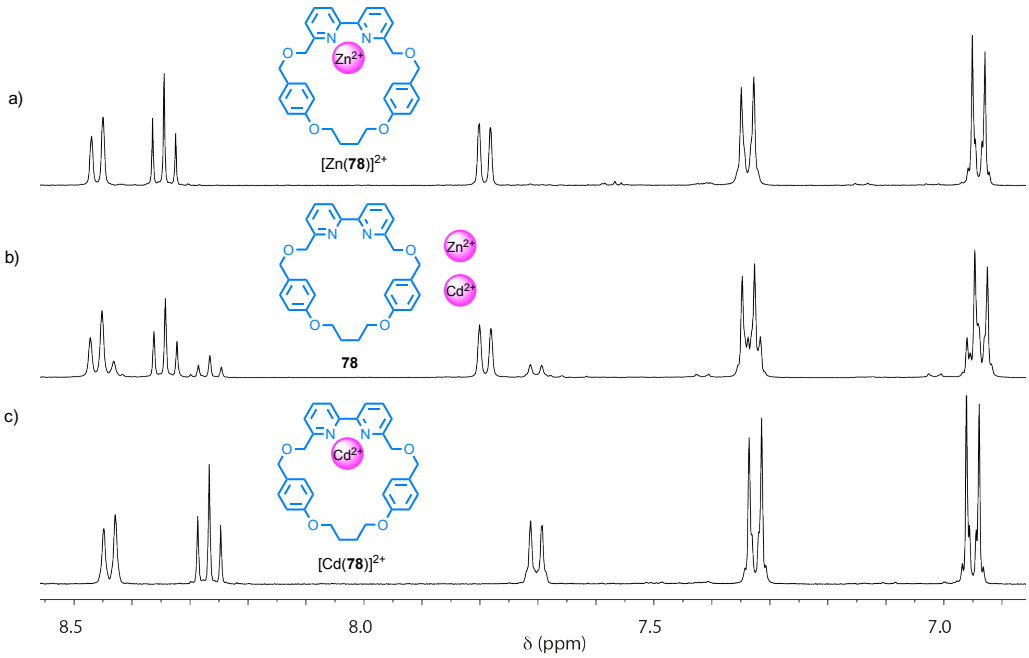

Figure 2. 14 Partial ^{1}H NMR stack plot (CD_3CN, 400 MHz, 298 K) of a) [Zn(**78**)]$^{2+}$ complex, b) **78** in the presence of Zn^{2+} and Cd^{2+} (1 equiv. of each) and c) [Cd(**78**)]$^{2+}$.

The strong binding observed for Zn^{2+} with rotaxane **83** convinced us to investigate the possibility of imparting selectivity using a more competitive solvent mixture. Therefore, UV-vis and fluorescence titrations were performed in a MeCN/H_2O (98:2) mix and similarly to the previous case, the data were fitted with non-linear regression analysis using both the

bipyridine absorption band and the maxima of emission. It appeared that the binding of both Zn^{2+} and Cd^{2+} was diminished in this new solvent mixture with dissociation constants of $K_d = 7.8 \times 10^{-5}$ and 1.8×10^{-3} M^{-1}, respectively (Figure 2. 15 c and d). Thus, whereas 1 equiv. of Zn^{2+} achieved 50% of Fmax and saturation occurred at ~12 equiv.; 20 equiv. were needed in the case of Cd^{2+} for a similar output of 50% and saturation could not be reached even in the presence of 100 equiv. of the metal ion (Figure 2. 15 e and f). Interestingly, macrocycle **78** still exhibits strong binding for both Zn^{2+} and Cd^{2+} under similar conditions ($K_d < 10^{-8}$, Figure 2. 15 a and b).

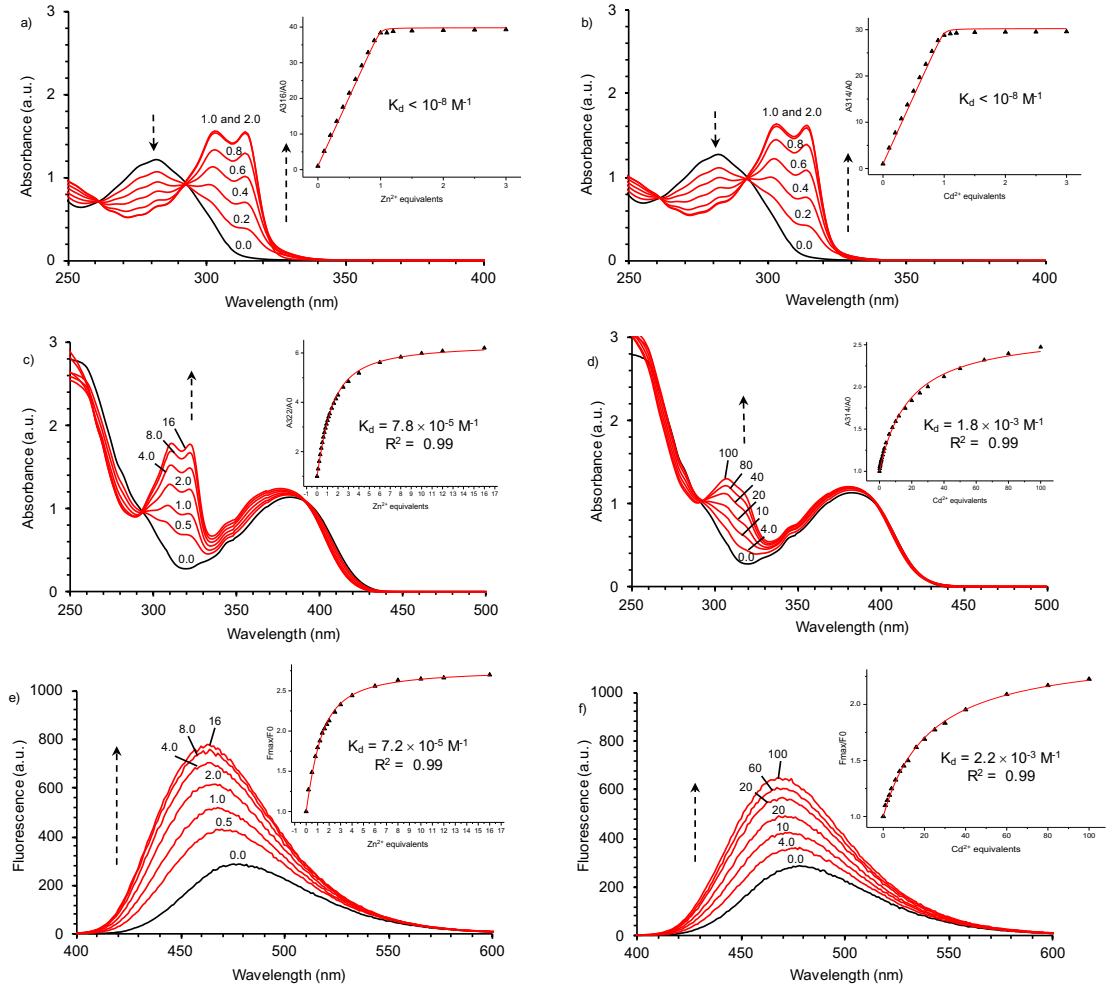

Figure 2. 15 UV-visible titrations of a) **78** with $Zn(ClO_4)_2.6H_2O$, b) **78** with $Cd(ClO_4)_2.6H_2O$, c) a) **83** with $Zn(ClO_4)_2.6H_2O$, b) **83** with $Cd(ClO_4)_2.6H_2O$, and fluorescence titrations of **83** with e) $Zn(ClO_4)_2.6H_2O$ and f) $Cd(ClO_4)_2.6H_2O$. ($MeCN/H_2O$ 98:2, 100 μM).

2.3. Conclusion and Future Work

We have demonstrated that small functional rotaxanes provided excellent scaffold for the design of metal ion sensors. Moreover, we have shown that the binding cavity provided by the mechanical bond determine not only the optical response but also the binding selectivity. Indeed, apart from **83** that demonstrated the desired selectivity for Zn^{2+} in MeCN/H_2O media, rotaxane **82** also appears to show a selective response (V^{2+} and Cd^{2+}).

Although **83** retains its selectivity in the presence of other divalent metal cations, it is still worth noticing that Cu^{2+}, V^{2+} and Ni^{2+} quench the fluorescence in a non-recoverable manner. However mechanically interlocked ligands possess a unique scaffold allowing for the tuning and functionalization of the cavity without affecting the binding site itself. Ultimately, this feature allows for the fine tuning of the optical and binding properties to perfect the system. For example, improving the selectivity or having an emission in a lower energy domain, which is more desirable than those in the UV-range in terms of biological applications are two aims to look for.

The mode of switching in the case of rotaxane **83** appeared to be reorientation of the interlocked components upon metal binding, which impact the relative positions of the macrocycle and the naphthalimide units. Nevertheless, given the scope of fluorescence outputs (i.e. enhancement, quenching and no effect) for various metal using the same probe, we cannot affirm it with certainty; more detailed computational studies would be needed in that regard in order to gather more information about the relative orbital energies and the processes controlling the fluorescent output.

This worked demonstrated promising results toward the use of the mechanical bond as a structural feature for the development mechanically chelating ligand capable of selective recognition of analytes of interest.

2.4. Experimental

General Experimental

Unless otherwise stated, all reagents and anhydrous solvents were purchased from commercial sources and used without further purification. All reactions were carried out under an atmosphere of N_2 using anhydrous solvents unless otherwise stated. Petrol refers to the fraction of petroleum ether boiling in the range 40-60 °C. DIPEA refers to N,N-diisopropylethylamine. NH_3-EDTA solution refers to an aqueous solution of NH_3 (17% w/w) with sodium-ethylenediaminetetraacetate (0.1 M). Flash column chromatography was performed using Biotage Isolera-4 automated chromatography system, employing Biotage SNAP or ZIP cartridges. Analytical TLC was performed on precoated silica gel plates (0.25 mm thick, 60F254, Merck, Germany) and observed under UV light. NMR spectra were recorded on Bruker AV400, AV3-400, AV500 or Bruker AV600 instrument, at a constant temperature of 298 K. Chemical shifts are reported in parts per million from low to high field and referenced to residual solvent. Coupling constants are reported in Hertz. Standard abbreviations indicating multiplicity were used as follows: m = multiplet, quint = quintet, q = quartet, t = triplet, d = doublet, s = singlet, app. = apparent, br = broad. Signal assignment was carried out using 2D NMR methods (HSQC, HMBC, COSY, NOESY) where necessary. In the case of some complex multiplets with contributions from more than one signal, absolute assignment was not possible, hence indicative assignments (e.g., H_A or H_B) are provided. All melting points were determined using a Griffin apparatus and are uncorrected. Low resolution mass spectrometry was carried out either by the mass spectrometry services at the Queen Mary University of London using an Agilent SL Ion Trap MSD instrument or at the University of Southampton using a Waters TQD mass spectrometer equipped with a triple quadrupole analyser with UHPLC injection (BEH C18 column, acetonitrile/hexane gradient with 0.2% formic acid). High resolution mass spectrometry (HRMS) was carried out either by the EPSRC National Mass Spectrometry in Swansea or by the mass spectrometry services at the University of Southampton with samples were analysed using a MaXis (Bruker Daltonics) with a Time of Flight (TOF) analyser; samples were introduced into the mass spectrometer via a Dionex Ultimate 3000 autosampler and a UHPLC pump using a 20-100% acetonitrile/hexane gradient with 0.2% formic acid over 5 min at 0.6 mL/min (column: Acquity UPLC BEH C18 (Waters) 1.7 μm 50 × 2.1 mm).

Macrocycle **78** was provided by members of the group. Alcohol **84** was synthesised by Dr Jessica Pancholi during her PhD**.** Ethynyl-3,5-di-*tert*-butylbenzene **88** was synthesised according to literature procedure.[24]

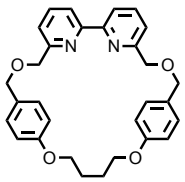

78

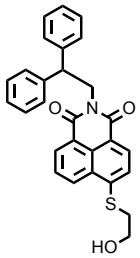

84

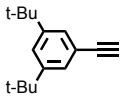

88

Experimental Data

*Compound (**85**)*

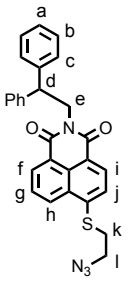

85

Alcohol **84** (130 mg, 0.3 mmol, 1 equiv.) and triphenylphosphine (220 g, 0.8 mmol, 3 equiv.) were combined in a sealed. THF (12 mL) was added, and the stirring solution was cooled to 0 °C. DEAD (0.13 mL, 0.8 mmol, 3 equiv.) was added to the reaction, followed by diphenyl phosphoryl azide (0.19 mL, 0.8 mmol, 3 equiv.), and stirred for 15 min. The reaction was then stirred at r.t. for 2 h, and then concentrated *in vacuo*. The resulting oil was purified by flash column chromatography, Petrol/CH_2Cl_2 1:1 to CH_2Cl_2 to CH_2Cl_2/EtOAc 8:2 to give azide **85** as an orange foam (0.095 g, 72%). ^{1}H NMR (400 MHz, $CDCl_3$, 298 K) δ 8.57-8.49 (m, 2H, H_f and H_h), 8.39 (d, *J* = 7.8, 1H, H_i), 7.71 (dd, *J* = 7.5, 8.2, 1H, H_g), 7.57 (d, *J* = 7.8, 1H, H_j), 7.40-7.31 (m, 4H, H_c), 7.27-7.18 (m, 4H, H_b), 7.16-7.10 (m, 2H, H_a), 4.85-4.80 (m, 3H, H_d and H_e), 3.58 (t, *J* = 6.7, 2H, H_l), 3.30 (t, *J* = 6.7, 2H, H_k).^{13}C NMR (101 MHz, $CDCl_3$) δ 163.9, 163.9, 142.6, 141.8, 131.8, 130.7, 130.3, 130.1, 129.8, 129.7, 128.6, 128.5, 127.1, 126.7, 124.7, 124.5, 123.1, 120.4, 120.3, 120.2, 49.8, 48.8, 44.6, 32.3. HRMS (ESI+) m/z = 501.1358 $[M+Na]^+$ (calc. for $C_{28}H_{22}N_4O_2SNa$ 501.1356). UV: λ_{max}(MeCN)/nm (ε / $mol^{-1}cm^{-1}dm^3$) 381 (6093).

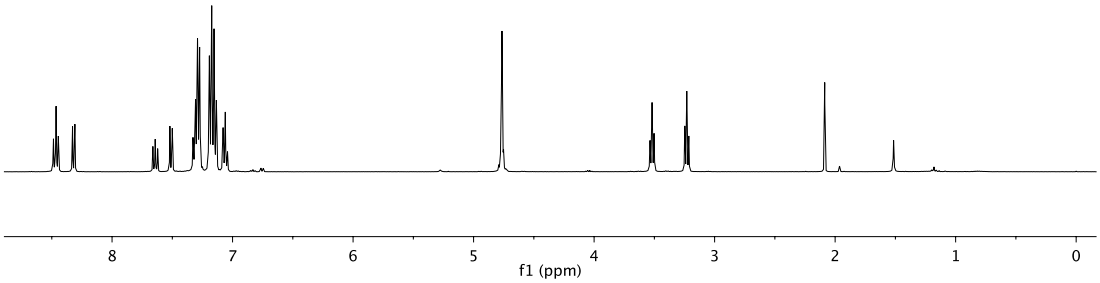

Figure S2. 1 ^{1}H NMR (400 MHz, $CDCl_3$, 298 K) of **85**.

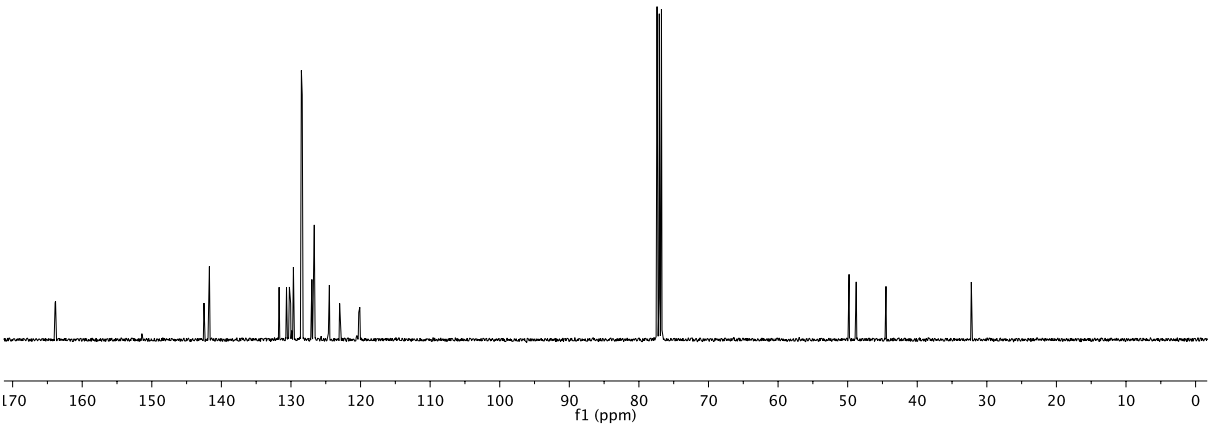

Figure S2. 2 ^{13}C NMR (101 MHz, $CDCl_3$, 298 K) of **85**.

*Rotaxane (**83**)*

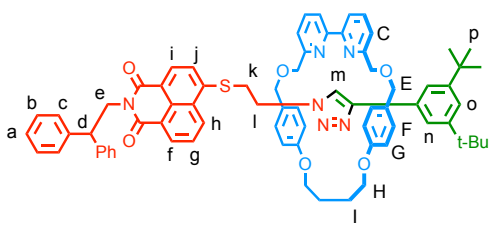

83

A dry CEM MW vial was charged with macrocycle **78** (25 mg, 0.05 mmol, 1 equiv.), azide **85** (25 mg, 0.05 mmol, 1 equiv.), alkyne **88** (11 mg, 0.05 mmol, 1 equiv.), and $[Cu(MeCN)_4]PF_6$ (18.6 mg, 0.049 mmol, 0.96 equiv.). CH_2Cl_2 (2.5 mL) was added, followed by DIPEA (9 µL, 0.05 mmol, 1 equiv.) and the reaction mixture stirred at r.t. for 16 h. NH_3-EDTA (5 mL) was added and the crude extracted with CH_2Cl_2 (3 x 5 mL). The combined organic layers were dried ($MgSO_4$) and concentrated *in vacuo* pressure. The crude was purified *via* flash column chromatography on silica gel using a linear gradient of MeCN (0 – 10%) in a mixture of petrol/CH_2Cl_2 1:1, affording product as a pale yellow foam (51 mg, 83%).^{1}H NMR ($CDCl_3$, 400 MHz, 298 K) δ 9.41 (s, 1H, H_m), 8.43 (d, *J* = 7.2, 1H, H_f), 8.33 (d, *J* = 8.3, 1H, H_h), 7.76 (d, *J* = 7.8, 1H, H_i), 7.67-7.61 (m, 3H, H_g and H_B), 7.61-7.59 (m, 2H, $H_{C,\ A}$), 7.47-7.42 (m, 4H, H_n and two of $H_{C,\ A}$), 7.41-7.37 (m, 4H, H_c), 7.27 (t, *J* = 1.6, 1H, H_o), 7.27-7.22 (m, 4H, H_b), 7.17-7.11 (m, 2H, H_a), 6.90 (d, *J* = 7.8, 1H, H_j), 6.82 (d, *J* = 8.5, 4H, H_F), 6.71 (d, *J* = 8.5, 4H, H_G), 4.87-4.83 (m, 3H, H_d and H_e), 4.62 (d, *J* = 11.8, 2H, H_E), 4.58-4.50 (m, 2H, H_H), 4.21 (d, *J* = 11.8, 2H, H_E), 4.14-4.07 (m, 2H, H_H), 4.09 (d, *J* = 12.2, 2H, two of H_D), 4.01 (d, *J* = 12.2, 2H, two of H_D), 3.18-3.12 (m, 2H, H_l), 2.38-2.23 (m, 2H, H_k), 2.30-2.19 (m, 2H, H_l), 2.06-1.94 (m, 2H, H_l), 1.85 (s, 18H, H_p).^{13}C NMR ($CDCl_3$, 101 MHz, 298 K) δ 164.0, 163.8, 159.0, 158.7, 155.6, 151.1, 147.5, 142.7, 141.7, 137.4, 131.3, 130.6, 130.5, 129.7, 129.5, 128.8, 128.5, 128.4, 127.9, 126.6, 126.5, 125.3, 125.3, 125.2, 122.8, 122.6, 121.7, 121.6, 120.7, 120.1, 120.0, 120.0, 119.8, 119.2, 114.9, 72.9, 70.8, 66.4, 48.8, 47.5, 44.4, 34.8, 31.5, 31.3, 29.4, 24.7. HRMS (ESI+) m/z = 1175.5479 $[M+H]^+$ (calc. for $C_{74}H_{73}N_6O_6S$ 1175.5463). UV: λ_{max}(MeCN)/nm (ε / $mol^{-1}cm^{-1}dm^3$) 381 (10674).

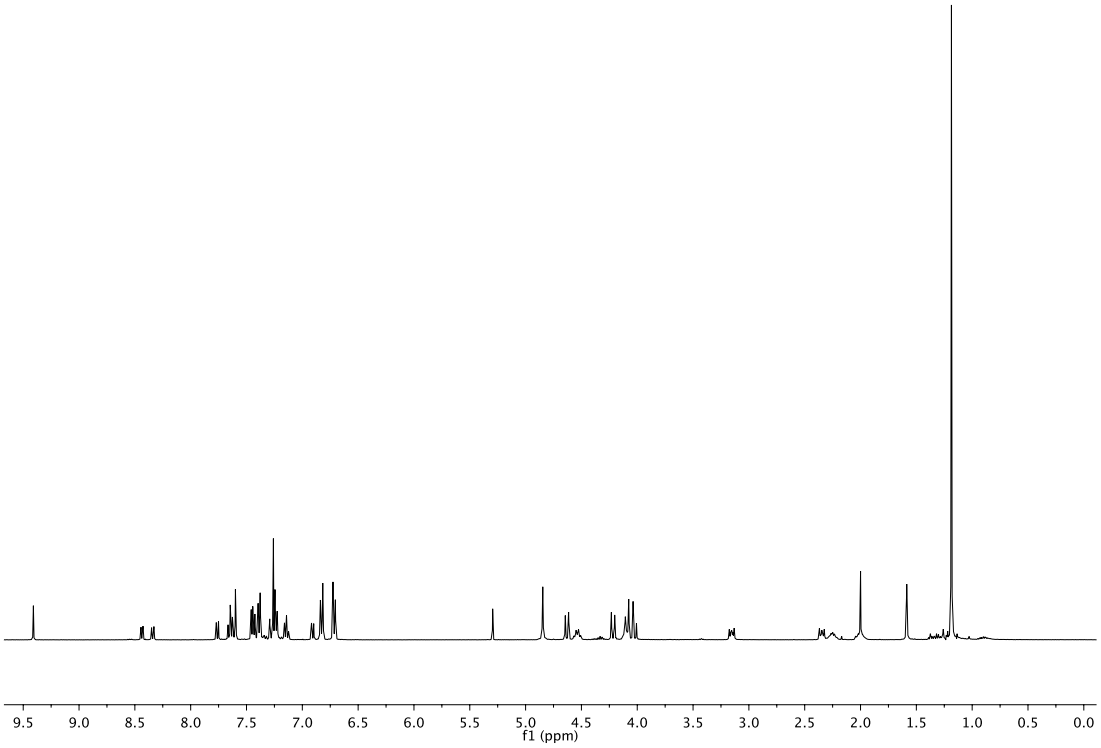

Figure S2. 3 ^{1}H NMR (400 MHz, $CDCl_3$, 298 K) of **83**.

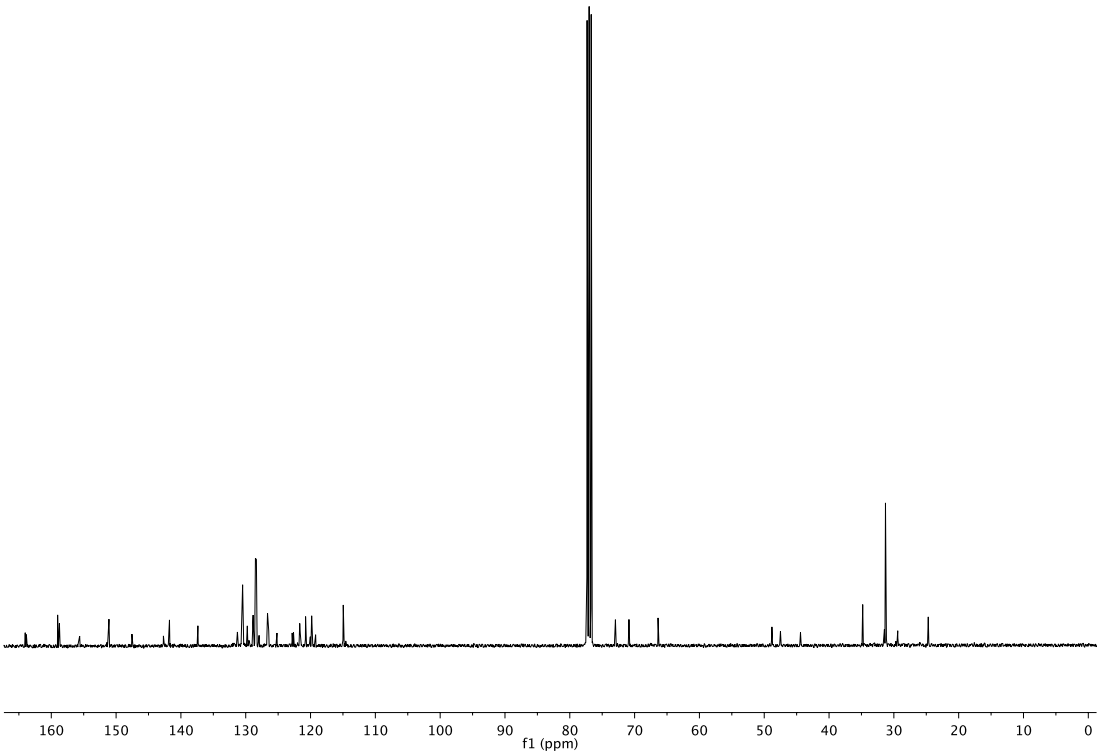

Figure S2. 4 ^{13}C NMR (101 MHz, $CDCl_3$, 298 K) of **83**.

UV-vis / Fluorescence titrations

Procedure: A 100 μM stock solution of the receptor was accurately prepared in the solvent of interest for the study using a volumetric flask. Solutions of metals with 100 μM of receptors to be titrated were prepared in separate 2.5 mL vials, and 1000 µL of the receptor solution were added using pipette (Eppendorf). The concentration of metal in the guest solutions was made 50 times that of the host (i.e. 5 mM). After each addition, the resulting solution was shaken vigorously and the absorbance/emission were recorded. UV-Vis data was recorded using a Varian Cary 4000 UV-Vis Spectrophotometer. Fluorescence titrations were carried out in parallel to the UV/Vis absorption measurements using a Cary Eclipse Fluorescence Spectrometer. Temperature control was provided by a Varian Cary PCB 150 Water Peltier System. The absorbance was recorded from 200 nm to 800 nm. Titrations were performed in triplicate to give K_d values. To determine association constants for the receptor-metal complexes, global analysis of the absorbance/emission data was carried out using a nonlinear least-squares curve fitting procedure with Origin 2016 software using the 1:1 global fitting model equation:

$$\frac{F}{F(0)} = 1 + \left(\frac{F(max)}{2F(0)} - 0.5\right) \times \left(1 + \frac{CM}{CL} + \frac{Kd}{CL} - \left[\left(1 + \frac{CM}{CL} + \frac{Kd}{CL}\right)^2 - \frac{4CM}{CL}\right]^{0.5}\right)$$

Equation 2.1 Equation used to determine K_d value for rotaxanes, where CM and CL concentrations of Zn^{2+} and rotaxane respectively, F is the observed absorbance, F(0) is the observed absorbance of the rotaxane alone (i.e. CM = 0). Non-linear regression analysis was used to determine F(max)/F(0) and K_d.

X-ray Data

For both **83** and [Zn(**83**)]$^{2+}$, crystals were grown by slow evaporation of MeCN solution. Data were collected at 100 K using a Rigaku 007 HF diffractometer equipped with a Saturn 944+ enhanced sensitivity detector. Cell determination and data collection were done using CrystalClear-SM Expert 3.1; data reduction, cell refinement and absorption correction were performed with CrysalisPro. The structure was solved using SUPERFLIP and refined against F_2 using anisotropic thermal displacement parameters for all non-hydrogen atoms using WINGX and software packages within. Hydrogen atoms were placed in calculated positions and refined using a riding model.

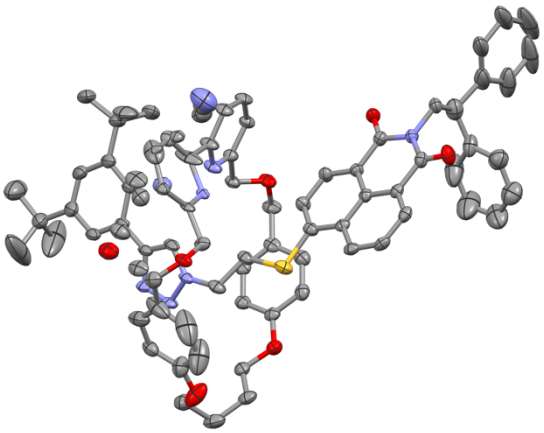

Figure S2. 5 Ellipsoid plot of rotaxane **83**. Ellipsoid are shown at 50% probability. Hydrogens were omitted for clarity.

Table S2. 1 Crystal data and structure refinement for cu_jp4_srot_2.

Identification code	cu_jp4_srot_2
Empirical formula	$C_{76}H_{77}N_7O_6S$
Formula weight	1216.50
Temperature/K	293(2)
Crystal system	monoclinic
Space group	$P2_1/c$
a/Å	10.4843(2)
b/Å	16.0918(4)
c/Å	40.1750(10)
α/°	90
β/°	90.865(2)
γ/°	90
Volume/Å^3	6777.2(3)
Z	4
ρ_{calc}g/cm^3	1.192
μ/mm^{-1}	0.879
F(000)	2584.0
Crystal size/mm^3	0.300 × 0.100 × 0.090
Radiation	CuKα (λ = 1.54184)
2Θ range for data collection/°	7.038 to 117.868
Index ranges	-11 ≤ h ≤ 11, -17 ≤ k ≤ 17, -44 ≤ l ≤ 34
Reflections collected	38747
Independent reflections	9659 [R_{int} = 0.0482, R_{sigma} = 0.0307]
Data/restraints/parameters	9659/24/890
Goodness-of-fit on F^2	1.062
Final R indexes [I>=2σ (I)]	R_1 = 0.0889, wR_2 = 0.2409
Final R indexes [all data]	R_1 = 0.1030, wR_2 = 0.2547
Largest diff. peak/hole / e Å^{-3}	1.56/-0.58

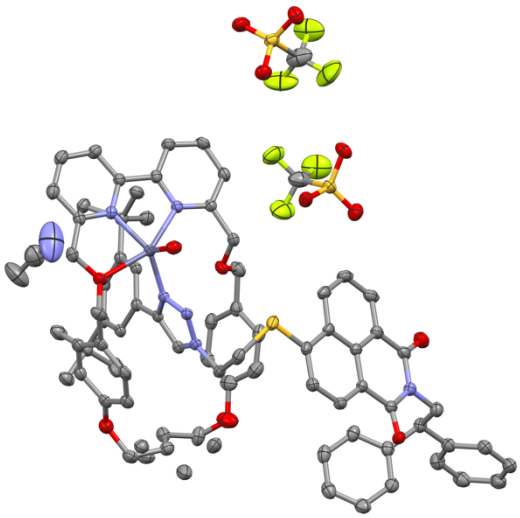

Figure S2. 6 Ellipsoid plot of rotaxane [Zn(**83**)](OTf)$_2$. Ellipsoid are shown at 50% probability. Hydrogens were omitted for clarity.

Table S2. 2 Crystal data and structure refinement for 2016md_III_095_100K.

Identification code	2016md_III_095_100K
Empirical formula	$C_{78}H_{79}F_6N_7O_{13}S_3Zn$
Formula weight	1598.03
Temperature/K	100(2)
Crystal system	triclinic
Space group	P-1
a/Å	15.1517(4)
b/Å	16.8905(4)
c/Å	17.4286(4)
α/°	111.628(2)
β/°	95.9721(19)
γ/°	111.463(2)
Volume/Å^3	3708.71(17)
Z	2
ρ_{calc}g/cm^3	1.431
μ/mm^{-1}	0.500
F(000)	1664.0
Crystal size/mm^3	0.100 × 0.060 × 0.050
Radiation	MoKα (λ = 0.71073)
2Θ range for data collection/°	3.006 to 64.312
Index ranges	-22 ≤ h ≤ 21, -25 ≤ k ≤ 25, -26 ≤ l ≤ 24
Reflections collected	94990
Independent reflections	24283 [R_{int} = 0.0572, R_{sigma} = 0.0631]
Data/restraints/parameters	24283/0/1017
Goodness-of-fit on F^2	1.015
Final R indexes [I>=2σ (I)]	R_1 = 0.0644, wR_2 = 0.1609
Final R indexes [all data]	R_1 = 0.1113, wR_2 = 0.1898
Largest diff. peak/hole / e Å^{-3}	1.60/-0.94

2.5. Bibliography

[1] J. Chan, S. C. Dodani, C. J. Chang, *Nature Chem.* **2012**, *4*, 973–984.

[2] K. P. Carter, A. M. Young, A. E. Palmer, *Chem. Rev.* **2014**, *114*, 4564–4601.

[3] Y. Pak, K. Swamy, J. Yoon, *Sensors* **2015**, *15*, 24374–24396.

[4] X. Qian, Z. Xu, *Chem. Soc. Rev.* **2015**, *44*, 4487–4493.

[5] J. Li, D. Yim, W.-D. Jang, J. Yoon, *Chem. Soc. Rev.* **2017**, *46*, 2437–2458.

[6] S. J. Rowan, J. F. Stoddart, *J. Am. Chem. Soc.* **2000**, *122*, 164–165.

[7] M. J. Langton, P. D. Beer, *Acc. Chem. Res.* **2014**, *47*, 1935–1949.

[8] S. Erbas-Cakmak, D. A. Leigh, C. T. McTernan, A. L. Nussbaumer, *Chem. Rev.* **2015**, *115*, 10081–10206.

[9] G. Baggi, S. J. Loeb, *Angew. Chem. Int. Ed.* **2016**, *55*, 12533–12537.

[10] S. S. Zhu, T. M. Swager, *J. Am. Chem. Soc.* **1997**, *119*, 12568–12577.

[11] K. Hiratani, M. Kaneyama, Y. Nagawa, E. Koyama, M. Kanesato, *J. Am. Chem. Soc.* **2004**, *126*, 13568–13569.

[12] Y. Nagawa, J. Suga, K. Hiratani, E. Koyama, M. Kanesato, *Chem. Commun.* **2005**, *3*, 749.

[13] N.-C. Chen, P.-Y. Huang, C.-C. Lai, Y.-H. Liu, Y. Wang, S.-M. Peng, S.-H. Chiu, *Chem. Commun.* **2007**, 4122.

[14] W. Zhou, J. Li, X. He, C. Li, J. Lv, Y. Li, S. Wang, H. Liu, D. Zhu, *Chem. Eur. J.* **2008**, *14*, 754–763.

[15] Y. Nakatani, Y. Furusho, E. Yashima, *Angew. Chem. Int. Ed.* **2010**, *49*, 5463–5467.

[16] S.-Y. Hsueh, C.-C. Lai, S.-H. Chiu, *Chem. Eur. J.* **2010**, *16*, 2997–3000.

[17] J. M. Baumes, I. Murgu, R. D. Connell, W. J. Culligan, A. G. Oliver, B. D. Smith, *Supramol. Chem.* **2012**, *24*, 14–22.

[18] J. Pancholi, D. J. Hodson, K. Jobe, G. A. Rutter, S. M. Goldup, M. Watkinson, *Chem. Sci.* **2014**, *5*, 3528–3535.

[19] K. J. Barnham, A. I. Bush, *Curr. Opin. Chem. Biol.* **2008**, *12*, 222–228.

[20] G. A. Rutter, *Islets* **2010**, *2*, 49–50.

[21] I. Lengyel, J. M. Flinn, T. Pető, D. H. Linkous, K. Cano, A. C. Bird, A. Lanzirotti, C. J. Frederickson, F. J. G. M. van Kuijk, *Exp. Eye Res.* **2007**, *84*, 772–780.

[22] H. Lahlali, K. Jobe, M. Watkinson, S. M. Goldup, *Angew. Chem. Int. Ed.* **2011**, *50*, 4151–4155.

[23] P. Thordarson, *Chem. Soc. Rev.* **2011**, *40*, 1305–1323.

[24] R. S. Stoll, M. V Peters, A. Kuhn, S. Heiles, R. Goddard, M. Bühl, C. M. Thiele, S. Hecht, *J. Am. Chem. Soc.* **2009**, *131*, 357–367.

Chapter 3: <<A Fluorescent Ditopic Rotaxane Ion Pair Host>>

Abstract: This chapter presents on the synthesis and study of a simple urea-based rotaxane that binds ion pairs (H^+X^-) and reports the binding event through a fluorescent switch on response. Interestingly, the response was the opposite for the axle on its own, which experience a quenching of the emission upon binding of anions. Moreover, the interlocked system appears to bind Cl^- selectively over more basic anions, another feature that differentiates it from its non-interlocked counterpart. Using x-ray crystallography techniques as well as fluorescence, NMR and UV-Vis spectroscopy analyses, we gathered evidence suggesting that the mechanical bond could explain the switch on response observed with the rotaxane and also imparts size selectivity which alter the relative binding constants of larger anions compared with the non-interlocked axle.

Acknowledgements: I would like to thank Mr Lei Qin and Prof Katrina Jolliffe for the expertise they provided in the anion binding study and for hosting me at the University of Sydney in November 2016.

I would like to thank the members of the Goldup Group for providing compound **104**.

I would like to thank the Royal Society for the funding.

Prior publication: None of this work has been previously published.

3.1. Introduction

Anion recognition has been a field of study of great interest for a few decades now due to the fundamental role negatively charged species play in biological, chemical, industrial and environmental processes.[1–3] Fluoride anions for example, although known for the positive role in dental health (e.g., fluoride containing toothpaste), can lead to detrimental effect such as debilitating skeletal defects and kidney failure under overexposure (warfare agent).[4] A number of excellent reviews cover the field of anion sensing using small[1,5,6] and macromolecules,[2,7] and how the process is done in Nature.[8,9] Nature's receptors possess a well-defined, three-dimensional cavity optimised and functionalised to accommodate a guest of interest and interact through a plethora of non-covalent interactions (HB, Van der waals, electrostatic…).

As mentioned in the previous chapter, the formation of the mechanical bond creates a three-dimensional space in which a variety of functionalities can be incorporated. For this reason, the field of mechanically interlocked molecule has experienced a growth of interest over the past 10 to 15 years for the development of anion sensors with high selectivity and sensitivity. In these systems, the output signal (redox, photophysic) is modulated upon binding of the negatively charged guest due to translational motions and/or structural rearrangement within the interlocked system, as well as changes in its electronic properties.[10–12]

We cannot talk about anion binding rotaxanes and catenanes without mentioning the work done by Beer and co-workers, pioneers in the field. In 2002, they published the first anion-templated formation of rotaxane in which the orthogonal coordination of a neutral hydrogen-bond (HB) donating isophthalamide receptor and pyridinium cation with chloride anion allowed efficient mechanical bond formation *via* a clipping approach using ring-closing metathesis chemistry (Scheme 3. 1 a).[13] Additional π-stacking and second sphere HB interactions between the cationic axle and neutral acyclic receptor also helped the templation. An interesting feature they quickly noticed with their anion templated interlocked systems is that the interaction between host and guest lives-on in the product. For example, in the case of rotaxane **90**, whereas the thread exhibited stronger binding affinity for AcO^- (K_{11} = 22 000 M^{-1}) the rotaxane was selective for Cl^- over more basic oxoanions by one order of magnitude due to the fact that these bigger guests would not fit in the cavity. Exploiting the feature to its full potential they developed in 2010 a series of rotaxanes based on a pyridinium axle and macrocycle incorporation various HB bond donors.[14] They demonstrated high degree of selectivity for chloride anions in aqueous solvent media (up to 35% water in acetone for rotaxane **91**, Scheme 3. 1 b).

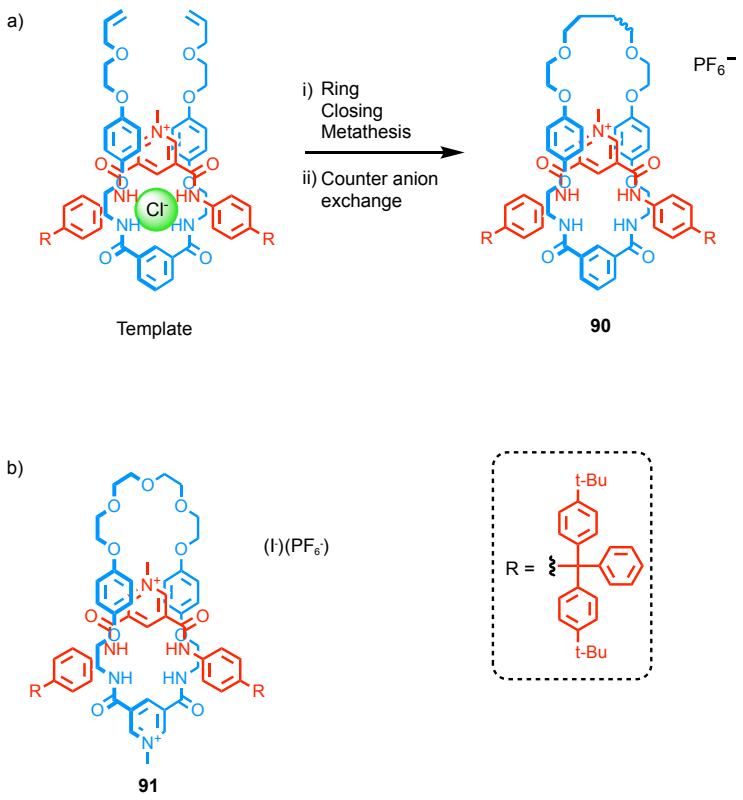

Scheme 3. 1 Examples of rotaxane sensors synthesised by beer and co-workers. a) First chloride-templated synthesis of rotaxane; b) Interlocked receptor **91** with high affinity for chloride in acetone/water 65:35.

In 2011 and they started investigating "higher-order" interlocked structures and published the first [3]rotaxane anion sensor **92** (Scheme 3. 2).[15] The methodology was similar to the previously reported one; chloride templation with subsequent isophthalamide formation in order to 'clip' the two macrocycles around the axle and final counter anion exchange for weakly coordinating PF_6^-. In this rotaxane they incorporated a ferrocene unit within the axle and were able to observe changes in the redox signal of **92** upon binding event (–55 mV in the case of Cl^-). They observed that whereas Cl^- formed a 1:2 complex where the anion sits in each of the interlocked cavities, sulfate displayed a strong 1:1 binding stoichiometry. They tentatively assigned it as resulting from the formation of a sandwich complex where the oxoanion is located in-between the two macrocycles.

In 2012, they made the receptor optically responsive by substituting a naphthalene unit for the ferrocene part (Scheme 3. 2).[16] Addition of Cl^-, Br^- and AcO^- to [3]rotaxane **93** revealed small blue-shift of the fluorescence property with a concomitant slight increase in intensity attributed to increase in rigidity of the system upon binding. In the case of SO_4^{2-} however, a four-fold decrease in the naphthalene emission intensity (λ_{em} = 410 and 432 nm in $CHCl_3$) was reported in the presence of 4 equivalents of the anion followed by an increase peaking at 15% of the initial value after 15 equivalents. The first quenching effect was assigned to the

formation of the sandwich complex resulting in close proximity of the two rings and the anion to the naphthalene moiety. When an excess of SO_4^{2-} was added, changes in conformation occurred in order to accommodate a second guest and the anion is no longer in close proximity to the emissive unit, restoring its optical properties.

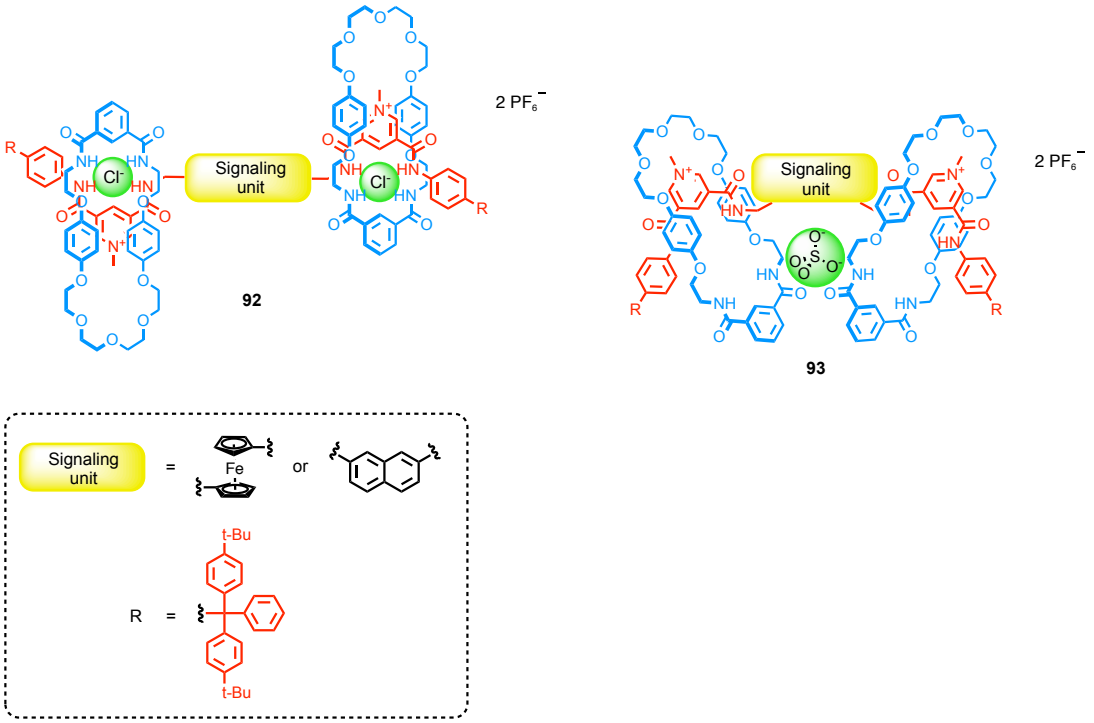

Scheme 3. 2 [3]rotaxanes receptors **92** and **93** by Beer and co-workers.

More recently they published the four-station [3]rotaxane molecular shuttles **94** that selectively recognised nitrate anions.[17] The binding occurred in this case through hydrogen-bond from the isophthalamide units in the macrocycles as well as halogen-bond provided by the bis-iodotriazolium incorporated in the axle. In the absence of coordinating anion, the two rings occupy the peripheral naphthalene diimide (NDI) stations due to charge-transfer interactions between the hydroquinone motifs and electron deficient NDI units. Upon addition of NO_3^- a 1:1 sandwich complex was formed in which the two macrocycles underwent a concerted molecular pincer motion to encapsulate the guest at the centre of the axle where the iodotriazolium stations are located (Scheme 3. 3). The high level of order and complexity of the binding cavity thus created resulted in the preferred binding of NO_3^- over more basic oxoanions (AcO^-, HCO_3^- and $H_2PO_4^-$) and notably Cl^- too, which formed a 1:2 complex. Furthermore, the shuttling of the macrocycle away from the NDI stations let to the disappearance of charge-transfer interactions that can be monitored by UV-vis spectroscopy, giving these systems potential as sensors.

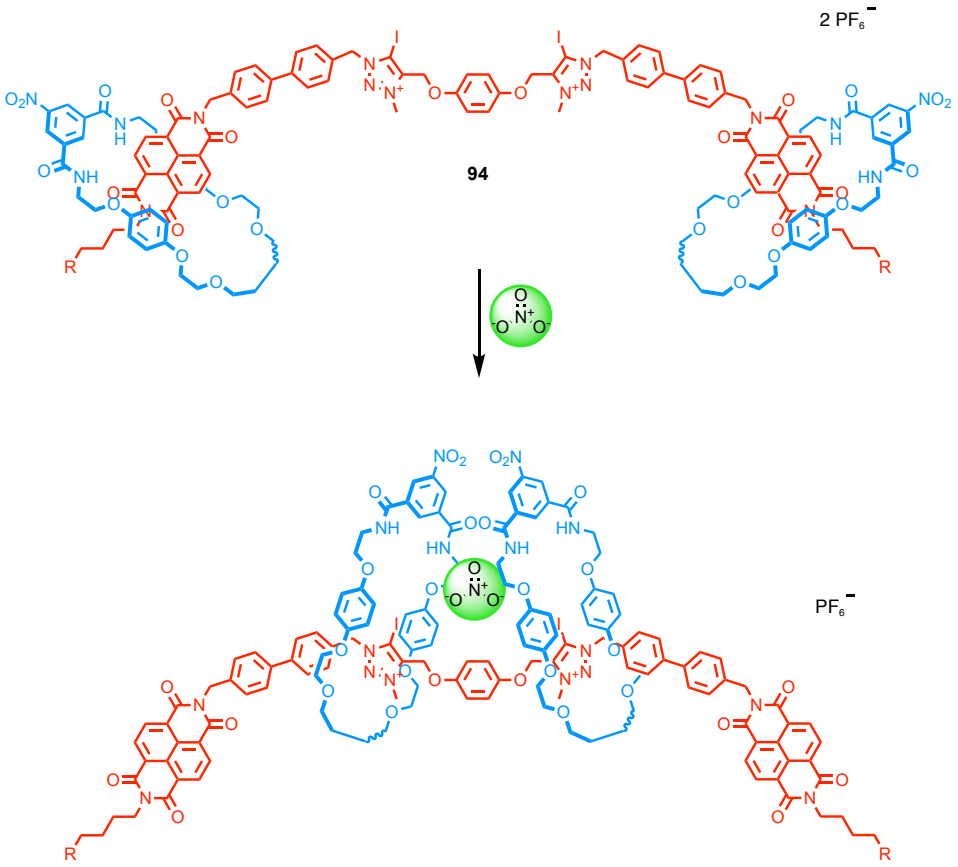

Scheme 3. 3 [3]rotaxane receptor **94** based on both hydrogen and halogen bonding interactions by Beer and co-workers.

Other groups have also shown interest in the development of mechanically interlocked sensors for anions. In 2013, Lin and co-workers synthesised diketopyrrolopyrrole (DPP) stoppered [2]rotaxane **95** incorporating an orthogonal bifurcated pyridine-pyridine hydrogen-bonded motif.[18] The system shown a selective optical response for F^- over other anions tested (Cl^-, Br^-, I^-, AcO-, NO_3^-, $H_2PO_3^-$) in DMSO. The mechanism of recognition proceeded in two cooperative steps. First the establishment of non-covalent interactions between the anion and the 2,6-dicarboxyamidopyridine ring unit, after which further addition of F^- led to deprotonation of the amide cleft (confirmed by ^1H and ^{19}F NMR spectroscopies) and shuttling of the ring toward the DPP unit (Scheme 3. 4). The closer proximity in space resulted in colour changes that were visible to the naked eye of the solution from pink to pale green with a concomitant quenching of the fluorescence.

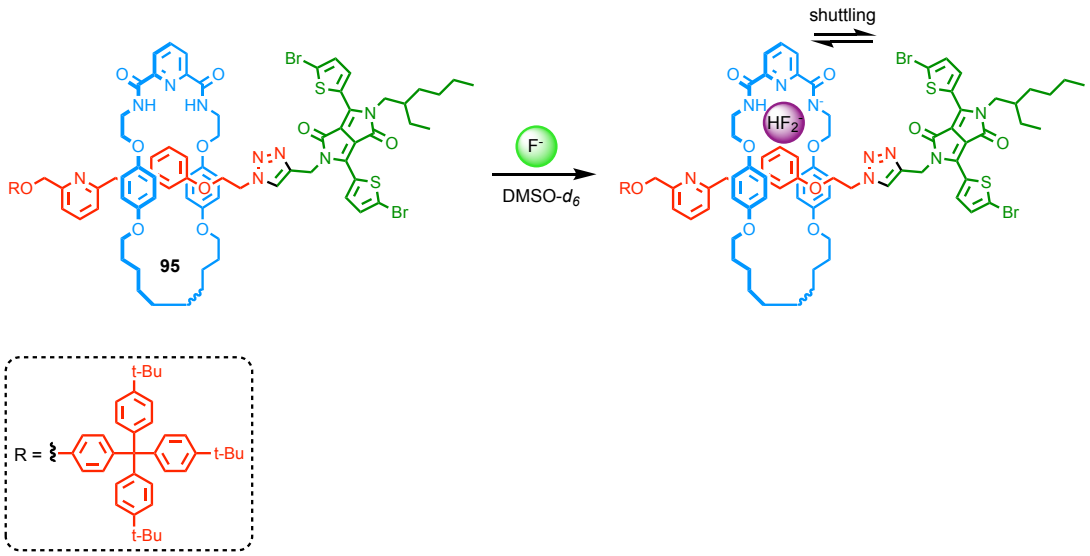

Scheme 3. 4 [2]rotaxane receptor **95** selective for F^- by Lin and co-workers.

The same year, Smith and co-workers reported the synthesis and study of squaraine rotaxane shuttles with deep-red fluorescence and colorimetric response to Cl^-.[19] The design was based on an anthracene containing tetralactam macrocycle and an axle incorporating a dihydroxyl substituted squaraine unit (Scheme 3. 5). Upon addition of chloride anions to a solution of rotaxane **96** in acetone, a colour change was easily distinguishable (from green to blue) due a decrease of the absorption at 663 nm with a concomitant appearance of a new band at 647 nm. The fluorescence was also affected with a decrease of the emission band at 698 nm and appearance of a new one at 665 nm. Those spectroscopic changes were assigned to Cl^- induced small amplitude displacement of the macrocycle away from the squaraine station, but still in close proximity to maintain an efficient energy transfer from the anthracene to the squaraine.

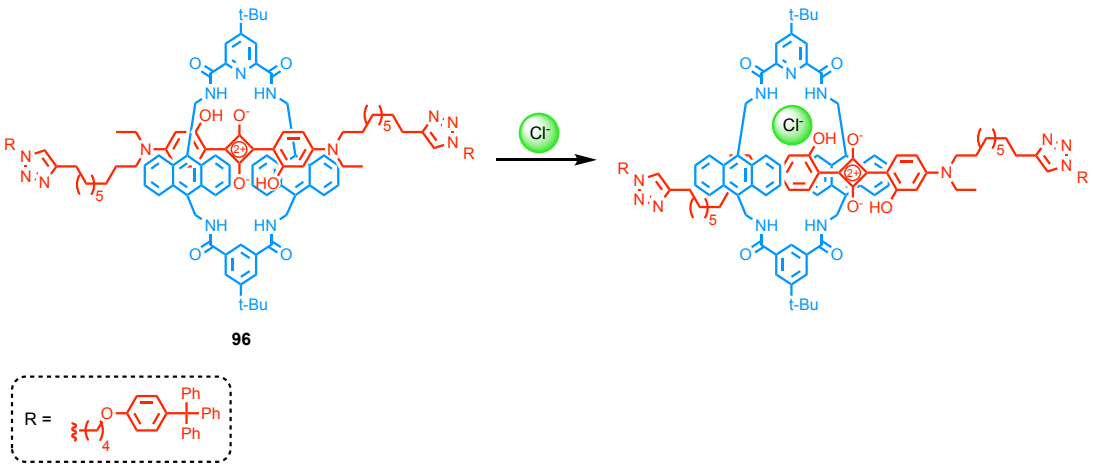

Scheme 3. 5 Squaraine based [2]rotaxane receptor **96** by Smith and co-workers.

Using a similar approach where binding event triggers molecular motion of the ring away from the photoresponsive unit, Berna and co-workers published the hydrogen-bonded [2]rotaxane **97**.[20] The hydrazodicarboxamide unit within the axle act as binding site for a tetralactam macrocycle, bringing the ring in close proximity to the anthracenyl stopper and quenching the fluorescence due to charge-transfer interactions. When benzoate anions were added, an enhancement of the fluorescence was observed in $CHCl_3$; it was assigned to the anion binding to the hydrazodicarboxamide site, consequently shuttling the ring further away from the anthracenyl to the solvophobic alkyl chain of the axle (Scheme 3. 6). It is noteworthy that the resulting enhanced fluorescence of the system (by ~10%) was still weaker than the one of the axle on its own by one order of magnitude, suggesting that the ring is still relatively close to the emissive stopper.

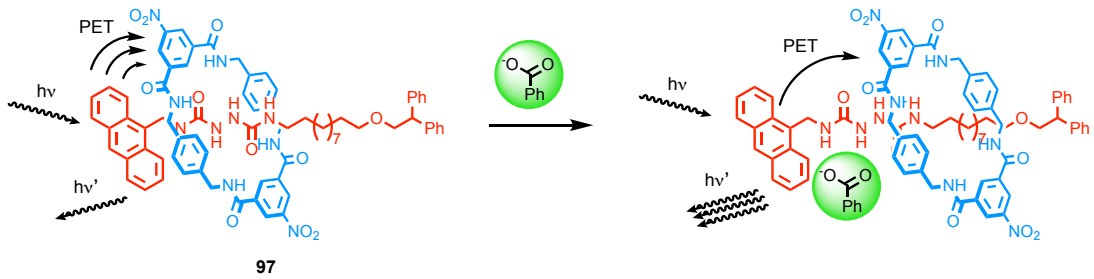

Scheme 3. 6 Fluorescent [2]rotaxane **97** receptor by Berna and co-workers.

Finally, a very recent example, slightly different that the previous ones discussed, was presented by Ballester and co-workers. They synthesised [2]rotaxane **98** *via* "capping" approach of a pseudorotaxane using click chemistry and demonstrated that the mechanically interlocked system acted as a heteroditopic receptor for ion pair (Scheme 3. 7).[21] Indeed, upon addition of tetraalkylammonium salts of Cl^-, NO_3^- and NCO^- they observed by ^1H NMR spectroscopy the formation of 1:1 complex where the anion is included inside the polar cavity where hydrogen bond interactions with various NH from both the axle and the ring occurred. In contrast, the cation sat in the electron-rich and shallow aromatic cavity defined by the calix[4]pyrrole core. Furthermore, they demonstrated that changing of the cation from tetrabutylammonium (TBA) to methyl trioctylammonium (MTOA), known to fit better within the pyrrole cavity, resulted in an increase of binding affinity for Cl^- by three orders of magnitude.

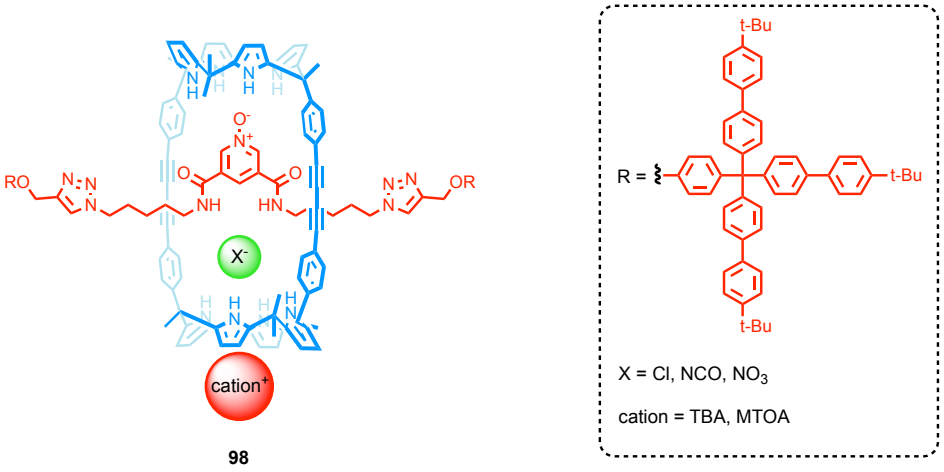

98

Scheme 3. 7 Heteroditopic [2]rotaxane ion-pair receptor by Ballester and co-workers.

Project Aim

There are no doubts regarding the efficacy of the anion templating approach developed by the group of Beer for the synthesis of anion responsive sensors. However, it possesses its limitation as only arrangements of anion-binding functionalities that are productive in the formation of the final interlocked system can be used.

The other common synthetic strategy relies on pseudorotaxane formation based on strong interactions between the respective binding sites of each component. These interactions live on in the final interlocked molecule, competing with the binding of the guest and/or diminishing the impact on the output recorded.

In this work, we aim to demonstrate an alternative approach to a simple anion binding rotaxane based on a urea H-bonding motive that plays no role in the rotaxane formation. Our aimed was to study the impact of the mechanical bond on the binding of anionic guest as well as exploring the possibility of functionalising the system in order to observe an optical response.

3.2. Results and Discussion

3.2.1. Preliminary results

3.2.1.1. Starting material and rotaxane synthesis

The two half-threads were readily synthesised in a single step from commercially available starting material (Scheme 3. 8). The urea-alkyne stopper **102** was obtained in 67% yield from the reaction of amine **99** with triphosgene in a CH_2Cl_2/$NaHCO_3$ 1:1 mixture followed by the addition of propargyl amine. The azide stopper **103** synthesis consisted in *in situ* lithiation of 3,5-di-*tert*-butylbromobenzene with n-BuLi followed by addition of *p*-toluenesulfonyl azide, affording **103** in 61% yield.

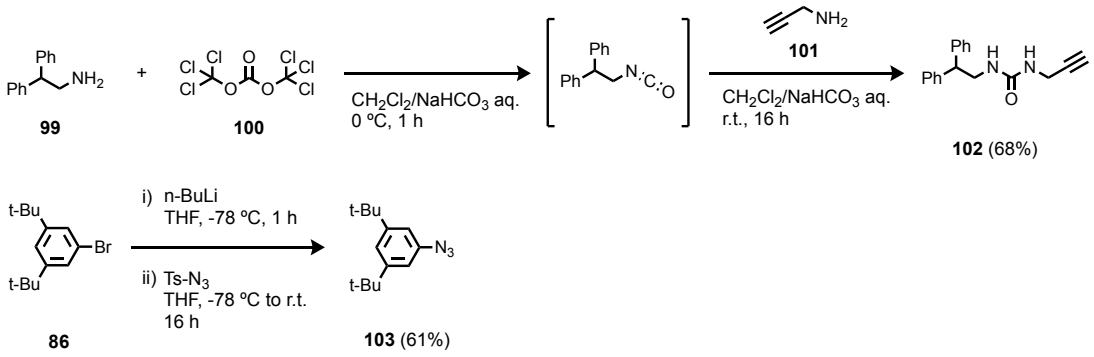

Scheme 3. 8 Synthesis of half-threads **102** and **103**.

The macrocycle **109** synthesis started with a Negishi-coupling reaction between the bromide derivative **104** and 2,6-dibromopyridine, affording the intermediate **106** (60%) that was then demethylated using aqueous HBr to give phenol derivative **107** (87%). Subsequent double Williamson ether formation with 1,4-dibromobutane provided macrocycle precursor **108** in acceptable yield (60%), which was converted to macrocycle **109** by a Nickel mediated bi-aryl coupling reaction (71%) (Scheme 3. 9).

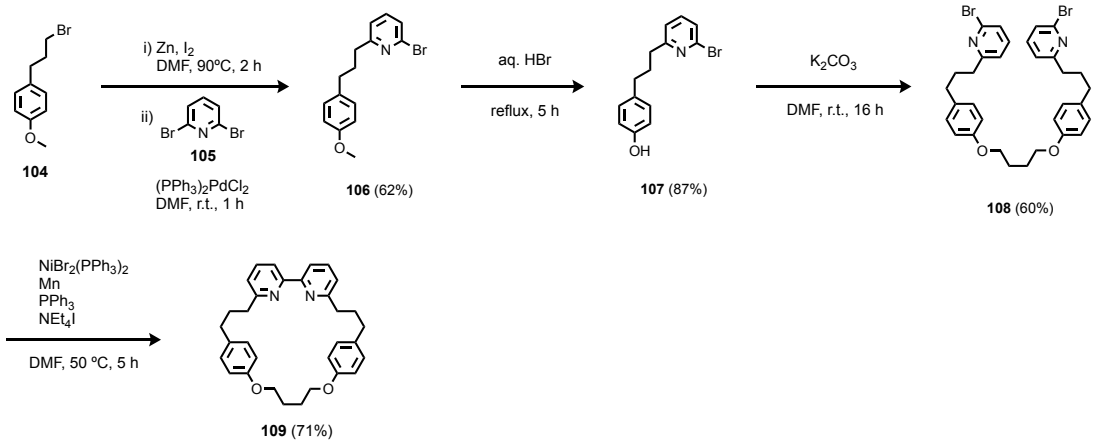

Scheme 3. 9 Synthesis of macrocycle **109**.

With the three starting materials in hands, rotaxane **110** was readily obtained in good yield (83%) using the AT-CuAAC click reaction. The axle **111** was synthesised under similar conditions in acceptable yield after purification (70%) (Scheme 3. 10).

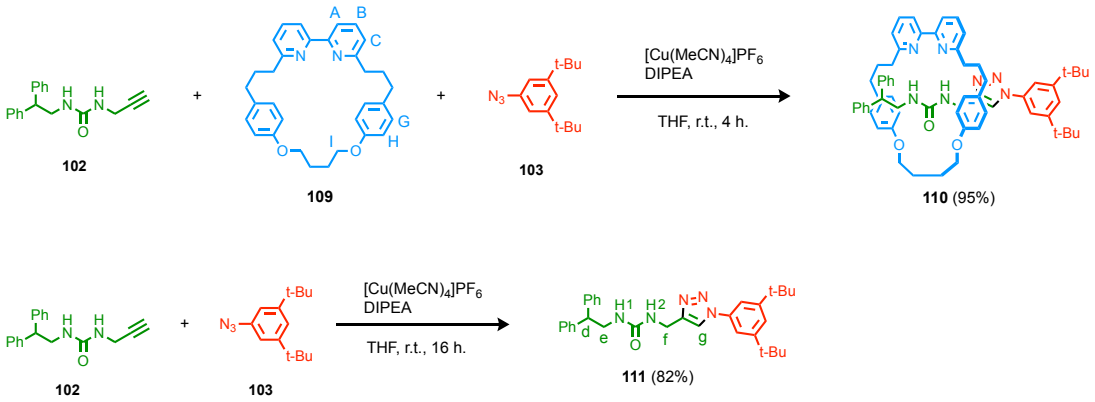

Scheme 3. 10 AT-CuAAC Synthesis of rotaxane **110** and axle **111**.

^{1}H NMR analysis of rotaxane **110** and axle **111** showed interesting differences (Figure 3. 1). Indeed, all of the macrocycle signals are affected and in particular protons H_l from the alkyl bottom chain that are now diastereotopic as a result of mechanical bond formation. Protons H_d, H_e and H_f are observed at higher field in rotaxane **110** compare to the non-interlocked axle **111** ($\Delta\delta$ = 0.95, 0.83 and 0.58 ppm) that could indicate CH-π interactions between the thread and the macrocycle. More interesting, the urea *-NH-* signals appears to be significantly deshielded ($\Delta\delta$ = 1.83 and 1.17 ppm) in **110** compare to **111**, whereas the triazole proton H_g is almost unaffected, suggesting that the bipyridine unit is actually interacting with the urea rather than the triazole station as typically observed in AT-CuAAC rotaxanes.[22]

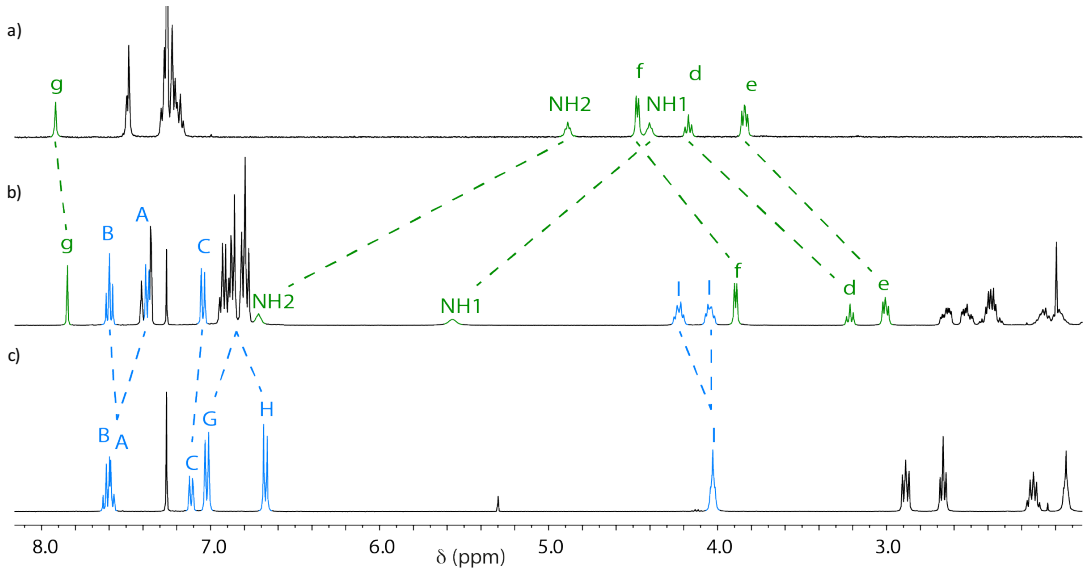

Figure 3. 1 Partial ^{1}H NMR stack plot ($CDCl_3$, 400 MHz, 298 K) of a) axle **111**, b) rotaxane **110** and c) macrocycle **109**.

Pleasingly, single-crystals suitable for X-ray diffraction were obtained from vapour diffusion of pentane into a solution of **110** in Et_2O. The solid-state analysis (Figure 3. 2) confirming our NMR conclusions. In particular, the fact that the bipyridine moiety is involved in a bifurcated hydrogen bonding interaction with the NH of the urea station.

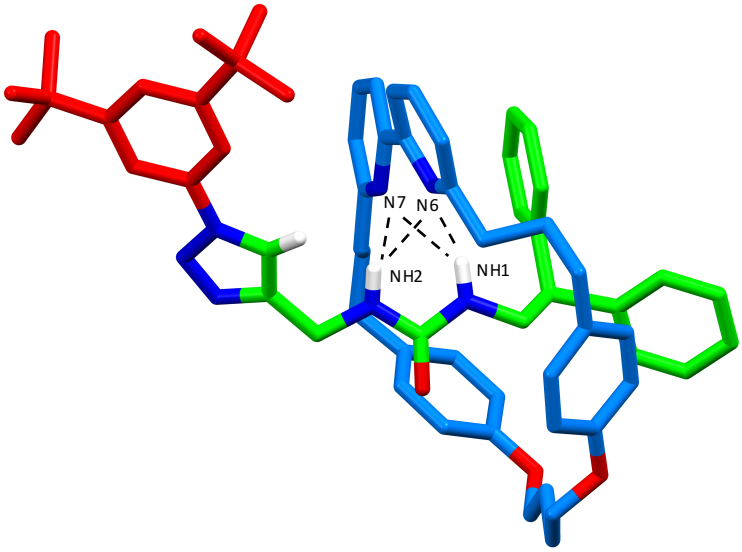

Figure 3. 2 Solid-state structure of rotaxane **110**.Non-relevant protons are not displayed for clarity. Black dotted lines correspond to short contact interactions. Selected distances in Å: N6•••NH1 = 2.43, N6•••NH2 = 2.56, N7•••NH1 = 2.78 and N7•••NH2 = 2.49.

*3.2.1.2. Preliminary binding studies with axle **111** and rotaxane **110***

Taking in account the previous observation, we anticipated that the addition of anions would lead to a competition for the urea H-bond donor. Ultimately, the ring could impart selectivity on the interlocked structure that would be absent on the axle.

However, preliminary results from our collaborator in Sydney revealed that whereas the axle **111** was binding anions such as Cl^- in $CDCl_3$ at 298 K, rotaxane **110** did not. It was demonstrated by the fact that in the case of **111**, clear movement downfield of the *-NH-* signals could be measured upon addition of Cl^- due to the establishment of N-H•••Cl^- hydrogen bond interaction (Figure 3. 3). But in the case of rotaxane **110** no changes were noticed for all the anions tested (AcO^-, F^-, Cl^-, MsO^-, TsO^-, HSO_4^-, Cl^-, Br^-, I^-). This indicates that the N-H•••anion interaction is unable to compete with the intramolecular hydrogen bond in place between the urea and bipyridine moieties.

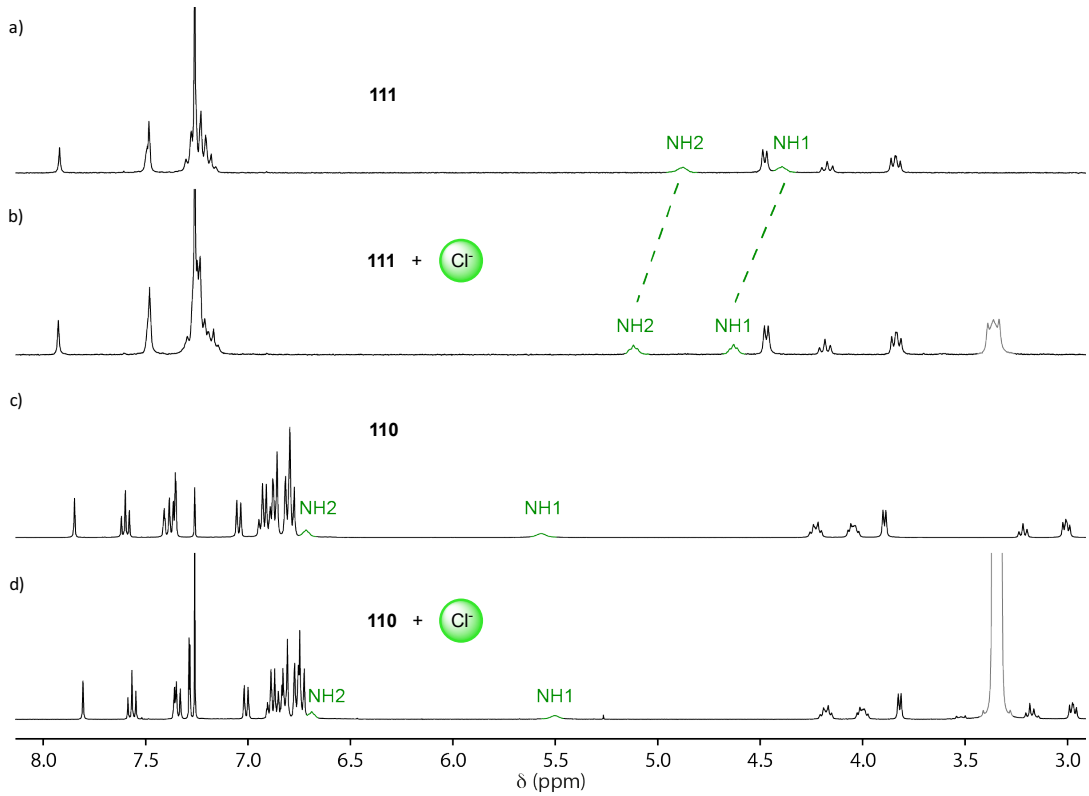

Figure 3. 3 Partial ^{1}H NMR stack plot ($CDCl_3$, 400 MHz, 298 K) of a) axle **111**, b) axle **111** in the presence of TBACl (1 equiv.), c) rotaxane **110** and c) rotaxane **110** in the presence of TBACl (10 equiv.). TBA signal in grey.

3.2.1.3. Protonation study

Previous work within the group has shown a similar inhibiting effect coming from the macrocycle; the activity of a Au^{I}-catalyst was inhibited due to Lewis basic interaction of the bipyridine unit with the metal ion.[23] In order to restore the catalyst activity, a cation was bound within the cavity of the rotaxane. We speculated that we could use a similar approach in the case of our urea-based rotaxane in order to turn-on its anion binding property. We selected a proton as a cationic guest and screened acids of different strength to see if they would behave differently. Pleasingly, we observed that upon addition of 1 equiv. of TsOH to a solution of rotaxane **110** in $CDCl_3$ at 298 K a new species, with a significantly different ^{1}H NMR spectrum, was formed (Figure 3. 4). The macrocycle aromatic signals were all affected to a certain degree, but more importantly the thread signals as well. The triazole proton H_g experiences a upfield shift ($\Delta\delta$ = 1.01 ppm), whereas alkyl proton H_d and H_e shifted to higher chemical shifts ($\Delta\delta$ = 0.85 and 0.51 ppm, respectively) that are similar to the ones found in the axle **111**. The latter observation is consistent with the macrocycle shuttling to the triazolium station. The broad signal at 5.85 ppm was tentatively assigned to urea *-NH-* signals.

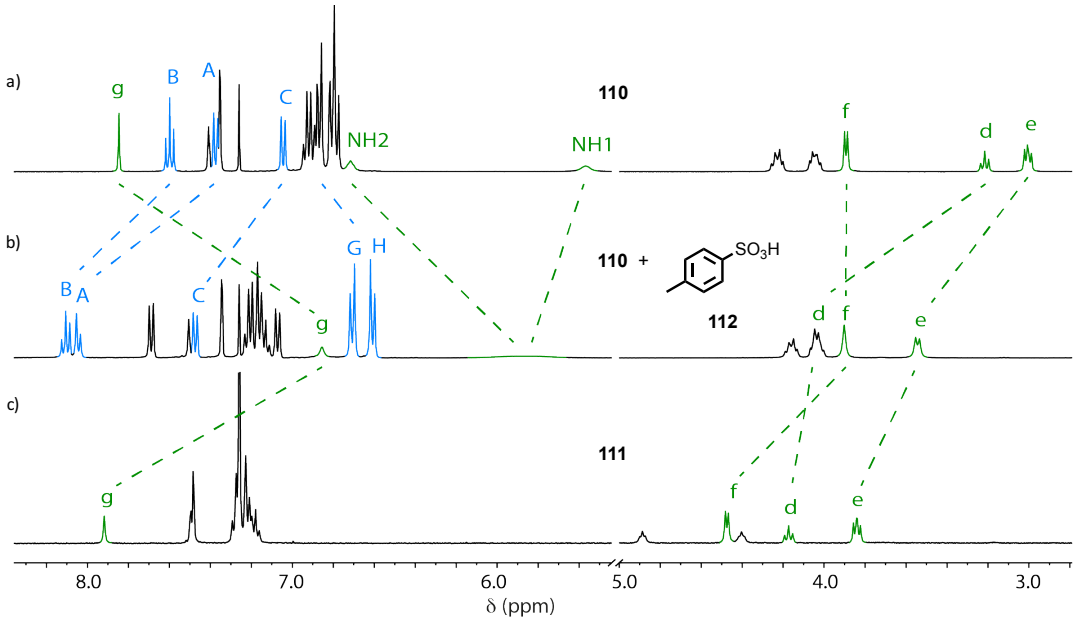

Figure 3. 4 Partial ^{1}H NMR stack plot ($CDCl_3$, 400 MHz, 298 K) of a) rotaxane **110**, b) rotaxane **110** with tosic acid (1 equiv.) and c) axle **111**.

In contrast, the same experiment performed with carboxylic acids gave different results. Addition of one equivalent of the pivalic acid to a sample of the rotaxane **110** created little change by ^{1}H NMR analysis (Figure 3. 5 b). Nonetheless the thread still seemed to be affected by the presence of the acid as H_d and He were slightly shielded ($\Delta\delta$ = 0.06 and 0.1 ppm) and H_d deshielded ($\Delta\delta$ = 0.1 ppm). More importantly the signals for triazole proton H_g and the urea -*NH*- shifted downfield, appearing at 8.08, 6.79 and 5.80 ppm, respectively. It was notable that further addition of carboxylic acid **113** amplified those effects (Figure 3. 5 c), the triazole and urea signals shifting to even higher values and eventually stabilizing with a 10:1 ratio of acid to rotaxane. It suggested that excess of acid was needed to drive the equilibrium towards completion. Similar results were obtained with acetic and 4-*tert*-butyl-benzoic acids (Figure 3. 5 d and e) although the shift observed were respectively larger and smaller compare to pivalic acid (Figure 3. 5 c), which could suggest that the bulkiness of the acid also plays a role.

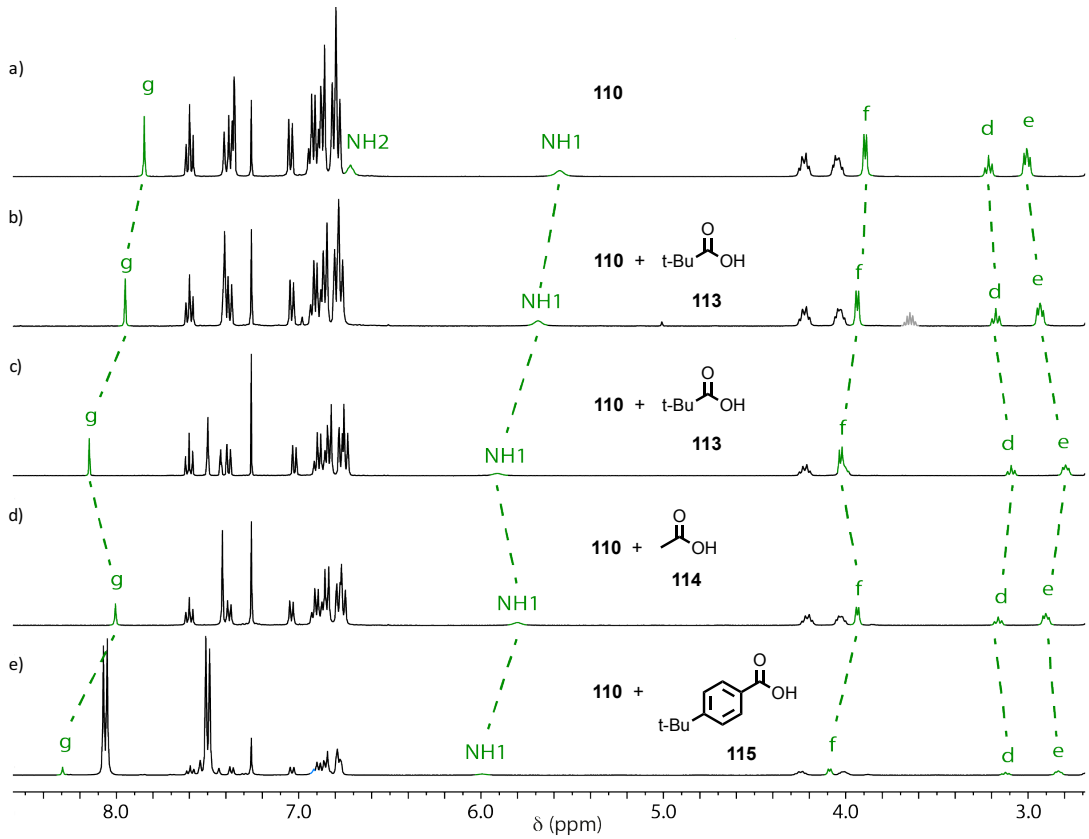

Figure 3. 5 Partial ^{1}H NMR stack plot ($CDCl_3$, 400 MHz, 298 K) of a) rotaxane **110**, b) rotaxane **110** with pivalic acid (1 equiv.), c) rotaxane **110** with pivalic acid (10 equiv.), d) rotaxane **110** with acetic acid (10 equiv.) and e) rotaxane **110** with 4-*tert*-butylbenzoic acid (10 equiv.).

This result was not the one we expected but still of interest. It suggested that carboxylic acids still interact with the rotaxane in a different fashion to stronger acids such as TsOH. Taking in account the shifts observed in the ^{1}H NMR for the axle signals (in particular H_d and H_e), we tentatively suggest that the macrocycle was displaced toward the diphenyl stopper as a similar upshield shift was observed for these protons going from the axle to the rotaxane (Figure 3. 6) (supposedly due to CH-π interactions). The deshielding of H_f, now being in an environment more similar to the non-interlocked thread, would further support this hypothesis. Finally, the deshielding effect on the triazole and urea protons suggested interactions between the acid and those two units in the thread (Figure 3. 6).

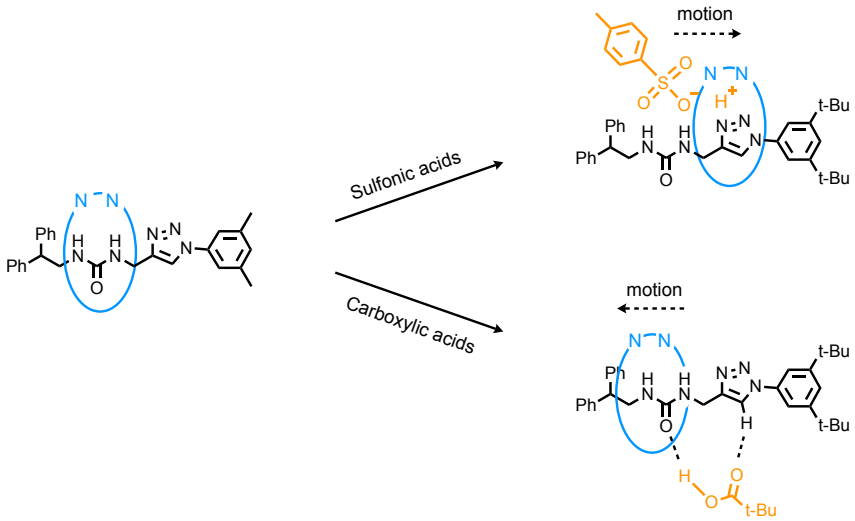

Figure 3. 6 Schematic of the two modes of interaction for both class of acids with rotaxane **110**.

*3.2.1.4. Synthesis and preliminary study of **110**.HBF_4*

Based on these results, it appeared that in order release the urea binding site from the bipyridine moiety, strong acids were needed. We opted for HBF_4 given its pK_a (0.5 in water) and the fact that being a weakling coordinating counter anion BF_4^- would not impact the binding of other anions.

Upon treatment of rotaxane **110** in CH_2Cl_2 with an aqueous solution of HBF_4, changes similar to the one seen in the case of TsOH acid were observed (Figure 3. 7 b). The macrocycle aromatic protons were all affected with H_A, H_B and H_C appearing at lower field ($\Delta\delta$ = 0.99, 0.87 and 0.72 ppm respectively) and H_H and H_G forming two sharp doublets at 6.63 and 6.75 ppm. Studying the axle signals, H_d and H_e were deshielded ($\Delta\delta$ = 0.66 and 0.09) whereas the proton signal for H_f was slightly shielded ($\Delta\delta$ = 0.14 ppm). Finally, the broad signals at 5.15 and 5.70 ppm were tentatively assigned to the urea whereas the triazole H_g could not be identified. Subsequent addition of Cl^- as its tetrabutylammonium (TBA) salt produced further changes in the ^{1}H NMR spectrum indicative of binding of the anion by the protonated receptor (Figure 3. 7 c). Consistent with this conclusion, treating the neutral rotaxane with HCl resulted in a very similar spectrum (Figure 3. 7 d).

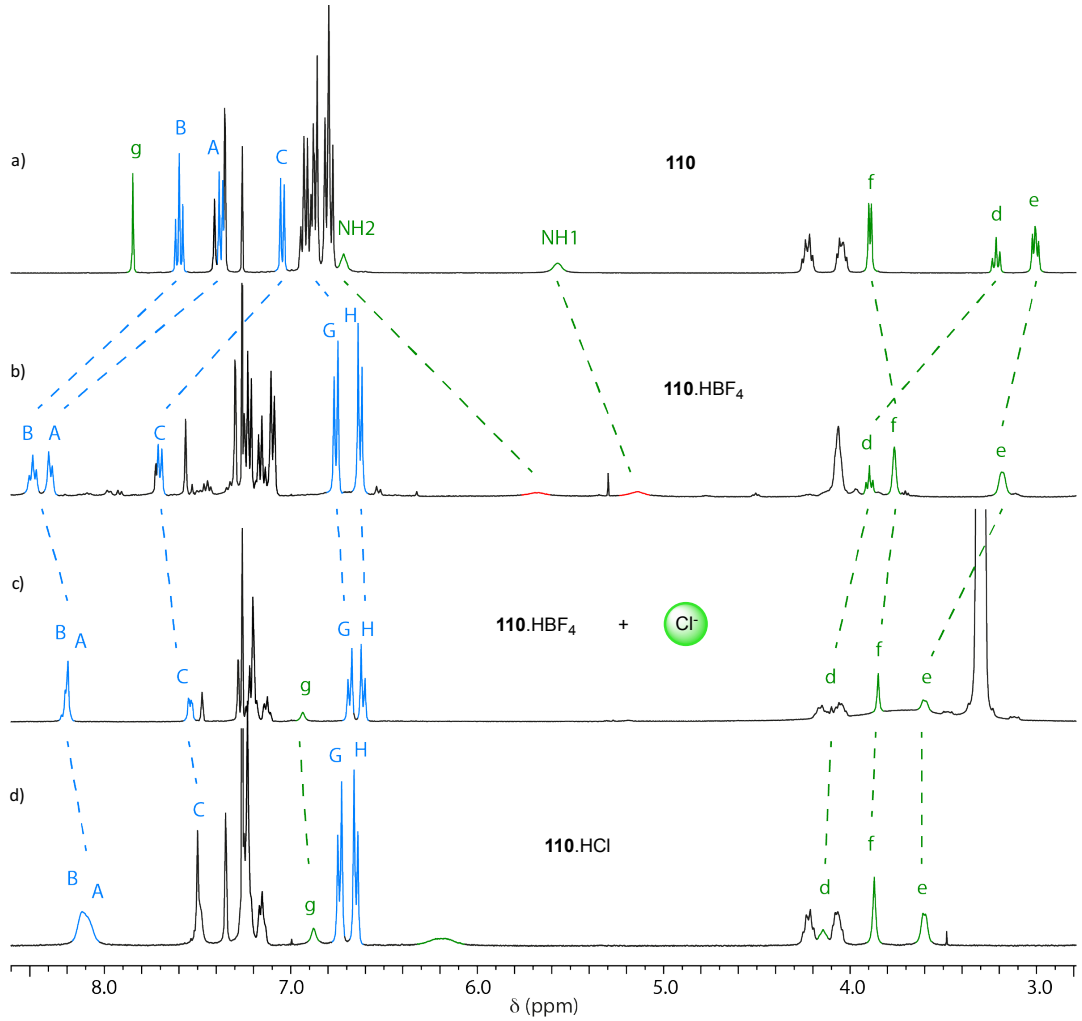

Figure 3. 7 Partial ^{1}H NMR stack plot ($CDCl_3$, 400 MHz, 298 K) of a) rotaxane **110**, b) **110**.HBF_4, d) **110**.HBF_4 with TBACl (5 equiv.) and d) **110**.HCl.

Although this is an exciting result, rotaxane **110** has major limitations as a sensing system: the lack of clear and detectable output signal. Indeed, the ^{1}H NMR spectrum was very broad and the fact that some of the signals appeared (triazole) or disappeared (NH) upon salt addition made it difficult to study and quantify the binding. For these reasons, we decided to build on these results and develop a system whose response upon binding would be observable not only by ^{1}H NMR but also UV-visible and fluorescence spectroscopies.

3.2.2. Fluorescent urea-based Rotaxane **120**

Based on our previous work on metal cation sensors as well as previous reports exploiting the naphthalimide urea core unit for the binding and transport of anions, we aimed to replace the diphenyl stopper with a naphthalimide.

*3.2.2.1. Synthesis and characterisation of fluorescent rotaxane **120** and axle **121***

The synthesis of the new naphthalimide urea alkyne half-thread started from 4-nitro naphthalic anhydride **116** and formation of the imide moiety in **117** with diphenyl ethylamine (90%). Subsequent reduction of the nitro group on Pd/C provided the amino naphthalimide **118** in excellent yield (94%), which was then reacted with triphosgene and propargyl amine in the presence of DMAP in order to afford the desired naphthalimide urea alkyne **119** (68%) (Scheme 3. 11). The synthesis of azide **103** and macrocycle **109** were discussed previously (Scheme 3. 8 and Scheme 3. 9).

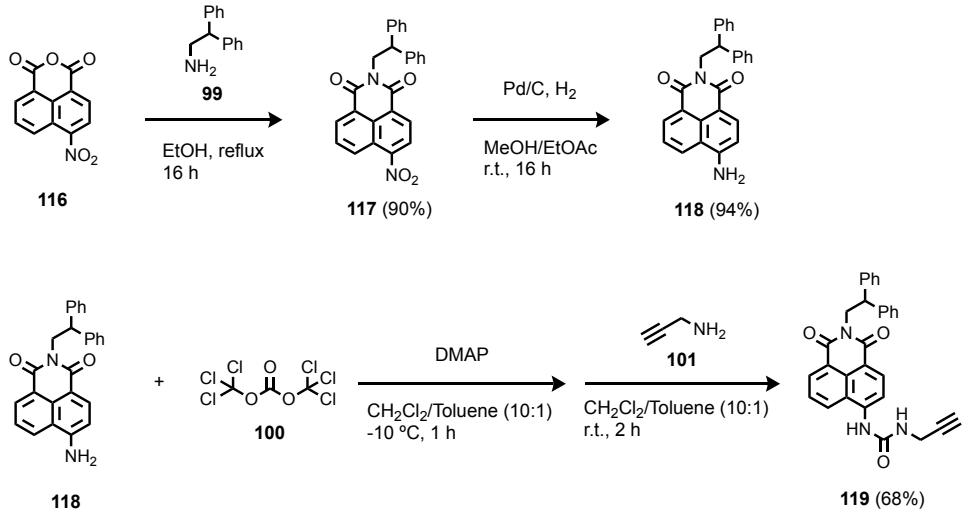

Scheme 3. 11 Synthesis of naphthalimide urea-alkyne **119**.

Rotaxane **120** was readily obtained in high yield (92%) using the AT-CuAAC click reaction. The non-interlocked counterpart **121** was synthesised in excellent yield (96%) using 0.2 equivalent of copper and heating at 50 °C for 2 h (Scheme 3. 12).

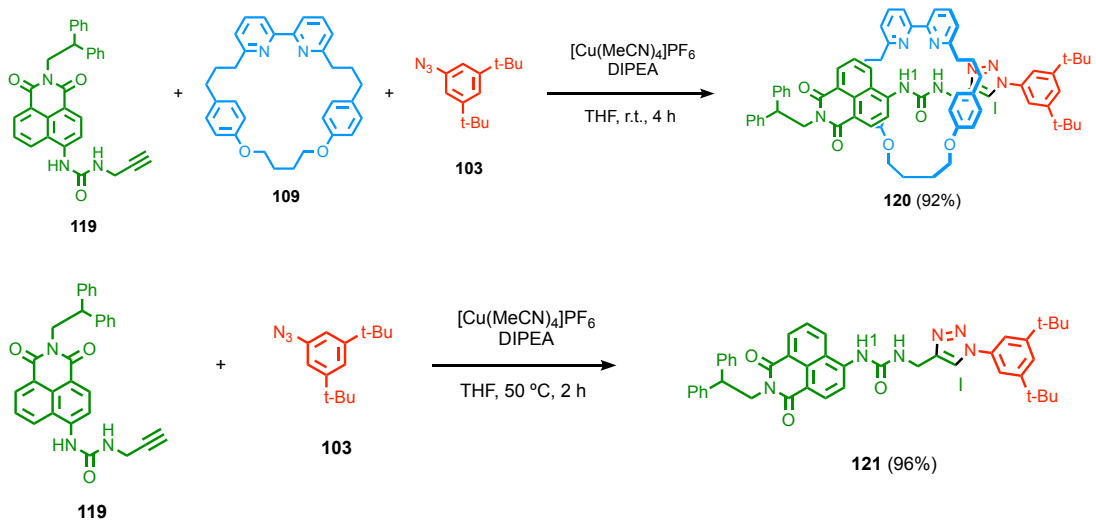

Scheme 3. 12 Synthesis of fluorescent rotaxane **120** and axle **121**.

We began the investigation of rotaxane **120** using ^{1}H NMR spectroscopy (Figure 3. 8). The urea -NHs appears downfield compare to the non-interlocked axle **121** ($\Delta\delta$ = 0.58 ppm) whereas the triazole proton H_I resonates at δ = 7.44 ppm (a shift upfield of 0.73 ppm in contrast to axle **121**). It provides strong evidence that the macrocycle is located around the urea station with the bipyridine hydrogen bonded to the urea moiety, in a similar fashion as it was seen with rotaxane **110**.

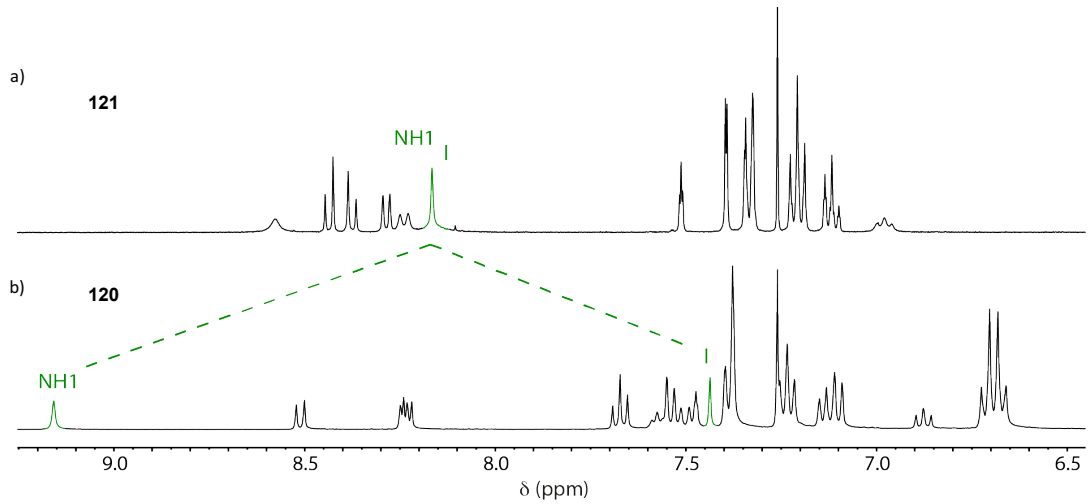

Figure 3. 8 Partial ^{1}H NMR stack plot ($CDCl_3$, 400 MHz, 298 K) of a) axle **121** and b) rotaxane **120**. For labelling see Scheme 3. 12.

Single crystals of **120** suitable for X-ray crystallography were obtained from slow cooling of a methanol/water mixture and confirmed our proposal. In the solid state (Figure 3. 9 a), the ring encircles the urea binding site to form two bifurcated H-bonds (N-H•••N distances of 2.45 (N8•••NH1), 2.89 Å (N8•••NH2), 2.33 Å (N7•••NH2) and 2.59 Å (N7•••NH1)). Interestingly, the naphthalimide peri proton H_h appears to be involved in short-contact interactions with N7 from the bipyridine (2.56 Å). Finally, the triazole is interacting with a molecule of water (C-H•••O = 2.62 Å) and the axle experiences a 90º bend, which appears to lock the ring close to the naphthalimide stopper.

However, a second set of single crystals was obtained under different conditions (vapor diffusion of Et_2O into a CH_2Cl_2 solution of **120** and notable differences were noticed between the two solid state structures (Figure 3. 9 b). In this new polymorph of **120** the axle has a linear geometry, giving the ring more freedom of motion. Perhaps related, the bipyridine now forms two bifurcated hydrogens bonds with both the urea and the triazole units (N7•••NH1 = 2.56 Å, N7•••NH2 = 2.33 Å, N8•••NH2 = 2.91 Å, N8•••H_I = 2.47 Å). Due to this change in conformation, the distance between naphthalimide peri proton H_h and N7 slightly increased by 0.3 Å.

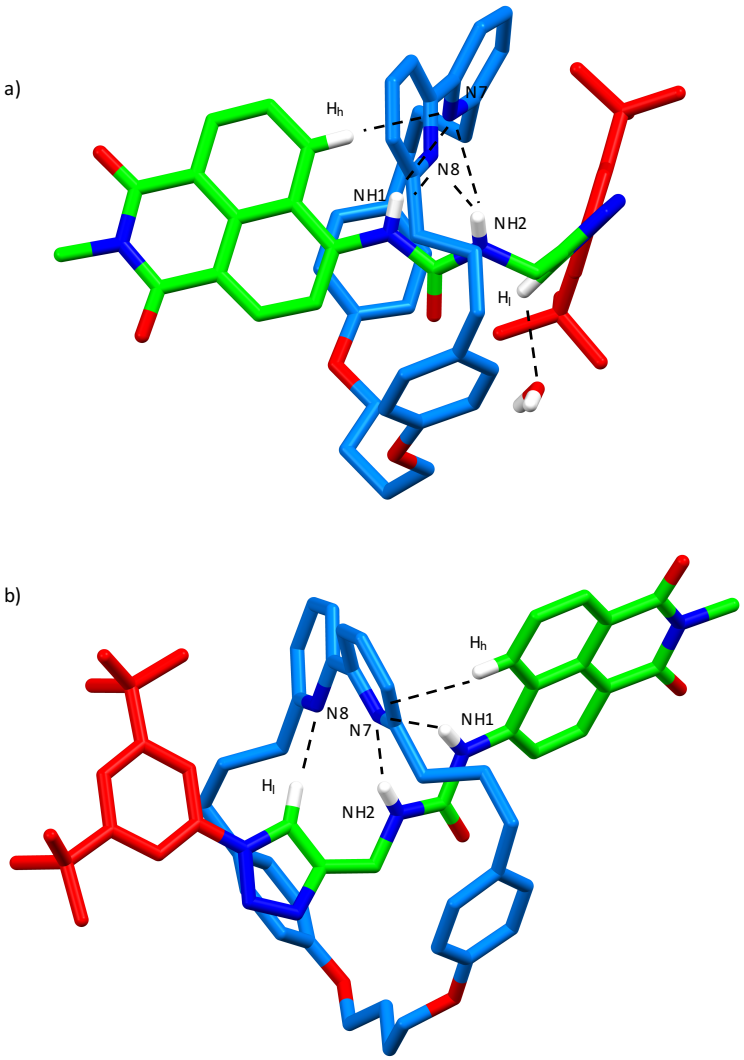

Figure 3. 9 Solid-state structures of the two polymorphs of rotaxane **120** obtained under different crystallisation conditions. The diphenyl head of the naphthalimide stopper has been truncated and the solvent and non-relevant hydrogen atoms hidden for clarity. Black dotted lines correspond to short-contact interactions. Selected distances in Å: a) N8•••NH1 = 2.45, N8•••NH2 2.89, N7•••NH2 = 2.33, N7•••NH1 = 2.59, C-H_h•••N7 = 2.56, C-H•••O = 2.62. b) N7•••NH1 = 2.56, N7•••NH2 = 2.33, N8•••NH2 = 2.91, N8•••H_l = 2.47, C-H_h•••N7 = 2.86.

3.2.2.2. UV-visible and fluorescence studies

Axle **121** and rotaxane **120** display absorbance bands in CH_2Cl_2 at 377 and 406 nm respectively attributed to the naphthalimide unit. This is consistent with the hydrogen bonding of the urea by the bipyridine that is expected to result in a bathochromic shift of the absorption maxima. A concentration dependent study was performed for the two systems in CH_2Cl_2 and revealed that both the axle **121** and rotaxane **120** form aggregates at concentration greater than 10^{-5} M in CH_2Cl_2. This was illustrated by the fact that their behaviors diverge from the Beer Lambert law at higher concentration with a decrease of the absorption coefficient (Figure 3. 10). Interestingly, the absorption which is broad at higher concentration sharpened upon dilution. This effect could tentatively be assigned to changes in conformations resulting from the dispersion process.

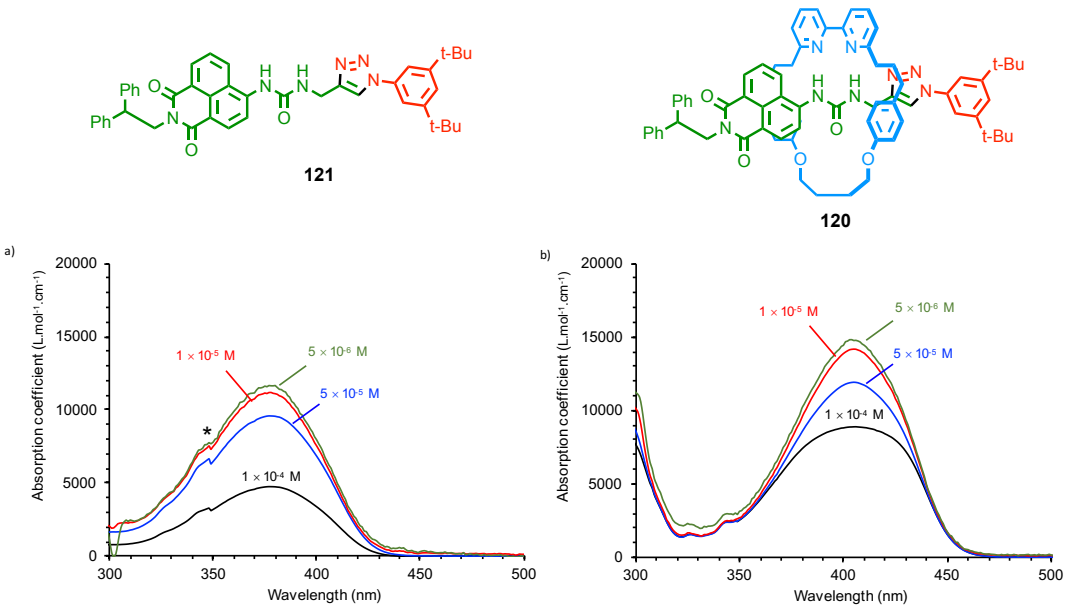

Figure 3. 10 Absorption coefficient spectra (CH_2Cl_2, 298 K) at various concentration for a) axle **121** and b) rotaxane **120**. Asterisk correspond to an artifact from the machine.

The fluorescence properties of both systems were studied in CH_2Cl_2 using their respective maxima of absorption. We observed an emission at 470 nm for axle **121** and 475 nm for the corresponding rotaxane **120** with similar intensities. In this case, the H-bond interactions seems to have a lesser impact on the behaviour.

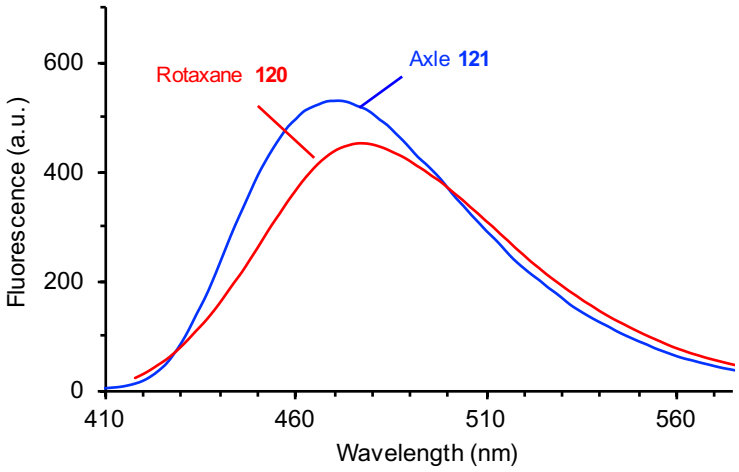

Figure 3. 11 Emission spectra of axle **121** (λ_{ex} = 378 nm) and rotaxane **120** (λ_{ex} = 388 nm) ($MeCN/CHCl_3$, 298 K, 130 μM).

*3.2.2.3. **120**.HBF_4 salt formation and characterisation*

Similarly to what was shown with rotaxane **110** incorporating a diphenyl stopper unit, addition of AcO^- as tetrabutylammonium salt to a sample of rotaxane **120** led to no observable changes by ^1H NMR, UV-visible or fluorescence spectroscopies suggesting that no anion binding was taking place. It indicates that in this system as well, the anion•••NH

interaction is unable to compete with the intramolecular hydrogen bond between the bipyridine moiety and urea station (Figure S3. 50). Therefore, we decided to move forward with the protonation of the system using HBF_4.

Upon treatment of rotaxane **120** in CH_2Cl_2 with an aqueous solution of HBF_4 a colour change from bright to pale yellow was observed (Figure 3. 12). Moreover, the ^1H NMR spectrum showed significant differences (Figure 3. 13) including a shift up-field of the two NH signals ($\Delta\delta$ = 1.07 and 0.29 ppm) consistent with the disappearance of the H-bonds with the bipyridine. The triazole proton H_I also experience a significant shift to lower values in ppm ($\Delta\delta$ = 1.11 ppm) that could indicate a shielding effect from the flanking aromatic rings of the macrocycle in the protonated species.

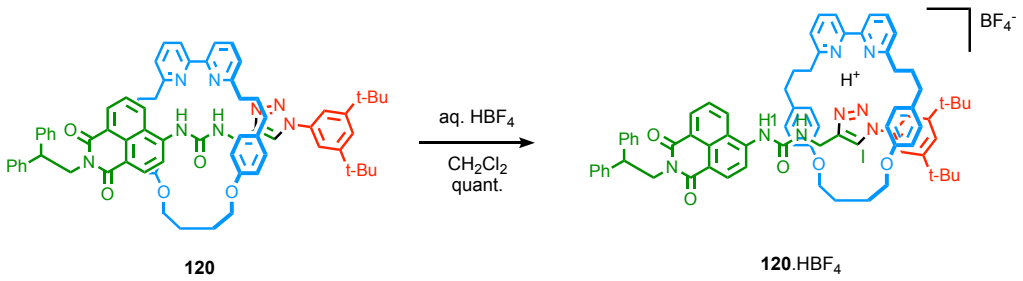

Figure 3. 12 Formation of **120**.HBF_4.

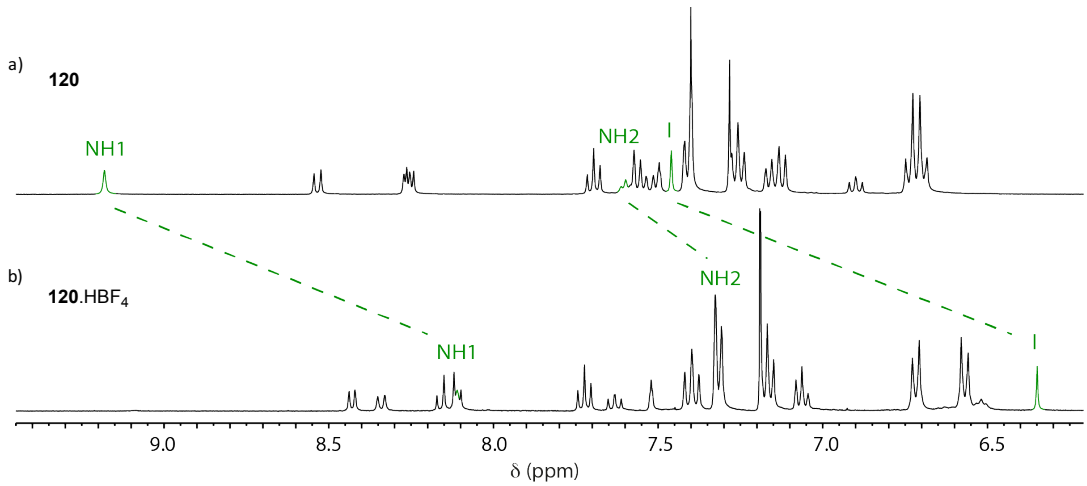

Figure 3. 13 Partial ^1H NMR stack plot ($CDCl_3$, 400 MHz, 298 K) of a) rotaxane **120** and b) **120**.HBF_4. For labelling see Figure 3. 12.

Pleasingly, single crystals suitable for X-ray crystallography were obtained from vapor diffusion of Et_2O into a solution of **120**.HBF_4 in CH_2Cl_2 and allowed us to confirm the salt formation. Upon protonation, the system experienced an important structural rearrangement. The bipyridine ring has now shuttled to the triazolium station, the two nitrogens being involved in bifurcated H-bonds with the triazolium proton (N7•••H_I = 2.04 Å

and N8•••H^{I} = 2.76 Å), freeing the urea NHs. Moreover, short-contact interactions can be observed between triazole proton H_I and one of the flanking aromatic from the ring (2.95 Å) (Figure 3. 14 a), which is in agreement with the shielding observed for its signal by ^{1}H NMR spectroscopy. Protonation also seems to induce π-stacking of the bipyridine unit and the naphthalimide core (3.28 Å between the two planes, Figure 3. 14 b). It is worth noticing that although located on the triazole ring in Figure 3. 14, it is not clear where the proton resides in the system and it is probably shared between the nitrogen atoms of the bipyridine and triazole units. Perhaps of interest, the urea adopts an orientation in the protonated system in which the oxygen atom is relatively close to the protonated triazole, suggesting a weak interaction with the proton.

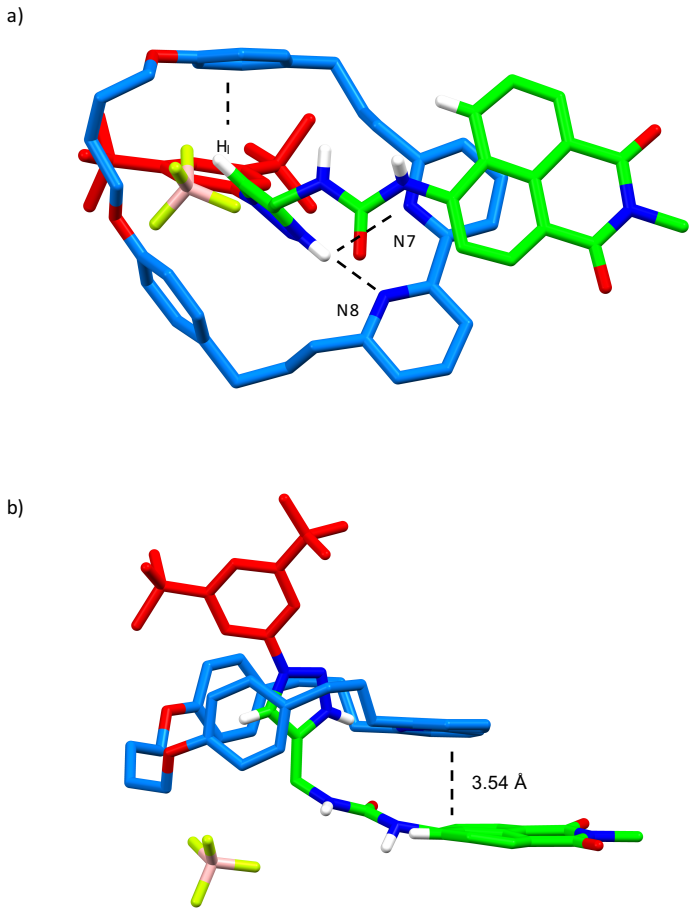

Figure 3. 14 Solid-state structure of **120**.HBF_4. The diphenyl head of the naphthalimide stopper has been truncated and the solvent hidden for clarity. Black dotted lines correspond to short-contact interactions. Selected distances in Å: N7•••H_I = 2.04, N8•••H^{I} = 2.76 and CH_I•••flanking aromatic = 2.95.

We then investigated the optical properties of **120**.HBF_4 using UV-vis and fluorescence spectroscopy techniques (Figure 3. 15). The absorbance spectra showed the appearance of a new band at 310 nm attributed to the bipyridine being engaged in strong H-bond with the protonated triazole unit. The absorbance band of the naphthalimide unit experiences a

hypsochromic shift of 25 nm, now exhibiting a maximum at λ_{abs} = 381 nm in a 1:1 mixture of MeCN/$CHCl_3$, similar to that of non-interlocked axle **121**. This observation is consistent with the urea NHs no longer being involved in H-bonding interactions. Upon excitation at 381 nm, **121**.HBF_4 displayed an emission centred on 462 nm, slightly blue-shifted comparing that of neutral rotaxane **120**.

However, a concentration study revealed an interesting behaviour. Upon dilution, a bathochromic shift of the naphthalimide absorption band was observed ($\Delta\lambda_{abs}$ = 11 nm) alongside a drop of the absorbance at 310 nm (Figure 3. 15 a). The fluorescence was also affected in an interesting way. When the concentration of the sample was reduced by a factor of 10, the intensity of the fluorescence stayed the same but was red-shifted ($\Delta\lambda_{em}$ = 16 nm, Figure 3. 15 b).

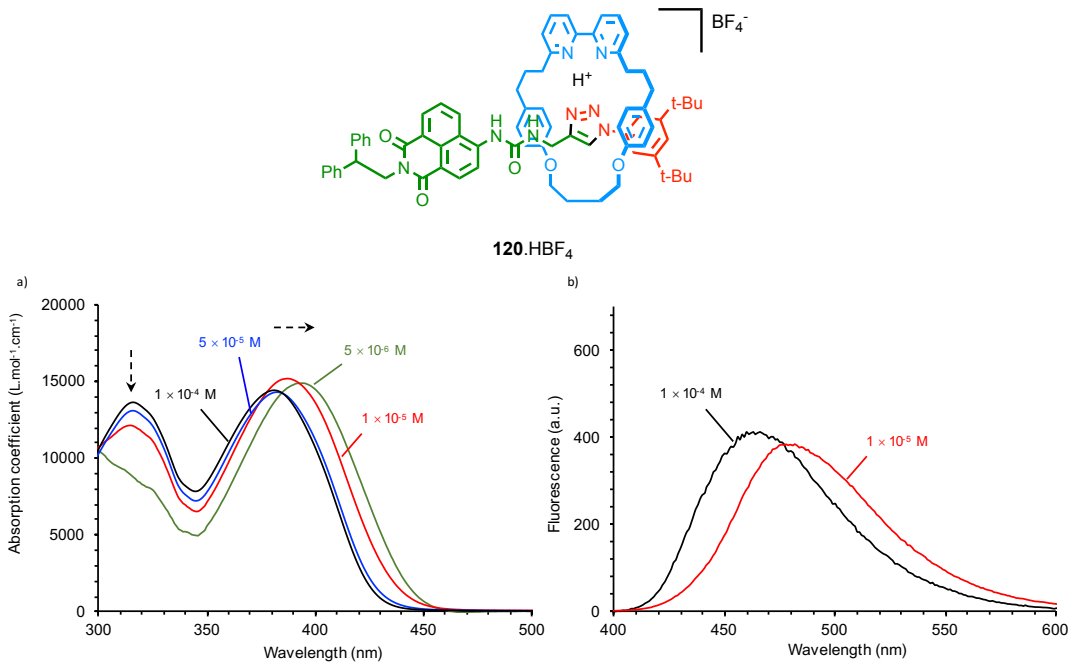

Figure 3. 15 UV-vis and fluorescence study of **120**.HBF_4 ($MeCN/CHCl_3$ 1:1, 298 K). a) absorption coefficient spectra of **120**.HBF_4 at various concentrations (see graphic), b) fluorescence spectra (λ_{ex} = 381 nm) of **120**.HBF_4 at various concentrations (see graphic).

Even more intriguingly, while the fluorescence was constant over time at 1×10^{-4} M (Figure 3. 16 a), an increase in intensity was observed on standing at 1×10^{-5} M (Figure 3. 16 b). One possible explanation would be that at lower concentration the system is being deprotonated by adventitious water being absorbed into the solvent. The disappearance of the bipyridine absorption band at 310 nm combined with the bathochromic and hyperchromic shift observed in fluorescence support this assumption.

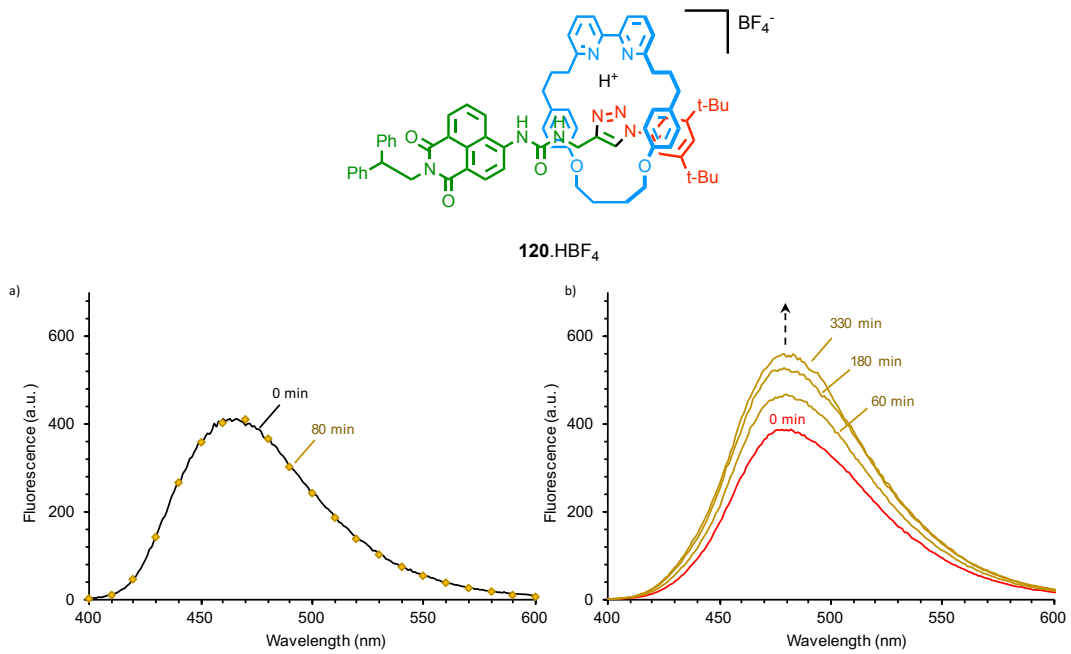

Figure 3. 16, a) fluorescence spectra of **120**.HBF_4 ($MeCN/CHCl_3$ 1:1, 298 K, C = 100 μM, λ_{ex} = 381 nm) at t = 0 (black curve) and 80 min (yellow markers), d) fluorescence spectra of **120**.HBF_4 ($MeCN/CHCl_3$ 1:1, 298 K, C = 10 μM, λ_{ex} = 381 nm) at t = 0 (red curve), 60, 180 and 330 min (yellow curves).

Importantly, the system did not reveal any stability issues at concentration of 1×10^{-5} M or higher, and thus this was selected as the concentration for the following titration studies.

*3.2.2.4. Binding studies with **120**.HBF_4*

We started with the study of the axle **121** toward a variety of anions, which produced the expecting binding behaviour. ^{1}H NMR spectroscopy titrations, performed at 298 K in 1:1 $CD_3CN/CDCl_3$, showed that portion-wise addition of the anions tested (AcO^-, MsO^-, TsO^-, HSO_4^-, F^-, Cl^-, Br^-, I^-) as their TBA salts to samples of **121** led to an increasing downfield shift of the urea -*NH*- signals as well as the naphthalimide *peri* proton H_I (Figure 3. 17). In terms of optical response, the binding event was associated with a red-shift of the naphthalimide absorbance band with a concomitant increase in intensity resulting in the formation of an isosbestic point (Figure 3. 18 a). This isosbestic point was used to perform fluorescent study and revealed that the interaction of the urea binding site with an anion caused a quenching of the emission (Figure 3. 18 b). Non-linear regression analysis of the data obtained *via* the three spectroscopic methods gave us an excellent fit for a 1:1 binding model and gave us the binding constant listed in Table 3. 1. It appears that the binding strength follows the hydrogen-bond acceptor strength, as it would be expected, with $AcO^- > F^- > Cl^- > MsO^- > TsO^- > HSO_4^- > Br^- > I^-$).

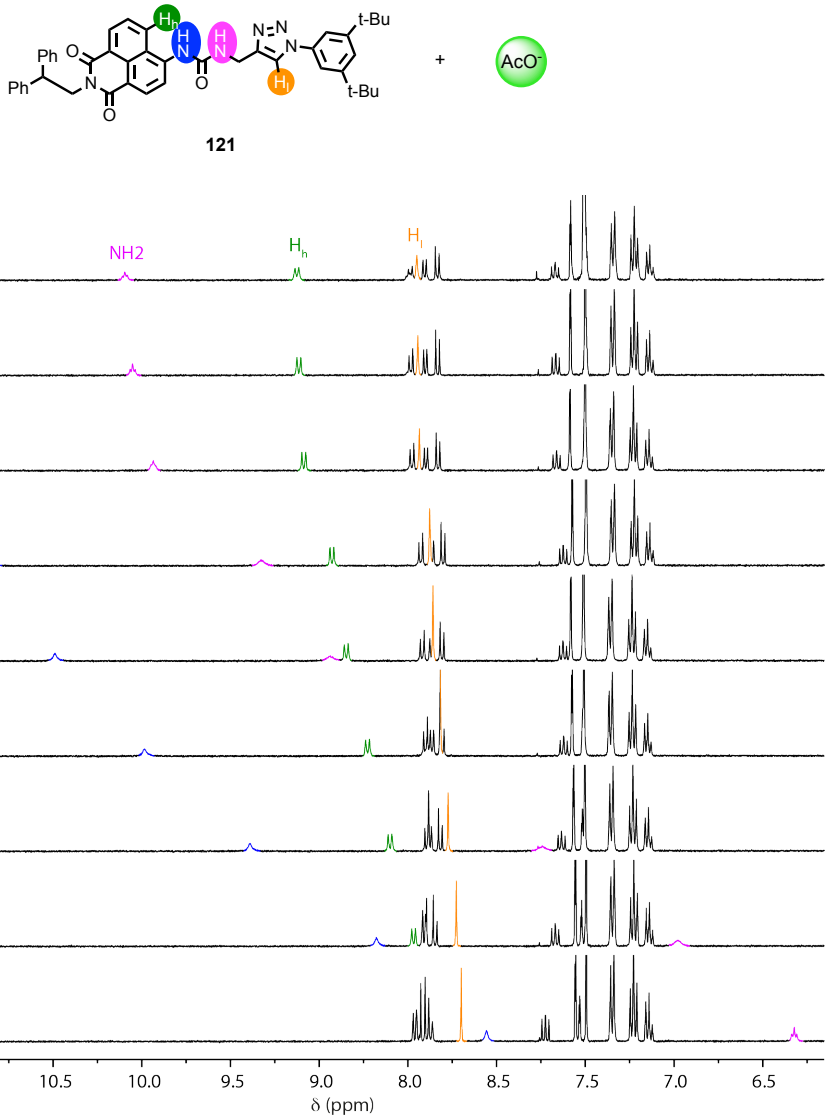

Figure 3. 17 Partial ^{1}H NMR titration ($CD_3CN/CDCl_3$ 1:1, 400 MHz, 298 K, 2.5 mM) of axle **121** with TBAAcO.

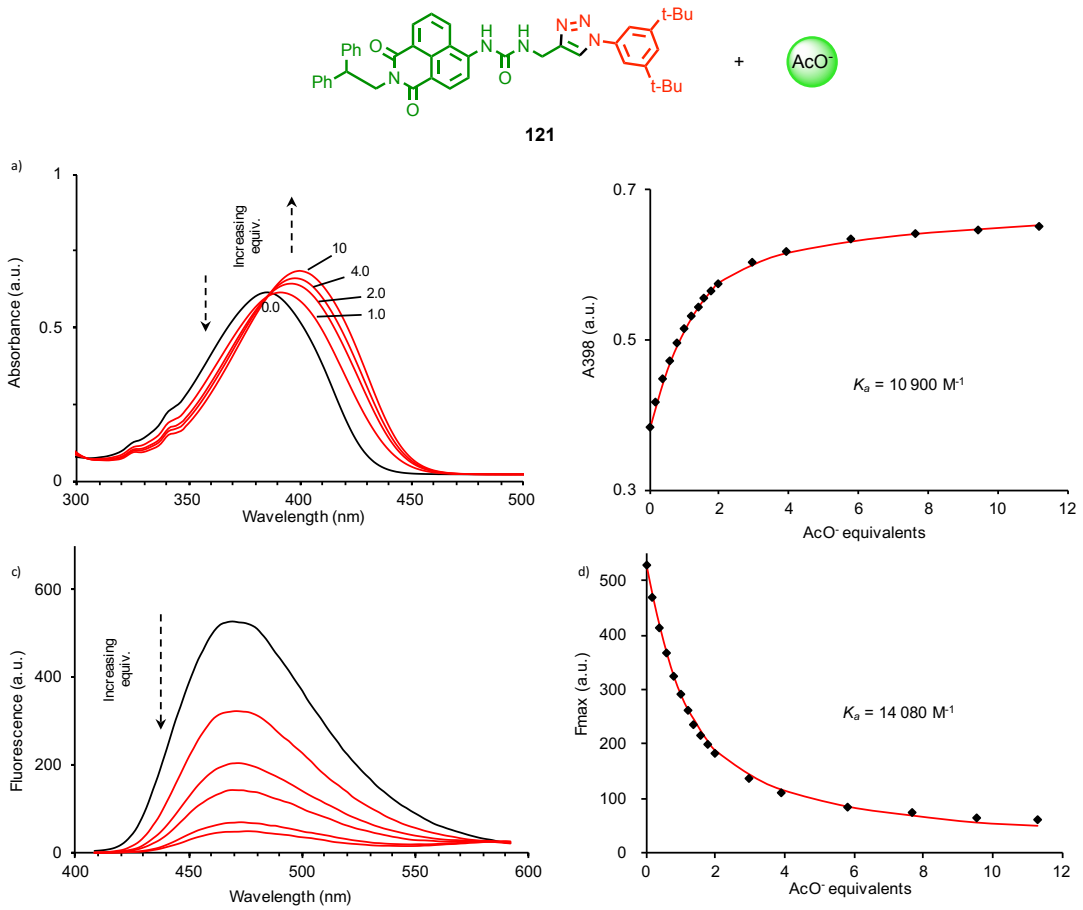

Figure 3. 18 UV-vis and fluorescence titration of axle **121** with TBAAcO (MeCN/$CHCl_3$, 298 K, C = 130 μM). a) absorption spectra of axle **121** in the presence of increasing equiv. of AcO^-, b) Fit for λ_{abs} = 398 nm versus equivalent of AcO^- added, c) fluorescence spectra (λ_{ex} = 381 nm) of axle **121** in the presence of increasing equiv. of AcO^- and d) Fit for F_{max} versus equivalent of AcO^- added.

We then moved on to studying the salt **120**.HBF_4 and observed a different behaviour. Treating it with basic anions such as AcO^- of F^- resulted in deprotonation of the system. This result is clear from the ^{1}H NMR titration that shows broadening of the signal to then recover the spectrum of **120** after addition of 1 equiv. of the anion (Figure 3. 19 b). The phenomenon was also observed by UV-vis spectroscopy by the progressive disappearance of the absorbance band at 310 nm upon the addition of increasing amounts of AcO^- (Figure 3. 19), a similar effect was observed with HO^- (Figure S3. 60).

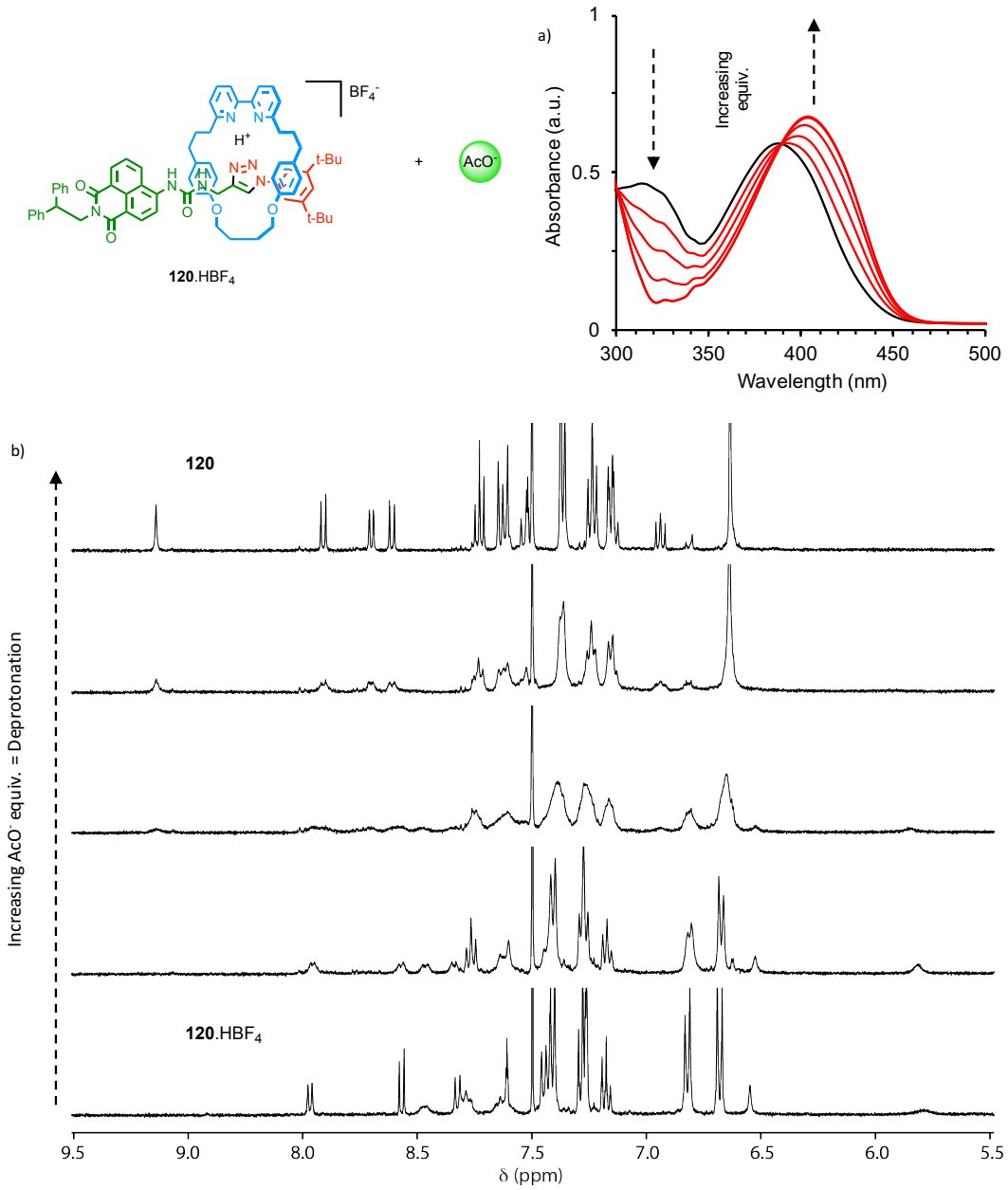

Figure 3. 19 a) UV-vis titration of **120**.HBF_4 with TBAAcO ($MeCN/CHCl_3$, 298 K, C = 130 μM). b) Partial ^{1}H NMR titration ($CD_3CN/CDCl_3$ 1:1, 400 MHz, 298 K, 2.5 mM) of **120**.HBF_4 with TBAAcO.

Conversely, when the protonated rotaxane **120**.HBF_4 was treated with less basic anions, such as Cl^-, changes consistent with binding of the anion by the urea moiety were observed in the ^{1}H NMR spectra (Figure 3. 20). Indeed, the signals attributable to the NH protons both shifted downfield due to the formation of NH•••Cl^- hydrogen bond interactions. Interestingly, the naphthalimide peri proton H_h experienced a similar effect suggesting the establishment of CH•••Cl^- hydrogen bond interactions here as well. It is also worth noticing the shift upfield of the triazole proton H_l, indicating a stronger CH•••π contact presumably due to the system being more restricted in the presence of an anionic guest binding.

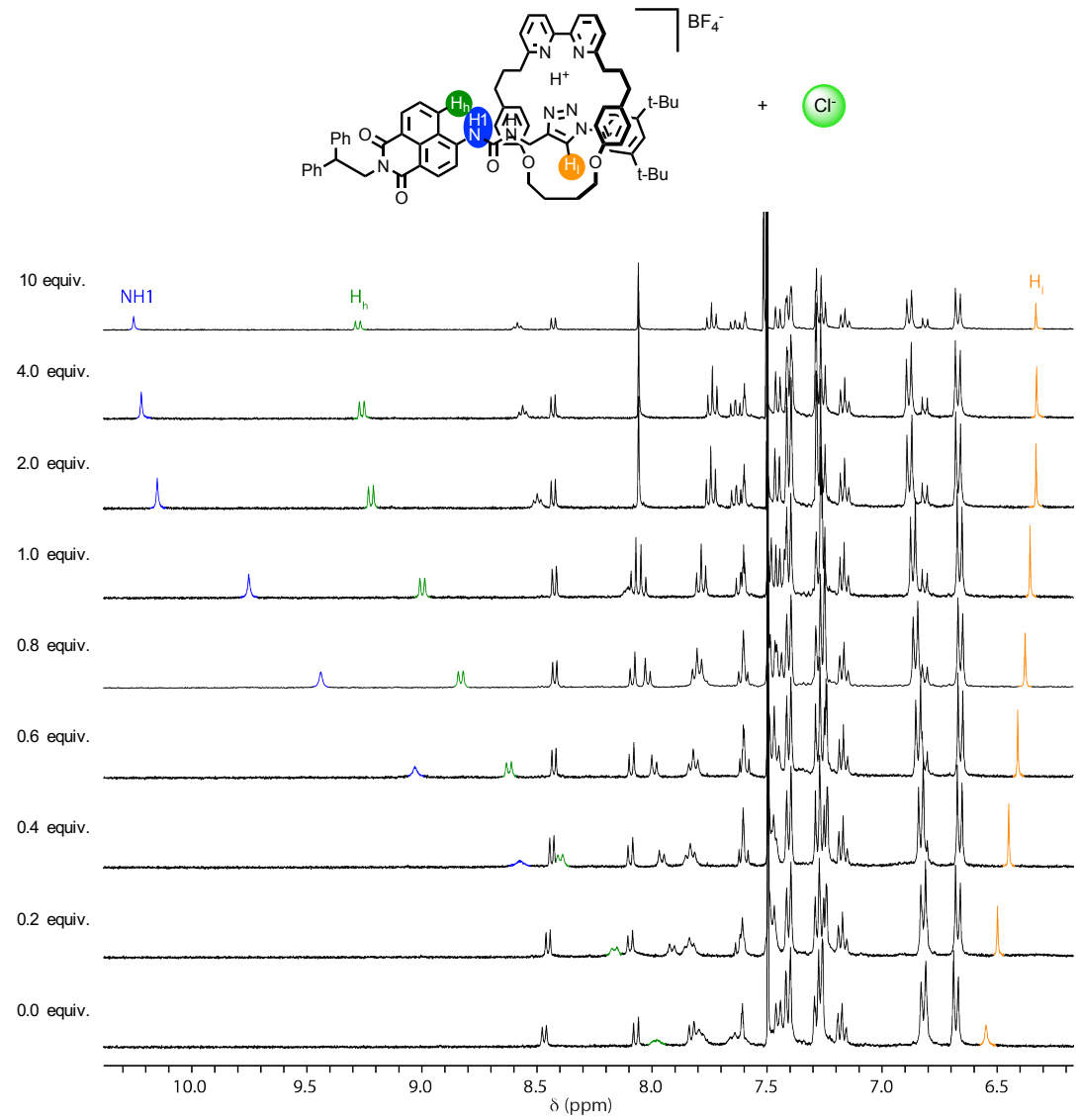

Figure 3. 20 Partial ^{1}H NMR titration ($CD_3CN/CDCl_3$ 1:1, 400 MHz, 298 K, 2.5 mM) of **120**.HBF_4 with TBACl.

X-ray analysis of single crystals obtained from slow evaporation of a solution of **120**.HBF_4 in $MeCN/CH_2Cl_2$ in the presence of 10 equivalent of TBACl allowed us confirm and observe the binding of anion by the receptor (Figure 3. 21). In the solid state, clear hydrogen-bond interactions can be observed between Cl^- and the urea NH as well as the naphthalimide proton H_h with distance of respectively 2.37 (NH2), 2.45 (NH1) and 2.63 Å. Moreover, the distance between the triazole proton H_l and the flanking aromatic of the macrocycle is shorter by 0.15 Å compare to **120**.HBF_4, suggesting stronger CH•••π contact (Figure 3. 21 a). These observations are consistent with the solution state observations made earlier. Interestingly, the π•••π interactions between the bipyridine moiety and the naphthalimide stopper seems to be enhanced upon binding of anion with a distance between the two planes shorter by 0.22 Å (Figure 3. 21 b).

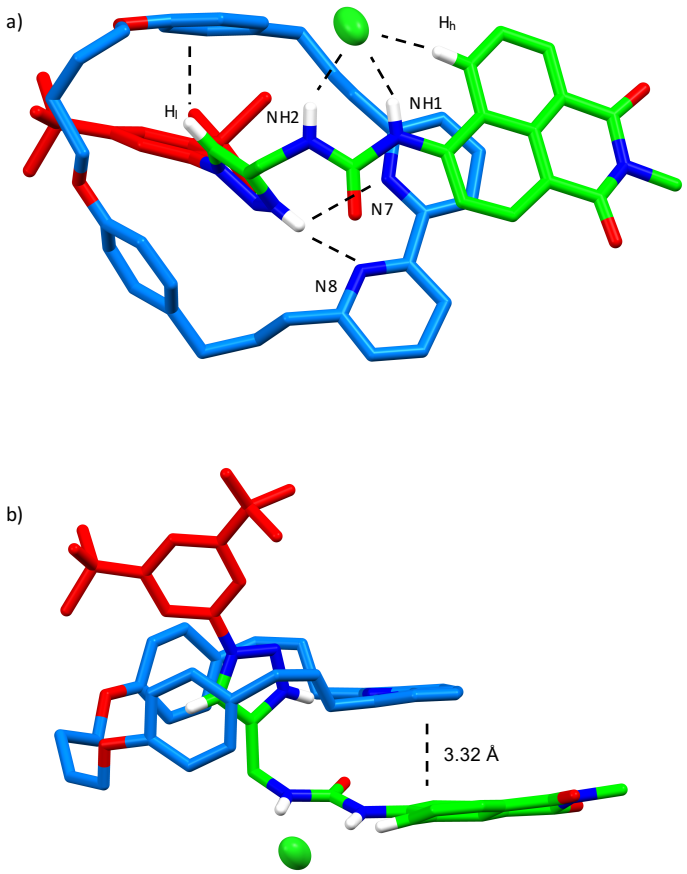

Figure 3. 21 Solid-state structure of **120**.HBF_4 binding chloride. The diphenyl head of the naphthalimide stopper has been truncated and the solvent as well as non-relevant hydrogens hidden for clarity. Black dotted lines correspond to short-contact interactions. Selected distances in Å: N7•••NH^+ = 2.04, N8•••H_l = 2.76, CH_l•••flanking aromatic = 2.80, NH1•••Cl = 2.46, NH2•••Cl = 2.38, CH_h•••Cl = 2.65.

Finally, we studied the optical response of the receptor. We observed that upon addition of increasing amount of Cl^- to a solution of **120**.HBF_4 the absorption of the naphthalimide unit was red shifted with a concomitant slight increase in intensity to create an isosbestic point, an outcome similar to that observed with non-interlocked axle **121**. Using this isosbestic for the fluorescence study, we noticed an increase in emission intensity upon binding of Cl^-, Br^-, HSO_4^-, MsO^- or TsO^- anions with a slight redshift (λ_{em} = 480 nm) (see ESI). However, although I^- displayed similar changes by ^1H NMR and UV-vis spectroscopy, the emission was quenched when binding to the receptor. We could tentatively assign this response as being due to Stern-Volmer-type collisional effect which competes with the switch-on response of weakly binding iodide.

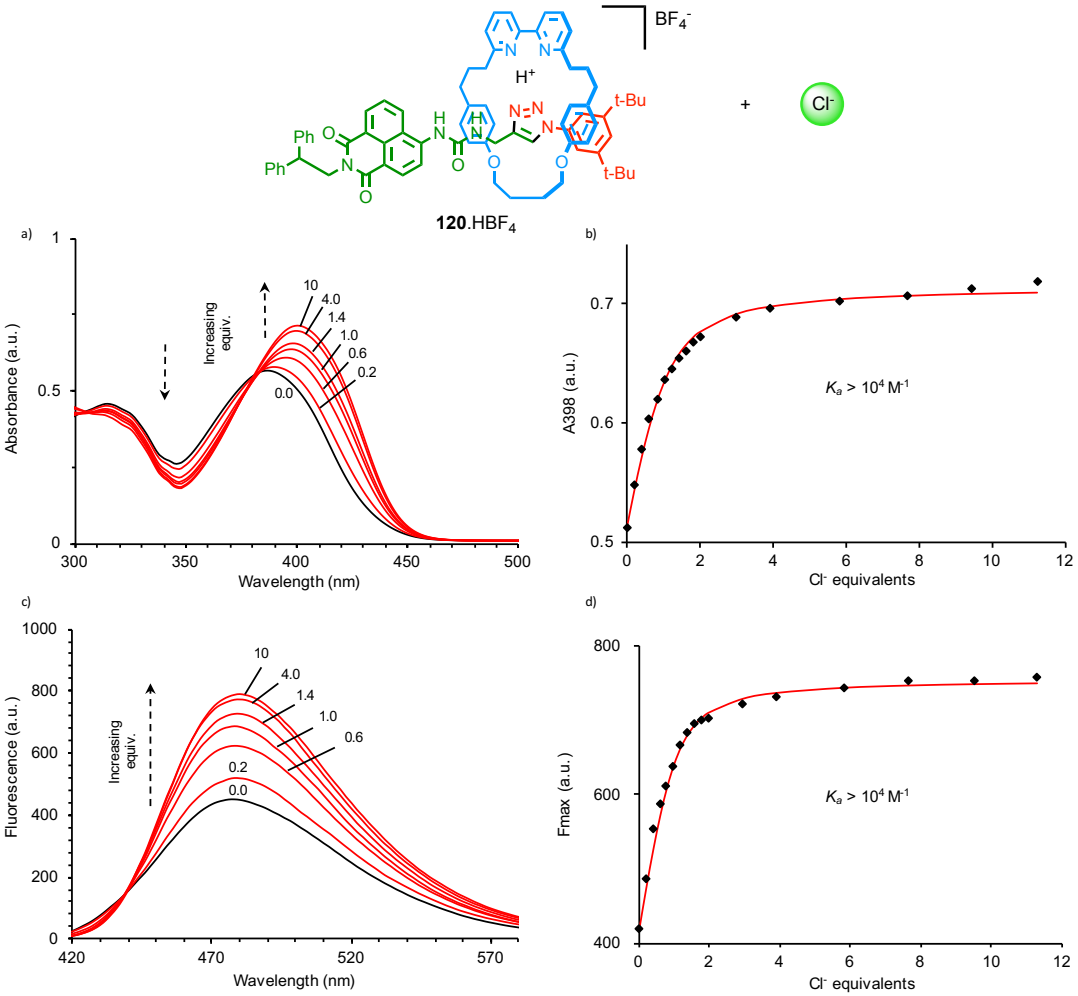

Figure 3. 22 UV-vis and fluorescence titration of **120**.HBF_4 with TBACl ($MeCN/CHCl_3$, 298 K, C = 130 μM). a) absorption spectra of **120**.HBF_4 in the presence of increasing equiv. of Cl^-, b) Fit for λ_{abs} = 398 nm versus equivalent of Cl^- added, c) fluorescence spectra (λ_{ex} = 381 nm) of **120**.HBF_4 in the presence of increasing equiv. of Cl^- and d) Fit for F_{max} versus equivalent of Cl^- added.

3.2.3. Comparison of the binding responses of rotaxane **120**.HBF_4 and axle **121**

Starting with the type of response, it is interesting to see that whereas **120**.HBF_4 exhibits a fluorescence switch-on response upon binding of anionic guests, the axle **121** fluorescence in contrast is switched-off. The reason behind this difference in behaviour is not clear at the moment. Indeed, in both cases the binding of the anion is expected to have a similar increasing effect on the electron density in the naphthalimide fluorophore and would be expected to enhance the stability of the excited state (on simple charge transfer grounds). The explanation probably is related to the bipyridine-naphthalimide π•••π interactions observed in both **120**.HBF_4 and **120**.HBF_4 bound to Cl^-, and obviously absent in the case of axle **121**. We have already observed that, in the solid state the distance between the two planes is reduced in the presence of an anionic guest. Moreover, it is possible that the binding event rigidifies the structure of the interlocked receptor thus reducing non-radiative decay pathways associated with bond rotation.

Anion	Binding constants (K_a) / M^{-1}		
	121	**120**.HBF_4	**120**
F^-	4930[a]	-[b]	-[d]
Cl^-	1780[a]	$>10^4$ ($28{,}000$[c])	-[d]
Br^-	390[a]	4660[a]	-[d]
I^-	70[a]	580[a]	-[d]
AcO^-	7770[a]	-[b]	-[d]
HSO_4^-	610[a]	2270[a]	-[d]
TsO^-	690[a]	1510[a]	-[d]
MsO^-	950[a]	2600[a]	-[d]

Table 3. 1 Binding constants of **120**, **120**.HBF_4 and **121** for a variety of anions. All titration experiments were carried out in 1:1 v/v $CDCl_3$-CD_3CN and the binding constants determined by non-linear regression analysis. Anions were added as their TBA salt. [a] Determined by ^1H NMR (c = 2.5 mM). [b] Deprotonation of the host was observed. [c] Determined by UV-vis (c = 130 μM). [d] No binding was observed.

Secondly, comparing the binding constants a clear number of differences appears. The first one being the possible deprotonation of **120**.HBF_4 to a state in which it does not possess any binding ability. This feature ensures that whereas the axle binds more basic anions with stronger affinity, it is not the case for the interlocked system which fails to bind AcO^- and F^-. The second difference is the fact that **120**.HBF_4 binds less basic anions much strongly than the neutral axle **121**. This is not so surprising as electrostatic interactions are expected to significantly stabilize the complex. However, it is noteworthy that **120**.BF_4 could not be synthesised, presumably due to the fact that the triazole moiety on its own is not basic enough to be protonated under these conditions, thus the presence of the threaded bipyridine ring is required.

Third and lastly, key differences observed in the relative order of binding strength of both receptors need to be highlighted. Whereas the binding affinity runs in the order $I^- < Br^- < HSO_4^- < TsO^- < MsO^- < Cl^-$ for axle **121**, the relative preference is the following for **120**.HBF_4 $I^- < HSO_4^- < TsO^- < MsO^- < Br^- < Cl^-$. Moreover, the difference in binding affinity between TsO^- and MsO^- is also more pronounced in the case of **120**.HBF_4 ($K_{a(MsO-)}/K_{a(TsO-)} = 1.72$) compared to the non-interlocked counterpart ($K_{a(MsO-)}/K_{a(TsO-)} = 1.38$). It would suggest that the presence of the mechanical bond provides a certain level of size selection in the case of the rotaxane. Br^- anion, with an anionic radius of 195 pm, is being preferred over the larger HSO_4^- (anionic radius of 206 pm), MsO^- and TsO^- anions. This goes in agreement with what has been previously reported in the field by Beer and co-workers.

3.3. Conclusions and Future Work

We have demonstrated that the AT-CuAAC reaction can be employed for the synthesis of mechanically interlocked receptor for anions in which functionalities used (bipyridine ligand) or generated (triazole unit) are not involved in the binding of the guest. This led to the serendipitous discovery of a mechanically interlocked system acting as a ditopic host for HX ion pairs. The binding strength is determined by two main factors: the strength of the hydrogen-bonding interaction between the host and the anion, and the pK_a of the anion itself.

We have shown that the rotaxane and the non-interlocked axle display opposite fluorescent responses to the binding of a guest. Whereas we are confident that the reason behind it lies in the interaction between the bipyridine and the naphthalimide units, more advanced computational studies will be needed to provide a better understanding of the system.

To conclude, there are several directions this project could follow. For example, it would be interesting to see, if by incorporating a longer spacer between the urea moiety and the triazole, the macrocycle could now be displaced to the triazole station in the presence of competitive hydrogen bond acceptor. In the current state of the system, even if the ring could be displaced to onto the triazole unit it would still be too close to the urea station to be able to neglect it entirely. This is even more true if we take in account that a triazole moiety is a relatively poor station for the bipyridine to bind to. Thus, another possibility would to incorporate within the thread a better competitive station such as an amide or a squareamide, and to see if in this case the macrocycle is able to impart selectivity. Finally, the receptor is at the moment specific to HX ion pairs. It would be useful to be able to expand the scope of ion-pairs guest by tuning the cavity so it can accommodate other cationic species of interest such as Li^+, Na^+ or K^+. In the long term, this would give us access to a family of receptors able to bind specific ion pairs depending on the nature of both the anion and cation which could have applications in the field of sensing and ion pair transport.

3.4. Experimental

General Experimental

Unless otherwise stated, all reagents and anhydrous solvents were purchased from commercial sources and used without further purification. All reactions were carried out under an atmosphere of N_2 using anhydrous solvents unless otherwise stated. Petrol refers to the fraction of petroleum ether boiling in the range 40-60 °C. DIPEA refers to N,N-diisopropylethylamine. NH_3-EDTA solution refers to an aqueous solution of NH_3 (17% w/w) with sodium-ethylenediaminetetraacetate (0.1 M). Flash column chromatography was performed using Biotage Isolera-4 automated chromatography system, employing Biotage SNAP or ZIP cartridges. Analytical TLC was performed on precoated silica gel plates (0.25 mm thick, 60F254, Merck, Germany) and observed under UV light. NMR spectra were recorded on Bruker AV400, AV3-400, AV500 or Bruker AV600 instrument, at a constant temperature of 298 K. Chemical shifts are reported in parts per million from low to high field and referenced to residual solvent. Coupling constants are reported in Hertz. Standard abbreviations indicating multiplicity were used as follows: m = multiplet, quint = quintet, q = quartet, t = triplet, d = doublet, s = singlet, app. = apparent, br = broad. Signal assignment was carried out using 2D NMR methods (HSQC, HMBC, COSY, NOESY) where necessary. In the case of some complex multiplets with contributions from more than one signal, absolute assignment was not possible, hence indicative assignments (e.g., H_A or H_B) are provided. Low resolution mass spectrometry (LRMS) was carried out by the mass spectrometry services at the University of Southampton using a Waters TQD mass spectrometer equipped with a triple quadrupole analyser with UHPLC injection (BEH C18 column, acetonitrile/hexane gradient with 0.2% formic acid). High resolution mass spectrometry (HRMS) was carried out by the mass spectrometry services at the University of Southampton using a MaXis (Bruker Daltonics) with a Time of Flight (TOF) analyser; samples were introduced into the mass spectrometer via a Dionex Ultimate 3000 autosampler and a UHPLC pump using a 20-100% acetonitrile/hexane gradient with 0.2% formic acid over 5 min at 0.6 mL/min (column: Acquity UPLC BEH C18 (Waters) 1.7 μm 50 × 2.1 mm).

3,5-di-*tert*-butylphenyl azide 103[24] and macrocycle 109[25] were synthesised following literature procedures.

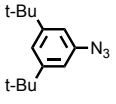

103

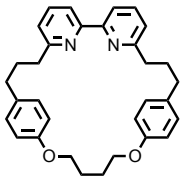

109

Experimental Data

*Compound (**102**)*

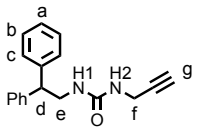

102

2,2-diphenylehtylamine (1.97 g, 10 mmol, 1 equiv.) was added in portions to a mixture of triphosgene (0.98 g, 3.3 mmol, 0.33 equiv.) in sat. $NaHCO_3/CH_2Cl_2$ (1:1, 70 mL) at 0ºC. The mixture was stirred at 0ºC for 1 h then propargylamine (0.63 mL, 10 mmol) was added and the reaction mixture was allowed to stir at room temperature for 16 h. The white precipitate formed was collected by suction filtration and dried under vacuum. The chlorinated layer from the filtrate was recovered, dried over $MgSO_4$, and concentrated. The resulting solid residue was washed with a petrol/CH_2Cl_2 mixture (2:1, 15 mL) affording more of **102** as a white solid (1.89 g, 68%). ^{1}H NMR ($CDCl_3$, 400 MHz, 298 K) δ 7.39 – 7.19 (m, 10H, H_a, H_b and H_c), 4.56 (m, 2H, -*NH*-), 4.19 (t, *J* = 7.9, 1H, H_d), 3.89 (dd, *J* = 5.5, 2.5, 2H, H_f), 3.83 (dd, *J* = 7.9, 5.7, 2H, H_e), 2.14 (t, *J* = 2.5, 1H, H_g). ^{13}C NMR ($CDCl_3$, 101 MHz, 298 K) δ 157.4, 142.1, 128.9, 128.3, 126.9, 80.6, 71.4, 51.2, 51.2, 45.0, 30.3. HRMS (ESI+) m/z = 279.1494 $[M+H]^+$ (calc. for $C_{18}H_{19}N_2O$ 279.1492).

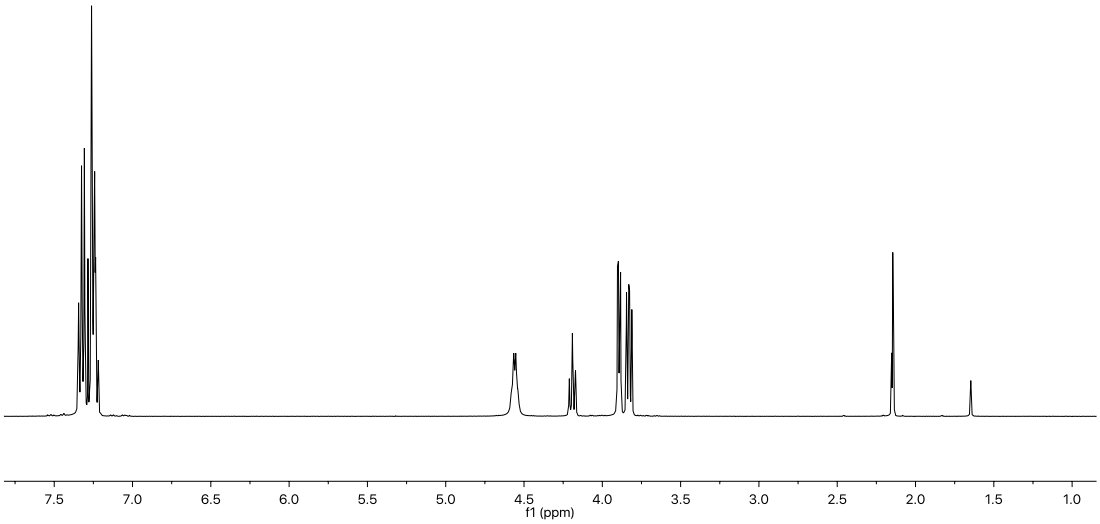

Figure S3. 1 ^{1}H NMR ($CDCl_3$, 400 MHz, 298 K) of **102**.

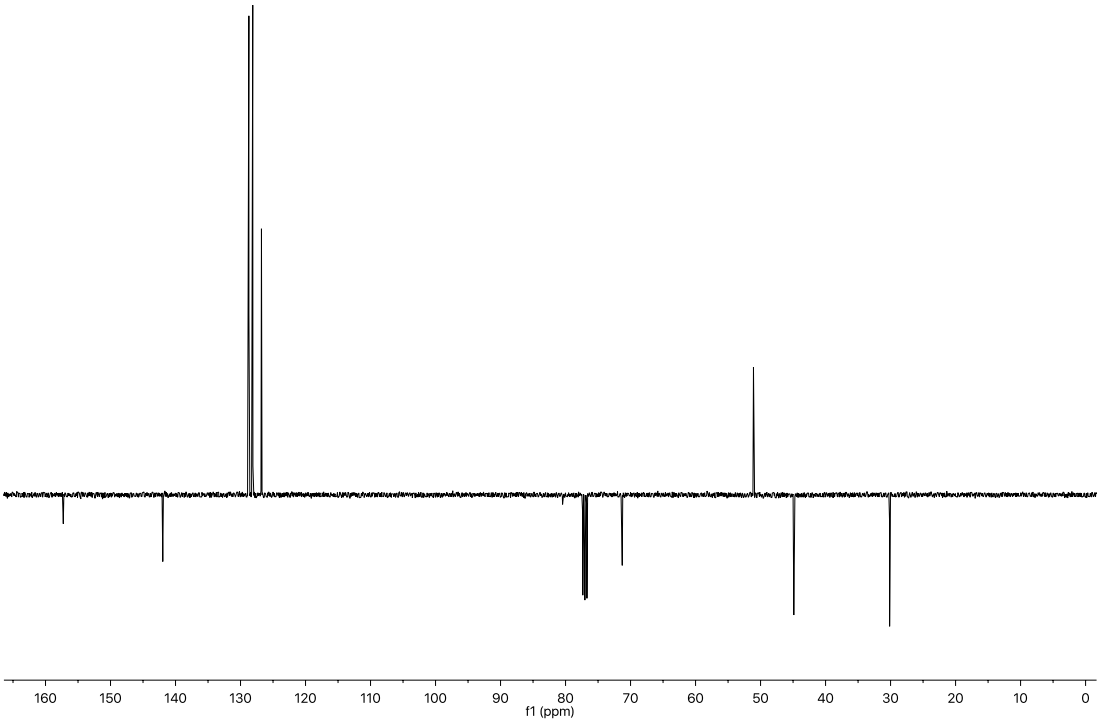

Figure S3. 2 J-MOD NMR ($CDCl_3$, 101 MHz, 298 K) of **102**.

*Rotaxane (**110**)*

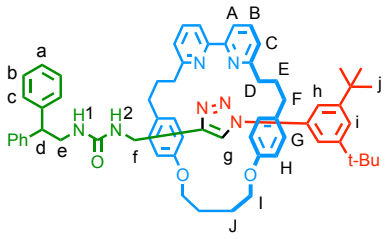

110

A dry CEM MW vial was charged with macrocycle **109** (47.8 mg, 0.1 mmol, 1 equiv.), azide **103** (23.1 mg, 0.1 mmol, 1 equiv.), alkyne **102** (27.8 mg, 0.1 mmol, 1 equiv.), and $[Cu(MeCN)_4]PF_6$ (35.7 mg, 0.096 mmol, 0.96 equiv.). THF (10 mL) was added, followed by DIPEA (18 µL, 0.025 mmol, 1 equiv.) and the reaction mixture stirred at r.t. for 4 h. NH_3-EDTA (20 mL) was added and the crude extracted with CH_2Cl_2 (3 x 25 mL). The combined organic layers were dried ($MgSO_4$) and concentrated *in vacuo*. The crude was purified *via* flash column chromatography on silica gel using a linear gradient of MeCN (0 – 15%) in a mixture of petrol/CH_2Cl_2 1:1, affording product **110** was obtained as a white foam (98 mg, 95%).^{1}H NMR ($CDCl_3$, 400 MHz, 298 K) δ 7.87 (s, 1H, H_g), 7.62 (t, *J* = 7.8, 2H, H_B), 7.43 (t, *J* = 1.8, 1H, H_i), 7.40 (d, *J* = 7.8, 2H, H_A), 7.38 (d, *J* = 1.8, 2H, H_h), 7.07 (d, *J* = 7.8, 2H, H_C), 7.00 – 6.86 (m, 10H, H_a, H_b and H_G), 6.86 – 6.78 (m, 8H, H_c and H_H), 6.74 (br s, 1H, -*NH2*-), 5.59 (s, 1H, -*NH1*-), 4.25 (m, 2H, H_I), 4.07 (m, 2H, H_I), 3.92 (d, *J* = 5.6, 2H, H_f), 3.24 (t, *J* = 7.9, 1H, H_d), 3.03 (dd, *J* = 7.9, 5.5, 2H, H_e), 2.67 (ddd, *J* = 13.4, 7.5, 3.9, 2H, H_F), 2.55 (ddd, *J* = 13.2, 8.7, 3.9, 2H, H_F), 2.49 – 2.32 (m, 4H, H_D), 2.18 – 1.94 (m, 4H, H_J), 1.89 – 1.66 (m, 4H, H_E), 1.32 (s, 18H, H_j). ^{13}C NMR ($CDCl_3$, 101 MHz, 298 K) δ 163.2, 157.7, 157.4, 155.9, 152.6, 148.1, 142.9, 137.1, 137.0, 132.6, 129.6, 128.0, 127.9, 126.0, 122.4, 121.7, 120.5, 119.6, 115.3, 115.1, 66.8, 51.5, 43.3, 36.1, 35.3, 31.4, 31.1, 25.2. HRMS (ESI+) *m/z* = 988.5831 $[M+H]^+$ (calc. for $C_{64}H_{74}N_7O_3$ 988.5848).

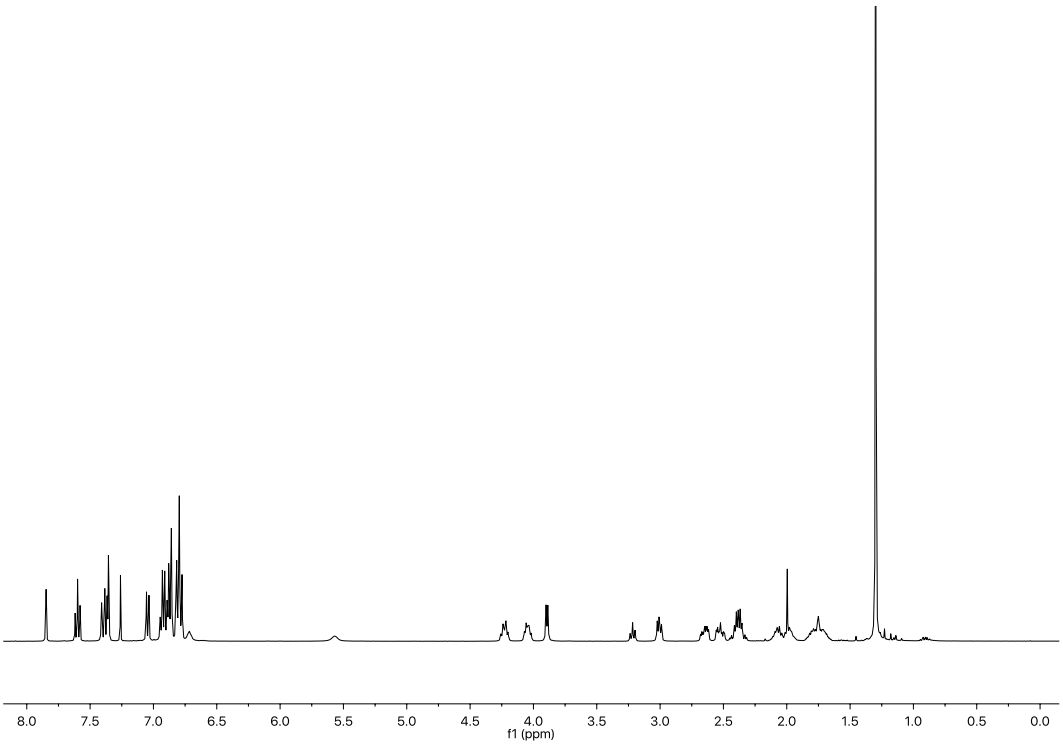

Figure S3. 3 ^{1}H NMR ($CDCl_3$, 400 MHz, 298 K) of **110**.

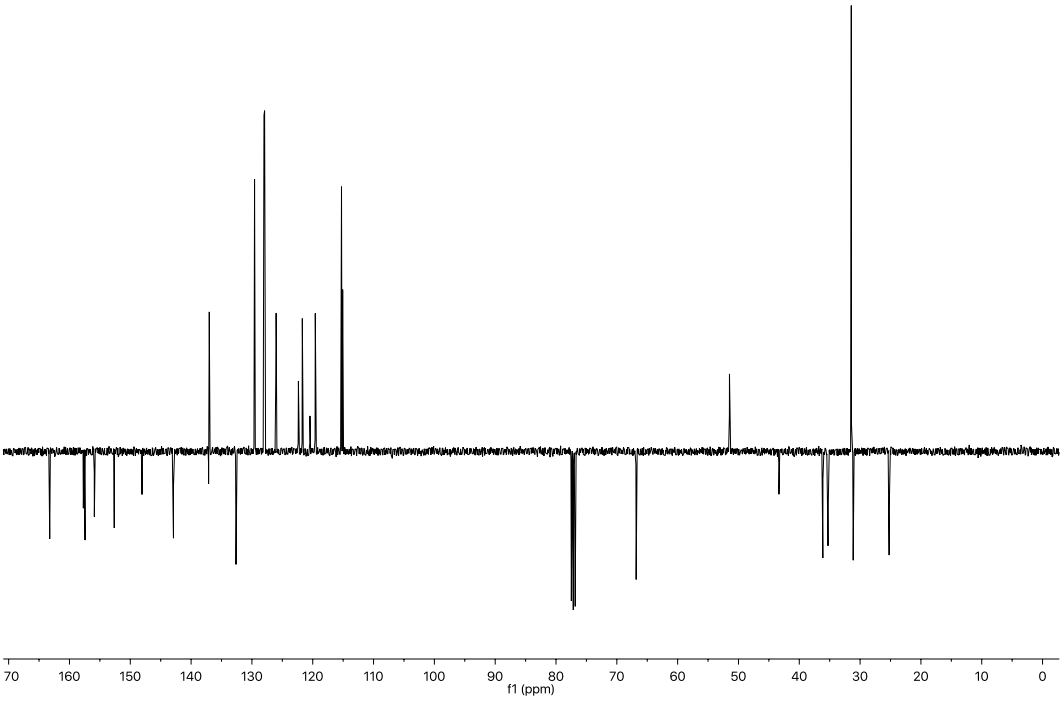

Figure S3. 4 J-MOD NMR ($CDCl_3$, 101 MHz, 298 K) of **110**.

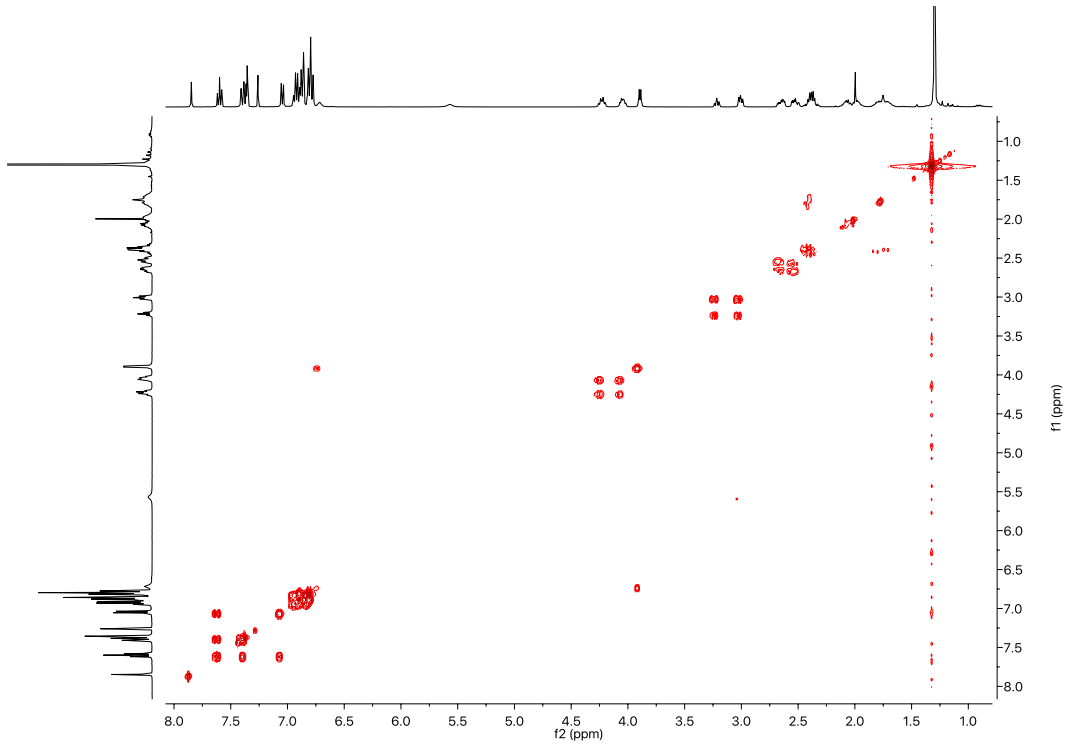

Figure S3. 5 COSY NMR ($CDCl_3$, 400 MHz, 298 K) of **110**.

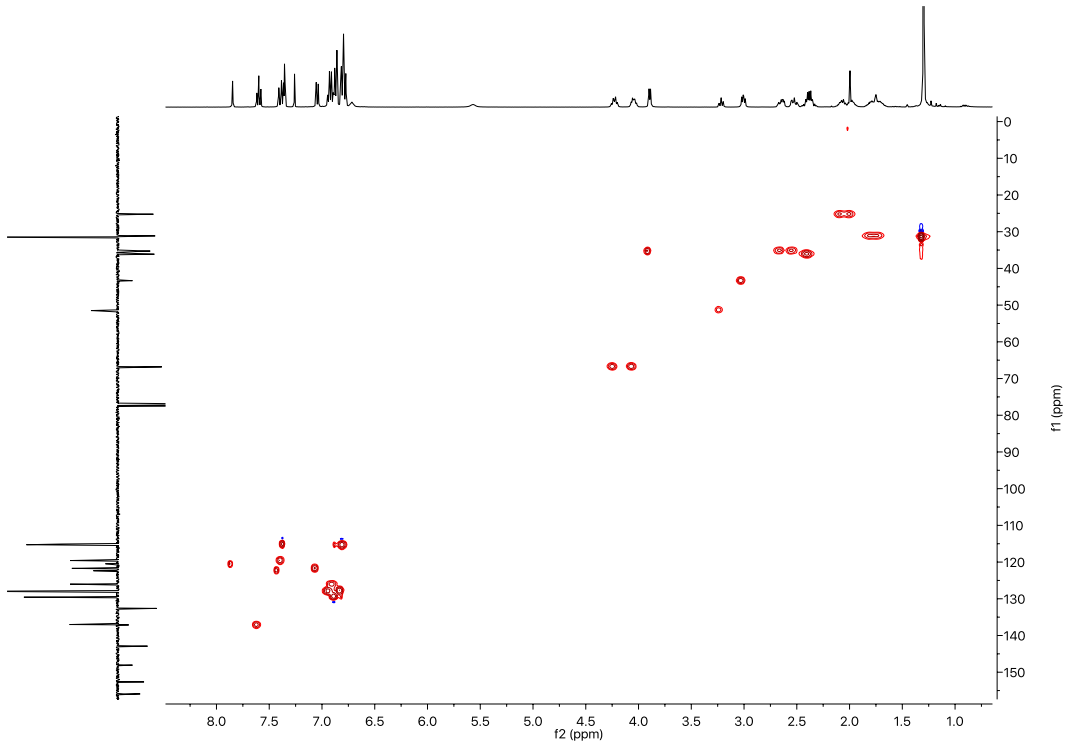

Figure S3. 6 HSQC NMR ($CDCl_3$, 400 MHz, 298 K) of **110**.

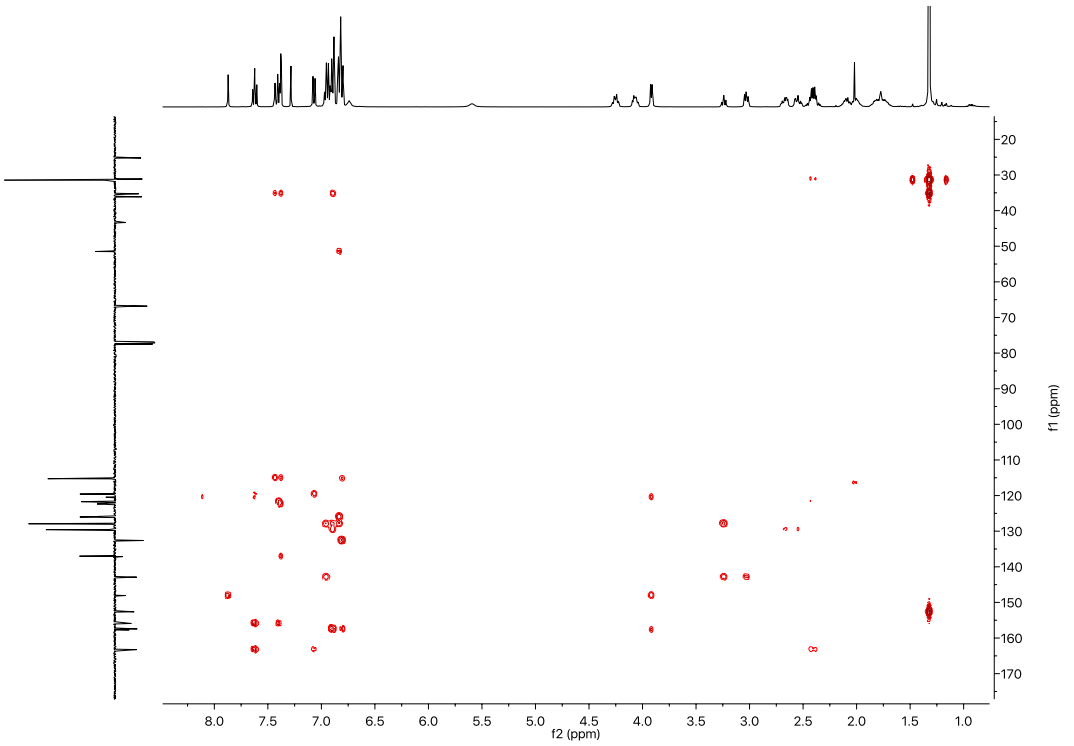

Figure S3. 7 HMBC NMR ($CDCl_3$, 400 MHz, 298 K) of **110**.

*Compound (**111**)*

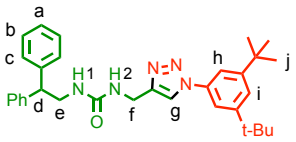

111

A dry CEM MW vial was charged with azide **103** (23.1 mg, 0.1 mmol, 1 equiv.), alkyne **102** (27.8 mg, 0.1 mmol, 1 equiv.), and $[Cu(MeCN)_4]PF_6$ (35.7 mg, 0.096 mmol, 0.96 equiv.). THF (10 mL) was added, followed by DIPEA (18 µL, 0.025 mmol, 1 equiv.) and the reaction mixture stirred at r.t. for 16 h. NH_3-EDTA (20 mL) was added and the crude extracted with CH_2Cl_2 (3 x 25 mL). The combined organic layers were dried ($MgSO_4$) and concentrated *in vacuo*. The crude was purified *via* flash column chromatography on silica gel using an isocratic elution of CH_2Cl_2/MeCN 3:1, affording product **111** was obtained as a white solid (42 mg, 82%).^{1}H NMR ($CDCl_3$, 400 MHz, 298 K) δ 7.93 (s, 1H, H_g), 7.51 (t, *J* = 1.7, 1H, H_i), 7.48 (d, *J* = 1.7, 2H, H_h), 7.26 – 7.11 (m, 10H, H_a, H_b and H_c), 5.38 (t, *J* = 5.9, 1H, -*NH2*-), 4.78 (t, *J* = 5.8, 1H, -*NH1*-), 4.42 (d, *J* = 5.9, 2H, H_f), 4.17 (t, *J* = 7.9, 1H, H_d), 3.83 (dd, *J* = 7.9, 5.8, 2H, H_e), 1.37 (s, 18H, H_j). ^{13}C NMR ($CDCl_3$, 101 MHz, 298 K) δ 158.0, 152.9, 146.4, 142.2, 136.9, 128.7, 128.2, 126.8, 123.1, 121.0, 115.6, 51.3, 45.0, 35.7, 35.3, 31.5. HRMS (ESI+) *m/z* = 510.3224 $[M+H]^+$ (calc. for $C_{32}H_{40}N_5O$ 510.3227).

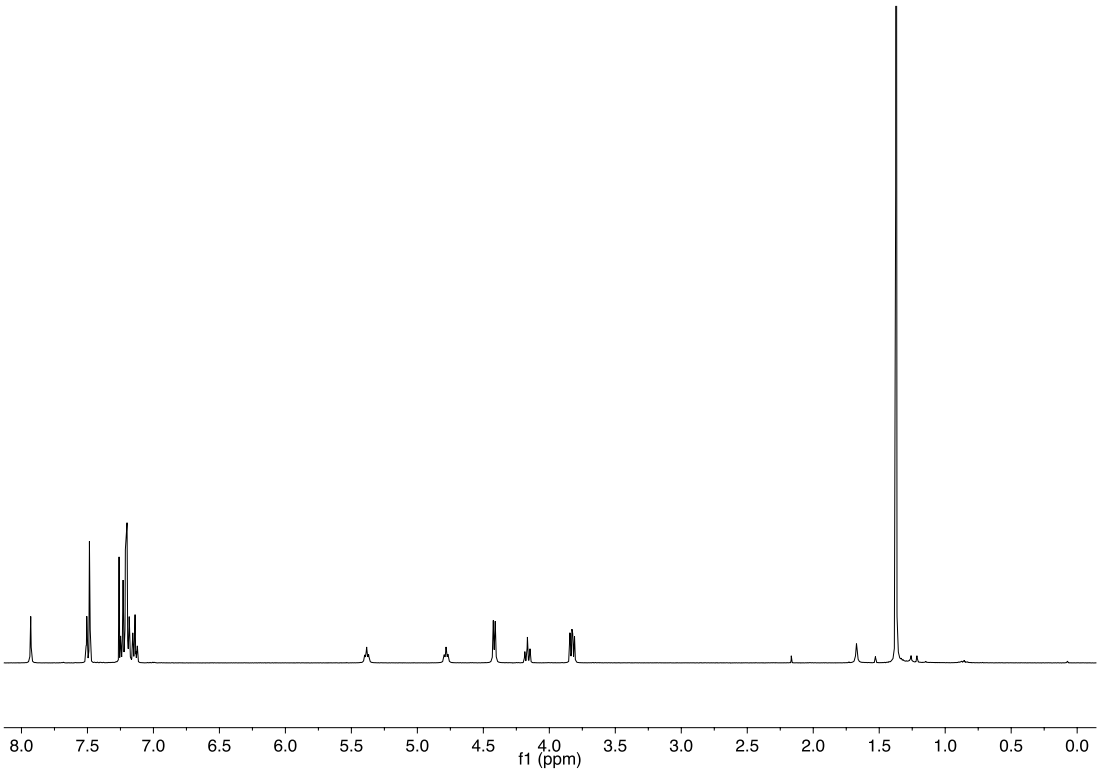

Figure S3. 8 ^{1}H NMR ($CDCl_3$, 400 MHz, 298 K) of **111**.

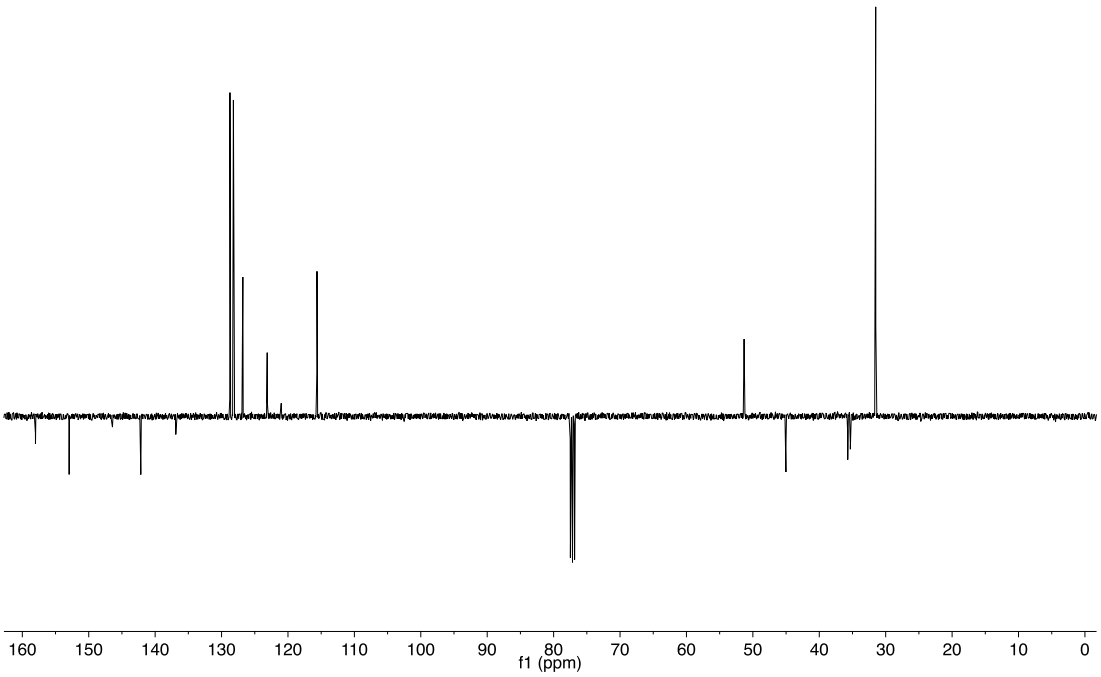

Figure S3. 9 J-MOD NMR ($CDCl_3$, 101 MHz, 298 K) of **111**.

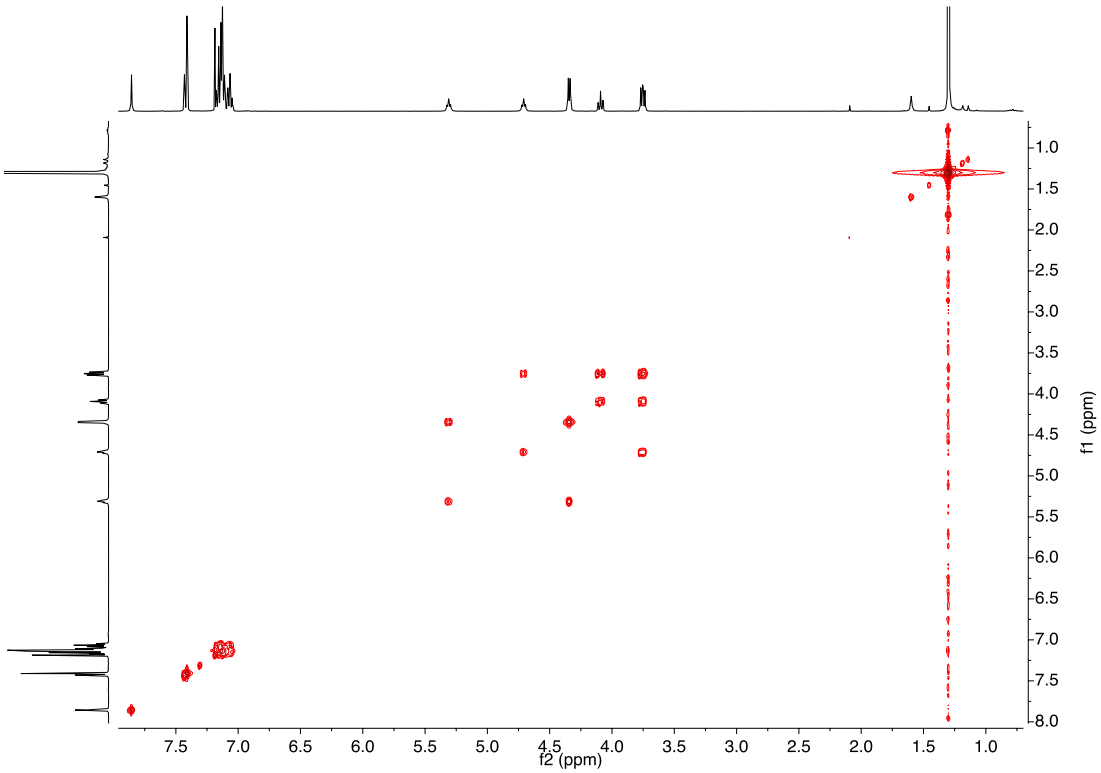

Figure S3. 10 COSY NMR ($CDCl_3$, 400 MHz, 298 K) of **111**.

*Compound (**117**)*

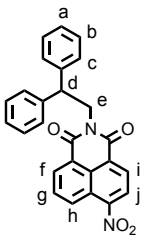

117

4-Nitro-1,8-naphthalic anhydride (500 mg, 2.1 mmol, 1 equiv.) was dissolved in EtOH (15 mL). Diphenyl ethylamine (490 mg, 2.5 mmol, 1.2 equiv.) was added to the solution and the mixture was refluxed at 80 °C for 18 h. After cooling to r.t., the crude mixture was evaporated *in vacuo* and purified by flash column chromatography using an isocratic elution of petrol/CH_2Cl_2 1:1, affording compound **117** as a yellow foam (750 g, 86%). ^{1}H NMR ($CDCl_3$, 400 MHz, 298 K) δ 8.79 (dd, *J* = 8.7, 1.0, 1H, H_h), 8.64 (dd, *J* = 7.3, 1.0, 1H, H_f), 8.58 (d, *J* = 8.0, 1H, H_j), 8.34 (d, *J* = 8.0, 1H, H_i), 7.93 (dd, *J* = 8.7, 7.4, 1H, H_g), 7.37-7.32 (m, 4H, H_c), 7.27-7.21 (m, 4H, H_b), 7.18-7.13 (m, 2H, H_a), 4.89-4.85 (m, 2H, H_e), 4.82-4.71 (m, 1H, H_d). ^{13}C NMR ($CDCl_3$, 101 MHz, 298 K) δ 163.3, 162.4, 149.5, 141.3, 132.4, 129.9, 129.7, 129.3, 128.9, 128.4, 128.4, 126.8, 126.7, 123.8, 123.6, 122.8, 48.5, 44.8. IR: (ν_{max}/cm^{-1}) 3405, 2905, 1692, 1620, 1577, 1520, 1375, 1313, 1226, 1181, 989. M.p. (°C) 40-43. LRMS (ESI+) m/z = 423 $[M+H]^+$.

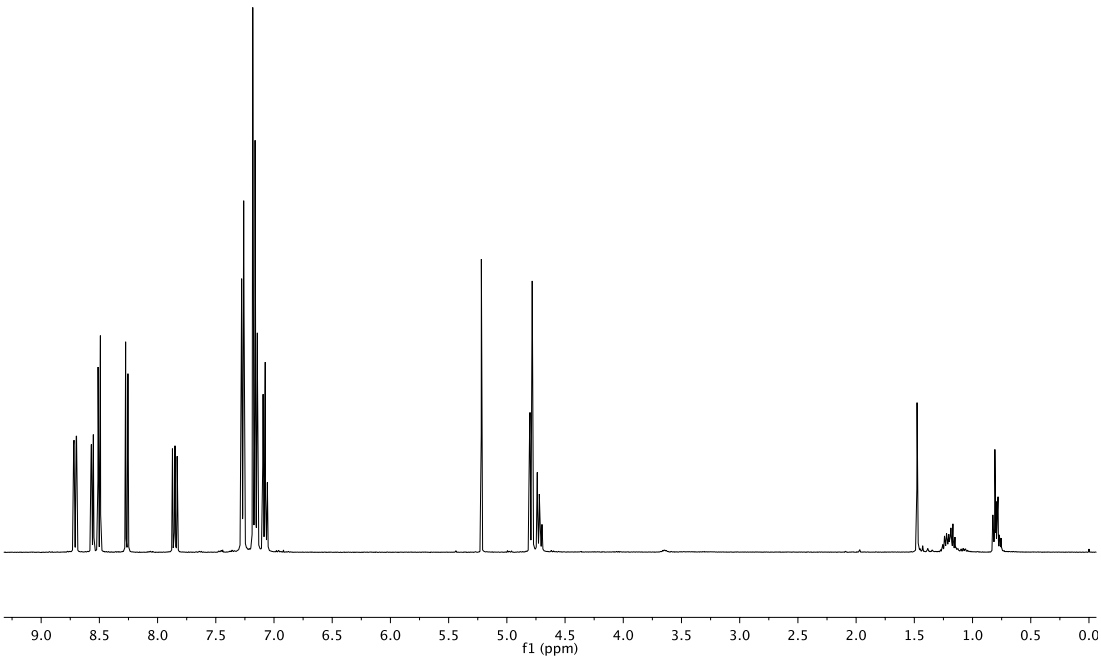

Figure S3. 11 ^{1}H NMR ($CDCl_3$, 400 MHz, 298 K) of **117**.

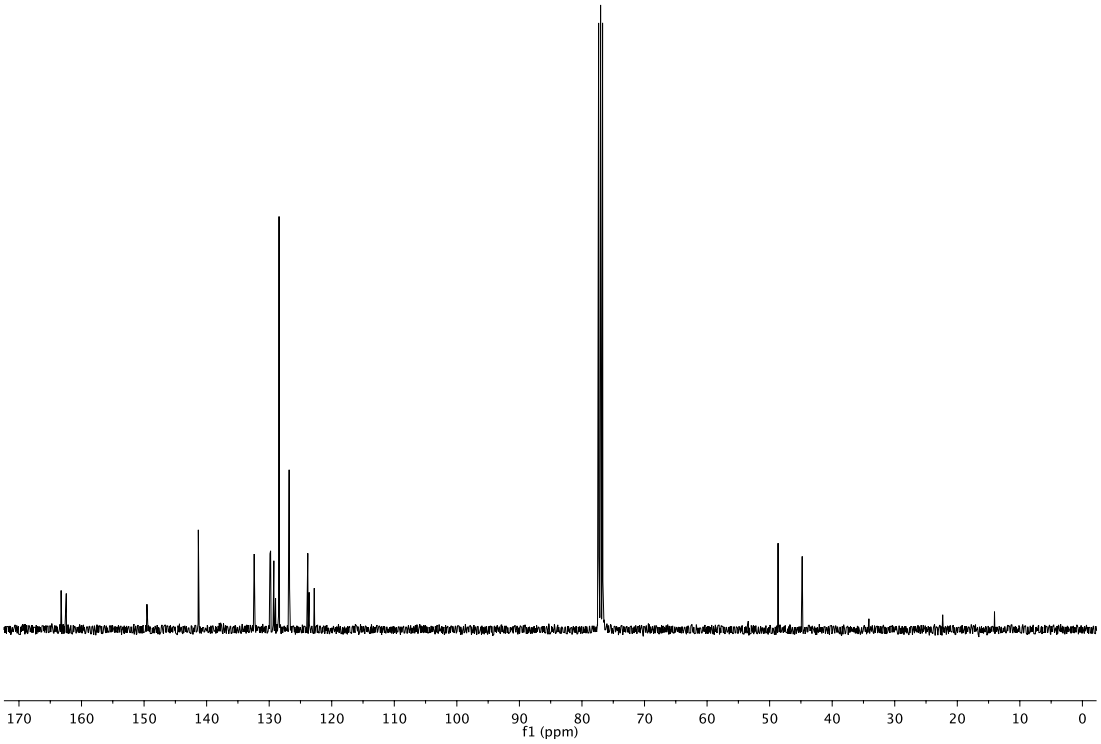

Figure S3. 12 ^{13}C NMR ($CDCl_3$, 101 MHz, 298 K) of **117**.

*Compound (**118**)*

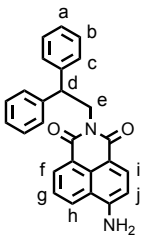

118

Nitro-compound **117** (360 mg, 0.95 mmol, 1 equiv.) was hydrogenated in MeOH/EtOAc (1:1, 20 mL) at r.t. under a hydrogen atmosphere, using a Pd/C catalyst (5%wt, 200 mg, 0.095 mmol, 0.1 equiv.). The reaction was monitored by TLC until all starting material had been consumed (~4 h). The reaction mixture was filtered through Celite, washed with MeOH/EtOAc (1:1), and the solvent evaporated *in vacuo,* affording aniline **118** as a yellow solid (0.36 g, 97%). ^{1}H NMR ($(CD_3)_2SO$, 400 MHz, 298 K) δ 8.57 (d, *J* = 8.0, 1H, H_h), 8.34 (d, *J* = 6.8, 1H, H_f), 8.12 (d, *J* = 8.4, 1H, H_i), 7.60 (dd, *J* = 7.7, 8.0, 1H, H_g), 7.42 (br s, 1H, -NH_2-), 7.35-7.30 (m, 4H, H_c), 7.26-7.20 (m, 4H, H_b), 7.16-7.11 (m, 2H, H_a), 7.80 (d, *J* = 8.4, 1H, H_j), 4.73-4.69 (m, 3H, H_d and H_e).^{13}C NMR ($(CD_3)_2SO$, 101 MHz, 298 K) δ 163.8, 162.9, 152.6, 142.2, 133.9, 130.9, 129.6, 129.3, 128.2, 128.0, 126.4, 123.9, 121.6, 119.2, 108.1, 107.3, 48.4, 43.3. IR: (ν_{max}/cm^{-1}) 3505, 3349, 3225, 2358, 1648, 1592, 1375, 1246, 1017. 982. M.p. (°C) 95-96. HRMS (ESI+) m/z = 393.1599 [M+H$^+$] (calc. for $C_{26}H_{21}N_2O_2$ 393.1598).

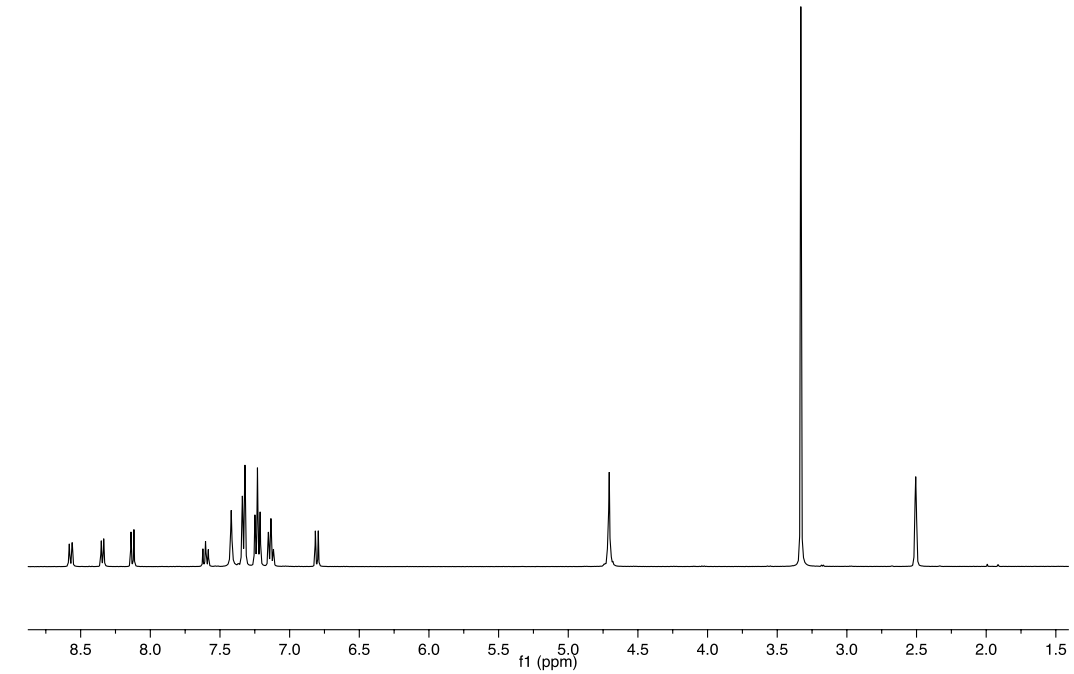

Figure S3. 13 ^{1}H NMR ($(CD_3)_2SO$, 400 MHz, 298 K) of **118**.

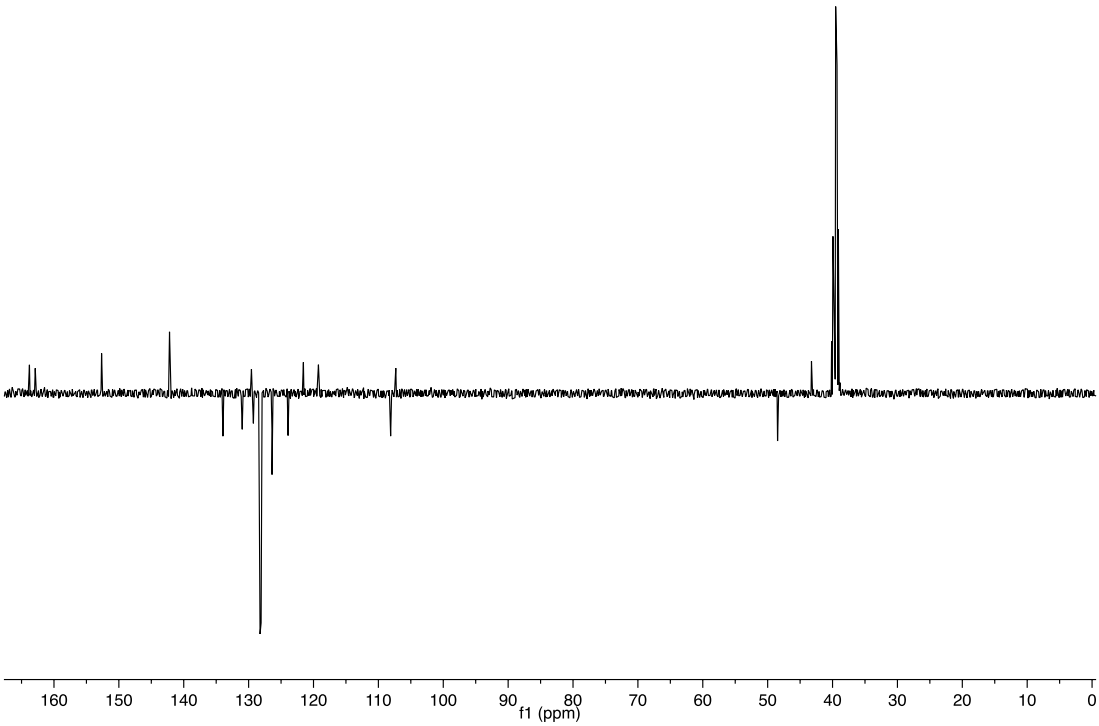

Figure S3. 14 J-MOD NMR ($(CD_3)_2SO$, 101 MHz, 298 K) of **118**.

*Compound (**119**)*

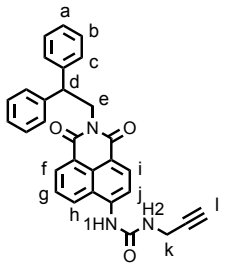

119

To a stirred suspension of amine **118** (98 mg, 0.25 mmol, 1 equiv.) and DMAP (61 mg, 0.5 mmol, 2 equiv.) in CH_2Cl_2 (10 mL) at -10 °C was added triphosgene (24 mg, 0.08 mmol, 0.33 equiv.) as a solution in toluene (1 mL). The resulting solution was kept -10 °C for 1 h. Propargylamine (32 μL, 0.5 mmol, 2 equiv.) was then added and the mixture allowed to stir at room temperature for 3 h. The solvent was concentrated *in vacuo* and the crude residue purified *via* flash column chromatography on silica gel using a linear gradient of EtOAc (5 – 20%) in petrol, affording pure product **119** as a pale yellow solid (77 mg, 65%).^{1}H NMR ($(CD_3)_2SO$, 400 MHz, 298 K) δ 9.31 (s, 1H, -*NH1*-), 8.56 (dd, *J* = 8.6, 1.0, 1H, H_h), 8.46 (d, *J* = 8.5, 1H, H_g), 8.43 (dd, *J* = 7.3, 1.0, 1H, H_j), 8.35 (d, *J* = 8.4, 1H, H_f), 7.83 (dd, *J* = 8.6, 7.3, 1H, H_i), 7.33 (d, *J* = 7.0, 4H, H_c), 7.23 (t, *J* = 7.6, 5H, H_b and -*NH2*-), 7.13 (t, *J* = 7.3, 2H, H_a), 4.80 – 4.61 (m, 3H, H_d and H_e), 4.01 (dd, *J* = 5.6, 2.5, 2H, H_k), 3.20 (t, *J* = 2.5, 1H, H_l) ^{13}C NMR ($(CD_3)_2SO$, 101 MHz, 298 K) δ 163.5, 162.9, 154.1, 142.0, 132.5, 130.8, 128.3 (overlap with quaternary according to HMBC), 128.1, 126.5, 126.1, 122.1, 121.9, 114.4, 114.4, 81.4, 73.4, 48.4, 43.5, 28.9. HRMS (ESI+) m/z = 474.1813 $[M+H]^+$ (calc. for $C_{30}H_{24}N_3O_3$ 474.1812).

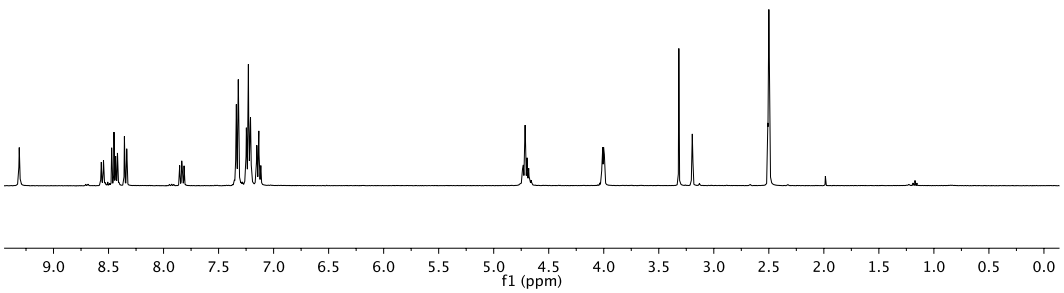

Figure S3. 15 ^{1}H NMR ($(CD_3)_2SO$, 400 MHz, 298 K) of **119**.

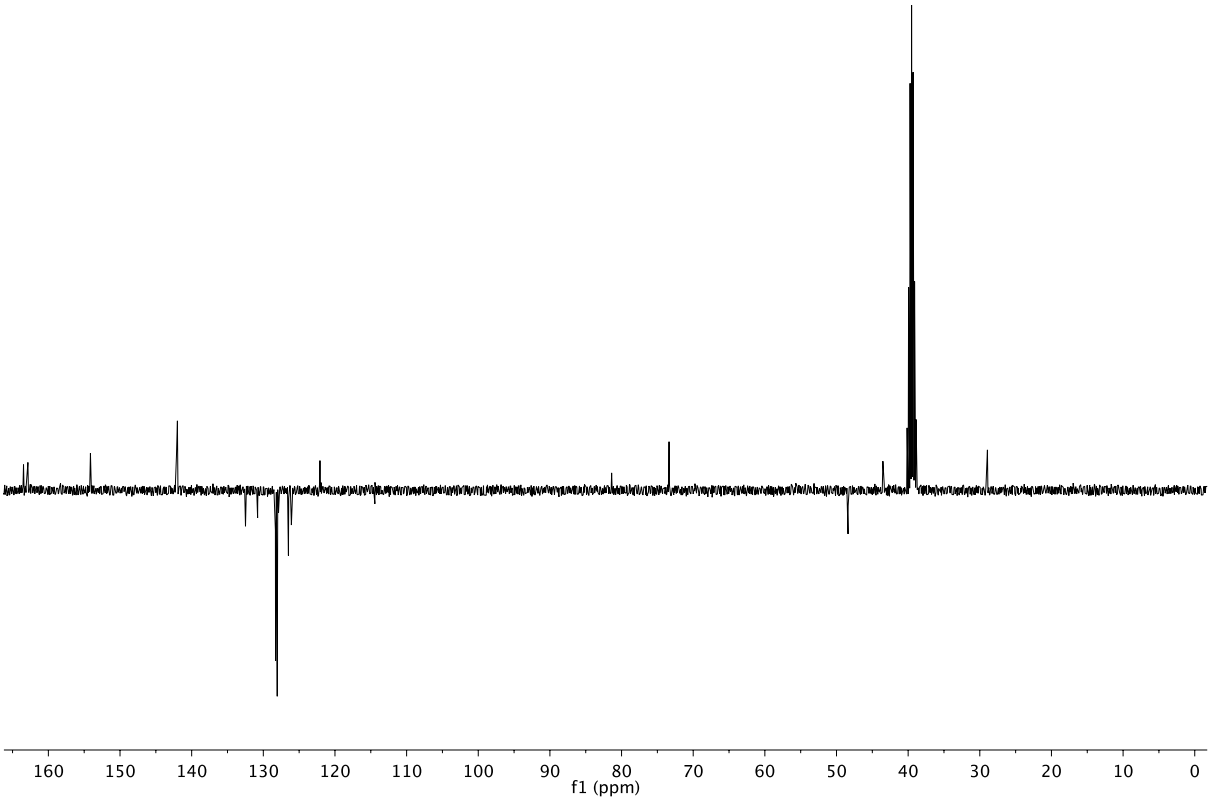

Figure S3. 16 J-MOD NMR ($(CD_3)_2SO$, 101 MHz, 298 K) of **119**.

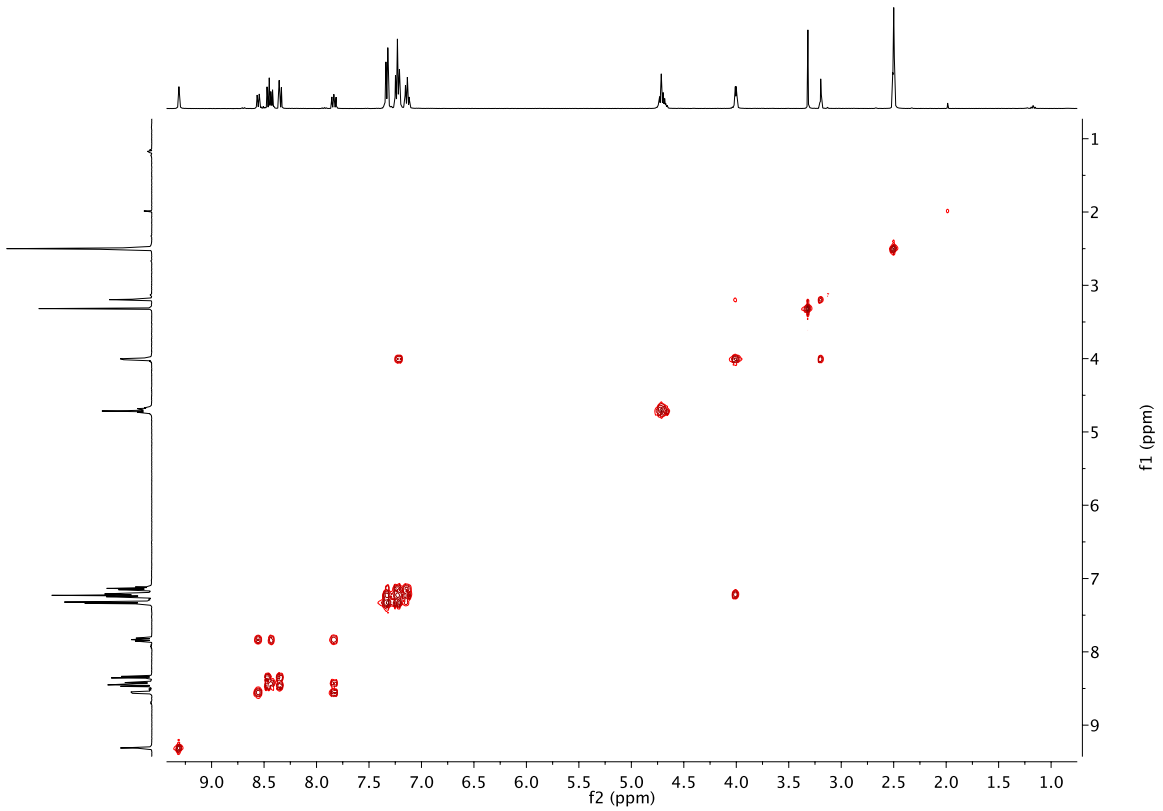

Figure S3. 17 COSY NMR ($(CD_3)_2SO$, 400 MHz, 298 K) of **119**.

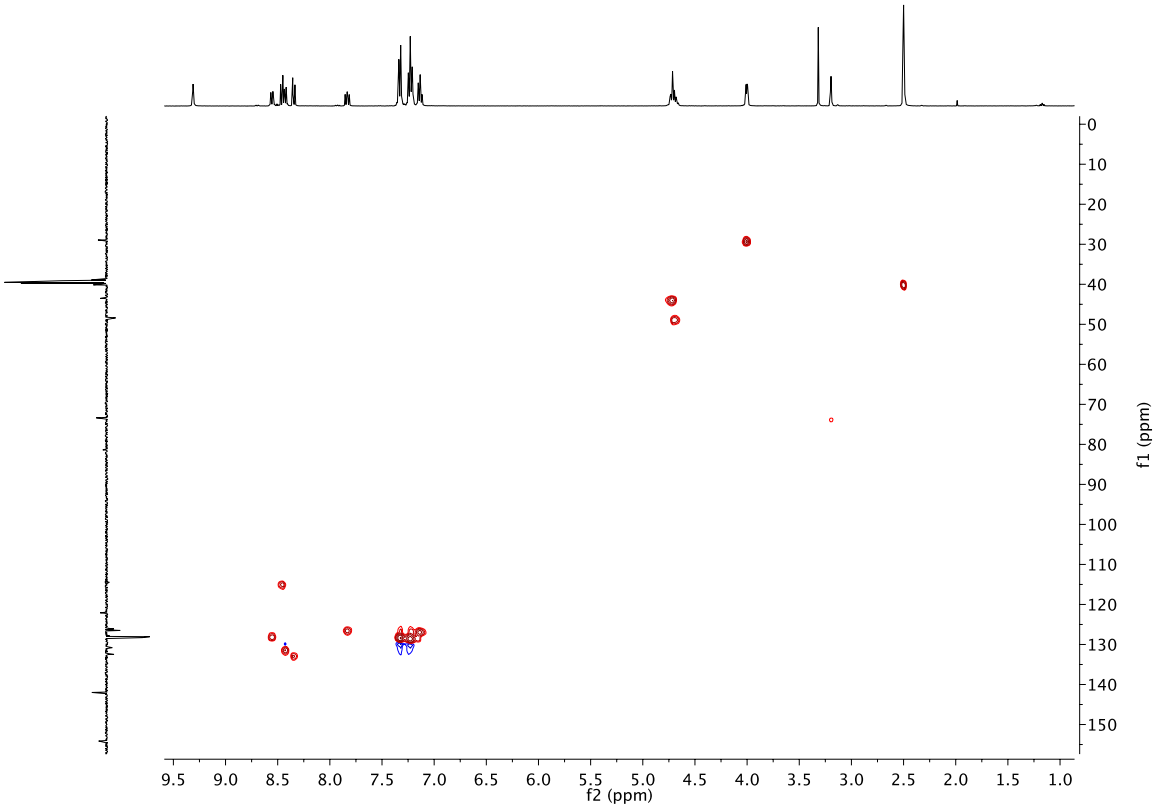

Figure S3. 18 HSQC NMR ($(CD_3)_2SO$, 400 MHz,298 K) of **119**.

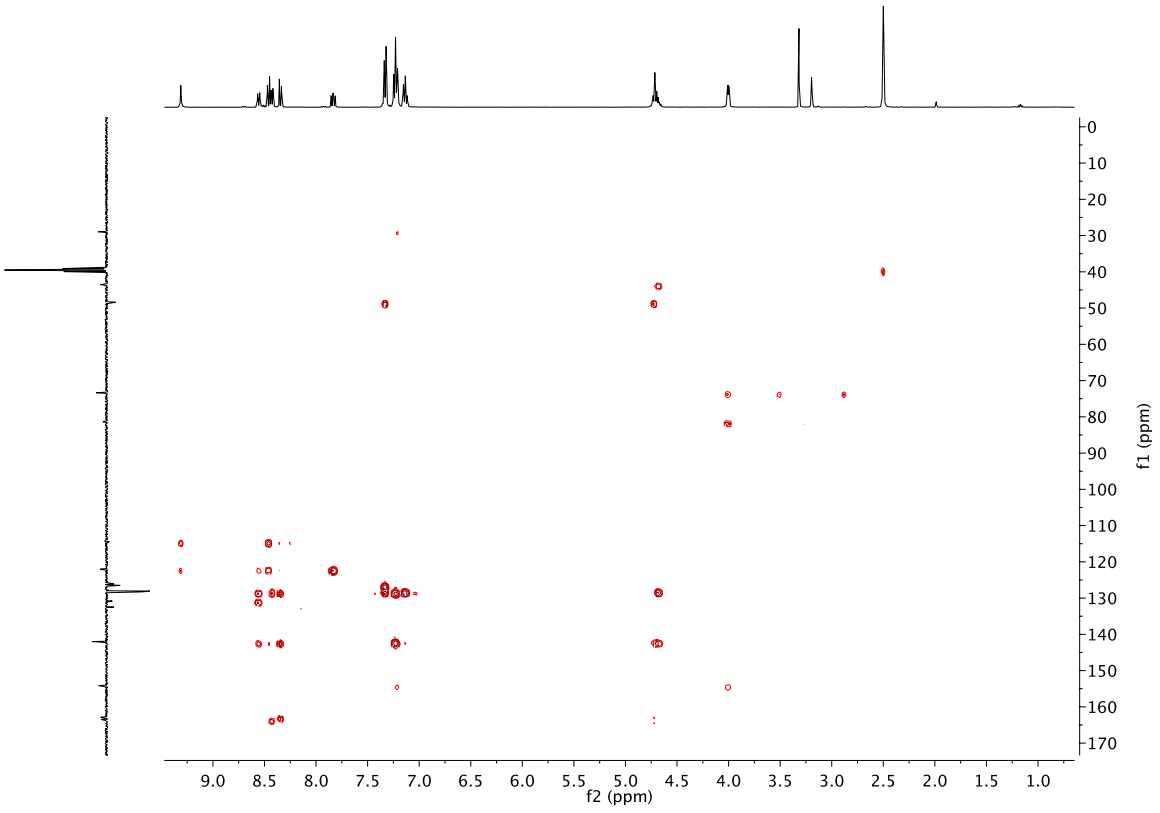

Figure S3. 19 HMBC NMR ($(CD_3)_2SO$, 400 MHz, 298 K) of **119**.

*Rotaxane (**120**)*

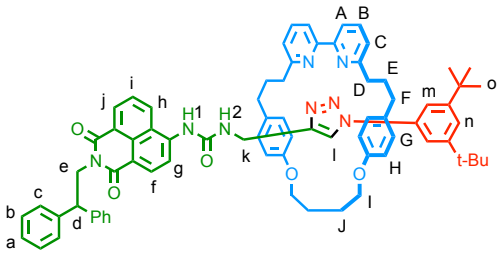

120

A dry CEM MW vial was charged with macrocycle **109** (12 mg, 0.025 mmol, 1 equiv.), azide **103** (5.8 mg, 0.025 mmol, 1 equiv.), alkyne **119** (12 mg, 0.025 mmol, 1 equiv.), and $[Cu(MeCN)_4]PF_6$ (8.9 mg, 0.024 mmol, 0.96 equiv.). CH_2Cl_2 (1 mL) was added, followed by DIPEA (4.4 µL, 0.025 mmol, 1 equiv.) and the reaction mixture stirred at r.t. for 4 h. NH_3-EDTA (5 mL) was added and the crude extracted with CH_2Cl_2 (3 x 5 mL). The combined organic layers were dried ($MgSO_4$) and concentrated *in vacuo*. The crude was purified *via* flash column chromatography on silica gel with an isocratic elution of petrol/CH_2Cl_2/MeCN/NH_3 46:46:7:1, affording product **120** was obtained as a yellow foam (27 mg, 92%).^{1}H NMR ($CDCl_3$, 400 MHz, 298 K) δ 9.16 (s, 1H, NH1), 8.51 (d, *J* = 8.5, 1H, H_f), 8.26 – 8.21 (m, 2H, H_j and H_g), 7.67 (t, *J* = 7.8, 2H, H_B), 7.57 (d, *J* = 5.5, 1H, NH2), 7.54 (d, *J* = 8.0, 2H, H_A), 7.50 (d, *J* = 8.5, 1H, H_h), 7.47 (t, *J* = 1.7, 1H, H_n), 7.44 (s, 1H, H_l), 7.41 – 7.36 (m, 6H, H_c and H_m), 7.23 (t, *J* = 7.9, 4H, H_b), 7.16 – 7.08 (m, 4H, H_C and H_a), 6.88 (dd, *J* = 8.5, 7.3, 1H, H_i), 6.71 (d, *J* = 8.7, 4H, H_H), 6.67 (d, *J* = 8.7, 4H, H_G), 4.92 – 4.80 (m, 3H, H_e and H_d), 4.34 – 4.21 (m, 4H, H_I), 3.81 (d, *J* = 5.5, 2H, H_k), 2.63 – 2.29 (m, 8H, H_D and H_F), 2.23 – 2.10 (m, 4H, H_J), 1.83 – 1.61 (m, 4H, H_E), 1.36 (s, 18H, H_o). ^{13}C NMR ($CDCl_3$, 101 MHz, 298 K) δ 164.8, 164.2, 163.9, 157.7, 156.0, 153.3, 152.8, 146.5, 143.0, 142.2, 138.0, 137.0, 133.7, 132.3, 130.4, 129.3, 129.1, 128.7, 128.4, 127.1, 126.6, 124.4, 122.7, 122.7, 122.6, 122.0, 120.1, 115.3, 115.2, 114.4, 114.1, 66.7, 49.0, 44.4, 36.1, 35.3, 35.0, 34.8, 31.5, 31.4, 25.2. LRMS (ESI+) m/z = 1184.1 $[M+H]^+$.

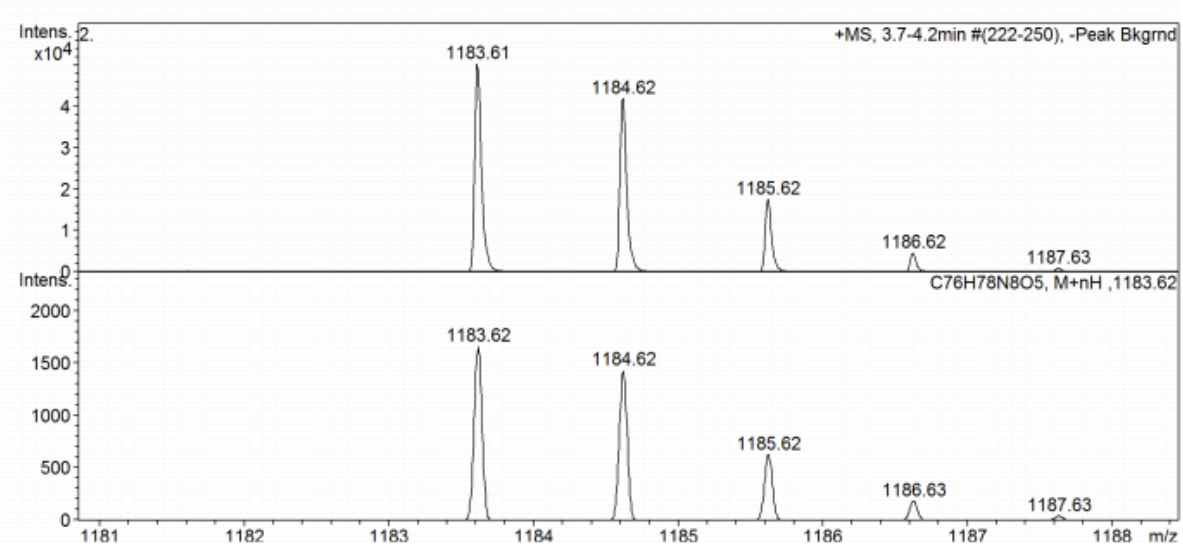

Figure S3. 20 Isotope pattern of **120**.

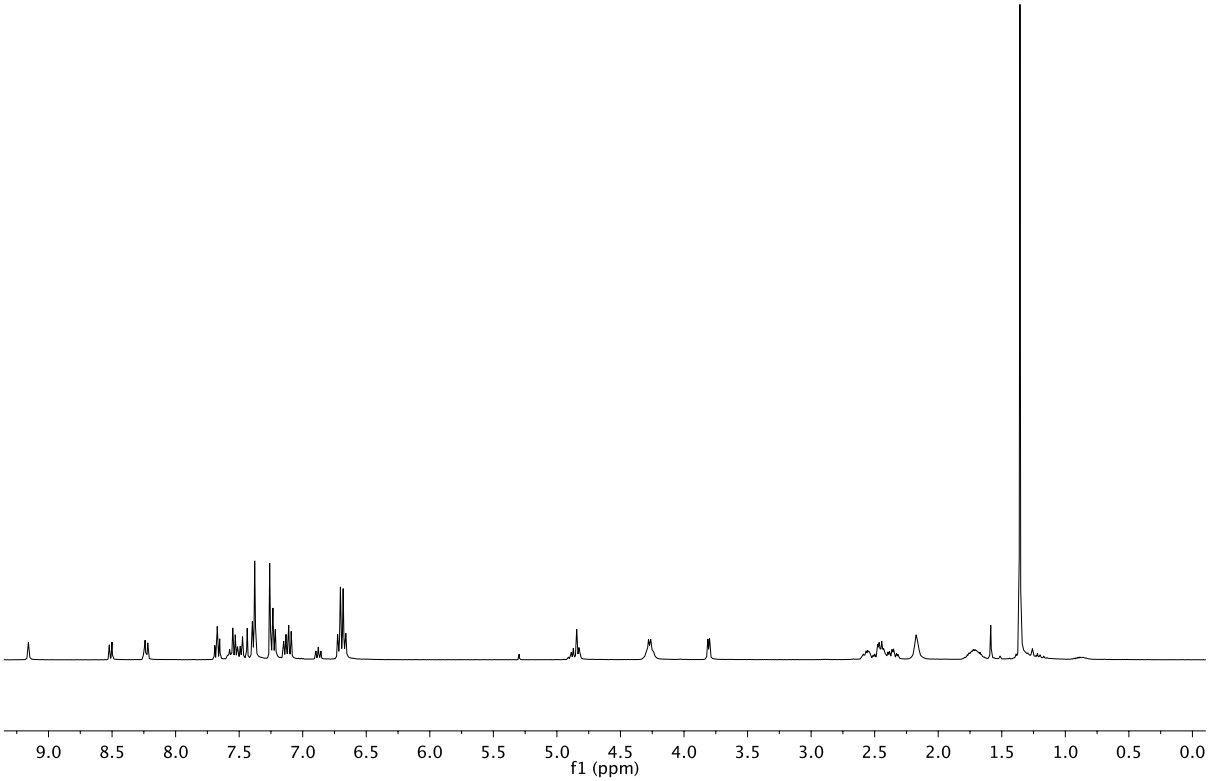

Figure S3. 21 ^{1}H NMR ($CDCl_3$, 400 MHz, 298 K) of **120**.

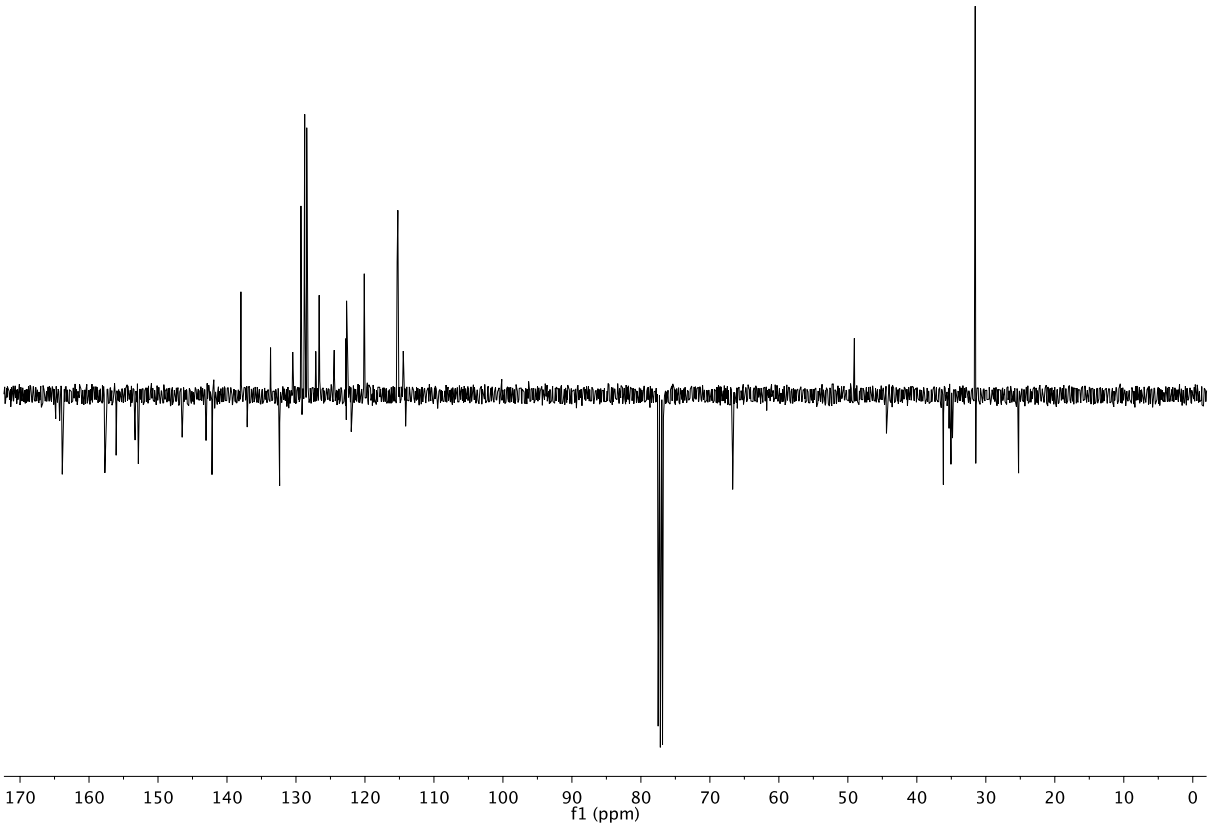

Figure S3. 22 J-MOD NMR ($CDCl_3$, 101 MHz, 298 K) of **120**.

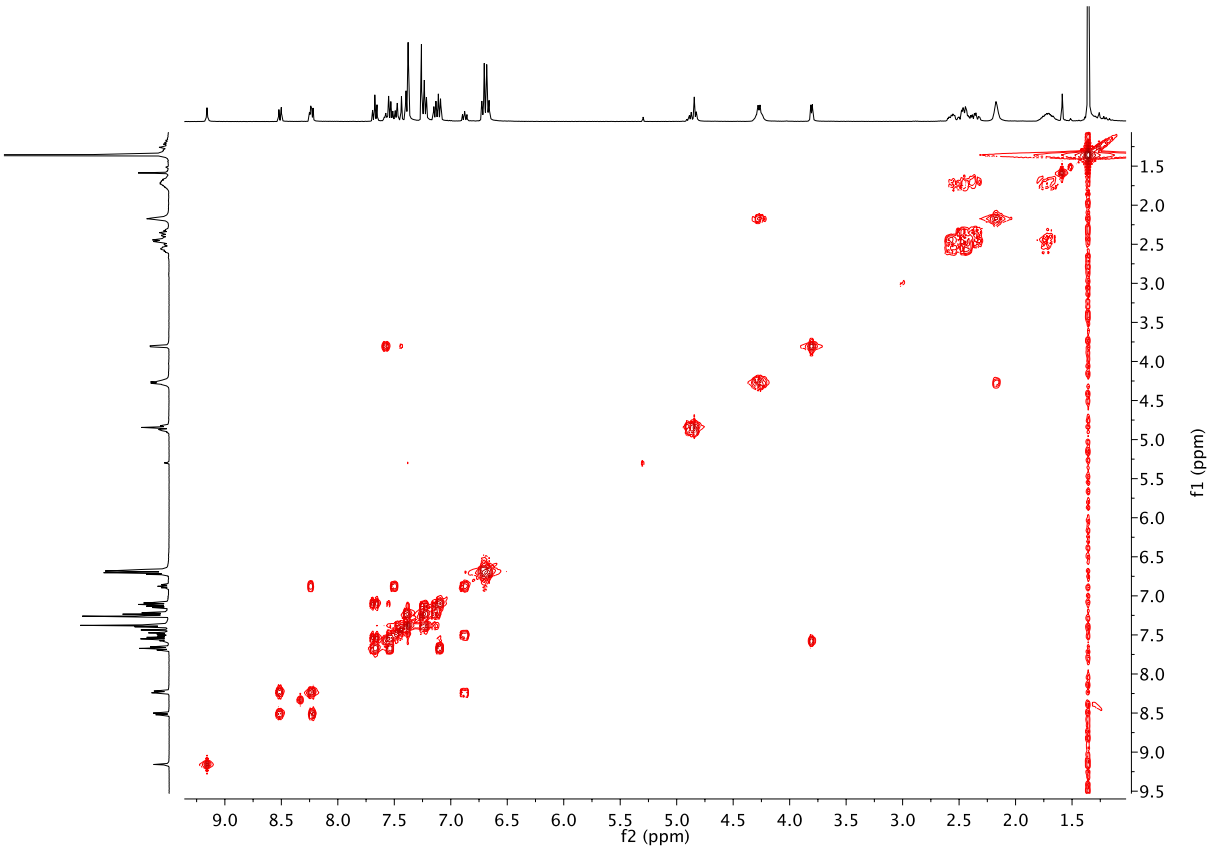

Figure S3. 23 COSY NMR ($CDCl_3$, 400 MHz, 298 K) of **120**.

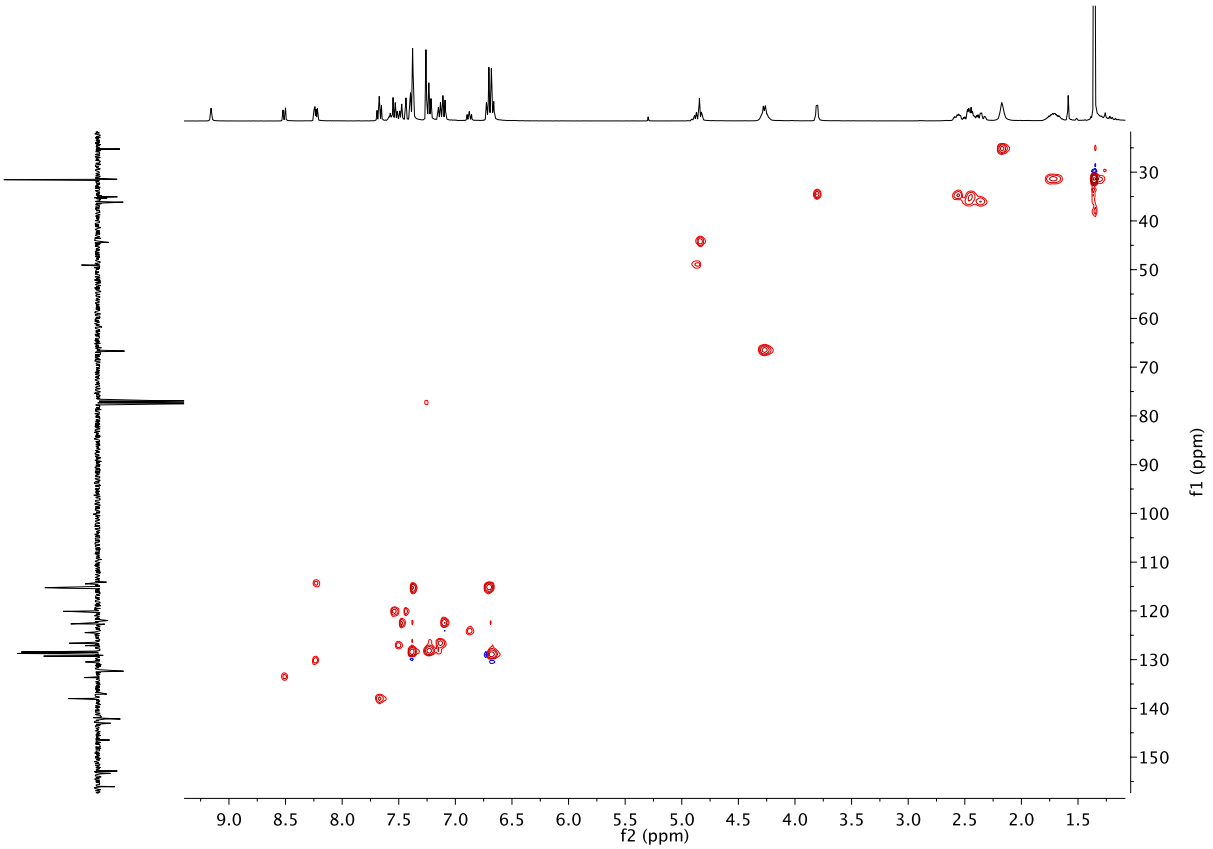

Figure S3. 24 HSQC NMR ($CDCl_3$, 400 MHz, 298 K) of **120**.

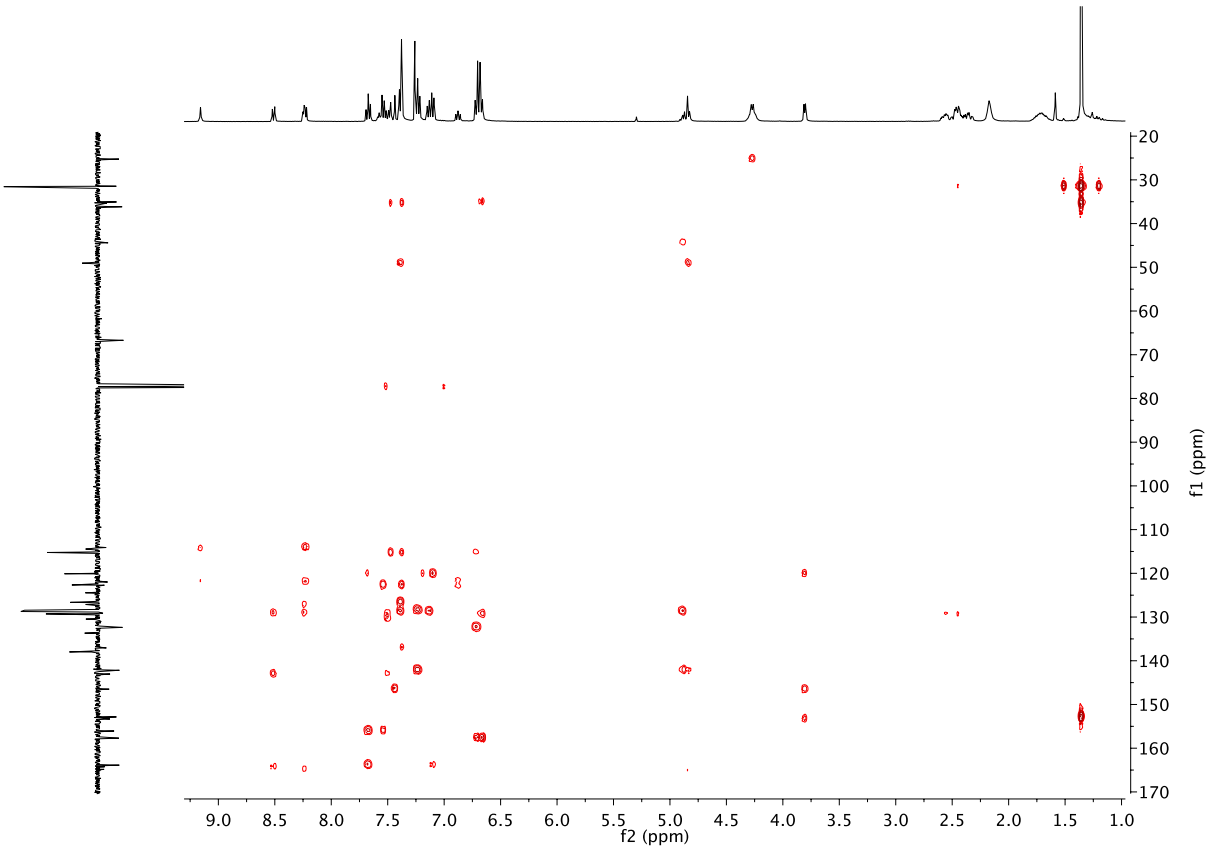

Figure S3. 25 26 HMBC NMR ($CDCl_3$, 400 MHz, 298 K) of **120**.

*Rotaxane (**120**.HBF_4)*

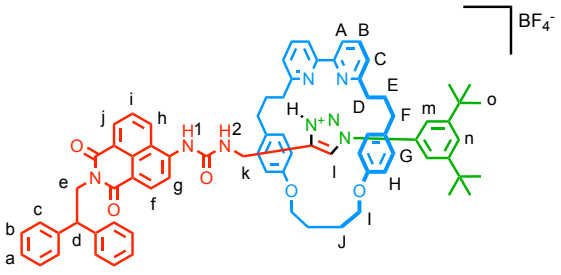

120.HBF_4

A solution of rotaxane **120** (20 mg, 0.017 mmol, 1 equiv.) in CH_2Cl_2 (2 mL) was washed with an aqueous solution of HBF_4 made of 5 drops of HBF_4 aq. (48 wt. %) in 2 mL of water. The pale yellow organic layer was recovered, dried ($MgSO_4$) and the solvent removed under vacuum, affording **120**.HBF_4 as a pale yellow solid (21 mg, 96%).^{1}H NMR ($CDCl_3$, 400 MHz, 298 K) δ 8.50 (d, *J* = 7.2, 1H, H_j), 8.41 (d, *J* = 8.6, 1H, H_h), 8.23 (d, *J* = 8.5, 1H, H_f), 8.18 (d, *J* = 8.5, 1H, H_g), 8.18 (s, 1H, -*NH1*-), 7.79 (t, *J* = 7.9, 2H, H_B), 7.70 (dd, *J* = 8.6, 7.3, 1H, H_i), 7.59 (t, *J* = 1.7, 1H, H_n), 7.48 (d, *J* = 8.7, 2H, H_A), 7.46 (d, *J* = 8.5, 2H, H_C), 7.42 – 7.33 (m, 6H, H_c and H_m), 7.28 – 7.18 (m, 4H, H_b), 7.17 – 7.08 (m, 2H, H_a), 6.79 (d, *J* = 8.3, 4H, H_G), 6.64 (d, *J* = 8.3, 4H, H_H), 6.59 (s, 1H, -*NH2*-), 6.42 (s, 1H, H_l), 4.92 – 4.79 (m, 3H, H_d and H_e), 4.34 – 4.10 (m, 4H, H_l), 4.06 (d, *J* = 6.1, 2H, H_k), 2.76 – 2.65 (m, 2H, H_F), 2.65 – 2.55 (m, 4H, H_D), 2.53 – 2.41 (m, 2H, H_F), 2.26 (m, 2H, H_J), 2.10 – 2.00 (m, 2H, H_J), 2.00 – 1.90 (m, 2H, H_E), 1.90 – 1.76 (m, 2H, H_E), 1.47 (s, 18H, H_o). ^{13}C NMR ($CDCl_3$, 101 MHz, 298 K) δ 164.7, 164.2, 162.6, 157.4, 154.9, 152.9, 148.3, 144.0, 142.3, 142.1, 141.3, 136.7, 132.6, 132.4, 131.4, 129.8, 129.0, 128.7, 128.4, 127.9, 126.7, 126.6, 126.0, 123.3, 122.5, 120.7, 120.6, 116.0, 115.3, 114.6, 114.1, 66.5, 48.9, 44.4, 34.9, 34.9, 34.3, 34.1, 31.7, 30.2, 25.0. ^{19}F NMR (376 MHz, $CDCl_3$, 298 K) δ -149.9, -150.0.

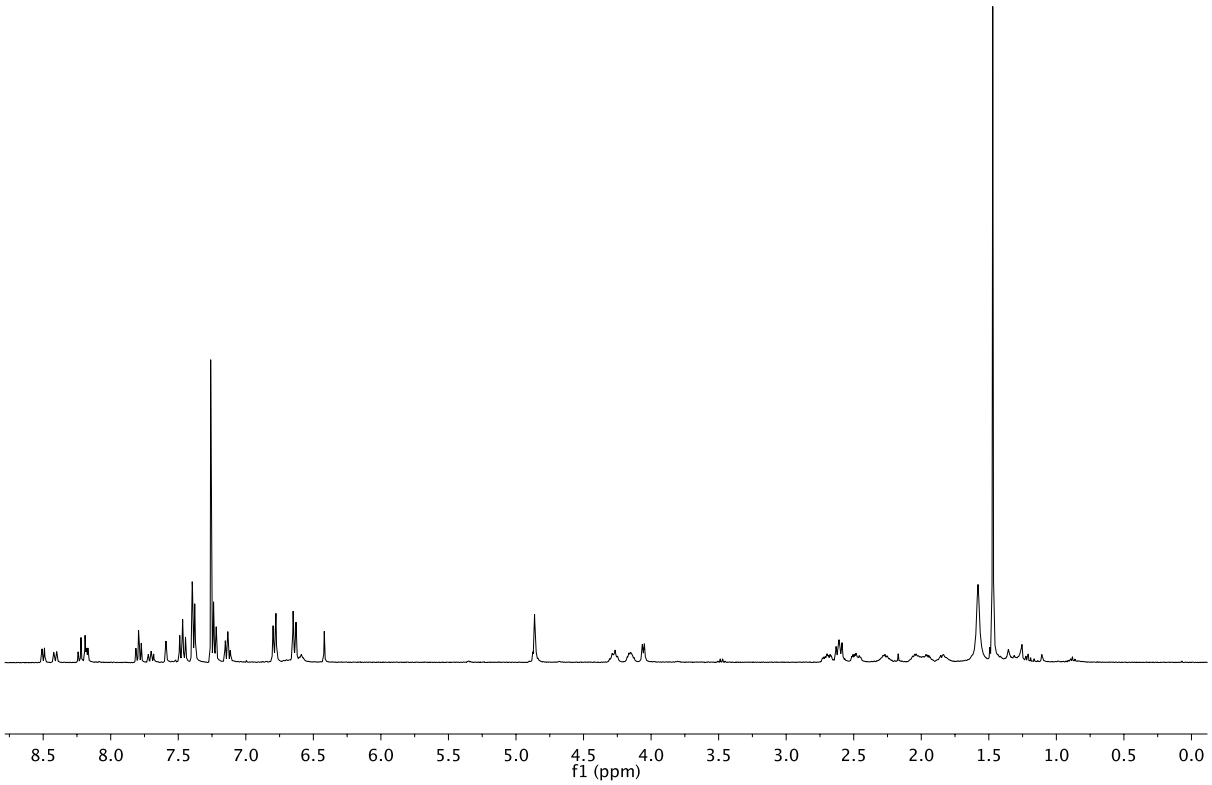

Figure S3. 26 ^{1}H NMR ($CDCl_3$, 400 MHz, 298 K) of **120**.HBF_4.

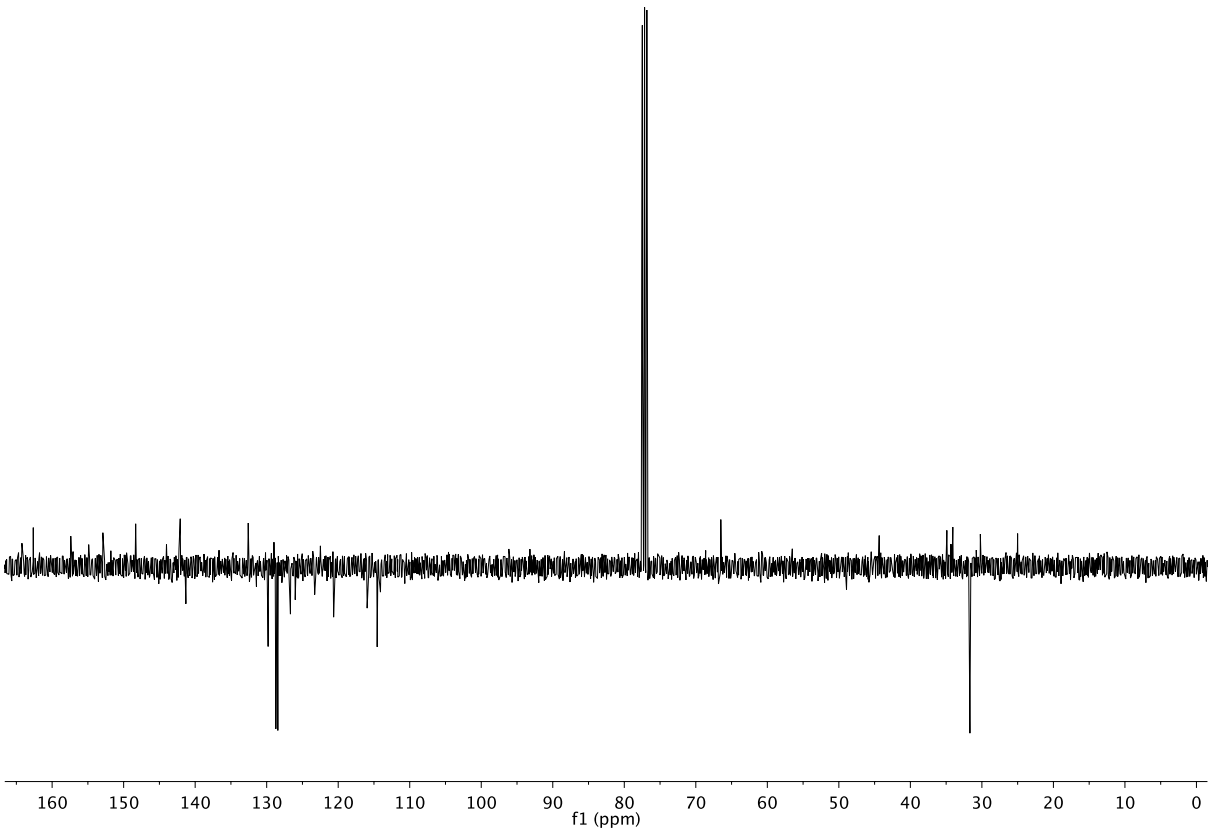

Figure S3. 27 J-MOD NMR ($CDCl_3$, 101 MHz, 298 K) of **120**.HBF_4.

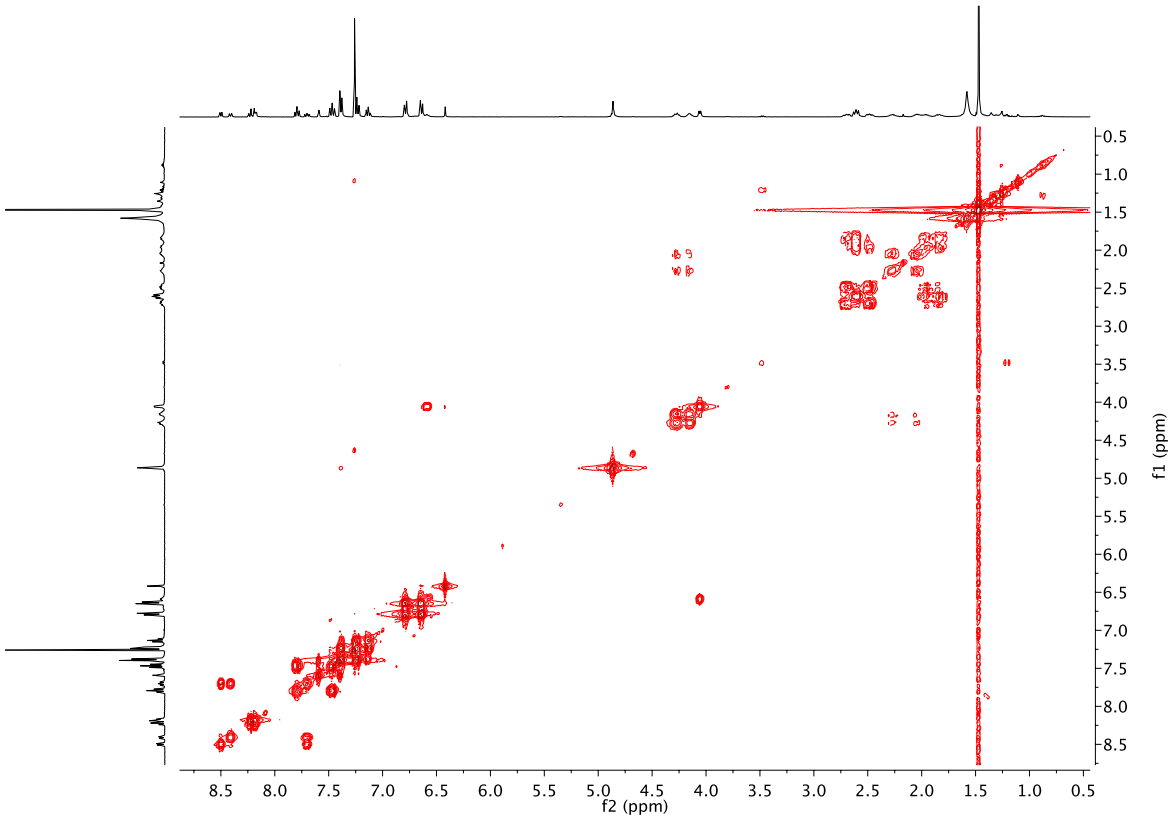

Figure S3. 28 COSY NMR ($CDCl_3$, 400 MHz, 298 K) of **120**.HBF_4.

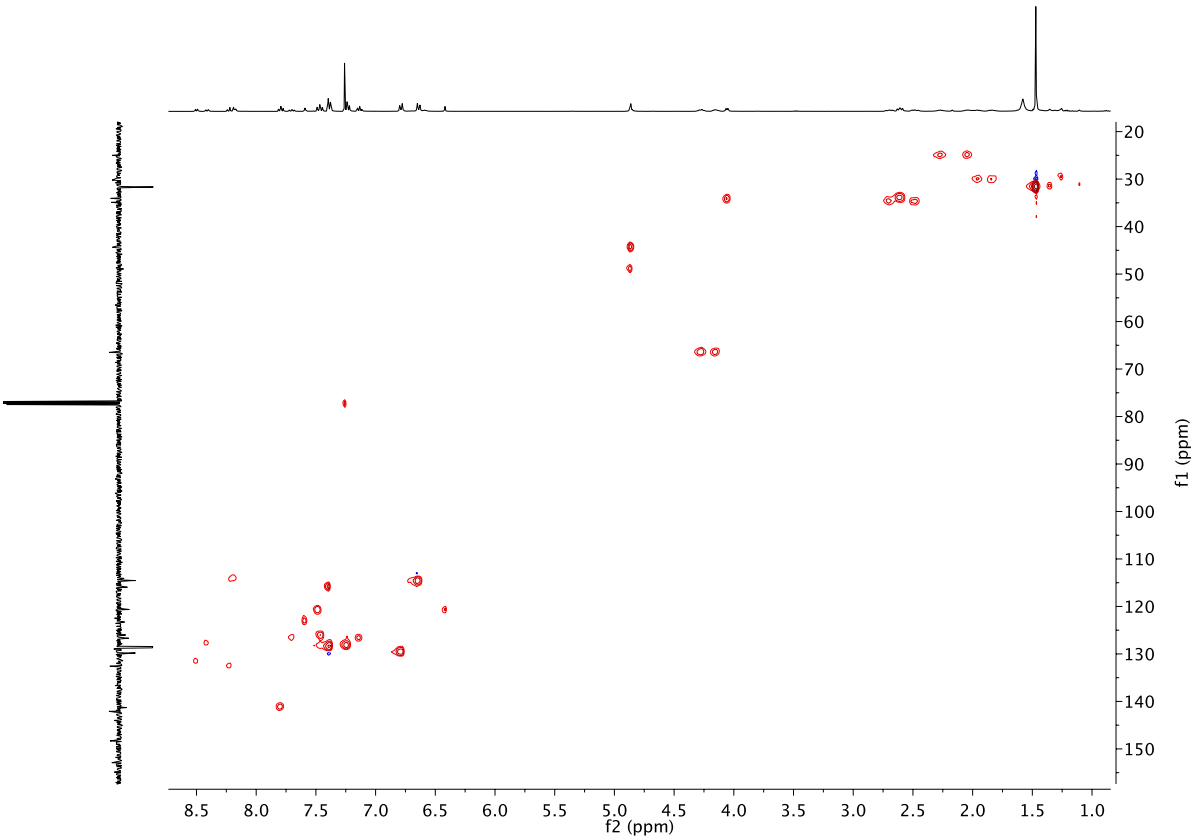

Figure S3. 29 HSQC NMR ($CDCl_3$, 400 MHz, 298 K) of **120**.HBF_4.

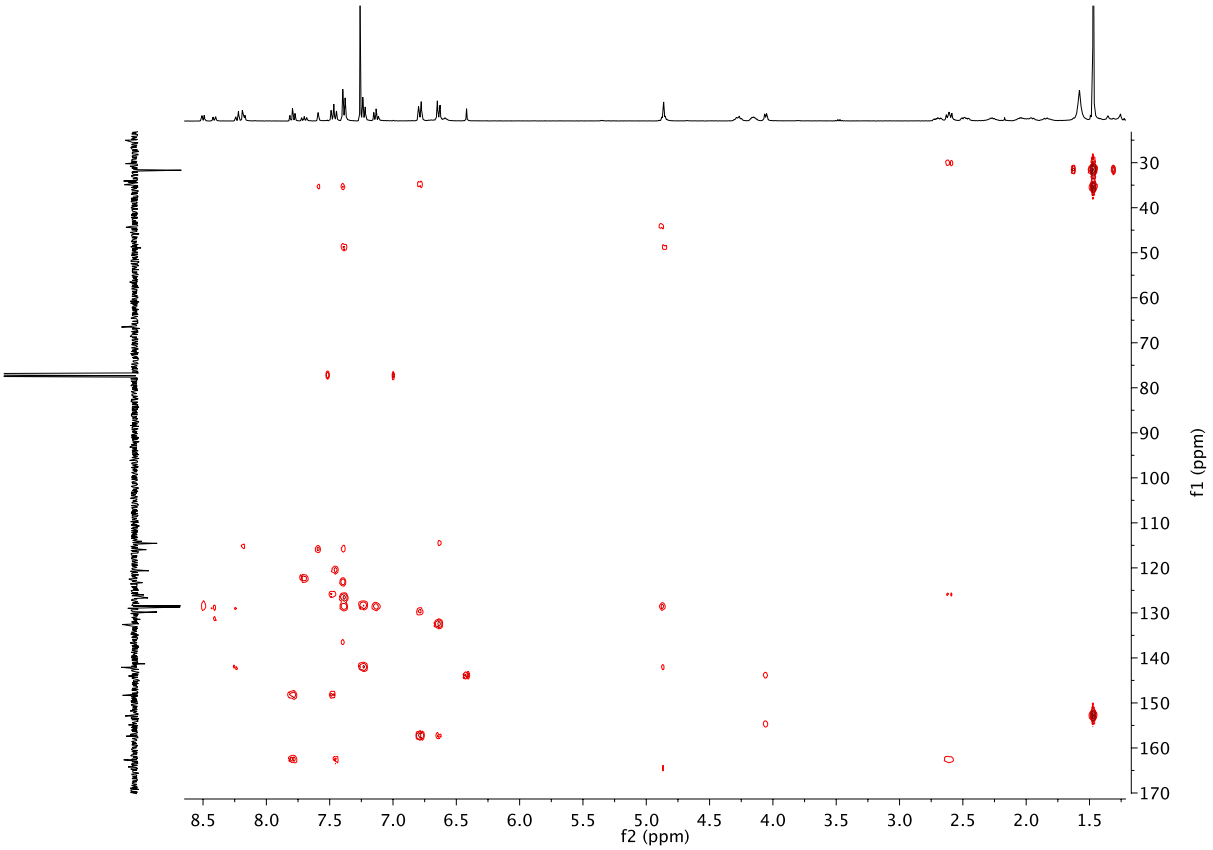

Figure S3. 30 HMBC NMR ($CDCl_3$, 400 MHz, 298 K) of **120**.HBF_4.

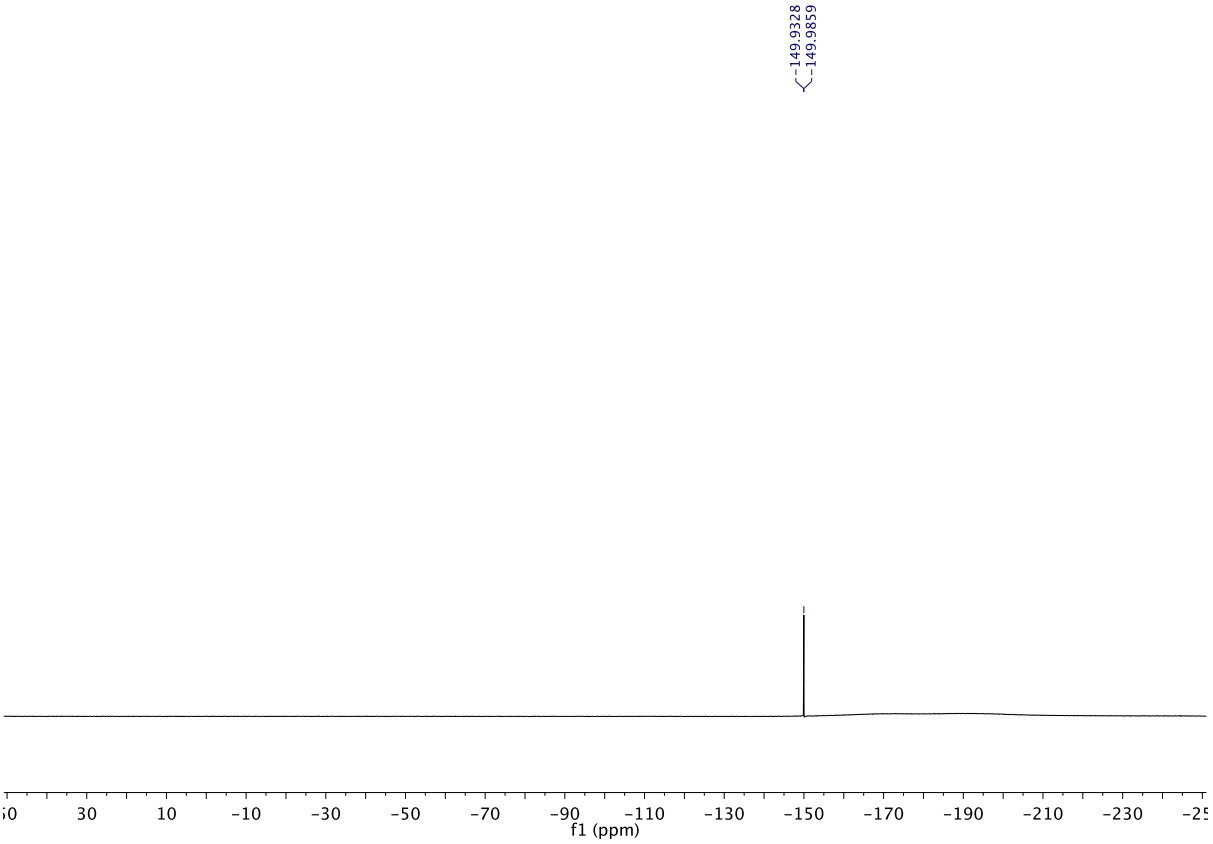

Figure S3. 31 ^{19}F NMR ($CDCl_3$, 376 MHz, 298 K) of **120**.HBF_4.

*Axle (**121**)*

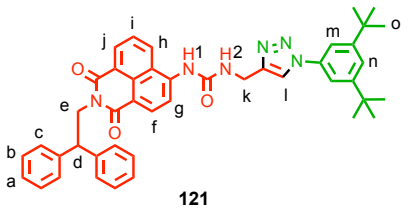

121

A dry CEM MW vial was charged with azide **103** (5.8 mg, 0.025 mmol, 1 equiv.), alkyne **119** (12 mg, 0.025 mmol, 1 equiv.), and $[Cu(MeCN)_4]PF_6$ (8.9 mg, 0.024 mmol, 0.96 equiv.). CH_2Cl_2 (1 mL) was added, followed by DIPEA (4.4 µL, 0.025 mmol, 1 equiv.) and the reaction mixture stirred at 50 °C for 4 h. EDTA-NH_3 (aq.) (5 mL) was added and the crude extracted with CH_2Cl_2 (3 x 5 mL). The combined organic layers were dried ($MgSO_4$) and concentrated *in vacuo*. The crude was purified *via* flash column chromatography on silica gel using an isocratic elution of CH_2Cl_2/MeOH 95:5, affording product **121** as a pale yellow solid (17 mg, 97%).^{1}H NMR ($CDCl_3$, 400 MHz, 298 K) δ 8.58 (s, 1H, -*NH1*-), 8.44 (d, *J* = 8.3, 1H, H_f), 8.38 (d, *J* = 8.3, 1H, H_g), 8.28 (d, *J* = 7.4, 1H, H_j), 8.24 (d, *J* = 8.5, 1H, H_h), 8.17 (s, 2H, H_l and -*NH2*-), 7.51 (t, *J* = 1.7, 1H, H_n), 7.39 (d, *J* = 1.7, 2H, H_m), 7.33 (dd, *J* = 8.2, 1.3, 4H, H_c), 7.21 (t app, *J* = 7.5, 4H, H_b), 7.12 (dd, *J* = 7.5, 1.3, 2H, H_a), 6.98 (t app, *J* = 7.9, 1H, H_i), 4.86 – 4.72 (m, 5H, H_d, H_e and H_k), 1.24 (s, 18H, H_o). ^{13}C NMR ($CDCl_3$, 101 MHz, 298 K) δ 164.4, 163.9, 153.4, 141.9, 141.2, 132.8, 130.9, 129.1, 128.6, 128.4, 127.3, 126.7, 125.7, 124.0, 123.3, 122.9, 117.2, 116.5, 116.1, 48.8, 44.5, 35.3, 31.3. HRMS (ESI+) m/z = 705.3556 $[M+H]^+$ (calc. for $C_{44}H_{45}N_6O_3$ 705.3548).

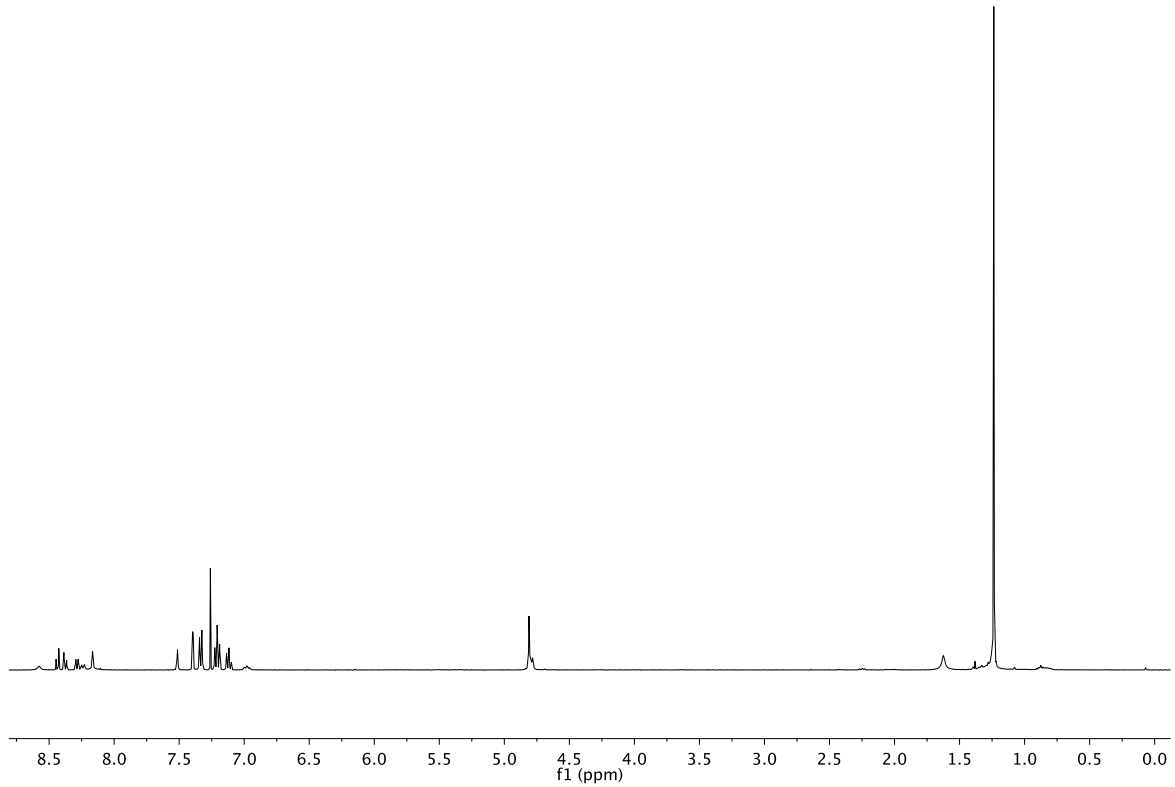

Figure S3. 32 ^{1}H NMR ($CDCl_3$, 400 MHz, 298 K) of **121**.

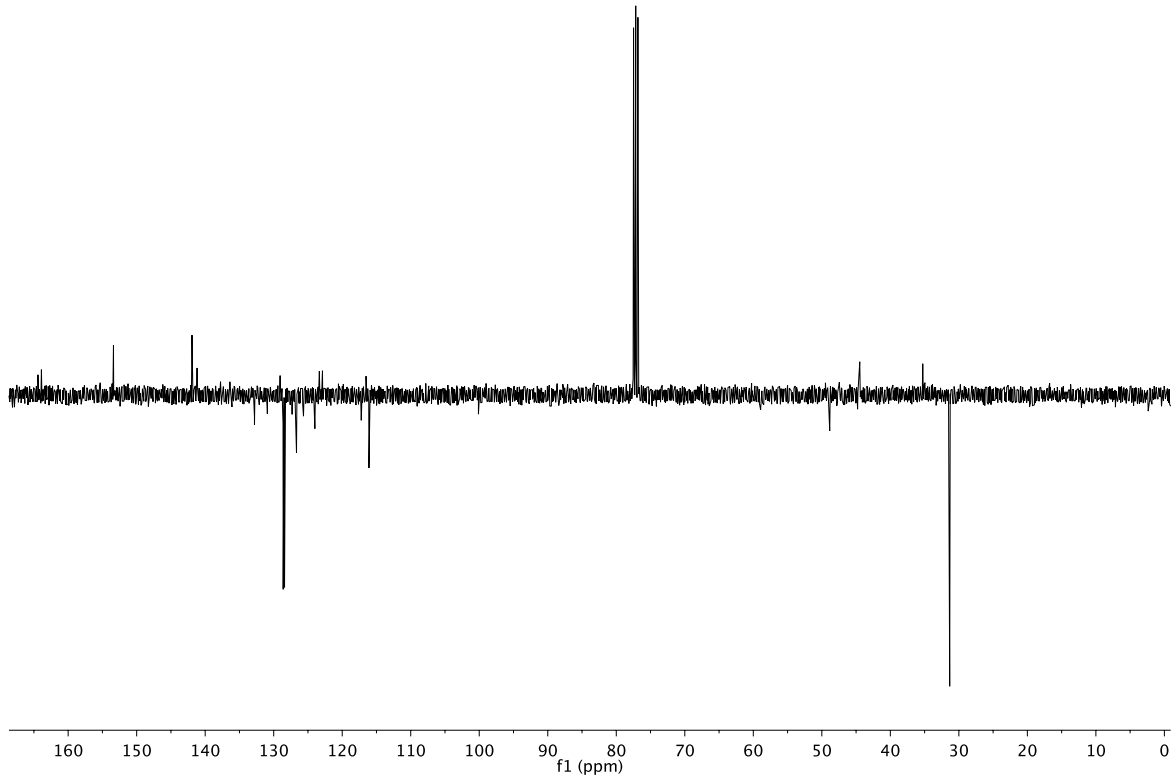

Figure S3. 33 J-MOD NMR ($CDCl_3$, 101 MHz, 298 K) of **121**.

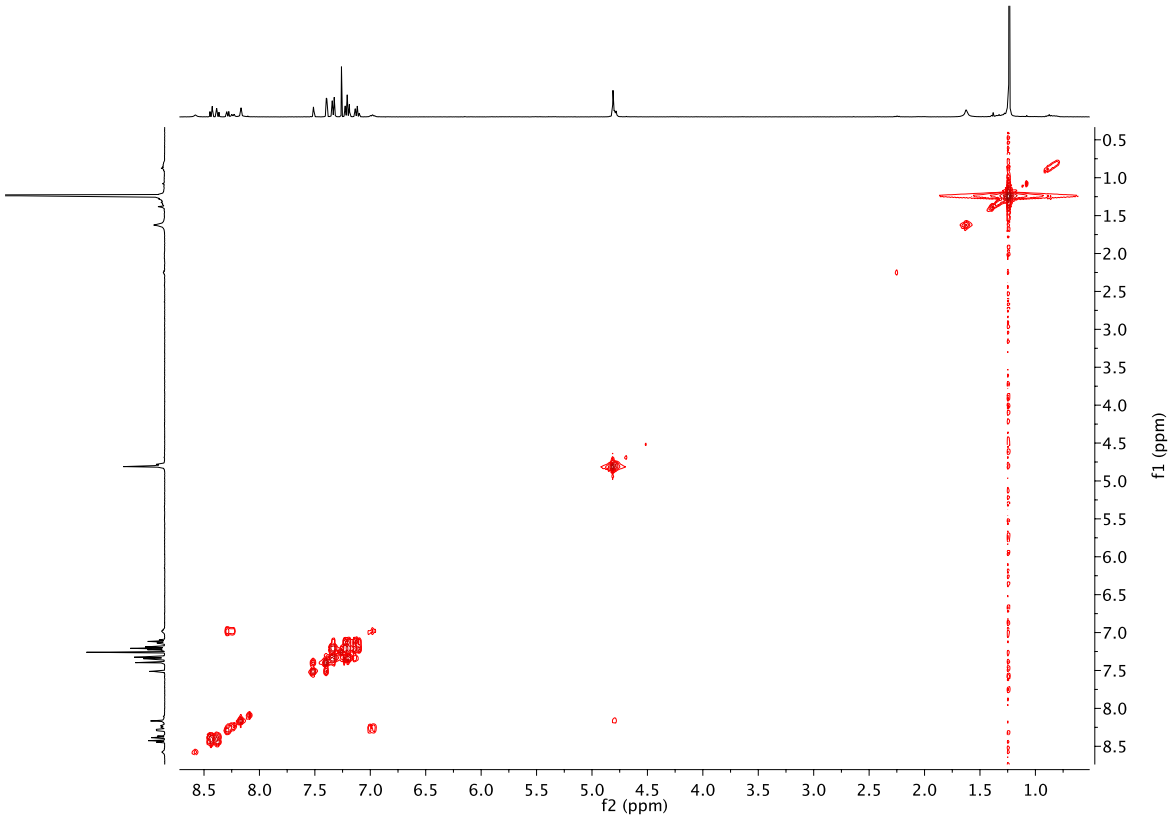

Figure S3. 34 COSY NMR ($CDCl_3$, 400 MHz, 298 K) of **121**.

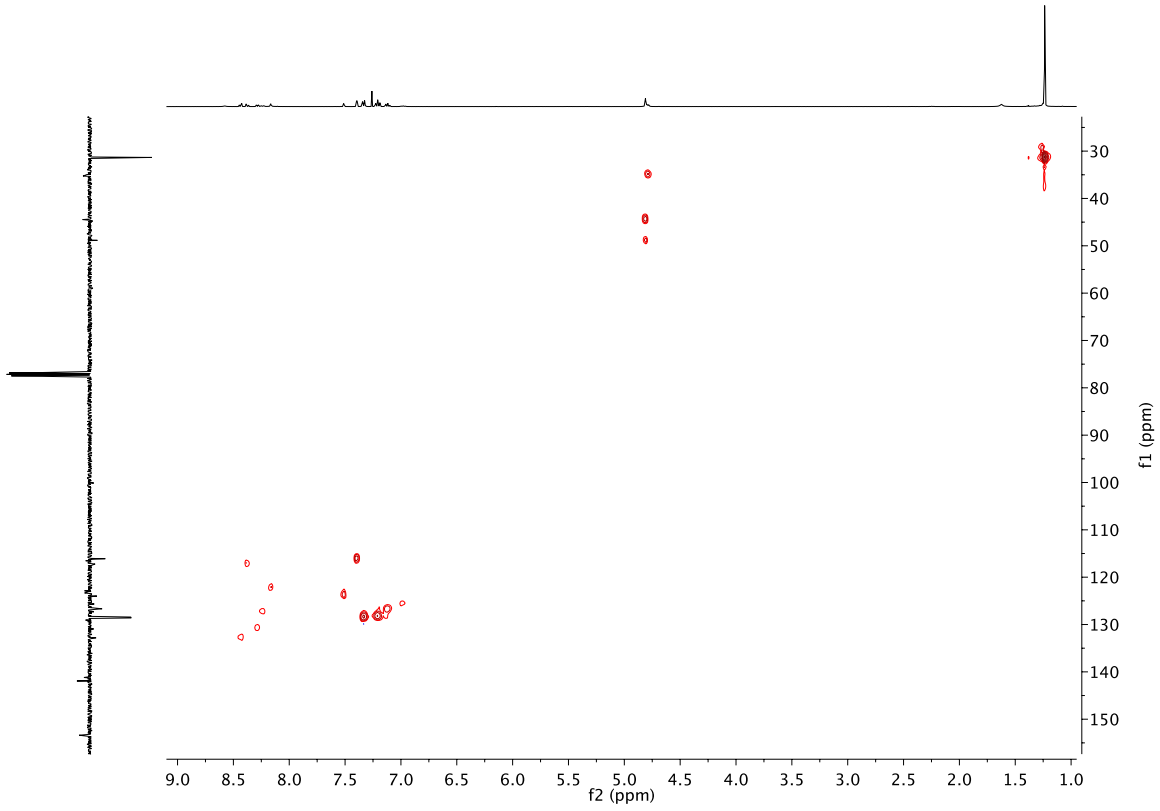

Figure S3. 35 HSQC NMR ($CDCl_3$, 400 MHz, 298 K) of **121**

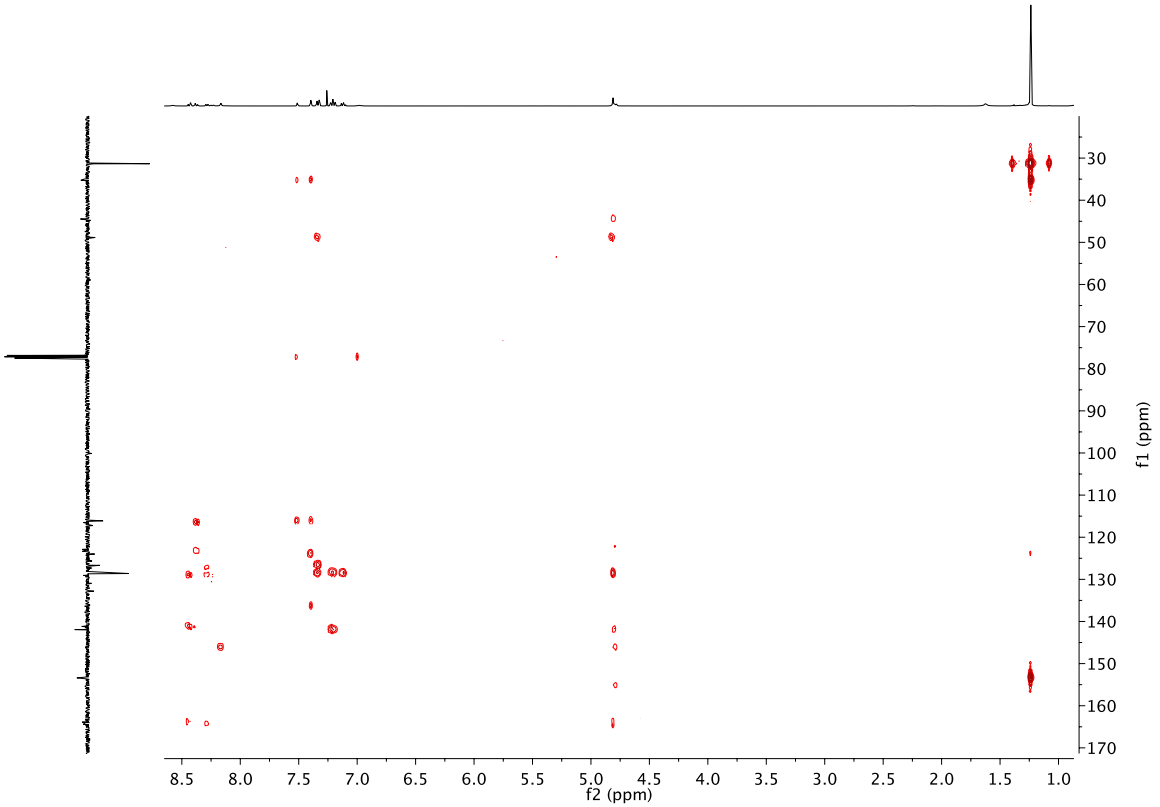

Figure S3. 36 HMBC NMR ($CDCl_3$, 400 MHz, 298 K) of **121**.

NMR and fluorescence titration data

^{1}H NMR Binding Studies Procedure: A 2.5 mM stock solution of the receptor was prepared in the stated deuterated solvent mixture using a volumetric flask. Solutions of anions with 2.5 mM of receptors to be titrated were prepared in separate 2 ml vials, and 200 µL of deuterated solvents (v/v) were added using pipettes (Eppendorf). The concentration of anion solutions was made 70 times that of the host (i.e. 160 – 180 mM). In each case, 550 µL of host solution in an NMR tube was titrated with aliquots of anion stock solution, and after each addition, the ^{1}H NMR spectrum was recorded on a Bruker Avance III 400 or Bruker Avance III 500 spectrometer after thorough mixing in 298K. This was performed in the following order: 10 × 1.5 µL, 2 × 7.5 µL, 4 × 14 µL (total 86 µL). Titrations were performed in triplicate to give K_a values. Typically, a total of at least 12 equiv. of anion was added. Non-linear curve fitting of the experimentally obtained titration isotherms (equivalents of anion vs chemical shift of NH and triazole proton) using the program HypNMR® (Hyperquad®) enabled the calculation of association constants (K_a/M^{-1}) using a 1:1 global fitting model.

Spectroscopic Binding Studies Procedure: A 0.13 mM stock solution of the receptor was prepared in the spectrophotometric solvents using a volumetric flask. Solutions of anions with 0.13 mM of receptors to be titrated were prepared in separate 2.5 ml vials, and 2000 µL of deuterated solvents (v/v) were added using pipettes (Eppendorf). The concentration of anion solutions was made 70 times that of the host (i.e. 8 – 10 mM). A total of at least 12 equiv. of anion was added, and this was performed in the following order: 10 × 1.5 µL, 2 × 7.5 µL, 4 × 14 µL (total 86 µL). After each addition, the resulting solution was stirred for at least 20 seconds, and the absorbance was recorded. Both salt and receptor were dried under high vacuum prior to use. UV-Vis data was recorded using a Varian Cary 4000 UV-Vis Spectrophotometer. Temperature control was provided by a Varian Cary PCB 150 Water Peltier System. The absorbance was recorded from 250 nm to 600 nm. Titrations were performed in triplicate to give K_a values. To determine association constants for the receptor-indicator complexes, global analysis of the absorbance data was carried out using a nonlinear least-squares curve fitting procedure using the online software http://supramolecular.org/ with a 1:1 global fitting model (Nelder-Mead method). Fluorescence titrations were carried out in parallel to the UV/Vis absorption measurements using a Cary Eclipse Fluorescence Spectrometer.

*^{1}H NMR titrations of axle (**121**)*

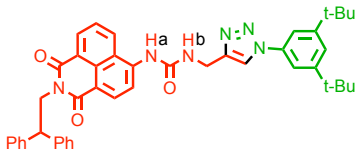

121

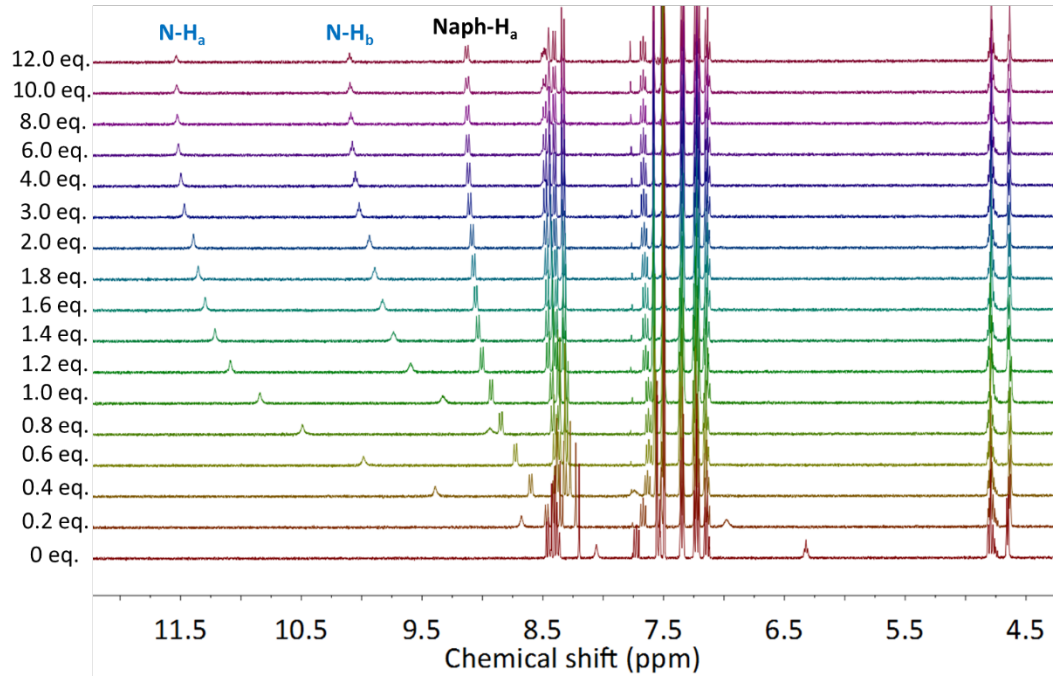

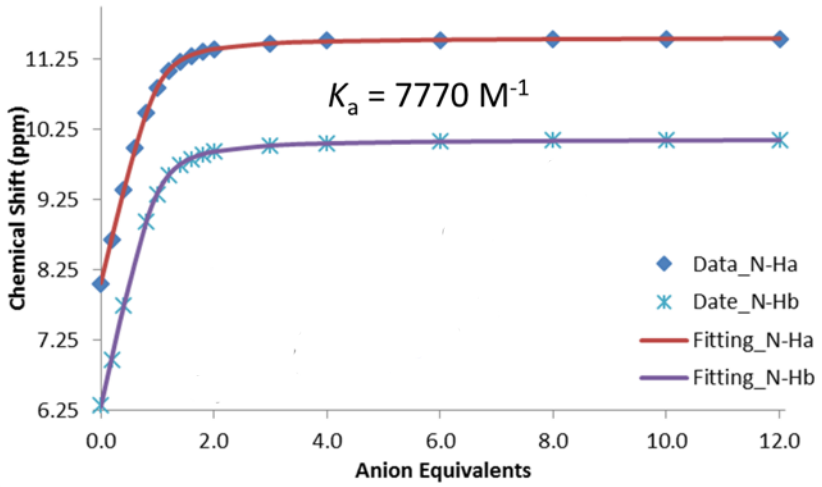

Figure S3. 37 ^{1}H NMR titration of 121 with TBAAcO (0-12 equiv.) in $CDCl_3/CD_3CN$ at 298 K

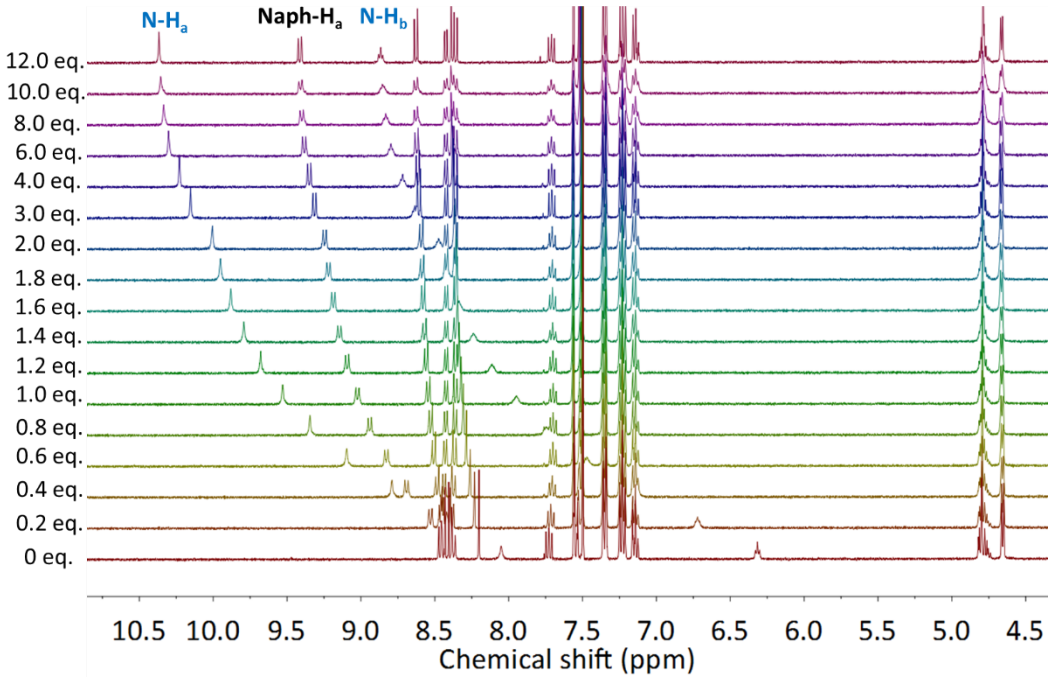

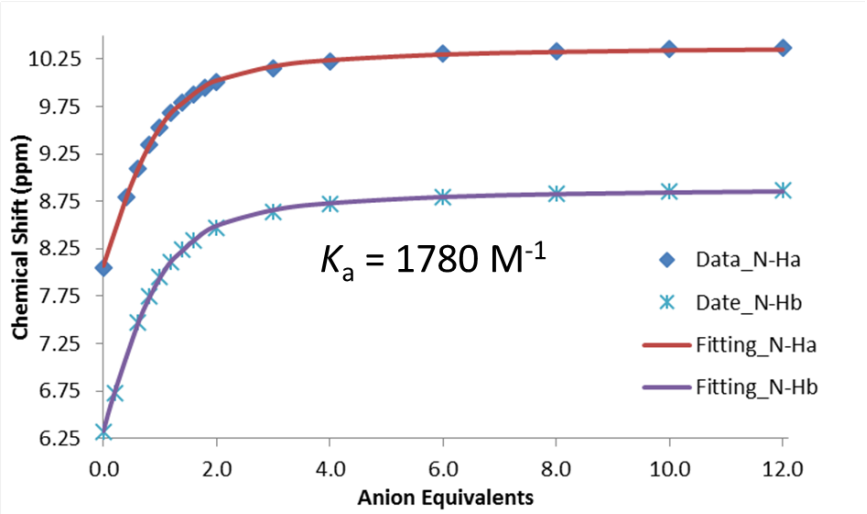

Figure S3. 38 ^{1}H NMR titration of **121** with TBACl (0-12 equiv.) in $CDCl_3/CD_3CN$ at 298 K.

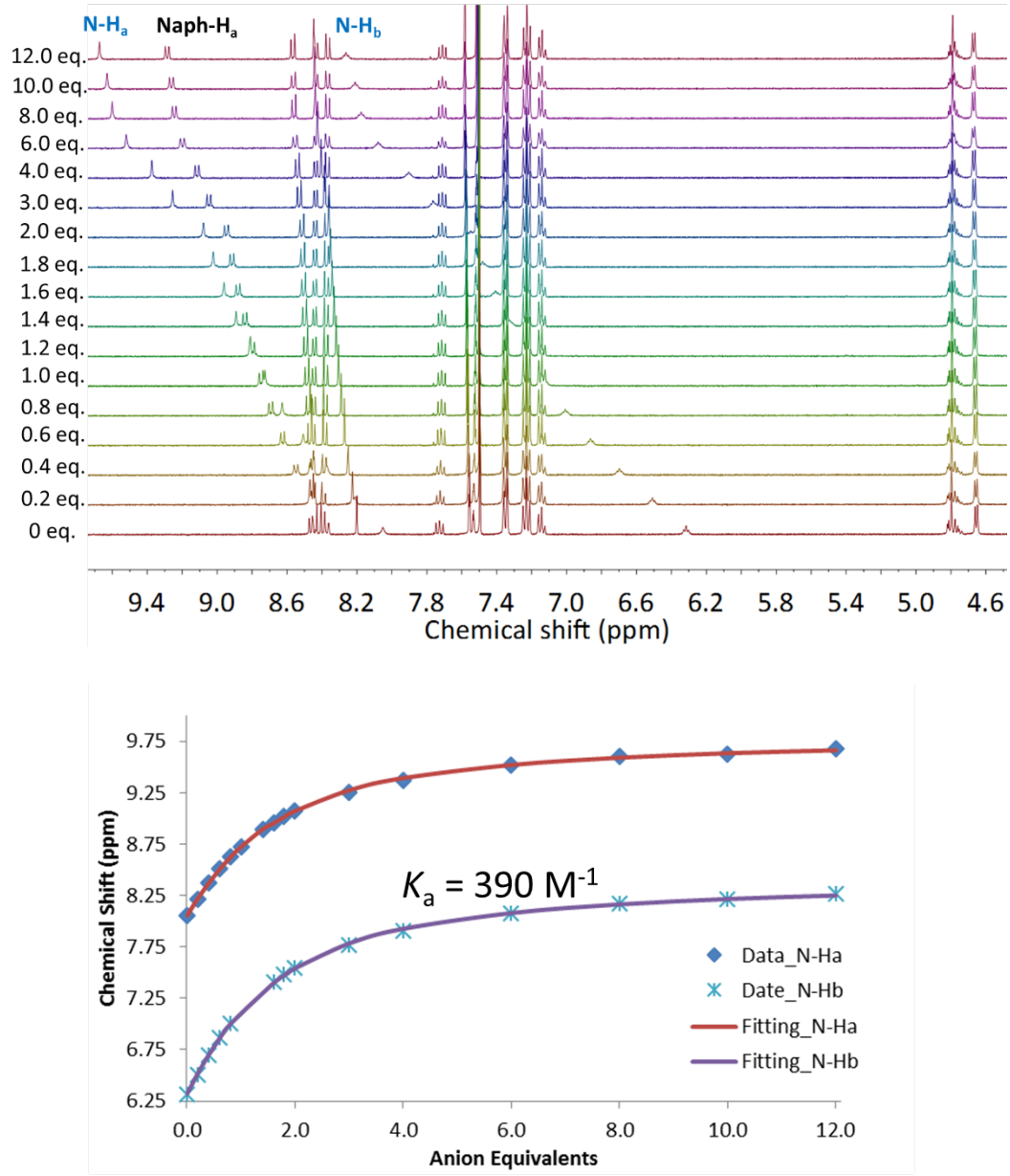

Figure S3. 39 ^{1}H NMR titration of **121** with TBABr (0-12 equiv.) in $CDCl_3/CD_3CN$ at 298 K.

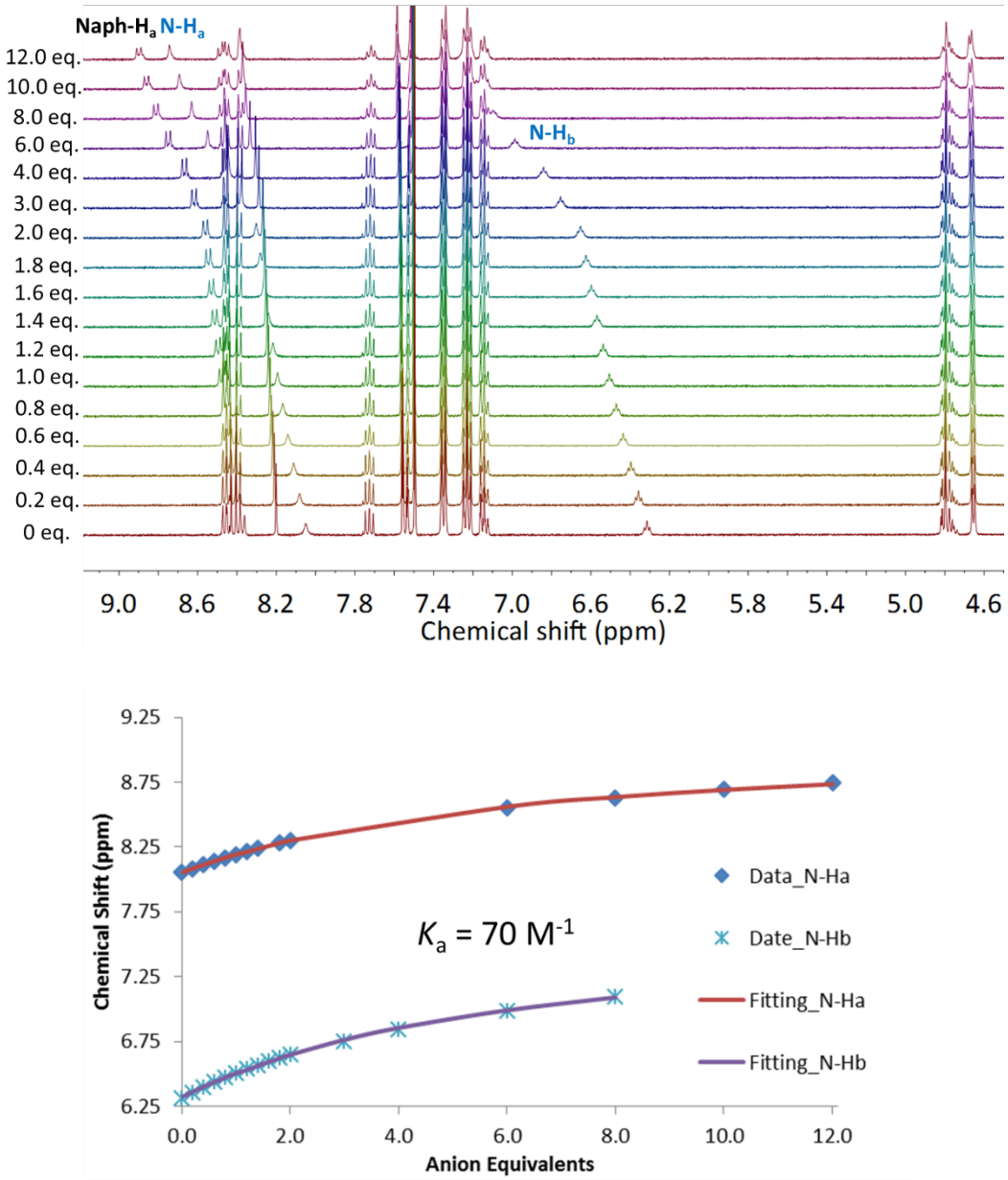

Figure S3. 40 ^{1}H NMR titration of **121** with TBAI (0-12 equiv.) in $CDCl_3/CD_3CN$ at 298 K

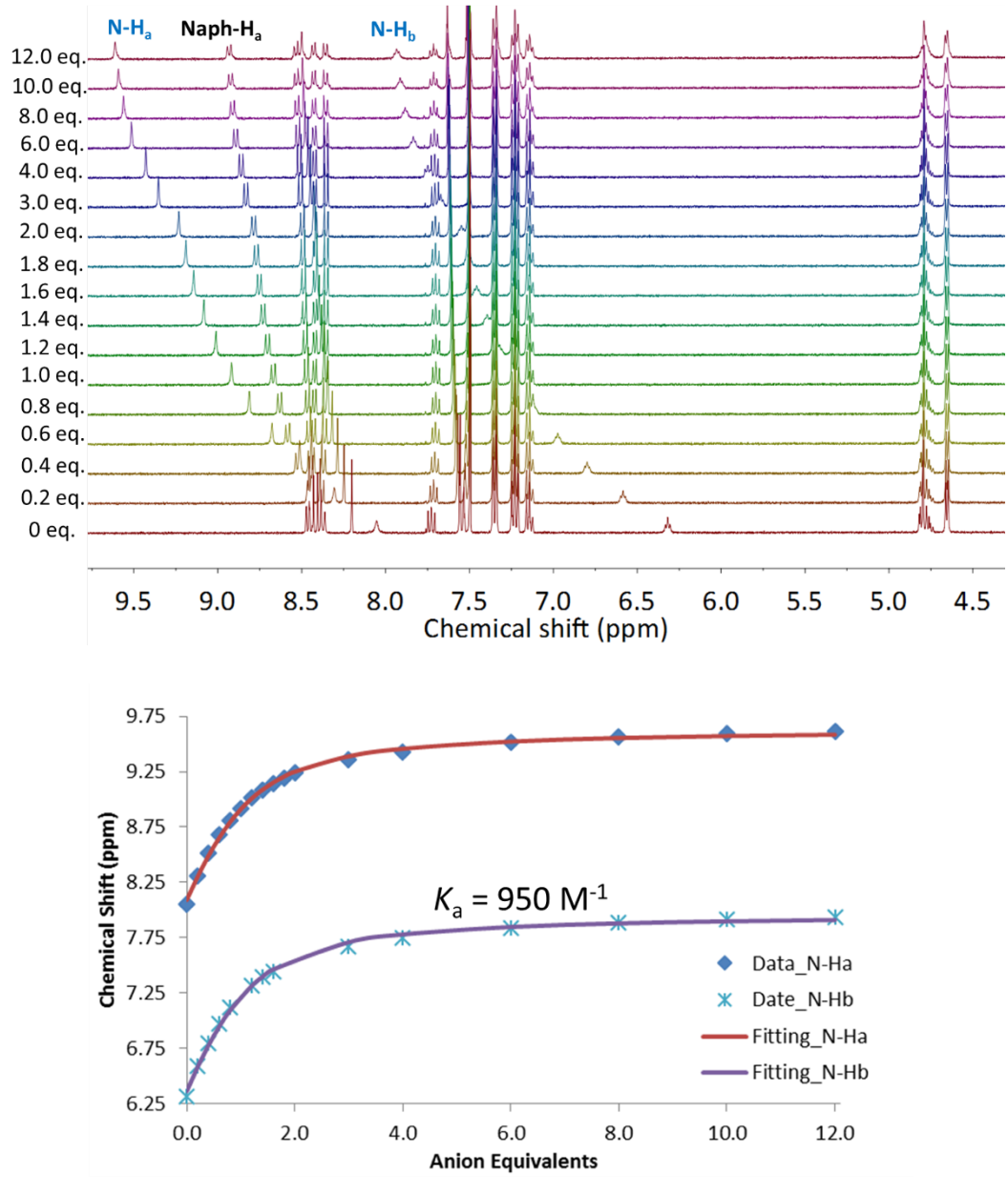

Figure S3. 41 ^{1}H NMR titration of **121** with TBAOMs (0-12 equiv.) in $CDCl_3/CD_3CN$ at 298 K.

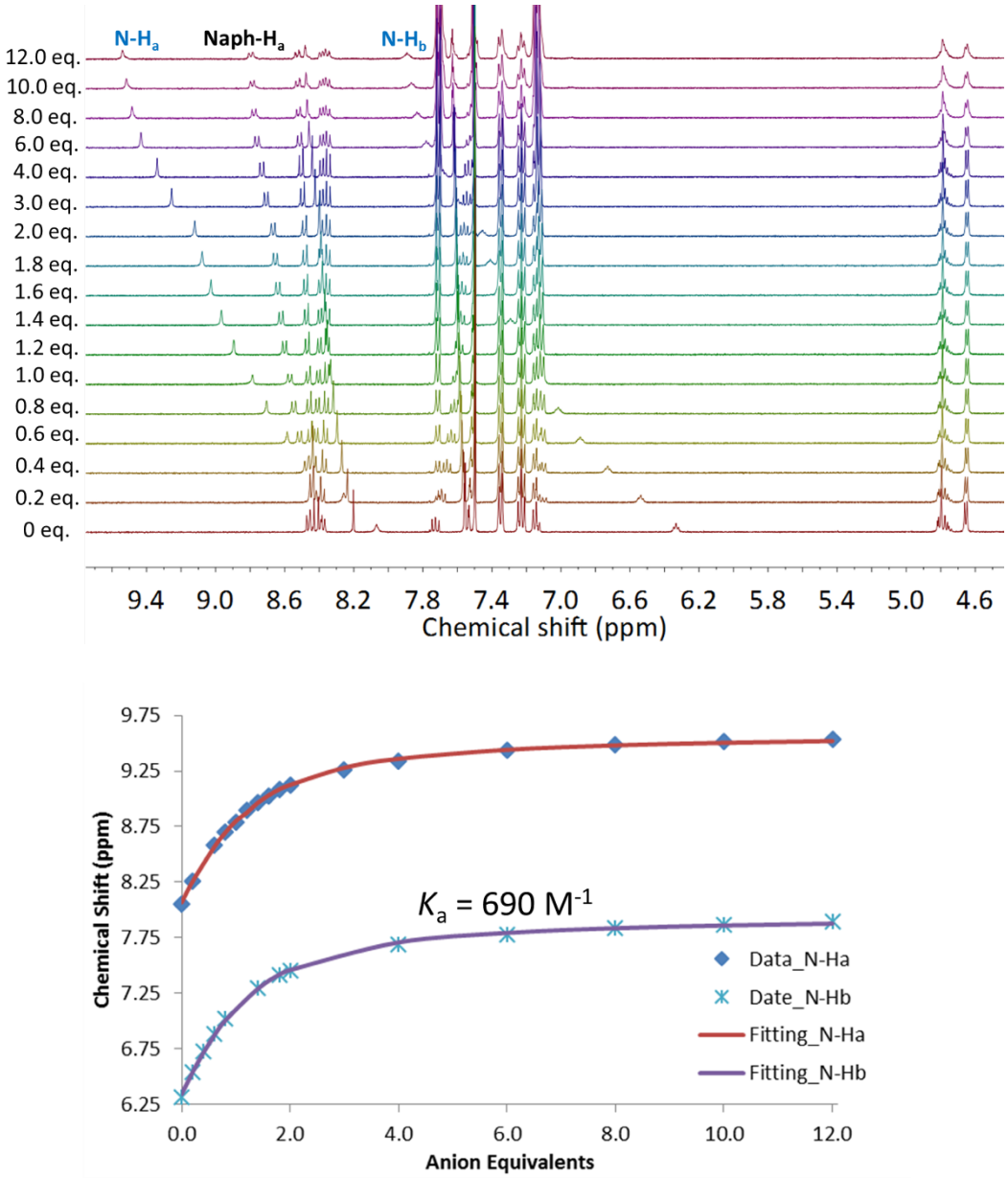

Figure S3. 42 ^{1}H NMR titration of **121** with TBAOTs (0-12 equiv.) in $CDCl_3/CD_3CN$ at 298 K.

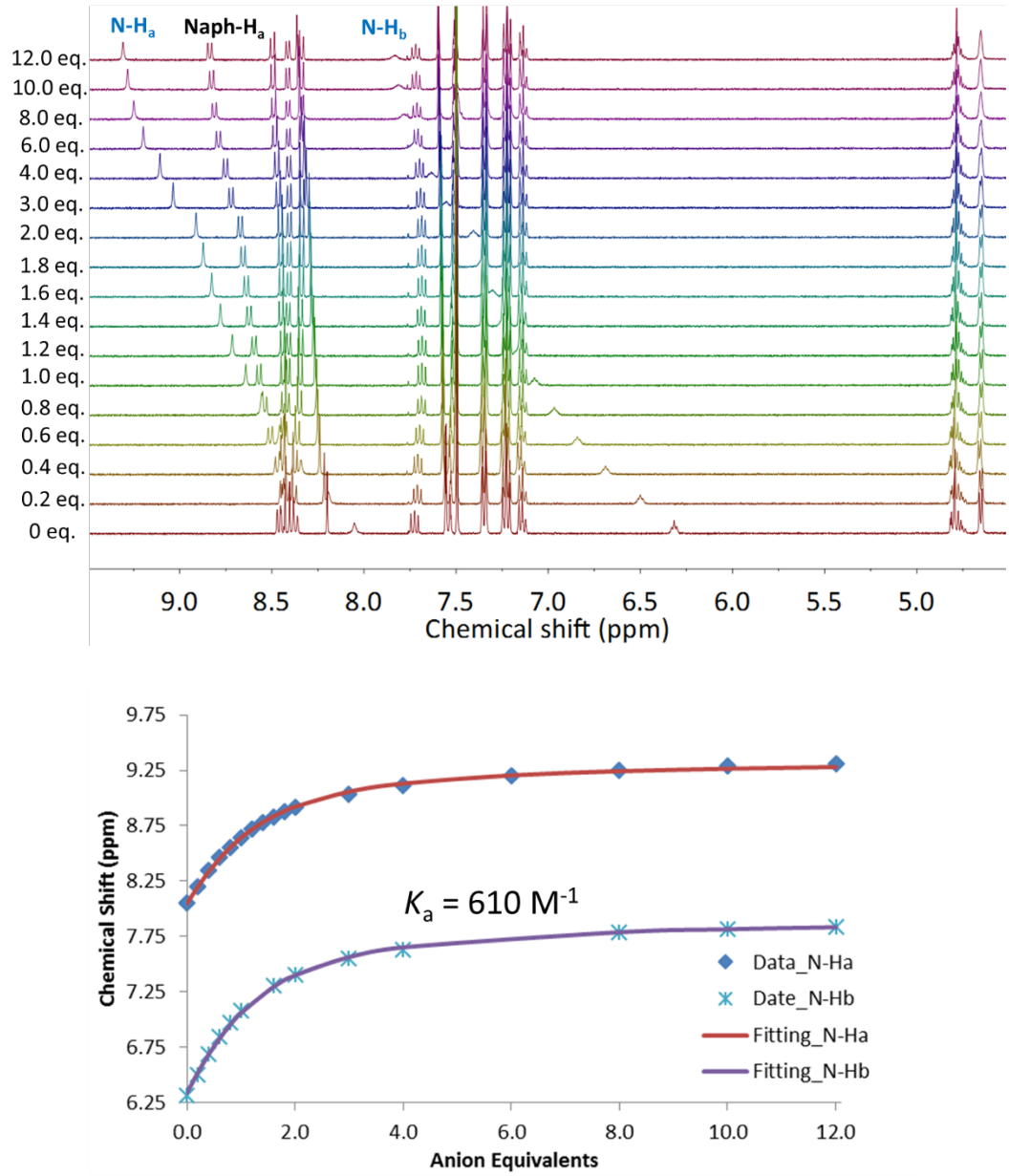

Figure S3. 43 ^{1}H NMR titration of **121** with $TBAHSO_4$ (0-12 equiv.) in $CDCl_3/CD_3CN$ at 298 K.

*UV-vis titrations of axle (**121**)*

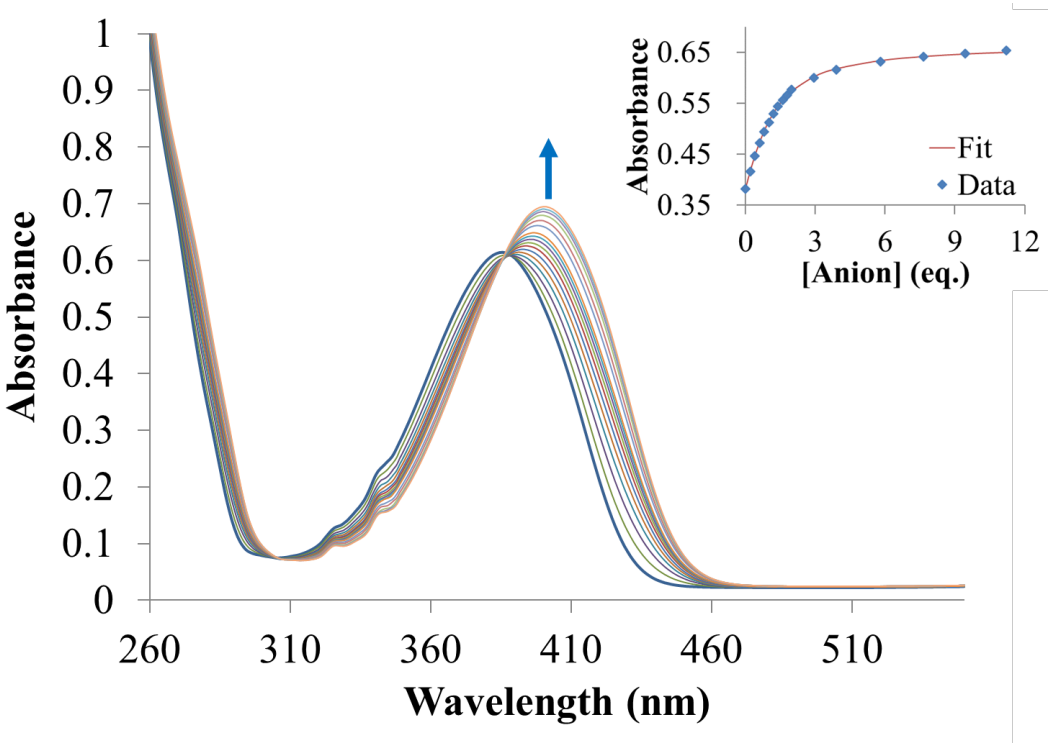

Figure S3. 44 UV-Vis titration of **121** with TBAOAc (0-12 equiv.) in $CHCl_3/CH_3CN$ at 298 K.

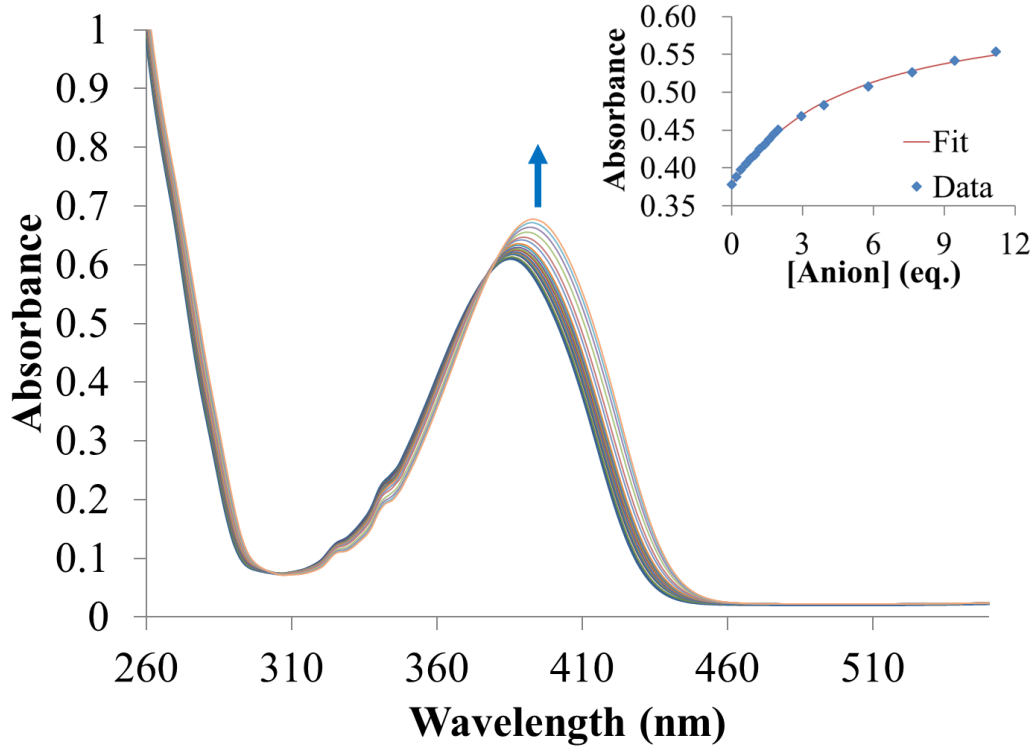

Figure S3. 45 UV-Vis titration of **121** with TBACl (0-12 equiv.) in $CHCl_3/CH_3CN$ at 298 K.

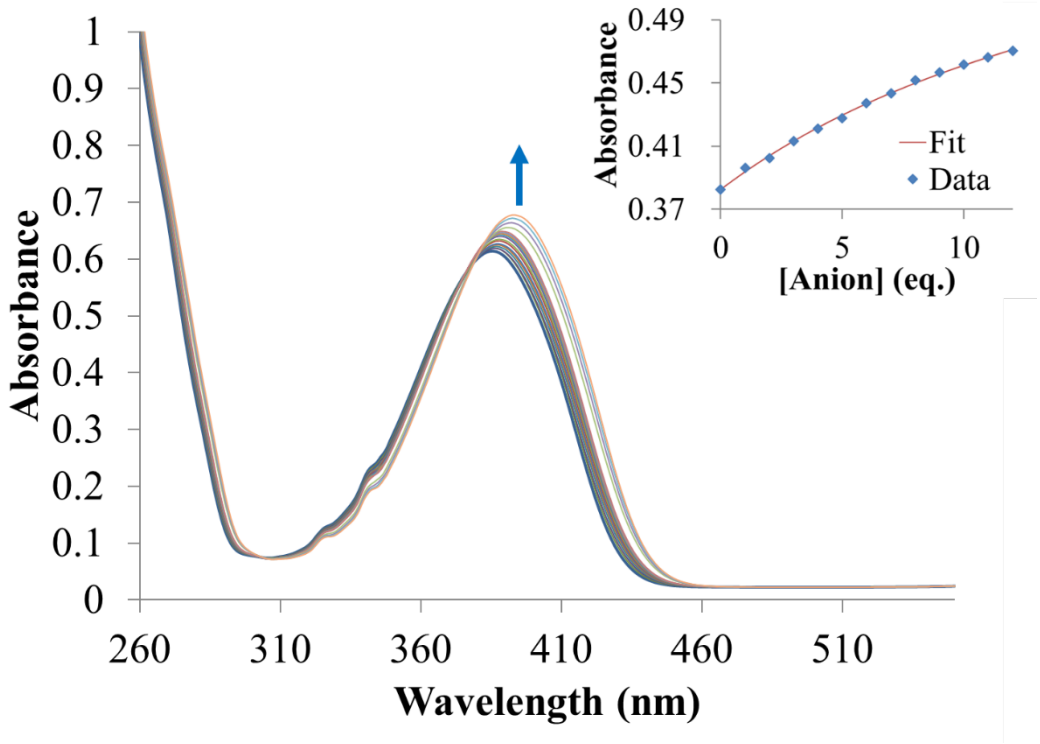

Figure S3. 46 UV-Vis titration of **121** with TBAOMs (0-12 equiv.) in $CHCl_3/CH_3CN$ at 298 K.

*Fluorescent titrations of axle (**121**)*

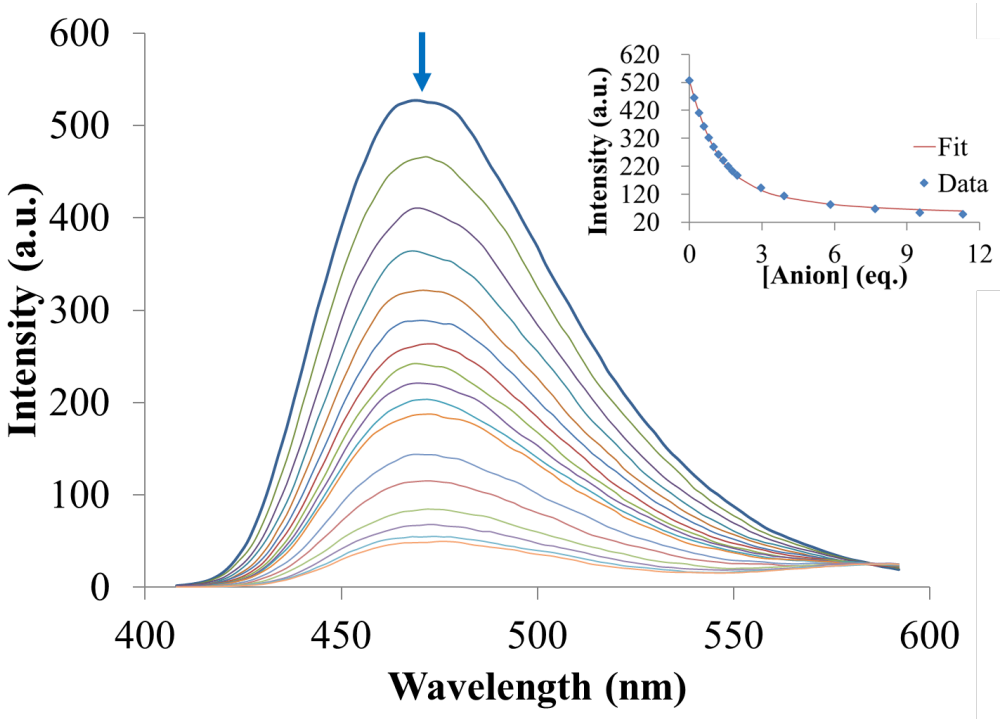

Figure S3. 47 Fluorescence titration of **121** with TBAOAc (0-12 equiv.) in $CHCl_3/CH_3CN$ at 298 K.

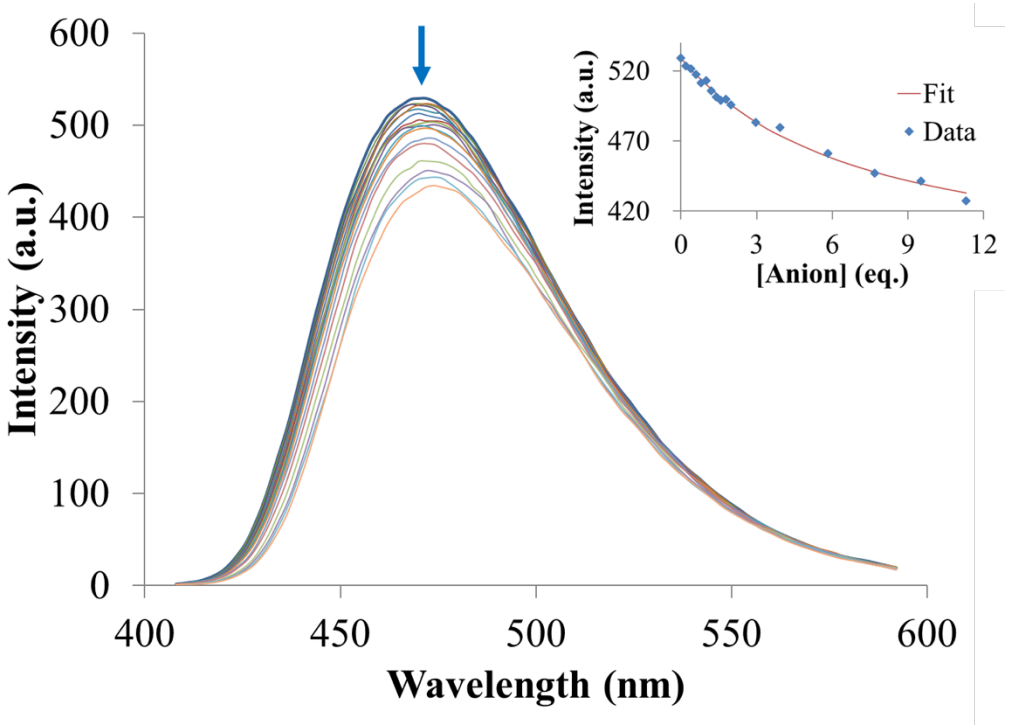

Figure S3. 48 Fluorescence titration of **121** with TBACl (0-12 equiv.) in $CHCl_3/CH_3CN$ at 298 K.

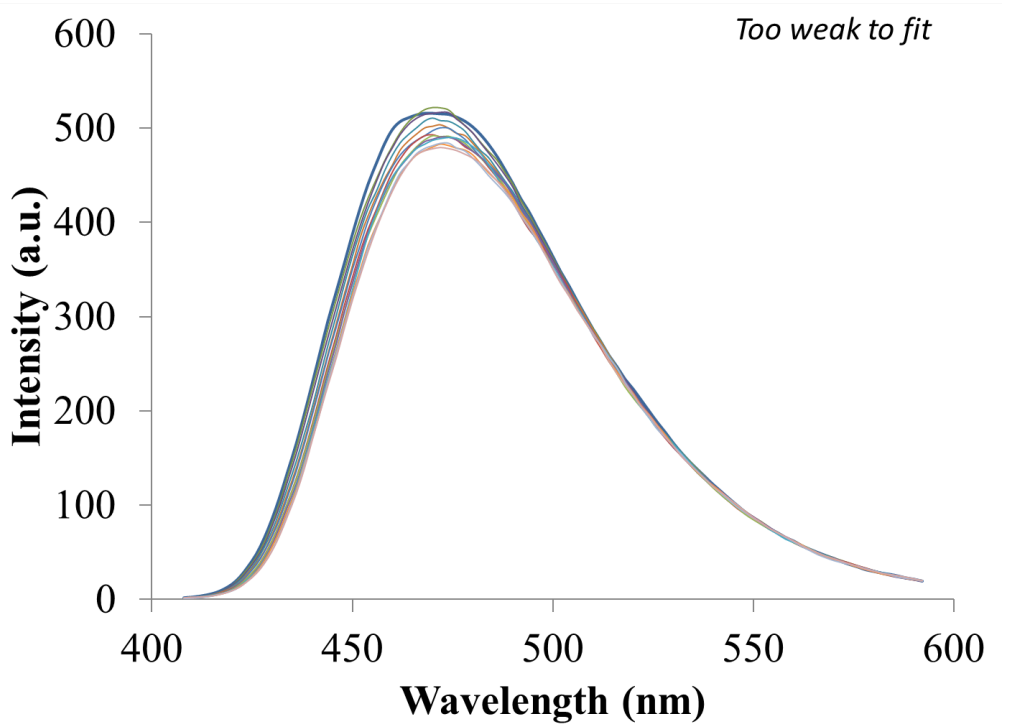

Figure S3. 49 Fluorescence titration of **121** with TBAOMs (0-12 equiv.) in $CHCl_3/CH_3CN$ at 298 K.

*^{1}H NMR titrations of rotaxane (**120**)*

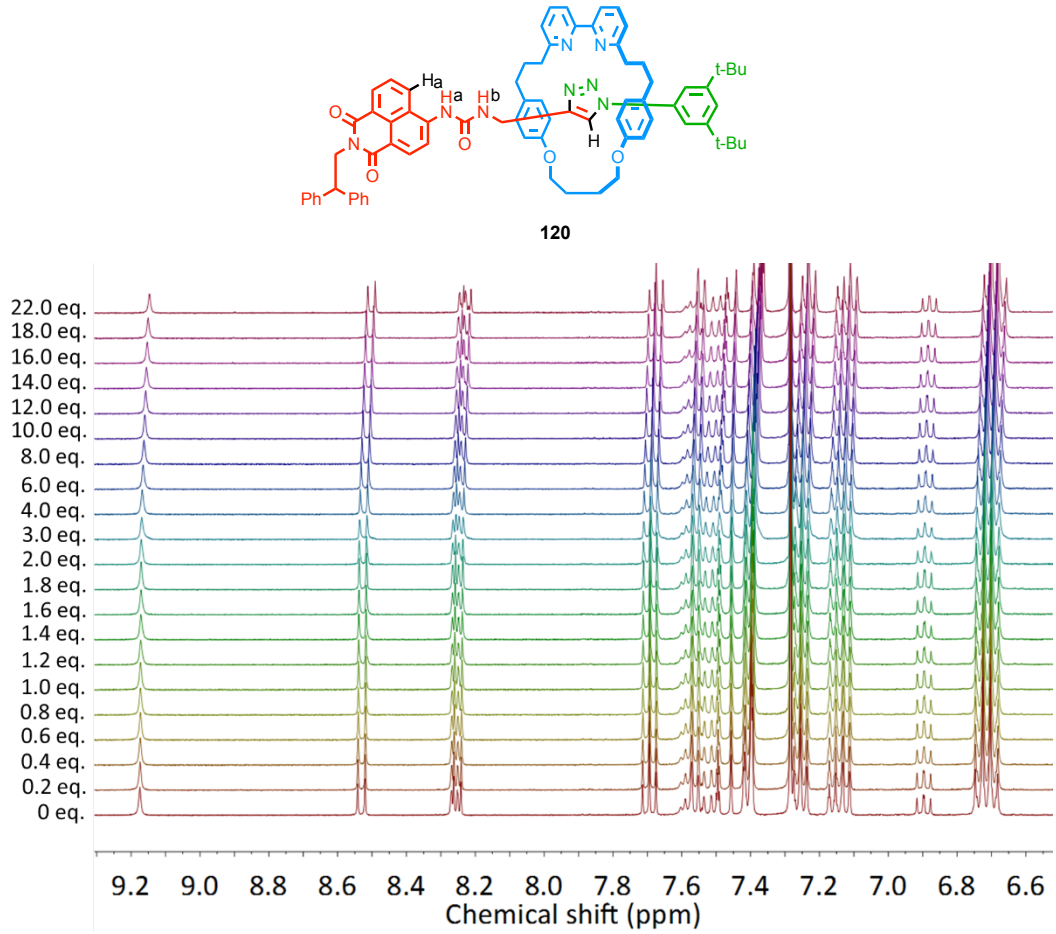

120

Figure S3. 50 ^{1}H NMR titration of **120** with TBAOAc (0-12 equiv.) in $CDCl_3/CD_3CN$ at 298 K.

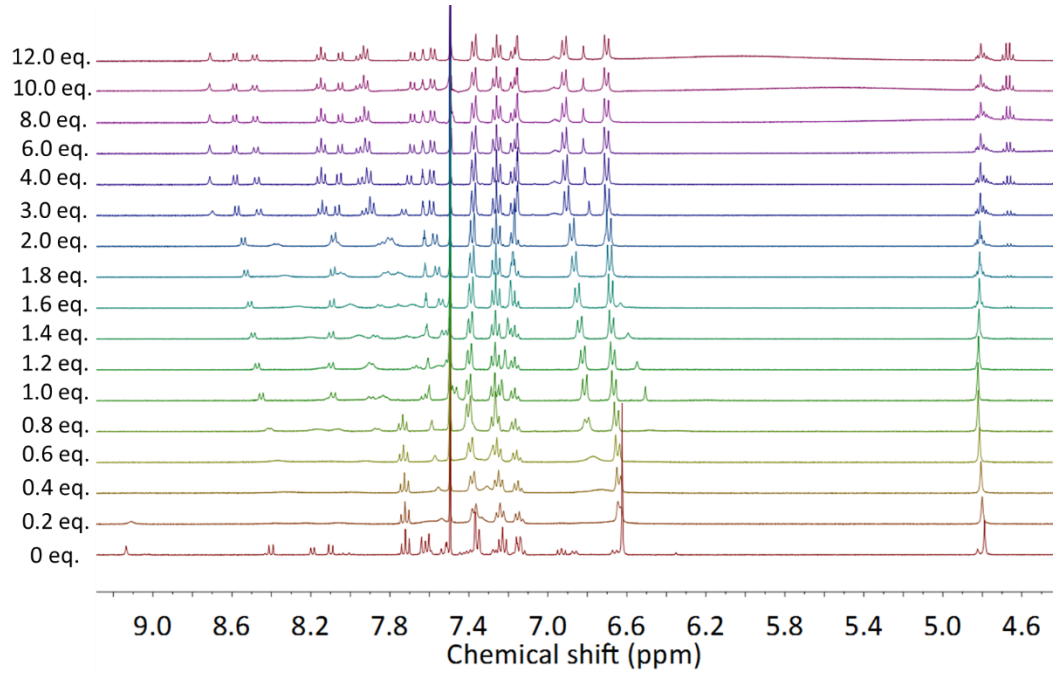

Figure S3. 51 ^{1}H NMR titration of **120** with HBF_4 (0-1 equiv.) in $CDCl_3/CD_3CN$ at 298 K.

*^{1}H NMR titrations of rotaxane **120**.HBF$_4$*

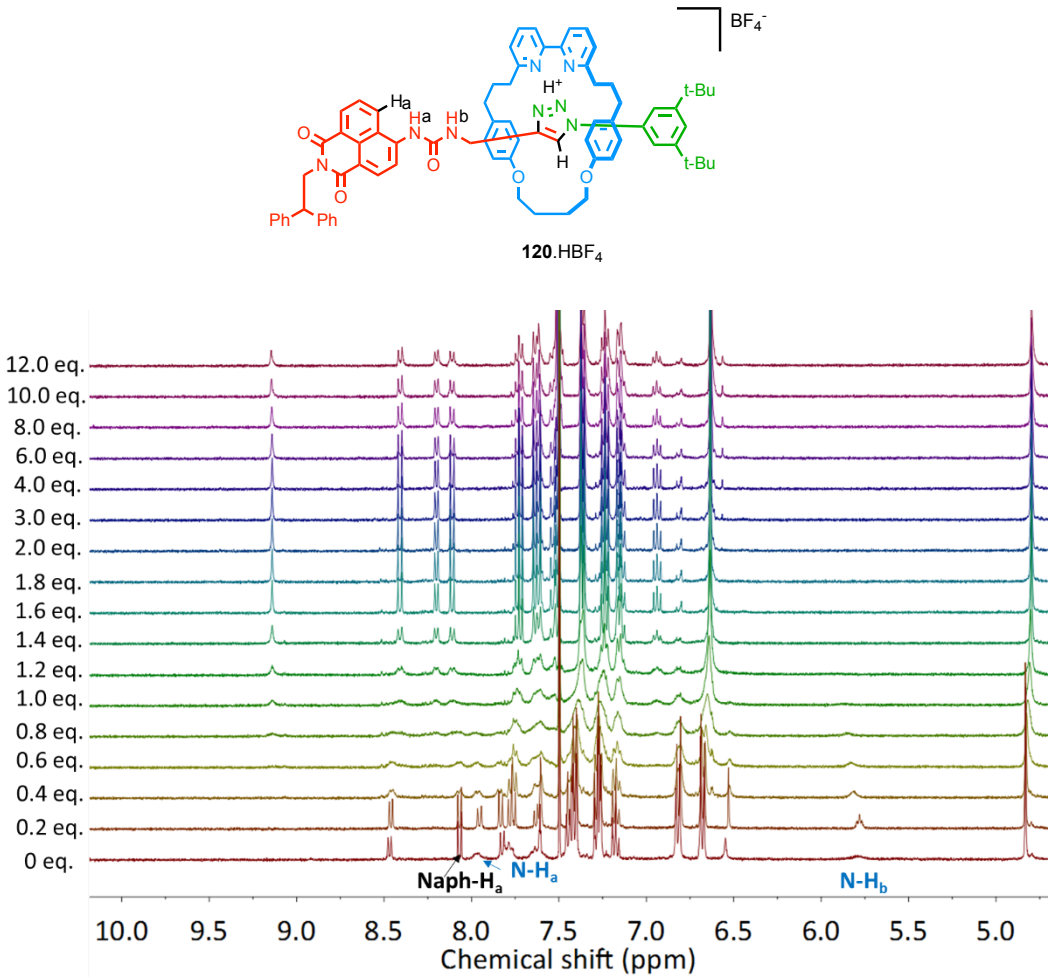

Figure S3. 52 ^{1}H NMR titration of **120**.HBF$_4$with TBAOAc (0-12 equiv.) in CDCl$_3$/CD$_3$CN at 298 K (Deprotonation).

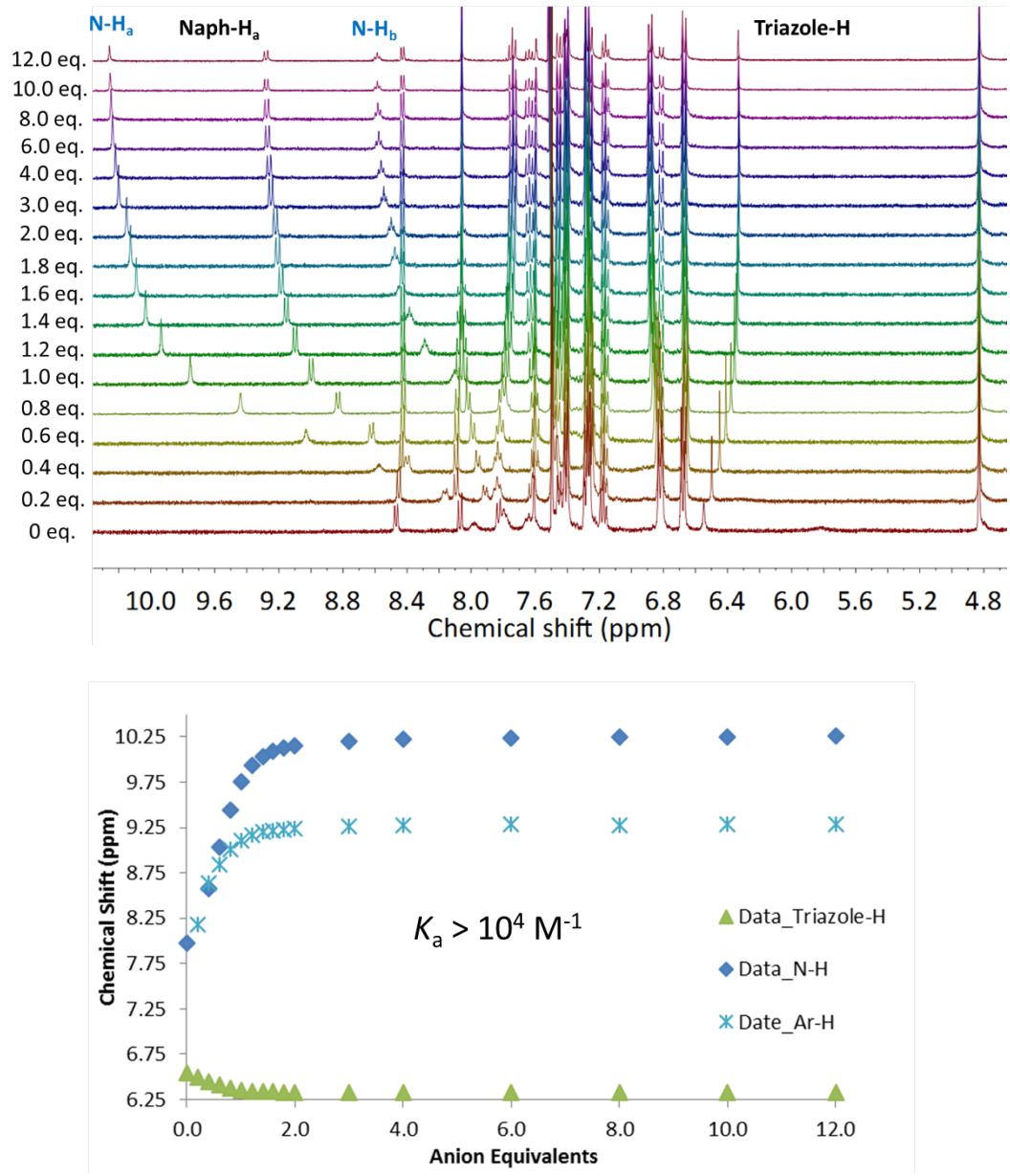

Figure S3. 53 ^{1}H NMR titration of **120**.HBF_4 with TBACl (0-12 eq.) in $CDCl_3/CD_3CN$ at 298 K.

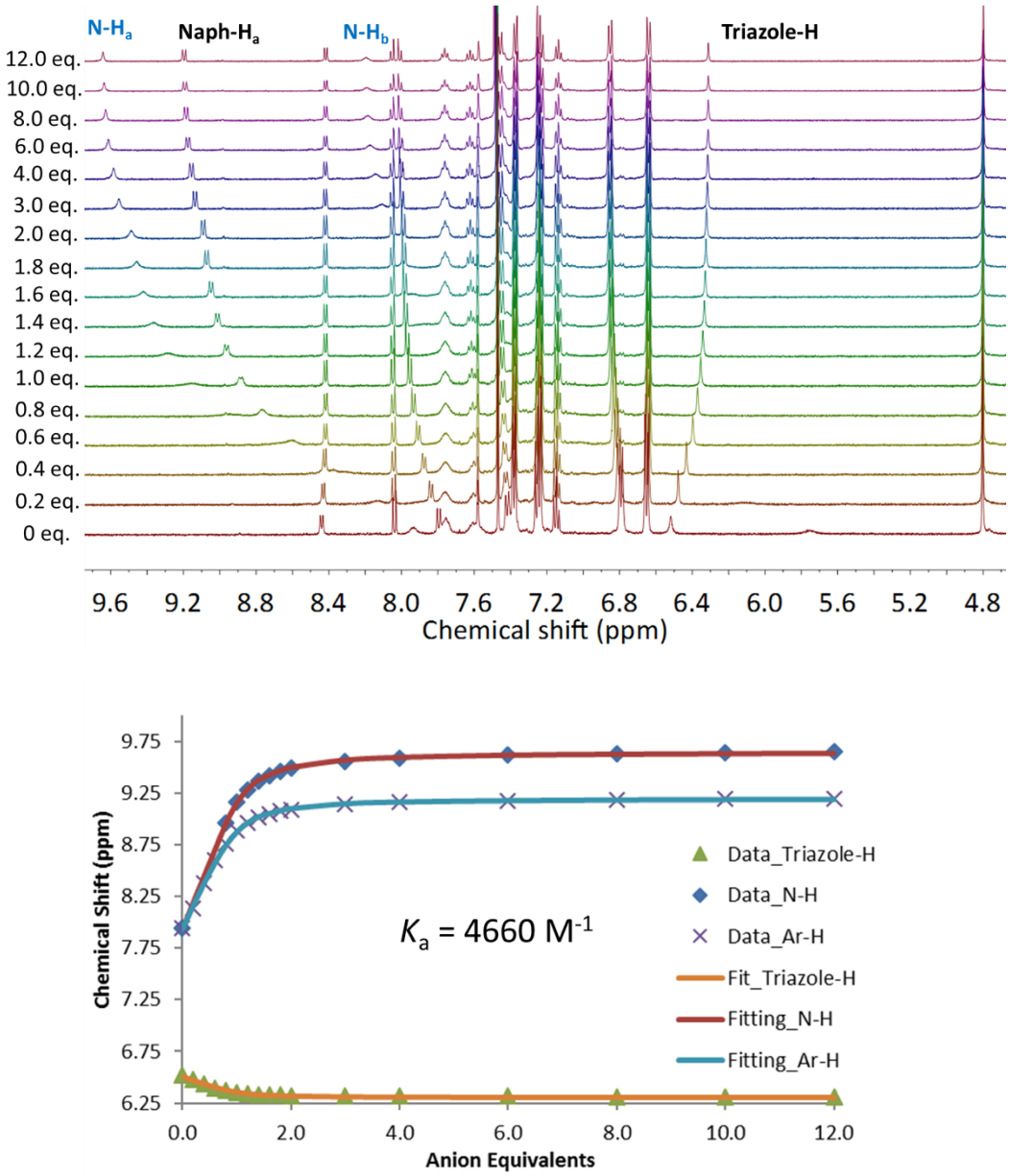

Figure S3. 54 ^{1}H NMR titration of **120**.HBF_4 with TBABr (0-12 equiv.) in $CDCl_3/CD_3CN$ at 298 K.

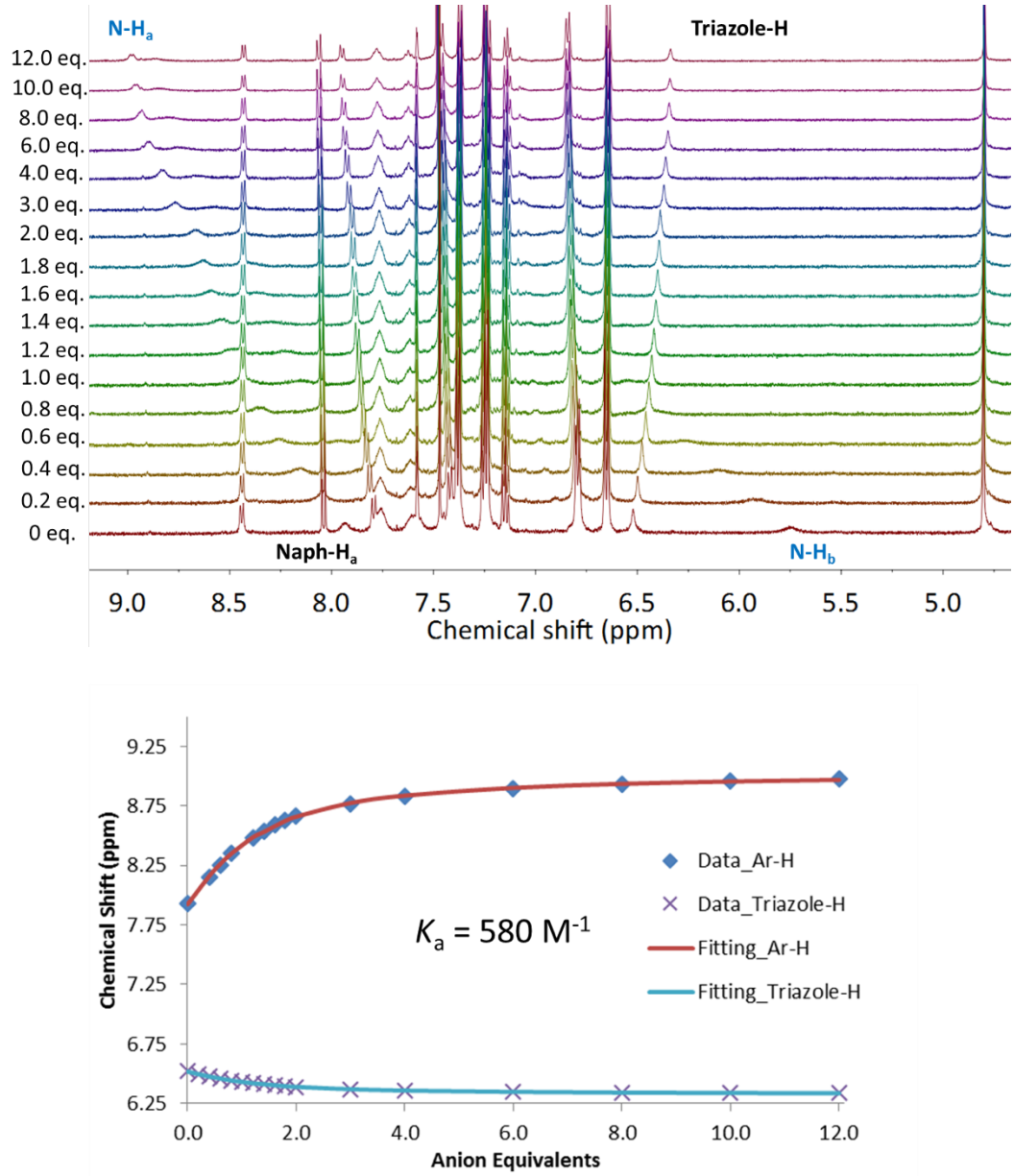

Figure S3. 55 ^{1}H NMR titration of **120**.HBF_4 with TBAI (0-12 equiv.) in $CDCl_3/CD_3CN$ at 298 K.

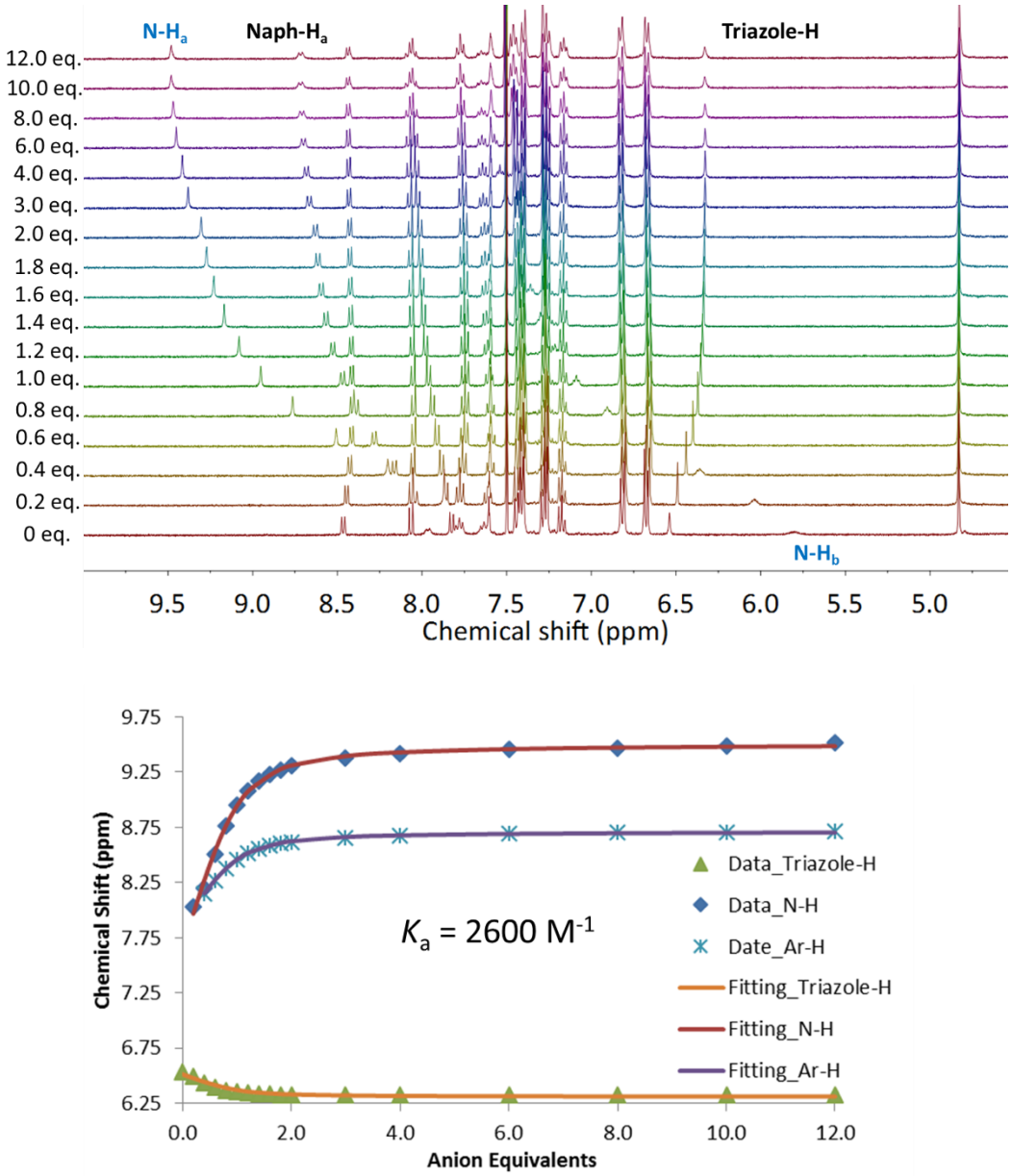

Figure S3. 56 ^{1}H NMR titration of **120**.HBF_4 with TBAOMs (0-12 equiv.) in $CDCl_3/CD_3CN$ at 298 K.

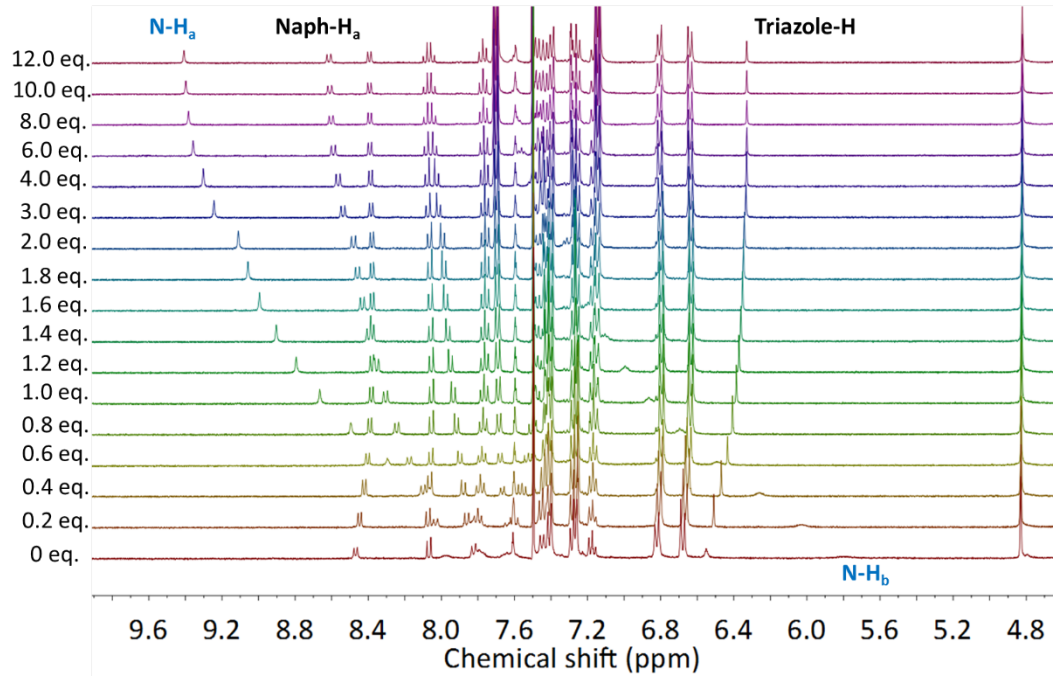

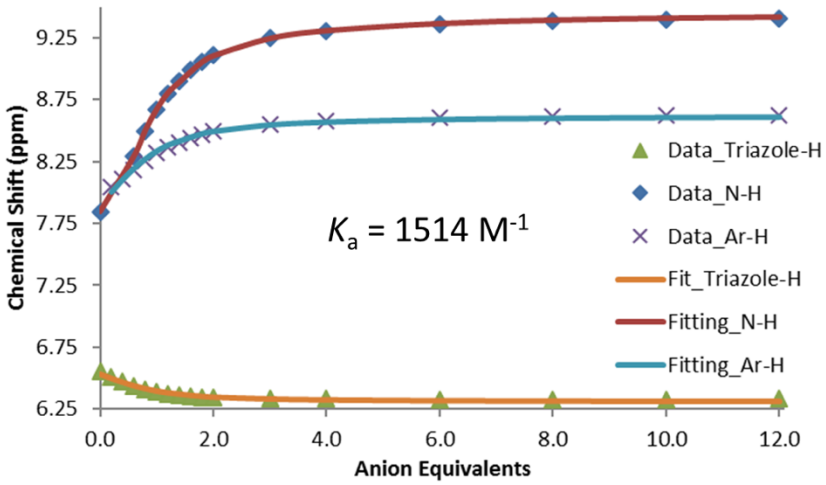

Figure S3. 57 ^{1}H NMR titration of **120**.HBF_4 with TBAOTs (0-12 equiv.) in $CDCl_3/CD_3CN$ at 298 K.

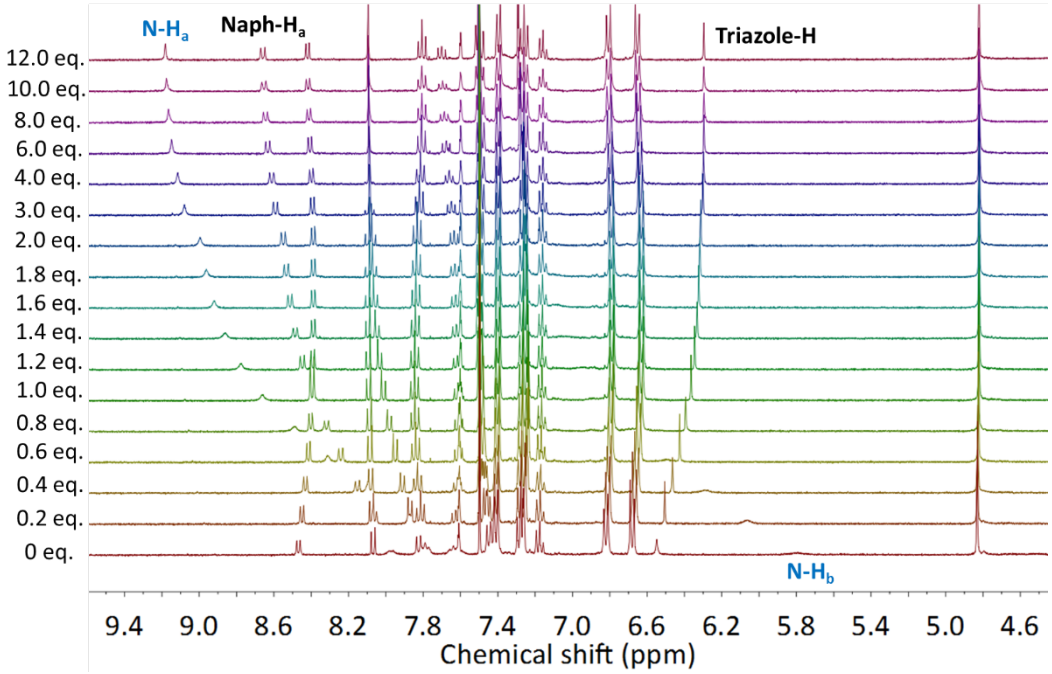

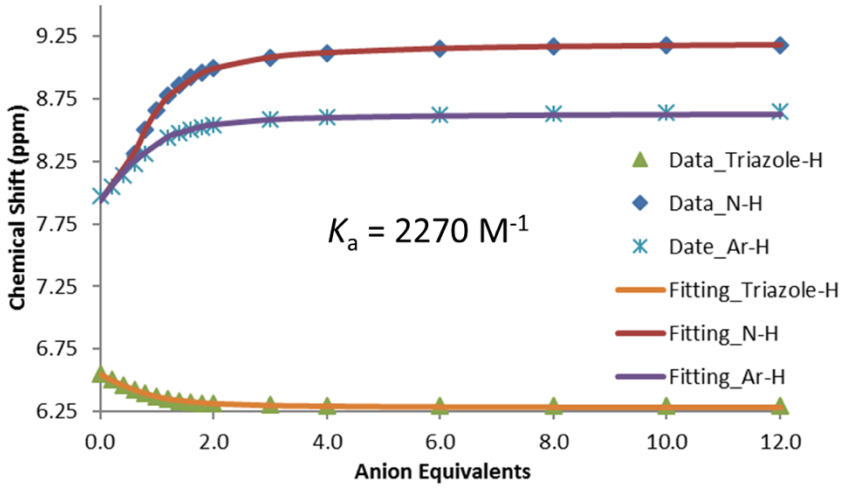

Figure S3. 58 ^{1}H NMR titration of **120**.HBF_4 with $TBAHSO_4$ (0-12 equiv.) in $CDCl_3/CD_3CN$ at 298 K.

*UV-Vis titrations of rotaxane **120**.HBF_4*

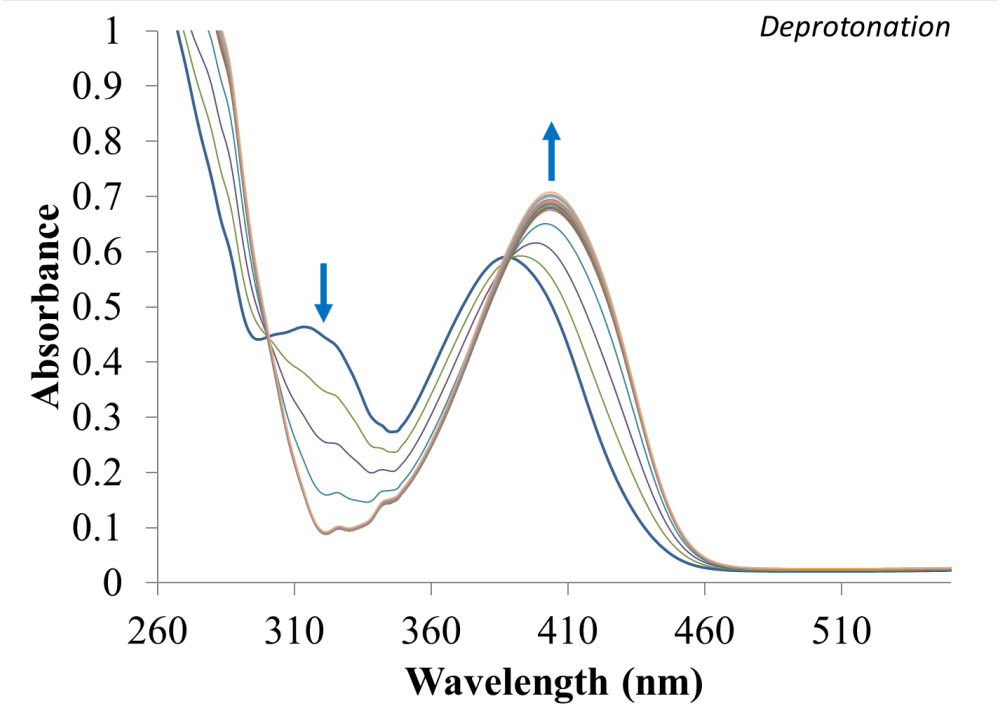

Figure S3. 59 UV-Vis titration of **120**.HBF_4 with TBAAcO (0-12 equiv.) in $CHCl_3/CH_3CN$ at 298 K.

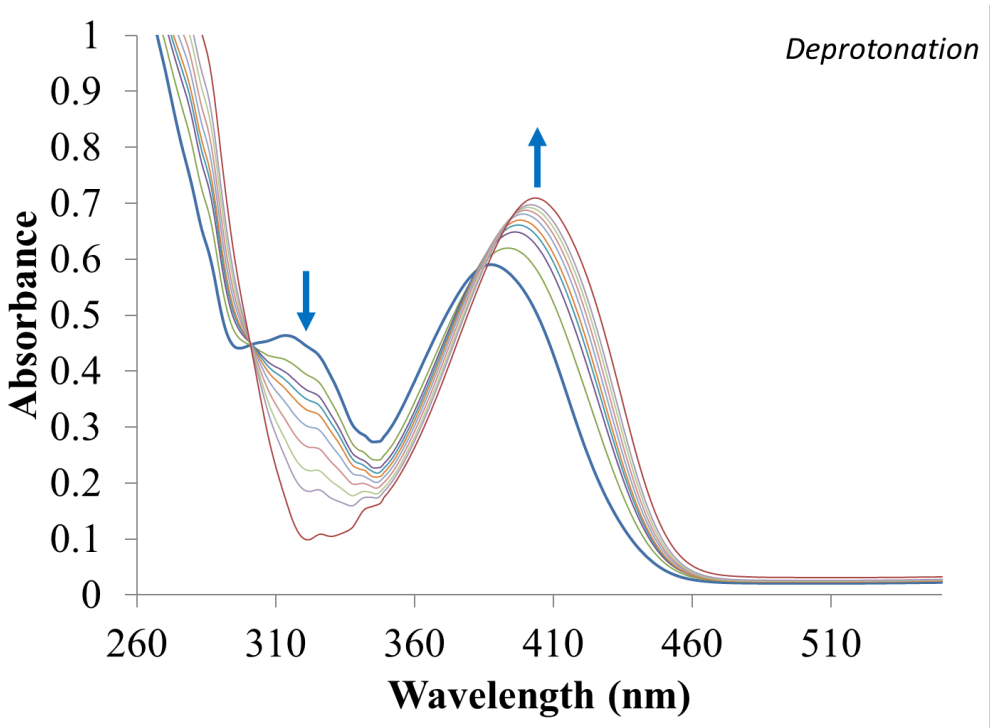

Figure S3. 60 UV-Vis titration of **120**.HBF_4 with TBAOH (0-12 equiv.) in $CHCl_3/CH_3CN$ at 298 K.

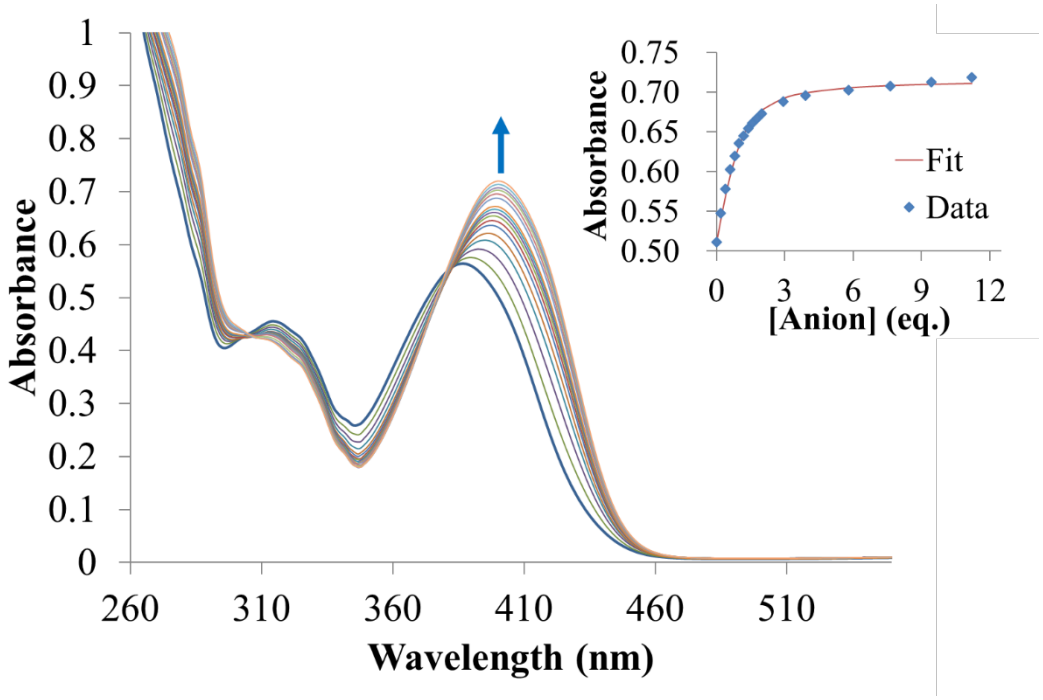

Figure S3. 61 UV-Vis titration of **120**.HBF_4 with TBACl (0-12 equiv.) in $CHCl_3/CH_3CN$ at 298 K.

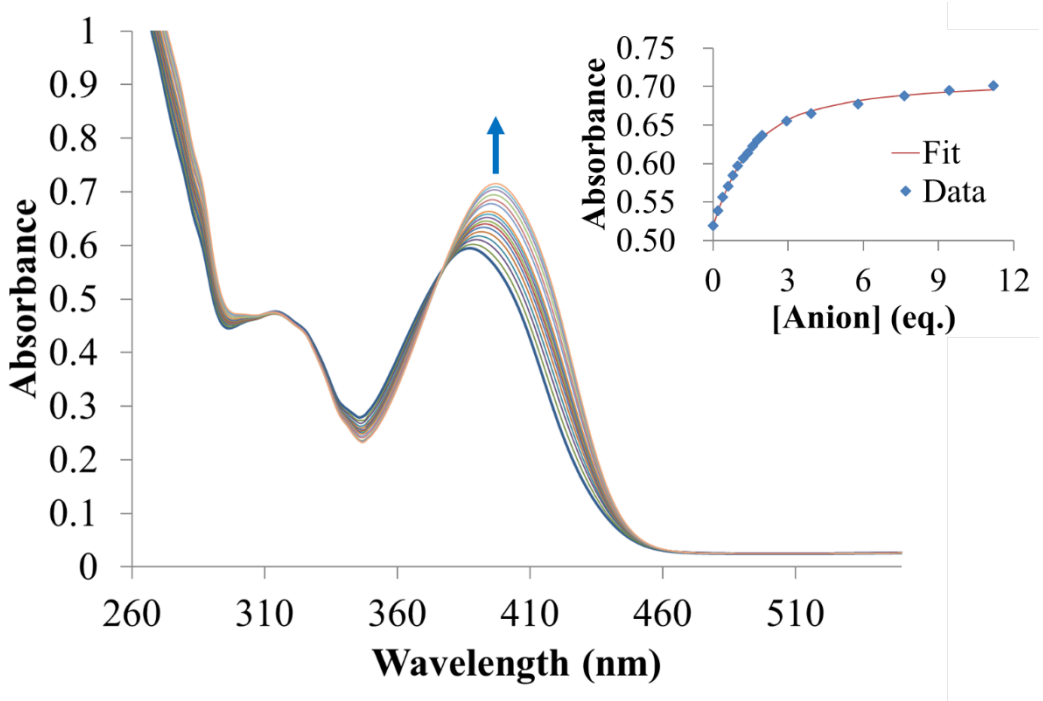

Figure S3. 62 UV-Vis titration of **120**.HBF_4 with TBABr (0-12 equiv.) in $CHCl_3/CH_3CN$ at 298 K.

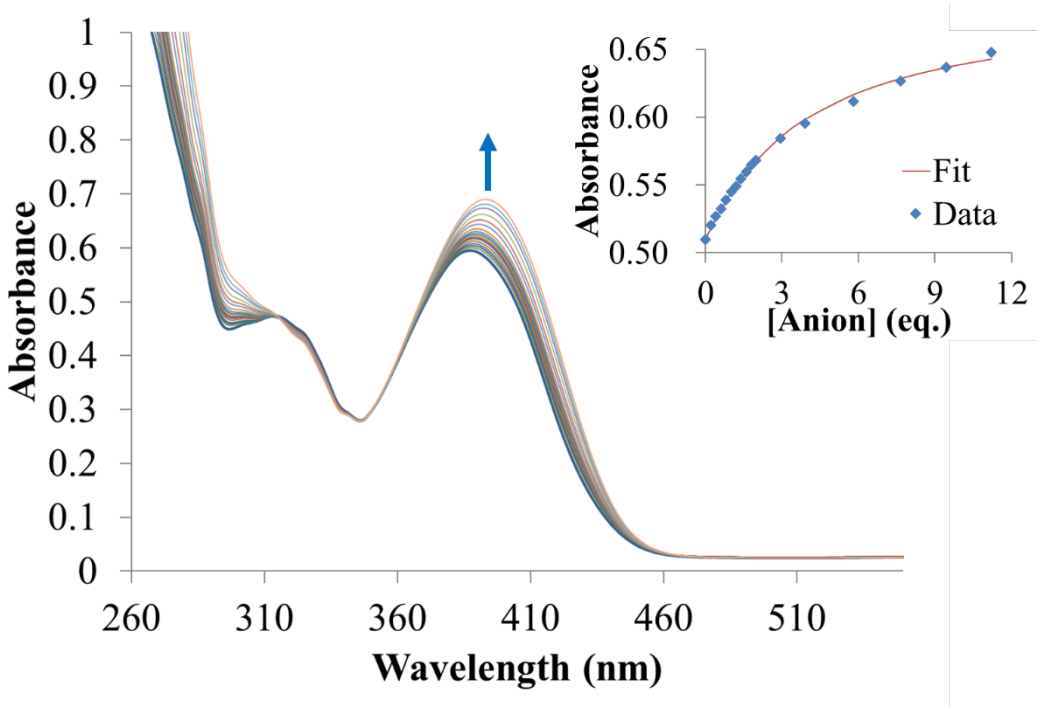

Figure S3. 63 UV-Vis titration of **120**.HBF_4 with TBAI (0-12 equiv.) in $CHCl_3/CH_3CN$ at 298 K.

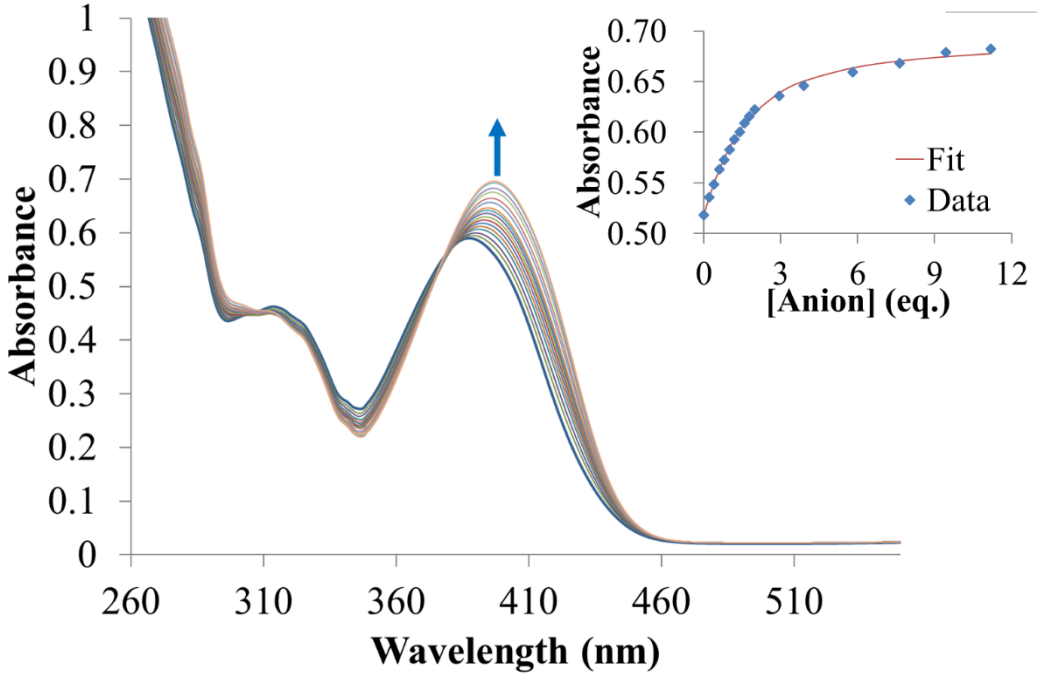

Figure S3. 64 UV-Vis titration of **120**.HBF_4 with TBAOMs (0-12 equiv.) in $CHCl_3/CH_3CN$ at 298 K.

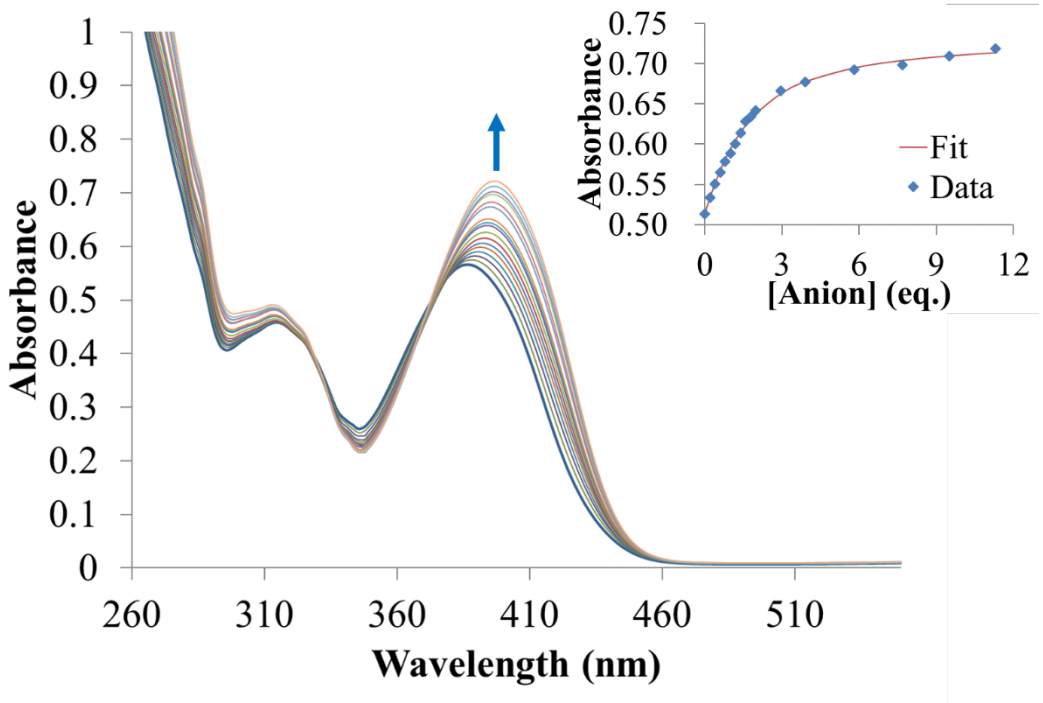

Figure S3. 65 UV-Vis titration of **120**.HBF_4 with TBAOTs (0-12 equiv.) in $CHCl_3/CH_3CN$ at 298 K.

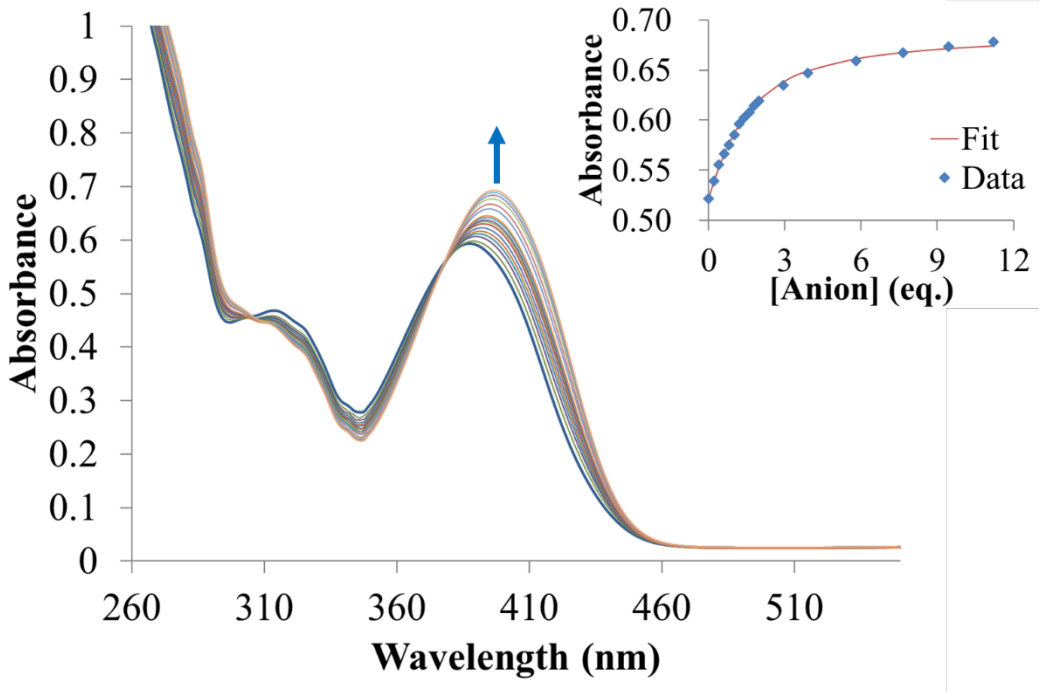

Figure S3. 66 UV-Vis titration of **120**.HBF_4 with $TBAHSO_4$ (0-12 equiv.) in $CHCl_3/CH_3CN$ at 298 K.

3.5. Fluorescence titrations of **120**.HBF_4

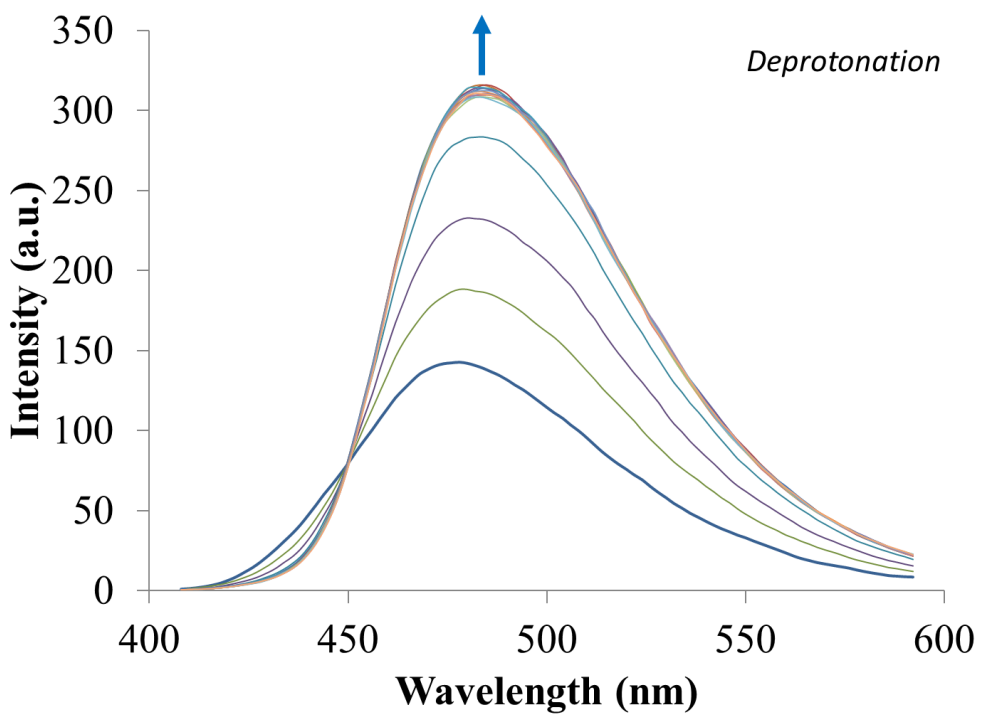

Figure S3. 67 Fluorescence titration of **120**.HBF_4 with TBAOAc (0-12 equiv.) in $CHCl_3/CH_3CN$ at 298 K.

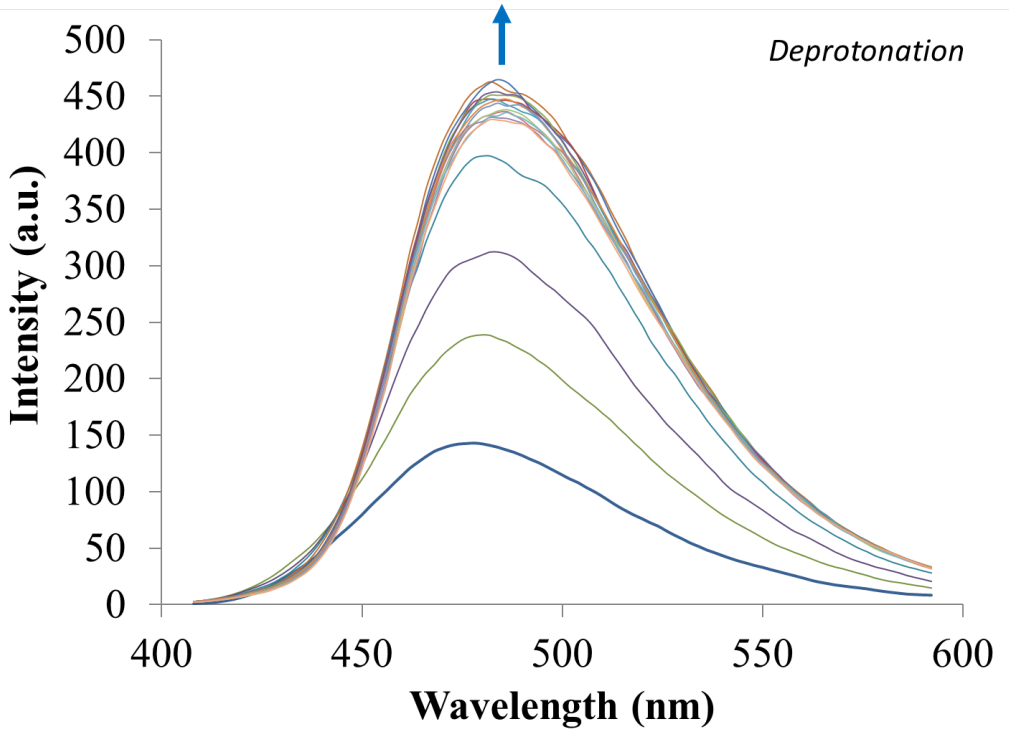

Figure S3. 68 Fluorescence titration of **120**.HBF_4 with TBAOH (0-12 equiv.) in $CHCl_3/CH_3CN$ at 298 K.

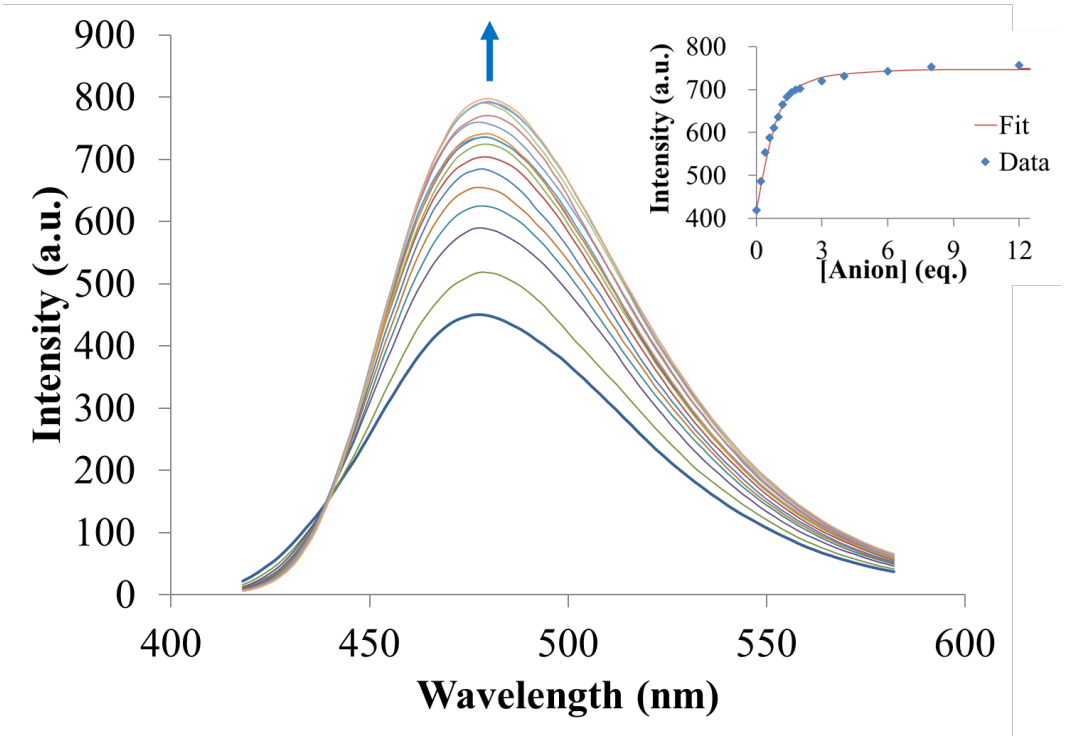

Figure S3. 69 Fluorescence titration of **120**.HBF_4 with TBACl (0-12 equiv.) in $CHCl_3/CH_3CN$ at 298 K.

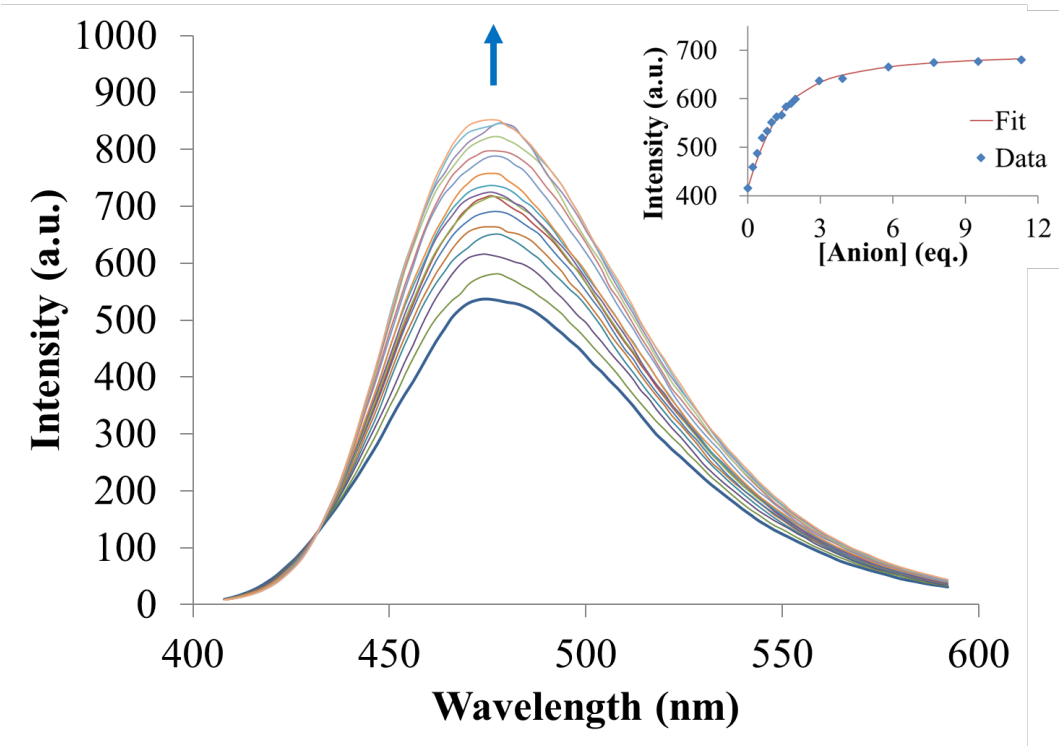

Figure S3. 70 Fluorescence titration of **120**.HBF_4 with TBABr (0-12 equiv.) in $CHCl_3/CH_3CN$ at 298 K.

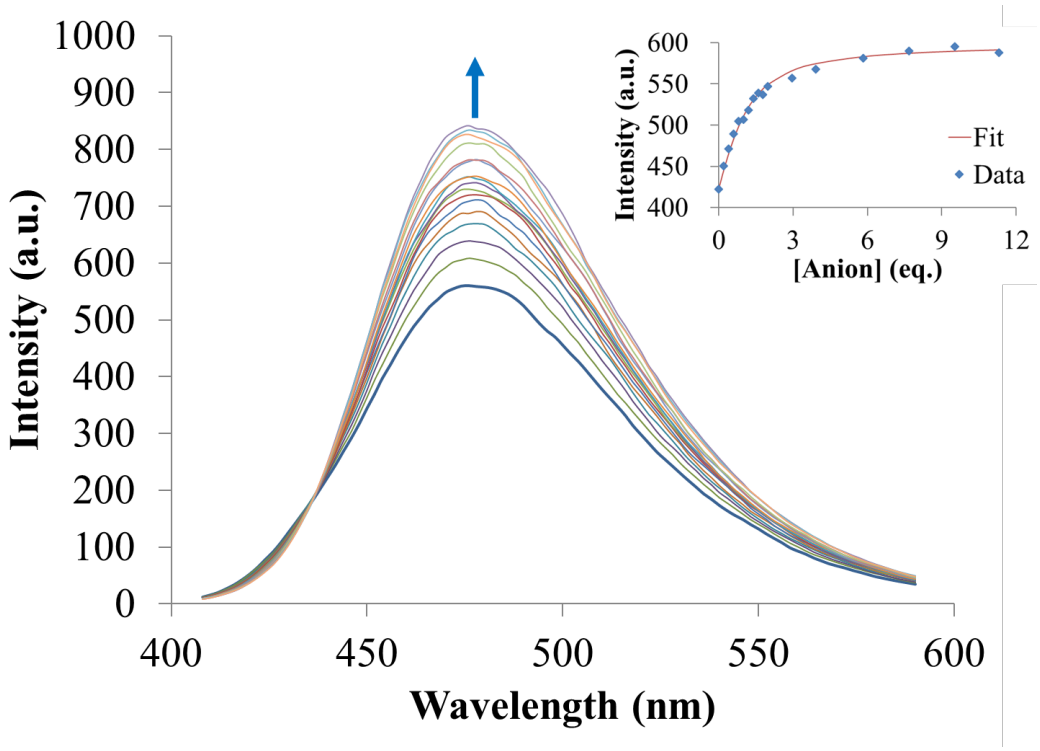

Figure S3. 71 Fluorescence titration of **120**.HBF_4 with TBAOMs (0-12 equiv.) in $CHCl_3/CH_3CN$ at 298 K.

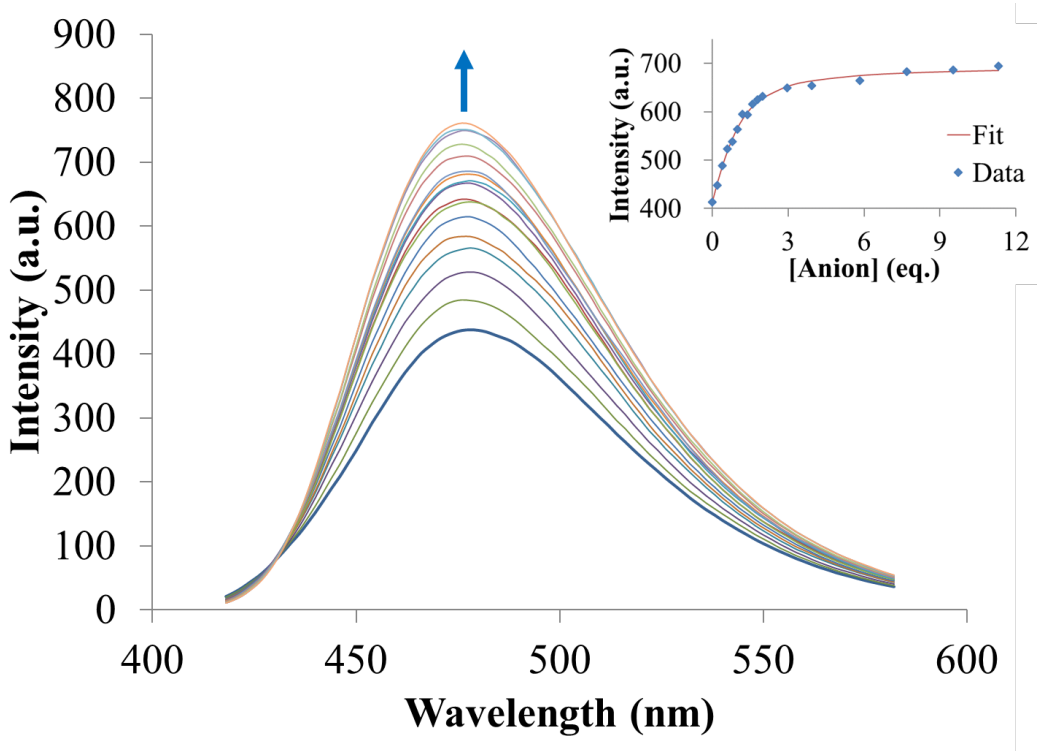

Figure S3. 72 Fluorescence titration of **120**.HBF_4 with TBAOTs (0-12 equiv.) in $CHCl_3/CH_3CN$ at 298 K.

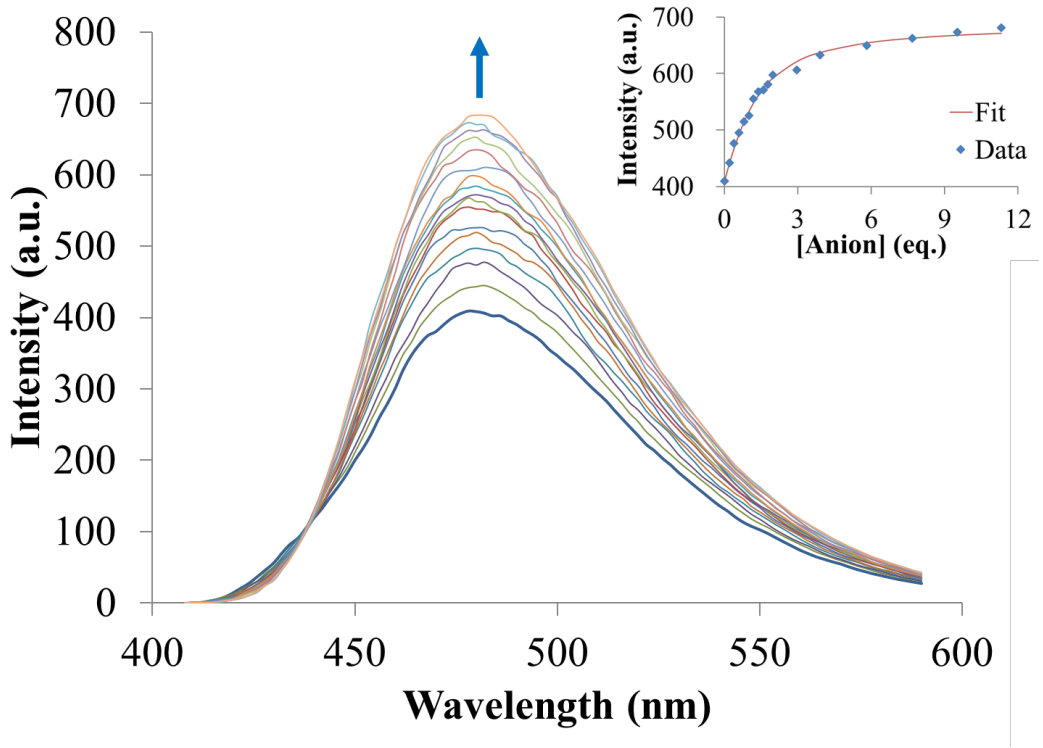

Figure S3. 73 Fluorescence titration of **120**.HBF_4 with $TBAHSO_4$ (0-12 equiv.) in $CHCl_3/CH_3CN$ at 298 K.

X-ray Data

Crystals of **110** were grown from vapour diffusion of pentane in a solution of **110** in Et_2O. Crystals of **120** were obtained from slow cooling of a $EtOH/H_2O$ mixture or by vapour diffusion of Et_2O in a solution of **120** in CH_2Cl_2. Crystals of **120**.HBF_4 were obtained from vapor diffusion of Et_2O into a solution of **120**.HBF_4 in CH_2Cl_2. Crystals of **120**.HBF_4 binding Cl were obtained from slow evaporation of a $MeCN/Et_2O$ mixture **120**.HBF_4 in the presence of TBACl (10 equiv.). Data were collected at 100 K using a Rigaku 007 HF diffractometer equipped with a Saturn 944+ enhanced sensitivity detector. Cell determination and data collection were done using CrystalClear-SM Expert 3.1; data reduction, cell refinement and absorption correction were performed with CrysalisPro. The structure was solved using SUPERFLIP and refined against F_2 using anisotropic thermal displacement parameters for all non-hydrogen atoms using WINGX and software packages within. Hydrogen atoms were placed in calculated positions and refined using a riding model.

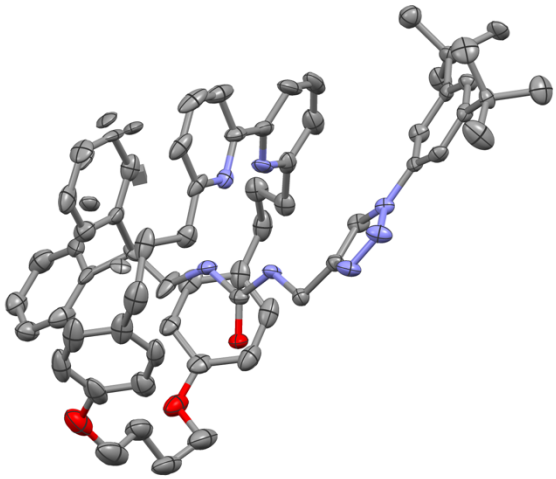

Figure S3. 74 Ellipsoid plot of rotaxane **110**. The diphenyl stopper still requires more refinement. Ellipsoid are shown at 50% probability. Hydrogens were omitted for clarity.

Table S3. 1 Crystal data and structure refinement for 2016md_urea_rotaxane_Estra4_100K.

Identification code	2016md_urea_rotaxane_Estra4_100K
Empirical formula	$C_{64}H_{74}N_7O_3$
Formula weight	988.29
Temperature/K	100(2)
Crystal system	monoclinic
Space group	$P2_1/c$
a/Å	10.5387(9)
b/Å	20.7568(19)
c/Å	25.412(3)
α/°	90
β/°	94.983(9)
γ/°	90
Volume/Å^3	5537.8(10)
Z	4
ρ_{calc}g/cm^3	1.185
μ/mm^{-1}	0.073
F(000)	2120.0
Crystal size/mm^3	0.050 × 0.030 × 0.030
Radiation	MoKα (λ = 0.71073)
2Θ range for data collection/°	3.218 to 52.744
Index ranges	-13 ≤ h ≤ 13, -25 ≤ k ≤ 19, -31 ≤ l ≤ 28
Reflections collected	48388
Independent reflections	11310 [R_{int} = 0.2943, R_{sigma} = 0.3442]
Data/restraints/parameters	11310/702/715
Goodness-of-fit on F^2	0.960
Final R indexes [I>=2σ (I)]	R_1 = 0.1080, wR_2 = 0.2184
Final R indexes [all data]	R_1 = 0.3003, wR_2 = 0.3234
Largest diff. peak/hole / e Å^{-3}	0.40/-0.54

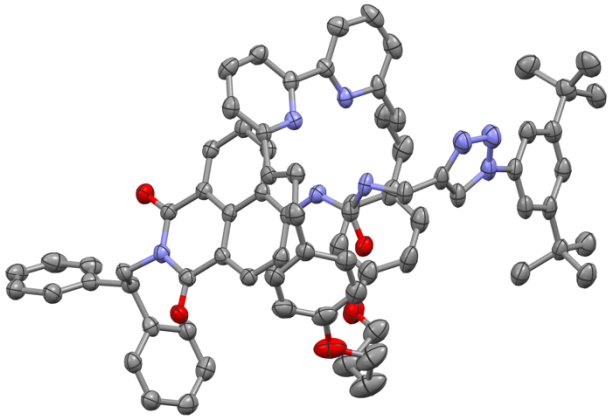

Figure S3. 75 Ellipsoid plot of rotaxane **120** for the crystals grown from a mixture MeOH/H_2O. Ellipsoid are shown at 50% probability. Hydrogens were omitted for clarity.

Table S3. 2 Crystal data and structure refinement for 2016md_V_029_MeOH_100K.

Identification code	2016md_V_029_MeOH_100K
Empirical formula	$C_{10}HN_{71}O_{11}$
Formula weight	1290.81
Temperature/K	100(2)
Crystal system	triclinic
Space group	P-1
a/Å	13.8653(8)
b/Å	15.7188(8)
c/Å	18.0898(7)
α/°	104.124(4)
β/°	94.099(4)
γ/°	114.898(5)
Volume/$Å^3$	3399.3(3)
Z	2
$\rho_{calc}g/cm^3$	1.261
μ/mm^{-1}	0.110
F(000)	1290.0
Crystal size/mm^3	0.040 × 0.020 × 0.010
Radiation	MoKα (λ = 0.71073)
2Θ range for data collection/°	2.998 to 52.744
Index ranges	-17 ≤ h ≤ 17, -19 ≤ k ≤ 19, -22 ≤ l ≤ 21
Reflections collected	60212
Independent reflections	13910 [R_{int} = 0.1013, R_{sigma} = 0.1175]
Data/restraints/parameters	13910/0/808
Goodness-of-fit on F^2	1.035
Final R indexes [I>=2σ (I)]	R_1 = 0.0903, wR_2 = 0.2100
Final R indexes [all data]	R_1 = 0.1752, wR_2 = 0.2649
Largest diff. peak/hole / e $Å^{-3}$	0.50/-0.31

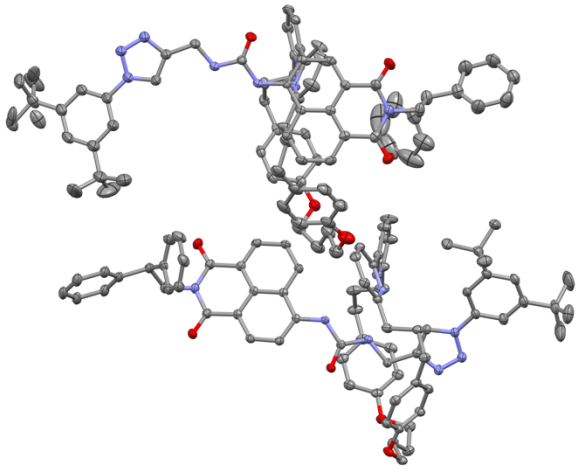

Figure S3. 76 Ellipsoid plot of rotaxane **120** for the crystals grown vapour diffusion of Et_2O in a solution of **120** in CH_2Cl_2. Ellipsoid are shown at 50% probability. Hydrogens were omitted for clarity.

Table S3. 3 Crystal data and structure refinement for 2015mdIII021_camphorsulfonicacid100K.

Identification code	2015mdIII021_camphorsulfonicacid100K
Empirical formula	$C_{152}H_{156}N_{16}O_{10}$
Formula weight	2366.92
Temperature/K	100(2)
Crystal system	triclinic
Space group	P-1
a/Å	16.0484(3)
b/Å	18.9960(3)
c/Å	23.1296(3)
α/°	83.2920(12)
β/°	80.9244(13)
γ/°	70.3923(14)
Volume/Å^3	6543.71(18)
Z	2
ρ_{calc}g/cm^3	1.201
μ/mm^{-1}	0.076
F(000)	2520.0
Crystal size/mm^3	0.100 × 0.060 × 0.050
Radiation	MoKα (λ = 0.71073)
2Θ range for data collection/°	3.056 to 52.744
Index ranges	-20 ≤ h ≤ 20, -23 ≤ k ≤ 23, -28 ≤ l ≤ 28
Reflections collected	118920
Independent reflections	26752 [R_{int} = 0.0286, R_{sigma} = 0.0221]
Data/restraints/parameters	26752/36/1645
Goodness-of-fit on F^2	1.019
Final R indexes [I>=2σ (I)]	R_1 = 0.0708, wR_2 = 0.1923
Final R indexes [all data]	R_1 = 0.0855, wR_2 = 0.2073
Largest diff. peak/hole / e Å^{-3}	1.39/-0.65

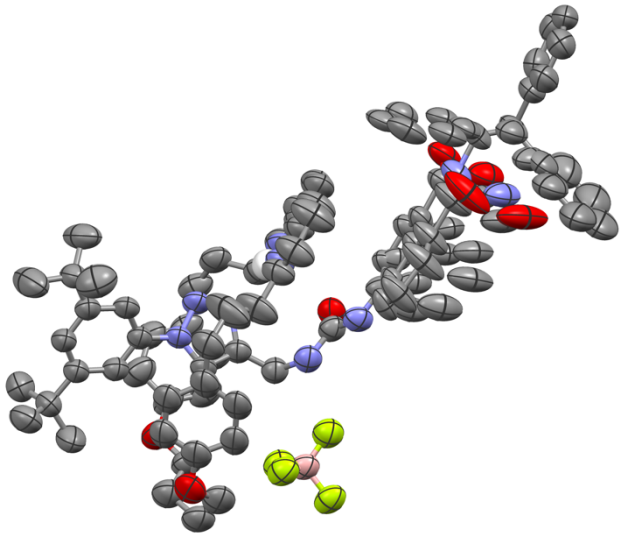

Figure S3. 77 Ellipsoid plot of rotaxane **120**.HBF_4. Ellipsoid are shown at 50% probability. Hydrogens were omitted for clarity.

Table S3. 4 Crystal data and structure refinement for 2017_md_naphtha_HBF4_dot_b_100K.

Identification code	2017_md_naphtha_HBF4_dot_b_100K
Empirical formula	$C_{76}H_{79}BF_4N_8O_5$
Formula weight	1271.28
Temperature/K	100(2)
Crystal system	triclinic
Space group	P-1
a/Å	12.6911(3)
b/Å	17.3702(5)
c/Å	19.0346(5)
α/°	100.235(3)
β/°	96.419(2)
γ/°	97.845(2)
Volume/Å^3	4050.7(2)
Z	2
ρ_{calc}g/cm^3	1.042
μ/mm^{-1}	0.584
F(000)	1344.0
Crystal size/mm^3	0.050 × 0.040 × 0.020
Radiation	CuKα (λ = 1.54184)
2Θ range for data collection/°	7.744 to 141.578
Index ranges	-12 ≤ h ≤ 15, -20 ≤ k ≤ 20, -22 ≤ l ≤ 22
Reflections collected	60879
Independent reflections	15147 [R_{int} = 0.0628, R_{sigma} = 0.0575]
Data/restraints/parameters	15147/2025/1027
Goodness-of-fit on F^2	1.307
Final R indexes [I>=2σ (I)]	R_1 = 0.1175, wR_2 = 0.3486
Final R indexes [all data]	R_1 = 0.1835, wR_2 = 0.4086
Largest diff. peak/hole / e Å^{-3}	1.05/-0.28

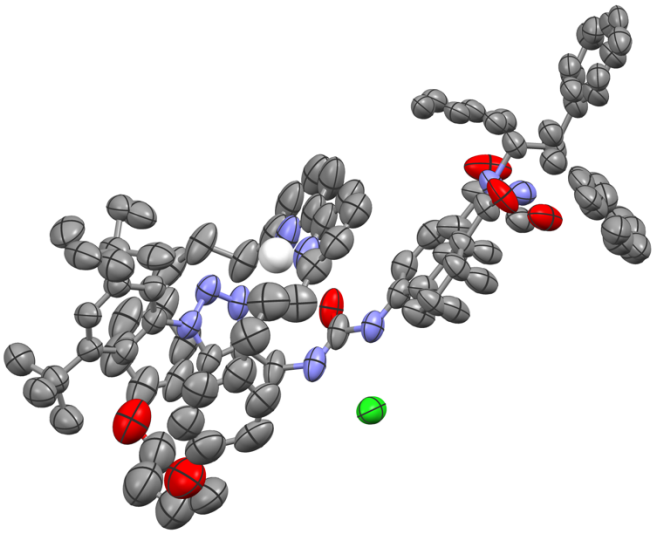

Figure S3. 78 Ellipsoid plot of rotaxane **120**.HCl. Ellipsoid are shown at 50% probability. Hydrogens were omitted for clarity.

Table S3. 5 Crystal data and structure refinement for 2017_md_naphtha_salt_Cl_b_dot_100K.

Identification code	2017_md_naphtha_salt_Cl_b_dot_100K
Empirical formula	$C_{76}H_{78.5}ClN_8O_5$
Formula weight	1217.90
Temperature/K	100
Crystal system	triclinic
Space group	P-1
a/Å	12.5002(2)
b/Å	17.8989(2)
c/Å	18.7000(3)
α/°	102.7550(10)
β/°	98.1480(10)
γ/°	97.0540(10)
Volume/Å^3	3987.71(10)
Z	2
ρ_{calc}g/cm^3	1.014
μ/mm^{-1}	0.804
F(000)	1292.0
Crystal size/mm^3	0.100 × 0.090 × 0.040
Radiation	CuKα (λ = 1.54184)
2Θ range for data collection/°	7.236 to 141.776
Index ranges	-14 ≤ h ≤ 14, -21 ≤ k ≤ 21, -22 ≤ l ≤ 22
Reflections collected	58570
Independent reflections	14945 [R_{int} = 0.0461, R_{sigma} = 0.0460]
Data/restraints/parameters	14945/2218/1045
Goodness-of-fit on F^2	2.081
Final R indexes [I>=2σ (I)]	R_1 = 0.1616, wR_2 = 0.4827
Final R indexes [all data]	R_1 = 0.2207, wR_2 = 0.5372
Largest diff. peak/hole / e Å^{-3}	1.09/-0.50

3.6. Bibliography

[1] F. P. Schmidtchen, M. Berger, *Chem. Rev.* **1997**, *97*, 1609–1646.

[2] N. Busschaert, C. Caltagirone, W. Van Rossom, P. a. Gale, *Chem. Rev.* **2015**, *115*, 8038–8155.

[3] P. Molina, F. Zapata, A. Caballero, *Chem. Rev.* **2017**, acs.chemrev.6b00814.

[4] L. S. Kaminsky, M. C. Mahoney, J. Leach, J. Melius, M. Jo Miller, *Crit. Rev. Oral Biol. Med.* **1990**, *1*, 261–281.

[5] R. Martínez-Máñez, F. Sancenón, *Chem. Rev.* **2003**, *103*, 4419–4476.

[6] P. A. Gale, N. Busschaert, C. J. E. Haynes, L. E. Karagiannidis, I. L. Kirby, *Chem. Soc. Rev.* **2014**, *43*, 205–241.

[7] M. J. Langton, P. D. Beer, *Acc. Chem. Res.* **2014**, *47*, 1935–1949.

[8] J. W. Pflugrath, F. A. Quiocho, *Nature* **1985**, *314*, 257–260.

[9] H. Luecke, F. a. Quiocho, *Nature* **1990**, *347*, 402–406.

[10] A. Caballero, F. Zapata, P. D. Beer, *Coord. Chem. Rev.* **2013**, *257*, 2434–2455.

[11] N. H. Evans, P. D. Beer, *Angew. Chem. Int. Ed.* **2014**, *53*, 11716–11754.

[12] M. Xue, Y. Yang, X. Chi, X. Yan, F. Huang, *Chem. Rev.* **2015**, *115*, 7398–7501.

[13] J. a. Wisner, P. D. Beer, M. G. B. Drew, M. R. Sambrook, *J. Am. Chem. Soc.* **2002**, *124*, 12469–12476.

[14] L. M. Hancock, L. C. Gilday, S. Carvalho, P. J. Costa, V. Félix, C. J. Serpell, N. L. Kilah, P. D. Beer, *Chem. Eur. J.* **2010**, *16*, 13082–13094.

[15] N. H. Evans, C. J. Serpell, P. D. Beer, *Chem. Commun.* **2011**, *47*, 8775.

[16] M. J. Langton, P. D. Beer, *Chem. Eur. J.* **2012**, *18*, 14406–14412.

[17] T. A. Barendt, A. Docker, I. Marques, V. Félix, P. D. Beer, *Angew. Chem. Int. Ed.* **2016**, *55*, 11069–11076.

[18] M. V. R. Raju, H.-C. Lin, *Org. Lett.* **2013**, *15*, 1274–1277.

[19] C. G. Collins, E. M. Peck, P. J. Kramer, B. D. Smith, *Chem. Sci.* **2013**, *4*, 2557.

[20] J. Berná, C. Franco-Pujante, M. Alajarín, *Org. Biomol. Chem.* **2014**, *12*, 474–478.

[21] J. R. Romero, G. Aragay, P. Ballester, *Chem. Sci.* **2017**, *8*, 491–498.

[22] H. Lahlali, K. Jobe, M. Watkinson, S. M. Goldup, *Angew. Chem. Int. Ed.* **2011**, *50*, 4151–4155.

[23] M. Galli, J. E. M. Lewis, S. M. Goldup, *Angew. Chem. Int. Ed.* **2015**, *54*, 13545–13549.

[24] W. Zhu, D. Ma, *Chem. Commun.* **2004**, 888.

[25] J. E. M. Lewis, R. J. Bordoli, M. Denis, C. J. Fletcher, M. Galli, E. A. Neal, E. M. Rochette, S. M. Goldup, *Chem. Sci.* **2016**, *7*, 3154–3161.

Chapter 4: A Mechanically Planar Chiral Rotaxane Host for the Enantioselective Sensing of Chiral Anions

Abstract: This chapter reports the synthesis of a simple urea-based mechanically planar chiral rotaxane host and the preliminary binding studies of chiral anions with it. During the investigation, we observed that the racemate of the receptor was capable of chiral descrimination as the two enantiomers of the receptor would not necesseraly bind a single enantiomer of a guest with identical association constants. Moving forward with this result, we developed a new chiral auxiliary that permitted the isolataton, using simple column chromatography techniques, of an enantioenriched sample (*ee* 90%) of the interlocked receptor. Interestingly, preliminary binding studies have shown that the latter binds preferentially one enantiomer of 1,1'-binaphthyl-2,2'-diyl hydrogen phosphate with a ratio K_R/K_S = 1.42.

Acknowledgements:

Prior publication: None of this work has been previously published.

4.1. Introduction

It is well known that chirality in chemistry can arise from a variety of factors related to the geometry of the molecule. For example, a molecule with a tetrahedral carbon atom with four non-equivalent substituents will be chiral. The presence of elements of asymmetry in a system such as an axis or plane will also result in chirality, namely axial and planar chirality (Scheme 4. 1).

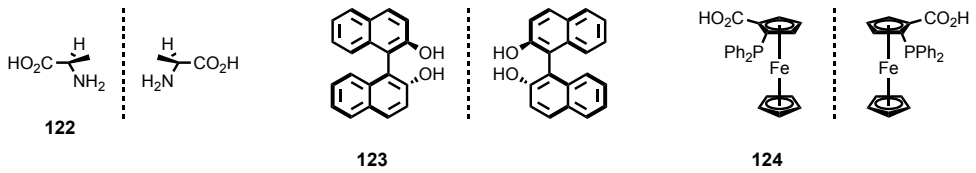

Scheme 4. 1 Three different types of chirality – point (left), axial (middle) and planar (right).

However, it is less commonly appreciated that the mechanical bond in catenanes and rotaxanes can impart chirality to the interlocked system. Taking the case of a [2]rotaxane made of a rotationally non-symmetrical macrocycle and a non-centrosymmetric axle as an example; both molecules on their own are devoid of any element of chirality. However, when mechanically bonded the final interlocked system exist as a pair of enantiomers due to the specific relative orientation of the two components (Figure 4. 1). It was proposed by Takata and co-workers to consider this form of chirality as planar chirality. However, to emphasise the role of the mechanical bond as the stereogenic element Goldup and co-workers suggested that such rotaxanes should be termed "mechanically planar chiral".

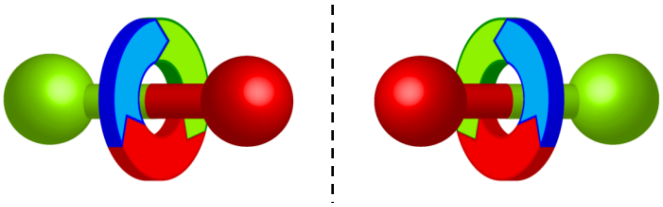

Figure 4. 1 Schematic representation of the two enantiomers of a mechanically planar chiral [2]rotaxane.

This unusual form of stereoisomerism was first discussed by Schill in 1971,[1] but it was only in 1997, three decades later, that Votgle and co-workers reported the first case of separation of both enantiomers of mechanically chiral rotaxane **125** (Scheme 4. 2) using chiral stationary phase HPLC.[2,3]

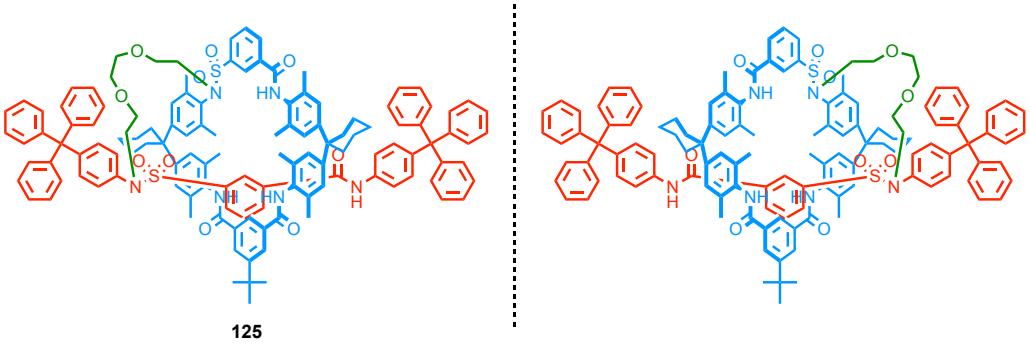

125

Scheme 4. 2 First isolated enantiomers of mechanically chiral pseudo rotaxane **125** by Votgle and co-workers.

10 years, later, Takata and co-workers published an enantioselective approach to mechanically planar rotaxane based on a dynamic kinetic resolution process (Scheme 4. 3).[4] They chose to use a chiral trialkylphosphane as a catalyst to mediate the end capping acylation reaction of enantiomeric pseudorotaxanes, which resulted in a 4.4 % enantiomeric excess (*ee*). The enantiomers still required chiral stationary phase to be separated, and the low *ee* obtained prevents the use of this method in a scalable synthetic manner.

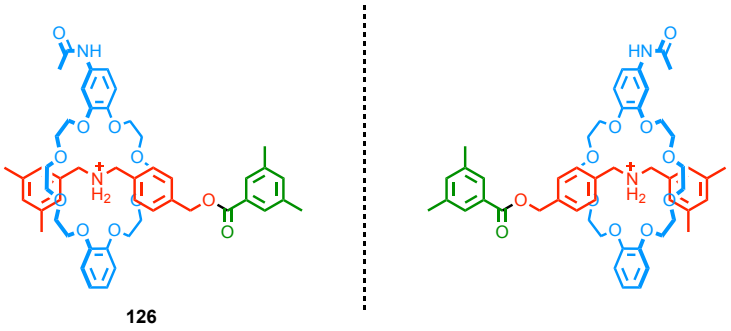

126

Scheme 4. 3 Enantio-enriched mechanically planar rotaxane **126** synthesised by Takata and co-workers.

In 2014 Goldup and co-workers developed a chiral auxiliary based approach towards the synthesis of mechanically planar rotaxanes.[5] By using an enantiopure covalently chiral stopper **127** and a non-C2 symmetrical macrocycle **128** they produced a pair of epimeric diastereoisomers (D-S_{mp})-**129** and (D-R_{mp})-**129** *via* AT-CuAAC methodology (Figure 4. 2). The two diastereoisomers could be separated using standard normal phase flash chromatography and were subsequently crystallised which allowed the unambiguous assignment of the mechanical stereochemistry. Finally, displacement of the chiral sugar auxiliary with an achiral bulky benzylamine *via* aminolysis, a process that preserves the mechanical bond, produced enantiopure mechanically planar chiral rotaxane (S_{mp})-**130** and (R_{mp})-**130**. The assignment of the absolute stereochemistry of both enantiomers is achieved by determining first the atom of highest priority using the Cahn-Ingold-Prelog (CIP) system in the axle and assigning it as A (the ester oxygen atom in this case). Then the highest priority

substituent of A is determined using the CIP system and labelled as B (carbonyl in the present case), which allows the assignment of the direction. This process is repeated in the macrocycle with the highest priority atom labelled as C and highest priority ligand as D (Figure 4. 2). The assembly is finally viewed along the direction A→B and the orientation of C and D observed as either clockwise (R_{mp} enantiomer) and anticlockwise (S_{mp} enantiomer).

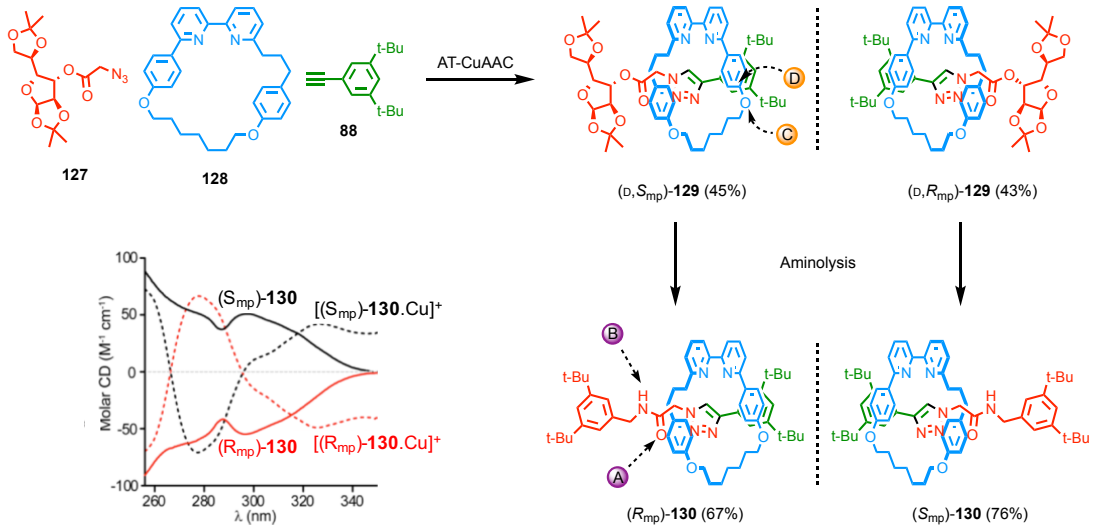

Figure 4. 2 Diastereomeric approach to enantiopure mechanically chiral rotaxanes by Goldup and co-workers and the chiroptical response of both enantiomers of **130** on their own and bound to Cu^{I}.

The study of the chiroptical properties of enantiopure rotaxane **130** revealed that, whereas **130** on its own displays mirror image CD spectra that are relatively featureless (Figure 4. 2), endotopic binding of Cu^{I} inside the cavity introduces an MLCT transition and the appearance of strong Cotton effects with two sign inversions (Figure 4. 2). The fact an inversion of the CD signal is observed upon binding of metal suggest that mechanically planar chiral metal complexes have potential applications in chiroptical switching.

To date, only one example of enantioselective sensing using mechanically planar chiral rotaxane has been reported. In this work, Kameta, Hiratani and co-workers synthesised a racemic sample of rotaxane **131** and studied its binding preference toward various amino acid derivatives.[6] Upon addition of phenylalaninol to an NMR sample of **131** they observed perturbation of the signals due to binding of the guest *via* the establishment of a multitude of hydrogen bonds and most probably π–π interactions. They could also follow the process using fluorescence spectroscopy where a decrease of the intensity of emission of the anthracene unit, with a concomitant increase for the one of the carbazole moiety, was observed. This effect was assigned to the fact that the guest induces motion of the macrocycle that induces changes in the charge transfer interactions between the naphtyl

units and the anthracene/carbazole moieties respectively. Their system was selective for phenylalaninol as no response was observed for the other amino acid derivatives tested (i.e., alaninol, prolinol, and tryptophanol). They investigated the case of phenylalaninol more in detail and reported that addition of 0.5 equiv. of (L)-phenylalaninol to a racemic sample of **131** resulted in the formation of two sets of signals by ^{1}H NMR spectroscopy, one matching the starting material and the second being assigned to the host-guest complex. Similarly, monitoring of the titration by fluorescence was proposed to lead to a titration curve consistent with binding of the guest and suggestive of a turning point when 0.5 equivalents of guest was added. They concluded that the system was able to recognize the chirality of phenylalaninol due to selective diastereomer formation. However, the data presented is not conclusive based on three factors: (i) ^{1}H NMR of the host in the presence of > 0.5 equiv. of (L)-phenylalaninol were not reported, (ii) the fluorescence titration data do not appear to fit any binding model.

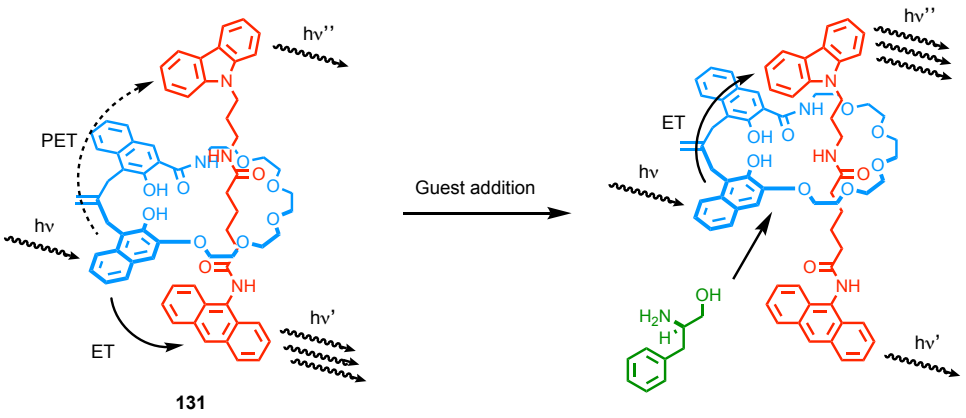

Scheme 4. 4 Mechanically planar chiral sensor **131** by Hiratani and co-workers.

Nevertheless, it does not undermine the fact that mechanically interlocked molecules have great potential in the field of chiral recognition. The well-defined chiral space the mechanical bond creates in a way mimics Nature's best receptors, which operate through the encapsulation of the target enantiomer inside a three-dimensional complementary chiral cavity, with a high level of functionalisation to maximise the number host-guest interactions. The importance of the encapsulation process has been demonstrated by high levels of selectivity displayed by synthetic chiral receptors such as macrocycles[7–9] and cryptand-like strapped calixpyrrole.[10] Very recently, it has been shown that the combination of chirality and mechanical bonding can produce a well-expressed chiral environment that can be exploited for the discrimination in binding of chiral analytes.

In 2016, Niemeyer and co-workers showed that catenane **132** featuring two chiral 1,1'-binaphthyl-phosphates was able to discriminate between the two enantiomers of dicationic amino acid guest derivatives (Scheme 4. 5) using ^{1}H NMR spectroscopy analysis.[11] Addition of both enantiomers of the guest induced changes in the ^{1}H NMR spectra of the host that could be quantified in order to determine association constants for each diastereomeric complex. At the end of this study they reported both higher binding affinities and diastereoselectivity for catenane **132** with doubly cationic anions than the macrocycle on its own.

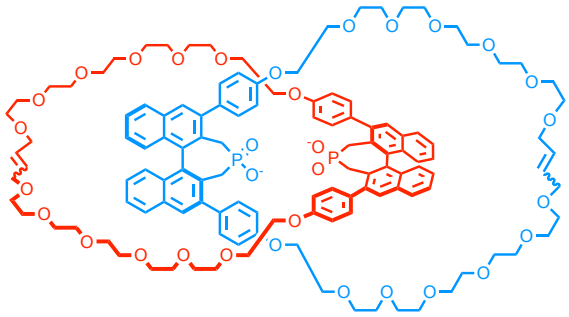

132

Scheme 4. 5 Chiral catenane receptor **132** by Niemeyer and co-workers.

Earlier this year, Beer and co-workers published rotaxane **133** (Scheme 4. 6) synthesised using their iodo-acetylene modification of the AT-CuAAC reaction.[12] Both components displayed elements of chirality in the form of a BINOL moiety in the macrocycle and two enantiopure (*S*)-serine units within the thread, thus forming a highly functional chiral cavity capable of multiple non-covalent interactions with guest molecules (hydrogen and halogen bonding, charge-charge interactions). The interlocked receptor was able to interact with both enantiomers of carboxylate salts of amino acid derivatives (leucine, tryptophan and proline) as well as BINOL-PO_4^- and every time displayed higher binding affinity for one of the two enantiomers. Indeed, a remarkable 3:1 selectivity was observed with proline whereas the other analytes still produced reasonable values (>1.5). Replacing the chiral axle with a non-chiral unit that lacked the hydrogen bond units resulted in a decrease in binding affinity (for carboxylate guests in particular) but still a good selectivity (3.4:1 in the case of leucine) albeit for the other enantiomer. Replacing the chiral macrocycle with an achiral analogue resulted in a loss and inversion of selectivity for the four analytes. Finally, they observed that the anion binding enantioselectivities of the non-interlocked axle and macrocycle were lower than those observed for **133**, thus demonstrating the impact of the mechanical bond in the creation of well-defined, highly functional, three-dimensional cavities.

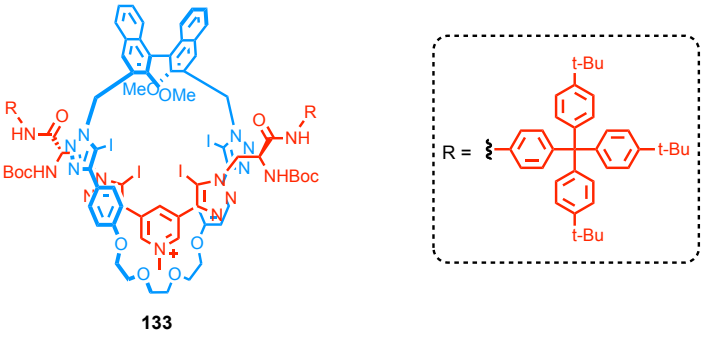

133

Scheme 4. 6 Chiral rotaxane receptor **133** by Beer and co-workers.

Project Aim

In the general context of growing interest in the development of novel chiral interlocked system, it is envisioned that mechanically planar chiral rotaxanes have potential applications in the field of enantioselective sensing due to the unique chiral environment surrounding the binding site. In fact, promising results have already been obtained with interlocked system incorporating covalent elements of chirality.[11,12] However, the synthesis and study of a mechanically planar chiral [2]rotaxane receptor yet still to be achieved.

Thus, we aimed to synthesise a novel mechanically planar chiral urea-based rotaxane receptor and to investigate its binding behaviour toward chiral anions. We based our work on the epimeric diastereoisomer methodology the group reported, the first objective being the development of a new chiral auxiliary that allows separation of diastereoisomers and brings anion binding functionality to the final interlocked product. Following this, we undertook the study of this new chiral receptor toward a variety of enantiopure guests and report on how the mechanical planar chirality affects the enantioselectivity of the sensor.

4.2. Results and Discussion

This chapter presents a study of enantioselective binding of chiral anions using mechanically planar chiral rotaxanes, which is still an on-going work. The results are not reported in the chronological order they were obtained and in places are preliminary and thus incomplete.

4.2.1. Binding study using racemic receptors rac-139 and rac-143.

4.2.1.1. Starting material and rotaxane synthesis

Non-C2 symmetrical macrocycle **128** was synthesised following a procedure published by the group (Scheme 4. 7).[13] Starting from boronic acid **134**, a Suzuki-coupling reaction (54%) followed by de-methoxylation using aqueous HBr provided **136** (88%). Two subsequent Williamson esterification reactions were then performed to provide first **137** and then macrocycle precursor **138** in 80 and 57% yield respectively (the synthesis of **107** is described in Chapter 3). Finally, the dibromide **138** was converted to macrocycle **128** *via* a Nickel mediated bi-aryl coupling (65%).

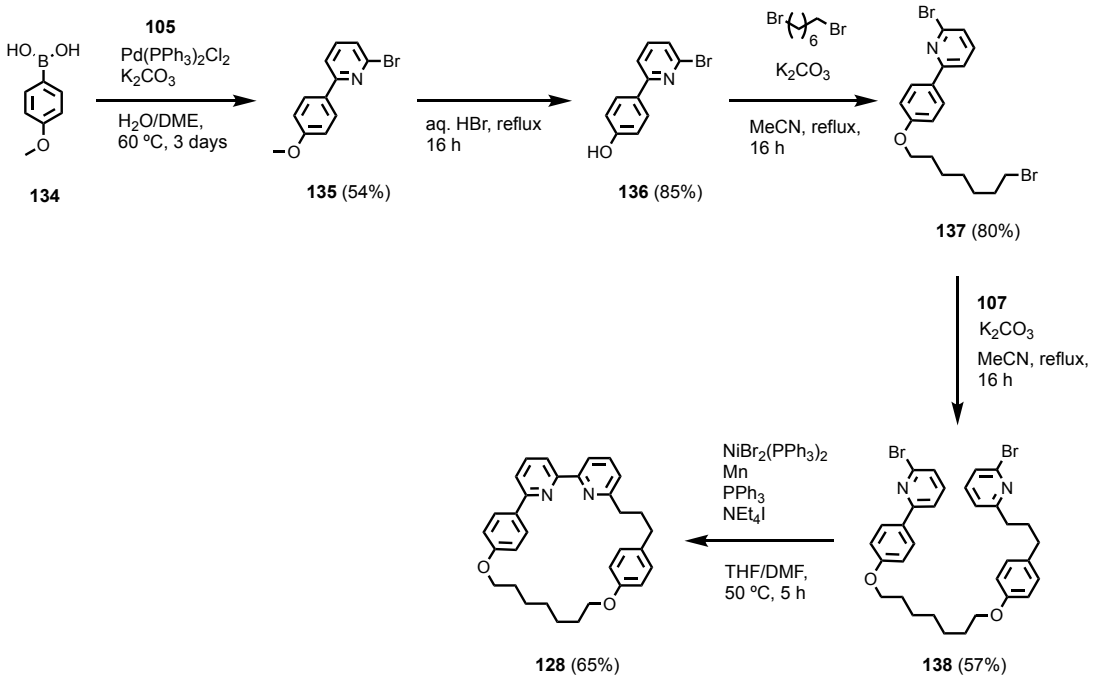

Scheme 4. 7 Synthesis of rotationally non-symmetrical macrocycle **128**.

The racemate of rotaxane rac-**139** was synthesised using the AT-CuAAC methodology in good yield (85%, Scheme 4. 8) using 1 equiv. of macrocycle **128** and both half-threads **103** and **119** with a substoichiometric amount of Cu^{I} (0.96 equiv.).

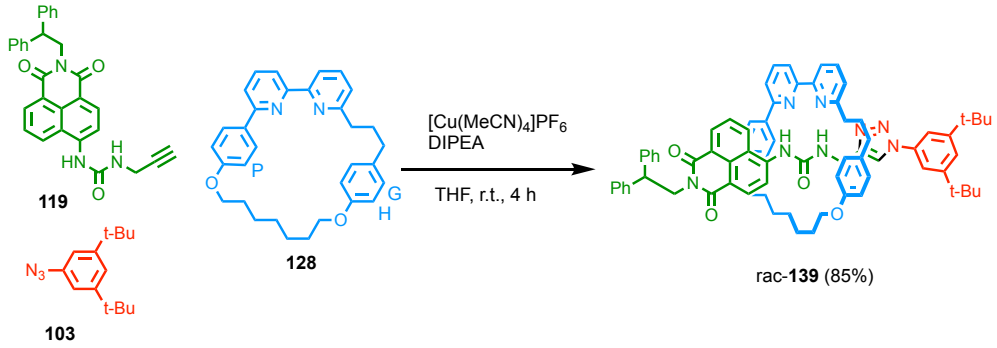

Scheme 4. 8 AT-CuAAC synthesis of rac-**139**.

4.2.1.2. Study of chiral neutral guests

In the previous chapter, we reported an unusual type of interaction between carboxylic acids and our urea-based interlocked receptor **110**. In this particular case, the acid did not protonate the rotaxane but still bound in some way the receptor, inducing shifts in the triazole and *-NH-* signals amongst others. We tentatively assigned it as shown below:

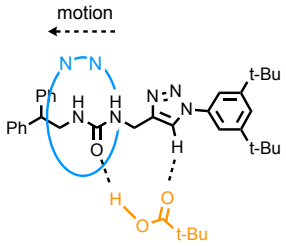

Scheme 4. 9 Schematic of the interaction of carboxylic acids with our urea-based interlocked receptor.

For that reason, we started investigating the possibility of having transfer of chiral information from a chiral guest (amino acid derivatives) to the achiral interlocked receptor **120** using ^{1}H NMR spectroscopy. Pleasingly, we observed that upon addition of 1 equiv. of commercially available enantiopure *N*-Boc-protected L-phenylalanine **140** to a sample of **120** in $CDCl_3$, similar shits to the one reported before occurred (Figure 4. 3). Both NH proton signals as well as the triazole proton H_I experienced a slight shift downfield ($\Delta\delta$ = 0.04, 0.04 and 0.02ppm respectively) whereas proton H_g from the naphthalimide unit resonated at lower value in ppm ($\Delta\delta$ = 0.06 ppm). But more interesting was the fact that the flanking aromatic proton H_G and H_H from the macrocycle experienced a diastereotopic split due to the close proximity of the chiral guest. A similar effect was observed with the commercially available protected tryptophan derivative **141** (Figure 4. 3).

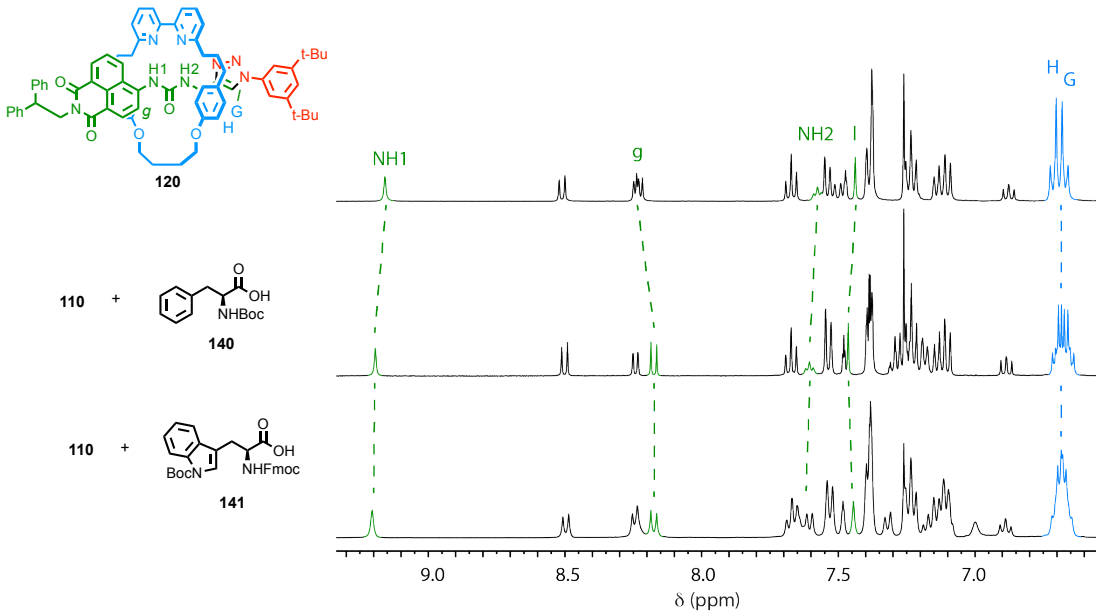

Figure 4. 3 Partial ^{1}H NMR stack plot ($CDCl_3$, 400 MHz, 298 K) of rotaxane **120** without any guest (top), with 1 equiv. of *N*-Boc-L-Phe-OH (middle) and 1 equiv. of Fmoc-L-Trp(Boc)-OH (bottom).

Building on this observation, we then performed the same experiment using rac-**139**. In the presence of 1 equiv. of *N*-Boc-phenylalanine **140**, a similar shift as the one reported above were observed but more importantly, proton H_g, H_k, from the axle and H_G, H_H and H_P from the macrocycle split into two signals due to the formation of two diastereomeric host-guest complexes (Figure 4. 4).

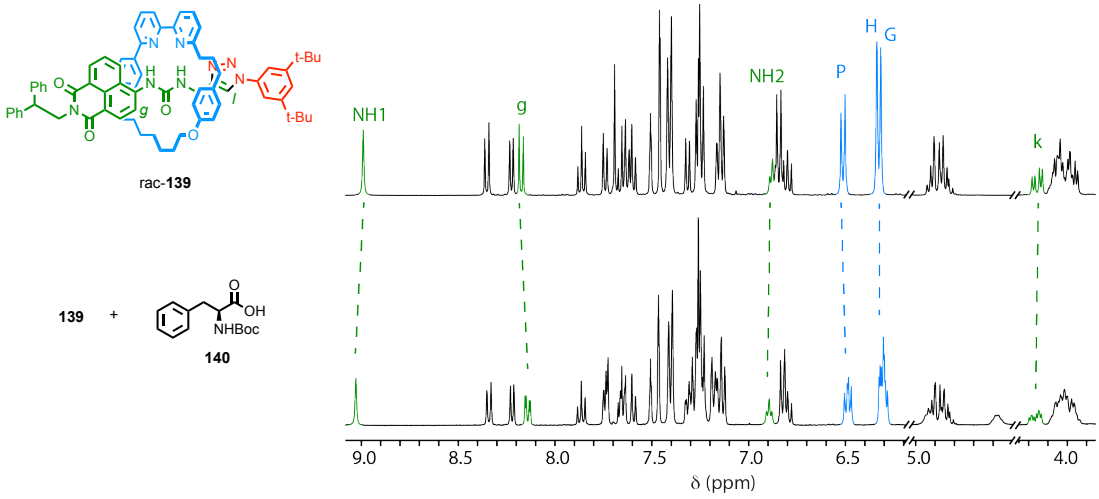

Figure 4. 4 Partial ^{1}H NMR stack plot ($CDCl_3$, 400 MHz, 298 K) of rotaxane rac-**139** without any guest (top) and with 1 equiv. of *N*-Boc-L-Phe-OH **140** (bottom). For labelling of H_P see Scheme 4. 8.

A ^{1}H NMR titration was performed ($CDCl_3$, 400 MHz, 298 K) by incremental additions of *N*-Boc-L-phenylalanine * (0-120 equiv.) to a solution of rac-**139** (C = 2.5 mM). Binding constants were calculated for each diastereomeric complexes using the variation of chemical shift for proton $H_{k/k'}$ and $H_{P/P'}$ applying a nonlinear least-squares curve fitting procedure using the

online software http://supramolecular.org/ with a 1:1 global fitting model (Nelder-Mead method).

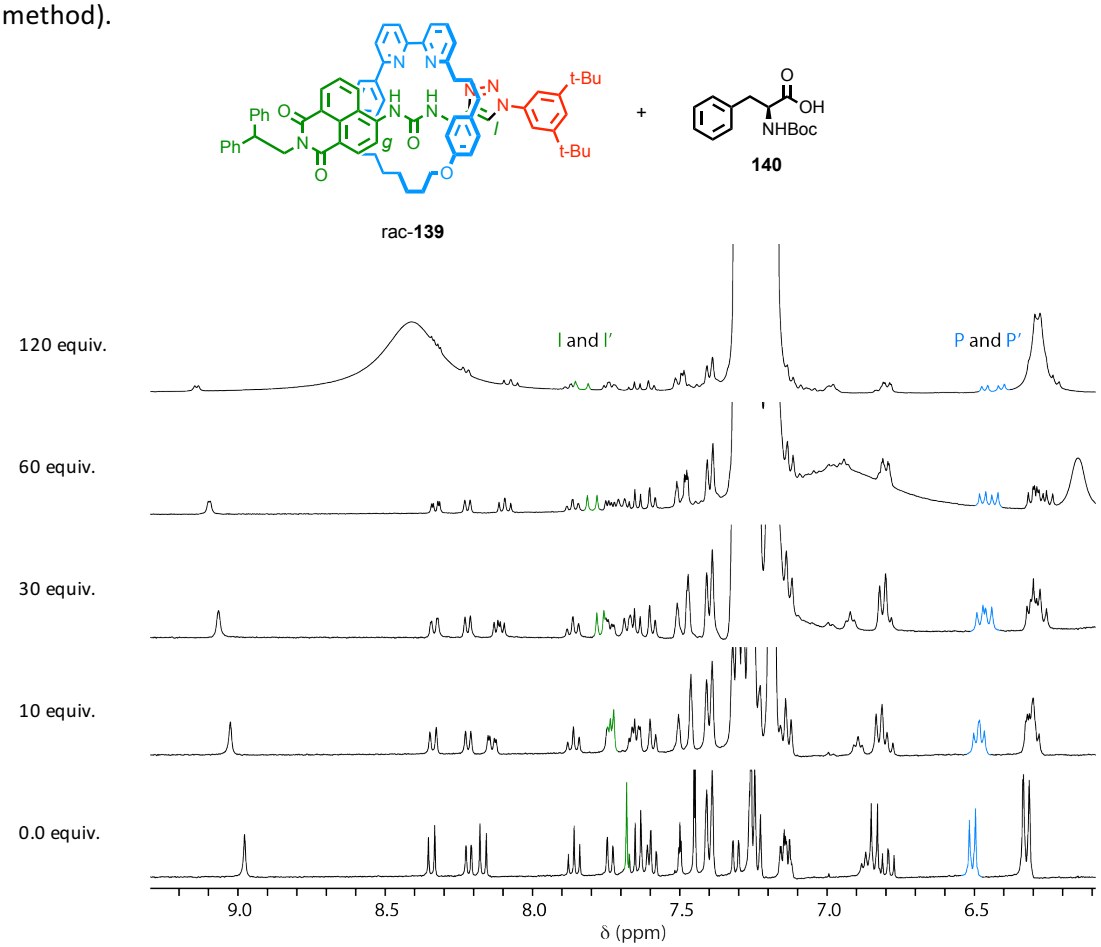

Figure 4. 5 Partial ^{1}H NMR titration ($CDCl_3$, 400 MHz, 298 K) of rotaxane rac-**139** with *N*-Boc-L-Phe-OH **140**. Increasing amount of guest (0-120 equiv.) from bottom to top. For labelling of proton H_P see Scheme 4. 8.

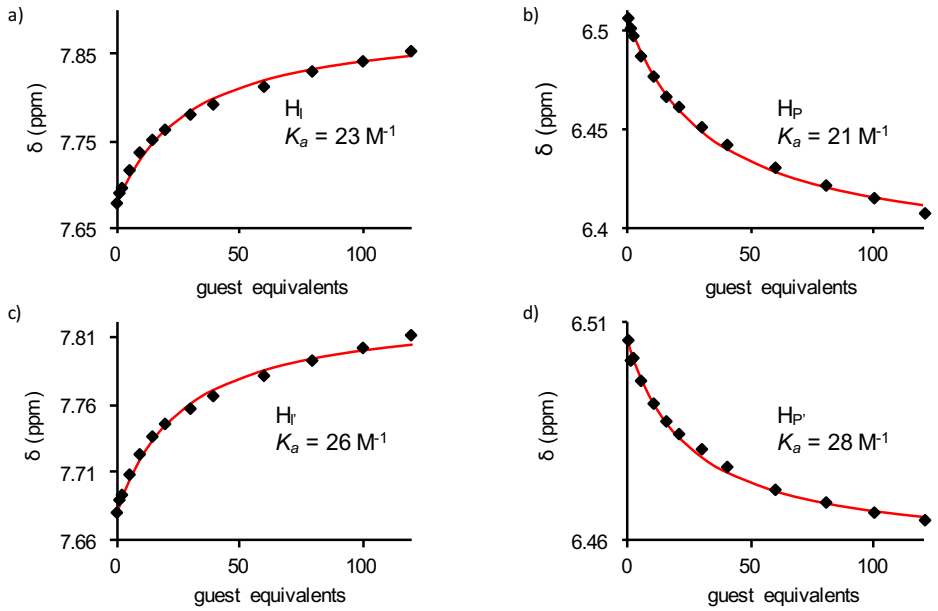

Figure 4. 6 Fitting curves with the corresponding calculated binding constants for the titration of rac-**139** with *N*-Boc-L-Phe-OH **140** ($CDCl_3$, 400 MHz, 298K) plotting the variation in chemical shift of a) proton H_I, b) proton H_P, c) proton $H_{I'}$ and d) proton $H_{P'}$.

However, the binding observed was very weak in both cases (K_a ~ 25 M^{-1}) and the values very close for each diastereoisomer complexes, making it impossible to conclude on an eventual enantioselectivity.

4.2.1.3. Study of chiral anionic guests

The observation of chiral information transfer was a promising first result. However, stronger host guest interactions were needed in order to accurately measure and quantify the binding of each enantiomer of the guests; the urea moiety needed to be properly involved in the process. To do so, a first approach would be to form rac-**139**.HBF_4 in a similar fashion to what have been shown in the previous chapter. But, we have also shown that **120**.HBF_4 was unable to bind carboxylate anions due to their high basicity leading to de-protonation of the receptor to a 'non-binding' state. Therefore, we decided to try methylating the triazole, expecting that a charged triazolium would be a much better competing station for the bipyridine to bind to.

First, a small-scale test reaction was performed on the achiral rotaxane **120** using 1 equiv. of Meerwein's reagent (Scheme 4. 10) and following the reaction by TLC. Although two spots could be seen after 2 h, one matching the starting material and the second expected to be the product **142**, the reaction did not evolve overnight. 2 more equiv. of the reagent were added but the outcome was similar 4 h. After treatment and purification, the desired product **142** was obtained in small quantity (2 mg, 34%), the rest being starting rotaxane **120**. At the moment, our hypothesis to explain the low conversion observed is the fact that Meerwein's salt is known to degrade at room temperature by hydrolysis to form diethyl ether, ethanol and HBF_4. We suspect the latter to protonate the starting rotaxane **120**, forming **120**.HBF_4, thus preventing methylation of the triazole ring even in the presence of an excess of reagent.

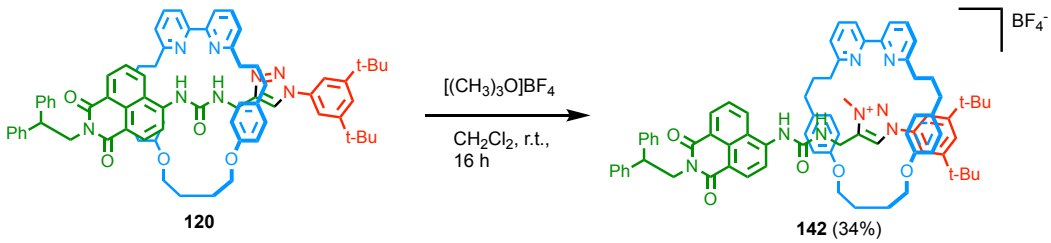

Scheme 4. 10 Synthesis of rotaxane **142**.

The small amount of material obtained was not enough to run a full NMR characterisation. However, single crystals suitable for x-ray crystallography were obtained from vapour diffusion of Et_2O into a solution of **142** in CH_2Cl_2 and confirmed the methylation of the triazole

moiety (Figure 4. 7). The solid-state structure is still under refinement but appears very similar to the one of **120**, the ring encircles the urea binding site to form two bifurcated H-bonds (N-H•••N distances of 2.51 Å (N8•••NH1), 2.73 Å (N8•••NH2), 2.33 Å (N7•••NH2) and 2.58 Å (N7•••NH1)). The naphthalimide peri proton H_h is also involved in short-contact interactions with bipyridine nitrogen N8 (N8•••CH_h = 2.59 Å). When viewed in space-fill mode (Figure 4. 7b), the steric hindrance brought by methyl group makes it unsure if it will be possible to shuttle the macrocycle onto the triazole station.

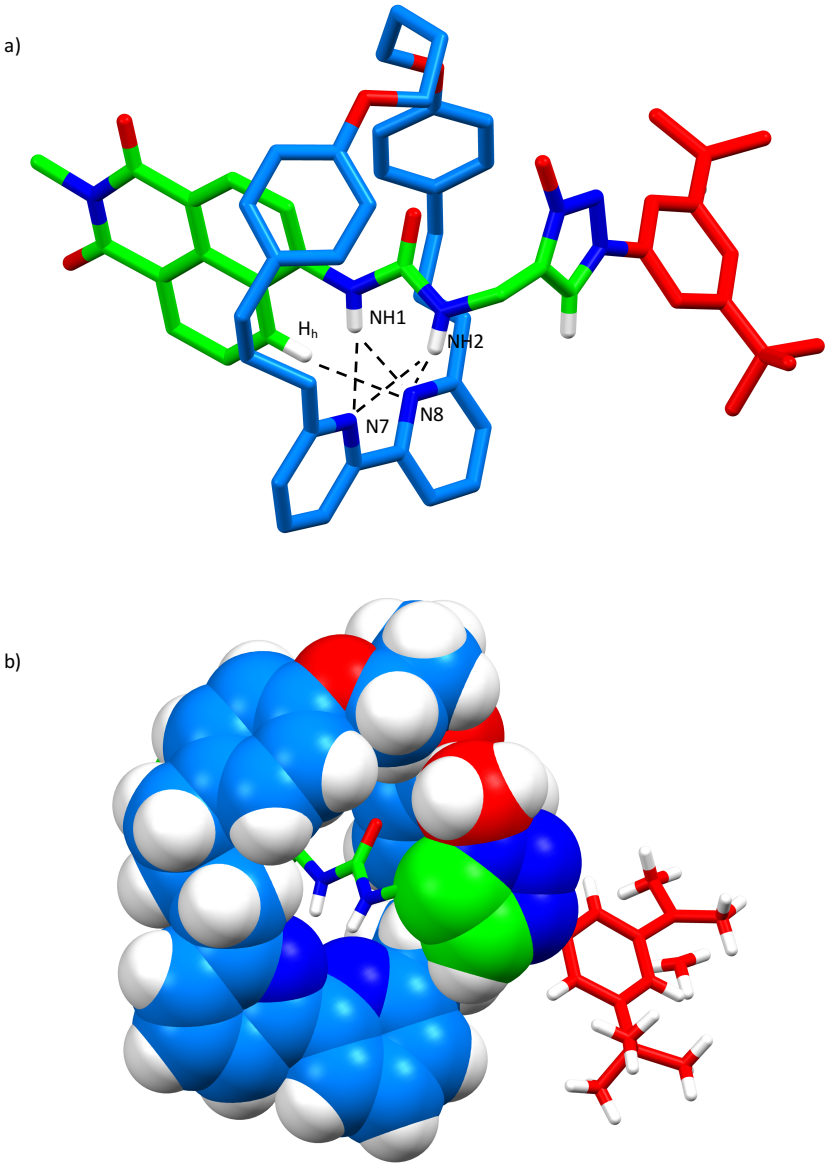

Figure 4. 7 Solid-state structure of rotaxane **142** still under refinement. Non-relevant protons, diphenyl unit of the naphthalimide and BF_4^- counter anion are not displayed for clarity. a) Black dotted lines correspond to short contact interactions, selected distances in Å: N8•••NH1 = 2.51, N8•••NH2 = 2.73, N7•••NH2 = 2.33, N7•••NH = 2.58 N7•••NH1 and N8•••CH_h = 2.59. b) Space-fill view for the macrocycle and the triazole unit.

Having confirmed that methylation of the triazole was possible, we applied this methodology to the racemate **139** using 2 equiv. of Meerwein's salt and obtained after counter-anion exchange the hexafluorophosphate salt rac-**143** in a moderate 48% yield.

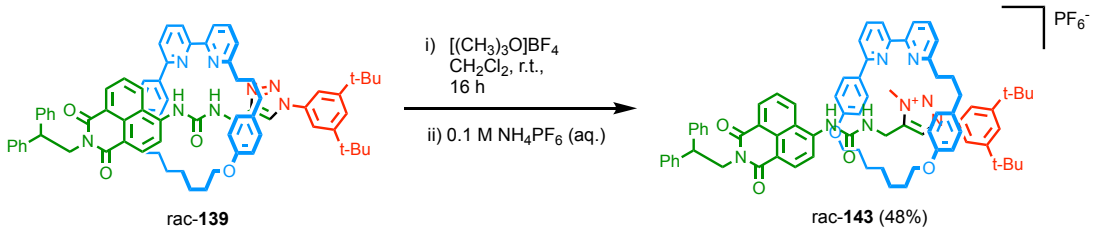

Scheme 4. 11 Synthesis of rotaxane rac-**143**.

We then investigated the binding behaviour of our new receptor rac-**143** toward a series of chiral anions consisting of TBA salts of *N*-Boc-L-phenylalanine (*N*-Boc-L-Phe-O$^-$) **144**, *N*-Boc-L-proline (*N*-Boc-L-Pro-O$^-$) **145** and (*R*)-(-)-1,1'-binaphthyl-2,2'-diyl hydrogen phosphate (*R*-BINOL-PO$_4^-$) **146**. Pleasingly, all three of them displayed strong binding in a competitive media made of acetone/water 98:2 (Figure 4. 8). Adding 1 equiv. of each guest to a sample of rac-**143** resulted notably in the urea NH1 proton and naphthalimide *peri* proton H$_h$ shifting downfield due to interactions with the anionic guest. The triazole proton H$_k$ also experienced a slight downfield shift that could be assigned to the shuttling of the bipyridine macrocycle from the urea to the triazolium station and the establishment of favourable hydrogen bond interactions with the triazole proton. Finally, the methyl group on the triazole and alkyl CH$_2$ from the axle was also affected and shifted upfield, which we could tentatively assign to the appearance of short-contact interactions with the flanking aromatic ring of the macrocycle after its translocation to the triazolium unit.

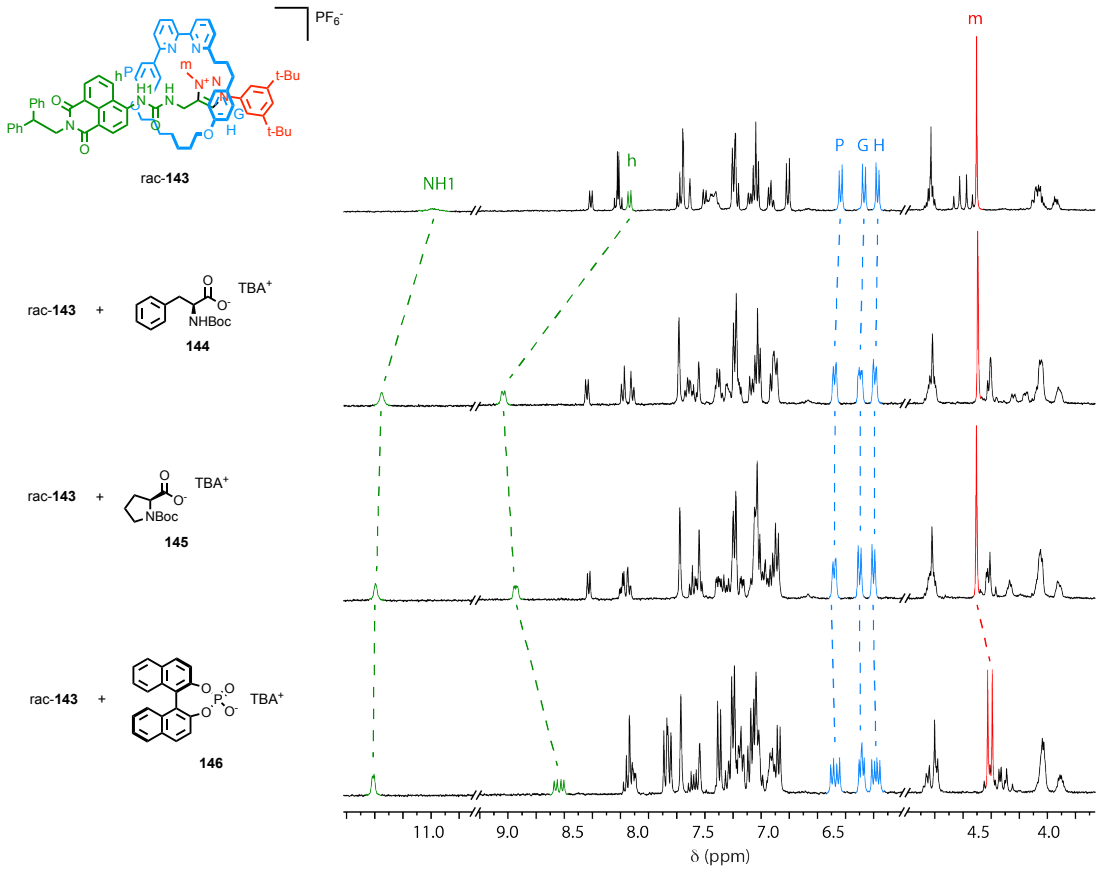

Figure 4. 8 Partial ^{1}H NMR stack plot ($(CD_3)_2CO$, 400 MHz, 298 K) of rotaxane rac-**143** with (from top to bottom) no guest, 1 equiv. of *N*-Boc-L-Phe-O$^-$ **144**, 1 equiv. of *N*-Boc-L-Pro-O$^-$ **145** and 1 equiv. of R-BINOL-PO_4^- **146**.

More importantly, the majority of the signal experienced a splitting due to the formation of two diastereoisomer host-guest complexes in solution. This feature, remarkably expressed in the case of the complex formed with *R*-BINOL-PO_4^- (Figure 4. 8), could be used to determine binding constants for each enantiomer and evaluate any potential enantioselectivity.

^{1}H NMR titration analysis was performed in a mixture of deuterated acetone/water 98:2 using rac-**143** as receptor (2.5 mM) and the two amino acid derivatives **144** and **145** as guest.

The data for phenylalanine derivative guest **144** showed a binding that was too strong to be fitted (K_a>10^4 M^{-1}). Moreover, the splitting of the signal was not significant enough to be able to differentiate both diastereoisomer complexes.

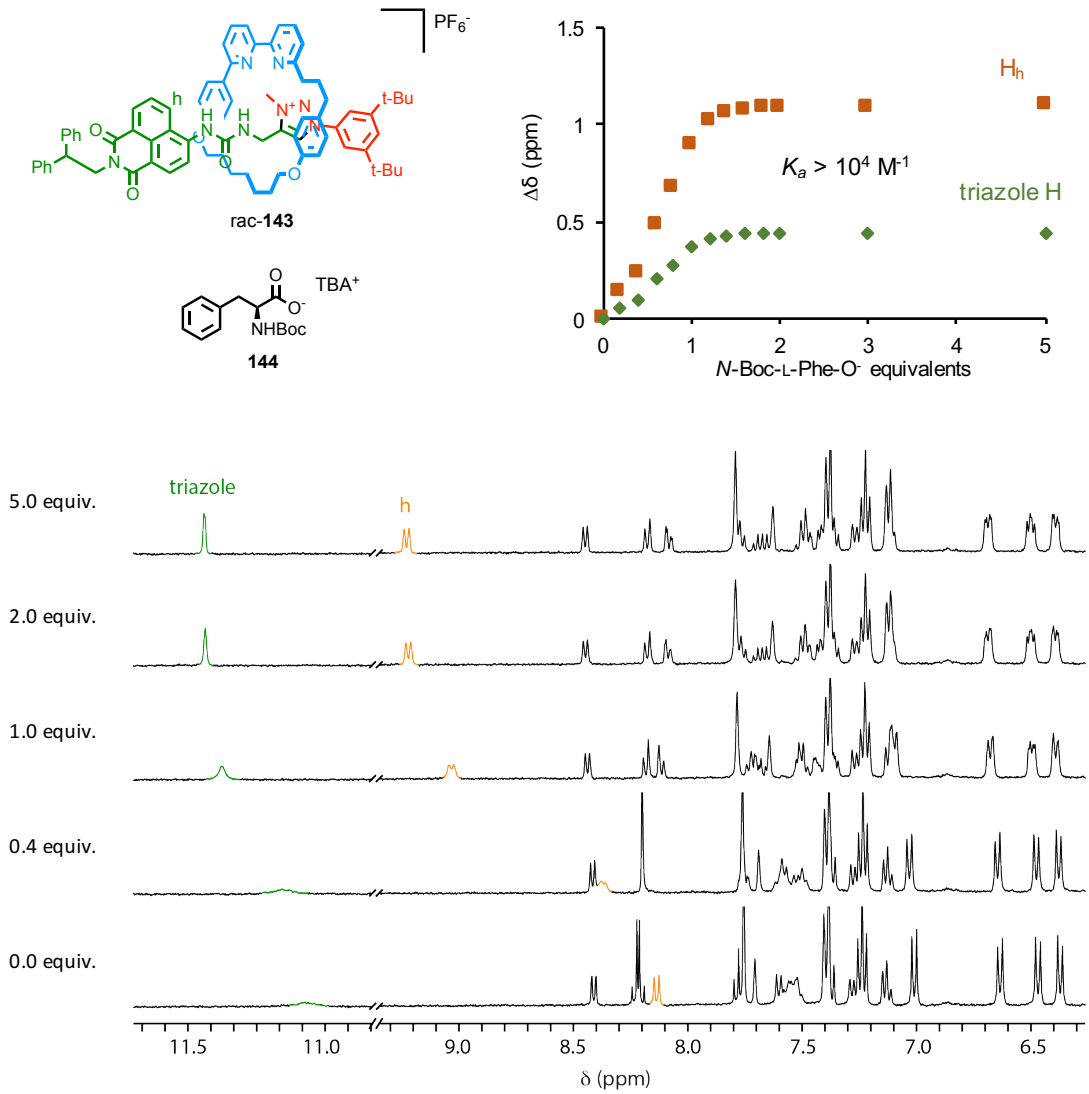

Figure 4. 9 ^{1}H NMR titration ($(CD_3)_2CO/D_2O$ 98:2, 400 MHz, 298 K) of rotaxane rac-**143** (2.5 mM) with *N*-Boc-L-Phe-O$^-$ **144**. Increasing amount of guest from bottom to top. Binding too strong to be fitted.

In the case of *N*-Boc-L-Pro-O$^-$ **145**, although the signals for the triazole and the naphthalimide proton H_k and H_h split, the binding was once again too strong ($K_a > 10^4$ M^{-1}) to be fitted.

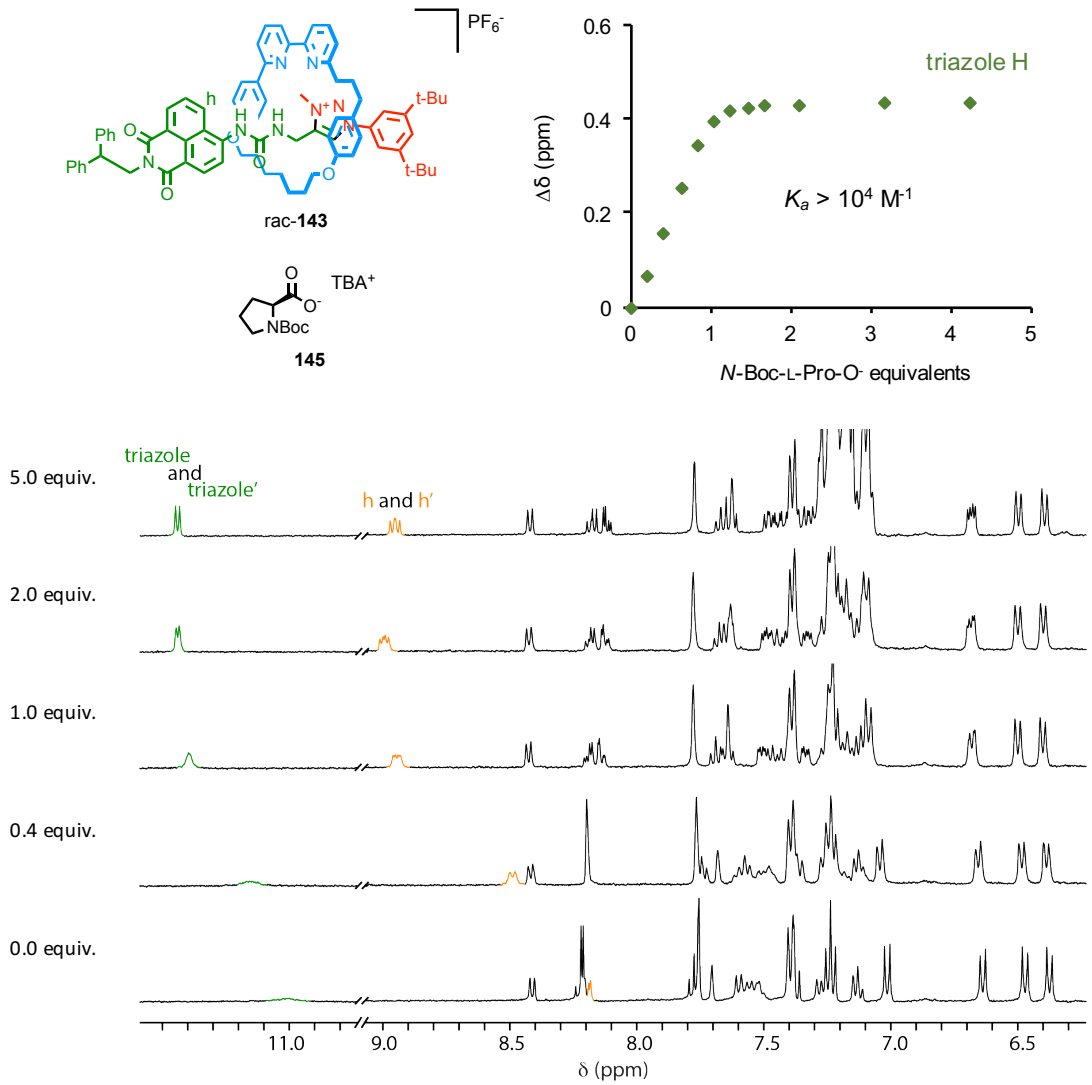

Figure 4. 10 ^{1}H NMR titration ($(CD_3)_2CO/D_2O$ 98:2, 400 MHz, 298 K) of rotaxane rac-**143** (2.5 mM) with *N*-Boc-L-Pro-O$^-$ **145**. Increasing amount of guest from bottom to top. Binding too strong to be fitted.

Taking these results into account, ^{1}H NMR titration analysis was performed in a more competitive solvent mixture consisting of deuterated acetone/water 95:5 and using rac-**143** as receptor (2.5 mM) and BINOL derivative **146** as guest (Figure 4. 11). Pleasingly, individual binding constants were obtained for each diastereoisomer complexes in this case using the variation of chemical shift for the methyl signal H_m applying a nonlinear least-squares curve fitting procedure using the online software http://supramolecular.org/ with a 1:1 global fitting model (Nelder-Mead method). These values revealed a slight selectivity in the binding with a ratio $K_a/K_{a'} = 1.3$ between the two enantiomers of **143**.

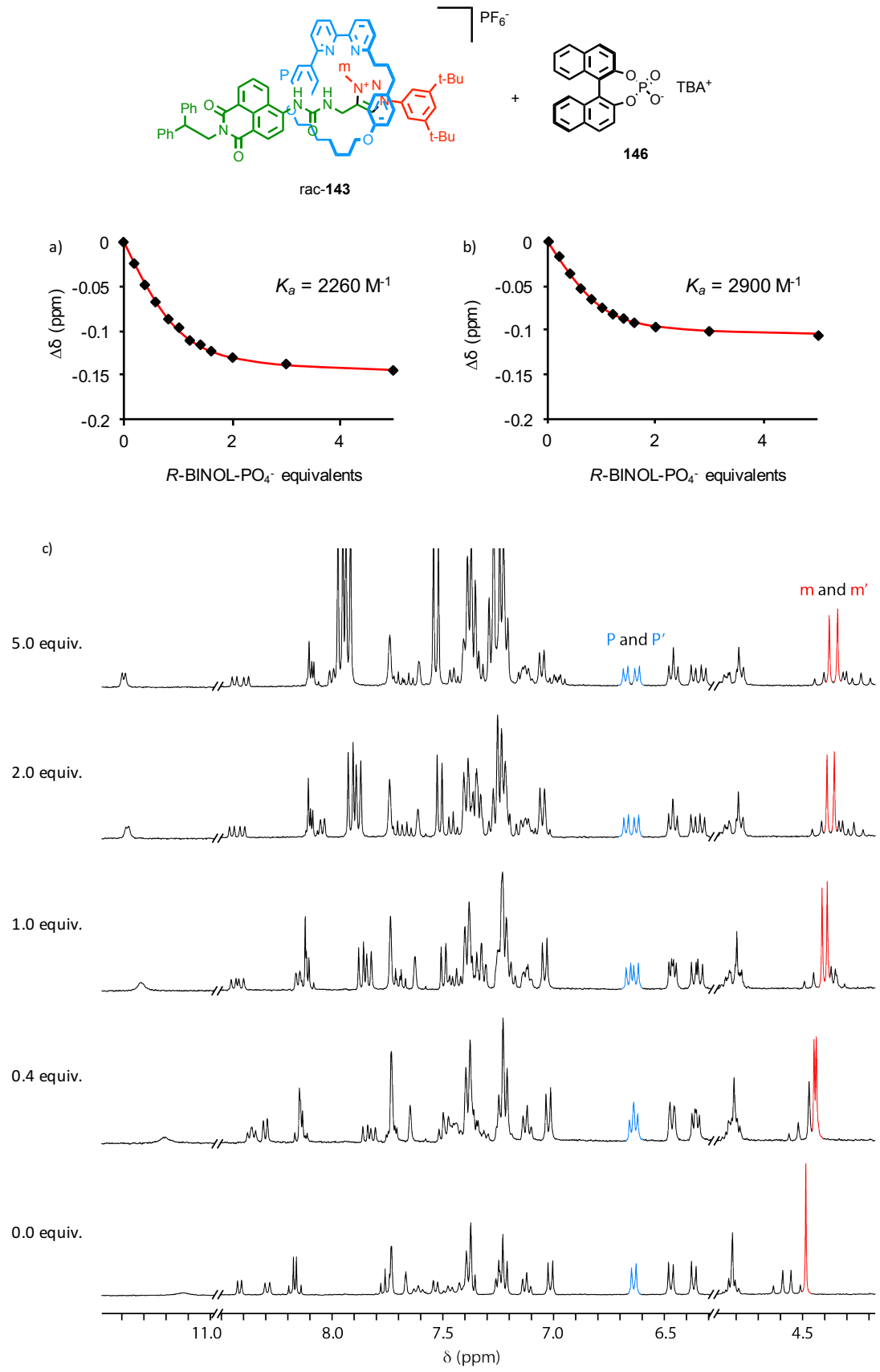

Figure 4. 11 ^{1}H NMR titration ($(CD_3)_2CO/D_2O$ 98:2, 400 MHz, 298 K) of rac-**143** (2.5 mM) with *R*-BINOL-PO_4^- **146**. a and b) Fitting curves with the corresponding calculated binding constants for each diastereoisomeric complexes plotting the variation in chemical shift of triazolium methyl proton H_m. c) ^{1}H NMR stack plot of rac-**143** with increasing amount of guest **146** (0-5 equiv.) from bottom to top.

Finally, an interesting observation was made while working with the rac-**143** in regards to its fluorescence response to binding. Studying the UV-vis and fluorescence response of the receptor (acetone/water 98:2, 298 K, C ~ 10^{-4} M range) we observed that whereas the addition of an excess of **144** and **145** triggers a similar increase in intensity of the naphthalimide absorption band at 387 nm with a slight red-shift in both cases, proline derivative **145** quenches the emission more efficiently than phenylalanine **144**. Moreover, a new absorbance band appeared at 560 nm in both cases. This result will need to be studied in more detail but suggests that it might be possible to differentiate between two guests of similar nature based on their structural backbone using fluorescence spectroscopy.

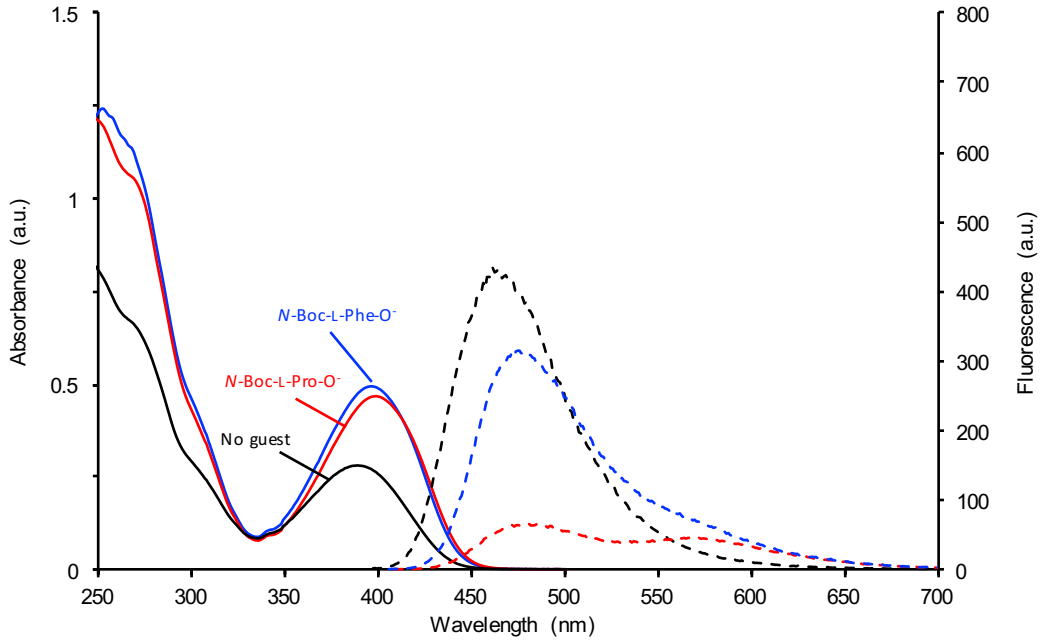

Figure 4. 12 UV-vis (plain lines) and fluorescence spectra (dotted lines) (acetone/water 98:2, 298 K, C ~ 100 μM) of rotaxane rac-**143** without any guest (black) and with 5 equiv. of *N*-Boc-L-Phe-O⁻ **144** (blue) or *N*-Boc-L-Pro-O⁻ **145** (red).

4.2.2. Development of a new chiral auxiliary

4.2.2.1. Pre-requisites

Having observed a potential positive effect of the mechanical planar chirality on the enantioselective binding process, we decided to synthesise the enantiopure form of rotaxane **143**. To do so, we needed to develop chiral auxiliary with specific features. First it had to be readily incorporated into the urea scaffold and stable under the AT-CuAAC reaction conditions. Second, it should allow for the separation of the two diastereoisomers of the corresponding rotaxane. Third and final, the integrity of the interlocked system must be maintained upon its removal.

For the development phase, a 3,5-di-*tert*-butylbenzyl unit was used instead of a naphthalimide for ease of synthesis and characterisation. All rotaxane formation reactions were performed on a small scale for screening purposes only. None of the final rotaxane products were fully characterised.

In the literature, it has been demonstrated that the methyl *p*-methoxybenzene (PMB) substituent is an efficient *N*-protecting group for amides or carbamates, which is readily cleaved under various conditions (TFA, DDQ, ammonium cerium (IV) nitrate).[14] The enantiopure version of the corresponding amine **151** is commercially available, so our work started from there.

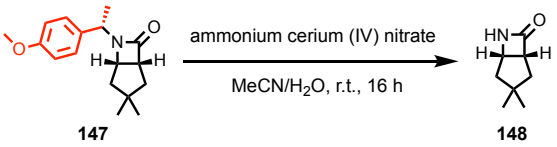

Scheme 4. 12 Example of the cleavage of the methyl PMB substituent by Bull and co-workers.

4.2.2.2. First-generation chiral auxiliary

We first designed the two urea-based alkyne stoppers **149** and **150** bearing the chiral group respectively on the nitrogen closer to the stopper (N1) or to the alkyne (N2).

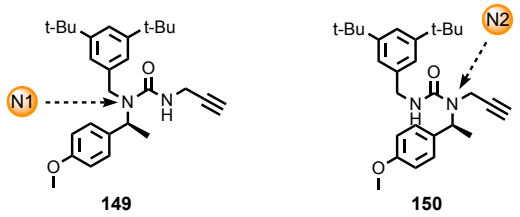

Scheme 4. 13 First-generation chiral urea-based stoppers

In both cases the synthesis started with an *N*-alkylation of the amine **151** to incorporate either 3,5-di-*tert*-butylbenzyl unit (**153**, 75%) or a propargyl group (**155**, 67%). From there the secondary amines were reacted with triphosgene under basic conditions followed by the addition of the desired bromide in order to afford the targeted urea stoppers **149** and **150** in 91% and 25% yield respectively (Scheme 4. 14). In the latter case, the significant decrease in yield can be explained by difficulty to isolate the product from un-reacted **155**.

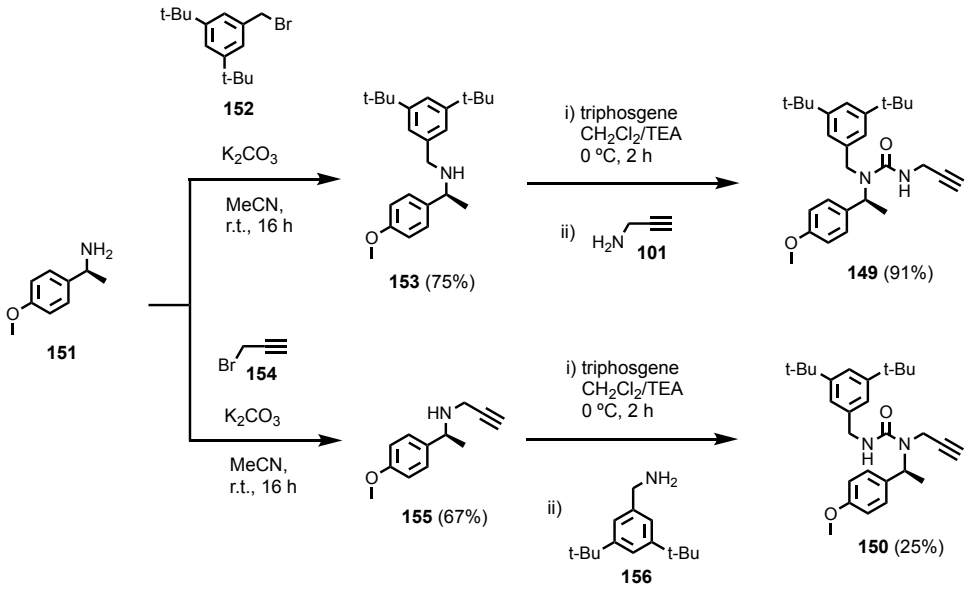

Scheme 4. 14 Synthesis of the first-generation chiral urea-based stoppers **149** and **150**.

We then made the corresponding rotaxanes using the AT-CuAAC methodology with 1 equivalent of desired alkyne, azide **103**, macrocycle **128** and DIPEA with a sub-stoichiometric amount of Cu^{I} (0.96 equiv.) in CH_2Cl_2 (0.025 M).

With alkyne stopper **150** (Scheme 4. 15), we hypothesised that the close proximity of the chiral auxiliary to the macrocycle would favour separation of the diastereoisomers. The ^{1}H NMR spectrum of the crude after NH_3-EDTA showed full conversion of both half-threads with only traces of the macrocycle left, but it also showed more species that what we would normally expect (Figure 4. 13). This fact, combined with the red colour of the crude (characteristic of the Cu^{I}-bipyridine complex), suggested that some copper ion was still coordinated inside the cavity of the rotaxane. It could be explained by the increase in steric bulk around the metal ion due to the close proximity of the chiral auxiliary (N2). Treatment of the crude with KCN in 1:1 CH_2Cl_2/MeOH resulted in a colour change of the solution to light red and changes in the ^{1}H NMR spectrum. Amongst them, the ratio between the two singlets at respectively 9.86 and 9.84 ppm that could potentially being assigned as triazole proton H_f for the two diastereoisomers as rotaxane and copper-complex, changed from 1:2 to 3:1 (Figure 4. 13). We decided to move forward with it and attempted purifying the crude but did not succeed in isolating either of the two diastereoisomers.

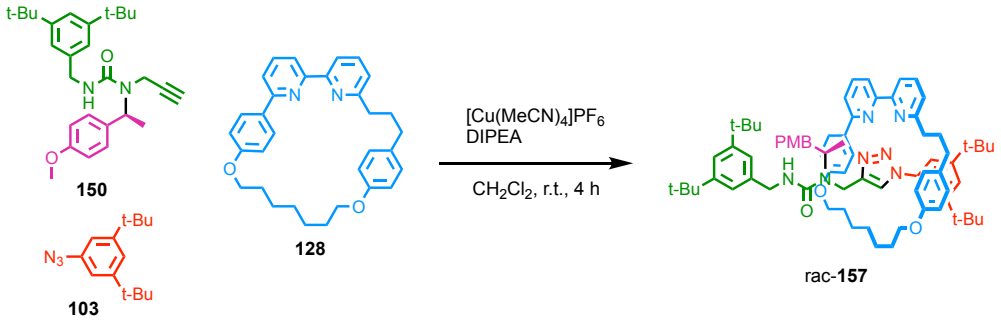

Scheme 4. 15 AT-CuAAC synthesis of rac-**157**.

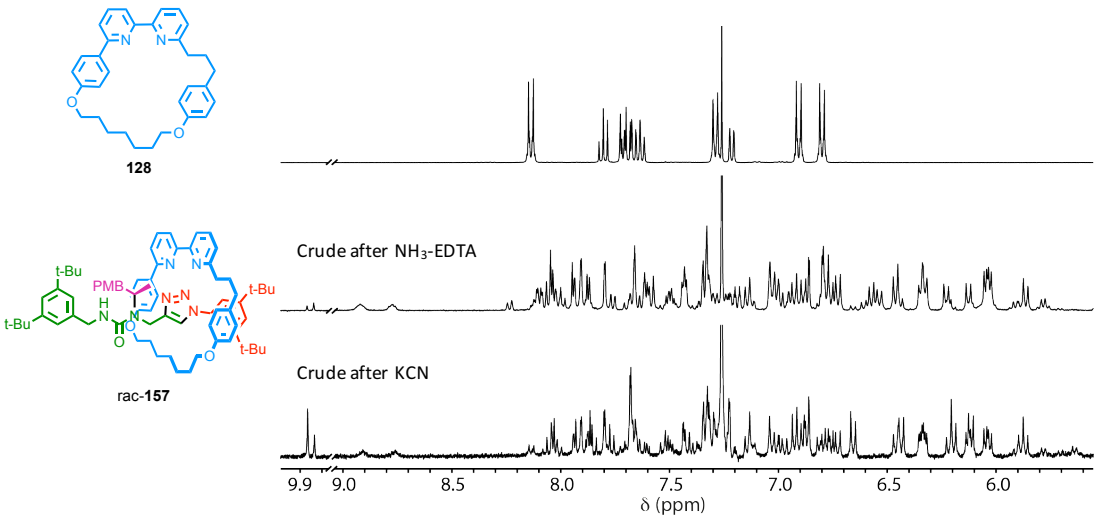

Figure 4. 13 ^{1}H NMR stack plot ($CDCl_3$, 400 MHz, 298 K) of macrocycle **128** (top), crude of the rotaxane formation of rac-**157** after EDTA-NH_3 treatment (middle) and after KCN treatment (bottom).

Moving on to half-thread **149** bearing the chiral auxiliary at the N1 position, we synthesised the corresponding rotaxane rac-**158** (Scheme 4. 16). After 4 h stirring at room temperature, the crude ^{1}H NMR showed excellent conversion (95%) of the macrocycle **128** to the rotaxane rac-**158** (Figure 4. 14). Attempts at isolating one diastereoisomer were unsuccessful using normal column chromatography techniques. However, after running three preparative thin layer chromatography with isocratic elution of Petrol/CH_2Cl_2 1:1 with 8% of MeCN, 5% of the first diastereoisomer (10% yield) was isolated (Figure 4. 14). As both diastereoisomers form a long streak on silica, the second one could not be isolated.

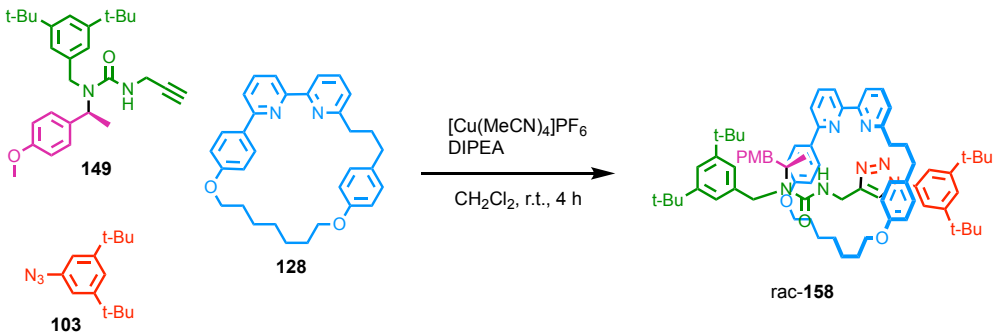

Scheme 4. 16 AT-CuAAC synthesis of rac-**158**.

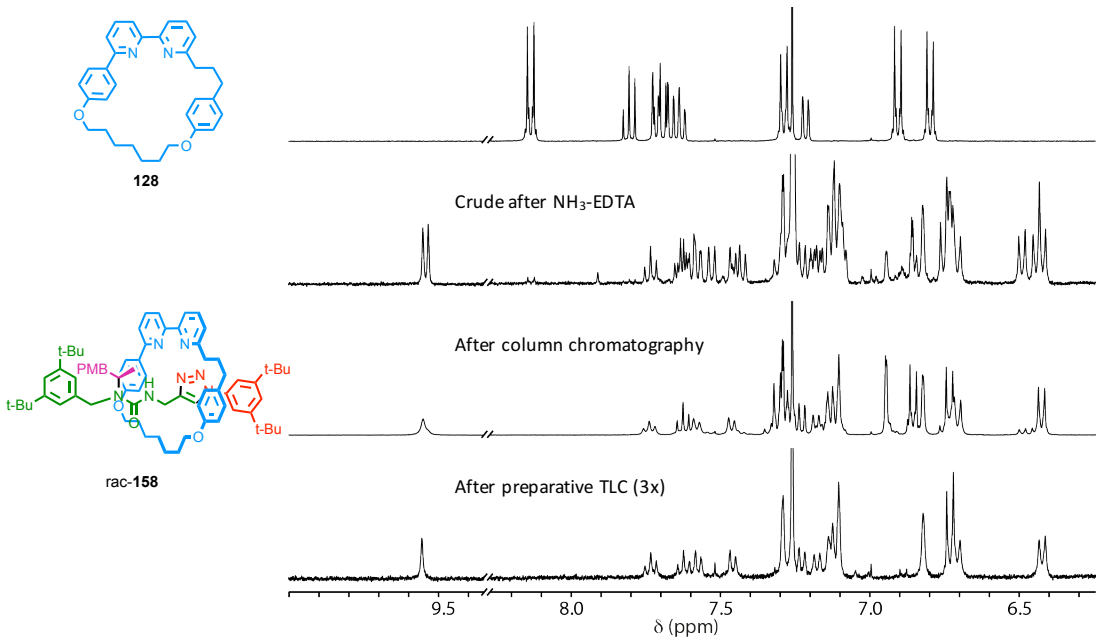

Figure 4. 14 ^{1}H NMR stack plot ($CDCl_3$, 400 MHz, 298 K) of (from top to bottom) macrocycle **128**, crude of the rotaxane formation of rac-**158**, mainly one diastereoisomer of **158** after column chromatography and one diastereoisomer of **158** isolated after preparative TLC.

Although low yielding, the fact that the new chiral auxiliary allowed for the separation of at least one of the two diastereoisomer was a promising result. We hypothesised that the separation was better in the case of the N1 substituted urea rotaxane **158** because the bipyridine unit could possibly be interacting with both the triazole and the urea *via* bifurcated hydrogen-bond interactions (seen in the previous chapter with naphthalimide rotaxane **120**). Such a structural conformation of the interlocked system could, in theory, improve the expression of chirality in **158** for two reason. First, it might result in an increase in rigidity of the system; and second it would bring the rotationally non-symmetrical macrocycle **128** closer to the stereogenic centre within the tread.

4.2.2.3. Second-generation chiral auxiliary

Our second design incorporated a hydroxyl unit, the aim being to increase the number of non-covalent interactions within the interlocked system. Starting from 4-hydroxy-D-phenylglycine **159**, *N*-Boc protection of the amine followed by methylation of the phenol unit and formation of the methyl ester using MeI afforded **160** in 93% yield over two steps. The Boc-protecting group was then removed under acidic conditions to give primary amine **161** in 96% yield after aqueous work up and flash chromatography on silica gel (Scheme 4. 17).

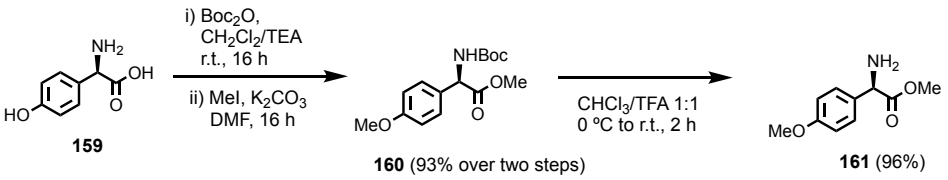

Scheme 4. 17 Synthesis of chiral primary amine **161**.

At this stage, the amine was N-alkylated with either a 3,5-di-*tert*-butylbenzyl unit or a propargyl group to give **162** and **164** in 65% and 61% yield respectively. In both cases, subsequent reduction of the methyl ester with lithium aluminium hydride (LAH) affording the hydroxyl derivatives **163** (94%) and **165** (95%) in excellent yields (Scheme 4. 18).

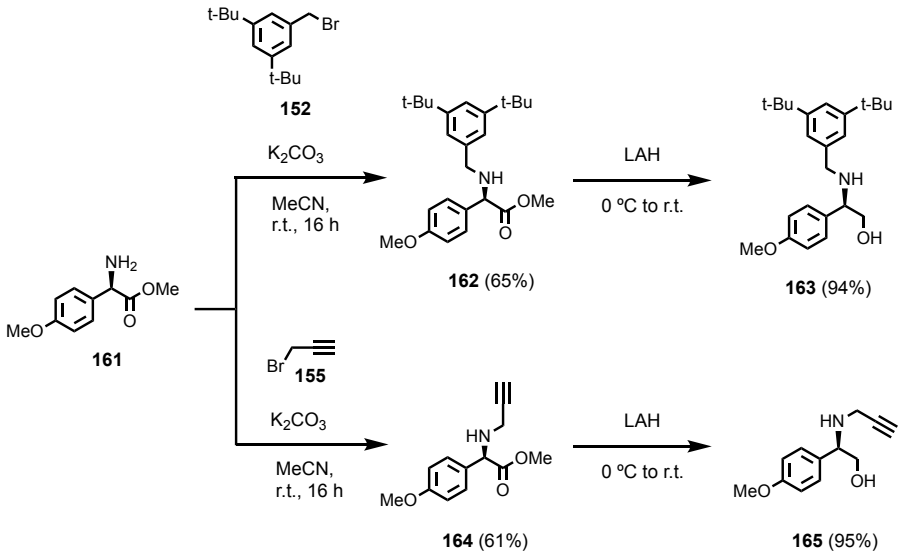

Scheme 4. 18 Synthesis of chiral secondary amines **163** and **165**.

For the final urea formation reaction, we opted for a different approach than before as the presence of the hydroxyl group made possible the formation of non-desired carbamate and carbonate esters derivative during the reaction using triphosgene. Therefore, we first synthesised the carbamoyl imidazole derivatives **167** (39%) and **169** (49%) from respective amines **101** and **156** with 1,1'-carbonyldiimidazole (CDI). Subsequent reaction with **163** and **165** respectively under basic conditions afforded the desired half-threads **168** (46%) and **170** (55%) (Scheme 4. 19).

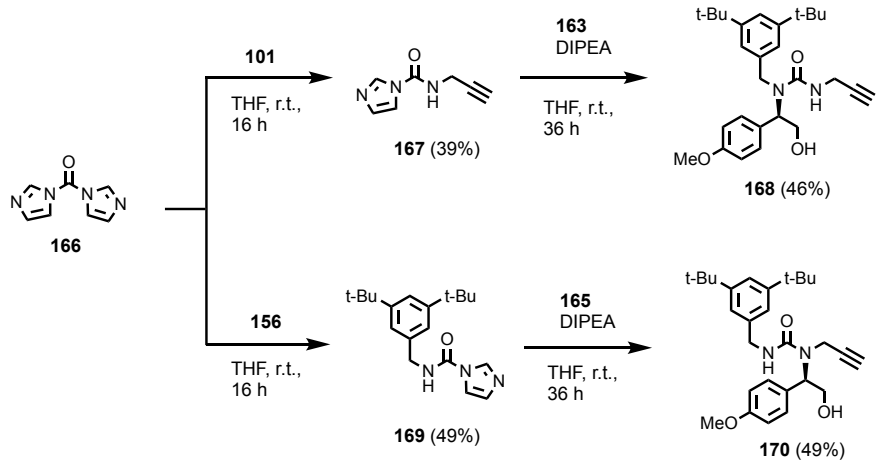

Scheme 4. 19 Synthesis of the second-generation chiral urea-based stoppers **168** and **170**.

Rotaxane rac-**171**, in which the chiral auxiliary occupies the N2 position, was first synthesised using our AT-CuAAC methodology (Scheme 4. 20) with 92% conversion of the macrocycle **128** to the interlocked system. The crude ^{1}H NMR after NH_3-EDTA treatment showed two singlets with a 1:1 ratio at respectively 9.86 and 9.80 ppm corresponding to the triazole proton H_I in each diastereoisomer. The two products produced a long streak on TLC under various solvent conditions. After three purifications *via* preparative thin layer chromatography, a small amount of the first diastereoisomer (5%) was obtained (Figure 4. 15). Far for being perfect, it was still an improvement when compared to the corresponding first-generation stopper that did not permit the separation of either diastereoisomer.

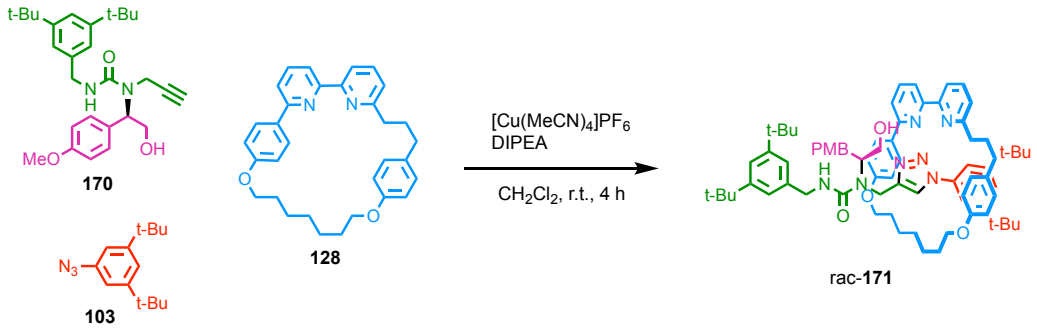

Scheme 4. 20 AT-CuAAC synthesis of rac-**171**.

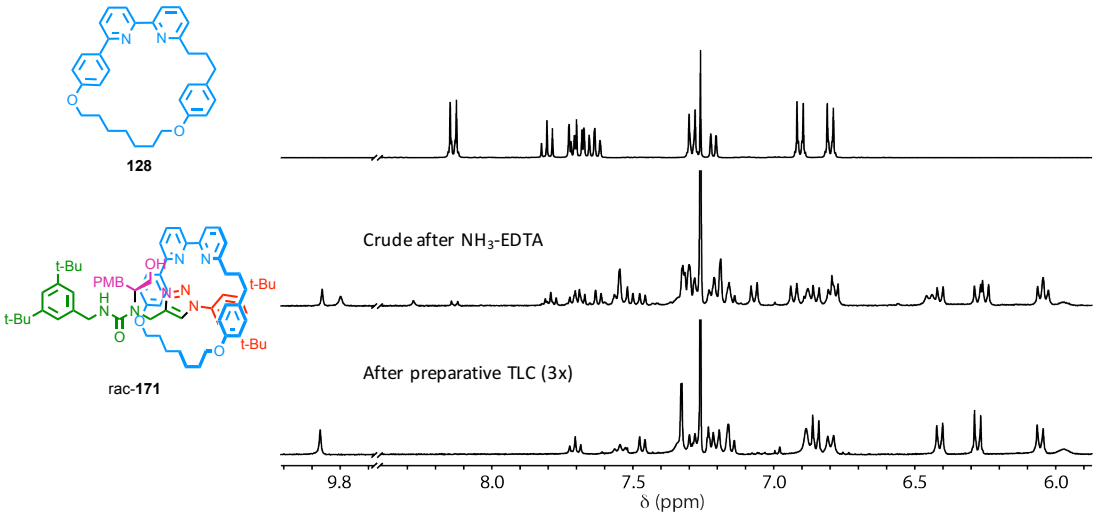

Figure 4. 15 ^{1}H NMR stack plot ($CDCl_3$, 400 MHz, 298 K) of macrocycle **128** (top), crude of the rotaxane formation of rac-**171** after NH_3-EDTA treatment (middle) and one diastereoisomer of **171** isolated after preparative TLC (bottom).

Single crystals of the racemate were obtain from vapour diffusion of Et_2O in a solution of the two diastereoisomers of **171** in CH_2Cl_2. Although the data we not strong enough to allow a complete refinement of the solid-state structure, interesting features are still worth noticing (Figure 4. 16). The axle experiences a 90º bend, which allow the establishment of hydrogen-bond interaction between the free urea NH and the triazole nitrogen N3 (N3•••NH1 = 2.14 Å) that would rigidify the structure. Although not occurring in the solid-state (most probably due to packing arrangement), it is not unlikely that in solution the hydroxyl would favor intramolecular hydrogen bonding interactions with the bipyridine unit (which appear possible Figure 4. 16 b). The latter would explain the slight separation observed for the two diastereoisomers with this system.

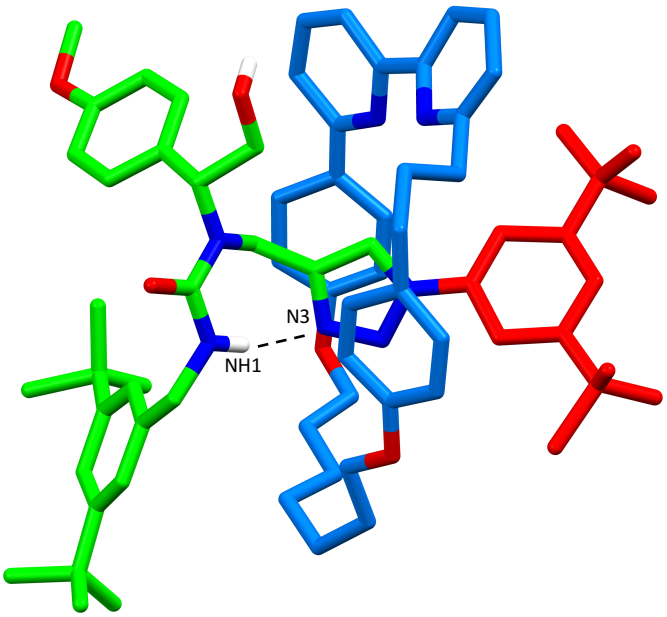

Figure 4. 16 Solid-state structure of rac-**171**. The data did not allow complete refinement of the structure. Non-relevant protons are not displayed for clarity. Black dotted lines correspond to short contact interactions. Selected distances in Å: N3•••NH1 = 2.14.

Rotaxane rac-**172**, in which the chiral auxiliary occupies the N1 position, was finally synthesised using our AT-CuAAC methodology with 95% conversion of the macrocycle **128** to the interlocked system (Scheme 4. 21). The crude NMR after NH_3-EDTA treatment showed two singlets with a 1:1 ratio at respectively 9.49 and 9.38 ppm corresponding to the triazole proton H_I for each diastereoisomer. Pleasingly in this case, two clear spots were observed on TLC corresponding to each diastereoisomer of rotaxane **172**. Column chromatography using a ratio product/silica of 500 and an eluent mixture consisting of Petrol/CH_2Cl_2 2:1 with 7% of Et_2O allowed to isolated pure fraction of the first diastereoisomer in reasonable yield (24%) (Figure 4. 17).

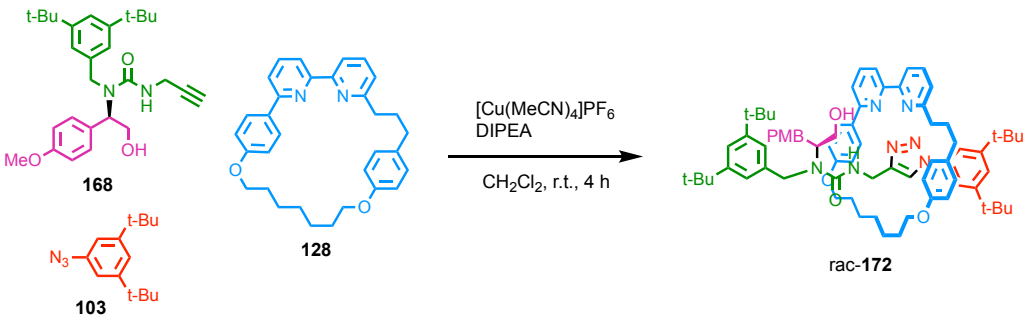

Scheme 4. 21 AT-CuAAC synthesis of rac-**172**.

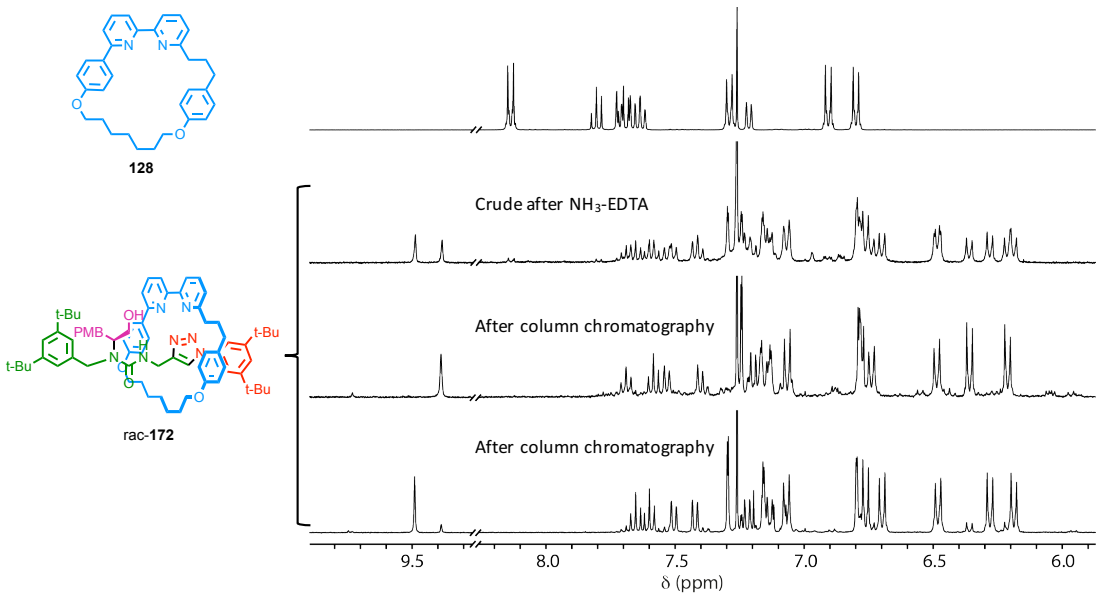

Figure 4. 17 ^{1}H NMR stack plot ($CDCl_3$, 400 MHz, 298 K) of (from top to bottom) macrocycle **128**, crude of the rotaxane formation of rac-**172** after NH_3-EDTA treatment, one diastereoisomer of **172** isolated after column chromatography and the other diastereoisomer at 95%.

Now that we had in our hands a chiral auxiliary that permitted separation of the two diastereoisomers of a rotaxane, we moved forward with it and applied the methodology to the synthesis a photo-responsive system.

4.2.3. Synthesis of mechanically planar chiral fluorescent rotaxane receptor

We started with the synthesis half-thread **174** incorporating the chiral auxiliary at the N2 position. However, we knew from previous attempts at making the naphthalimide urea alkyne stopper **119** that the reaction of the amino naphthalimide with CDI would not occur.

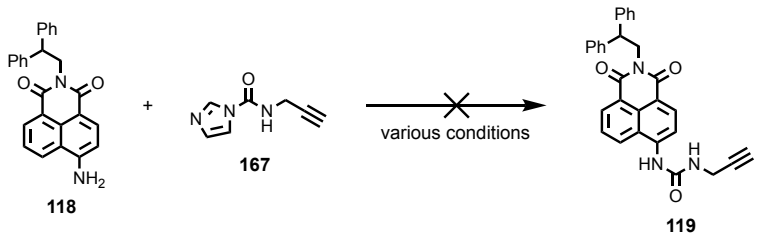

Scheme 4. 22 Failed attempts at synthesising **119** using the carbamoylimidazole approach.

Therefore, we opted for the use of triphosgene but protecting first the alcohol to prevent side-reactions. The protecting group needed to be removable under basic conditions since acidic ones would also cleave the chiral auxiliary, so we decided to use a *tert*-butyldimethylsilyl (TBDMS) group. Alcohol protection was achieved using TBDMSCl in the presence of imidazole, affording amine **173** in 95% yield (Scheme 4. 23). The urea synthesis using triphosgene and DMAP in a mixture CH_2Cl_2/toluene 10:1 gave the desired half-thread **174** in acceptable 54% yield (Scheme 4. 23).

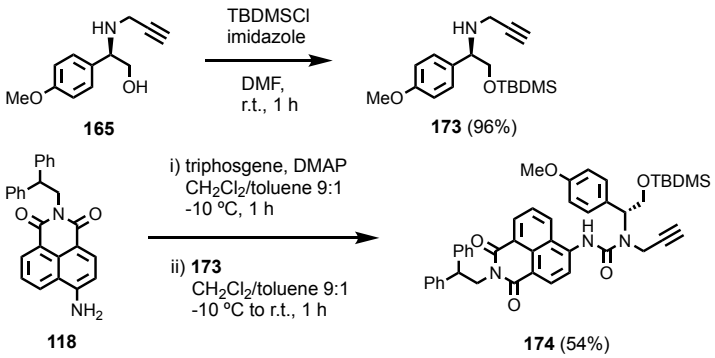

Scheme 4. 23 Synthesis of the protected chiral amine **173** and the fluorescent chiral urea stopper **174**.

A rotaxane formation reaction was performed with the protected version of the stopper to see if the TBDMS group would influence the separation of the two diastereoisomers. However, using our standard conditions with 1 equiv. on each half-thread only 18% conversion of the macrocycle **128** into rotaxane rac-**176** was achieved (Table 4.1 entry 2). The phenyl azide stopper **103** was still present in the reaction mixture but the chiral alkyne **174** had decomposed to form what we suspect to be the product **175** (Scheme 4. 24) *via* an intramolecular 5-exo-dig cyclisation of the urea onto the alkyne. This hypothesis is supported by a similar outcome being observed by our collaborators in Sydney working on thiourea derivatives. It appears that the presence of the naphthalimide unit as well as the chiral substituent onto the urea unit increases its acidity enough for the rearrangement to occur under basic conditions.

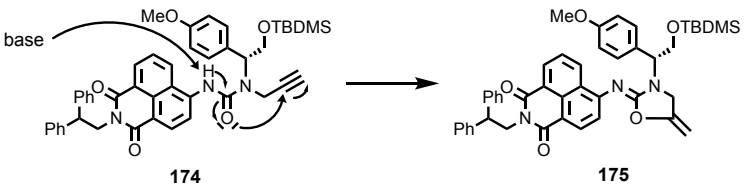

Scheme 4. 24 base mediated 5-exo-dig cyclisation of **174**.

We screened different reaction conditions, starting with base-free conditions with microwave heating. However, after 1 h at 100 °C we observed only decomposition of the starting material (Table 4.1 entry 1). Changing from CH_2Cl_2 to THF or a mixture of CH_2Cl_2/EtOH (1:1) with 1 equiv. DIPEA decreased the conversion (respectively 12 and 15%) most probably due to solubility issues (Table 4.1 entries 5 and 6). Decreasing the amount of DIPEA used during the reaction reduced the conversion to 12% (0.5 equiv., Table 4.1 entry 3) whereas increasing it to 3 equiv. gave result similar to 1 equiv. (18%, Table 4.1 entry 4). Finally, replacing DIPEA (pKaH of the conjugated acid of 18 in MeCN) with aniline (pKaH of

the conjugated acid of 11 in MeCN) gave 75% conversion of the macrocycle **128** to rotaxane product rac-**178** (Table 4.1 entry 7).

entry	solvent[a]	base (equiv.)	Conversion (%)[b]
1	CH_2Cl_2	--[c]	0
2	CH_2Cl_2	DIPEA (1)	18
3	CH_2Cl_2	DIPEA (0.5)	12
4	CH_2Cl_2	DIPEA (3)	18
5	THF	DIPEA (1)	12
6	CH_2Cl_2/EtOH	DIPEA (1)	15
7	CH_2Cl_2	Aniline (1)	75

Table 4. 1 Screening of the reaction conditions for the formation rac-**176**. [a] 1 equiv. of alkyne **174**, azide **103**, macrocycle **128** and 0.96 equiv. of $[Cu(MeCN)_4]PF_6$ at r.t. [b] conversion of **128** to **176** after 4 h determined by ^1H NMR of the crude following NH_3-EDTA treatment. [c] microwave reaction, 100 °C, 1 h.

Using our optimized conditions, rotaxane rac-**176** was synthesised and isolated as a mixture of the two diastereoisomers that did not separate during the purification process. The remaining macrocycle **128** co-eluted with rotaxane rac-**176** but, as it should not be an issue for the next step, we carried on with the synthesis. TBDMS removal was done using tetrabutylammonium fluoride (TBAF) in THF to give rotaxane rac-**177**. At this stage, it was possible to remove the left-over macrocycle **128** but also to isolate the first of the two diastereoisomers. Indeed, both diastereoisomers of **177** appeared as distinct spots on TLC and column chromatography with a ratio silica/product of 500 using an isocratic elution of Petrol/CH_2Cl_2 2:1 with 20% of Et_2O, afforded 30 mg (24%) of the first diastereoisomer and 21 mg (17%) of a mixture of the two in which the second diastereomer predominated (95%). The chiral auxiliary was then cleaved by stirring the rotaxane in a 1:1 mixture of CH_2Cl_2/TFA for 30 min, to give the rotaxane **139** in 95% yield (Scheme 4. 25, Figure 4. 19). At this stage, we decided to investigate the enantiopurity of both our chiral auxiliary (**164**) and rotaxane and measured for both an *ee* of 90% (although the HPLC conditions still require optimisation, Figure 4. 18 HPLC traces of a) amine derivative **164** in 90% *ee* and b) of rotaxane **139** as a racemate (bottom) and at the end of the synthetic route using the chiral auxiliary (top).). Working with a different batch of starting material or modifying our reaction conditions produced a similar result, which makes it reasonable to assume that it originates from the commercially available starting material (it was not possible to directly assess the ee of the commercial sample using HPLC). The rest of the study was carried out with this entioenriched version of **139**. However, very recent work focused on solving this issue and we managed to crystallise the intermediate **165** (following reduction of the ester group to the alcohol) to an *ee*>99.5% from a mixture of cyclohexane/Et_2O. In the future, this essentially enantiopure source of starting material should allow isolation of enantiopure **139**.

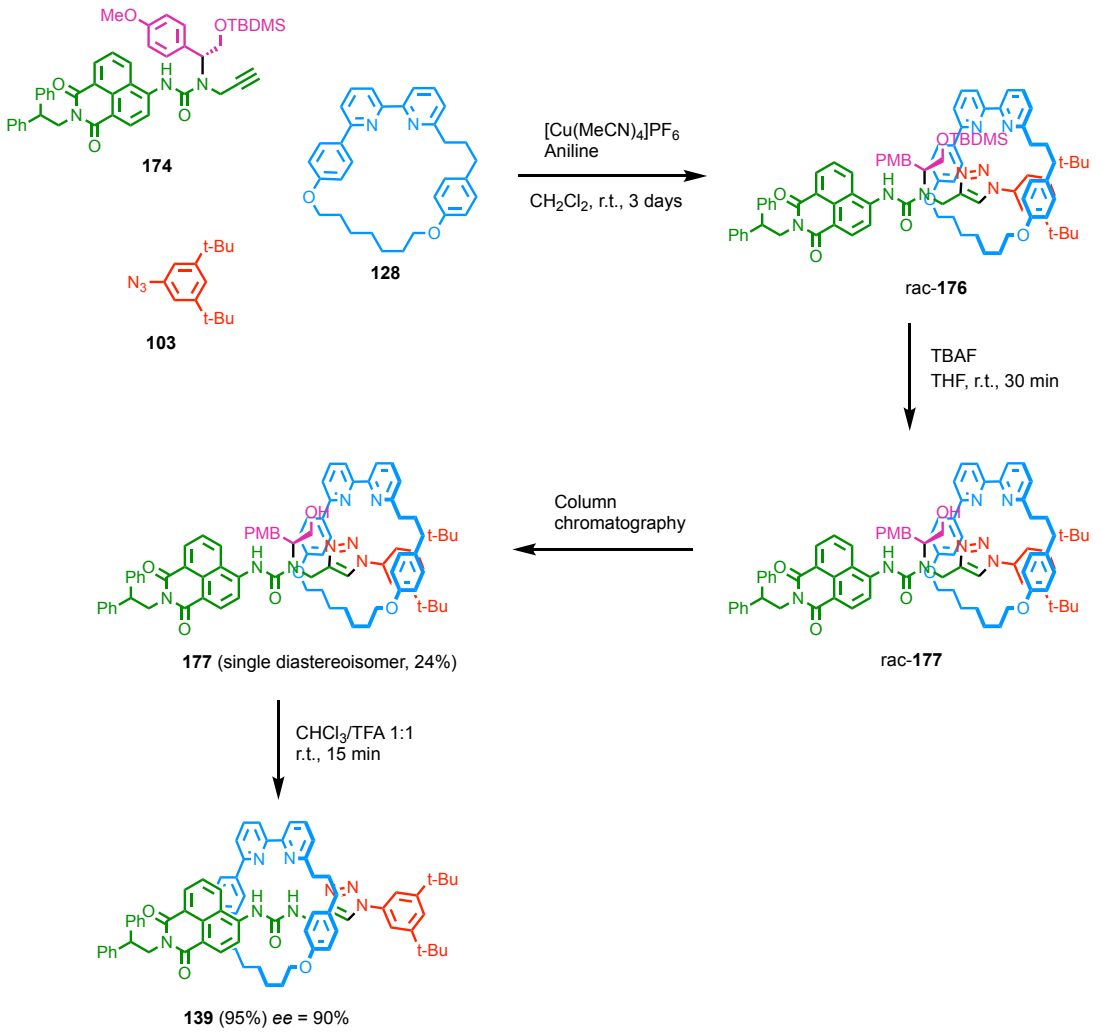

Scheme 4. 25 Synthetic route to obtain enantio-enriched rotaxane **139**.

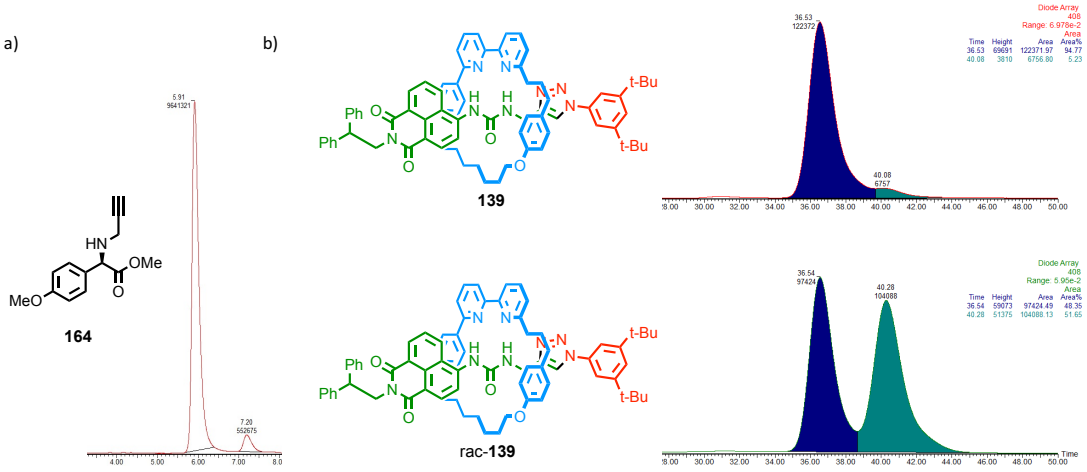

Figure 4. 18 HPLC traces of a) amine derivative **164** in 90% *ee* and b) of rotaxane **139** as a racemate (bottom) and at the end of the synthetic route using the chiral auxiliary (top).

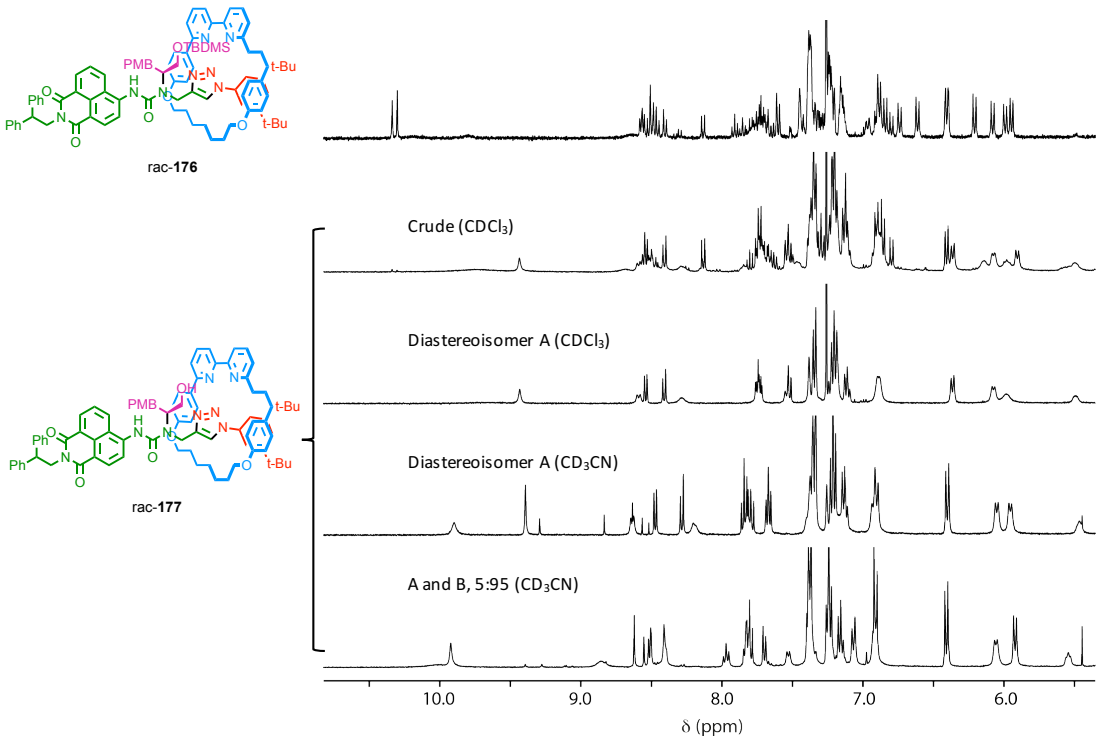

Figure 4. 19 ^{1}H NMR stack plot ($CDCl_3$, 400 MHz, 298 K) of (from top to bottom) TBDMS protected rotaxane rac-**178** contaminated with macrocycle **128**, crude TBDMS deprotection of rac-**178**, first diastereoisomer of **179** isolated after column chromatography, first diastereoisomer of **179** isolated after column chromatography (CD_3CN), second diastereoisomer of **179** at 95% (CD_3CN).

Finally, methylation of the triazole which was achieved using the conditions previously reported to give rotaxane **180** in 40% yield after purification and counter anion exchange of BF_4^- for PF_6^- (Scheme 4. 26).

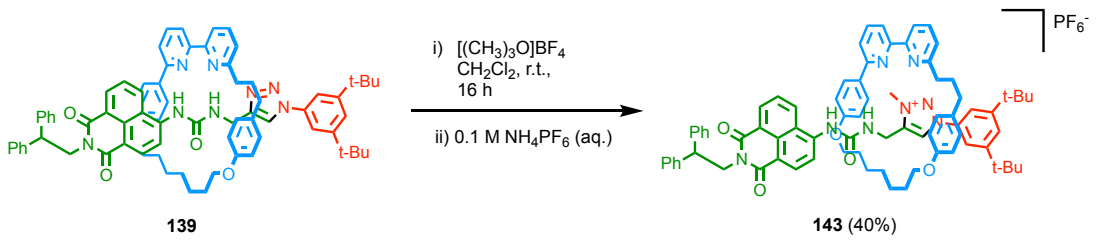

Scheme 4. 26 Synthesis of the enantio-enriched rotaxane **143**.

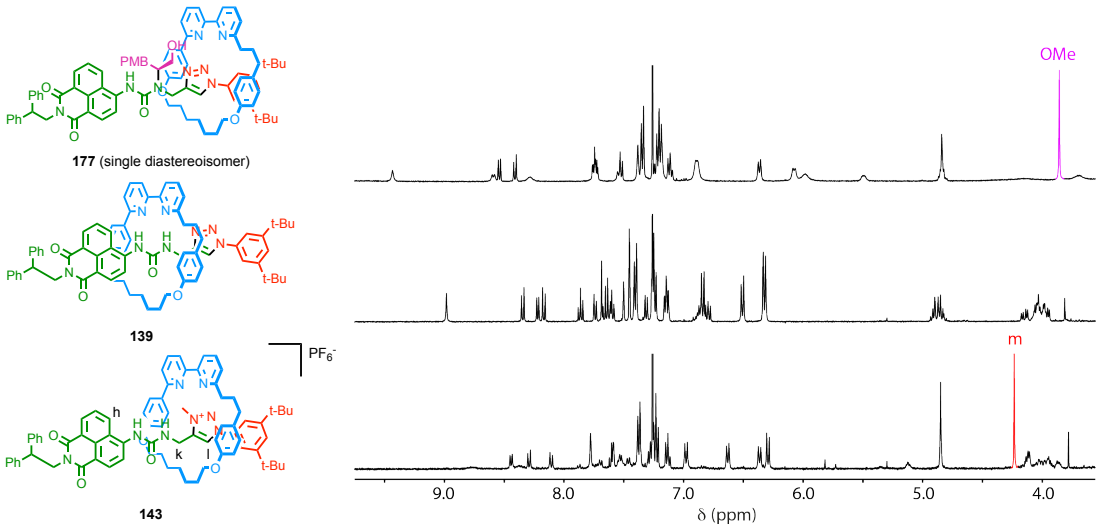

Figure 4. 20 ^{1}H NMR stack plot (CD_3CN, 400 MHz, 298 K) of isolated diastereoisomer of **179** (top), enantioenriched rotaxane **139** after cleavage of the protecting group (middle) and enantio-enriched rotaxane **143** after methylation of the triazole unit (bottom).

4.2.4. Anion binding Study

^{1}H NMR titrations were performed with the enantio-enriched rotaxane **143** using both enantiomers of *N*-Boc-PheO^{-} and BINOL-PO_4^{-} as their TBA salts. Binding constants were calculated for each enantiomer of the guest applying a nonlinear least-squares curve fitting procedure using the online software http://supramolecular.org/ with a 1:1 global fitting model with selected proton signals (Nelder-Mead method).

The study with Boc-Phe-O^{-} was performed in deuterated acetone/water 9:1 at a host concentration of 1 mM (Figure 4. 21, Figure 4. 22). Portion-wise addition of the guest molecule induced various shifts in the ^{1}H NMR spectrum of **143**, notably for the alkyl proton H_k, the triazole proton H_l and the naphthalimide proton H_h. Using a global fitting method, we measured binding constants of 220 M^{-1} and 195 M^{-1} for the D and L enantiomer respectively, suggesting no selectivity for one of the enantiomers of the guest.

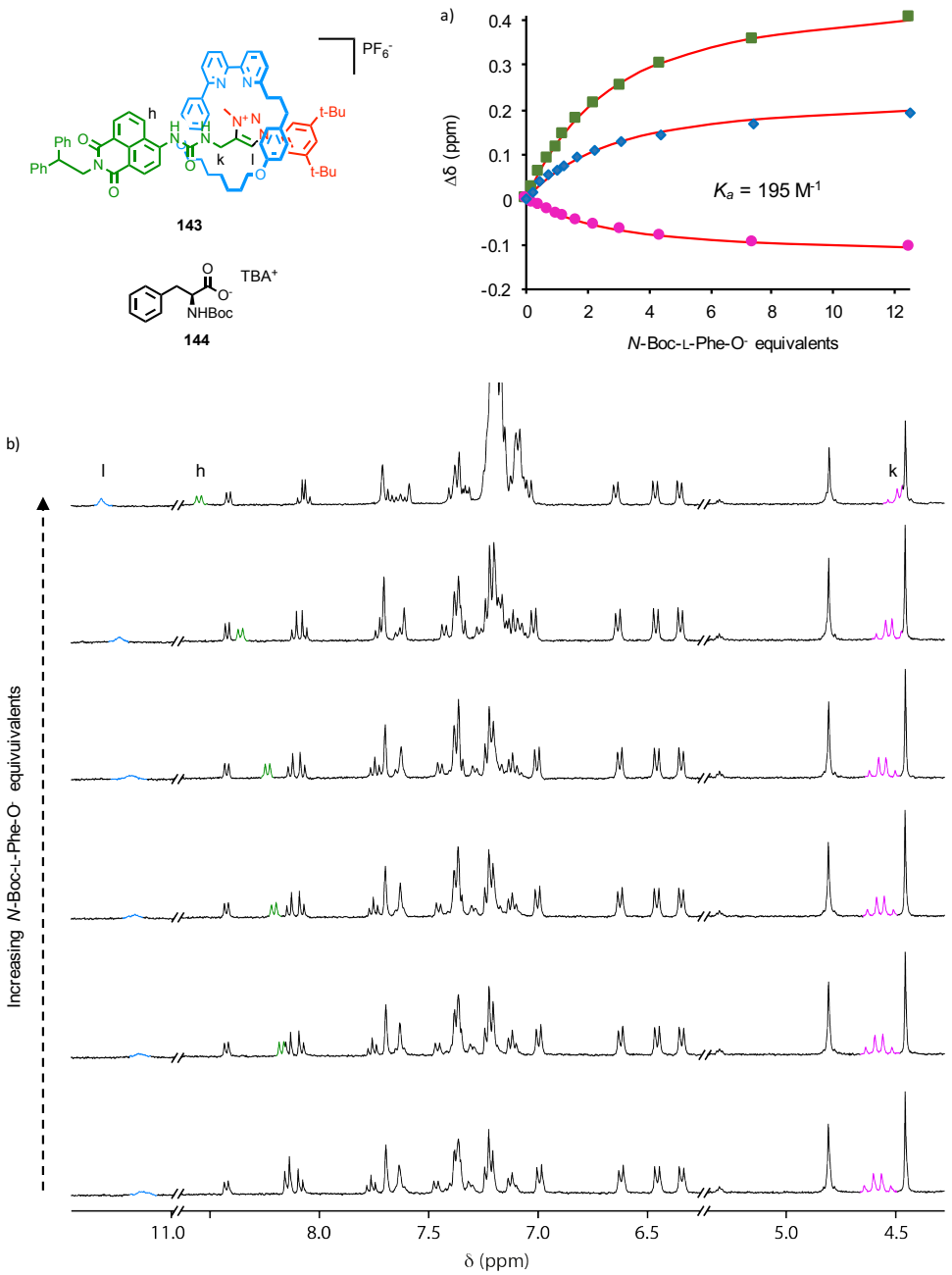

Figure 4. 21 ^{1}H NMR titration ($(CD_3)_2CO/D_2O$ 9:1, 400 MHz, 298 K) of rotaxane **143** (1 mM) with *N*-Boc-L-Phe-O$^-$ **144**. a) Global fitting curves with the calculated binding constant using the variation in chemical shift of protons H_k, H_h and H_l. c) ^{1}H NMR stack plot of **143** with increasing amount of *N*-Boc-L-Phe-O$^-$ **144** (0-3.5 equiv.) from bottom to top.

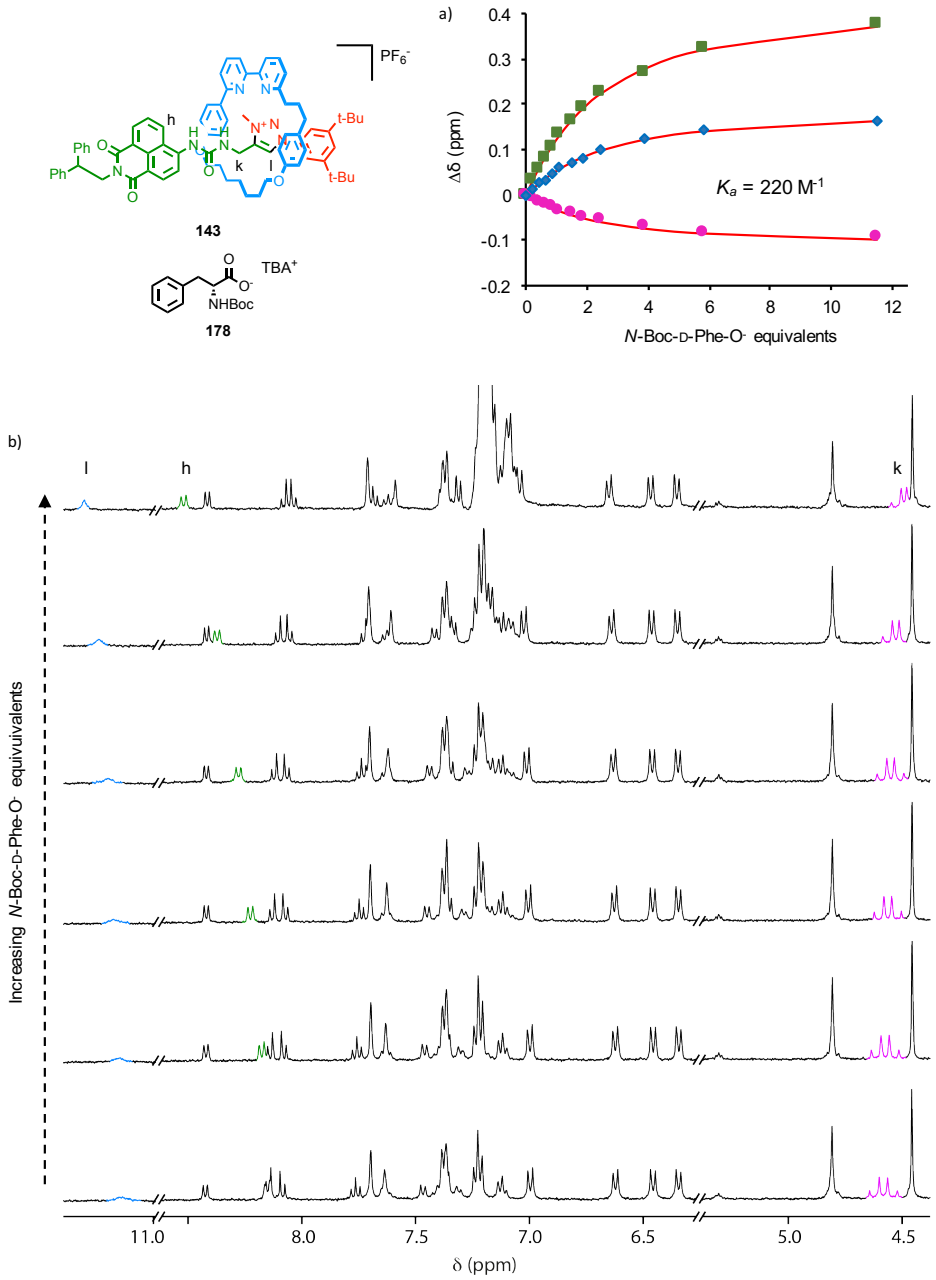

Figure 4. 22 ^{1}H NMR titration ($(CD_3)_2CO/D_2O$ 9:1, 400 MHz, 298 K) of rotaxane **143** (1 mM) with *N*-Boc-D-Phe-O$^-$ **178**. a) Global fitting curves with the calculated binding constant using the variation in chemical shift of protons H_k, H_h and H_l. c) ^{1}H NMR stack plot of **143** with increasing amount of *N*-Boc-D-Phe-O$^-$ **178** (0-3.5 equiv.) from bottom to top.

However, a similar study done with BINOL-PO_4^- acetone/water 95:5 at a host concentration of 1 mM (Figure 4. 23, Figure 4. 24) showed more promising results. Portion-wise addition of the guest molecule induced various shifts in the ^{1}H NMR spectrum of **143**, notably for the triazolium methyl protons H_m and the two naphthalimide protons H_h and H_j. Applying a global fitting method, we measured binding constants of 920 M^{-1} and 650 M^{-1} for the *R* and *S* enantiomer respectively, thus a slight enantioselectivity of K_R/K_S = 1.42.

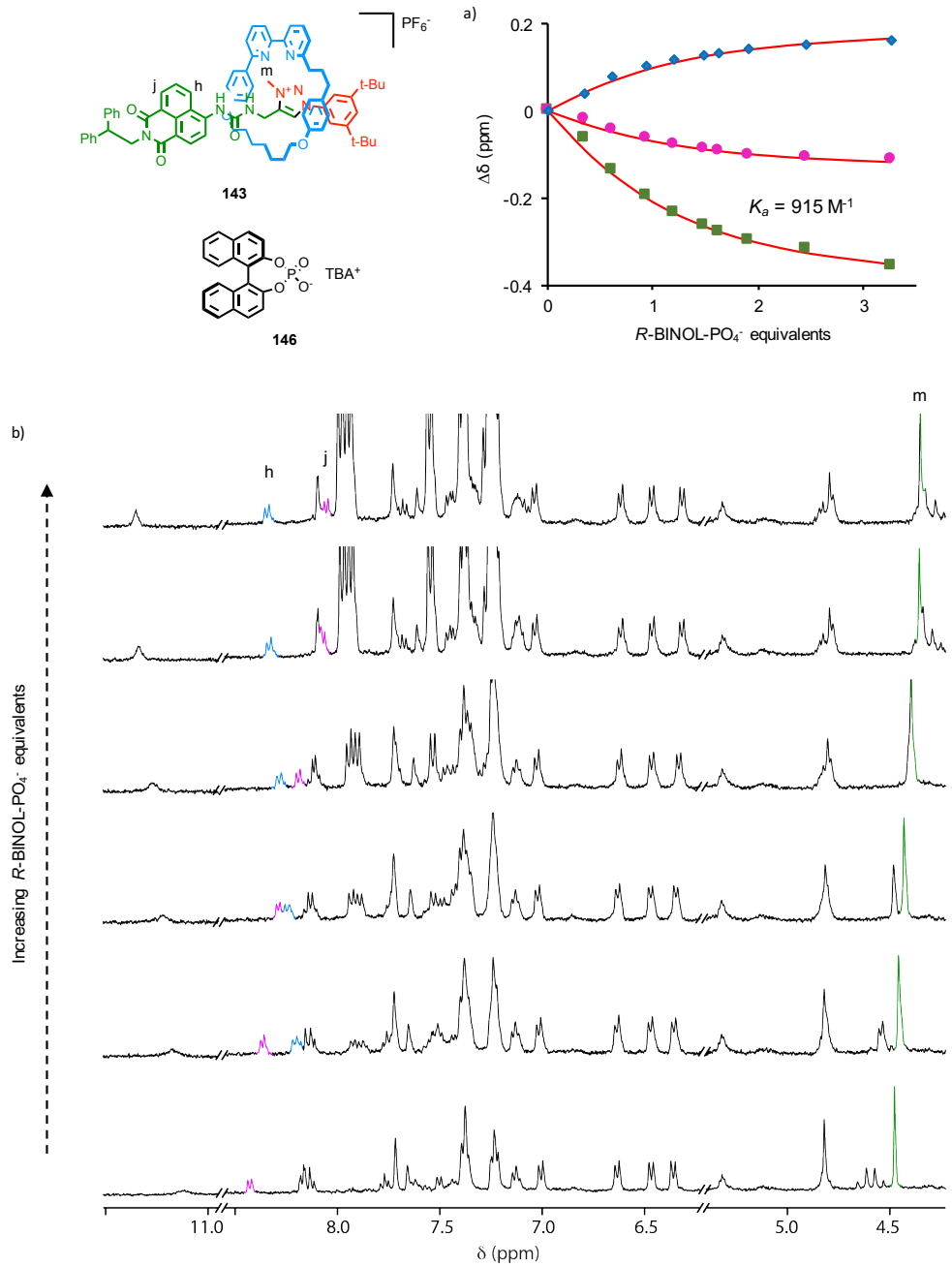

Figure 4. 23 ^{1}H NMR titration ($(CD_3)_2CO/D_2O$ 92:8, 400 MHz, 298 K) of rotaxane **143** (1 mM) with *R*-BINOL-PO_4^- **146**. a) Global fitting curves with the calculated binding constant using the variation in chemical shift of protons H_m, H_h and H_j. c) ^{1}H NMR stack plot of **143** with increasing amount of *R*-BINOL-PO_4^- **146** (0-3.5 equiv.) from bottom to top.

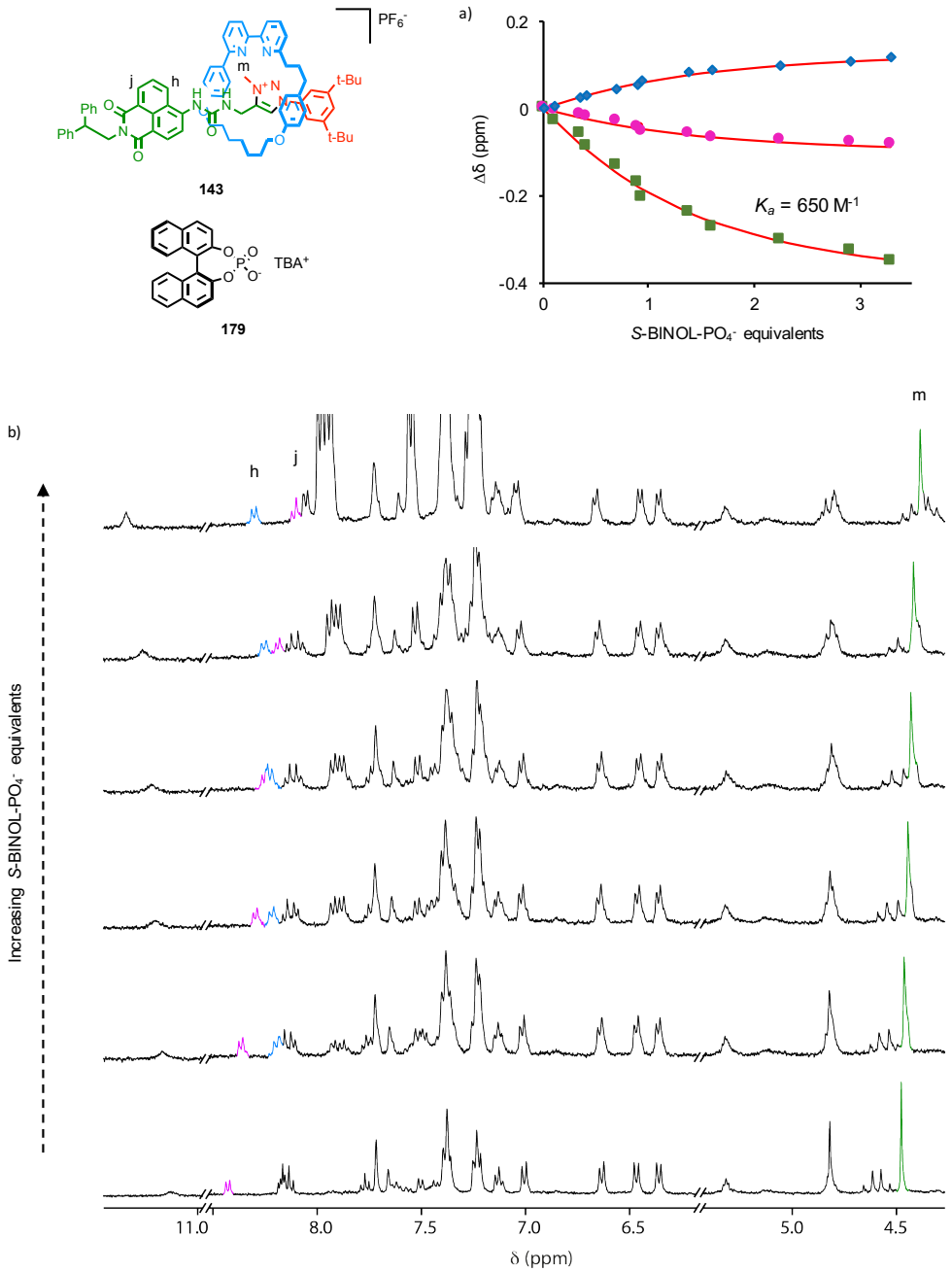

Figure 4. 24 ^{1}H NMR titration ($(CD_3)_2CO/D_2O$ 92:8, 400 MHz, 298 K) of rotaxane **143** (1 mM) with *S*-BINOL-PO_4^- **179**. a) Global fitting curves with the calculated binding constant using the variation in chemical shift of protons H_m, H_h and H_j. c) ^{1}H NMR stack plot of **143** with increasing amount of *S*-BINOL-PO_4^- **179** (0-3.5 equiv.) from bottom to top.

This is a promising first result for the application of mechanically planar chirality in the development of chiral sensors as it shows that it can impart selectivity to the system. Although it is still early in the study to have any certainty, it is not unlikely that both the steric and rigidity of the guests influence the selectivity observed in the binding event. Indeed, our system is relatively simple in that it consists of a simple binding motif, the urea, around which the mechanical bond creates a chiral three-dimensional environment. In contrast to receptor

developed **133** by Beer and co-workers, the number of non-covalent interactions possible between the anionic guest and **143** is limited making the steric influence of the mechanical bond the main contributor to the enantioselectivity.

4.3. Conclusions and Future Work

During this work, we have demonstrated the transfer of chiral information from a neutral or charged chiral guest to an interlocked receptor devoid of any chirality. Moving forward in the study we have shown that the racemate of mechanically planar rotaxane demonstrated slight enantioselectivity in the binding of an enantiopure BINOL-PO_4^- guest.

We then developed a new chiral auxiliary giving us access, by simple column chromatography processes, to functional mechanically planar chiral rotaxane receptors incorporating a urea binding site. With our enantioenriched system preliminary binding studies suggest the selective binding of one enantiomer of BINOL-PO_4^- with a ratio K_R/K_S = 1.42 in acetone/water 95:5.

This is a promising result but the study is just started and the scope of chiral anionic guest need to be expanded. Moreover, the synthesis of the receptor in higher enantiomeric excess (>99%) is also a requirement in order to get a better idea of the enantioselectivity and start investigating the reason behind it. At the moment, it would appear that the steric and rigidity of the guest play an important role in it, which would not be so surprising as our receptor mainly consists in a well-defined three-dimensional chiral pocket with a limited number non-covalent secondary interactions. However, it is too early in this project to have any certainty over the origins of selectivity. Detailed computational studies would perhaps bring a better understanding of the system.

The UV-vis, fluorescence and CD spectroscopic responses upon guest binding have to be recorded as well and could prove to be interesting given the difference in fluorescent response already observed with the racemate **143**.

Finally, it is worth noticing that this methodology could be apply to other field of study such as catalysis, in which we have already demonstrated the unambiguous impact of the mechanical bond with our gold catalyst.[15] Our new chiral auxiliary makes it possible to build mechanically planar rotaxane bearing a secondary amine that could be used enantioselective organocatalysis.

4.4. Experimental

General Experimental

Unless otherwise stated, all reagents and anhydrous solvents were purchased from commercial sources and used without further purification. All reactions were carried out under an atmosphere of N_2 using anhydrous solvents unless otherwise stated. Petrol refers to the fraction of petroleum ether boiling in the range 40-60 °C. DIPEA refers to N,N-diisopropylethylamine. NH_3-EDTA solution refers to an aqueous solution of NH_3 (17% w/w) with sodium-ethylenediaminetetraacetate (0.1 M). Flash column chromatography was performed using Biotage Isolera-4 automated chromatography system, employing Biotage SNAP or ZIP cartridges. Analytical TLC was performed on precoated silica gel plates (0.25 mm thick, 60F254, Merck, Germany) and observed under UV light. NMR spectra were recorded on Bruker AV400, AV3-400, AV500 or Bruker AV600 instrument, at a constant temperature of 298 K. Chemical shifts are reported in parts per million from low to high field and referenced to residual solvent. Coupling constants are reported in Hertz. Standard abbreviations indicating multiplicity were used as follows: m = multiplet, quint = quintet, q = quartet, t = triplet, d = doublet, s = singlet, app. = apparent, br = broad. Signal assignment was carried out using 2D NMR methods (HSQC, HMBC, COSY, NOESY) where necessary. In the case of some complex multiplets with contributions from more than one signal, absolute assignment was not possible, hence indicative assignments (e.g., H_A or H_B) are provided. Low resolution mass spectrometry (LRMS) was carried out by the mass spectrometry services at the University of Southampton using a Waters TQD mass spectrometer equipped with a triple quadrupole analyser with UHPLC injection (BEH C18 column, acetonitrile/hexane gradient with 0.2% formic acid). High resolution mass spectrometry (HRMS) was carried out by the mass spectrometry services at the University of Southampton using a MaXis (Bruker Daltonics) with a Time of Flight (TOF) analyser; samples were introduced into the mass spectrometer via a Dionex Ultimate 3000 autosampler and a UHPLC pump using a 20-100% acetonitrile/hexane gradient with 0.2% formic acid over 5 min at 0.6 mL/min (column: Acquity UPLC BEH C18 (Waters) 1.7 μm 50 × 2.1 mm).

3,5-di-*tert*-butylphenyl azide 103[16] and macrocycle 128[13] were synthesised following literature procedures.

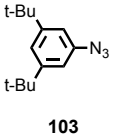

103

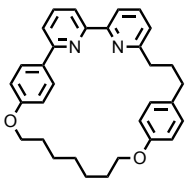

128

General Rotaxane Procedure

The macrocycle **128** (1 equiv.), azide **103** (1 equiv.), alkyne (1 equiv.), $[Cu(MeCN)_4]PF_6$ (0.96 equiv.) were weighed dry into a sealed flask and purged with N_2. Solvent was added to make a 0.02 M solution (wrt. macrocycle), followed by DIPEA (1 equiv.) and the mixture stirred at r.t. for 4 h. The crude reaction was diluted with CH_2Cl_2 and washed with 16% aqueous NH_3-EDTA solution. The organic layer was retained and the aqueous layer extracted twice further with CH_2Cl_2. The organic extracts were combined, dried over $MgSO_4$, filtered and dried *in vacuo*. The crude mixture was purified by flash column chromatography to yield the desired [2]rotaxane.

Preparation of chiral tetrabutylammonium (TBA) salts of anions

The method employed was reported Beer and co-workers.[17]

The appropriate commercially-available *N*-Boc-amino acid or BINOL-PO_4H derivative (1 equiv.) was mixed with methanol (1.0 mL) and cooled to 0 ^oC. To this solution was added a 1.0 M solution of Bu_4NOH (1 equiv.) in methanol dropwise and the resulting solution was stirred at r.t. for 30 min. The solvent was then removed *in vacuo* and the product dried on a high vacuum for 1 day before usage. The hygroscopic TBA salts were stored in a vacuum desiccator between usage.

Experimental Data

*Compound (**153**)*

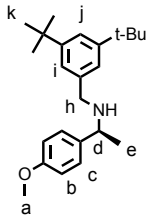

153

To a stirred solution of amine **151** (151 mg, 1 mmol, 1 equiv.) in MeCN (10 mL) at r.t. was added K_2CO_3 (173 mg, 1.25 mmol, 1.25 equiv.) followed after 15 min by 3,5-di-*tert*-butylbenzyl bromide **152** (283 mg, 1 mmol, 1 equiv.). The resulting solution was stirred for 16 h then filtered through celite and concentrated *in vacuo*. The crude residue was purified *via* flash column chromatography on silica gel with a linear gradient of EtOAc in petrol 0 to 40%, providing the pure product **153** as colourless oil (265 mg, 75%). ^{1}H NMR ($CDCl_3$, 500 MHz, 298 K) δ 7.31 (t, *J* = 1.9, 1H, H_j), 7.29 (d, *J* = 8.8, 1H, H_c), 7.10 (d, *J* = 1.9, 2H, H_i), 6.90 (d, *J* = 8.7, 2H, H_b), 3.82 (s, 3H, H_a), 3.78 (q, *J* = 6.6, 1H, H_d), 3.65 (d, *J* = 13.1, 1H, H_h), 3.59 (d, *J* = 13.1, 1H, H_h), 1.35 (d, *J* = 6.6, 3H, H_e), 1.33 (s, 18H, H_k). ^{13}C NMR ($CDCl_3$, 126 MHz, 298 K) δ 158.7, 150.8, 139.8, 138.0, 127.9, 122.5, 121.0, 113.9, 56.9, 55.4, 52.4, 35.0, 31.7, 24.7. HRMS (ESI+) m/z = 354.2794 $[M+H]^+$ (calc. for $C_{24}H_{36}NO$ 354.2791).

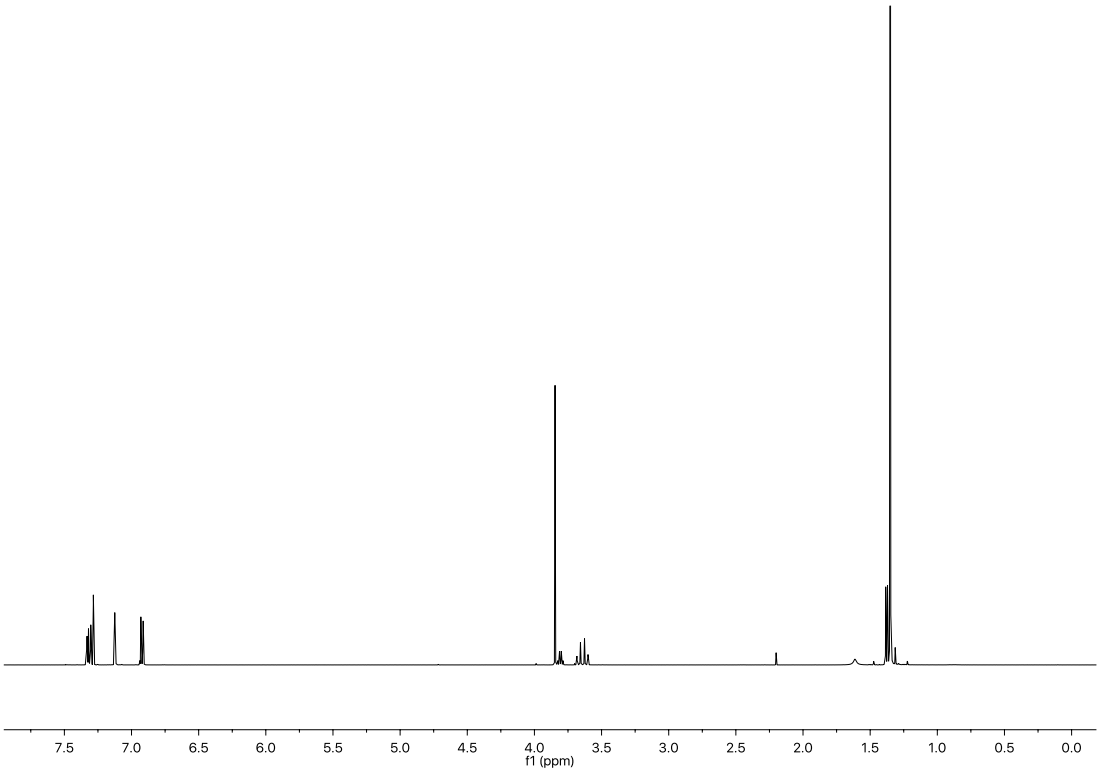

Figure S4 1 ^{1}H NMR ($CDCl_3$, 500 MHz, 298 K) of **153**.

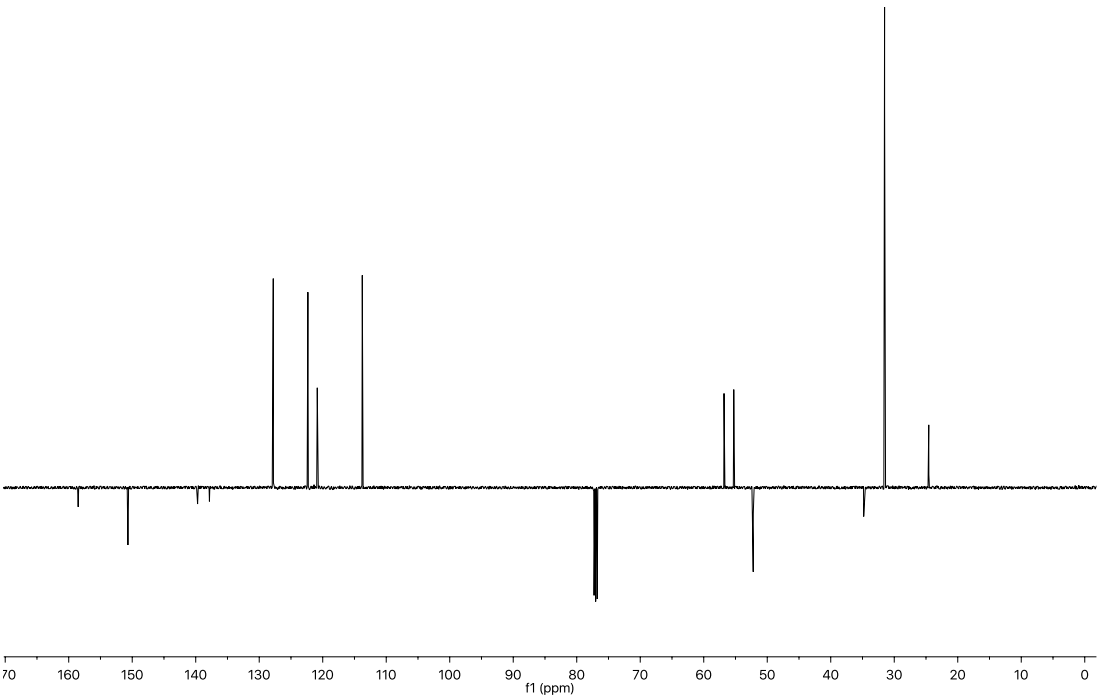

Figure S4 2 J-MOD NMR ($CDCl_3$, 126 MHz, 298 K) of **153**.

*Compound (**149**)*

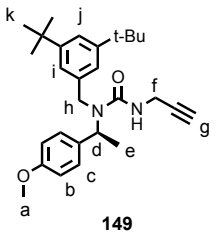

149

To a stirred solution of triphosgene (80 mg, 0.3 mmol, 0.4 equiv.) in CH_2Cl_2 (3 mL) at - 10 °C was added drop-wise amine **153** (228 mg, 0.68 mmol, 1 equiv.) as a solution in CH_2Cl_2 (1 mL) and TEA (0.14 mL, 1.0 mmol, 1.5 equiv.). After 2 h stirring in an ice bath was added propargylamine (0.05 mL, 0.8 mmol, 1.1 equiv.) and TEA (0.1 mL, 0.7 mmol, 1 equiv.). The solution was stirred at r.t. for 16 h then diluted with CH_2Cl_2 (10 mL) and sat. $NaHCO_3$ (aq.) (10 mL). The organic layer was washed with water (5 mL), dried ($MgSO_4$) and concentrated *in vacuo*. The crude was purified *via* flash chromatography on silica gel using a linear gradient of EtOAc in petrol 0 to 20%, affording product **149** as colourless oil (130 mg, 25%). ^{1}H NMR ($CDCl_3$, 400 MHz, 298 K) δ 7.31 (d, *J* = 8.8, 1H, H_c), 7.28 (t, *J* = 1.8, 1H, H_j), 6.95 (d, *J* = 1.8, 1H, H_i), 6.85 (d, *J* = 8.8, 2H, H_b), 5.89 (q, *J* = 7.1, 1H, H_d), 4.43 (t, *J* = 5.3, 1H, -*NH*-), 4.25 – 4.05 (m, 2H, H_h), 4.03 – 3.84 (m, 2H, H_f), 3.79 (s, 3H, H_a), 2.07 (t, *J* = 2.5, 1H, H_g), 1.52 (d, *J* = 7.1, 3H, H_e), 1.27 (s, 18H, H_k). ^{13}C NMR ($CDCl_3$, 101 MHz, 298 K) δ 158.9, 158.6, 151.6, 136.9, 133.8, 128.9, 121.5, 120.8, 114.0, 70.8, 55.4, 52.3, 47.1, 35.0, 31.6, 30.7, 17.4. (alkyne quaternary carbon not detected). HRMS (ESI+) m/z = 435.3010 $[M+H]^+$ (calc. for $C_{28}H_{39}N_2O_2$ 435.3006).

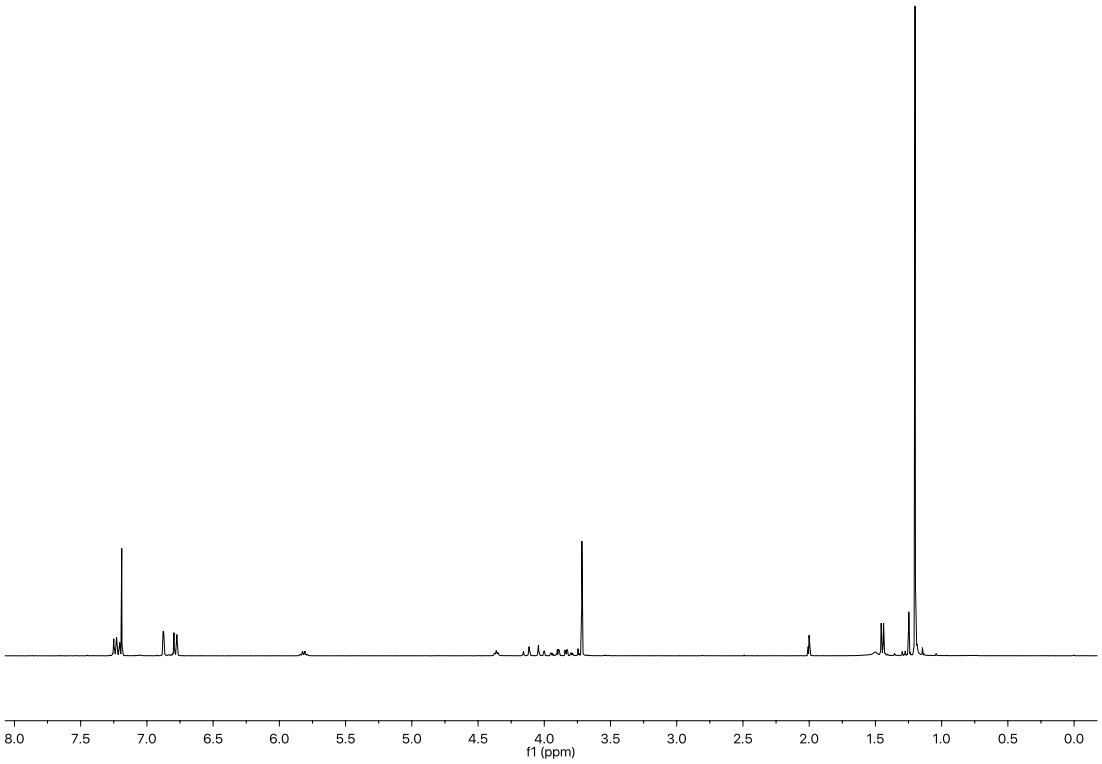

Figure S4 3 ^{1}H NMR ($CDCl_3$, 400 MHz, 298 K) of **149**.

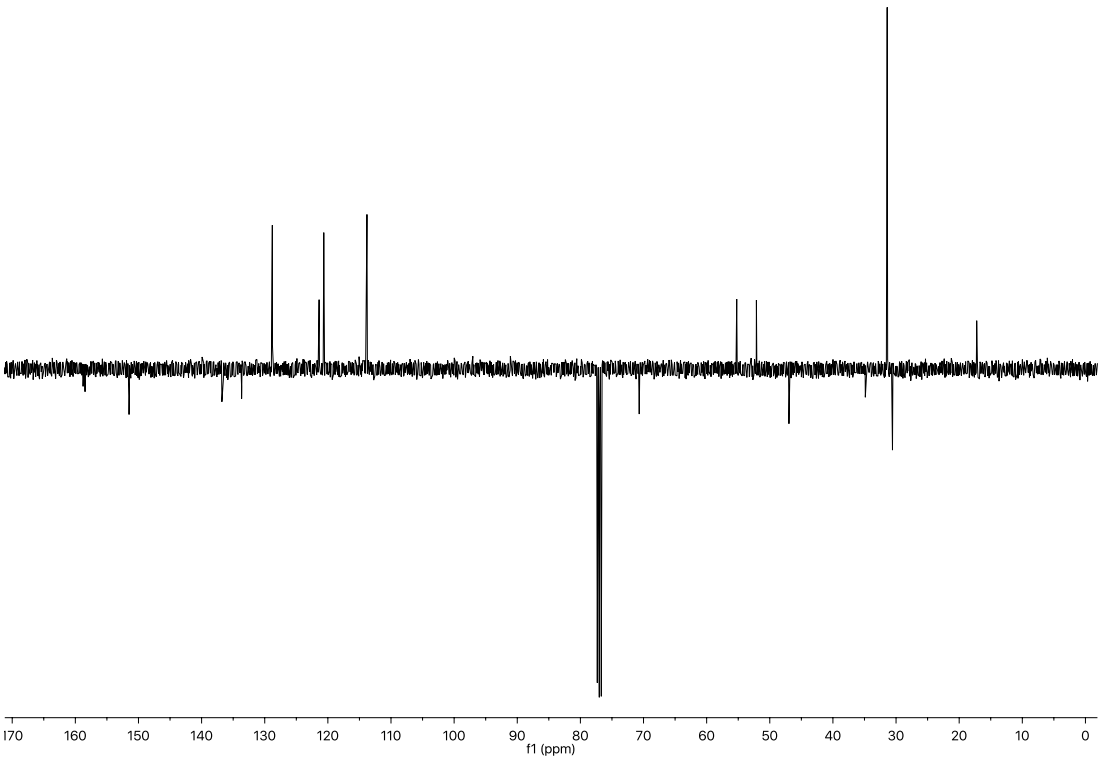

Figure S4 4 J-MOD NMR ($CDCl_3$, 101 MHz, 298 K) of **149**.

*Compound (**155**)*

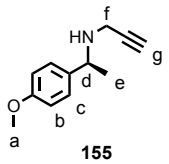

155

To a stirred solution of amine **151** (318 mg, 2.1 mmol, 1.05 equiv.) in MeCN (10 mL) at r.t. was added K_2CO_3 (346 mg, 2.5 mmol, 1.25 equiv.) followed after 15 min by propargyl bromide (80 wt. % in toluene, 0.22 mL, 2 mmol, 1 equiv.). The resulting solution was stirred for 16 h then filtered through celite and concentrated *in vacuo*. The crude residue was purified *via* flash column chromatography on silica gel with a linear gradient of petrol/EtOAc 0 to 30%, providing the pure product **155** as colourless oil (252 mg, 67%). ^{1}H NMR ($CDCl_3$, 500 MHz, 298 K) δ 7.26 (d, *J* = 8.8, 1H, H_c), 6.87 (d, *J* = 8.8, 1H, H_b), 3.97 (q, *J* = 6.6, 1H, H_d), 3.80 (s, 3H, H_a), 3.34 (dd, *J* = 17.1, 2.4, 1H, H_f), 3.15 (dd, *J* = 17.1, 2.4, 1H, H_f), 2.21 (t, *J* = 2.4, 1H, H_g), 1.57 – 1.48 (br s, 1H, *-NH-*), 1.34 (d, *J* = 6.6, 3H, H_e). ^{13}C NMR ($CDCl_3$, 126 MHz, 298 K) δ 158.9, 136.6, 128.1, 114.0, 82.5, 71.3, 55.8, 55.4, 36.0, 24.1. LRMS (ESI+) m/z = 190.3 [M+H].

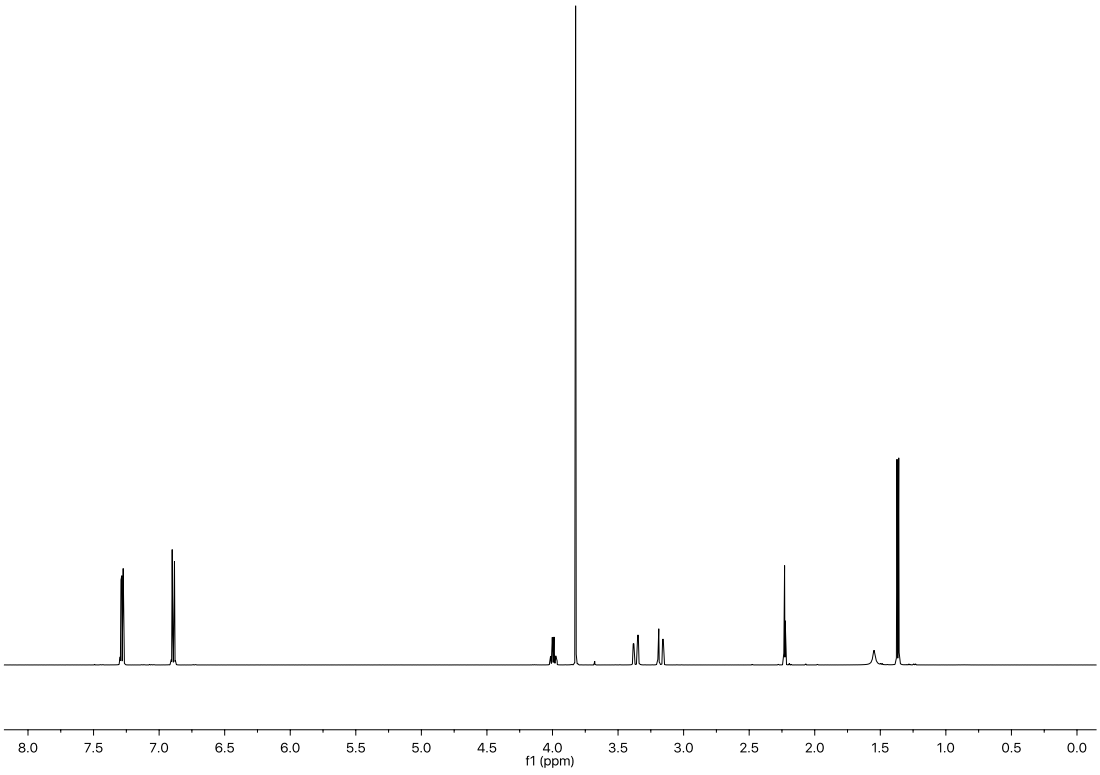

Figure S4 5 ^{1}H NMR ($CDCl_3$, 500 MHz, 298 K) of **155**.

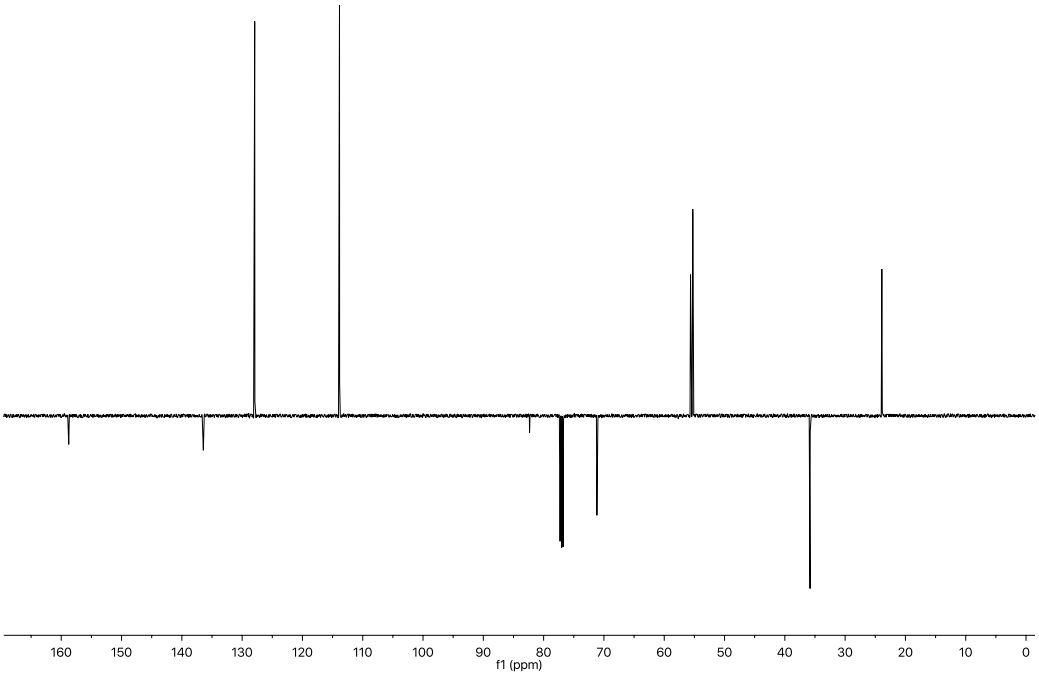

Figure S4 6 J-MOD NMR ($CDCl_3$, 126 MHz, 298 K) of **155**.

*Compound (**150**)*

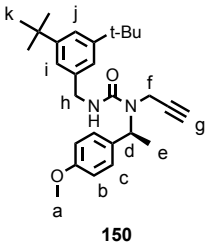

150

To a stirred solution of triphosgene (59 mg, 0.2 mmol, 0.4 equiv.) in CH_2Cl_2 (3 mL) at - 10 °C was added drop-wise amine **155** (95 mg, 0.5 mmol, 1 equiv.) as a solution in CH_2Cl_2 (0.5 mL) and TEA (0.1 mL, 0.8 mmol, 1.5 equiv.). After 2 h stirring in an ice bath was added 3,5-de-*tert*-butylbenzyle amine (117 mg, 0.6 mmol, 1.1 equiv.) and TEA (0.04 mL, 0.6 mmol, 1.1 equiv.). The solution was stirred at r.t. for 16 h then diluted with CH_2Cl_2 (10 mL) and sat $NaHCO_3$ (10 mL). The organic layer was washed with water (5 mL), dried ($MgSO_4$) and concentrated *in vacuo*. The crude was purified *via* flash chromatography on silica gel using a linear gradient of EtOAc in petrol 0 to 20%, affording product **150** as colourless oil (210 mg, 97%). ^{1}H NMR ($CDCl_3$, 400 MHz, 298 K) δ 7.45 (t, *J* = 1.8, 1H, H_j), 7.42 (d, *J* = 8.8, 2H, H_c), 7.26 (d, *J* = 1.8, 2H, H_i), 6.99 (d, *J* = 8.8, 2H, H_b), 5.76 (q, *J* = 7.1, 1H, H_d), 5.12 (t, *J* = 5.4, 1H, -*NH*-), 4.68 – 4.55 (m, 2H, H_h), 3.95 (dd, *J* = 18.7, 2.5, 1H, H_f), 3.93 (s, 3H, H_a), 3.80 (dd, *J* = 18.7, 2.5, 1H, H_f), 2.35 (t, *J* = 2.5, 1H, H_g), 1.72 (d, *J* = 7.1, 3H, H_e), 1.45 (s, 18H, H_k). ^{13}C NMR ($CDCl_3$, 101 MHz, 298 K) δ 159.0, 157.8, 151.1, 138.5, 133.3, 128.5, 121.7, 121.3, 114.0, 80.7, 72.5, 55.4, 52.5, 45.7, 35.0, 32.3, 31.6, 17.3. HRMS (ESI+) m/z = 435.3008 $[M+H]^+$ (calc. for $C_{28}H_{39}N_2O_2$ 435.3006).

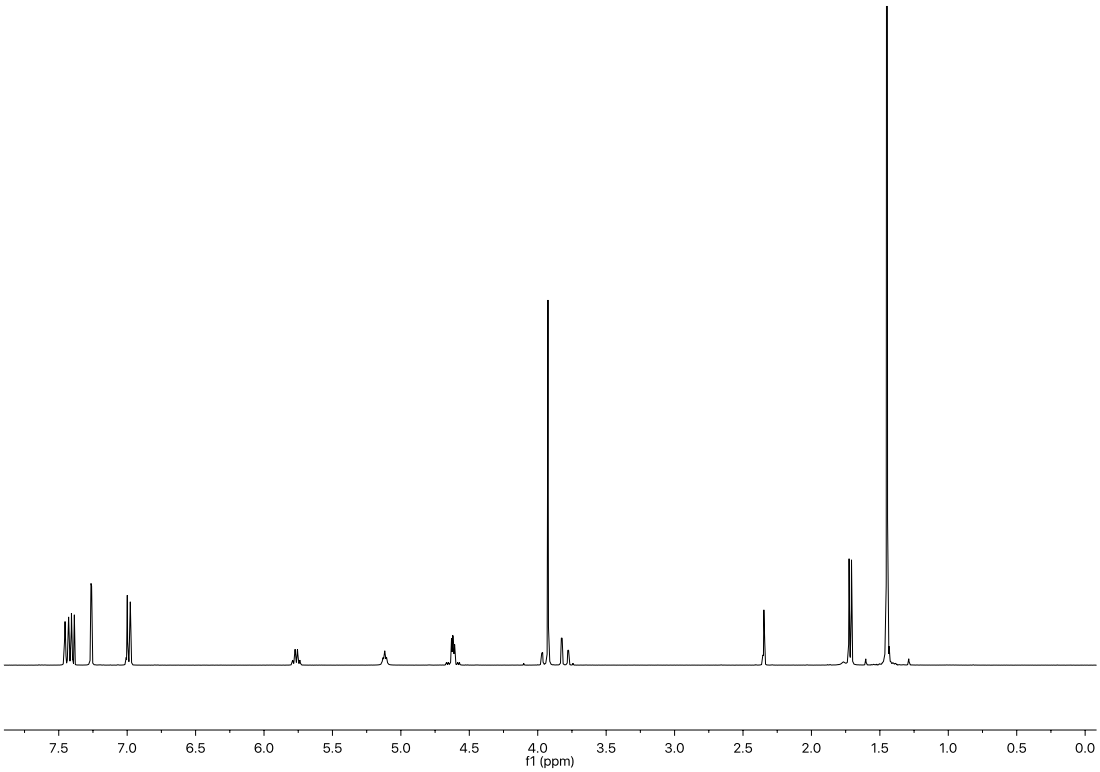

Figure S4 7 ^{1}H NMR ($CDCl_3$, 400 MHz, 298 K) of **150**.

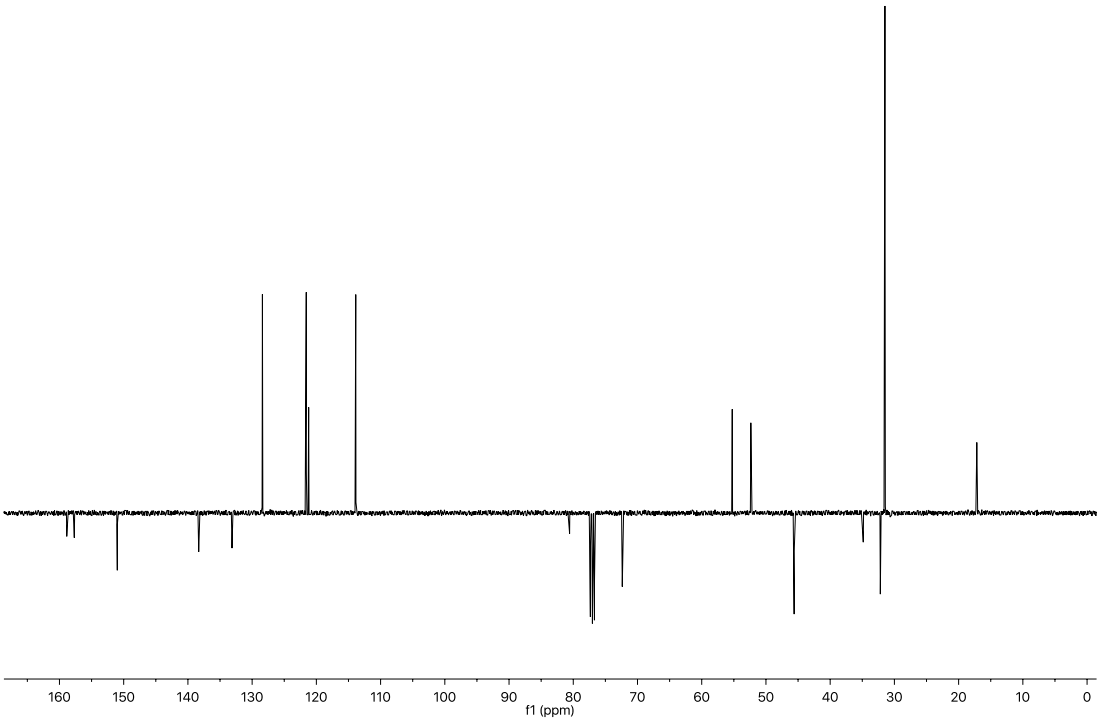

Figure S4 8 J-MOD NMR ($CDCl_3$, 101 MHz, 298 K) of **150**.

*Compound (**167**)*

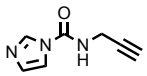

167

To a solution suspension of CDI (778 mg, 4.8 mmol, 1.2 equiv.) in THF (8 mL) was slowly added propargylamine (220 mg, 4 mmol, 1 equiv.) as a solution in THF (1 mL) over the course of 1 h. The solution was then stirred at r.t. for 16 h, concentrated *in vacuo* and the crude purified *via* flash chromatography on silica gel with a step-wise gradient of CH_2Cl_2/EtOAc 2:1 -> 1:1 -> 1:3. The pure product was obtained as colourless oil that crystallises on standing (235 mg, 39%). ^{1}H NMR ($CDCl_3$, 400 MHz, 298 K) δ 8.21 (br s, 1H, H_a or H_b or H_c), 7.43 (t app, *J* = 1.5, 1H, H_a or H_b or H_c), 7.14 (br s, 1H, H_a or H_b or H_c), 6.86 (br s, 1H, -*NH*-), 4.25 (dd, *J* = 5.3, 2.5, 2H, H_d), 2.36 (t, *J* = 2.5, 1H, H_e). ^{13}C NMR ($CDCl_3$, 101 MHz, 298 K) δ 148.6, 130.5, 116.1, 78.1, 72.8, 30.7.

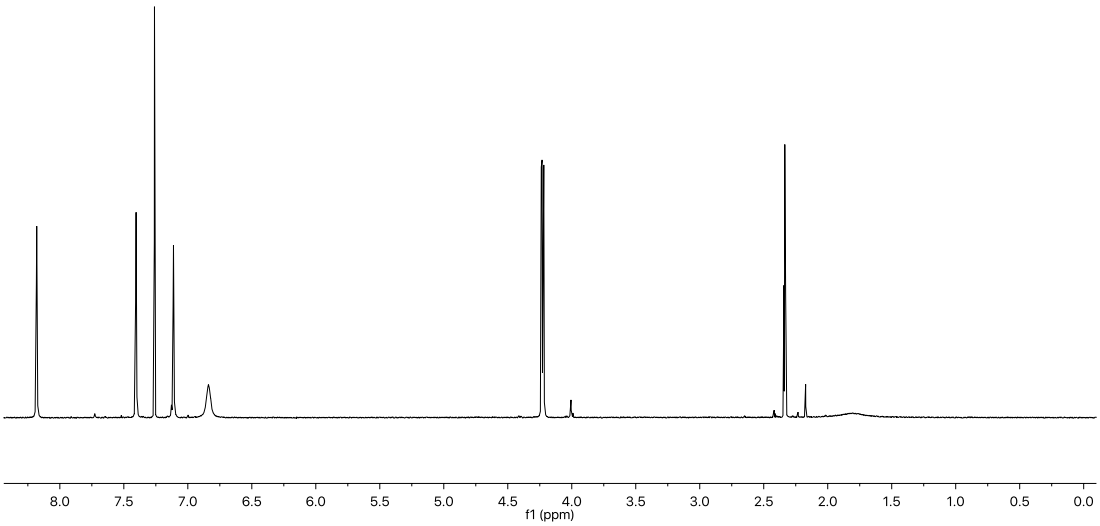

Figure S4 9 ^{1}H NMR ($CDCl_3$, 400 MHz, 298 K) of **167**.

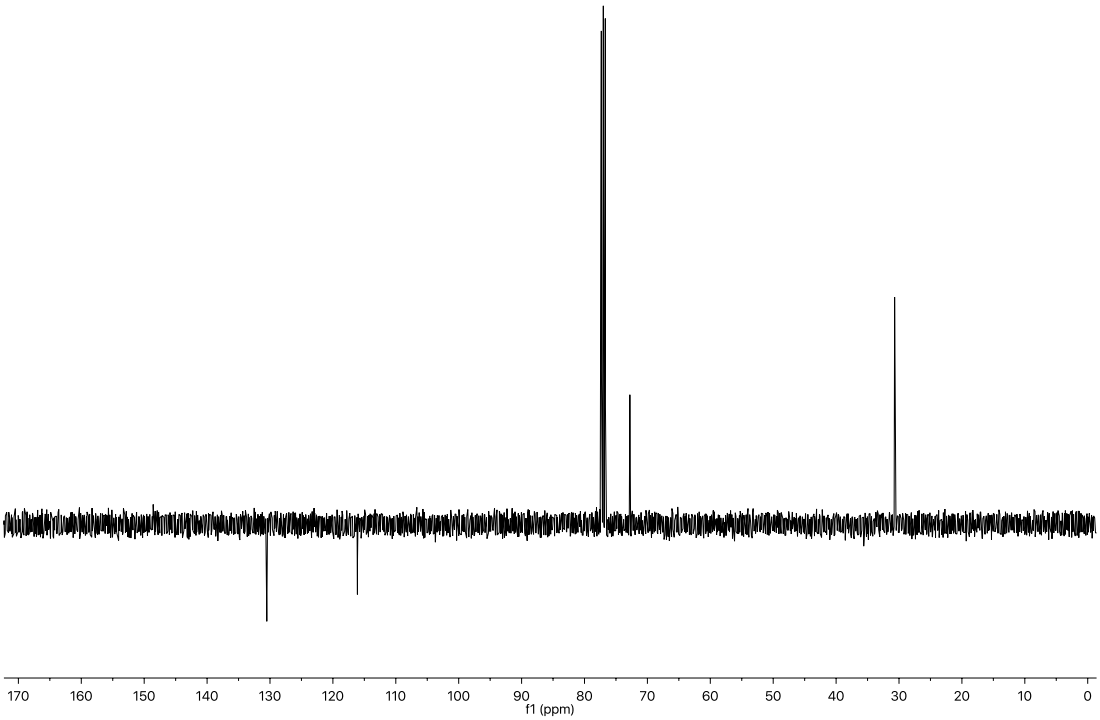

Figure S4 10 J-MOD NMR ($CDCl_3$, 101 MHz, 298 K) of **167**.

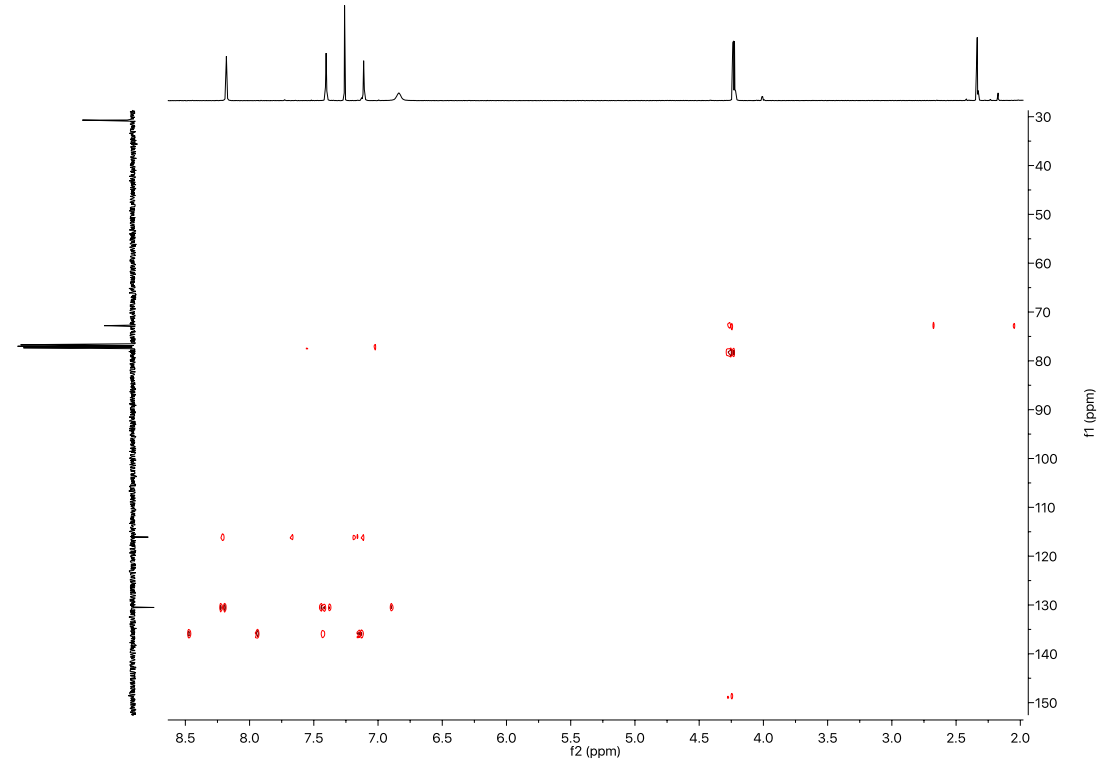

Figure S4 11 HMBC NMR ($CDCl_3$, 400 MHz, 298 K) of **167**.

*Compound (**162**)*

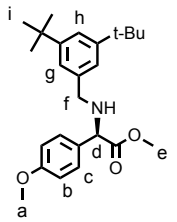

162

To a stirred solution of amine **161** (190 mg, 1.0 mmol, 1 equiv.) in MeCN (5 mL) at r.t. was added K_2CO_3 (168 mg, 1.25 mmol, 1.25 equiv.) followed after 15 min by 3,5-di-*tert*-butylbenzyl bromide (275 mg, 1.0 mmol, 1 equiv.). The resulting solution was stirred for 16 h then filtered through celite and concentrated *in vacuo*. The crude residue was purified *via* flash column chromatography on silica gel with a linear gradient of EtOAc in petrol 0 to 10%, providing the pure product **162** as yellow oil (250 mg, 65%). ^{1}H NMR ($CDCl_3$, 400 MHz, 298 K) δ 7.34 – 7.27 (m, 3H, $H_{c,\ h}$), 7.12 (d, *J* = 1.8, 2H, H_g), 6.93 – 6.85 (m, 2H, H_b), 4.35 (s, 1H, H_d), 3.81 (s, 3H, H_a), 3.69 (m, 5H, H_e and H_f), 1.32 (s, 18H, H_i). ^{13}C NMR ($CDCl_3$, 101 MHz, 298 K) δ 173.9, 159.6, 150.9, 138.6, 130.4, 128.9, 122.7, 121.3, 114.2, 63.9, 55.4, 52.0, 35.0, 31.7. HRMS (ESI+) m/z = 398.2693 $[M+H]^+$ (calc. for $C_{25}H_{36}NO_3$ 398.2690).

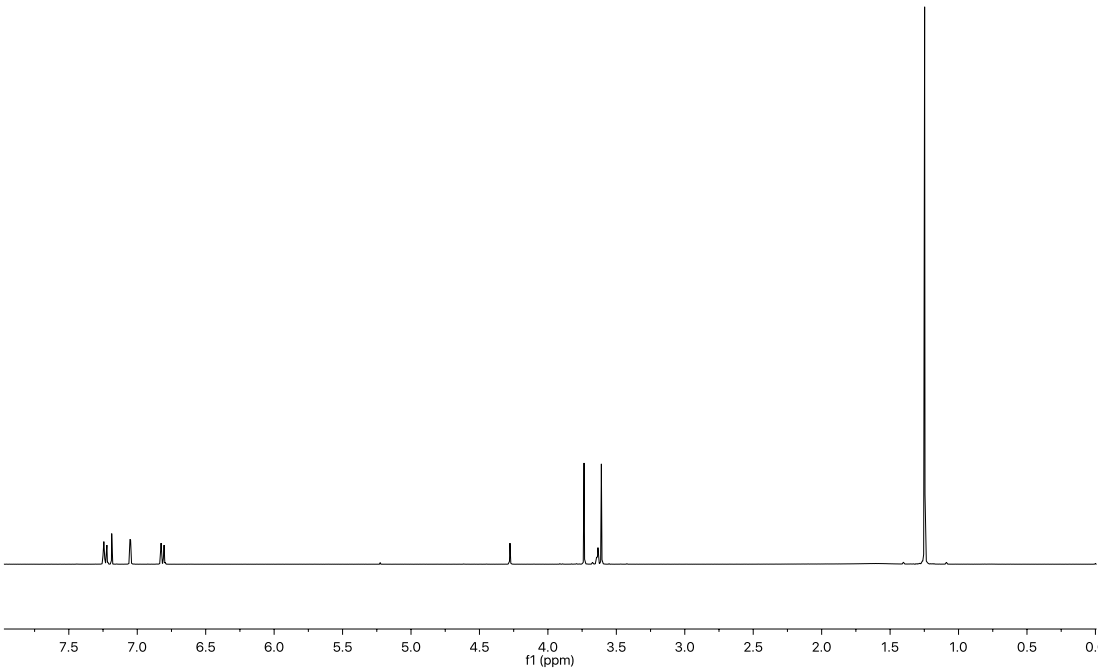

Figure S4 12 ^{1}H NMR ($CDCl_3$, 400 MHz, 298 K) of **162**.

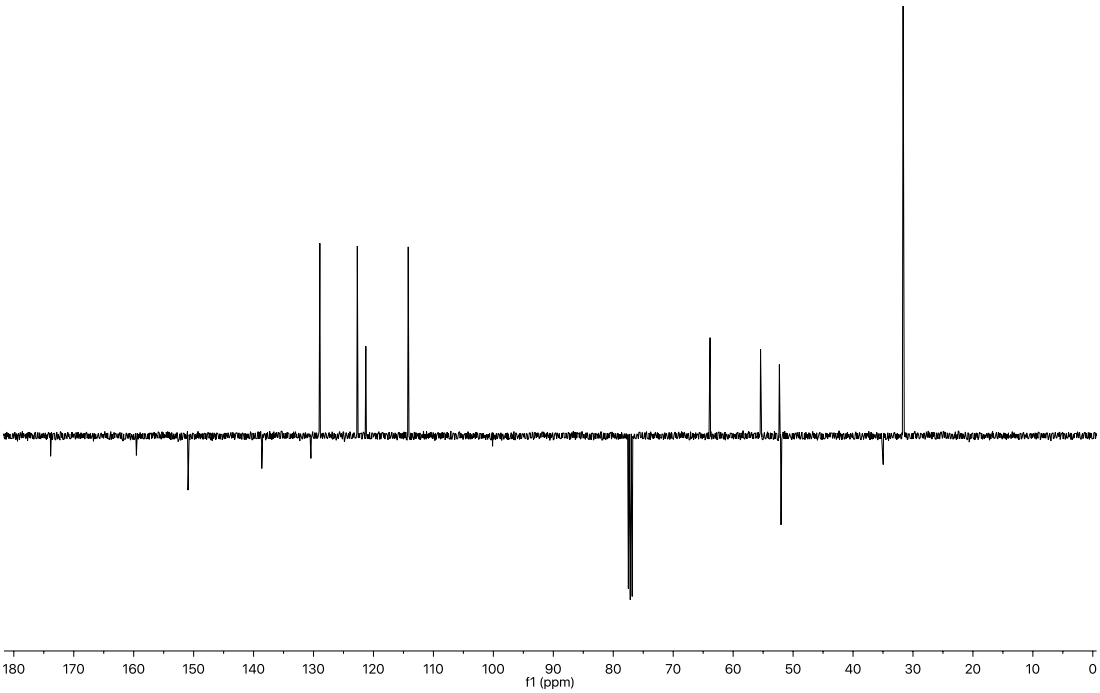

Figure S4 13 J-MOD NMR ($CDCl_3$, 101 MHz, 298 K) of **162**.

*Compound (**163**)*

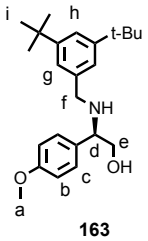

163

To a stirred suspension of $LiAlH_4$ (140 mg, 3.7 mmol, 3 equiv.) in THF (6 mL) at 0 °C was added drop-wise a solution of amino ester **162** (492 mg, 1.24 mmol, 1 equiv.) as a solution in THF (2 mL). The reaction mixture was allowed to warm up to r.t. and stirred at that temperature for 1 h. The reaction was cooled to 0 °C and carefully quenched with the drop-wise addition of water (0.75 mL) followed by 10M NaOH (aq.) (0.75 mL). After 15 min stirring at r.t., the mixture was filtered through $MgSO_4$ and the filtrate concentrated *in vacuo*. The crude was purified *via* flash chromatography on silica gel with an isocratic elution of Petrol/EtOAc 1:1, affording the pure amino alcohol **163** as a white solid (430 mg, 94%). ^{1}H NMR ($CDCl_3$, 400 MHz, 298 K) δ 7.33 (t, *J* = 1.8, 1H, H_h), 7.25 (d, *J* = 8.7, 2H, H_c), 7.12 (d, *J* = 1.8, 2H, H_g), 6.92 (d, *J* = 8.7, 2H, H_f), 3.83 (s, 3H, H_a), 3.80 – 3.72 (m, 2H, H_d and H_f), 3.69 (dd, *J* = 10.7, 4.5, 1H, H_e), 3.61 (d, *J* = 12.8, 1H, H_h), 3.55 (dd, *J* = 10.7, 8.7, 1H, H_e), 2.27 (br s, 1H, -*OH*), 1.33 (s, 18H, H_i). ^{13}C NMR ($CDCl_3$, 101 MHz, 298 K) δ 159.2, 150.9, 139.3, 132.8, 128.5, 122.6, 121.2, 114.2, 66.9, 63.3, 55.4, 51.9, 31.6. HRMS (ESI+) m/z = 370.2739 $[M+H]^+$ (calc. for $C_{24}H_{36}NO_2$ 370.2741).

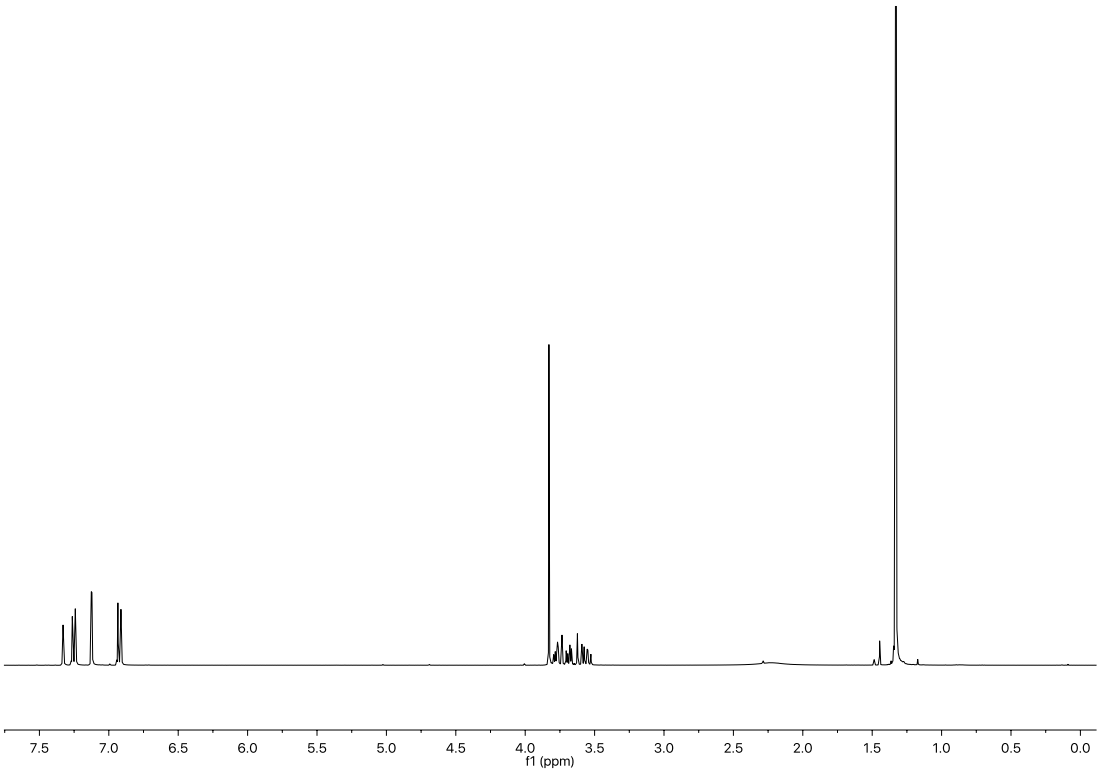

Figure S4 14 ^{1}H NMR ($CDCl_3$, 400 MHz, 298 K) of **163**.

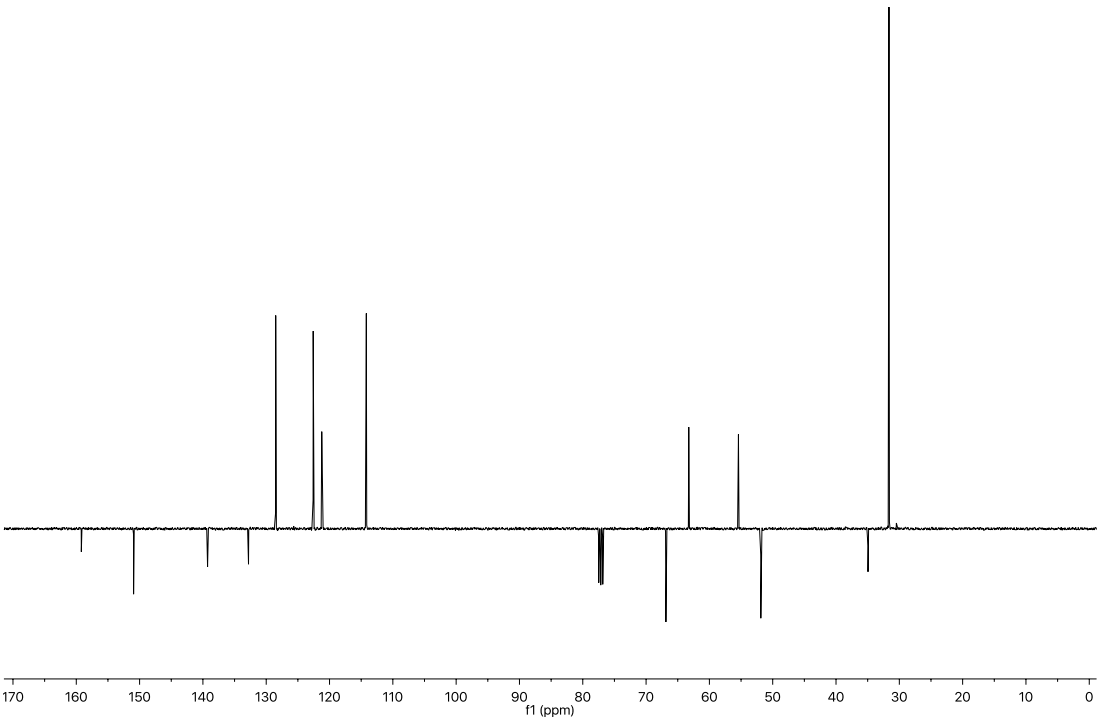

Figure S4 15 J-MOD NMR ($CDCl_3$, 101 MHz, 298 K) of **163**.

*Compound (**168**)*

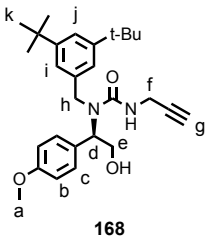

168

A solution of hydroxyl amine **163** (357 mg, 1.0 mmol, 1 equiv.), carbamoyl imidazole **167** (144 mg, 1.0 mmol, 1 equiv.) and DIPEA (0.25 mL, 1.4 mmol, 1.5 equiv.) in THF (10 mL) was stirred at r.t. for 36 h before being concentrated *in vacuo*. The crude was purified *via* flash chromatography on silica gel with a step-wise gradient of EtOAc in petrol 40 to 50%, affording the pure alkyne stopper **168** as a colourless oil (200 mg, 46%). ^{1}H NMR ($CDCl_3$, 400 MHz, 298 K) δ 7.28 (t, *J* = 1.8, 1H, H_j), 7.25 (d, *J* = 8.7, 2H, H_c), 6.97 (d, *J* = 1.8, 2H, H_i), 6.86 (d, *J* = 8.7, 2H, H_b), 5.55 (dd, *J* = 7.9, 5.9, 1H, H_d), 4.70 (t, *J* = 5.3, 1H, -*NH*-), 4.32 (d, *J* = 17.2, 1H, H_h), 4.19 (d, *J* = 17.2, 1H, H_h), 4.09 (m , 2H, H_e), 3.96 (dd, *J* = 5.3, 2.5, 2H, H_f), 3.78 (s, 3H, H_a), 2.77 (s, 1H, -*OH*), 2.10 (t, *J* = 2.5, 1H, H_g), 1.27 (s, 18H, H_k). ^{13}C NMR ($CDCl_3$, 101 MHz, 298 K) δ 159.9, 159.3, 151.9, 136.5, 129.7, 129.6, 121.7, 120.8, 114.3, 80.7, 71.1, 63.6, 60.8, 55.4, 48.5, 35.0, 31.5, 30.8. HRMS (ESI+) m/z = 451.2959 $[M+H]^+$ (calc. for $C_{28}H_{39}N_2O_3$ 451.2955).

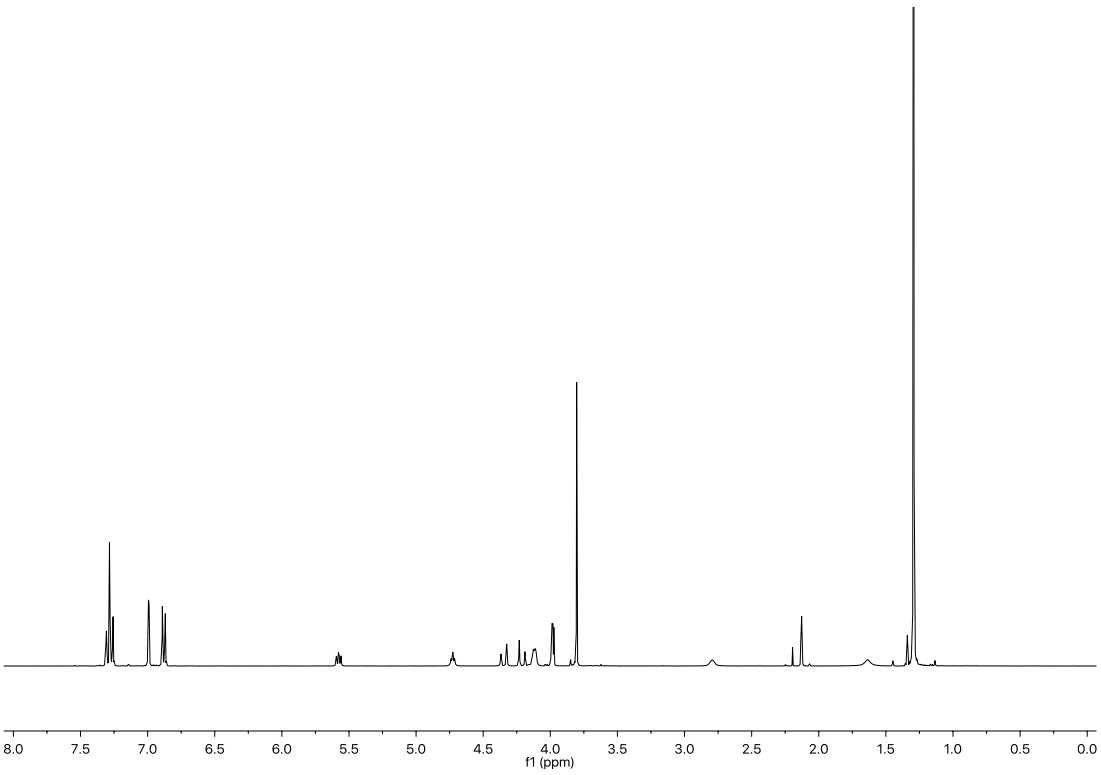

Figure S4 16 ^{1}H NMR ($CDCl_3$, 400 MHz, 298 K) of **168**.

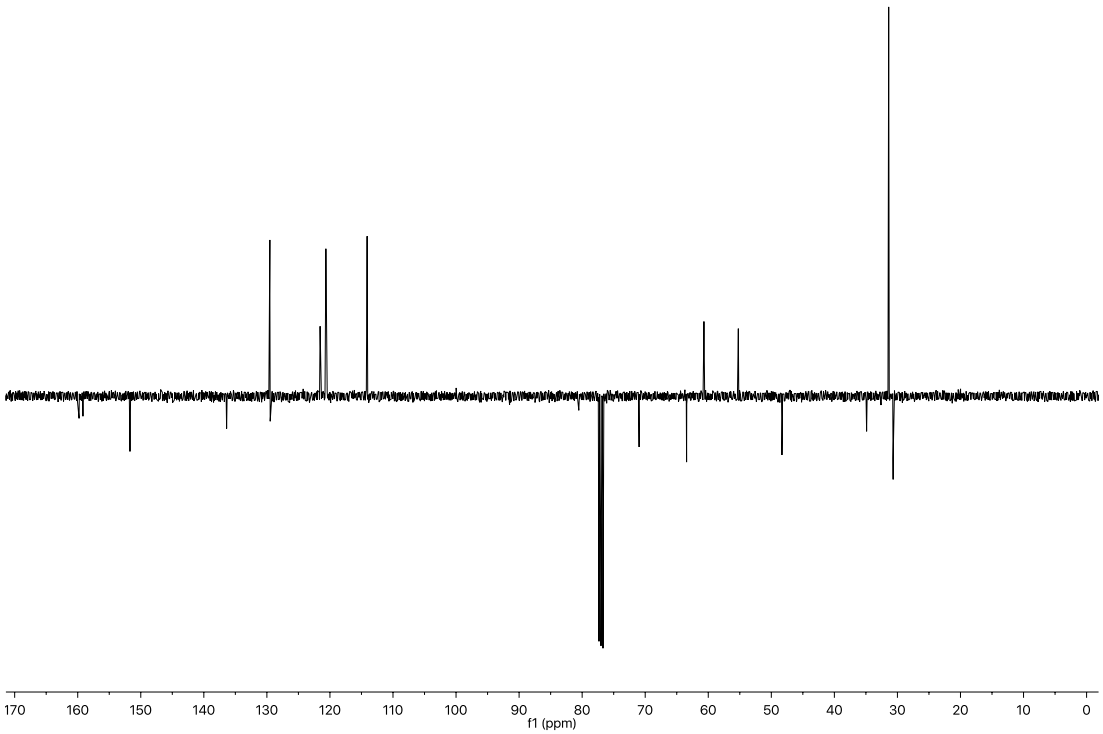

Figure S4 17 J-MOD NMR ($CDCl_3$, 101 MHz, 298 K) of **168**.

*Compound (**169**)*

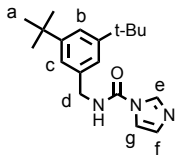

169

To a suspension of CDI (89 mg, 0.6 mmol, 1.1 equiv.) in THF (1 mL) was added 3,5-di-*tert*-butylbenzyl amine (110 mg, 0.5 mmol, 1 equiv.) and the resulting mixture was stirred a 45 ºC for 16 h. The crude was concentrated *in vacuo* and purified *via* flash chromatography on silica gel with a linear gradient of EtOAc in petrol 50 to 75% to give **169** as a white solid (77 mg, 49%). ^{1}H NMR ($CDCl_3$, 400 MHz, 298 K) δ 8.08 (br s, 1H, H_e or H_f or H_g), 7.39 (m, 2H, H_b and H_e or H_f or H_g), 7.28 (br s, 1H, -*NH*-) 7.18 (d, *J* = 1.8, 2H, H_c), 6.87 (br s, 1H, H_e or H_f or H_g), 4.56 (d, *J* = 5.4, 2H, H_d), 1.32 (s, 18H, H_a). ^{13}C NMR ($CDCl_3$, 101 MHz, 298 K) δ 151.7, 149.0, 136.2 (2 signals overlapping according to HSQC analysis), 130.0, 122.7, 122.3, 116.4, 45.8, 35.0, 31.5. HRMS (ESI+) m/z = 336.2044 $[M+Na]^+$ (calc. for $C_{19}H_{27}N_3NaO$ 336.2046).

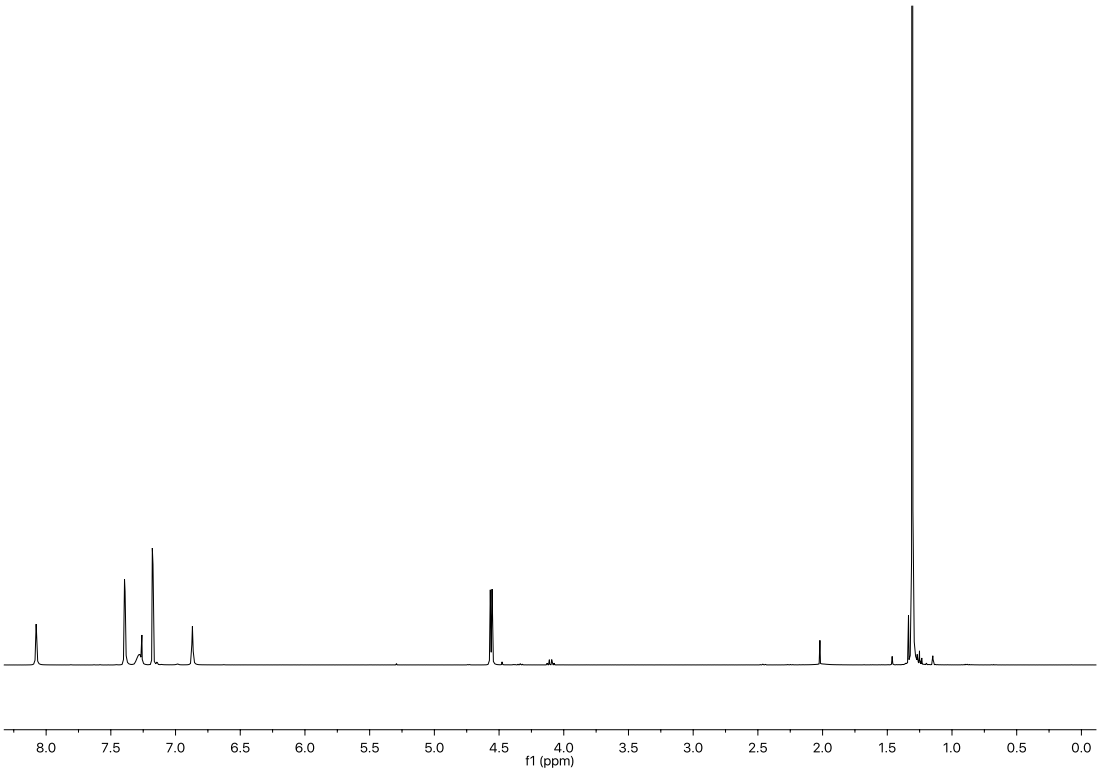

Figure S4 18 ^{1}H NMR ($CDCl_3$, 400 MHz, 298 K) of **169**.

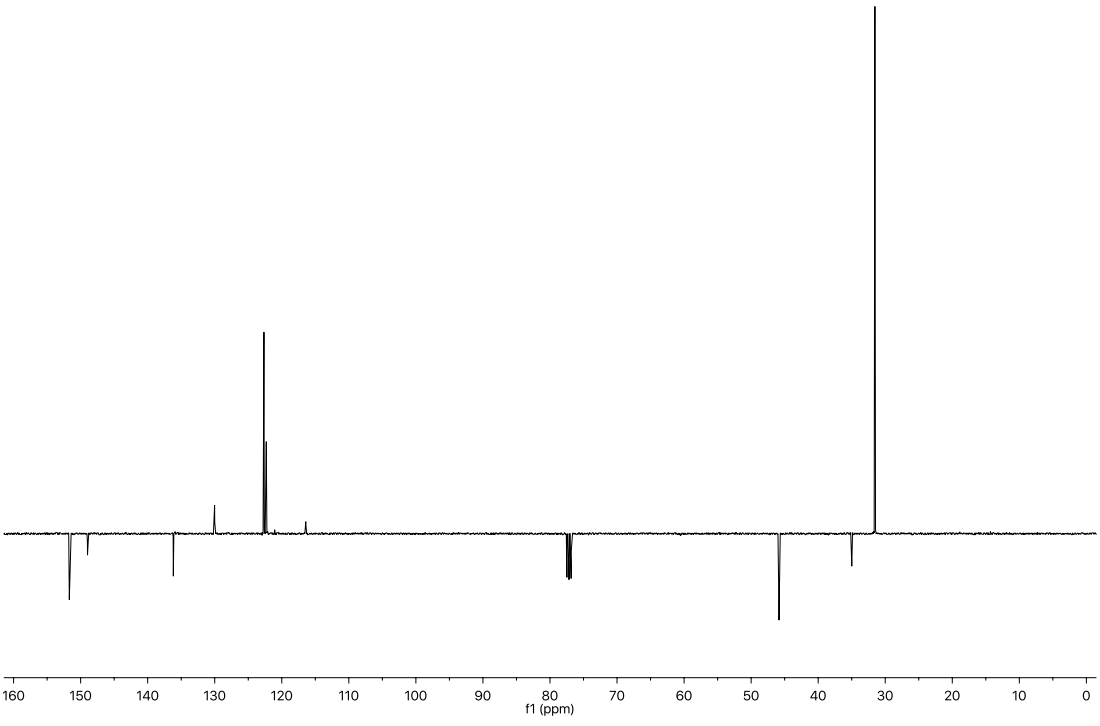

Figure S4 19 J-MOD NMR ($CDCl_3$, 101 MHz, 298 K) of **169**.

*Compound (**164**)*

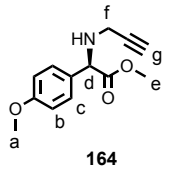

164

To a stirred solution of amine **161** (310 mg, 1.6 mmol, 1 equiv.) in MeCN (8 mL) at r.t. was added K_2CO_3 (3.29 mg, 2.4 mmol, 1.5 equiv.) followed after 15 min by propargyl bromide (80 wt. % in toluene, 0.28 mL, 1.6 mmol, 1 equiv.). The resulting solution was stirred for 16 h then filtered through celite and concentrated *in vacuo*. The crude residue was purified *via* flash column chromatography on silica gel with a step-wise gradient of EtOAc in petrol 0 - 15 - 25%, providing the pure product **164** as yellow oil (226 mg, 61%). ^{1}H NMR ($CDCl_3$, 400 MHz, 298 K) δ 7.31 (d, *J* = 8.7, 2H, H_c), 6.88 (d, *J* = 8.7, 2H, H_b), 4.59 (s, 1H, H_d), 3.80 (s, 3H, H_a), 3.69 (s, 3H, H_e), 3.45 (dd, *J* = 17.1, 2.4, 1H, H_f), 3.27 (dd, *J* = 17.1, 2.4, 1H, H_f), 2.24 (t, *J* = 2.4, 1H, H_g), 1.90 (s, 1H, -*NH*-). ^{13}C NMR ($CDCl_3$, 101 MHz, 298 K) δ 173.2, 159.7, 129.4, 129.2, 114.3, 81.3, 72.2, 63.0, 55.4, 52.5, 35.8. HRMS (ESI+) m/z = 234.1126 $[M+H]^+$ (calc. for $C_{13}H_{16}NO_3$ 234.1125).

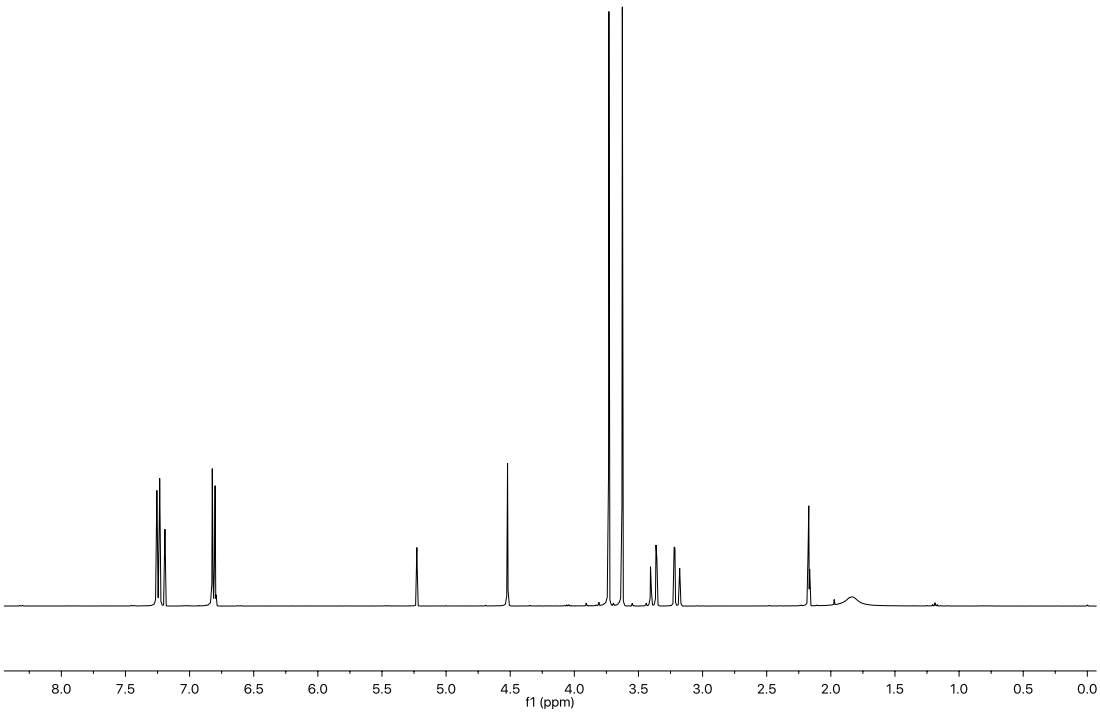

Figure S4 20 ^{1}H NMR ($CDCl_3$, 400 MHz, 298 K) of **164**.

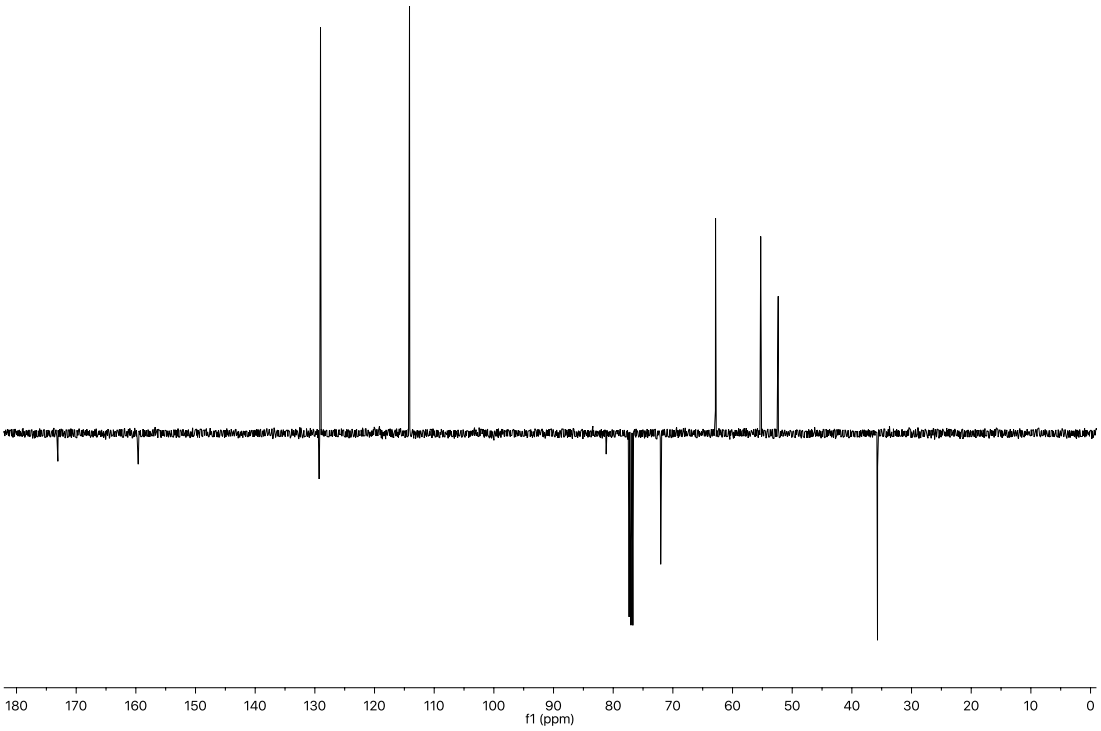

Figure S4 21 J-MOD NMR ($CDCl_3$, 101 MHz, 298 K) of **164**.

*Compound (**165**)*

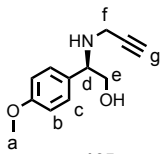

165

To a stirred suspension of LAH (25 mg, 0.7 mmol, 2.2 equiv.) in THF (2 mL) at 0 °C was added drop-wise a solution of amino ester **164** (70 mg, 0.3 mmol, 1 equiv.) as a solution in THF (0.5 mL). The reaction mixture was allowed to warm up to r.t. and stir at that temperature for 1 h. The reaction was cooled to 0 °C and carefully quenched with the drop-wise addition of water (0.2 mL) followed by 10M NaOH(aq.) (0.2 mL). After 15 min stirring at r.t., the mixture was filtered through $MgSO_4$ and the filtrate concentrated *in vacuo*. The crude was purified *via* flash chromatography on silica gel with an isocratic elution of CH_2Cl_2/MeOH 98:2, affording the pure amino alcohol **165** as a yellow oil (59 mg, 95%). ^{1}H NMR ($CDCl_3$, 400 MHz, 298 K) δ 7.26 (d, *J* = 8.7, 2H, H_c), 6.89 (d, *J* = 8.7, 2H, H_b), 3.96 (dd, *J* = 8.3, 4.5, 1H, H_d), 3.80 (s, 3H, H_a), 3.73 (dd, *J* = 10.8, 4.5, 1H, H_e), 3.60 (dd, *J* = 10.7, 8.3, 1H, H_e), 3.42 (dd, *J* = 17.0, 2.4, 1H, H_f), 3.20 (dd, *J* = 17.0, 2.4, 1H, H_f), 2.21 (t, *J* = 2.4, 1H, H_g), 1.79 (s, 1H, -*NH*-). ^{13}C NMR ($CDCl_3$, 101 MHz, 298 K) δ 159.4, 131.6, 128.8, 114.2, 82.1, 71.6, 67.0, 62.4, 55.4, 35.8. HRMS (ESI+) m/z = 206.1173 $[M+H]^+$ (calc. for $C_{12}H_{16}NO_2$ 206.1176).

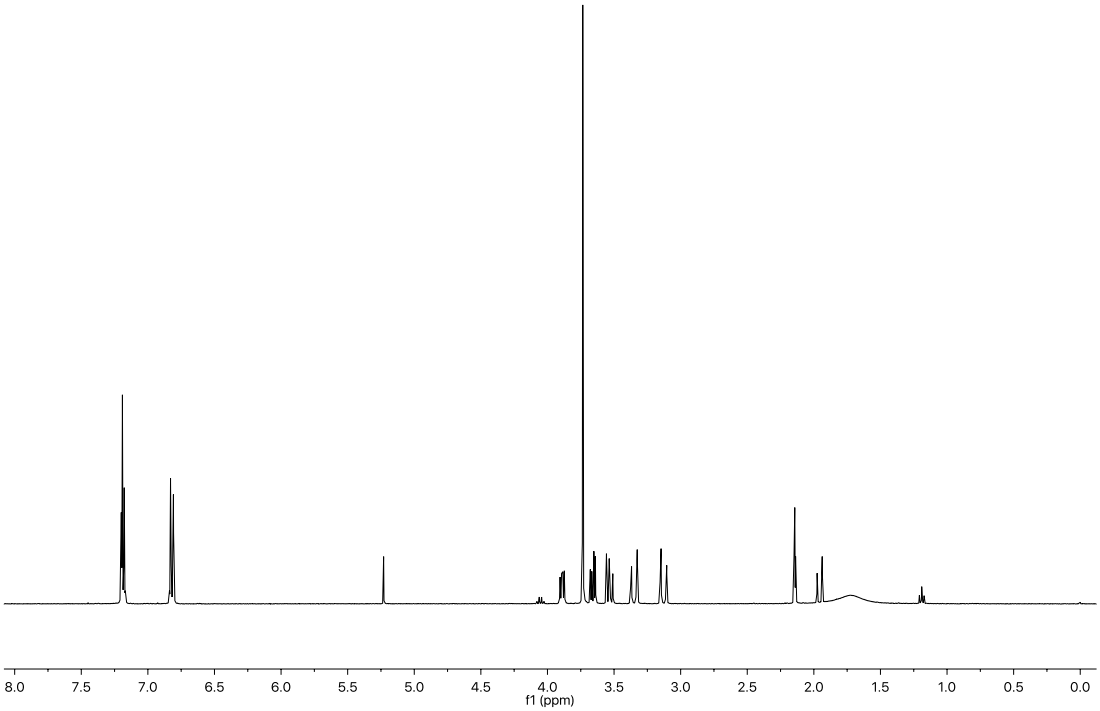

Figure S4 22 ^{1}H NMR ($CDCl_3$, 400 MHz, 298 K) of **165**.

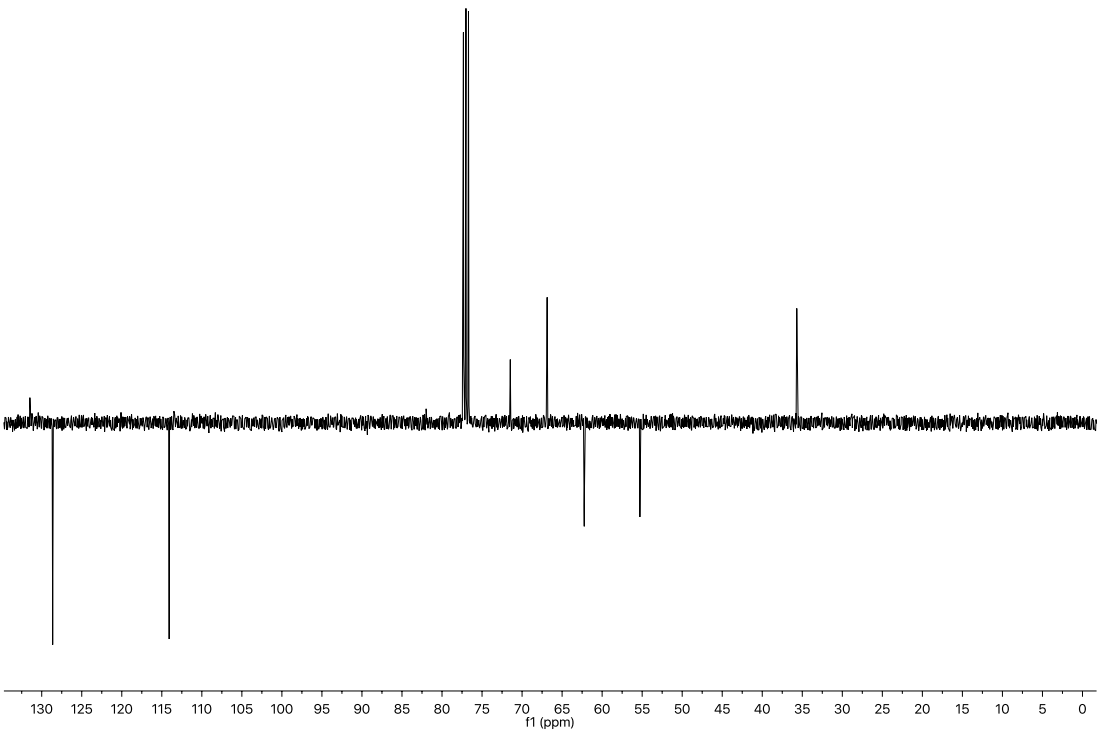

Figure S4 23 J-MOD NMR ($CDCl_3$, 101 MHz, 298 K) of **165**.

*Compound (**170**)*

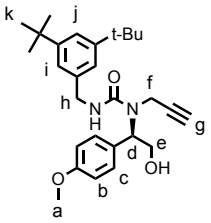

170

A solution of hydroxyl amine **165** (45 mg, 0.2 mmol, 1.1 equiv.), carbamoyl imidazole **169** (63 mg, 0.2 mmol, 1 equiv.) and DIPEA (0.04 mL, 0.2 mmol, 1.1 equiv.) in THF (3 mL) was stirred at r.t. for 36 h before being concentrated *in vacuo*. The crude was purified *via* flash chromatography on silica gel with a linear gradient of Et_2O (0 to 20%) in a 1:1 mixture of petrol/CH_2Cl_2, affording the pure alkyne stopper **170** as a colourless oil (44 mg, 49%).^{1}H NMR ($CDCl_3$, 400 MHz, 298 K) δ 7.34 (t, *J* = 1.8, 1H, H_j), 7.24 (d, *J* = 8.8, 1H, H_c), 7.15 (d, *J* = 1.8, 2H, H_i), 6.88 (d, *J* = 8.8, 2H, H_b), 5.46 (dd, *J* = 8.3, 5.3, 1H, H_d), 5.25 (t, *J* = 5.3, 1H, -*NH*-), 4.57 – 4.42 (m, 2H, H_h), 4.23 – 4.09 (m, 2H, H_e), 3.94 (dd, *J* = 18.7, 2.5, 1H, H_f), 3.80 (s, 3H, H_a), 3.72 (dd, *J* = 18.7, 2.5, 1H, H_f), 2.70 (br s, 1H, -*OH*), 2.27 (t, *J* = 2.5, 1H, H_g), 1.32 (s, 18H, H_k). ^{13}C NMR ($CDCl_3$, 101 MHz, 298 K) δ 159.4, 159.0, 151.2, 138.2, 129.1, 129.1, 121.8, 121.5, 114.3, 80.3, 72.8, 63.0, 59.8, 55.4, 45.9, 35.0, 33.0, 31.6. HRMS (ESI+) m/z = 451.2959 $[M+H]^+$ (calc. for $C_{28}H_{39}N_2O_3$ 451.2955).

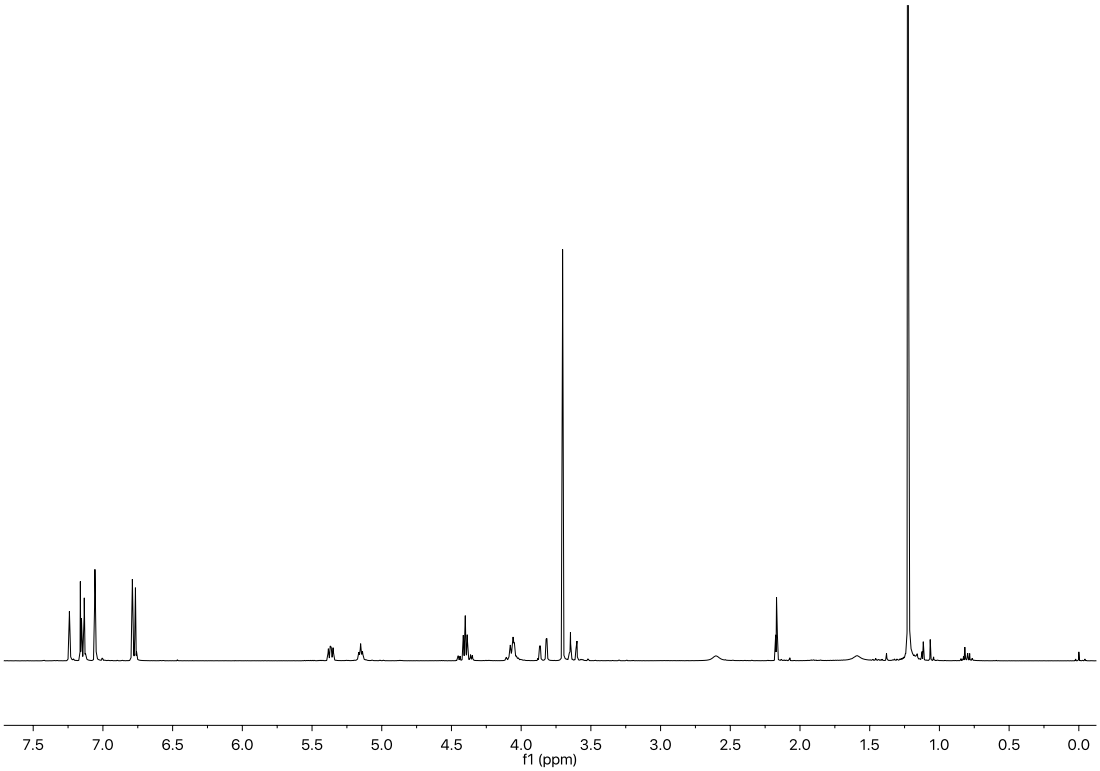

Figure S4 24 ^{1}H NMR ($CDCl_3$, 400 MHz, 298 K) of **170**.

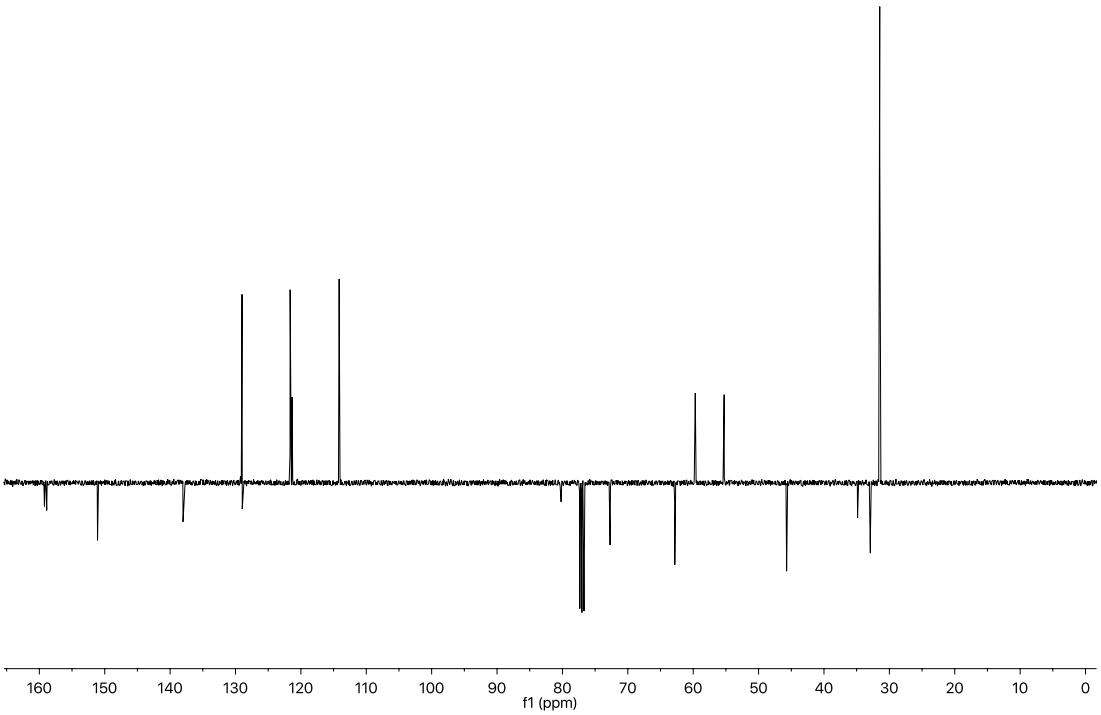

Figure S4 25 J-MOD NMR ($CDCl_3$, 101 MHz, 298 K) of **170**.

*Compound (**173**)*

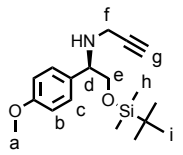

173

To a stirred solution of amino alcohol **167** (291 mg, 1.4 mmol, 1 equiv.) and imidazole (290 mg, 4.26 mmol, 3 equiv.) in DMF (14 mL) was added TBDMSCl (642 mg, 4.3 mmol, 3 equiv.) and the reaction was allowed to stir at r.t. for 1 h. Sat. $NaHCO_3$ (aq.) (50 mL) was added and the mixture was extracted with EtOAc (3 x 20 mL). The combined organics were washed with water (20 mL) and brine (20 mL), dried ($MgSO_4$) and concentrated *in vacuo*. The residue was then dissolved in Et_2O (25 mL) and washed with water (2 x 10 mL) to remove the traces of DMF. The organic layer was dried ($MgSO_4$) and concentrated *in vacuo*, affording the product that was used in the next step without further purification (435 mg, 96%). ^{1}H NMR ($CDCl_3$, 400 MHz, 298 K) δ 7.28 (d, *J* = 8.8, 2H, H_c), 6.87 (d, *J* = 8.8, 2H, H_b), 3.97 (dd, *J* = 9.5, 3.9, 1H, H_d), 3.80 (s, 3H, H_a), 3.64 (dd, *J* = 10.0, 3.9, 1H, H_e), 3.58 – 3.49 (m, 1H, H_e), 3.41 (dd, *J* = 17.1, 2.4, 1H, H_f), 3.10 (dd, *J* = 17.1, 2.4, 1H, H_f), 2.19 (t, *J* = 2.4, 1H, H_g), 0.91 (s, 9H, H_i), 0.05 (s, 6H, H_h). ^{13}C NMR ($CDCl_3$, 101 MHz, 298 K) δ 159.3, 131.7, 129.1, 114.0, 82.5, 71.3,

68.3, 62.6, 55.4, 35.7, 26.1, 18.4, -5.2. HRMS (ESI+) m/z = 320.2036 $[M+H]^+$ (calc. for $C_{18}H_{30}NO_2Si$ 320.2040).

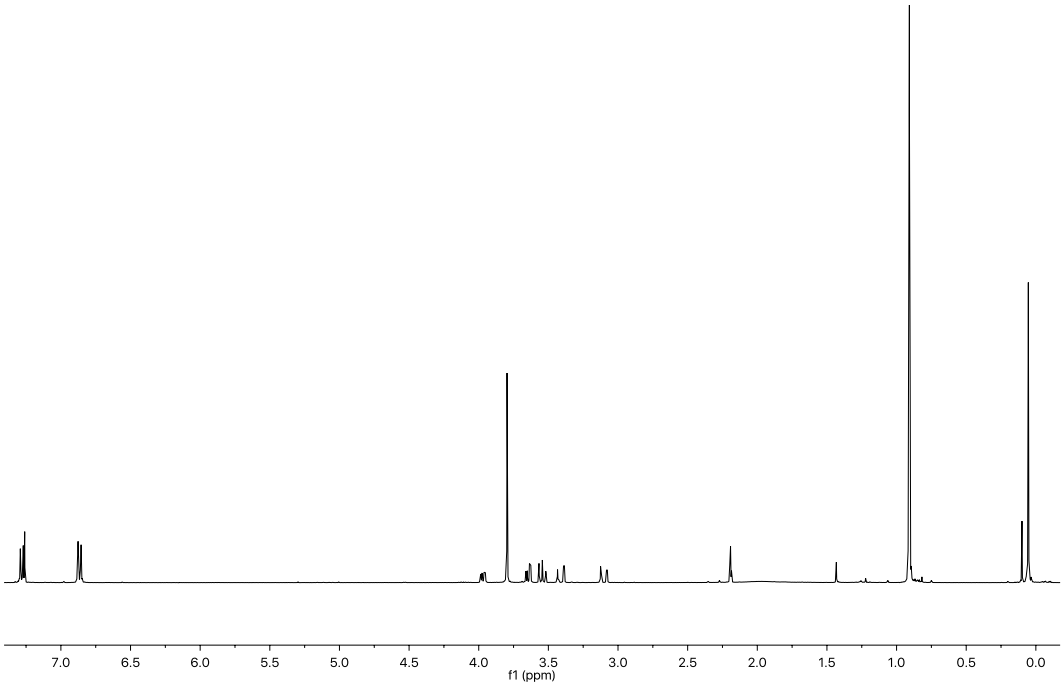

Figure S4 26 ^{1}H NMR ($CDCl_3$, 400 MHz, 298 K) of **173**.

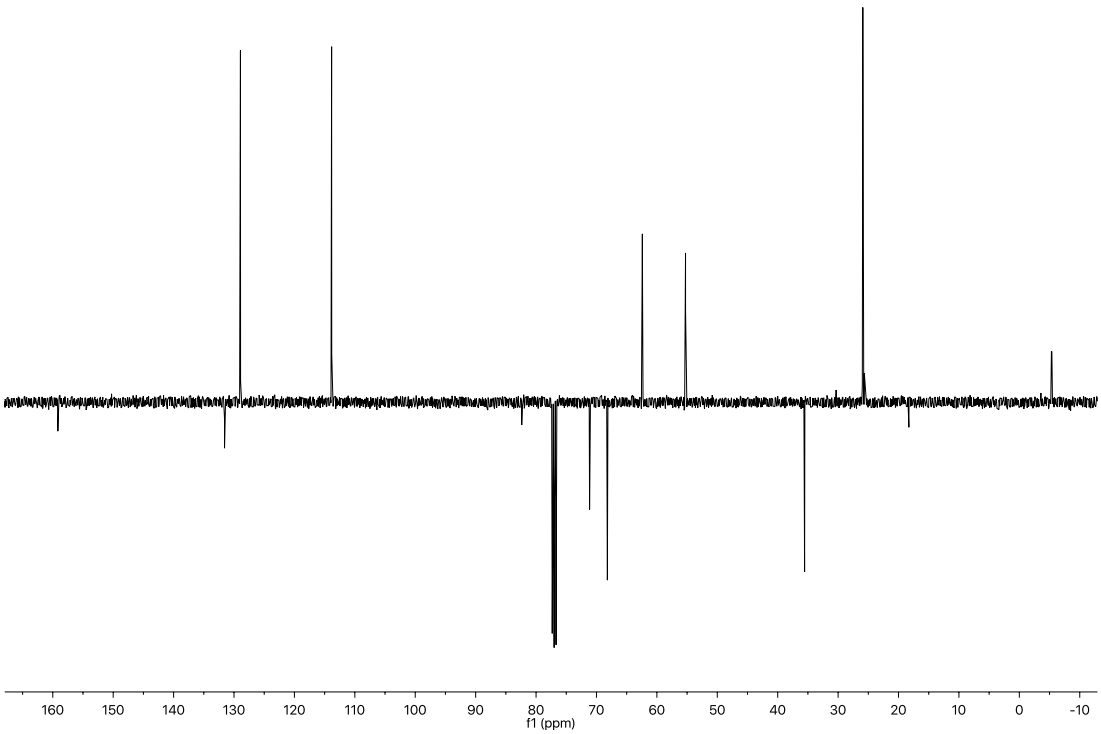

Figure S4 27 J-MOD NMR ($CDCl_3$, 101 MHz, 298 K) of **173**.

*Compound (**174**)*

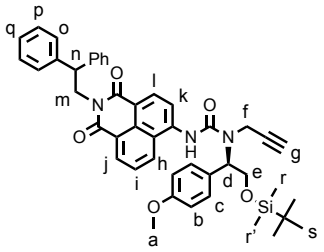

174

To a stirred suspension of amine **118** (98 mg, 0.25 mmol, 1 equiv.) and DMAP (61 mg, 0.5 mmol, 2 equiv.) in CH_2Cl_2 (10 mL) at -10°C was added triphosgene (24 mg, 0.1 mmol, 0.33 equiv.) as a solution in toluene (1 mL). The resulting solution was kept at that temperature for 1 h before addition of amine **173** (159 mg, 0.5 mmol, 2 equiv.), after which the mixture was allowed to stir at room temperature for 2 h. The solvent was concentrated *in vacuo* and the crude residue purified *via* flash column chromatography on silica gel with an isocratic elution of Petrol/CH_2Cl_2/Et_2O 45:45:10, affording the pure product **174** as yellow oil (100 mg, 54%). ^{1}H NMR ($CDCl_3$, 400 MHz, 298 K) δ 8.50 – 8.43 (m, 2H, H_j and H_l), 8.36 (d, *J* = 8.3, 1H, H_k), 8.26 (br s, 1H, -*NH*-), 7.56 (d, *J* = 8.5, 1H, H_h), 7.49 (dd, *J* = 8.5, 7.1, 1H, H_i), 7.41 (d, *J* = 8.7, 2H, H_c), 7.35 (d, *J* = 7.5, 4H, H_o), 7.22 (t, *J* = 7.6, 4H, H_p), 7.17 – 7.08 (m, 2H, H_q), 6.95 (d, *J* = 8.8, 2H, H_b), 5.29 (dd, *J* = 6.9, 3.8, 1H, H_d), 4.83 (s, 3H, H_m and H_n), 4.57 – 4.48 (m, 1H, H_f), 4.47 (dd, *J* = 10.7, 6.9, 1H, H_e), 4.32 (dd, *J* = 10.7, 3.8, 1H, H_e), 4.06 (dd, *J* = 18.1, 2.4, 1H, H_f), 3.82 (s, 3H, H_a), 2.37 (t, *J* = 2.4, 1H, H_g), 0.87 (s, 9H, H_s), 0.08 (s, 3H, H_r), 0.06 (s, 3H, $H_{r'}$). ^{13}C NMR ($CDCl_3$, 101 MHz, 298 K) δ 164.4, 163.9, 159.8, 155.2, 142.0, 141.0, 132.9, 131.0, 129.4, 129.0, 128.6, 128.5, 128.4, 126.8, 126.7, 125.9, 123.4, 123.2, 117.2, 116.7, 114.6, 80.5, 72.8, 64.3, 61.3, 55.5, 48.9, 44.5, 35.3, 26.1, 18.6, -5.2, -5.2. Mass spectrometry analysis (ESI+) showed only product **119** in which the chiral auxiliary has been cleaved. Better conditions to detect compound **173** are currently under investigation.

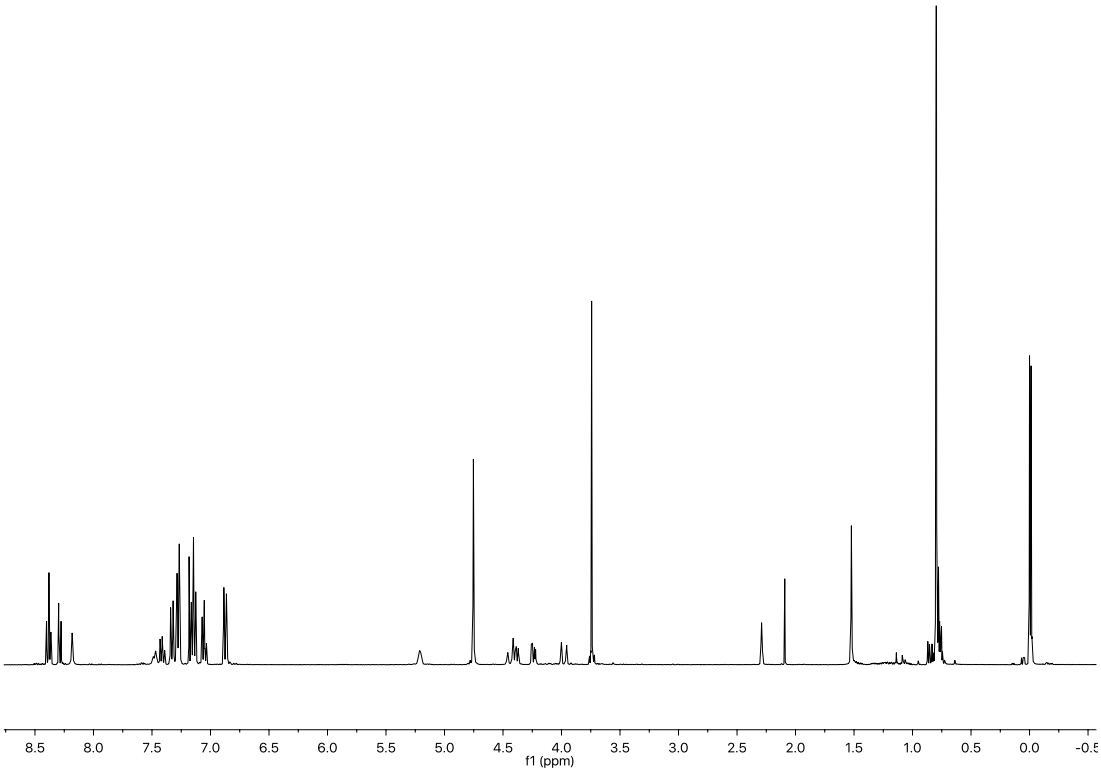

Figure S4 28 ^{1}H NMR ($CDCl_3$, 400 MHz, 298 K) of **174**.

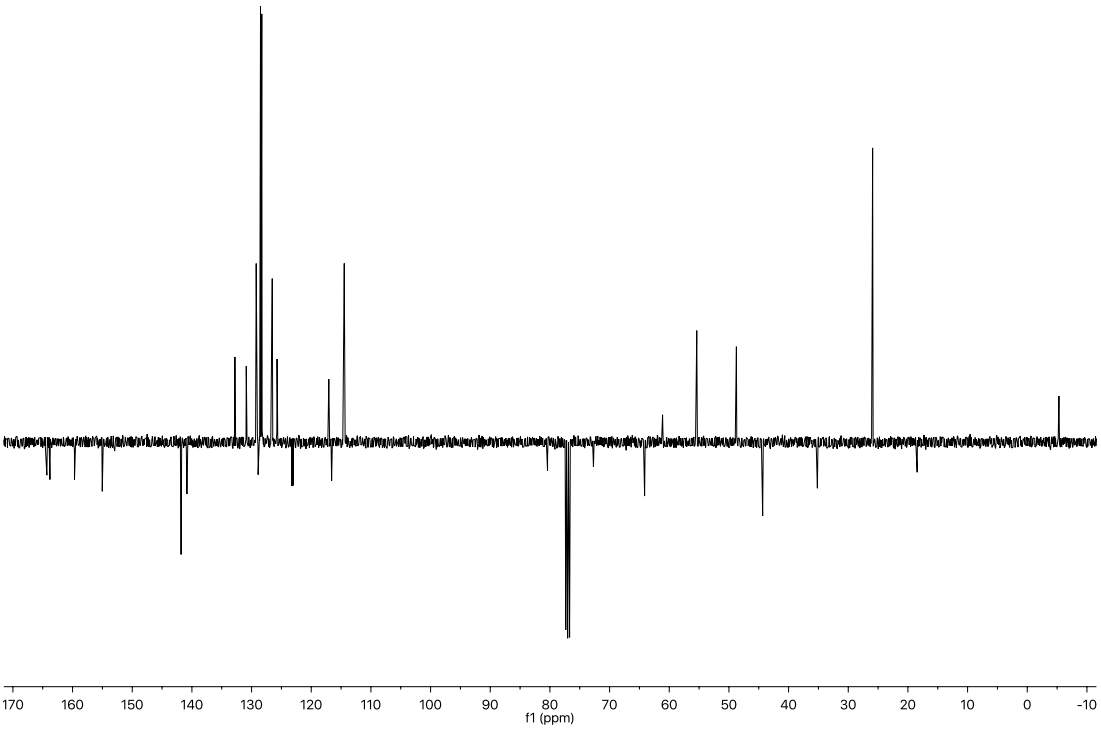

Figure S4 29 J-MOD NMR ($CDCl_3$, 101 MHz, 298 K) of **174**.

*Rotaxane (rac-**139**)*

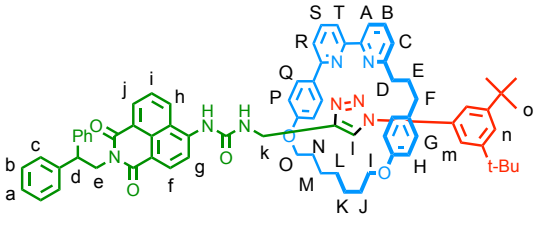

rac-**139**

Rotaxane rac-**139** was synthesised according to general rotaxane formation procedure with macrocycle **128** (96 mg, 0.2 mmol, 1 equiv.), alkyne **119** (95 mg, 0.2 mmol, 1 equiv.), azide **103** (27 mg, 0.2 mmol, 1 equiv.), $[Cu(MeCN)_4]PF_6$ (71 mg, 0.19 mmol, 0.96 equiv.), DIPEA (35 μL, 0.2 mmol, 1 equiv.) in THF. The crude was purified using a gradient of MeCN (0 to 5%) in a mixture of petrol/CH_2Cl_2 1:1, affording the desired rotaxane as a yellow foam (200 mg, 85%). ^{1}H NMR ($CDCl_3$, 400 MHz, 298 K) δ 8.98 (s, 1Hn -*NH1*-), 8.35 (d, *J* = 8.5, 1H, H_f), 8.22 (dd, *J* = 7.3, 1.0, 1H, H_j), 8.17 (d, *J* = 8.5, 1H, H_g), 7.86 (t, *J* = 7.8, 1H, H_B), 7.74 (dd, *J* = 7.8, 1.0, 1H, H_A), 7.68 (s, 1H, H_I), 7.66 – 7.61 (m, 2H, H_h and H_S), 7.59 (dd, *J* = 7.8, 1.0, 1H, H_T), 7.50 (t, *J* = 1.7, 1H, H_n), 7.46 (d, *J* = 1.7, 2H, H_m), 7.41 (dd, *J* = 7.9, 1.4, 4H, H_c), 7.31 (dd, *J* = 7.8, 1.0, 1H, H_C), 7.25 (t app, *J* = 7.6, 4H, H_b), 7.18 – 7.11 (m, 3H, H_a and H_R), 6.90 – 6.83 (m, 3H, -*NH2*- and H_Q), 6.80 (dd, *J* = 8.5, 7.3, 1H, H_i), 6.51 (d, *J* = 8.5, 2H, H_G), 6.36 – 6.28 (m, 4H, H_H and H_P), 4.96 – 4.79 (m, 3H, H_d and H_e), 4.15 (dd, *J* = 15.2, 6.0, 1H, H_k), 4.11 – 3.92 (m, 5H, H_I, H_k and H_O), 2.72 – 2.40 (m, 4H, H_D and H_F), 2.05 – 1.91 (m, 2H, H_J and H_N), 1.90 – 1.69 (m, 4H, H_E, H_J and H_N), 1.68 – 1.44 (m, 6H, H_K, H_L and H_M), 1.37 (s, 18H, H_o). ^{13}C NMR ($CDCl_3$, 101 MHz, 298 K) δ 164.9, 164.5, 164.3, 160.1, 159.0, 157.5, 156.9, 156.4, 153.5, 153.0, 146.5, 143.0, 142.2, 142.1, 138.5, 137.8, 137.0, 133.5, 131.7, 131.2, 130.3, 128.8, 128.8, 128.7 (overlap with one quaternary according to HMBC analysis), 128.4, 128.4, 127.0, 126.7, 126.6, 123.9, 123.5, 123.0, 122.4, 121.4, 121.2, 121.1, 120.2, 120.1, 115.4, 115.0, 114.4, 113.5, 113.4, 67.5, 66.4, 48.9, 44.3, 36.7, 35.3, 35.2, 35.0, 33.2, 31.5, 29.5, 28.7, 28.5, 26.2, 26.1. LRMS (ESI) m/z = 1184.1 $[M+H]^+$.

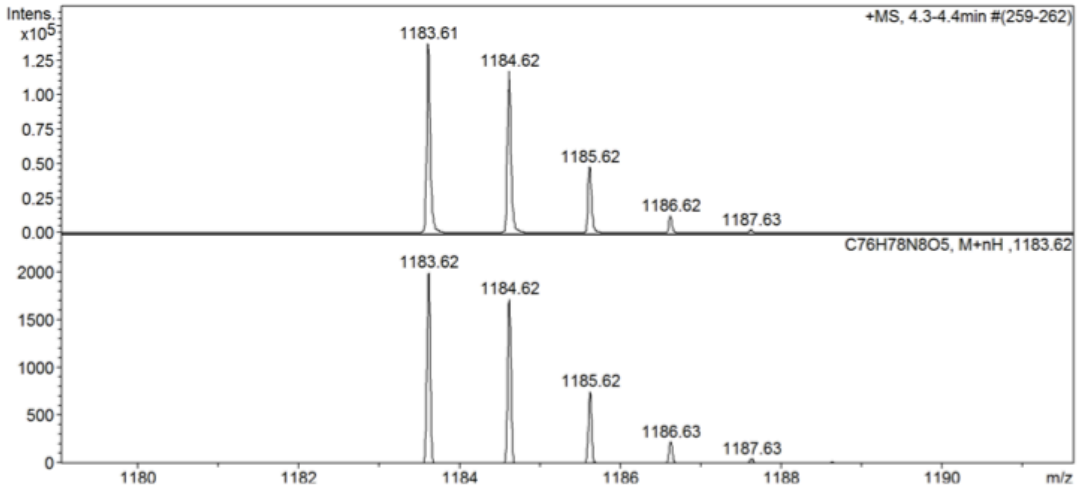

Figure S4 30 Isotope pattern of rac-**139**.

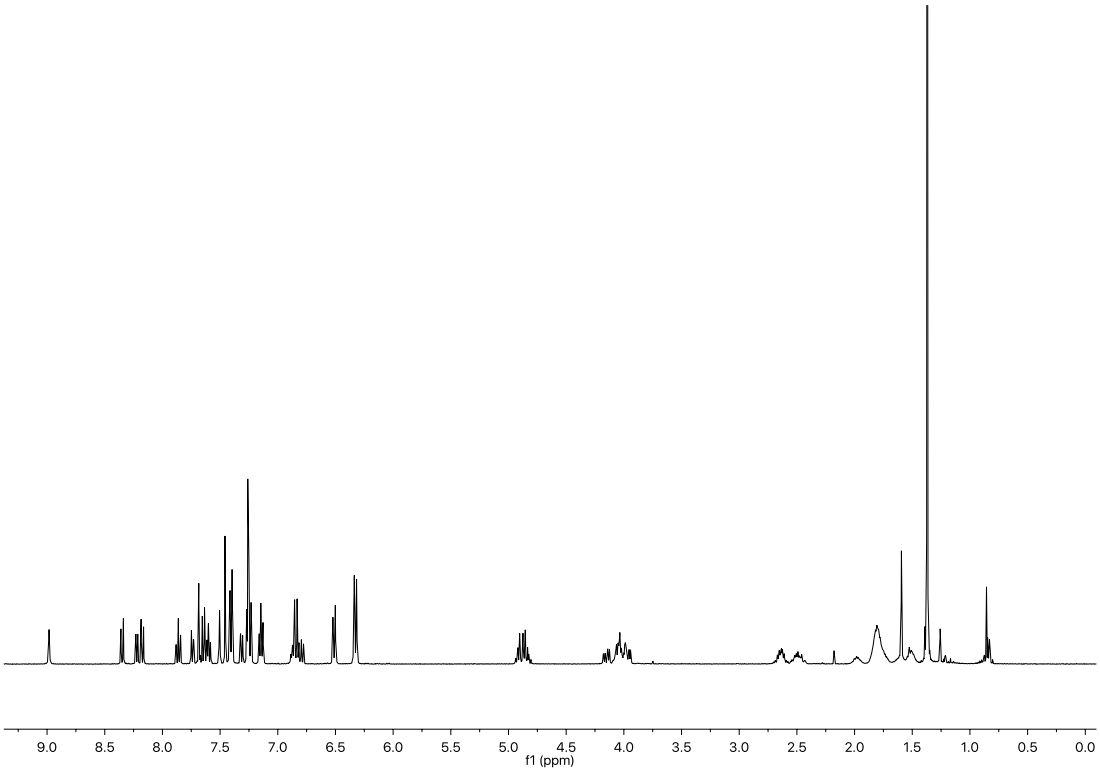

Figure S4 31 ^{1}H NMR ($CDCl_3$, 400 MHz, 298 K) of rac-**139**.

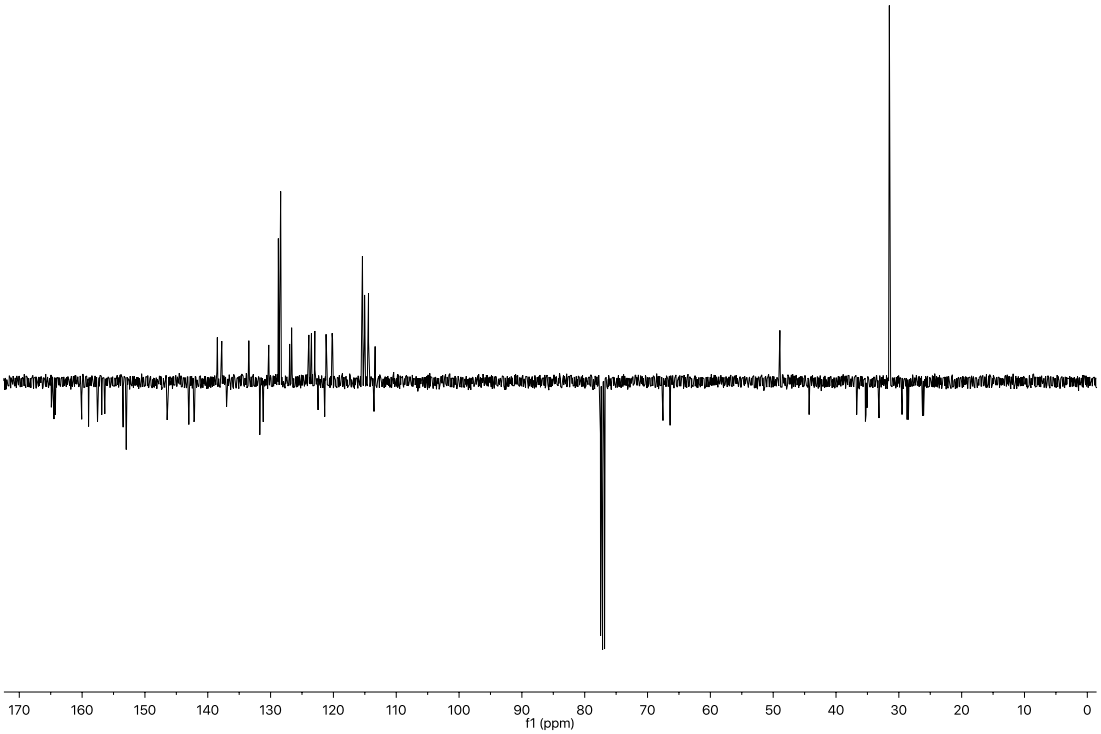

Figure S4 32 J-MOD NMR ($CDCl_3$, 101 MHz, 298 K) of rac-**139**.

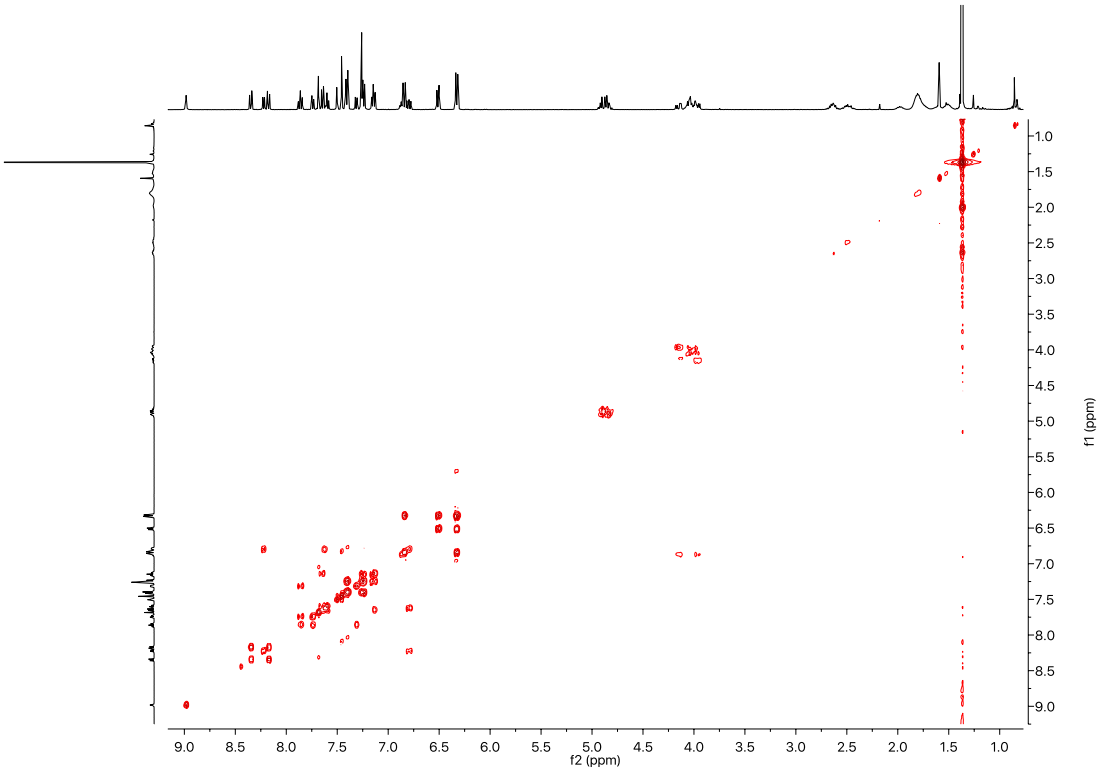

Figure S4 33 COSY NMR ($CDCl_3$, 400 MHz, 298 K) of rac-**139**.

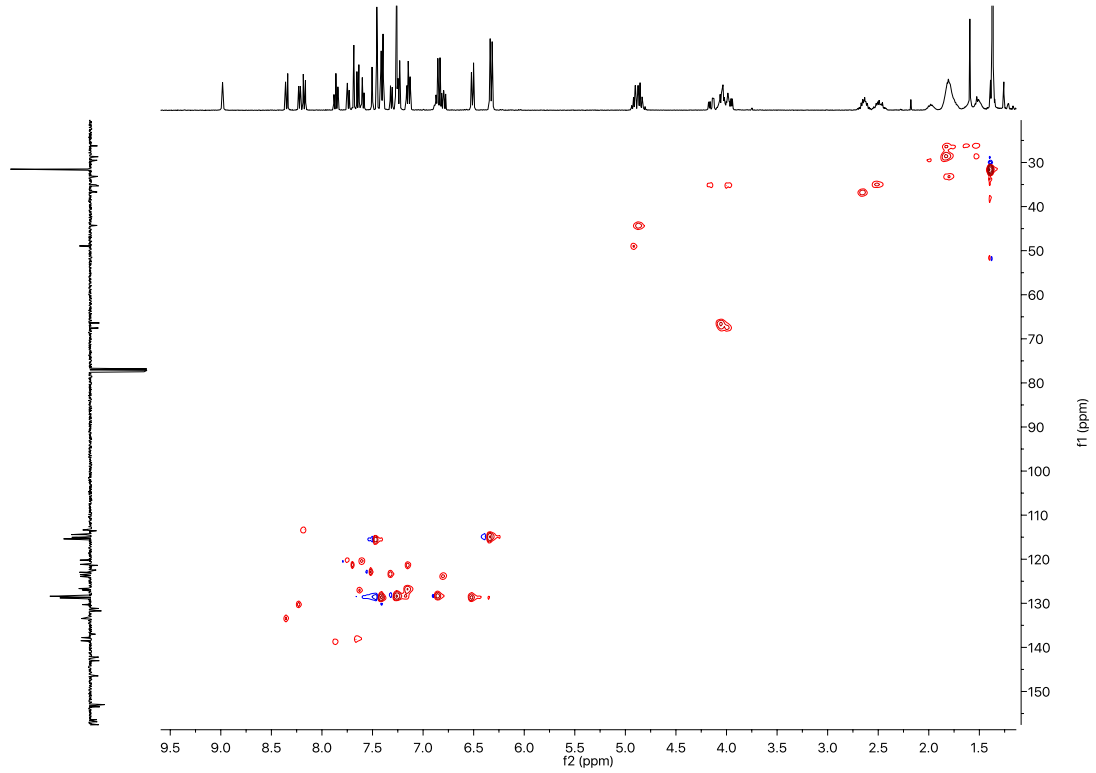

Figure S4 34 HSQC NMR ($CDCl_3$, 400 MHz, 298 K) of rac-**139**.

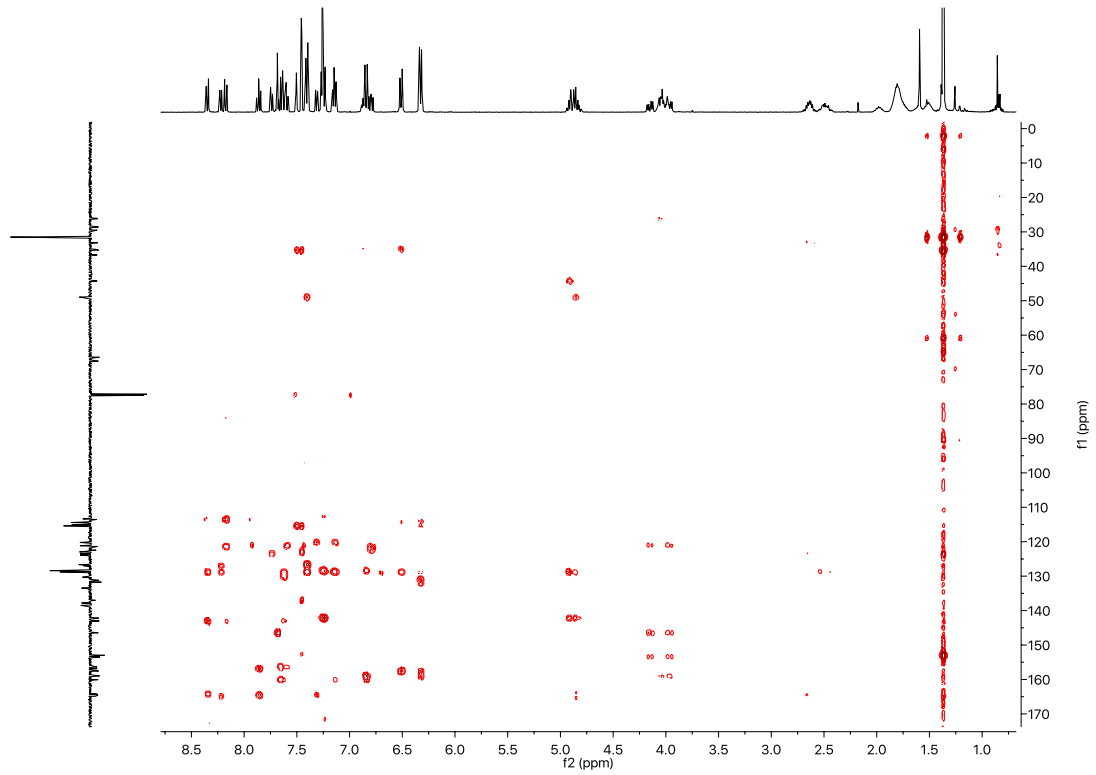

Figure S4 35 HMBC NMR ($CDCl_3$, 400 MHz, 298 K) of rac-**139**.

*Rotaxane (rac-**143**)*

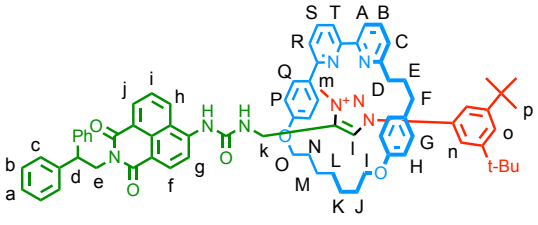

rac-**139**

Rotaxane rac-**139** (15 mg, 0.01 mmol, 1 equiv.) and $[(CH_3)_3O]BF_4$ (3.9 mg, 0.02 mmol, 2 equiv.) were stirred in CH_2Cl_2 (1 mL) at r.t. for 16 h. A drop of MeOH was added to quench the reaction and the solvent was removed under vacuum. The crude was purified *via* flash chromatography on silica gel with a step-wise gradient of MeCN (0 – 20 – 25 – 35%) in a mixture of petrol/CH_2Cl_2 1:1. The solid residue was dissolved in CH_2Cl_2 (5 mL) and washed with a 0.1 M NH_4PF_6 (aq.) (3 x 5 mL) to give rac-**143** a pale yellow solid (8 mg, 48%). ^{1}H NMR ($(CD_3)_2CO$, 400 MHz, 298 K) δ 10.70 (s, 1H, H_l), 8.80 (s, 1H, *-NH1-*), 8.39 (d, *J* = 7.3, 1H, H_j), 8.31 – 8.25 (m, 2H, H_f and H_g), 8.04 (d, *J* = 8.4, 1H, H_h), 7.83 – 7.78 (m, 3H, H_n and H_S), 7.77 (br s, 1H, H_o), 7.71 (d, *J* = 7.9, 1H, H_T), 7.66 (br s, 2H, H_A and H_B), 7.49 (br s, 1H, H_i), 7.43 – 7.39 (m, 4H, H_c), 7.38 (dd, *J* = 7.7, 0.9, 1H, H_R), 7.34 (br s, 1H, H_C), 7.28 – 7.22 (m, 4H, H_b), 7.18 – 7.12 (m, 2H, H_a), 7.07 (br s, 1H, *-NH2-*), 7.01 (d, *J* = 8.6, 2H, H_Q), 6.63 (d, *J* = 8.2, 2H, H_G), 6.46 (d, *J* = 8.6, 2H, H_P), 6.37 (d, *J* = 8.2, 2H, H_H), 4.91 – 4.80 (m, 3H, H_d and H_e), 4.72 – 4.63 (m, 1H, H_k), 4.62 – 4.54 (m, 1H, H_k), 4.52 (s, 3H, H_m), 4.15 – 4.01 (m, 3H, H_l and H_O), 4.00 – 3.93 (m, 1H, H_l), 2.81 – 2.66 (m, 2H, H_D), 2.55 – 2.37 (m, 2H, H_F), 2.10 – 1.82 (m, 6H, H_E, H_N and H_J), 1.82 – 1.34 (m, 6H, H_K, H_L and H_M), 1.27 (s, 18H, H_p). ^{13}C NMR ($(CD_3)_2CO$, 101 MHz, 298 K) δ 164.7, 164.2, 164.1, 160.3, 159.8, 157.8, 157.5, 157.3, 155.1, 154.1, 143.2, 143.1, 142.2, 139.2, 138.9, 133.9, 133.1, 132.9, 131.3, 130.2, 129.5, 129.3, 129.3, 129.3, 129.1, 129.1, 127.6, 127.4, 126.6, 126.4, 124.6, 123.8, 122.8, 122.3, 121.7, 121.0, 116.3 (assigned *via* HMBC analysis), 115.8, 115.4, 114.7, 114.1, 67.2, 66.4, 49.7, 44.6, 38.8, 37.8, 36.0, 35.5, 34.1, 33.9, 31.4, 28.4, 26.7, 26.5. (signal for carbons N and J overlap with acetone signal according to HMBC analysis). ^{31}P NMR ($(CD_3)_2CO$, 162 MHz, 298 K) δ -144.21 (sept, *J* = 707.8). ^{19}F NMR ($(CD_3)_2CO$, 162 MHz, 298 K) δ -72.64 (d, *J* = 707.8). LRMS (ESI+) m/z = 1198.22 $[M]^+$.

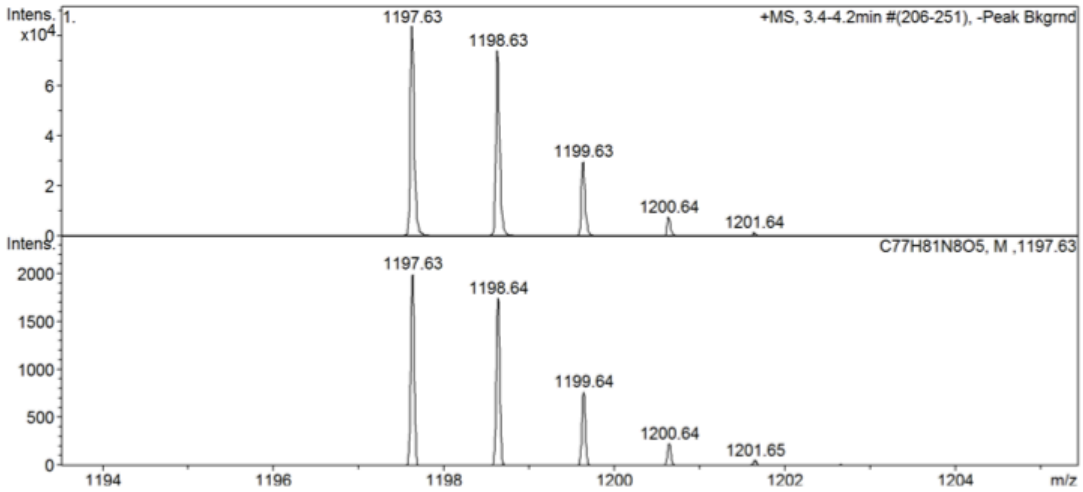

Figure S4 36 Isotope pattern of rac-**143**.

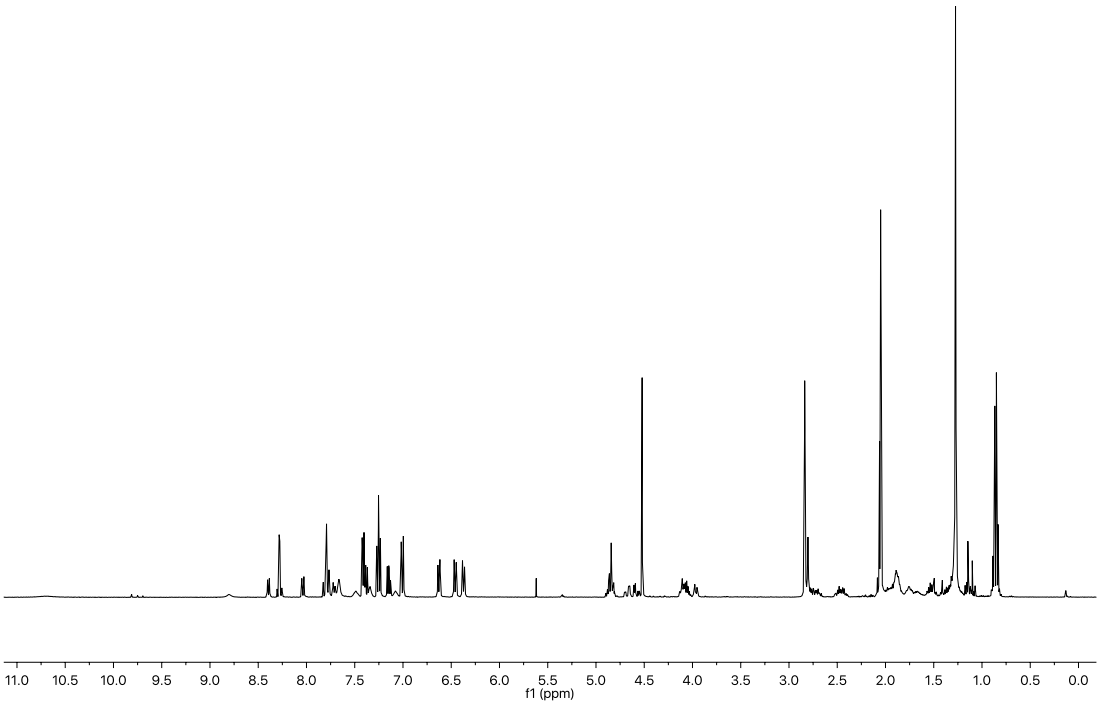

Figure S4 37 ^{1}H NMR ($(CD_3)_2CO$, 400 MHz, 298 K) of rac-**143**.

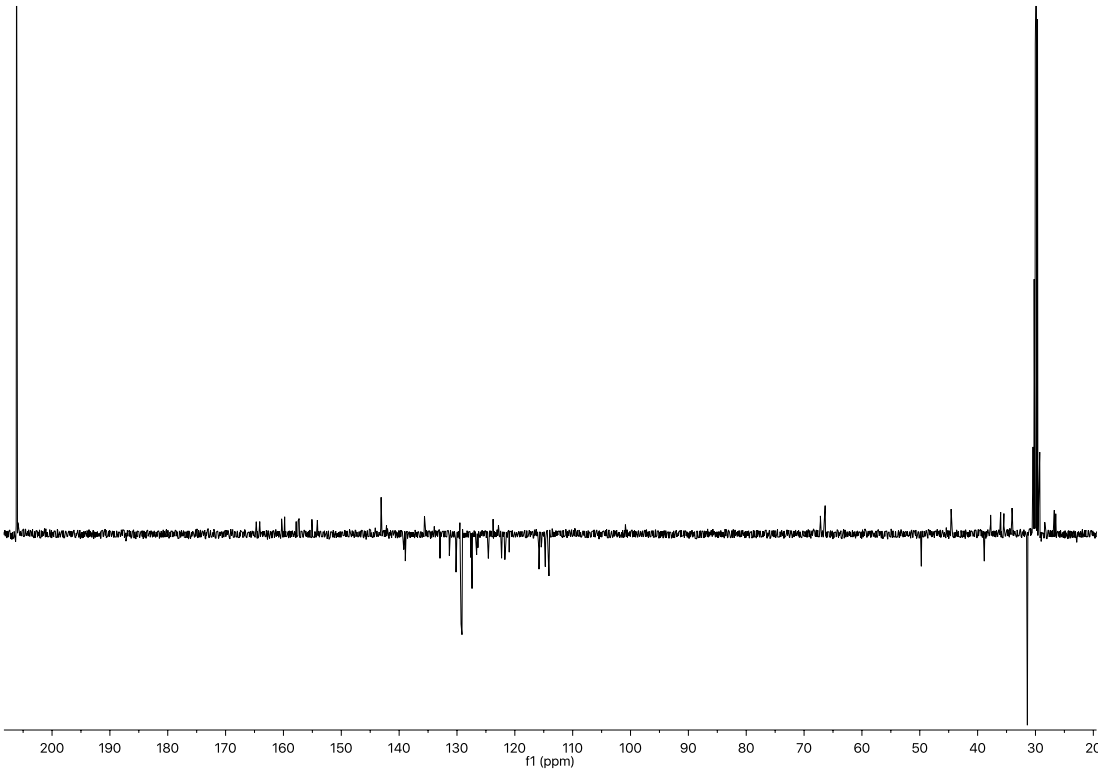

Figure S4 38 J-MOD NMR ($(CD_3)_2CO$, 101 MHz, 298 K) of rac-**143**.

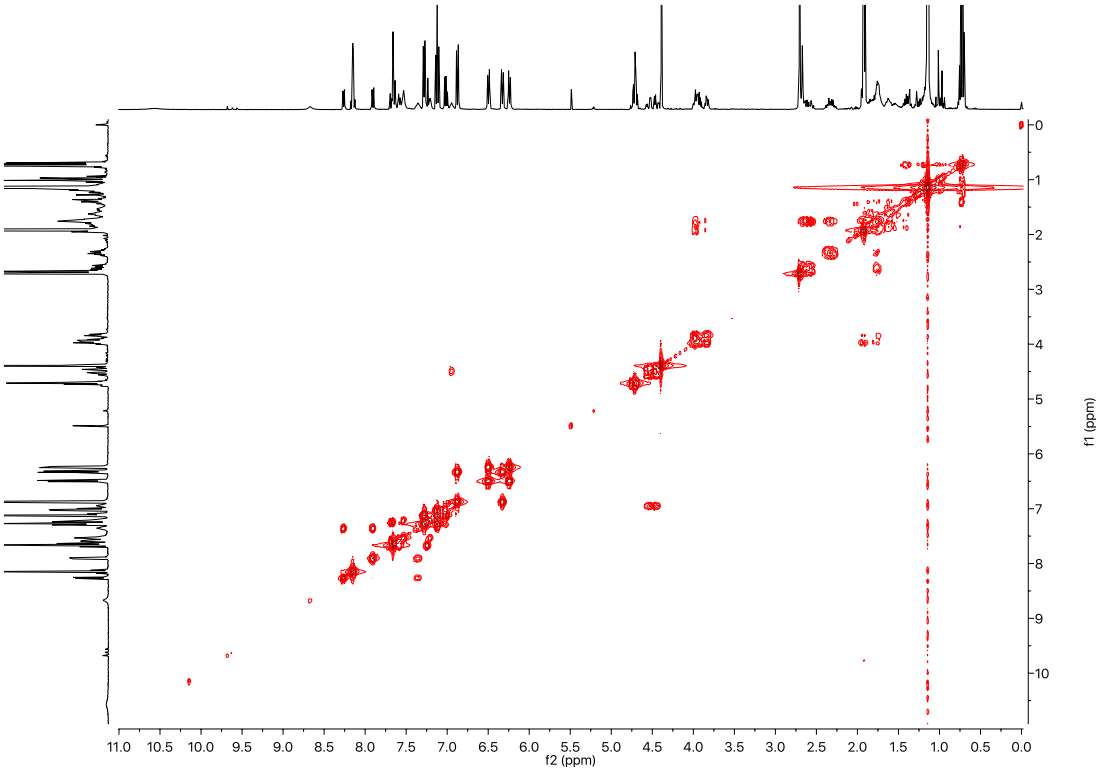

Figure S4 39 COSY NMR ((CD_3), 400 MHz, 298 K) of rac-**143**.

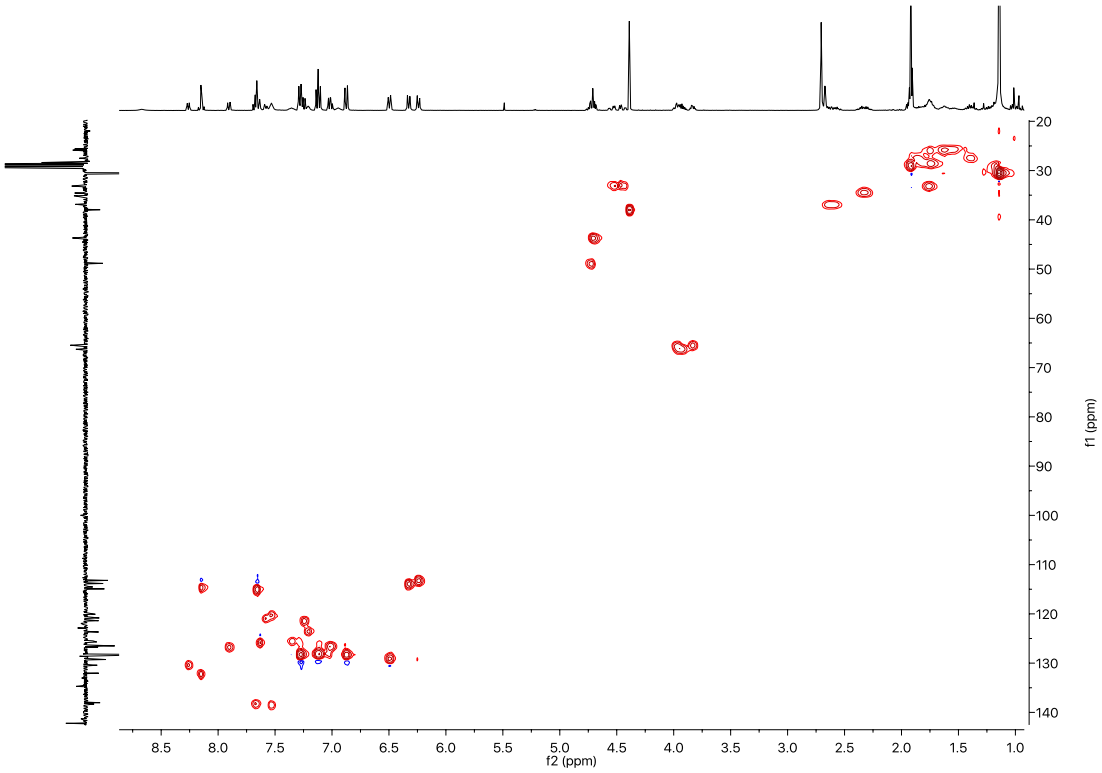

Figure S4 40 HSQC NMR ($(CD_3)_2CO$, 400 MHz, 298 K) of rac-**143**.

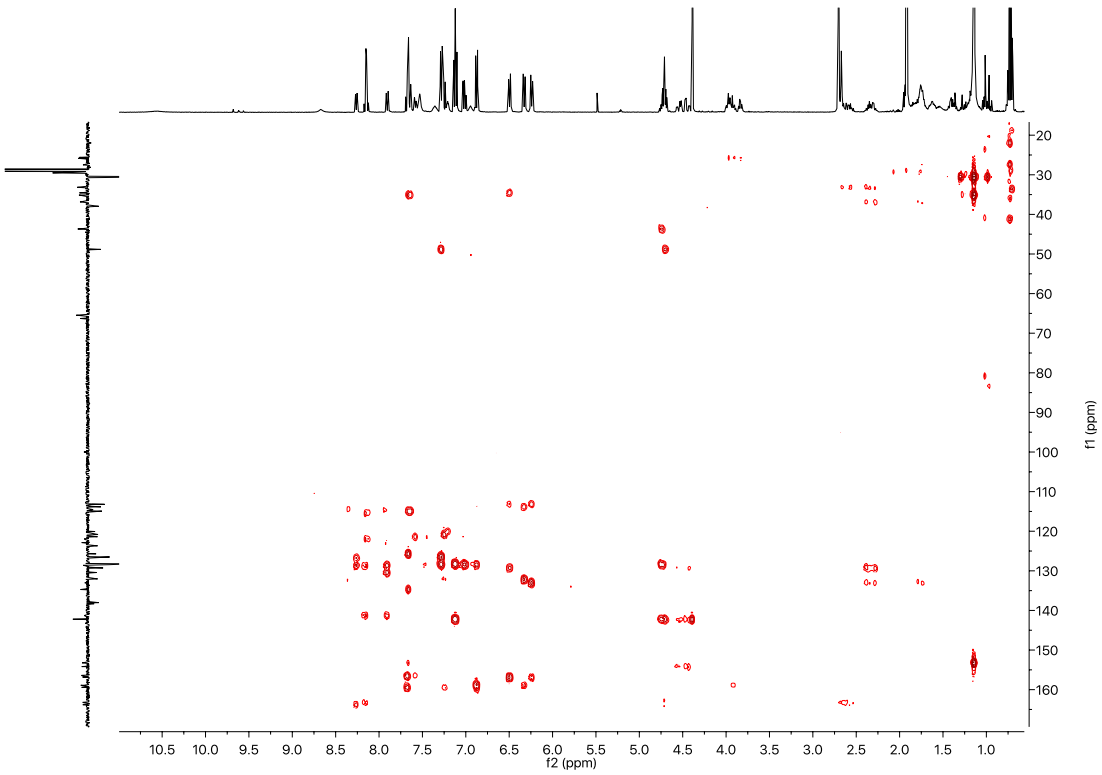

Figure S4 41 HMBC NMR ($(CD_3)_2CO$, 400 MHz, 298 K) of rac-**143**.

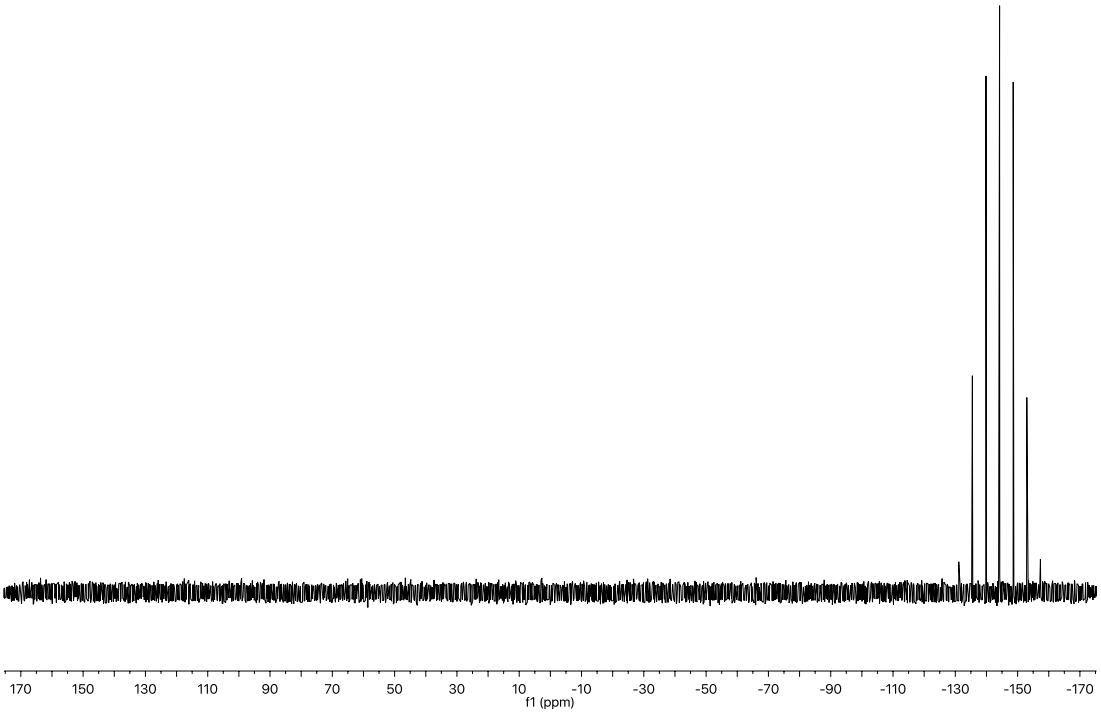

Figure S4 42 ^{31}P NMR ($(CD_3)_2CO$, 162 MHz, 298 K) of rac-**143**.

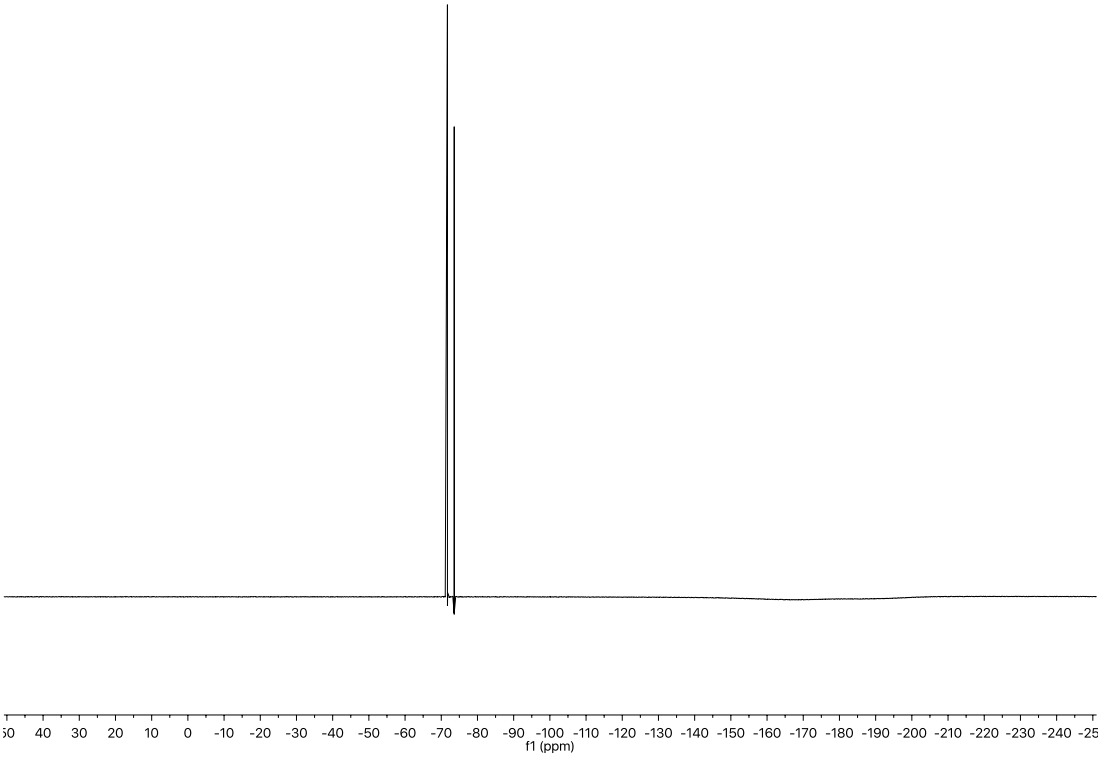

Figure S4 43 ^{19}F NMR ($(CD_3)_2CO$, 162 MHz, 298 K) of rac-**143**.

*Rotaxane (**177**)*

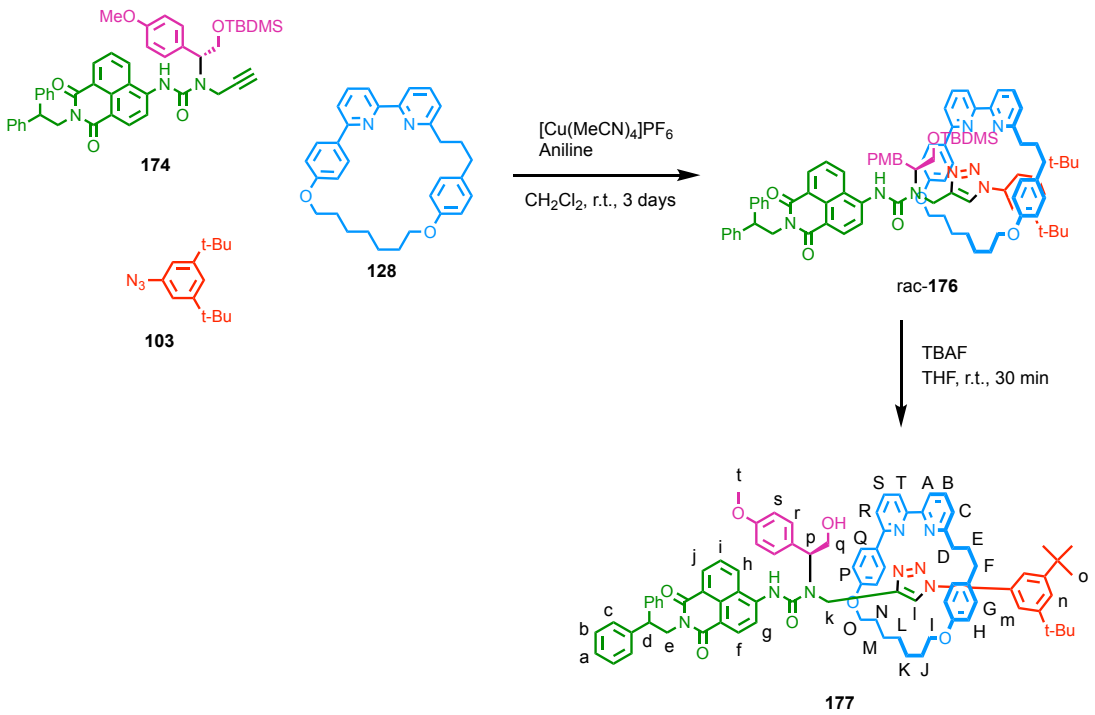

Rotaxane rac-**176** was synthesised according to general rotaxane formation procedure with macrocycle **128** (65 mg, 0.14 mmol, 1 equiv.), alkyne **174** (100 mg, 0.14 mmol, 1 equiv.), azide **103** (31 mg, 0.14 mmol, 1 equiv.), $[Cu(MeCN)_4]PF_6$ (49 mg, 0.13 mmol, 0.96 equiv.), aniline (0.02 mL, 0.2 mmol, 1.5 equiv.) in CH_2Cl_2. The crude was isolated as a mixture of the two diastereoisomers with the remaining macrocycle **128** *via* flash column chromatography on silica gel with an isocratic elution of petrol/CH_2Cl_2/Et_2O 10:10:1. (150 mg, 70% yield of rotaxane). The mixture was then dissolved in THF (1 mL) and TBAF (0.19 mL, 0.19 mmol, 2 equiv.). The reaction was stirred at r.t. for 30 min then diluted with CH_2Cl_2 (5 mL) and washed with 1M NH_4Cl (aq.) (4 x 5 mL). The organic layer was recovered, dried ($MgSO_4$) and concentrated before being submitted to flash column chromatography purification (silica/product = 500) with an isocratic elution of petrol/CH_2Cl_2 2:1, Et_2O 20%, which provided the pure first diastereoisomer (32 mg, 0.024 mmol, 18%). Unfortunately, the majority of the compound was used in the next step prior to full assignment of the ^{1}H NMR ^{1}H NMR ($CDCl_3$, 400 MHz, 298 K) δ 9.43 (s, 1H), 8.59 (d, *J* = 8.5, 1H), 8.54 (d, *J* = 7.4, 1H), 8.41 (d, *J* = 8.3, 1H), 8.28 (br s, 1H), 7.81 – 7.68 (m, 2H), 7.59 – 7.49 (m, 2H), 7.38 (s, 2H), 7.37 – 7.30 (m, 4H), 7.25 – 7.16 (m, 6H), 7.15 – 7.08 (m, 2H), 6.96 – 6.82 (m, 4H), 6.37 (d, *J* = 7.9, 2H), 6.07 (d, *J* = 8.1, 2H), 5.98 (br s, 2H), 5.49 (br s, 1H), 4.90 – 4.76 (m, 3H), 4.15 (br s, 2H),

3.86 (s, 3H), 3.54 (m, 4H), 2.80 – 2.58 (m, 2H), 2.57 – 2.45 (m, 1H), 2.27 (s, 1H), 1.98 – 1.19 (m, 18H), 1.11 (s, 18H). LRMS (ESI+) m/z = 1334.28 $[M+H]^+$.

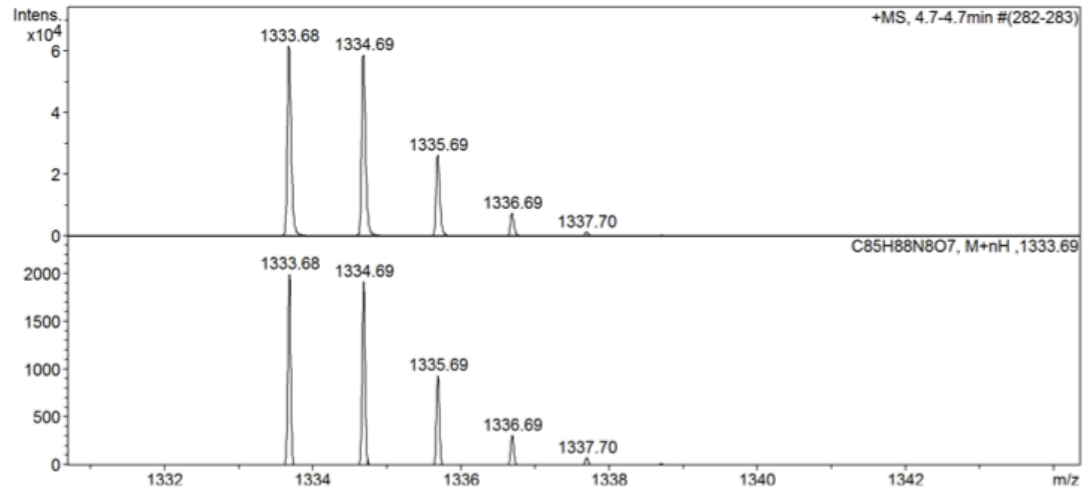

Figure S4 44 Isotope pattern for **177**.

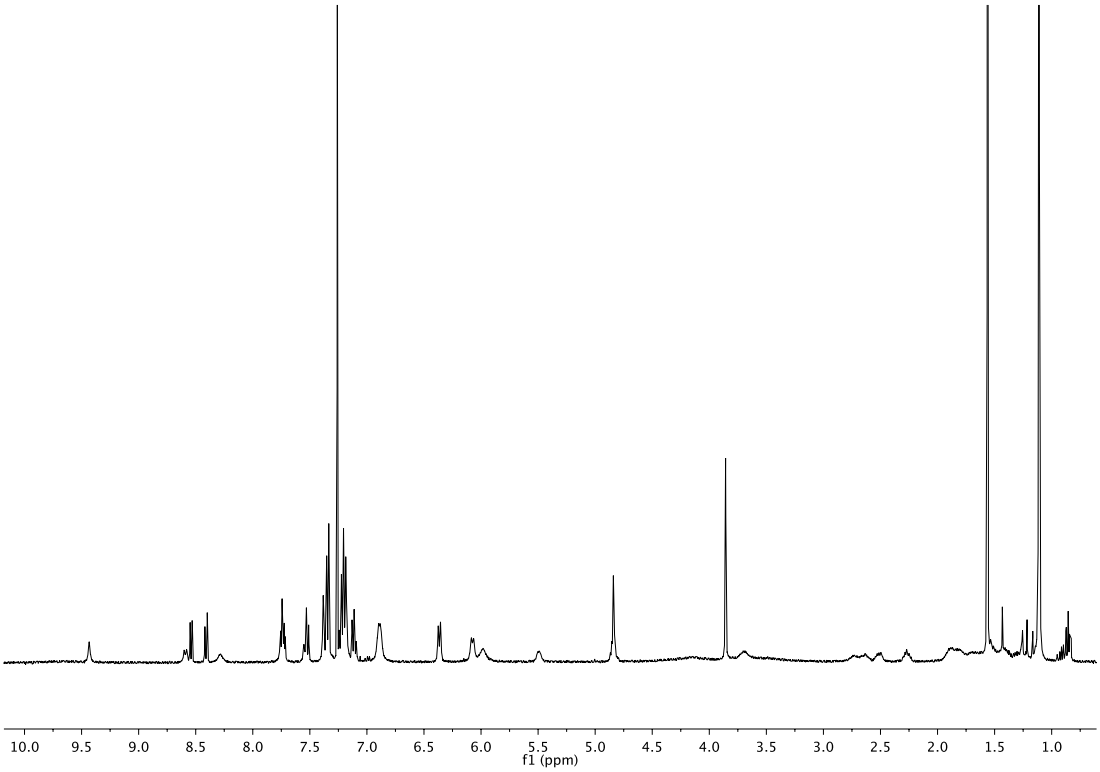

Figure S4 45 ^{1}H NMR ($CDCl_3$, 400 MHz, 298 K) of the first enantiomer of **177**.

*Compound (**143**)*

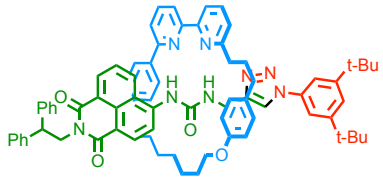

139 *ee* = 90%

To a stirred solution of the first enantiomer of **177** (30 mg, 0.023 mg, 1 equiv.) in $CHCl_3$ (0.5 mL) at 0 ºC was added TFA (0.5 mL). The resulting solution was allowed to stir at r.t. for 15 min. The crude was diluted with CH_2Cl_2 (2 mL) and washed with sat. $NaHCO_3$ (aq.) (2 mL). The organic layer was dried ($MgSO_4$) and the solvent removed *in vacuo*. The crude residue was purified *via* flash chromatography on silica gel, affording **139** as a yellow solid (26 mg, 95%). *ee* 90% [Whelk-O 1® (EtOH); flow rate 0.2 mL/min, ***t1* = 35.5 min**, *t2* = 40.1 min]. NMR data matches that of rac-**139**.

4.5. Bibliography

[1] G. Schill, A. Lüttringhaus, *Angew. Chem. Int. Ed. Engl.* **1964**, *3*, 546–547.

[2] C. Yamamoto, Y. Okamoto, T. Schmidt, R. Jäger, F. Vögtle, *J. Am. Chem. Soc.* **1997**, *119*, 10547–10548.

[3] C. Reuter, C. Seel, M. Nieger, F. Vögtle, *Helv. Chim. Acta* **2000**, *83*, 630–640.

[4] Y. Makita, N. Kihara, N. Nakakoji, T. Takata, S. Inagaki, C. Yamamoto, Y. Okamoto, *Chem. Lett.* **2007**, *36*, 162–163.

[5] R. J. Bordoli, S. M. Goldup, *J. Am. Chem. Soc.* **2014**, *136*, 4817–4820.

[6] N. Kameta, Y. Nagawa, M. Karikomi, K. Hiratani, *Chem. Commun.* **2006**, 3714.

[7] J. L. Sessler, A. Andrievsky, V. Král, V. Lynch, *J. Am. Chem. Soc.* **1997**, *119*, 9385–9392.

[8] Z.-B. Li, J. Lin, L. Pu, *Angew. Chem. Int. Ed.* **2005**, *44*, 1690–1693.

[9] T. Ema, K. Okuda, S. Watanabe, T. Yamasaki, T. Minami, N. A. Esipenko, P. Anzenbacher, *Org. Lett.* **2014**, *16*, 1302–1305.

[10] J. Yoo, M. Kim, S. Hong, J. L. Sessler, C. Lee, *J. Org. Chem.* **2009**, *74*, 1065–1069.

[11] R. Mitra, M. Thiele, F. Octa-Smolin, M. C. Letzel, J. Niemeyer, *Chem . Commun.* **2016**, *52*, 5977–5980.

[12] J. Y. C. Lim, I. Marques, V. Félix, P. D. Beer, *J. Am. Chem. Soc.* **2017**, *139*, 12228–12239.

[13] J. E. M. Lewis, R. J. Bordoli, M. Denis, C. J. Fletcher, M. Galli, E. A. Neal, E. M. Rochette, S. M. Goldup, *Chem. Sci.* **2016**, *7*, 3154–3161.

[14] C. D. Evans, M. F. Mahon, P. C. Andrews, J. Muir, S. D. Bull, *Org. Lett.* **2011**, *13*, 6276–6279.

[15] M. Galli, J. E. M. Lewis, S. M. Goldup, *Angew. Chem. Int. Ed.* **2015**, *54*, 13545–13549.

[16] W. Zhu, D. Ma, *Chem. Commun.* **2004**, 888.

[17] J. Y. C. Lim, I. Marques, L. Ferreira, V. Félix, P. D. Beer, *Chem . Commun.* **2016**, *52*, 5527–5530.